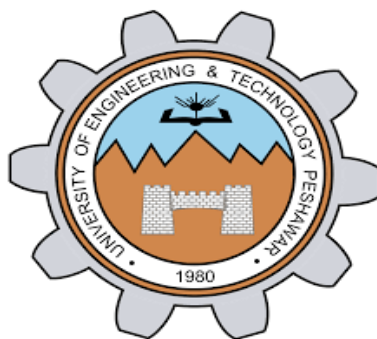# 5TH ONLINE INTERNATIONAL CONFERENCE

SUSTAINABILITY IN PROCESS INDUSTRY

(SPI-2020)

DECEMBER 15-16, 2020

Organized By

DEPARTMENT OF CHEMICAL ENGINEERING

UNIVERSITY OF ENGINEERING AND TECHNOLOGY, PESHAWAR
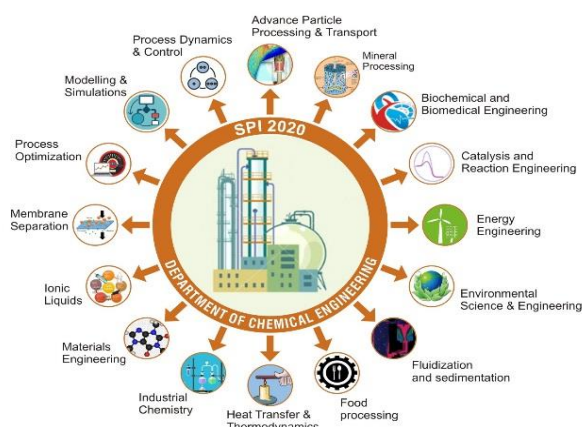
5th Online International Conference on

SUSTAINABILITY IN PROCESS INDUSTRY
(SPI-2020)

December 15-16, 2020

Organized By:

DEPARTMENT OF CHEMICAL ENGINEERING
UNIVERSITY OF ENGINEERING AND TECHNOLOGY, PESHAWAR

Editorial Board

Prof. Dr. Muddasar Habib
Dr. S. Naveed ul Hasan
Dr. Naseer Ahmed Khan
Dr. Hayat Khan
Dr. Maryum Ibrar Shinwari

Organizing Committee

Patron-in-Chief

Vice Chancellor, UET Peshawar

General Chair / Guest of Honor

Prof. Dr. Iftikhar Hussain   (Vice Chancellor, UET Peshawar)
Prof. Dr. Qaisar Ali   (Pro-Vice Chancellor, UET Peshawar)

Conference Advisor

Prof. Dr. Muhammad Abdul Aziz Irfan
(Senior Dean, Faculty of Mechanical, Chemical and Industrial Engineering, UET Peshawar)

Conference Chair

Prof. Dr. Muddasar Habib   (Chairman, Department of Chemical Engineering, UET Peshawar)

Conference Co-Chair

Prof. Dr. Saeed Gul   (Department of Chemical Engineering, UET Peshawar)
Prof. Dr. Mohammad Younas (Department of Chemical Engineering, UET Peshawar)

Conference Secretaries

Dr. S. Naveed ul Hasan
Dr. Hayat Khan

Steering Committee

Dr. Naseer Ahmad Khan
Ms Ghazala Malik
Dr. Imran Ahmad
Dr. S. Naveed ul Hasan
Dr. Hayat Khan
Dr. Mansoor ul Hassan

Protocol and Registration Committee

Dr. Nehar Ullah
Dr. Irshad Ali
Dr. Asmat Ullah

Media and Publications Committee

Dr. Naseer Ahmed Khan
Dr. S. Naveed ul Hassan
Dr. Hayat Khan
Dr. Mansoor ul Hassan
Ms Ghazala Ali Khan

Food and Entertainment Committee

Engr. Amad Ullah Khan
Engr. Wajid Ali

Conference Hall and Stage Committee

Dr. Imran Ahmad
Engr. Amad Ullah Khan

Scientific Expert Committee

Prof. Dr. Naveed Ramzan	(UET Lahore)
Prof. Dr. Khadija Qureshi	(MUET, Jamshoro)
Prof. Dr. Suleman Tahir	(University of Gujrat)
Prof. Dr. Shahid Maqsood	(UET Peshawar)
Prof. Dr. Abdul Shakoor	(UET Peshawar)
Dr. Atta Ullah	(PIEAS Islamabad)
Dr. Tanveer Iqbal	(UET, Lahore, KSK campus)
Dr. Saima Yasin	(UET, Lahore, KSK campus)
Dr. Muhammad Najam Khan Malghani	(BUITEMS, Quetta)
Dr. Faisal Mushtaq	(BUITEMS, Quetta)
Dr. Muhammad Yasir Khan	(Karachi University, Karachi)
Dr. Iftikhar Ahmad	(NUST Islamabad)
Dr. Ishaq Ahmad	(UET Peshawar)
Dr. Khan Muhammad	(UET Peshawar)

Members

Prof. Dr. Iftikhar Hussain	Member
Prof. Dr. Sahar Noor	Member
Prof. Dr. Farid Khan	Member
Prof. Dr. Zia-ul-Haq	Member
Prof. Dr. Abdul Shakoor	Member
Prof. Dr. Misbah Ullah	Member
Prof. Dr. Khan Shahzada	Member
Dr. Shumaila Farooq	Member
Ms. Ghazala Malik	Member
Dr. Jamil Ahmad	Member
Dr. Nehar Ullah	Member
Dr. Imran Ahmad	Member
Engr. Imran Khan Swati	Member
Engr. Sultan Ali	Member
Engr. Amad ullah Khan	Member
Dr. Irshad Ali	Member
Dr. Muhammad Daud	Member
Dr. Nasser Ahmed Khan	Member
Dr. Asmat Ullah	Member
Dr. Muazzam Arshad Paracha	Member
Dr. Mansoor ul Hassan	Member
Engr. Unsia Habib	Member
Engr. Wajid Ali	Member

Invited Speakers

Prof. Dr. Najma Memon	(National Centre of Excellence in Analytical Chemistry, University of Sindh, Jamshoro, Pakistan)
Prof. Dr. Khadija Qureshi	(Mehran University of Engineering and Technology Jamshoro, Pakistan)
Prof. Dr. Nadia Tahir	(QAA, HEC Islamabad, Pakistan)
Dr. Neslihan Yuca	(Maltepe University Enwair Energy Technologies Corporation Istanbul, Turkey)
Dr. Tanveer Iqbal	(University of Engineering and Technology Lahore Pakistan)
Dr. Afrasyab Khan	(SUS University, Russia & PIEAS Islamabad Pakistan)
Dr. Muhammad Zaman	(PIEAS Islamabad, Pakistan)
Dr. Sofia Chaudry	(Punjab University Pakistan & Murdoch University Western Australia)
Dr. Thi Bang Tuyen Nguyen	(University of Newcastle Australia)
Dr. Muhammad Shehzad Kamal	(KFUPM, Kingdom of Saudi Arabia)
Dr. Iftikhar Ahmad	(NUST, Islamabad Pakistan)
Dr. Muhammad Yasir Khan	(University of Karachi, Pakistan)
Engr. Hafiz Zeeshan Ahmad	(Tronox Management Pty Ltd, Western Australia)
Engr. Fazli Amin	(Deputy General Manager (Production), Askari Cement Nizampur, Pakistan)

Sponsors and Partners

Established in 1957 as Pakistan National Scientific & Technical Documentation Centre, (PANSDOC) by UNESCO under PCSIR, later on project was formulated and it was converted to Pakistan Scientific & Technological Information Centre (PASTIC) and transferred under the administrative control of Pakistan Science Foundation in 1973.

PASTIC is committed to serve Scientific and Technological Information needs of R&D and Industrial Community through Anticipatory and Responsive Information Services. PASTIC collects information from within the country as well as from abroad, processes and organizes the same and disseminate to its users. PASTIC is the premier organization for dissemination of Scientific and Technological Information to the citizens of Pakistan through a network of its Centers located at Islamabad, Karachi, Lahore, Peshawar, Quetta, Faisalabad and Muzaffarabad. PASTIC clients include Scientists, Researchers, Engineers, Entrepreneurs and Industry people.

To begin with PASTIC supported research community across the country when S&T research infrastructure in Pakistan was at a nascent stage and provided facilities including supply of scientific and technical documents, abstracts and indexes, bibliographies, translations, patent information and patent indexes, science reference library service, technological information transfer service, dissemination of computer based information services, reprographic and publication services.

PASTIC Objectives

- National S&T/R&D Information Repository of indigenous information resources (databases)
- S&T/R&D information dissemination through contemporary reference information tools
- Strengthen National Science Reference Library for resource sharing & Inter-library collaborations (consortium) and empowerment of information professionals.
- Promotion of R&D based industrial development
- Facilitate printing of S&T/R&D Publications
- Capacity/skill development of researchers & entrepreneurs
- Develop collaborations with national and international information networks

PASTIC Activities/Functions

PASTIC Online databases

Pakistan Science Abstracts (PSA): National research published in Pakistani S&T Journals & Conference Proceedings etc.

PakCat: Union online Public Access Catalogue (OPAC) of Books available in Science and technology Libraries of Pakistan.

DSpace full text digital repository of indigenous S&T literature.

Database of R&D Projects executed in Pakistan & Industry related databases.

S&T Publications
- Pakistan Journal of Computer & Information Systems (PJCIS): A biannual Open Access primary Journal meant for researchers from Computer Science & Engineering, Information & Communication Technologies (ICTs), Information Systems, Library and Information Science.
- Technology Roundup: Publish bi-monthly bulletin by repackaging of latest global Trade and Technology information.
- Union Catalogue: Provide information on research materials (books/journals/conference proceedings/reports, etc) available in different S&T libraries of Pakistan.
- Scientific Periodicals of Pakistan: A handy guide of scientific periodicals published in Pakistan.
- Abstract Books of Conferences: PASTIC support publication/printing of Abstract Books organized by various S&T universities (on request).

Promotion of Commercializable Technologies & Industrial Products
Organize STEM and IT Expo to promote local Research and Development, SMEs, technologies/products/services/industrial R&D challenges/issues as well as empowering youth and general public on new and faster ways of delivering and accessing information.

National Science Reference Library Facility
A state of the art Traditional Library facilitating the researcher through following services: Reference & Referral Services; Reader Service; Internet Service, Journal Listings; Photocopying & Scanning Services.

Human Resource Development (Capacity Building)
Organize Seminars/Workshops /Trainings/ for capacity building of:
- Young Researchers on Data Analysis and bibliographic citation Tools (SPSS, EndNote, Mendeley)
- Women Entrepreneurs on e-marketing and e business skills
- Library Professionals on Library Information Management Tools & techniques (Koha, D-space etc)
- Researchers and entrepreneurs on Intellectual Property Rights, Media Information Literacy

Preface

There has never been a time where the need for sustainability has been felt as profoundly as is evident from the global events of today. The global geo-political situation, emergence of new world players, decline in influence of current super powers, struggle for controlling the worlds resources, emergence of new economic blocks, utilization of resources to their optimum in today's changing world all dictate that our survival lies in a renewed strategy to use our limited resources especially in a sustainable way. Hence the new industrial, social, cultural, and environmental scenarios has to be analyzed and new strategies are to be devised so as to make our living sustainable. This need has been felt and thought after since last two decades and recognized in our Department which plays a vital role in indigenous and global research to contribute towards the sustainable development of Pakistan in the areas of vital importance such as process industries, use of natural resources, recycling, and reuse.

This international event of **"Sustainability in Process Industry (SPI-2020)**, (15-16, Dec. 2020) hosted by the Department of Chemical Engineering, University of Engineering and Technology Peshawar, has been a regular bi-annual event attracting the cutting edge research from the renowned researchers of both national and international repute since its first inception in 2012. Until now this has been an on-campus participating event however with the adaptation of new norms due to COVID-19, this year's event is being held online which we hope will bring new horizons in our intellectual and professional interaction on national and international level.

The 1st conference on **"Sustainability in Process Industry (SPI-2012)**, was held at UET, Peshawar on March 28, 2012, 2nd on **"Sustainability in Process Industry (SPI-2014**)", on May 22, 2014, 3rd conference in this series, **"Sustainability in Process Industry (SPI 2016)"** was held on October 19-20, 2016 and 4th conference on **"Sustainability in Process Industry (SPI 2018)"** was organized on October 24-25, 2018 with the support of Higher Education Commission (HEC), Frontier Works Organization (FWO), and in collaboration with PASTIC.

We hope that you will find this 5th conference on **"Sustainability in Process Industry (SPI 2020)",** being held on our Departments Silver Jubilee (1995-2020), intellectually stimulating with provision of valuable opportunities to share ideas with other researchers and industrial practitioners.

Prof. Dr. Muddasar Habib
Conference Chair

Acknowledgement

It is our great pleasure to welcome you to the SPI-2020 5th online International conference of the series, "Sustainability in Process Industry (SPI-2020)". Putting together SPI-2020 was a team effort. We greatly appreciate all the authors/researchers for providing the content of the program in the form of oral presentations and the other participants. We are also grateful to the keynote speakers from academia and various industries in Pakistan and overseas. These valuable talks can and will guide us to a better understanding of "Sustainability in Process Industry". We also thank the host organization, UET, Peshawar, our generous sponsors PASTIC and Rizvi & Company without their support it would not be possible to hold this conference. We are grateful to all organizers, who worked hard in order to make this conference successful.

Table of Contents

Technical Session 1-A (Google meet/Zoom)
MATERIAL ENGINEERING-1

Session Chair: **Dr. Afrasyab Khan**
Session Co-Chair: **Dr. Hayat Khan**

Presenter	Paper Title
Engr. Ihsan ur Rehman *(USPCASE UET Peshawar)*	Fabrication and Characterization of Porous Alumina and Fly Ash Based Filtering Membrane Through Appending Pore Forming Agent Technique
Engr. Mohammad Azad Alam *(UTP Malaysia)*	Investigation on the impact strength of the stir casted Al/SiC/Gr hybrid composite for automotive applications
Sher Afgan *(Dept. of Chem Eng., UET Peshawar)*	Poly Ethylene Terephthalate (PET) Recycling as Composite Sheets and its Characterization using Nano Indentation
Nishat Riaz *(GIKI, Topi)*	Corrosion behavior of Nitinol after aging treatment in simulated body fluid.
Nosheen Naz *(UET, Peshawar)*	Investigating suitable polymer for cap of neutral safety switch used in agricultural tractors.
Maqsood ur Rehman *(UET, Peshawar)*	Industrial Wastewater Irrigation effect on Quality of Local Soil and Vegetables of Mingora, Swat.

Fabrication and Characterization of Porous Alumina and Fly Ash Based Filtering Membrane through Appending Pore Forming Agent Technique

Ihsan Ur Rahman [A,*], Khurshid Ahmad [A], Muhammad Hassan [A], Misbah Ullah [A], Muhammad Sohail [A]
and Muhammad Farooq Siddique [A]

[A] =U.S.-Pakistan Center for Advanced Studies in Energy (USPCAS-E), University of Engineering and Technology Peshawar
[A,*] Email: ihsanrahman.uspcase@uetpeshawar.edu.pk

Abstract— **Rapid industrialization has posed global challenges such as pollution, waste disposal, and severe environmental degradation. Consequently, Pakistan has also been facing severe environmental degradation. Particularly, combustion emissions from small and medium-sized industries in Pakistan contain particulate in quantities that are far larger than the acceptable ranges set by national and international environmental protection as well as health organizations. Therefore, various methods are needed to reduce emissions to the minimum acceptable standards. Membrane separation technology has been widely used for the treatment of industrial effluents. However, the selection of appropriate membrane material with high thermal, chemical, and mechanical stability is critical while using membrane separation technology in treating combustion products. In this study, porous membranes were fabricated from, ceramics materials which are not only cost-effective but also known for high chemical and mechanical stability and longer life. The appending pore-forming agent technique was used for the fabrication of membrane, where porous alumina and fly ash were used as a base material. A 30 vol% starch solution was used as a pore-forming agent. Moreover, 1M solution of NaOH and Na_2CO_3 in combination with 3 ml of ethyl silicate and 2 drops of carbonic acid were used as binders. The membrane recipe was mixed at 22 ºC and poured in the mold and kept for 24 hours to dry. Afterward, it was de-moisturized at 105 ºC for 20 hours. The membrane was then sintered in a furnace at 1250 ºC. The porosity of the final products ranged from 62.2 to 75.1% with an average pore size ranged from 7.6 to 10 μm. The measured bulk densities were 4.5- 4.05 g/cm³ with linear shrinkage of 5.3-3.4%. Moreover, the mechanical strength was 2.7 MPa. The visual permeability of the membrane showed a significant reduction of the particulate in the combustion products, after passing through the membrane.**

Keywords—**Air pollution, appending pore forming agent technique, porosity, porous ceramic membrane, sintering.**

I. INTRODUCTION

According to the worldometer reports the worldwide population growth rate is 1.01% in 2020, where Pakistan is placed at 5th position [1]. Due to this rapid increase in population it is of utmost importance to fulfil the needs of human lives. Which caused industrialization and development in infrastructure. Consequently it engendered many environmental calamities e.g. global warming, air and water pollution, waste disposal and reduction in human life resources [2].

More specifically talking about the air pollution according to WHO's report the air pollution has been augmented by 8% in the previous 5 years, while the Peshawar city is ranked second among all the air polluted cities in the world. Approximately 98% of towns having population of 100,000 in little and intermediate income countries, containing Pakistan are not meeting the air quality standards according to WHO reports [3]. The level of particulate matter ($PM_{2.5}$) in Peshawar is 40-90 micrograms per cubic meter while according to the National Environmental Quality Standards (NEQS) the limit is 15 micrograms per cubic meter [4].

To contribute to the reduction of air pollution, membrane purification technology is considered worldwide the most effective, reliable, highly energy efficient and simple in operation [5]. Polymeric or organic membranes have been used previously [6] but their major drawback is the inability to withstand severe conditions like high temperatures and high chemical and corroded environment

Ceramic or inorganic membranes on other hand are considered for such uses because of low thermal expansion coefficient, high corrosion stability, high mechanical bending strength, good specific surface area, good thermal resistance to high temperature, good permeability feature and light weight compare to metals [7]. The porous ceramic materials used for the manufacturing of porous ceramic filtering

membranes are those, whose morphology varying depend upon the fabrication techniques, those materials are [8]; aluminum oxide or alumina [9], zirconium oxide [10], silica or silicon oxide [11], silicon carbide [12], mullite, magnesium oxide, silicon oxy-carbide, cordierite, titanium oxide [13]. The melting points described for these ceramics are very high i.e. for Alumina melting point is 2050 ºC, for zirconia 2770 ºC, for titania 1605 ºC and for silicon Carbide 2500 ºC [14]. In these materials the mostly used is alumina for its excellent nature of chemical and thermal stability and good structure [15]. But the issue associated with it is high temperature of sintering i.e. ≥ 1500 ºC [16] which make it less economical. To reduce the cost of raw material and using low temperature sintering, different techniques are in use [17].

Studies shown that fly ash which is the byproduct of many combustion process specifically of coal fired power plants, also causes environmental pollution [18], this fly ash would be utilized because it contain mostly alumina and silica which consequently will reduce the cost of raw materials, also fly ash disposal issue will be reduced [19]. The addition of starch to this type of ceramic membrane will reduce the mechanical strength of it, which is the basic intrinsic property of the ceramic membranes [20]. It is of utmost importance to develop such a ceramic membrane which have high mechanical strength and good porosity properties [21].

In this research, a porous alumina and fly ash based membrane is fabricated (for treatment of flue gases of tyres powder combustion) through low sintering temperature by appending pore-forming agent technique where starch is used as pore former, to maintain good porosity and mechanical strength some binding material i.e. Ethyl silicate, sodium carbonate and sodium hydroxide are also used. Different composition are made and then characterized at the end.

II. Methodology

A. Material Selection

Porous alumina with a chemical formula Al_2O_3. Having melting point and boiling point 2030°C, 2977°C respectively while the density is 3.0-4.0 gm/cm^3. It is in pure white powder form. Porous alumina is one of the base material used for having excellent structure and good thermal and mechanical properties [15] and for pore size distribution. Fly ash is brought from Lakhra Coal-Fired Power Plant, Sindh, Pakistan. After X-ray florescence spectroscopy the main constituents found were SiO_2 63 wt%, and Al_2O_3 22 wt% etc. Fly ash is used to reduce the cost of fabricated membrane and help in ash disposal management also it has internal bonding with alumina in making mullite too [22]. Starch is an organic compound having chemical formula of $(C_6H_{10}O_5)_n$. It is in white amorphous powder form. The melting point of this starch is 256 °C while the density is 1.5 gm/cm^3. This organic compound is used as pore forming agent which upon burning during sintering process left pores behind [23] also it is used as binder too. Ethyl silicate is used in combination with sodium carbonate and sodium hydroxide as a binder to maintain the proper mechanical strength of the fabricated membrane [24]- [25].

B. Fabrication steps

In this research work for the fabrication of ceramic membrane 'appending pore for agent Technique' was used. The steps followed during fabrication are shown in Figure 1. All the reactants are first made active. 100 gm of porous alumina was taken and placed in furnace at 600 ºC for 2 hours to calcine it, during calcination the pure white alumina changed to brownish color. 100 gram of fly ash was first washed through HCl leaching and again washed with NaCl Leaching. Then washed fly ash sample was placed in furnace at 105 ºC for 6 hours where its original black color changed into grey. 30 Vol% solution of starch was prepared and placed on hot plate for mixing at 960 rpm and heating at 80 ºC for 24 hours where the starch solution becomes thick, setup is shown in figure 2. Afterall 1M binder solution of Na_2CO_3 and NaOH was prepared by mixing at 1200 rpm at room temperature for 24 hours on hot plate. Starch solution is used, 2.3 gm of base material per 1 ml of starch solution while same combination is applied for binder solution too. After the activation of reactants 4 samples were prepared in slurry form shown in table 1.

The prepared 4 membrane samples were then passed through different treatments like mixing all the reactants, where calcined alumina and activated fly ash were mixed manually, in parallel starch solution
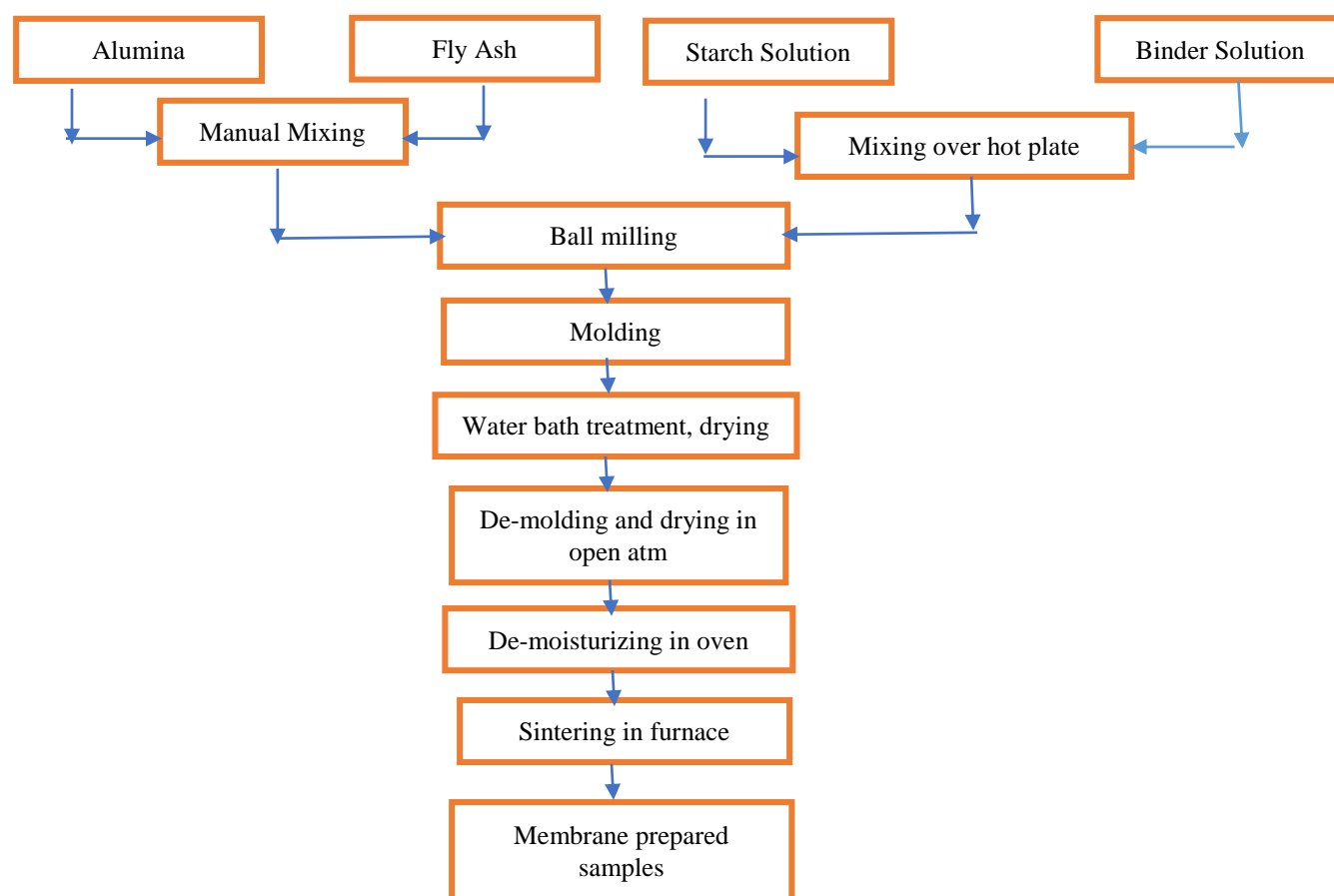
Fig. 1. Steps followed during fabrication of porous alumina and fly ash based filtering membrane through appending pore-forming agent technique

.

and binder solution were mixed on hot plate magnetic stirrer speed of 1200 rpm. Then both the mixed reactants are ball milled for 1 hour to get uniform slurry. Once all the membrane samples were mixed homogenously it was forwarded for next treatment of molding. The membrane slurries were poured into molds, two types of molds were used i.e. polyethylene and steel mold of 0.061 m. petri dishes were used as a base for putting mold into it, while peace of A-4 sheets were place in between molds and petri dishes. The surface were properly oiled in case de-molding. Molding setup having sample-04 is shown in figure 3.

TABLE I: COMPOSITION OF FOUR MEMBRANE SAMPLES

Reactants	Sample-01	Sample-02	Sample-03	Sample-04
Alumina	5 g	10 g	15 g	20 g
Fly Ash	5 g	5 g	5 g	0
Starch solution	5 ml	6.53 ml	8.7 ml	8.7 ml
Binder solution	4.5	6.53 ml	8.7 ml	8.7 ml
Ethyl Silicate	3 ml	3 ml	3 ml	3 ml
Carbonic Acid	2 drops	2 drops	2 drops	2 drops
Water	10 ml	0	0	0

Fig. 2. Experimental setup of preparing 30 Vol% starch solution, hot plate is used with magnetic stirrer, the temperature was kept constant at 80 ºC while mixing speed was 960 rpm for 24 hours.

Fig. 3. Molding setup for sample-01 where polyethylene mold of 0.061 is used.

The molds are then covered fully and placed in water bath set a temperature of 80 ºC for 1 hour. The purpose of treating the membrane samples in molds is to avoid uneven shrinkage and segregation. Once it's done the membrane samples molds are then uncovered and treated at 13 ºC for few minutes for sudden quenching, after all the samples are placed in open atmosphere at 22 ºC for 24 hours, at last the samples were demolded and placed in open atmosphere for 3 hours. All the membrane green bodies were then treated at 105 ºC for 20 hours in furnace to remove the moisture content. Finally the moisture free membrane samples were sintered till the temperature reached 1250 ºC in stepwise temperature rise and fall i.e. from 20 to 500 ºC the heating rate was 2 ºC/min so that the combustion of starch occur, then temperature was maintained at 500 ºC for 2 hours. From 500 to 900 ºC the temperature rate was 2 ºC/min again to decompose other unwanted substances present in the samples, now from 900 ºC till 1250 ºC the heating rate was 1 ºC/min. Once the last temperature was attained, it is finally decreased in the similar manner to avoid any uneven rise or fall in temperature.

All 4 membrane samples are cured and fabricated in the similar type of fabrication steps, sample-01 and sample-04 are shown in figure 4 and figure 5.

Fig. 4. Front side view of sample-01 (50 wt% alumina and 50 wt% fly ash) membrane sintered at 1250 ºC

Fig. 5. *Top side view of sample-04 (66.3 wt% alumina and 33.3 wt% fly ash) membrane sintered at 1250 ºC*

III. RESULTS AND DISCUSSION

A. *Loss in Mass*

All 4 membranes samples after drying and de-moisturizing in oven at 105 ºC for 20 hours, sintering at 1250 ºC in furnace through stepwise manner, are examined for percentage loss in mass using (1).

$$\%age\ loss\ in\ mass\ \ = $$
$$\frac{initial\ mass\ of\ the\ sample\ (gm) - sample\ mass\ after\ drying\ (gm)}{Initial\ mass\ of\ the\ sample\ (gm)}\ x\ 100 \qquad (1)$$

Loss in mass, due to de-moisturization in oven and sintering in furnace for all 4 samples is shown in figure 6, where sample-01 shows higher percentage of de-moisturization as it contain additional water content. While the other samples show a gradual increase in percentage loss in mass as the porous alumina content increases. Similar pattern is followed in sintering process too.
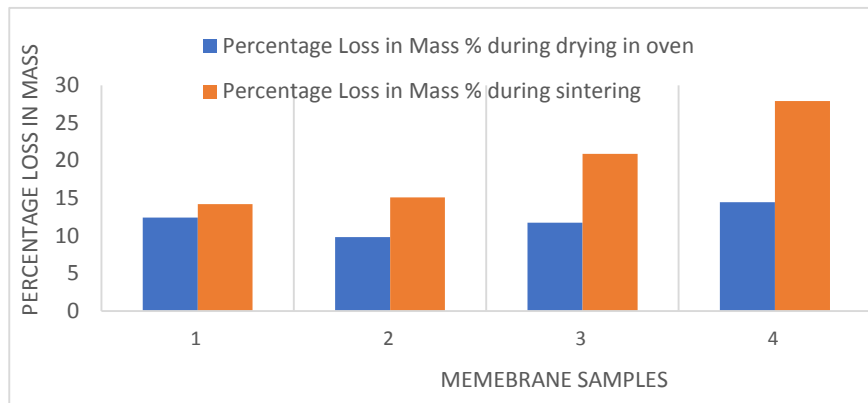
Fig. 6. Percentage loss in mass of all 4 samples during drying in oven at 105 ℃ for 20 hours and sintering in furnace at 1250 ℃ (stepwise heating and cooling)

B. Bulk Density, Percentage Porosity and Percentage Linear Shrinkage Measurement

The bulk densities and percentage porosities of all 4 membrane samples were examined by arranging experimental setup for applying Archimedes Principle. While percentage linear shrinkage was determined by using (2).

$$Percentage\ Linear\ Shrinkage = \frac{D1 - D2}{D1}\ x\ 100 \qquad (2)$$

Where D1 is the diameter of membrane sample before sintering process while D2 is diameter after sintering process. As shown in table 2, the percentage porosities are increased gradually from sample-01 to sample-04 while bulk densities and percentage linear shrinkages are decreased. The reason is increase of alumina and starch content in all samples.

TABLE II: PERCENTAGE POROSITIES, PERCENTAGE LINEAR SHRINKAGE AND BULK DENSITIES OF ALL CURED MEMBRANE SAMPLES

Membrane samples	Percentage Porosity	Percentage linear shrinkage	Bulk density (gm/cm^3)
Sample-01	62.4	5.3	4.48
Sample-02	65.2	4.4	4.33
Sample-03	68.9	4.0	4.21
Sample-04	75.01	3.4	4.05

C. Optical Microscopy

All the membrane samples are then passed through optical microscopy test. The optical microscope was set at 500X. The average pore sizes determined from sample-01 to sample-04 were, 7.6 µm, 8.4 µm, 9.1 µm and 10 µm respectively. Sample-01 and sample-04 optical microscope structures are shown in figure 7 and figure 8 respectively. The largest average pore size was determined for sample-04 while there is uniformity in the pore structure too.
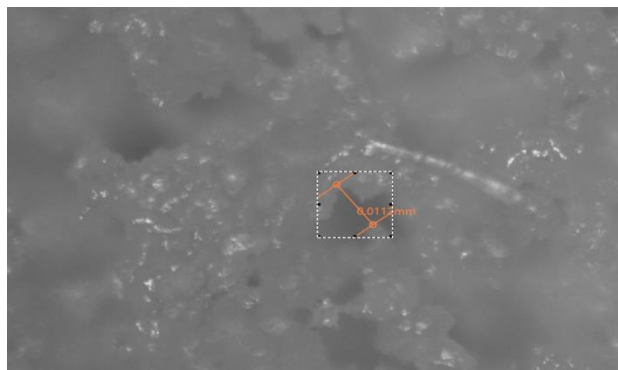
Fig. 7. Optical microscopy of sample-01 with average pore size of 7.6 micrometer. (Test is conducted for cured membrane sample sintered at 1250 ℃ in furnace).
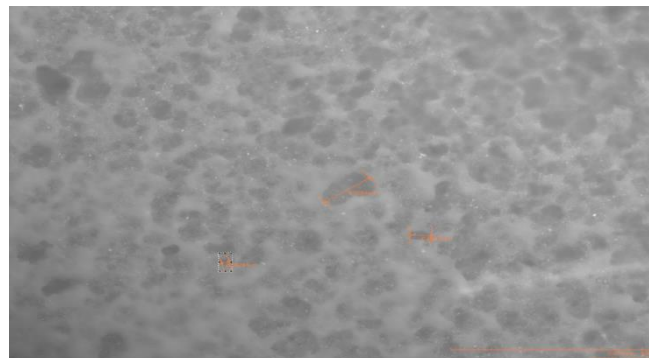
Fig. 8. Optical microscopy of sample-04 with average pore size of 10 micrometer. (Test is conducted for cured membrane sample sintered at 1250 ℃ in furnace.

D. Compressibility and TGA Analysis

Compressive strength test is carried out for all samples to check its strength, the highest was found for sample-01 which is 2.7 MPa. For sample-02 the strength was 1.2 MPa while for other 2 samples the mechanical strength was less than 1 MPa.

Thermal gravimetric analysis (TGA) is conducted for sample-01 before curing it fully. From figure 9 its disclosed that the loss in mass is higher in early stages till 600 ℃ as in beginning there is de-moisturization and after it combustion of starch starts. Then at higher temperature the loss in mass is reduced to low. This shows how efficient and stable ceramic membranes are, using at high temperatures.
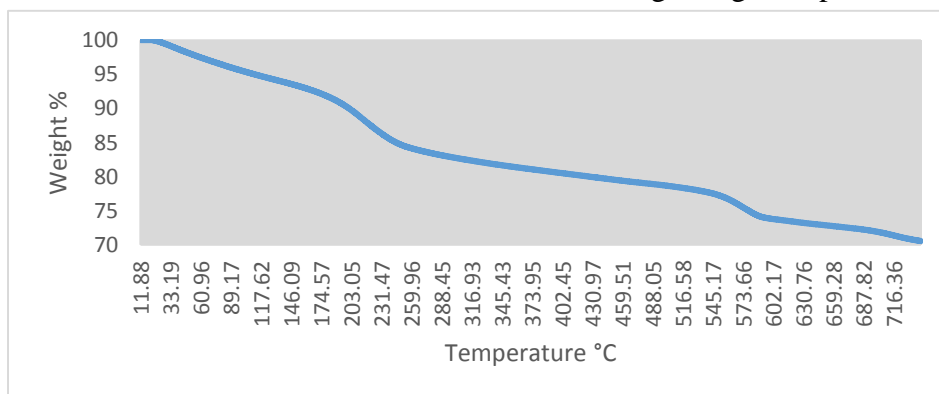
Fig. 9. Thermal Gravimetric Analysis (A 8.5 mg of sample in powder is taken after that nitrogen is admitted into the apparatus at rate of 30 ml/min for 30 mints. 20 °C/min heating rate is fixed till 750 °C for the removal volatile components).

E. Visual Permeability Test

At last a visual permeability test was performed. The experimental setup made for this test is shown in the figure 10. The glass tube has two parts, upper and lower part the porous ceramic membrane was fixed in between these two parts. And the lower end of the glass tube was fixed on the combustion chamber chimney. While the upper end of the glass tube was tightened with the vacuum pump inlet. The vacuum pump sucks the exhaust gases from the combustion chamber which passes through the membrane and released to the atmosphere through the outlet of the vacuum pump. The fuel used here for the test was powdered tyre in combustion chamber. As shown in figure 11 & 12, a cake is found of blackish

particulates on the exposed surface of membrane to the flue gases from combustion chamber. While the upper surface of membrane is found quite neat and clean.

Fig. 10. Visual Permeability Test Setup, All the dimensions of the glass tube is according to the dimensions of the prepared membrane samples. The height of the lower glass tube is 10 inch while the upper glass tube part have 6 inch in length.

Fig. 11. Cake of blackish particulates over the lower surface of membrane exposed to flue gases   from

Fig. 12. Upper surface of membrane after testing it for flue gasses passage

IV. CONCLUSION

The porous-alumina and fly ash based membrane is fabricated through appending pore-forming agent technique. 4 samples were prepared and analyzed through different characteristic measurements, the mechanical strengths determined were 2.7 MPa, 1.2 MPa and so on for all samples respectively. The porosity ranged from 62.2 % to 75.01%. The increase in the amount of porous alumina resulted in a decrease in the bulk density from 4.5 g/cm^3 to 4.05 g/cm^3 while linear shrinkage also decreased from 5.3% to 3.4%. Thermal gravimetric analysis shows high stability of porous alumina and fly ash based membrane at higher temperatures. The visual permeability test as showed a good filtering of the flue gases at high temperatures.

ACKNOWLEDGMENT

.

V. REFERENCES

[1] "population," 5 11 2020. [Online]. Available: https://www.worldometers.info/world-population/#:~:text=Population%20in%20the%20world%20is,it%20was%20at%20around%202%25..

[2] Van Bavel J, "The world population explosion: causes, backgrounds and projections for the future," *NCBI,* vol. 5, no. 4, p. 281–291, 2013.

[3] News Corrspondent, "Most Polluted Cities: Peshawar ranks second in WHO report," The Express Tribune, 14 May 2016. [Online]. Available: https://tribune.com.pk/story/1103464/most-polluted-cities-peshawar-ranks-second-in-who-report. [Accessed 5 November 2020].

[4] Zulfiqar Ali, "Particulate air pollution growing in Peshawar," Dawn, 4 December 2016. [Online]. Available: https://www.dawn.com/news/1300411. [Accessed 5 November 2020].

[5] M. Mulder, Basic Principles of Membrane Technology, Netherland: Springer Netherlands, 1996.

[6] E. Favre, "Polymeric Membranes for Gas Separation," *Comprehensive Membrane Science and Engineering,* pp. 155-212, 2010.

[7] A. S.Gopi and S.Thomas, "11 - Synthesis, microstructure, and properties of high-strength porous ceramics," *Fundamental Biomaterials: Ceramics,* pp. 265-271, 2018.

[8] P Colombo, "Ceramic Foams: Fabrication, Properties and Applications," *Key Engineering Materials,* pp. 1913-1918, 2001.

[9] D. Ivanov, S. Shlyapin., G. Val'yano and L. Fedorova, "Structure and Physicomechanical Properties of Porous Ceramic Based on Al2O3 Prepared Using a Filtration Combustion Method.," *Refract. Ind. Ceram,* no. 58, pp. 538-541, 2018.

[10] J. Han, C. Hong, X. Zhang, J. Du and W. Zhang, "Highly Porous ZrO2 Ceramics Fabricated by a Camphene-Based Freeze-Casting Route: Microstructure and Properties.," *J. Eur. Ceram. Soc.,* no. 30, pp. 53-60, 2010.

[11] Z. Sun, C. Lu, J. Fan and F. Yuan, "Porous Silica Ceramics with Closed-Cell Structure Prepared by Inactive Hollow Spheres for Heat Insulation," *J. Alloy. Compd,* no. 662, pp. 157-164, 2016.

[12] J. Shin, B. Kumar, J. Kim and S. Hong, "Tribological Properties of Si3N4/SiC Nano–Nano Composite Ceramics," *J. Am. Ceram. Soc,* no. 94, pp. 3683-3686, 2011.

[13] J. Chen, G. Liu and T. W. Button, "Mechanical Properties of Porous TiO2 Ceramics Fabricated by Freeze Casting Process," *Adv. Appl. Ceram,* no. 112, p. 436–441, 2013.

[14] Wyatt O.H and Dew- Hughes D, "Metals, ceramics and polymers," *Journal of Applied Crystallography,* vol. 9, no. 1, 1976.

[15] Z. Wei, J. Hou and Z. Zhu, "High-aluminum Fly Ash Recycling for Fabrication of Cost-effective Ceramic Membrane Support," *Journal of Alloys and Compounds,* no. 683, pp. 474-480, 2016.

[16] L. Li, M. Chen, Y. Dong, X. Dong, S. Cerneaux, S. Hampshire, J. Cao, L. Zhu, Z. Zhu and j. Leu, "A low-cost alumina-mullite composite hollow fiber ceramic membrane fabricated via phase-inversion and sintering method," *Journal of the European Ceramic Society,* no. 36, pp. 2057-2066, 2016.

[17] F. Jiang, L. Zhang, E. Mukiza, Z. Qi and D. Cang, "Formation Mechanism of High Apparent Porosity Ceramics Prepared From Fly Ash Cenosphere," *J. Alloy. Compd,* pp. 750-757, 2018.

[18] I. Jedidi, S. Saïdi, S. Khemakhem, A. Larbot, N. Elloumi-Ammar, A. Fourati, A. Charfi, A. Salah and R. Amar, "Elaboration of New Ceramic Microfiltration Membranes from Mineral Coal Fly ash Applied to Waste Water Treatment," *J. Hazard. Mater.,* no. 172, p. 152–158, 2009.

[19] Yang Y, Liu F, Chang Q, Hu Z, Wang Q and Wang Y, "Preparation of Fly Ash-Based Porous Ceramic with Alumina as the Pore-Forming Agent," *Ceramics,* pp. 1-10, 2019.

[20] A. Jamaludin, S. Kasim, M. Abdullah and Z. Ahmad, "Sago Starch as Binder and Pore-Forming Agent for the Fabrication of Porcelain Foam," *Ceram. Inter,* no. 40, p. 4777–4784, 2014.

[21] P. Biesheuvel, H. Verweij and P. Biesheuvel, "Design of Ceramic Membrane Supports: Permeability, Tensile Strength and Stress," *J. Membr. Sci,* no. 156, pp. 141-152, 1999.

[22] J. Jung, H. Park and R. Stevens, "Mullite Ceramics Derived from Coal Fly Ash," *J. Mater. Sci. Lett,* no. 20, pp. 1089-1091, 2001.

[23] E. Tynova, W. Pabst, E. Gregorova and H. J, "Starch Consolidation Casting of Alumina Ceramics—Body Formation and Microstructural Characterization," *Key Eng Mat,* vol. 13, no. 206, pp. 1969-1972, 2002.

[24] L. Wang, J. Ning and Z. Yao, "Development of porous ceramics materials," *Bull Chin Ceram Soc,* vol. 1, no. 41, 1998.

[25] J. Yang, G. Zhang and T. Ohji, "Porosity and Microstructure Control of Porous Ceramics by Partial Hot Pressing," *J Mater Res,* vol. 7, no. 16, 2001.

Investigation on the impact strength of the stir casted Al/SiC/Gr hybrid composite for automotive applications

Mohammad Azad Alam[A,B],*, Lovejeet Gerewal[B], H.H Ya[A], Mohammad Yusuf[C], Faisal Masood[D]

[A]*Mechanical Engineering Department, Universiti Teknologi Petronas, Seri Iskandar, Perak, Malaysia*
[B]*Mechanical Engineering Department, IFTM University, Moradabad, U.P India*
[C]*Chemical Engineering Department, Universiti Teknologi Petronas, Seri Iskandar, Perak, Malaysia*
[D]*Electrical Engineering Department, Universiti Teknologi Petronas, Seri Iskandar, Perak, Malaysia*

* Corresponding author: **azadalam.mech3@gmail.com**

Abstract— **The present research investigates the impact strength behaviour of AA6063 casted composites reinforced with varying percentages of micron SiC particles and 5 wt. % graphite. AA6063/SiC/Gr hybrid composites were fabricated via liquid metallurgy route. The standard charpy impact testing was performed on the various fabricated samples and impact strength was evaluated. The significant improvement in impact strength was observed by adding SiC and graphite as a reinforcement in the aluminum matrix. The pure Aluminium's average Impact strength was found to be 7 Joule for the three samples used for testing. For aluminium with 10 percent Silicon Carbide, the average Impact strength was found to be 8 Joule, which is 14.28 percent higher compared to pure aluminium. For aluminium with 20 percent Silicon Carbide, the average Impact strength was 10 Joule for the three samples, showing increase of 42.85 percent in strength compared to pure aluminium.**

Keywords— **Hybrid composites, Impact strength, SiC and graphite particles**

I. INTRODUCTION

The progress of science and technology needs to use advanced and latest materials for structural applications. A unique degree of properties unattainable in traditional non-reinforced metals and alloys is offered by metal matrix composites. The most important advantage associated with composites is their high strength and stiffness along with low weight. Due to their exceptional mechanical properties, the interest in the industrial use of aluminum (Al) and its alloys based composites in the automotive and aircraft sectors has gradually increased significantly in recent years [1]. AA6063 is an aluminum alloy of superior performance with adequately suitable mechanical characteristics. The motivation for substituting ferrous metals with versatile aluminum alloys can be increased by these exceptional attributes [2]. Taking into consideration their low weight, Al has poor hardness and strength for the mentioned objective. The addition of reinforcing particles to the matrix aluminum alloys introduces aluminum matrix composites, a fruitful approach to improving the mechanical properties of aluminum alloys [3]. As a reinforcement particle for AMCs, nitrides, carbides, oxides and few compounds of intermetallic have been extensively used. Among the carbide particles, Silicon carbide (SiC) is terribly attractive owing to its excellent physical and mechanical properties and, most of all, sufficient wet-ability with aluminum [4].

Although, there are various processing route for the development of AMCs such as powder metallurgy, squeeze casting, spray casting, ball milling, stir casting and friction stir processing. Among these, the stir casting process for nanocomposite products are more competent, reliable and less expensive as compared to the products manufactured by other processes [5][6]. Mazahery et al. [7] fabricated the high performance A356 –Nano Al2O3 composites by vortex method. They revealed that the hardness of the composites increased with increasing volume fraction of nano-particles. Tensile test results of as-cast and heat-treated SiC-reinforced Al 7075 matrix composites reported and found the increased UTS at 10% micro size SiC. Compressive and tensile properties of Al and Al–AlN nanocomposites have been studied. They proposed that compressive strength was enhanced by the addition of AlN nanoparticles. Pre-synthesized composite reinforcement prepared via milling of alumina with Al and Mg powders (master metal matrix composite) were anticipated. They have concluded that fabrication of Al-A206/ alumina composites by master metal

matrix composite with an addition of 100 nm alumina particles in the semi-solid state leads to considerable improvement in strength. By choosing proper combination of matrix and reinforcement material, a composite material can be developed that precisely meets the requirements of a specific application. Previous researches are limited in delivering constant and satisfactory exploration of A356 reinforced with SiC nanoparticles produced through two-step stir casting process. Although, some investigations have been reported the manufacturing of aluminium alloy reinforced SiC composites through double stir casting. Former researches are absence specially AA6063 reinforced with previously mechanically milled aluminium fine powder with SiC and Graphite nanoparticles through ball milling process using ball mill followed by two-step stir casting process. This work focuses to explore the fabrication process of AA6063/SiC/Gr hybrid composites through stir casting process. Mechanical behavior and morphology of AA6063 reinforced with SiC nanoparticles are also discussed in detail.

II. METHODOLOGY

Aluminium 6063 T5 is used as a matrix material and the Silicon carbide (Sic) and Graphite (Gr) is used as reinforcement.

Table1: Chemical composition of aluminium 6063T5

Component	Al	Cr	Cu	Fe	Mg	Mn	Other each	Other total	Si	Ti	Zn
Wt.%	Max 97.5	Max 0.1	Max 0.1	Max 0.35	0.45-0.9	Max 0.1	Max 0.05	Max 0.15	0.2-0.6	Max 0.1	Max 0.1

Aluminium alloy in fixed amount is placed in a crucible furnace

Aluminium alloy melted in furnace at 800 °C

Addition of preheating of weighed Sic and Graphite in fixed quantity to 200°C for 1 hour

Manual Mechanical stirring to proper mixing

Then the liquid (molten metal and molten reinforcement particles) is usually poured into a mould, which contains a hollow cavity of the desired shape and then allowed to solidify

After solidification the specimen is drawn and testing of mechanical properties is evaluated

Fig. 1 Flow chart for experimental plan

A. Impact Test

To determine the charpy test parameter following ASTM E23 Standard are used. The sample for charpy test was prepared by manual stir casting method. The charpy test was done on Impact test machine. Standard specimen was used to find out impact strength of the composite. The comparison of the properties of the pure aluminium 6063T5 with the properties of the composite materials. The charpy test specimen was 55mm long with 10 · 10mm2 cross section, having a standard 45 notch 2mm deep.

Fig. 2: Charpy test specimen before testing
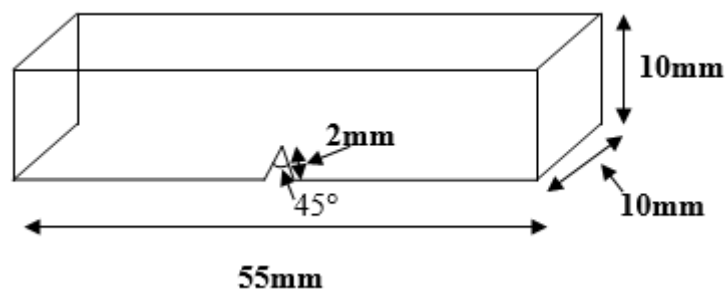
Fig. 3: Dimension of Charpy test specimen

III. RESULTS AND DISCUSSION

A. *Impact strength*

The pure Aluminium's average Impact strength was found to be 7 Joule for the three samples used for testing. Aluminium with 10 percent Silicon Carbide, the average Impact strength was found to be 8Joule, which is 14.28 percent higher compared to pure Aluminium. Aluminium with 20 percent Silicon Carbide the average Impact strength was 10Joule for the three samples, showing increase of 42.85 percent in strength compared to pure aluminium. Aluminium with 10 percent Graphite, the average Impact strength for the three samples was found to be 12Joule, which is 71.42 percent higher compared to pure aluminium. For Aluminium with 20 percent graphite, the average Impact strength for the three samples was found to be 8Joule, which is 14.28 percent higher compared to Pure aluminium. Average Impact strength for aluminium with 10 percent Silicon Carbide and 5 percent graphite was found to be 11.33 which is 61.85 percent higher compared to pure Aluminium. Aluminium with 10 percent Graphite and 5 percent Silicon Carbide, the Impact strength for the three samples was found to be 8, 14.28 percent higher than the pure Aluminium. Aluminium with 20 percent Silicon Carbide and 5 percent Graphite, the average Impact strength for the three samples was 14, which is 100 percent higher than that of pure aluminium. Aluminium with 20 percent Graphite and 5 percent Silicon Carbide, the average Impact strength for the three samples was 10, 42.85 percent higher than that of pure Aluminium.
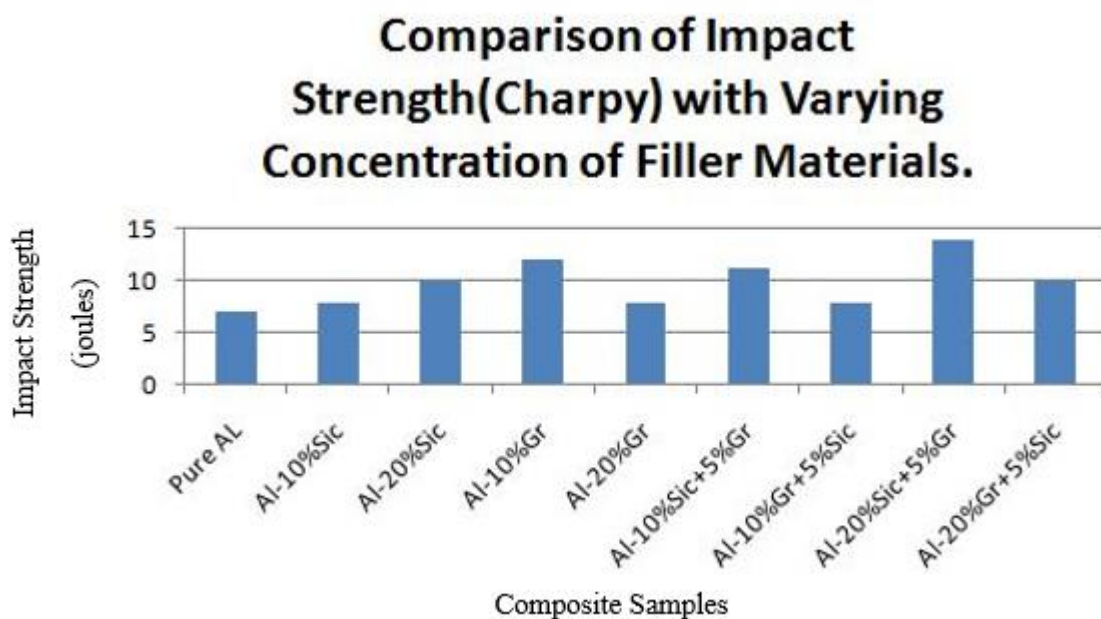
Fig. 4 Average Impact Strength Comparison of pure Al

B. *Fracture Behaviour*

To understand the unusual mechanical behaviour of this composite the fractography performed on the specimen fig (a-b) shows the micrograph of fracture surface of the specimen containing different percentage of silicon and graphite.

Fracture normally occur as a result of one or the combination of the following mechanism

1. Fracture reinforcing particle
2. Particle debonding of reinforcement-matrix interface and nucleation of voids
3. Development of the voids and ignition of cracks in the matrix

Various type of factor is responsible for the composite fracture. They are the processing methods, the applied stress, reinforcement distribution and morphology of the reinforcing particle. The overall fracture is ductile in nature. The fracture behaviour of any material depend on a number of things like shape, size and its processing methods as it decides strength at the interface, its porosity and so on.
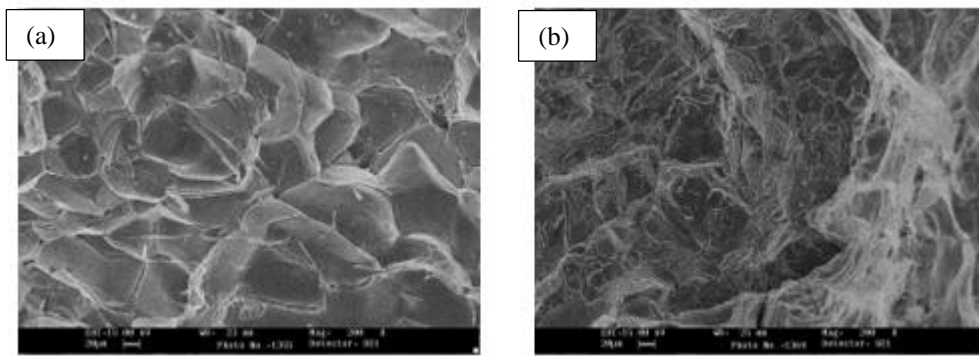
Fig. 4 SEM micrograph of fracture surface of Al/SiC/Gr composites.

IV. CONCLUSION

Stir casting process is well suited and economical for the preparation of AMMC's with desired properties. The impact strength of MMC increases with increase in weight percentage of Sic & Gr and it is maximum for sample 8 (Al-20%Sic+5%Gr). The best result has been obtained at Al-20%Sic+5%Gr weight fraction of Silicon carbide & Graphite particles. Maximum Impact Strength = 14 Joules.

ACKNOWLEDGMENT

REFERENCES

[1]   H. Fallahdoost, A. Nouri, and A. Azimi, "Journal of Physics and Chemistry of Solids Dual functions of TiC nanoparticles on tribological performance of Al / graphite composites," *J. Phys. Chem. Solids*, vol. 93, pp. 137–144, 2016, doi: 10.1016/j.jpcs.2016.02.020.

[2]   A. Azimi, A. Shokuhfar, and O. Nejadseyfi, "Mechanically alloyed Al7075 – TiC nanocomposite : Powder processing , consolidation and mechanical strength," *Mater. Des.*, vol. 66, pp. 137–141, 2015, doi: 10.1016/j.matdes.2014.10.046.

[3]   K. Haider, M. A. Alam, A. Redhewal, and V. Saxena, "Investigation of Mechanical Properties of Aluminium Based Metal Matrix Composites Reinforced With Sic & Al2O3," *Int. J. Eng. Res. Appl.*, vol. 5, no. 9, pp. 63–69, 2015.

[4]   M. A. Alam *et al.*, "Modelling and optimisation of hardness behaviour of sintered Al/SiC composites using RSM and ANN: A comparative study," *J. Mater. Res. Technol.*, vol. 9, no. 6, pp. 14036–14050, 2020, doi: 10.1016/j.jmrt.2020.09.087.

[5]   M. T. Alam, S. Arif, A. H. Ansari, and M. N. Alam, "Optimization of wear behaviour using Taguchi and ANN of fabricated aluminium matrix nanocomposites by two-step stir casting," *Mater. Res. Express*, vol. 6, no. 6, p. 65002, 2019.

[6]   M. T. Alam, A. H. Ansari, S. Arif, and M. N. Alam, "Mechanical properties and morphology of aluminium metal matrix nanocomposites-stir cast products," *Adv. Mater. Process. Technol.*, vol. 3, no. 4, pp. 600–615, 2017, doi: 10.1080/2374068X.2017.1350543.

[7]   A. Mazahery, H. Abdizadeh, and H. R. Baharvandi, "Development of high-performance A356/nano-Al2O3 composites," *Mater. Sci. Eng. A*, vol. 518, no. 1–2, pp. 61–64, 2009.

Poly Ethylene Terephthalate Recycling as Composite Sheets and its Characterization using Nano Indentation

Sher Afgan [A], Nehar Ullah [B], Muhammad Sualiman[C], Tanveer Iqbal [D],

[A, B] =*Department of Chemical Engineering, University of Engineering and Technology, Peshawar, Pakistan*

Abstract— **This paper focuses on utilization of post-consumer poly ethylene terephthalate (PET) bottles for the fabrication of newly developed high strength, optimized insulating composite sheets as an effective, ecofriendly process of recycling. In order to reinforce the strength and aesthetics of the reclaimed material it is integrated with coupling agent known as talc. The impact of talc on the mechanical properties of the composite was studied in this research. It was concluded that talc of optimized size 45µm attributes high strength, high lubricity and surface homogeneity to the material. Talc to plastic ratio was 1:4. Strength and thermal conductivity results reveals that by adding filler material talc and virgin PET in recycled PET high mechanical strength, low thermal conductivity is obtained. Nano-indentation technique was used to analyze further the mechanical properties of the composite sheets at nano scale level. Load-displacement curves displayed the harder behavior of 80% RPET and 20% talc as it needed 100 µN load to impose a low penetration depth while the sheet without talc observed softer behavior.**
Keywords— **Composite, Nano Indentation, Poly ethylene terephthalate, Recycled, Talc**

I. INTRODUCTION

Poly ethylene terephthalate (PET) is widespread used polymer which is used in profusion in bottles manufacturing for water containment and beverages of carbonated drinks. [1] Post-consumer PET is discarded as dumps in landfills which is an environmental threat of global nature. The harm associated with PET are severe to humanity and aquatic life. The universal demand for PET based materials has been expedited so much that Pakistan annually generates 3.3 million tons of plastic waste, of which 60% is recycled, mostly mechanical. According to a report PET accounted about Pakistan produces 18.8 million tons which constitutes nearly 7% out of the total plastic production of 269 million tons. [2] By 2021 this annual consumption of PET bottles is set to pinnacle more than half of a trillion i.e. 583.3bn, according to the recent most estimates. [3] Economic and environmental aspect plays integral part in the use of reclaimed materials material and impart better insulating and compressive strength [4] In current era many researchers studied proved that additive materials can play a vital role in imparting strength to composite materials made up of recycled PET content. These binding/ filler materials are used as additive material to improve some properties of theses polymeric materials.[5] Collection of post-consumer PET bottles**,** the recycling process and finally which market for the end product of recycling is to be targeted. Firstly, in this study only homogeneous waste is collected which is only discarded PET bottles. Secondly, mechanical recycling is preferred as the collected waste is of homogeneous nature. Thirdly and most importantly market for the end product is selected that is as a substitute for expensive insulating materials. [6] In this study it is feasible to perform mechanical recycling due to the collection of homogeneous plastics i.e. only one kind of PET bottles. Pretreatment is necessary to make good separation of each component. [7] Polystyrene and polyurethane foams whole life cycle has bad footprints on environment and cause serious health issues in case of fire, thereby contributing in the rise of global warming potential.[8] These factors play a vital role to substitute these polymers with bio-renewable resources also called the recyclable materials Talc being the soft metal in a family has many uses as an industrial mineral.[9] Talc is abundantly available mineral

and an important filler in plastic, paint, and rubber as a filler material especially for softness works as it is also. This peculiar compound gave a few dominant characteristics to material which is softness, high strength, and purity. It is mixed in a ratio of 1:4 with the PET bottles. [10] Incorporation of talc and RPET as a substitute of expensive filler materials and virgin polymers will help to cope with high energy demand for the manufacturing of these polymeric materials and CO_2 release associated with these polymer manufacturing companies to make sheets of virgin materials will be minimized up to certain extent.[11]

Poly ethylene terephthalate integrated with talc and impact of talc on the properties of PET was studied in this research. Talc ratio in sheets when kept greater than 20% will result in the longer setting time and lower compressive strength .[10] Researchers have confirmed that up to to some extent of substituting the high cost virgin polymers with recycled polymers reinforced with additives such as tire rubber, waste marble dust, fly ash, rice husk, saw dust, etc induce distinctive properties to reclaimed and helps in a alot of energy savings because of less manufacturing of virgin polymers. The effect of practically utilizing talc in composite insulating sheets, cement, tiles, self-compacting concrete, agglomerate marble, pavements, embankment, glues and paints with fruitful outcomes were demonstrated [11]–[13] During mechanical recycling, the stumbling block of RPET is hydrolysis and thermal degradation of RPET due to the residual moisture, contaminants and adhesives which causes the decrease in intrinsic viscosity and molecular weight.[14] To overcome this drawback VPET is mixed with RPET with varying percent. Studies shown that by increasing the percentage of RPET in composite sheets there will be decreasing intrinsic viscosity, thereby decreasing environmental footprints and economically feasible. The results of substitution of 20% of talc with 80% PET was investigated which gives maximum compressive strength compared to that of virgin PET. Researchers have studied that degradation of RPET leads to molecular weight loss & mechanical properties deterioration, hydrolytic chain scission, thermal exposure and shear degradation due to contaminants & moisture during reprocessing. Intrinsic viscosity of RPET is 0.76-0.84 dl/g[15]Studies reveals that 100% VPET is costly, not ecofriendly, non-sustainable, lower melt flow index and higher molecular weight, viscosity aesthetics of products. Intrinsic viscosity of VPET is 0.98 - 1 dl/g[6] Researchers have studied that composites of R/V PET prepared in defined conditions show certain rheological and mechanical properties similar to those of virgin polymers with better aesthetics, higher molecular weight and viscosity, ecofriendly nature, less costly, and better aesthetics. [15] Compressive strength, aesthetics, low thermal conductance and smoothness of surface of sheets increases with the substitution of abundantly available talc. [12]. The results revealed that virgin polymers can be an alternative to reclaimed polymers up to the range of 60- 80% recycled material.[15]

This huge amount of post-consumer PET bottles needs to be utilized as a substitute material in preparation of composite sheets which will be used in the construction of sustainable sheets used in homes/ buildings, which in turn will help in minimizing this raw product and reducing environment threat.
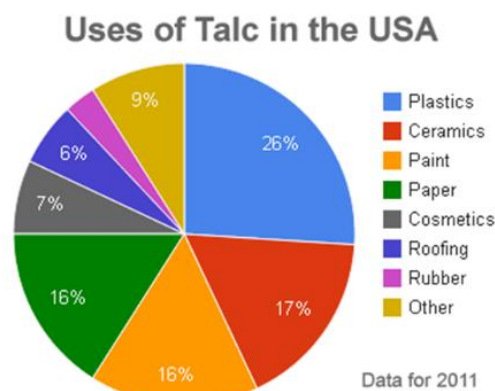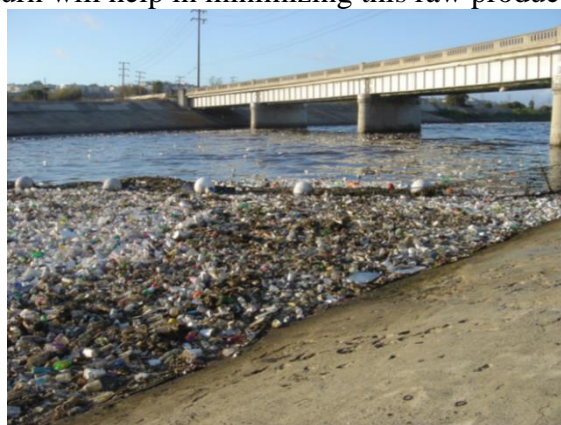
Fig 1. a) PET bottles waste b) Uses of Talc

II. Methodology

The materials used in this research were talc, waste PET, virgin PET.

A. Talc

Hydrous Magnesium Silicate $Mg_3 Si_4O_{10}(OH)_2$ also known as talc (Soap Stone) is incorporated in this research work was collected from Mingora emerald mines quarry. Talc was found in the form of irregular lumps o but for optimized conditions it is needed in powder form. Therefore it was crushed and grinded into

powder form using the hammer mill (FT2 Armfield, UK) thereby increasing surface area. Further sorting and screening by vibratory sieve shaker (Retsch AS200 Digit) to get a sample size of 45μm. The ratio of talc to PET is optimized at 1:4 which will yield an optimum product for that specific additive.

B. Recycled PET Pretreatment

Recycled PET bottles of grade 1 are used in a major ratio as it is the main ingredient of the composite material. These are collected from scrap dealer at the cost of Rs 60/Kg. Firstly pre-treatment of these bottles was done where they were washed with tap water. Then PET bottles were shredded into small flakes for prompt melting. Furthermore these flakes were rinsed with RO hot water followed by caustic soda for thorough cleaning and got cleared of contaminants and adhesives. These clean flakes were then subjected into tray drier to remove any retained moisture for further processing.

C. Virgin PET

It was purchased form PEPSICOLA Company Limited. The properties of reclaimed polymers due to rigorous recycling procedures and environmental effects are lost and deteriorated which can be overcome by the inclusion of some amount of virgin polymers in the reclaimed material.

D. Mixture Proportioning

The tests were carried out on a variety of samples of varying ratio ranging from 80 %R PET to 100 %R PET with small amount of VPET i.e. up to 20% and a fixed ratio of talc i.e. with one part of talc and four parts of PET (1:4) as per the ASTM standards optimized in previous research. [10]

E. Molding

Materials were casted in metallic mold of 3x3 in. The mold was covered with aluminum foil, so the molten plastic slurry does not stick to the metallic mold. After the material was poured in the mold it was then covered with its head piece and was then removed from the respective molds after 24 hours of casting period.

F. Experimental Procedure

A non-stick metallic pot was selected for the melting process of plastic as it can sustain the severe temperature. The pot was filled with the raw materials and kept for pre-heating in a furnace set for 330°C.The required amount of plastic was added to pot and it is introduced into the furnace for 20min at temperature of 330°C. Firstly, virgin PET was added into the pot then it is heated at about 330°C then RPET was added at temperature of 390°C. The waste plastic was kept in the furnace for 25-30 mins so that the plastic melts completely into molten form.

After 20 min, the substrate changed into molten state, subsequently the filler material talc was added through constant mixing, and keeping utmost care so that the molten PET does not gets hard. Finally the molten plastic was poured into the mold. The mold was already packed with aluminum foil, which has much higher temperature than the plastic, to avoid any type of sticking with the surface of mold. Without any further delay quickly the mold was put into the hydraulic press and compressed to get smooth and strengthened surface. Then it was kept for cooling under room temperature for 3 Hrs. Then the side surface was smoothened by sand paper. Hence the molten plastic solidified into thick insulating composite sheets.

Fig 2. Schematic of fabrication of composite sheet

G. Characterization

1. Compressive Strength Test

Compressive strengths tests of the composite samples were conducted using Universal Testing Machine (UTM), model number UH-200A, with a capacity of 200 tons according to ASTM D3410 standard. Cylindrical samples of diameter 1 in and length double of diameter 2 in were prepared as per required standard. UTM top plate was allowed to move at constant speed to apply an axial compressive load on the surface of the sample. The UTM provides an optimum value of compressive load (P) at failure. The compressive strength was then calculated by the given equation.

$$Compressive\ Strength = \frac{Pressure}{Area}$$

Fig 3. Universal testing machine

2. Thermal Conductivity Test

Thermal conductivity tests were performed on the heat conduction unit (P.A. Hilton Ltd).Samples of composite insulated material having diameter 30mm were fabricated and were placed in between the apparatus and the heat transfer rate at different point was noted. The thermal conductivity was determined as per the extent of heat conduction by each material.

Fig 4. Thermal Conductivity Unit

3. SEM Analysis

To get the morphological images of the samples **SEM JSM-IT100, JEOL, Japan** is used. SEM is a kind of electron microscope. SEM produce image of sample surface by very high energy beam of electrons. The composite surface is analyzed for the surface deformation. 15 KV voltage was needed in order to excite the electrons. The samples were gold coated first to provide the conductive characteristics to the composite surface. Samples were placed on steel stubs with aid of adhesive tape. Silver coating paint worked as a bridge of conduction between steel stub and the composite surface. SEM images shows the ductile or brittle deformations and presence of cracks etc on the surface of sample.

4. Water Testing

The method ASTM D 570-98 was utilized for observing the water absorption effect on the strength of the composite sheet. For this purpose samples were firstly dried in the tray drier. Keeping precision of 0.01g in consideration the samples were weighted through analytical weight balance. The samples were then immersed in normal distilled water at ambient/room temperature conditions. The samples were then weighed after removing from water, dried out with drier and then compared to the initial weight before immersion in water. Composite sheet sample was weighed before immersion into the water. It was then left for 24 hours of immersion in water and then weighed again.
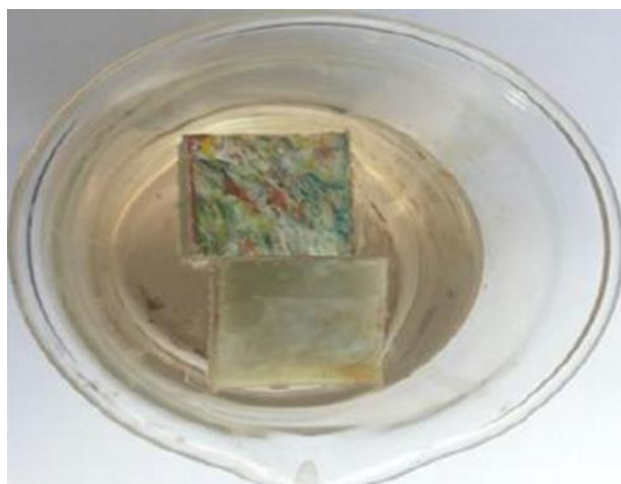
Fig 5. Sample immersed in water

5. Nano Indentation

Nano indentation also called as depth sensing indentation. It is used to analyze nano scale mechanical properties of materials for instance, metals, biological tissues and polymers. Nano-indentation analysis was performed on the developed composite using MTS Nano-Indenter IIs (Nano Instruments Ltd., USA). The load was imposed via the Berkovich Indenter for some specified time. Subsequently the residual indentation dimension was measured. The load was imposed on the composite sheet sample which then imposes an

indent on the surface by covering a displacement also known as indentation depth displacement. This load could be a function of the indentation depth or vice versa. Every indentation experiment gives a set of loading and unloading curves which are use to analyze hardness of the material.[16]

Fig. 6 MTS Nano-Indenter IIs, (NANO INDENTERVR IIs machine, supplied by Nano Instruments Ltd., Tennessee, USA)

III. RESULTS AND DISCUSSION

A. Compressive Strength Test

These compressive strength results shows the comparison of two PET polymers one obtained from recycled bottles RPET and the other was with virgin VPET and talc. In order to improve properties and cut out the drawbacks of RPET at high temperatures, recycled polymers were melted along with VPET. Due to less molecular weight and less intrinsic properties of RPET it shows lesser strength. It is clear from the figure 7 that the compressive strength of composite sheets is increased when some of the reclaimed material is replaced with 20% new material and 20% optimized filler/coupling agent compared to the sheets made of RPET only. This is due to the fact that the compressive bonding forces formed after the incorporation of coupling agent and filler material talc is stronger than normal.
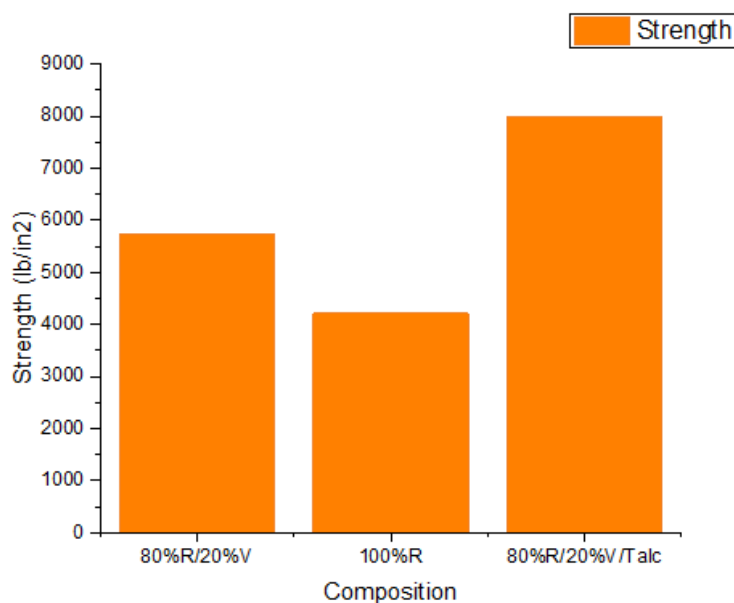
Fig 7. Composition of V/R PET -talc composite sheets vs Compressive Strength of composite sheets

B. Thermal Conductivity Analysis

Figure 8 illustrates three curves, where each of the curves is an insulating material made of different compositions. The only process parameter kept constant was the degree of compression of each insulating product. Talc to plastic ratio was optimized as 1:4. Figure 8 shows that material made of 100% RPET with no additives has the most steeper slope and the material with 80% recycle PET and 20% V PET incorporated with and without talc has a less steeper slope comparatively. Hence the newly developed optimized sheet having 80% RPET/VPET and 20% talc shows the least steepness and represented the lowest gradient value of K = 0.0214 W/m.k which is the most preferable material composition as it gives the best insulating property which means the temperature drop is low as one moves along the length/thickness of the material. These results indicated the importance of reinforcing filler material. Pores conductivity was reduced due to entrapped air in the pores. Composite sheets with reinforcing talc particles shows better thermal insulation due to preservation of pores. These talc particles restricts the movement of the gas particles, reducing the heat transfer through the base polymer. The correlation between these values may be attributed to the geometrical complexity of the composite sample for instance, particles shape and size, distribution and orientation of the dispersed particles, packing fraction, trapped air within the composite etc

TABLE I: THERMAL CONDUCTIVITY OF COMPOSITE SHEETS

Length	Temperature		
(mm)	**80 % RPET**	**100%RPET**	**80% RPET + Talc**
10	112.8	107.5	120.1
20	108.2	96.2	104.5
30	98.7	93.8	95.2
70	23.8	23.9	24.8
80	23.2	22	22.4
90	22.4	21.9	21
K (W/m. k)	0.0243	0.314	0.0214
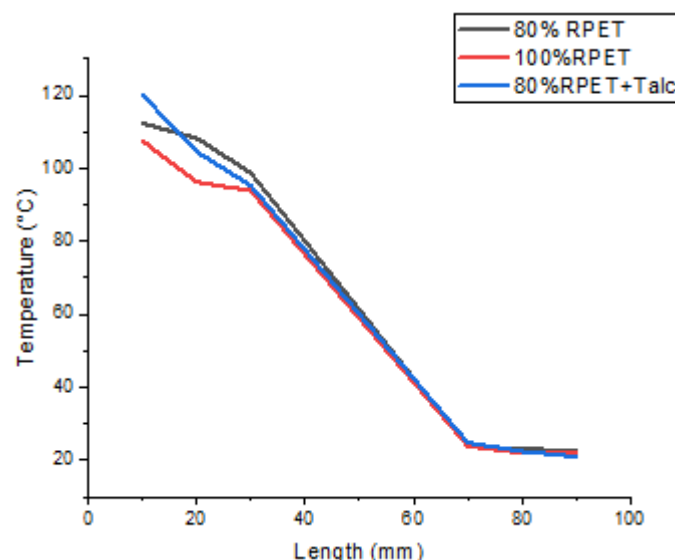
Fig 8. Temperature gradient across the length of the sample

C. SEM

SEM images in figure 9 (a) amply reveals the talc blended intimately in the PET plastic but of less aesthetics. Figure 9 (b) shows a uniform distribution of talc throughout the composite. Pores can also be observed upon the surface. Bubbles formed are due to the injection of talc to the PET plastic. Void space and the porous structure helps to generate vacuum inside the material enhancing its insulating properties. Figure 9 (b) indicates appreciable adhesion between the materials used. The aesthetic properties of figure 9(b) is improved due to the inclusion of talc and virgin PET polymer and lower formation of talc agglomerates were visible which contributes to its hardness. Whereas 100 % R PET has low aesthetic properties and low strength compared to V/R-talc composite sheets which took integral part to lower elastic modulus and compressive strength.
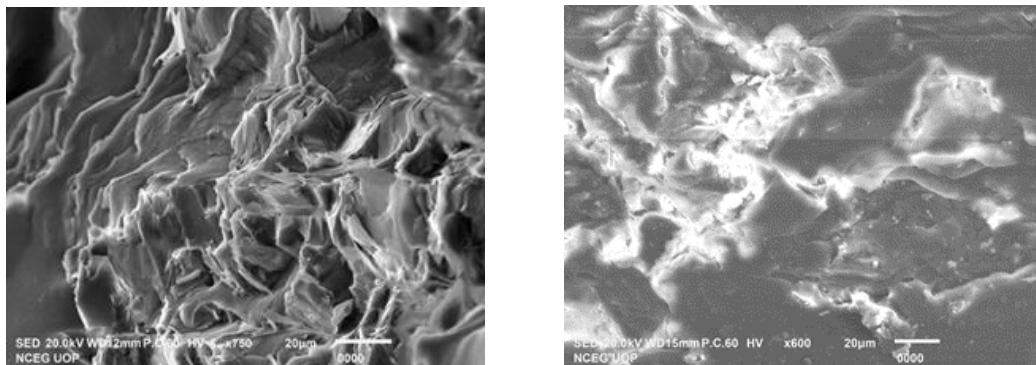
Fig. 9 a) 80%Recycle + Virgin PET b) 80% R + Virgin PET+ Talc

D. Water Absorption Test

The composite samples after the immersion in water shows the following results:
Weight of the composite before immersion in water = Wi = 135 g
Weight of the composite sample after immersion in water = Wf = 135g
Amount of water absorbed = Wi − Wf = 135g − 135g =0.00 kg
Thus it was concluded that these newly developed composite sheets are water proof in nature and can be used in the buildings and homes for insulation purposes safely.

E. Particle Size of Talc

Effect of particle size on the strength of insulating material is shown in figure 10. It is noted that as the particle size was decreased the material had greater strength and by increasing the mesh size the strength was decreased. The material having mesh size of 45 μm had maximum strength.
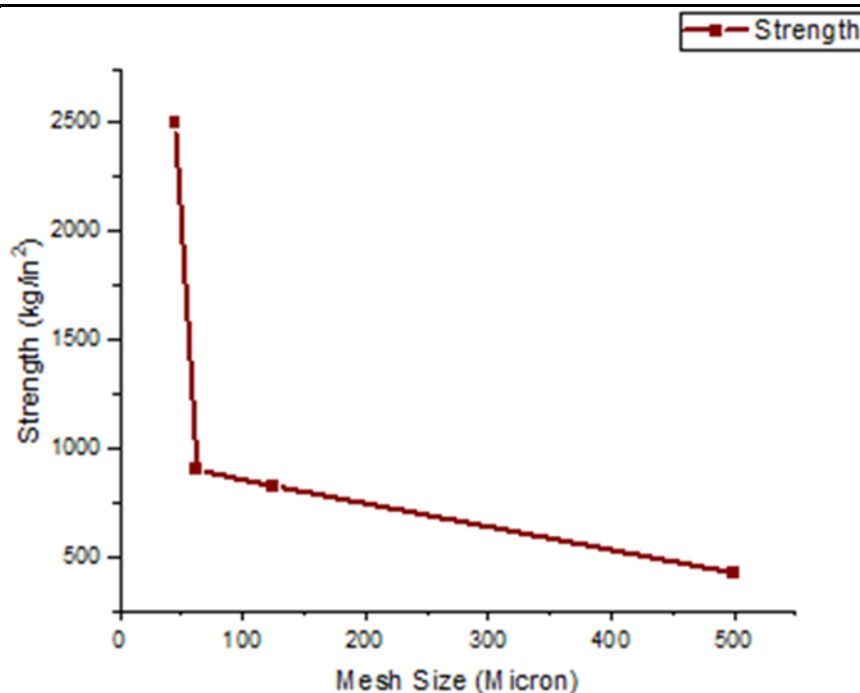
Fig 10. Particle size of different mesh size vs strength of the material

F.   Nano Indentation

The mixing of talc to the composite sheets can have a sturdy effect including stiffness, softening or swelling of the sheets showing increasing volume. Nano-indentation analysis was performed on different samples and loading and un loading cycle curves were obtained. Figure 11 represents load vs displacement curves of composite samples. Both the curves observed similar pattern and 100 mN load was imposed on the samples to produce an exceptional range of penetration depths. The observed high values of peak load are due to stiffness and strength caused by filler material talc. The maximum displacements were in the range of 10 μm to 16 μm. It was concluded that composite sheets having some amount of Virgin PET, 20% talc and maximum amount of R content that is up to 60 to 80% represented a harder behavior as it required a load of 100 mN to impose a penetration depth of 9μm whereas a similar value of load was observed for greater penetration depths in the range of 13 μm which represents the softer material.
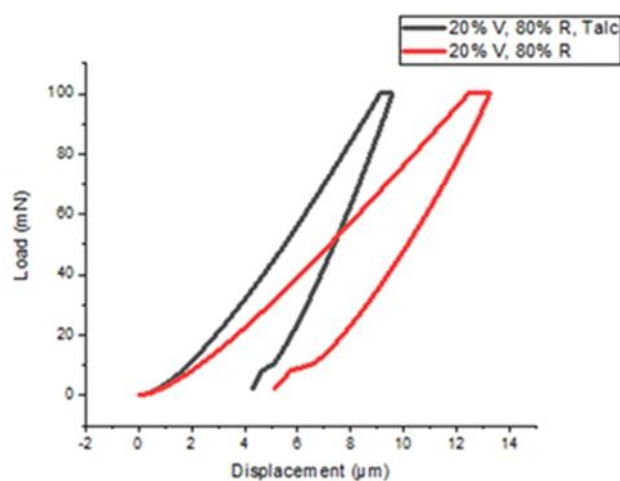
Fig. 11 Load –displacement curves for PET samples of different compositions

IV. CONCLUSION

This research work presented a value-added approach to facilitate recycling of discarded PET bottles by transforming them into greater strength, eco-friendly, and economically affordable talc-reinforced composite sheets. Compressive strength of the optimized composite sheet was increased and it was 7597 lb/in^2. Composite sheets fabricated from reclaimed material has many advantages that is these are light weight, helps to keep the buildings thermally insulated and help noise reduction which proved to be favorable for the purpose of insulation in homes and its sustainable for the environment. Results show that additive talc provides smoothness and porosity further enhancing the thermal insulation capability of the sheets. Nano indentation tests revealed that 20% of substitution of talc and 60 to 80% provides competent results and requires a load of 100mN to impose an indent of 9 μm compared to the sheets made up of only recycled PET which needs the same 100 mN load to impose indent of 13 μm. Thus these newly developed insulating composite sheets are one of the promising cost-effective recycling technologies for reduction of enormous amount of PET bottles and a way to cope with environmental threat associated with it.

V. REFERENCES

[1]   T. AK, A. OO, and R. AO, "A Pilot Recycling of Plastic Pure Water Sachets/Bottles into Composite Floor Tiles: A Case Study from Selected Dumping Site in Ogbomoso," *J. Mater. Sci. Eng.*, vol. 04, no. 06, 2015.

[2]   I. Taniguchi, S. Yoshida, K. Hiraga, K. Miyamoto, Y. Kimura, and K. Oda, "Biodegradation of PET : Current Status and Application Aspects," 2019.

[3]   A. Angus and G. Westbrook, "Top 10 Global Consumer Trends 2019," *Euromonitor Int.*, 2019.

[4]   J. Hopewell, R. Dvorak, and E. Kosior, "Plastics recycling: Challenges and opportunities," *Philos. Trans. R. Soc. B Biol. Sci.*, vol. 364, no. 1526, pp. 2115–2126, 2009.

[5]   G. Lonca, P. Lesage, G. Majeau-Bettez, S. Bernard, and M. Margni, "Assessing scaling effects of circular economy strategies: A case study on plastic bottle closed-loop recycling in the USA PET market," *Resour. Conserv. Recycl.*, 2020.

[6]   A. Oromiehie and A. Mamizadeh, "Recycling PET beverage bottles and improving properties," *Polym. Int.*, vol. 53, no. 6, pp. 728–732, 2004.

[7]   M. P. Aznar, M. A. Caballero, J. A. Sancho, and E. Francés, "Plastic waste elimination by co-gasification with coal and biomass in fluidized bed with air in pilot plant," *Fuel Process. Technol.*, vol. 87, no. 5, pp. 409–420, 2006.

[8]   A. Oushabi, S. Sair, Y. Abboud, O. Tanane, and A. El Bouari, "An experimental investigation on morphological, mechanical and thermal properties of date palm particles reinforced polyurethane composites as new ecological insulating materials in building," *Case Stud. Constr. Mater.*, vol. 7, no. June, pp. 128–137, 2017.

[9]   B. Yesilata, Y. Isiker, and P. Turgut, "Thermal insulation enhancement in concretes by adding waste PET and rubber pieces," *Constr. Build. Mater.*, vol. 23, no. 5, pp. 1878–1882, 2009.

[10]   N. Mohammad, S. Hussain, and N. Mohammad, "Optimization of flotation parameters for talc carbonates of Mingora emerald mine (Swat), Khyber Pakhtunkhwa, Pakistan," *J. Himal. Earth Sci.*, vol. 48, no. 2, pp. 26–31, 2015.

[11]   Y. W. Leong, Z. A. M. Ishak, and A. Ariffin, "Mechanical and thermal properties of talc and calcium carbonate filled polypropylene hybrid composites," *J. Appl. Polym. Sci.*, 2004.

[12]   H. E. Wiebking, "Increasing the flexural modulus of rigid PVC at elevated temperatures," *J. Vinyl Addit. Technol.*, 2006.

[13]   Y. Endo, D. R. Chen, and D. Y. H. Pui, "Effects of particle polydispersity and shape factor during dust cake loading on air filters," *Powder Technol.*, vol. 98, no. 3, pp. 241–249, 1998.

[14]   D. H. Kang, R. Auras, K. Vorst, and J. Singh, "An exploratory model for predicting post-consumer recycled PET content in PET sheets," *Polym. Test.*, vol. 30, no. 1, pp. 60–68, 2011.

[15]   a Elamri, K. Abid, O. Harzallah, and a Lallam, "Characterization of Recycled/ Virgin PET Polymers and their Composites," *Am. J. Nano Res. Appl. Am. J. Nano Res. Appl. Spec. Issue Nanocomposites Coat. Manuf.*, vol. 3, no. 11, pp. 11–16, 2015.

[16]   S. Yasin *et al.*, "Effect of experimental conditions on nano-indentation response of low density polyethylene (LDPE)," *J. Macromol. Sci. Part A Pure Appl. Chem.*, 2019.

Corrosion behavior of Nitinol after aging treatment in simulated body fluid

Nishat Riaz [A], Muhammad Imran Khan [B]

[A, B] =*Faculty of materials and chemical engineering, GIK institute, Topi, Distt. Swabi, 23640, KPK*

Abstract—**Nitinol as a biomaterial has gained significant importance because of its unique properties like superelasticity, shape memory effect and biocompatibility. They find extensive applications in cardiovascular devices, medical implants, bone fixation plates, staples, and orthodontic wires. The major concern for nitinol usage is their corrosion resistance because of large content of Ni i.e. 50 at% which can cause mechanical deterioration of implant and also inflammations inside the body. Therefore, present work aimed development of nitinol (50at%Ti-50at%Ni) alloy and its corrosion study in simulated body fluid. Optical microscopy and Potentio-dynamic polarization test in furnace cooled and aged form was done. It was found that corrosion resistance of aged alloy is higher as compare to furnace cooled sample.**

Keywords— **Biomaterial, Corrosion resistance, Nitinol, Shape memory effect, Simulated body fluid**

I. INTRODUCTION

Biomaterials are continuously developed to counter need for the biocompatibility and improved mechanical properties. Nitinol, a group of equiatomic, Ni-Ti alloys is largely recognized and accepted for the biomedical use[1-4]. Nitinol's superelasticity, shape memory effect, and wear resistance[5] have made them to be widely used as an implant in surgery fields including orthopedics, vascular interventions, orthodontics and laparoscopy tools[6].

Nitinol shows shape memory behavior which is mainly because of crystallography and thermodynamics of these SMA's. They are characterized by two solid phases: martensitic phase (M) and high temperature austenitic phase (A)[7]. In particular, the martensite can be present in two forms: First is stress-free martensite, which is characterized by the twinned martensite (M), which shows minimum misfit with parent phase. Therefore no macroscopic deformation is associated to it. Second configuration is the stress-induced martensite, that is characterized by the detwinned single-variant (S) martensite structure, which line up the variants along a particular direction, which shows macroscopic deformation. The transformation between austenite and the martensite phase is a stress-temperature induced athermal diffusionless thermoelastic martensitic transformation (TMT). If material goes to original shape upon heating, it's called shape memory effect while if the stress loading and unloading is responsible for the effect, it is called superelasticity[8-10]. NiTi alloy show good mechanical properties to be used as biomaterial but at present, there is still little research is done on biocompatibility of Nitinol. Nickel present in Nitinol may dissolve from the material because of corrosion and can cause allergic reactions[11]. Therefore, to have information about corrosion resistance of these alloys before their use inside the human body is important. Different mechanical and thermomechanical treatments were done to improve their properties. In the present work, corrosion properties of the Nitinol in the simulated body fluids are studied in the furnace cooled and aged samples.

II. METHODOLOGY

Ni_{50}-Ti_{50} (at%) binary alloy was developed in Mini arc Melter MAM–1 having tungsten electrode for the melting of metals. Alloy was homogenized at 1000°C in quartz tube for 3 hours and then cooled in the furnace. Samples were cut using EDM machine into small samples. Aging treatment was done on the samples at 500°C for 3 hours in argon atmosphere in tube furnace followed by water quenching. Optical microscopy was done to study their microstructure. Gamry Potentiostat was used for electrochemical polarization tests. OCP and Tafel plots were taken to understand behavior of alloy in furnace cooled and aged form in the SBF.

III. RESULTS AND DISCUSSION

Optical microscopy was done to study microstructure of the sample after grinding and polishing the samples. Fig.1 shows microstructures in both furnace cooled and aged form after etching. Fig.1(a) shows microstructure of furnace cooled sample showing polycrystalline structure. These grains are of different sizes and orientation. Whereas aged sample shows grain coarsening as observed from Fig.1(b) because of aging treatment at 500°C.
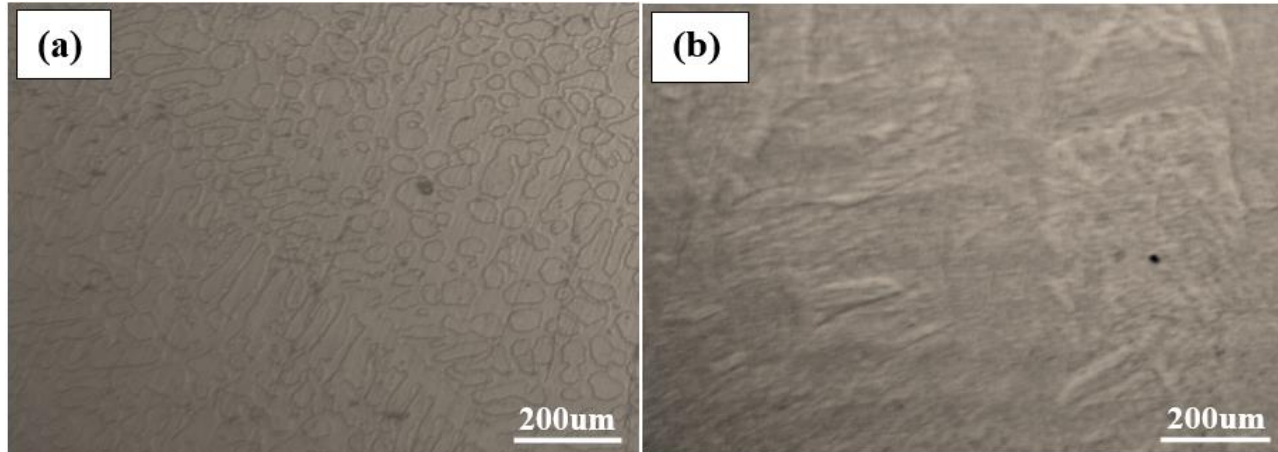
Fig. 1. Optical Micrograph for Nitinol a) Furnace cooled b) Aged.

Potentiodynamic polarization test was performed to assess corrosion behavior of the sample in the simulated body fluid. Tafel extrapolation was done to find corrosion current (I_{corr}) and corrosion rate. Fig.2 shows the curves obtained while values of corrosion rates are given in the table 1. It is seen that furnace cooled sample shows higher corrosion rate i.e. 1.201 mpy as compare to aged sample. A small polarizing effect is also seen in aged sample which shows an increase in potential value while no change in corrosion current value showing that sample attained passivation during reaction for some time. This can be because of the reason that furnace cooled sample have more grain boundaries which provide more active sites for corrosion, causing more dissolution by corrosion. While in the case of aged sample, it is expected that more stable oxide layer after heat treatment is formed and also grain coarsening occurred which decreases the corrosion current (I_{corr}) value while potential (E_{corr}) goes to positive side.
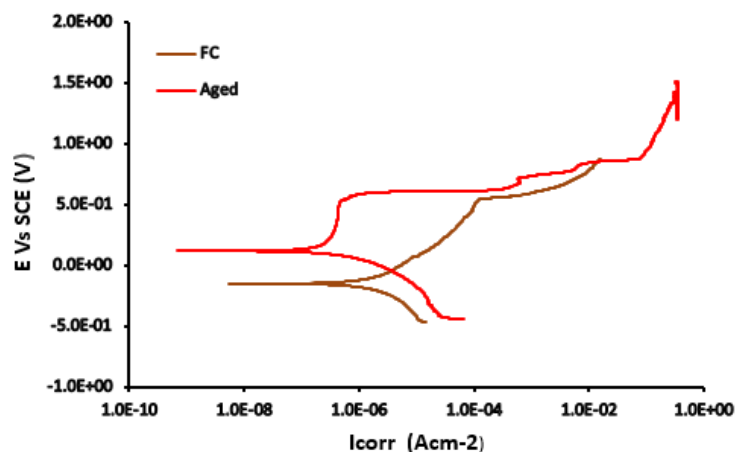
Fig. 2. Tafel curves of furnace cooled and aged samples.

TABLE I: TAFEL RESULTS OF FC AND AGED SAMPLES

Sr. No	Sample	βa (V/decade)	βc (V/decade)	Icorr (μA)	Ecorr (mV)	CR (mpy)
1	Fc	$381×10$	$364×10^{-3}$	2.590	-153	1.201
2	Aged	$16.9×10^{-3}$	$225×10^{-3}$	0.577	177	$245×10^{-3}$

IV. CONCLUSION

1. Optical microscopy shows that aging treatment results in increase in grain size as compare to furnace cooled sample. While Furnace cooled sample show smaller grains of different sizes and orientation.
2. Corrosion resistance of aged sample is found higher than FC sample in Potentiodynamic polarization test. The reason can be coarser grains in aged condition which provides less dissolution sites for corrosion as well as it can be due to stable oxide layer after aging heat treatment.

V. REFERENCES

[1] L. Delaey, R. Krishnan, H. Tas, and H. Warlimont, "Thermoelasticity, pseudoelasticity and the memory effects associated with martensitic transformations," *Journal of Materials Science,* vol. 9, no. 9, pp. 1521-1535, 1974.
[2] T. W. Duerig, K. Melton, and D. Stöckel, *Engineering aspects of shape memory alloys*: Butterworth-Heinemann, vol.6, pp. 18-23 2013.
[3] K. Otsuka, and K. Shimizu, "Pseudoelasticity and shape memory effects in alloys," *International Metals Reviews,* vol. 31, no. 1, pp. 93-114, 1986.
[4] J. Perkins, *Shape memory effects in alloys*: Springer Science & Business Media, 2012.
[5] P. Filip, "Titanium-nickel shape memory alloys in medical applications," *Titanium in Medicine*, pp. 53-86: Springer, 2001.
[6] M. I. Khan, H. Y. Kim, T.-h. Nam, and S. Miyazaki, "Formation of nanoscaled precipitates and their effects on the high-temperature shape-memory characteristics of a Ti50Ni15Pd25Cu10 alloy," *Acta materialia,* vol. 60, no. 16, pp. 5900-5913, 2012.
[7] N. Sharma, T. Raj, and K. Jangra, "Applications of nickel-titanium alloy," *Journal of Engineering and Technology,* vol. 5, no. 1, pp. 1, 2015.
[8] K. Tsuchiya, "Mechanisms and properties of shape memory effect and superelasticity in alloys and other materials: A practical guide," *Shape Memory and Superelastic Alloys*, pp. 3-14: Elsevier, 2011.
[9] L. Petrini, and F. Migliavacca, "Biomedical applications of shape memory alloys," *Journal of Metallurgy,* vol. 2011, 2011.
[10] H. Karaca, S. Saghaian, B. Basaran, G. Bigelow, R. Noebe, and Y. Chumlyakov, "Compressive response of nickel-rich NiTiHf high-temperature shape memory single crystals along the [1 1 1] orientation," *Scripta Materialia,* vol. 65, no. 7, pp. 577-580, 2011.
[11] J. Ryhänen, "Biocompatibility of nitinol," *Minimally Invasive Therapy & Allied Technologies,* vol. 9, no. 2, pp. 99-105, 2000.

Comparison of acetal and nylon for cap of neutral safety switch used in agricultural tractors

Nosheen Naz*, Afzal Khan,
Department of Mechanical Engineering,
University of Engineering & Technology Peshawar,
KPK, Pakistan.

Abstract-Neutral safety switch is installed in agriculture and other purpose agricultural machinery to specify the working of neutral gear. Neutral safety switch comprises of acetal cap with crimped copper terminal, plunger, main cover body, and spring. However, acetal (POM) is used in production of these caps. Acetal manufactured caps usually fractures and cracks due to some unidentified reasons. Some caps may be received in fractured and burnt form. However, the market claim $\geq 10\%$ per month which is substantially higher market failure. Therefore, proper material is needed to replace acetal material in aforementioned application. This research validates more nylon as material in comparison to acetal (POM) using several field tests on cap. Caps were assembled with the switch assembly and tested on endurance testing machines. Each cap was subjected to severe heating and cooling cycles and afterwards tested on endurance testing machine. Hence, the results depicted that nylon is better material in comparison to acetal.
Keywords: Safety switch, Acetal, endurance testing machine, material.

I. Introduction

Automotive switches play a vital role in making this facility more comfortable and safe. Shifting of automotive from purely mechanical to electro-mechanical assemblies has made auto industry more and more challenging. However, still problems related to design, processing, materials and process remains intact with the components involved in auto-motives. These switches includes door locking, light indicator[1-3], mirror indicator, hand brake indicator switch and neutral gear indication switches accordingly [4] etc.

These switches consists of several components made from several materials i.e., metals, plastics and ceramics (in rare cases). These components were assembled together in making these switches. However, some components or their materials may not perform adequately in harsh or normal environmental conditions. Ultimately, due to specific reasons these components can fail. Hence, the appropriate material is very crucial in this process.

In our case the cap of neutral safety switch has been returned in guarantee claim in substantial quantity. Therefore, we compared the used material i.e., acetal with nylon. 100 switches were taken and subjected to heating and cooling cycles. Heating and cooling cycles were performed at several temperatures. The results helped to identify that nylon based caps were better in comparison to acetal.

II. Methodology

100 caps were manufactured from acetal and nylon based caps each. Experiments were performed at various heating cooling temperatures ranging from 263 - 283, 293, 303, 313, 323, 333, 343, 353K for 1, 2 and 3 hours for 10, 20 and 30 days. Additionally, switches were exposed to endurance testing machine.

III. Results and Discussions

Results show that percentage of failed caps increased when the temperature gradient between heating and cooling cycle enhanced. Initially there were < 1% cracked caps of acetal. However, with increase in gradient from 20K to 30, 40, 50, 60, 70 and 80K increased the cracking of cap to 1.8, 2.2, 3.1, 3.6, 3.8, 4.05 and 4.21 % respectively (heating and cooling cycle for one hour). In contrast, further increasing the heating or cooling cycle time to 2 hours has no significant effect on the cracking percentage. The cracked percentage remained between 1.2, 1.9, 3.15, 3.5, 3.83, 4.17 and 4.3 % respectively. Further increase in heating or cooling cycle for approximately 3 hours subsequently caused slight increase in cracked percentage of 1.5, 2.29, 3.35, 4.09, 4.83 and 5.2 % respectively at temperature gradients of 20, 30, 40, 50, 60, 70 and 80K.
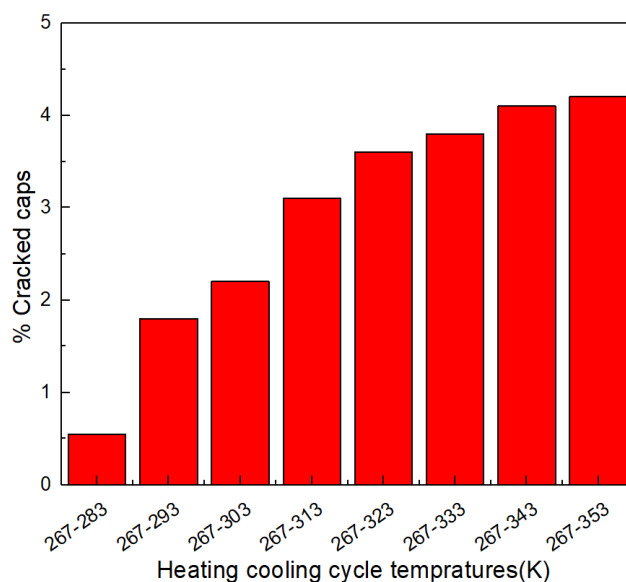
Fig. 1. Cracked caps during heating /cooling cycles at various temperatures for 1 hour and continued for 10 days.
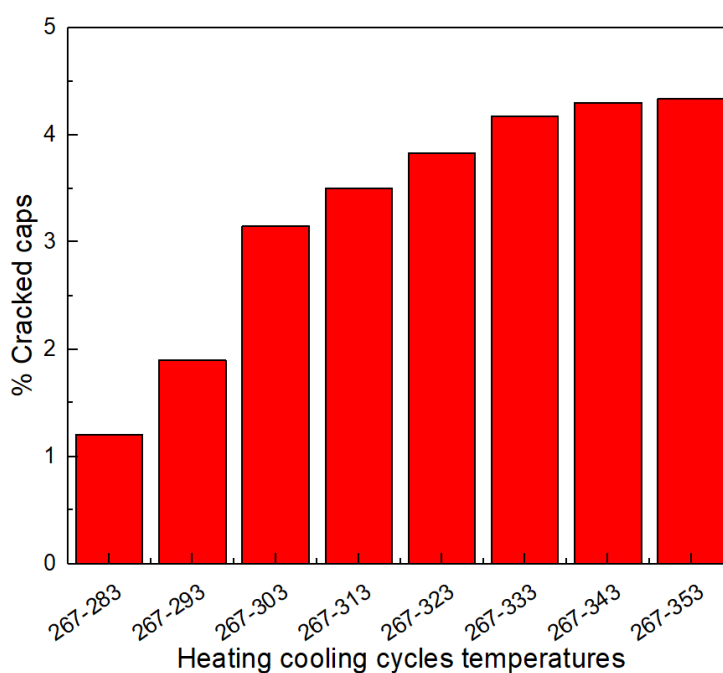
Fig. 2. Cracked caps during heating /cooling cycles at various temperatures for 2 hour and continued for 20 days.
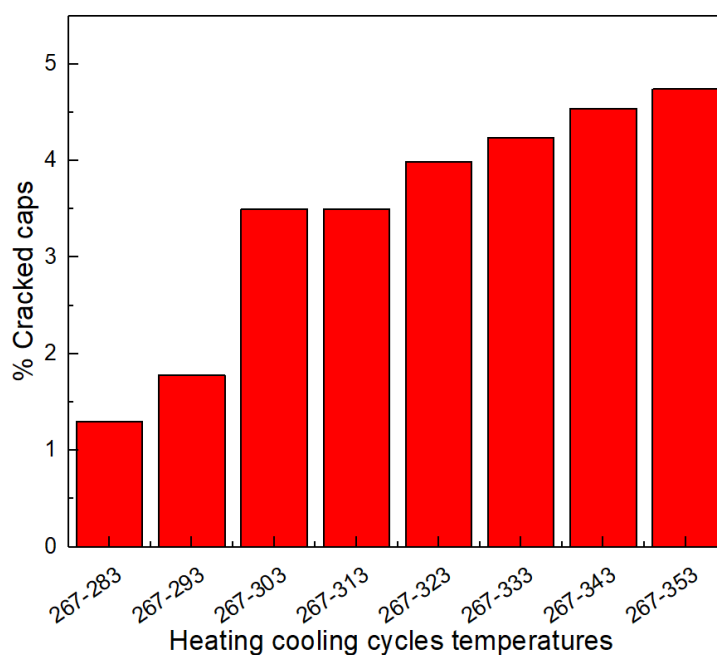
Fig. 3. Cracked caps during heating /cooling cycles at various temperatures for 3 hour and continued for 30 days.

IV.   Conclusion

Increase in temperature gradient in heating and cooling cycles significantly affect the cracking percentage of the caps of acetal. However, the effect on nylon caps was much lower in comparison to the acetal based caps.

References

1. Rosso, V.D., Combined automotive light switch, US patent 5736696, 1998.
2. Tonar, W.L., Bugno, M.D., Roth, M.R., Cammenga, D.J., Minikey, D.L., Stray, J.A., Neuman, G.A., Automotive rear view mirror with capacitive switches, US Patent 9134585B2, 2015.
3. Leung, C.H., Wang, B.H. Thermal modeling of electrical switches and relays, IEEE transactions on components, packaging, and manufacturing technology part A,19(3), 346-352, 1996.
4. Ashby, M., Cebon, D. Materials selection in mechanical design, Journal de Physique 111, 3, 1993, C7-1-C7-9.

Effect of Industrial Wastewater Irrigation on Quality of Local Soil and Vegetables in Mingora city swat.

Maqsood ur Rahman [1], Nehar Ullah [1], Irshad Ali [1]

[1] Department of Chemical and Materials Engineering, University of Engineering & Technology, Peshawar, Pakistan

Abstract- **Industrialization shows an important position in the development of the country. Besides development there are other aspects too that industrialization brings with itself. Increases number of industries discharge unwanted substances. A large amount of wastewater is discharged without any proper treatment into the environment. Excess amount of toxic heavy metals from these industrial processes are added into the soil, ground and source water that are consequently used for agricultural irrigation purposes. Discharge of untreated effluents causes severe adverse effect on eco system containing humans, plants, and animal as well. The current research work is to study the consequence of industrial wastewater used for local agriculture and their impact on quality of soil and vegetable i.e. onion, pumpkin, tomato, lady finger and green paper. Before atomic absorption spectrophotometer wet digestion method was used for heavy metals detection. The concentration of heavy metals in wastewater follow the order: Fe >Cr>Pb> Ni> Co> Mn. The investigation further shows that the amount of iron and lead in wastewater has the dominant effects on vegetables in Mingora city Swat. Lead has the highest level of accumulation in the soil. Iron and lead have the highest transfer factor for pumpkin and lady finger. The study will help the local former to cultivate proper crops in the area where it is irrigated through industrial wastewater in Mingora city Swat. It also creates public awareness to select that types of vegetable which effect less. This study also provides practically applicable solution to the local industry for the treatment of effluents.**

Key words: heavy metals, wastewater, soil, vegetable, health risk.

I. INTRODUCTION

Vegetable contain carbohydrates protein vitamin which are the essential fraction for the growth of human health. [1]. To get pure vegetable it requires the area where soil and water are free from unwanted impurities. But now a day that type of land and water are difficult to finds. With the development of industries due to human needed in all over the world the discharge of wastewater increases and due to scarcity of pure water, farmer uses wastewater for agriculture.

Heavy metals have the specific gravity of five times that of water [2]. The effluent waste from industries contain toxic heavy metals which is most serious environmental concern of the present day. The accumulated heavy metals in soil create huge health problems. For irrigation, the use of wastewater which contains heavy metals for a long time increase the concentration above the allowable range [3, 4]. The heavy metal presence in soil play dynamic rule in controlling metal bioavailability to plants [5]. Heavy metals present in the wastewater had highest concentration which is used for irrigation. Continuously used for irrigation increase its amount in soil [6].

Untreated discharging of wastewater from Municipal and industries contain toxic material which creates major water pollution. In Pakistan there is no proper water treatment facility available [7, 8]. The accessibility of soil metals to plants is a function of soil properties like Ph., organic carbon cat ion exchange capacity. The metal concentration decreases when going in depth while higher on the topsoil [9]. Large number of toxic chemical which are identified in water from textile dying in which some cannot be removed which represent a worrying environmental problem for the clothing manufacturing [10]. In plants heavy metals accumulated which depend upon plants species and efficiency [11].

Soil has the capability to absorb toxic chemical but decreases its ability of captivation continuously, but after saturation it will occupy by vegetable. As long the use of wastewater makes the metals accumulates in the soil and increase its absorption and accumulation in plants. For every type of organism and plants water is a main source of life and energy, but people mostly suffer from clean drinking water. Due to shortage of clean water high % of all illnesses in developing countries are related to wastewater [12]. Different types of diseases and health problems cause by wastewater which contain heavy metals above permissible limit [13]. Water treatment process involving the calculation of many factors, the treatment of wastewaters to make them suitable for irrigation. Several technologies are available with varying degree of success to control

water pollution [14]. Chosen quality for irrigation aims, representing an economic benefit in the area where low-cost wastewater treatment systems [15, 16, 17]. With rate of fast growth wastewater which contain heavy metal in soil become increasing and create major environmental anxiety and its direct effect on human health [18].The total land irrigated wastewater has been estimated to be about 50 million acres in fifty countries, which is about 10% of whole irrigated land (FAO, 2003). The wastewater from textile mill, the propagation ratio and evolution were comparatively greater than the control, at small amount but with the increase in the effluent concentrations these parameters were decreased. Away from 25% discharge, the length of root and shoot decreased. The discharge from textile mills will reduced seed development and initial growth of all vegetable's plants [19, 8].

According to An visa, the allowable limits for Cd, Ni, Pb and Cr are 1.0, 5.0, 0.5 and 0.1 mg/kg, separately (fresh weight) [20]. Proteins, lipids, and DNA are damage by reactive oxygen which are produced in large quantity by oxidation [17]. The problems associated with industrial pollutants, there is need to monitor water in which industrial effluents are discharged [21]. Use of industrial effluents for irrigation purposes is a highly warranted effectiveness of water pollutants concept [22].The wastewater is rises due to industrialization being used for agricultural fields. Vegetable crops cultivated in suburban areas absorb metals from contaminated soil due to wastewater irrigation. The metals also   deposit on plant's parts unprotected to the polluted air [23]. Contaminated land which grow crops like vegetables, fruits and nuts can collect toxic heavy metals [24]. Our Area of interest is Mingora city, KPK, to highlight the harmful effects of heavy metals accumulation due to industrial wastewater irrigation. In this research article we will point out the amounts of heavy metals present in Industrial wastewater, their adverse effect and apply any one of the treatment techniques to remove how much concentration of heavy metals.

II. MATERIAL AND EXPERIMENTS
2.1 Sampling Area

2.1.1 Mingora

Mingora is the capital city of district Swat. It is located at an altitude of 984 m. The average annual temperature in Mingora is 19.3℃. November is the driest while August has the highest precipitation month with rain of 22 and 134 mm. Chitral districts is bounded by North, Kohistan and Shangla districts in the East, Buner district and Malakand protected area in the South. Both upper and lower Dir districts in west. While Indus disconnects it from Hazara in the east. The district is enclosed by the sky-high mountains [22].

| Different sites of Mingora city | Location of Mingora city swat [22]. | sample collection point |
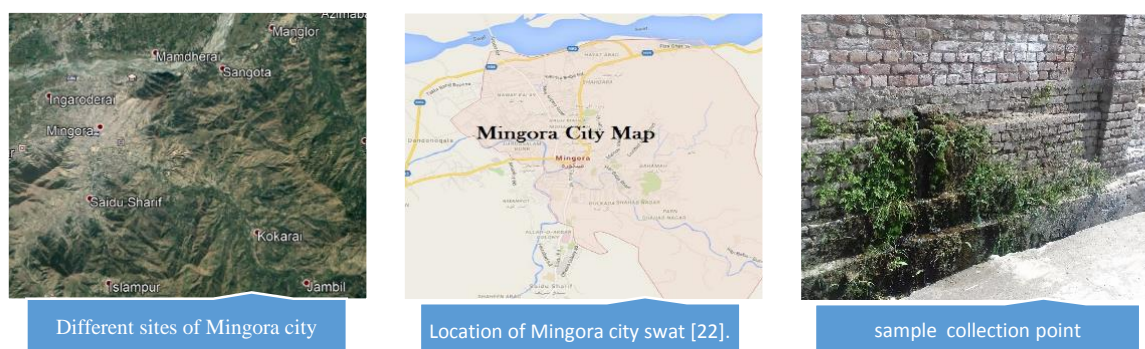
Fig 1:Diferent location and sampling point in Mingora city.
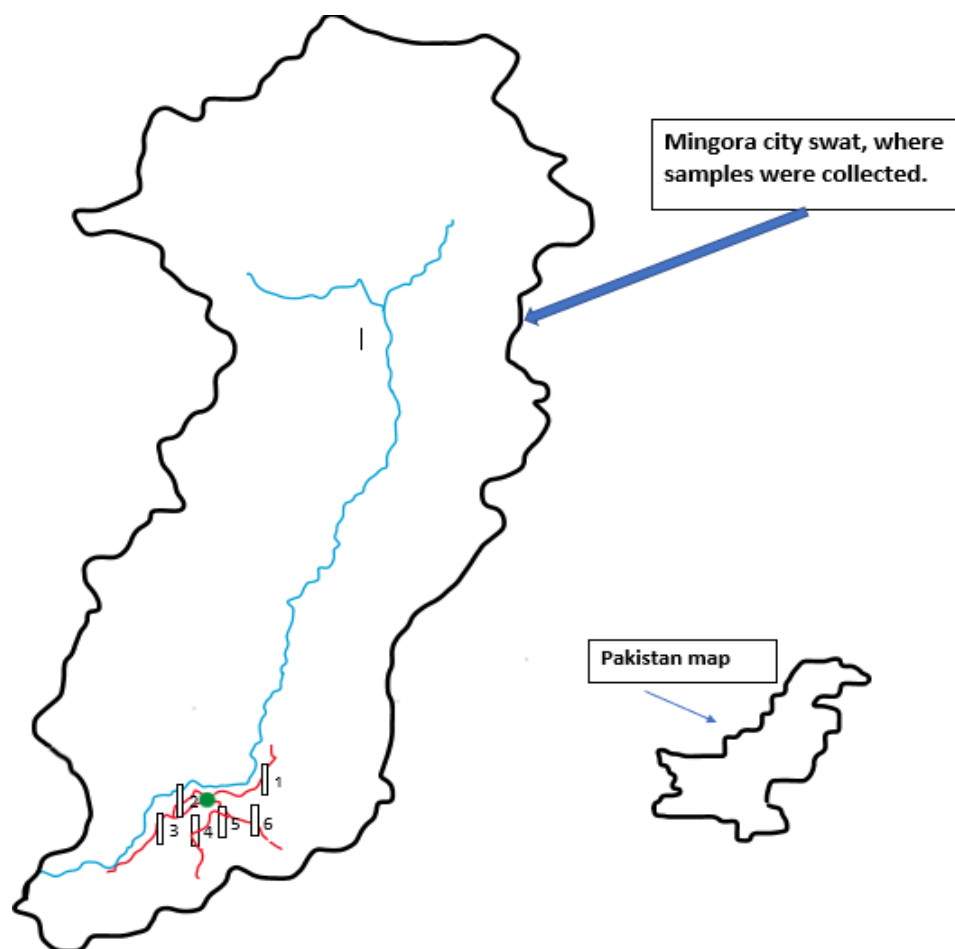
Fig 2: Site map of the samples where it was taken.

The box in above sketch of Swat Mingora represent the area from which samples has been taken.

1. Fizagat.   4. Saidu sharif.
2. Mingora City.   5. Shahab Nagar.
3. Rahim abad.   6. Kokarai.

The above mention area there are different types such as plastic, paper, chemicals, petroleum, rubber, pharma, cosmetics, textiles, steel, and other industries are working.

2.1.2 Research Location

The drain water irrigation area in Mingora around where most of the industrial wastewater are run-offs and the water use for agriculture purpose. The farming occupation in the area consist of lady finger, tomato, onion cucumber, pumpkin, radish, and turnip. These wastewaters are used for many years, due scarcity of pure water.

2.2 Samples collection

Different samples were collected from area where different industrial effluent were drain .These industries discharge huge amount of wastewater in which soil and vegetables are directly affected.

2.2.1 Water samples

Wastewater samples from different area were collected from different places (sites) at Mingora city. The samples were put in a small   clean bottle which were washed by distilled water and these were sealed and labellate. These sample were transported to chemistry lab to ready for Atomic absorption spectrophotometer (AAS).

2.2.2 Vegetable samples

The samples of vegetables (ladyfinger, tomato, pumpkin, and onion) were composed from cultivated fields in the study area in the month of October November, where it is irrigated by industrial wastewater. The samples were taken in a small clean bottle and these were sealed and labeled. Sample of vegetables were also collected from control agricultural field. These sample were transported to chemistry lab for preparation and analysis.

2.2.3 Soil samples

Different Soil samples were taken from farming field present in the study area. The samples were kept in new plastic bottles and brought to the chemistry lab for analyses. Samples of different area from top and depth was taken and collected.

2.3. Chemical Reagents

Distilled water was use throughout in the lab work. Analytical grade chemicals were used. HCL HNO3 and perchloric acid were reagent of analysis. These reagents were used for preparation of water, soil, and vegetable samples.

2.4.1 Water samples Preparation

Water sample up to 50ml was collected in washed and cleaned beaker. Concentrated nitric acid of 10ml was added to water sample beaker and heated it up till the total solution remains 40 ml. after cooling using Whatman NO.42 filter paper was used . After filtration 10 ml of distilled water was added to dilute the filtrate. In this way all the samples were prepared.

2.4.2 Vegetable samples preparation

Each sample of vegetable was scrubbed with distilled water to remove dirt and unwanted particles. With the help of knife, the washed sample was then cut to separate the roots, stems and leaves. After cleaning, each sample was dried in air and then put in oven at 80 °C for 24 Hrs. followed by heating at 100 °C in electric oven. Vegetables samples were then converted into a powder form (80 mesh) using a commercial mixer (TSK- WestPoint, France) and kept in plastic bags for acid digestion.

2.4.3 Soil samples preparation

Soil samples from different areas were taken. Wet sample were dried in the oven until it become dry. Aqua regia of HNO3 and HCL of (1:3) were prepared in the round bottom flask. Two grams of each sample was taken, and 10 ml prepared sample were put into the soil and gently shaken. Then the sample was heated through oven at temperature of 90 deg °C for 20 to 25 mins. After cooling it was filtered through Whatman 42 filter paper. 20 ml of distilled water was added after filtration. Thus, all samples of soil were prepared. After preparation further investigation of heavy metals concentration.

2.5 Risk assessment

Khan et al using equations to calculate Health risk assessments (HRAs) for heavy metals through the ingesting of contaminated food crops.

HRA = DIM / Rf D

HRA is the human risk assessments through the ingesting of vegetables, the daily intake of metal (DIM) (mg metal/kg body weight/day) and Rf D is the reference dose. The reference dose values for Zn, Pb, Ni, Cr and Mn were 0.30, 0.004, 0.02,1.5 and 0.033 mg/kg bw/day, respectively [25, 26, 27].

III: RESULTS AND DISCUSSION

Table 1: Concentration of Heavy Metals in Industrial Wastewater and Tube Well Water.

Heavy Metals (mg/L)	Fe	Pb	Cr	Ni	Mn	Co
Industrial Wastewater	6.72	0.395	0.539	0.122	0.128	0.203
S. Deviation	0.0255	0.129	0.013	0.0131	0.0207	0.026
Tube well-Water.	1.17	0.043	0.416	0.096	0.033	0.116
S. Deviation	0.0787	0.235	0.0536	0.017	0.0106	0.0275

3.1 wastewater of Industries and tube well water

The order of heavy metals concentration in Industrial Wastewater follows as Fe>Cr>Pb> Co>Mn. >Ni. The heavy metals concentration is high in effluents from industries as compared to Tube well water. The wastewater is directly use for irrigation purposes. The concentration of heavy metals is higher than permissible limit. People use wastewater for vegetables growing from long time.
The Congregation of Heavy metals in Industrial effluents and Tube Well water (controlled samples) were compared. All the heavy metals in tested wastewater in selected area of Mingora, where it is used for vegetable irrigation were higher than permissible limit. Iron and chromium show highest result compare to other heavy metals. The value of iron is (6.72 mg/l) which is greater than tube well water of (1.17 mg/l) and cross the allowable limit of (5 mg/l) by WHO. Different area where samples were collected are higher than control water. Lead concentration is (0.393 mg/l) which is above the permissible limit of (0.01mg/l) by WHO. Cobalt also cross, the acceptable limit of (0.025 mg/l).

Table 2: Heavy metal concentrations (mg/L) Comparison of different area studies [28].

S. No	Fe	Pb	Ni	Cr	References
Charsadda	0.01	0.075	0.002	0.007	Khan et al. 2013a
Kohistan	--	0.009	0.004	0.007	Muhammad et al. 2011
Quetta	0.64	0.07	0.09	0.04	Khanoranga and Khalid 2019
Southwest, Nigeria	0.20	-	ND	0.19	Titilawo et al. 2018
Khorramabad, Iran	-	0.001	-	0.05	Ghaderpoori et al. 2018

Khan et al. 2013a study in District Charsadda and they found Iron concentration of 0.01mg/L, Pb 0.0075mg/L, Ni of 0.002mg/L and Cr 0.005 mg/L. Similarly, Muhammad et al. 2011 reported the heavy metals concentration as Pb 0.009, Ni 0.004 and Cr 0.007 mg/L in district Kohistan wastewater. Khanoranga and Khalid 2019 reported concentration of heavy metals as Iron 0.064 mg/L, Lead 0.07mg/L,

Nickle 0.04 mg/L and Chromium 0.09 mg/L. Titilawo et al. 2018 reported concentration of heavy metals as Iron 0.2 and Chromium 0.19 mg/L. Ghaderpoori et al. 2018 also analyzed the wastewater of Khorramabad, Iran for heavy metals concentration and they found Pb concentration of 0.001mg/L (which was too low compared to other studies), and Chromium concentration of 0.05 mg/L.

Table 3: Soil Contains heavy metals irrigated with industrial effluents and Tube Well water.

Heavy Metals (mg/L)	Fe	Pb	Cr	Ni	Mn	Co
Soil (IWW)	47.27 ±0.109	2.92 ±0.092	2.90 ±0.038	1.013 ±0.02	0.901 0.014±	0.679 ±0.053
Soil (TWW)	17.12 ±0.27	2.12 ±0.21	2.03 ±0.03	0.76 ±0.04	0.23 ±0.012	0.49 ±0.01

Continuous use of wastewater lead to enrichment of heavy metals in soil. The high amount, of Heavy metals strongly affects their availability to soil. In case of soil samples, metal bio available section was higher in wastewater wetted soil as compared to pure water saturated. Fe Concentration was the highest for industrial wastewater followed by Pb>Cr>Ni>Mn>Co. All the values from results are above the allowable limit. The increase in amount, of Heavy metals in soil is mainly due to soil irrigation with untreated industrial effluents from different industries of the Industrial area Mingora city.

Table 4: Concentration of heavy metals in wastewater irrigated vegetables.

Heavy Metals(mg/L)	Fe	Pb	Cr	Ni	Mn	Co
Lady Finger Mean+ S.d	8.09 ±0.056	3.51 ±0.27	0.43 ±0.04	0.17 ±0.05	0.21 ±0.004	0.086 ±0.046
Pumpkin Mean+ S.d	24.9 ±0.18	1.61 ±0.21	0.51 ±0.032	0.39 ±0.04	0.973 ±0.01	0.072 ±0.01
Onion Mean+ S.d	3.6 ±0.04	0.67 ±0.025	0.44 ±0.06	0.25 ±0.04	0.155 ±0.02	0.138 ±0.006
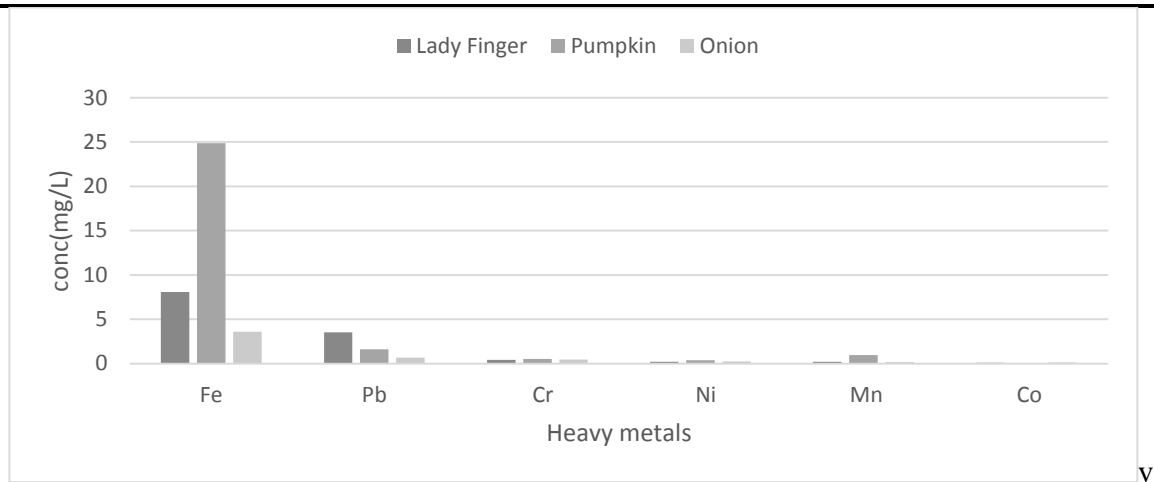
Fig 3: Comparative plot of heavy metals concentration (mean) in vegetable irrigated through Industrial wastewater.

From the above table it concluded that industrial wastewater not only affect the soil quality but also the vegetables irrigated through it. To compare these results with vegetables irrigated with tube well water (as a control samples), we performed the analysis. For pumpkin iron (Fe) has the highest value compare to other vegetables. For pumpkin Ni, Mn show high concentrations compared to other vegetable. For onion cobalt value is the greater than other. Onion is more resistive to lead. Lady finger resistive to Nickel.

IV.TREATMENT PROCESS

4.1 Nanofiltration

There are many wastewater purification techniques which are using in many parts of the world. such as activated sludge, adsorption, advanced oxidation process, reverse osmosis, and nanofiltration. However, it removes insecticides, biological matter, salt removing of sea water, oil process heavy metals ions and pollutants from industrial wastewater.

4.2 Process description

Membranes have pore sizes from 1-10 nanometer, created from polymer thin film. Feed passes through pump to semi-permeable membrane. The stream is separated into two portions permeate and retentate. The former is filter portion while later is the rejected non-filtered portion. In concern research nanofiltration was applied for the removal of wastewater effluent from industries. The pure water flux (J, $L \cdot m^{-2} \cdot h^{-1}$) and permeability ($L \cdot m^{-2} \cdot h^{-1} \cdot bar^{-1}$) were obtained from the following equations:

$$J=(\Delta V)/(A \cdot \Delta t)$$

$$Permeability=J/(\Delta P)$$

Where ΔV is the volume (L) of the permeate; A is the effective membrane filtration area (m^2), and Δt is the experimental time (h). ΔP is the transmembrane pressure applied by diaphragm pumps (bar). The salt rejection was obtained by using the following equation.

$$R (\%) =(C_f-C_P)/C_f \times 100\%$$

Where C_f and C_p, determined by the solution conductivity monitor (FE 38-Standard/Conductometer, Mettler, Switzerland), are the solute concentrations of the feed and permeate, respectively. Each experiment was carried out at least three times, and a mean value was taken.
The recovery of feed sample was determined by the following equation.

$$R\% = (Q_p/Q_f) * 100$$

Where, Q_p and Q_f is the volumetric flow rate of permeate and feed (L). Some results of nanofiltration is given as.

Table 5: Rejection of heavy metals from wastewater using nanofiltration of different pressure at

Heavy metals(mg/L)	Fe	Pb	Cr	Ni	Mn	Co
Ind wastewater	6.70	0.292	0.515	0.107	0.123	0.181
Tube-Well-Water	1.17	0.043	0.416	0.091	0.033	0.116
Results of NF	Fe	Pb	Cr	Ni	Mn	Co
Pressure (2 bar)	0.393	0.290	0.013	0.102	0.019	0.157
Pressure (3 bar)	0.373	0.274	0.015	0.096	0.017	0.146
Pressure (4 bar)	0.354	0.228	0.021	0.090	0.016	0.142
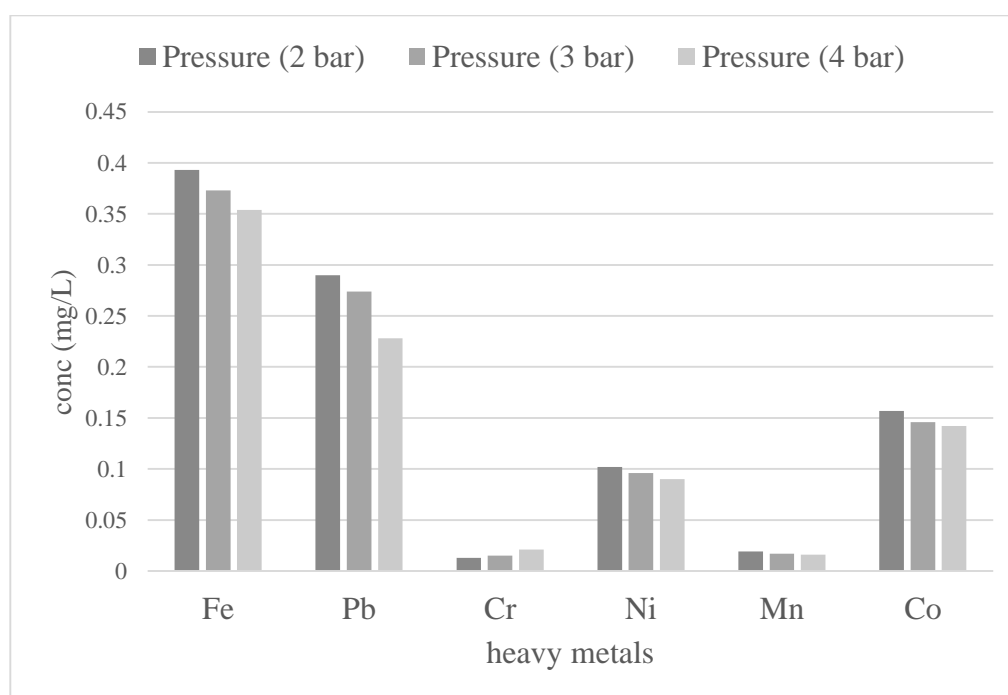
Fig:4 Removal of heavy metals through Nanofiltration process.

By applying one of the treatments such as nanofiltration are effective in removing mostly heavy metals from wastewater. Others treatment equipment may also be used. The result shown by nanofiltration can show that heavy metals can be removed.

V. Conclusions

Industrial wastewater concentration to tube well water is high and cross the allowable limit by WHO. The iron value is 6.72(mg/L) which is too high to 0.3(mg/L) assign by WHO. The value of lead is 0.393(mg/L) greater to 0.01(mg/L) by WHO. Chromium concentration is 0.537(mg/L) greater than 0.05(mg/L). The nickel is 0.121(mg/L) greater than 0.02(mg/L). manganese value is 0.125(mg/L) less than 0.5(mg/L) by WHO but greater than 0.05(mg/L) kept by USEPA. Results showed that Industrial wastewater irrigation changes soil quality, increase in heavy metals concentration in vegetables (Fe, Ni, Mn, Pb, Co and Cr). Industrial effluent which has highest concentration of heavy metals is unfit for vegetable growing. Uninterrupted uses of wastewater results to the enhancement of heavy metals in soil. The concentration of heavy metals in soil and vegetables cross the allowable limit. The use of any type of filtration outside each industry can removes it successfully so govt if apply strict rules for industries then it will reduce the hazards of wastewater.

VI. REFERENCES

[1]. Bigdeli M, Seilsepour M. Investigation of metals accumulation in some vegetables irrigated with waste water in Shahre Rey-Iran and toxicological implications. Am Eurasian J Agric Environ Sci. 2008;4(1):86-92.

[2]. Bharti R, Ajay S. Assessment of spatio-temporal changes in characteristics of industrial waste water in Dehradun region of Uttarakhand. Environ Conserv J. 2013;14(3):51-60.

[3]. Zhou Z-Y, Fan Y-P, WANG M-J. Heavy metal contamination in vegetables and their control in China. Food Rev Int. 2000;16(2):239-55.

[4]. Manzoor J, Sharma M, Wani KA. Heavy metals in vegetables and their impact on the nutrient quality of vegetables: A review. J Plant Nutr. 2018;41(13):1744-63.

[5]. Khan MJ, Jan MT, Farhatullah N, Khan MA, Perveen S, Alam S, et al. The effect of using waste water for tomato. Pak J Bot. 2011;43(2):1033-44.

[6]. Singh A, Sharma RK, Agrawal M, Marshall FM. Risk assessment of heavy metal toxicity through contaminated vegetables from waste water irrigated area of Varanasi, India. Trop Ecol. 2010;51(2):375-87.

[7]. Nasrullah RN, Bibi H, Iqbal M, Durrani MI. Pollution load in industrial effluent and ground water of Gadoon Amazai Industrial Estate (GAIE) Swabi, NWFP. Journal of agricultural and biological science. 2006;1(3):18-24.

[8]. Hossain MA, Uddin MK, Molla A, Afrad M, Rahman M, Rahman G. Impact of industrial effluents discharges on degradation of natural resources and threat to food security. The Agriculturists. 2010;8(2):80-7.

[9]. Chaney R. Crop and food chain effects of toxic elements in sludges and effluents. IN: RECYCLING MUNICIPAL SLUDGES AND EFFLUENTS ON LAND. 1973.

[10]. Kant R. Textile dyeing industry an environmental hazard. 2011.

[11]. Pandey G, Madhuri S. Heavy metals causing toxicity in animals and fishes. Research Journal of Animal, Veterinary and Fishery Sciences. 2014;2(2):17-

[12]. Roy S, Gupta S. Effect of wastewater irrigation on soil and some selected vegetables grown in Asansol, West Bengal. International Journal of Environmental Sciences. 2016;6(5):894-904.

[13]. Abdulla M, Chmielnicka J. New aspects on the distribution and metabolism of essential trace elements after dietary exposure to toxic metals. Biol Trace Elem Res. 1989;23(1):25-53.

[14]. Farooq M, Anwar F, Rashid U. Appraisal of heavy metal contents in different vegetables grown in the vicinity of an industrial area. Pakistan Journal of Botany. 2008;40(5):2099-106.

[15]. Jaishankar M, Tseten T, Anbalagan N, Mathew BB, Beeregowda KN. Toxicity, mechanism and health effects of some heavy metals. Interdisciplinary toxicology. 2014;7(2):60-[72].

[16]. Jan FA, Ishaq M, Khan S, Ihsanullah I, Ahmad I, Shakirullah M. A comparative study of human health risks via consumption of food crops grown on wastewater irrigated soil (Peshawar) and relatively clean water irrigated soil (lower Dir). J Hazard Mater. 2010;179(1-3):612-21.

[17]. Tariq M, Ali M, Shah Z. Characteristics of industrial effluents and their possible impacts on quality of underground water. Soil Environ. 2006;25(1):64-

[18]. Liu W-h, Zhao J-z, Ouyang Z-y, Söderlund L, Liu G-h. Impacts of sewage irrigation on heavy metal distribution and contamination in Beijing, China. Environ Int. 2005;31(6):805-12.

[19]. ul Islam E, Yang X-e, He Z-l, Mahmood Q. Assessing potential dietary toxicity of heavy metals in selected vegetables and food crops. Journal of Zhejiang University Science B. 2007;8(1):1-13.

[20]. Jamali M, Kazi T, Arain M, Afridi H, Jalbani N, Memon A. Heavy metal contents of vegetables grown in soil, irrigated with mixtures of wastewater and sewage sludge in Pakistan, using ultrasonic- assisted pseudo- digestion. Journal of Agronomy and Crop Science. 2007;193(3):218-28.

[21]. Marr K, Fyles H, Hendershot W. Trace metals in Montreal urban soils and the leaves of Taraxacum officinale. Can J Soil Sci. 1999;79(2):385-7.

[22]. Imran S, Bukhari L, Gul S. Water Quality Assessment Report: Mingora City District Swat Khyber Pakhtunkhwa 2018. Pakistan Council of Research in Water Resources (PCRWR). All rights reserved by PCRWR The authors encourage fair use of this material for non-commercial purposes with proper citation Authors: Saiqa Imran, Lubna Naheed Bukhari and Samar Gul, Pakistan Council of Research in Water Resources, Pakistan. 2018:40.

[23]. Sharma R, Agrawal M, Marshall F. Heavy metal contamination in vegetables grown in wastewater irrigated areas of Varanasi, India. Bull Environ Contam Toxicol. 2006;77(2):312-8.

[24]. Tasrina R, Rowshon A, Mustafizur A, Rafiqul I, Ali M. Heavy metals contamination in vegetables and its growing soil. J Environ Anal Chem. 2015;2(142):2.

[25]. Joint F, Additives WECoF, Organization WH. Toxicological evaluation of certain food additives and naturally occurring toxicants: World Health Organization; 1993.

[26]. Council NR. Review of EPA's Integrated Risk Information System (IRIS) Process. 2014.

[27]. Hassan N, Ahmad K. Intra-familial distribution of food in rural Bangladesh. Institute of Nutrition and Food Science, University of Dhaka, Bangladesh. Internet pages. Internet pages (http://www unu edu/unpress/food/8F064e/8F064E05 htm)(11/9/01). 2000.

[28]. Mahfooz Y, Yasar A, Sohail MT, Tabinda AB, Rasheed R, Irshad S, et al. Investigating the drinking and surface water quality and associated health risks in a semi-arid multi-industrial metropolis (Faisalabad), Pakistan. Environmental Science and Pollution Research. 2019;26(20):20853-65.

Technical Session 1-B (Google meet/Zoom)
MATERIAL ENGINEERING-2

Session Chair: **Dr. Muhammad Yasir Khan** (engryasir28@gmail.com)
Session Co-Chair: **Dr. Nehar Ullah**

Presenter	Paper Title
M. Sohail (USPCAS-E UET Peshawar)	Analysis of thermally conductive polymer-metal composite material
Engr. Raza A.A (Ameer Ahmad Raza) (UET Peshawar)	Production of White Cement by substituting Limestone with Waste Marble Powder
Tariq Aziz (Dept. of Civil Eng., UET Peshawar)	Experimental Investigation of Mechanical Properties of Cement Stabilized Low-Pressure Compressed Earth Blocks Masonry: An Approach towards the Low-Cost-Green-building Technology
Zahoor Ali (Dept. of Mech Eng., UET Peshawar)	Effects of cooling techniques on the secondary hardening behavior of 15crmnmov6 steel
Habib Ahmad (Dept. of Civil Eng., UET Peshawar)	To Assess the Effect of Industrial Waste on The Quality of Ground Water. A Case Study of Hayatabad Industrial Estate, Peshawar, Pakistan.

Analysis of Thermally Conductive Polymer Metal Composite Material

Muhammad Sohail [A], Khurshid Ahmad [A], Muhammad Hassan [A], Ihsan Ur Rahman [A], Fahad Ullah Zafar [A], Hassam Naeem [B]

[A] US-Pakistan Center for Advance Studies in Energy (USPCAS-E), University of Engineering and Technology Peshawar (UET), Pakistan
[B] *The EPSRC Centre-LiME, BCAST, Brunel University, Uxbridge UB8 3PH, UK*

Abstract- **In recent years, the design and development of packaging electronic devices have encountered a growing challenge as the power levels and the performance of the devices increases. As the size of such devices decrease, ensuring reliability in the operation of the devices is becoming a challenge. Thermal interface material offers significantly less thermal resistance and therefore avoids excessive heating of the interfaces. In this research, thermal interface materials were prepared by mixing polydimethylsiloxane (PDMS) with copper (Cu) and graphite (Gr) powder. Various samples including pure PDMS, PDMS-Cu, PDMS-Gr, and PDMS-Cu-Gr were prepared. The thermal conductivity, thermal diffusivity, volumetric heat capacity, and thermal effusivity were measured. The results showed that pure PDMS exhibited the lowest thermal conductivity of 0.20 $wm^{-1}k^{-1}$, while PDMS-Cu-Gr exhibited the highest thermal conductivity of 2.711 $wm^{-1}k^{-1}$. Similarly, PDMS-Cu-Gr and PDMS exhibited a thermal diffusivity of 1.43 mm^2/s and 0.26 mm^2/s respectively. The thermogravimetric analysis (TGA) showed that the PDMS-Cu-Gr composite can withstand a maximum operating temperature of about 280°C. The results suggest that PDMS-Cu-Gr composite has good potential of being used as thermal interface material.**

Keywords—Heat Transfer, Electronic Cooling, Thermal Interfaces, Thermal Conductivity, Thermal Resistance

I. INTRODUCTION

Thermal interface material (TIM) refers to a class of material that is often utilized at the interface of two or more components to improve the thermal coupling of electronic devices. A TIM is considered highly efficient especially in devices that dissipate heat such as heat sinks whose key role is to remove heat from electronic devices. For heat to be removed efficiently from electronic devices, the design of a TIM must ensure that the material used provides a better life cycle with enhanced reliability [1]. The non-planarity and surface roughness at the microscopic level of the surfaces of the heat-dissipating devices and the heat spreader is often associated with asperities occurring between the interfaces of the mating components. These astringencies act as inhibitors to the two joining surfaces thereby preventing them from providing good thermal contact owing to the ineffective thermal conductivity resulting from the air gaps between the mating pair of components [2].

Owing to the surface irregularities, the performance of electronic devices is limited. This is where the thermal interface materials come into play by providing an effective conductive path between the two mating components. As such, the TIMs provide an excellent material confirmation by eliminating the surface irregularities between the joining surfaces of the material through the action of high pressure imposed between the mating material surfaces thus yielding high thermal conductivity [3].

The thermal resistance of TIMs is also a major consideration. The effective thermal resistance is closely associated with the total resistance between the mating surfaces and the TIM as well as the thermal conductivity of the same. Equation 1 is employed in determining the effective thermal resistance [1].

$$R_{Effective} = \frac{BLT}{K_{TIM}.A} + R_{C_1} + R_{C_2} \qquad (1)$$

Where R effective is the effective thermal resistance,
BLT represents the bold line thickness
K_{TIM} designates the interface thermal conductivity
A represents the Area
R_{c1} and R_{c2} denote the contact resistance between the mating surfaces and the TIM.

Studies have determined that the effective thermal resistance shown to be minimized to limit the rate of heat dissipation when the device is in operation. This is done by reducing the value of BLT by employing a material with relatively high thermal conductivity. More also, by reduction of surface irregularities through the application of high pressure between the TIM and the mating materials can significantly reduce the surface resistance [2].

The main challenges in the development of thermal interface materials are related to the thermal management of electronic systems as reported in various studies [2, 4] For instance, the work of Kafil [5] identified that the degree of interconnectivity between the mating surfaces in electronic systems influences the performance of these devices, and with the recent growth in the production of electronic devices for industrial and domestic applications, thermal management is very essential. The authors reported that using TIMs energy consumption by electronic devices can be enhanced.

Auciello and Sumant [6] carried out a comprehensive study on the application of ultra-nanocrystalline diamond films in multifunctional devices. The authors reported that if the heat transfer through radiation between the mating surfaces is neglected, the heat flux at the interface often takes place in two different conduction paths. The conduction paths involve solid-solid at the contact points and solid-air conduction within the non-contacting points. In the later conducting path, the air is a poor conductor of heat reduced the efficiency of heat transfer. The decrease in heat transfer is attributed to the contact resistance. To overcome temperature build-up at the junction, contact thermal resistance should be reduced by replacing the air gap using a material with higher thermal conductivity such as TIMs. The study concluded that the use of thermal interface materials enhances the conductivity and effective heat transfer.

The work of Hopkins [7] investigated the thermal transport across solid interfaces with nanoscale imperfections such as surface roughness, dislocations, and their effects on thermal boundary conductivity. The researcher employed the concept of time-domain thermal reflectance to investigate the factors that influence the junction's thermal resistance. The study reported that conductance is affected by surface roughness, disorder, joining process as well as dislocations. As such, the existence of surface irregularities such as roughness limits the performance of the thermal junction of the two joining components in electronic components.

Thermal interface material addresses the challenges associated with the contact area between the mating surfaces. As such, they often replace the air voids induced by surface roughness. In this sense, TIMs often deform under assembling pressure to fill up the voids thereby improving the conductivity between the mating material components. Their ability to deform under pressure provides an engineering trade-off. This desirable characteristic of TIMs is attributed to their low shear stress which allows them to easily change shape to conform to the shape of the contacting surfaces [8].

Recent improvements on the TIMs include the development of deformable TIMs through the reduction of the thickness of the bond line. This reduction is associated with increased thermal conductivity and deformability of TIMs. Several authors have suggested that the largest percentage of the research done aims at improving the thermal conductivity of thermal interface materials by using more advanced filler material to the existing matrix which is polymer-based [1] The work of Hamasaiid et al [9] investigated the effects of surface roughness on the thermal interface made of aluminum blocks bonded with silicon oil and grease using a model based on the common flux tube. The study reported that the contact thermal resistance is affected by the surface roughness, applied pressure capillary pressure, and air backpressure. From their comprehensive mechanical investigation, the researchers pointed out that the liquid surface energy, contact surface angle, and the behavior of trapped gas are highly dependent on the wetting, applied pressure, surface topology, temperature, and the thermal conductivity of the material. From the results, the study concluded that the heat transfer from the flux tube to the heat sink was lower for TIMs.

Notably, the material properties are essential when selecting a thermal interface material. Thermal conductivity comes out as one of the most important considerations, but it does not show the actual performance of the material to transfer heat energy in real applications [10]. Therefore, conditions should be considered when selecting a thermal interface material. A thin bond line of thickness is desired to attain very low thermal impedance [11].

In commercial applications, the characterization of thermal interface material is done as per ASTM D5470

[12]. This is a standard method that dictates the apparatus used to determine the BLT and thermal impedance of TIMs in a regulated pressure condition. Further, the work of Lee [13] depicted that adhesive strength of thermal interface material influences vibrations and rework ability hence it should be considered over the whole range of temperature in thermal interface material selection. A TIM with high adhesive strength has been shown to induce difficulties not only in reworking but also it makes it hard to cut through a TIM with small bold line thickness [14].

This work focuses on the development and fabrication of a polymer-based TIM using Poly dimethyl siloxane (PDMS) polymer, copper (Cu), and graphite (Gr) fillers. The study aims to achieve a thermal interface material with increased thermal conductivity and reduced thermal contact resistance.

II. METHODOLOGY

Four samples were prepared comprising PDMS, PDMS-Cu, PDMS-Gr, and PDMS-Cu-Gr. PDMS was first mixed with curing agent and mixed for 10 minutes at a magnetic stirrer at 330rpm. The resulting solution was cured for 24hours. Similarly, PDMS-Cu, PDMS-Gr, and PDMS-Cu-Gr were mixed in ratios 1:4, 1:1, and 3:4:3 respectively with 1g of curing agent in each. The samples were then poured into 4×3 mm rectangular molds with uniform thickness and allowed to cure for 24hours at room temperature after which they were then cured at 105 ℃ in a hot plate for 2 hours and allowed to cool for the next 24hours at room temperature. Finally, the cured samples were then extracted from the mold. Figure 1 illustrates the process flow diagram of the sample preparation.
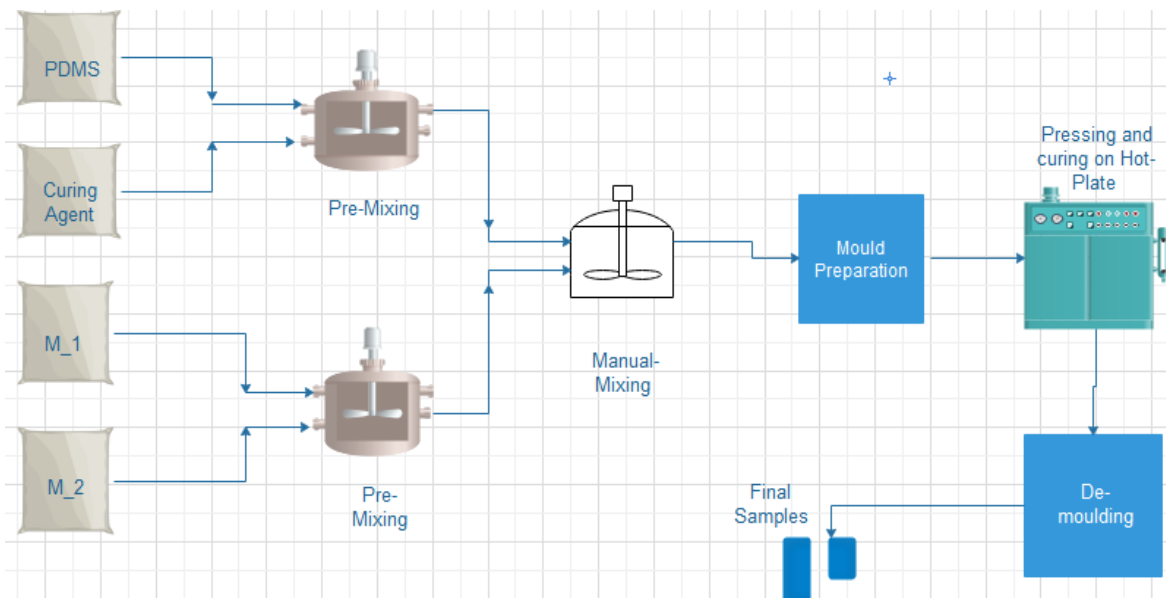
Figure 1: The process flow diagram of the sample preparation.

III. CHARACTERIZATION

A. HOT DISK TPS 2500 S APPROACH

This project employed Hot Disk TPS 2500S for transient measurements of thermal conductivity of the sample composites prepared. Kapton sensors was clamped between an insulator and the samples. The thermal-physical properties constituting the heating power and time were measured and recorded as illustrated in table 1.

Table 1: The thermal-physical properties constituting the heating power and time

Parameters	PDMS	PDMS-Cu	PDMS-Gr	PDMS-Cu-Gr
Heating Power (mW)	3 mW	2.5 mW	3 mW	15 mW
Time (sec)	5 sec	5 sec	2 sec	3 sec

B. THERMOGRAVIMETRIC ANALYSIS (TGA) APPROACH

This technique was used to analyze the material changes in weight with time and specified temperature to give a clear idea of the thermal stability of the developed TIM composites. This test was performed in the material characterization laboratory USPAC-E UET Peshawar. During the analysis, 6mg of each sample was heated at a constant rate of 20 ^{0}C/min to a maximum temperature of 600 ºC.

IV. RESULTS AND DISCUSSION

A. Thermal Analysis

From the Hot disk TPS 2500 S results, the thermal conductivity of the samples was determined. To start with, the PDMS sample exhibited a thermal conductivity of 0.20 $wm^{-1}k^{-1}$. The PDMS-Cu recorded a thermal conductivity of 0.62 $wm^{-1}k^{-1}$. While PDMS-Gr and PDMS-Cu-Gr exhibited a thermal conductivity of 2.41 $wm^{-1}k^{-1}$ and 2.71 $wm^{-1}k^{-1}$ respectively. It was determined that copper and graphite filler improved the thermal conductivity of PDMS. As such, it was shown that the thermal conductivity of PDMS increased from 0.20 $wm^{-1}k^{-1}$ to 2.71 $wm^{-1}k^{-1}$ which was about 13.12 times the initial thermal conductivity. Figure 2 illustrates the thermal conductivity of the various samples.
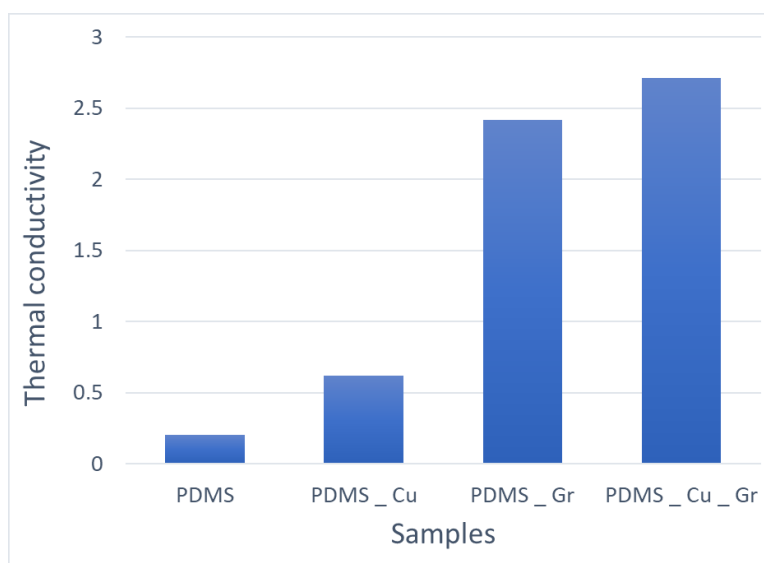
Figure 2: Thermal conductivity of the samples

The thermal diffusivity of the samples was also obtained from the Disk TPS 2500 S. Pure PDMS exhibited a thermal diffusivity of 0.26 mm^2/s while PDMS-Cu, PDMS-Gr, and PDMS-Cu-Gr recorded thermal diffusivity of 0.13, 1.02, and 1.43 mm^2/s respectively. Despite PDMS-Cu recording high thermal diffusivity as compared to PDMS, the thermal diffusively of PDMS is higher than that of PDMS-Cu. The controversial results were attributed to the fact that PSMS-Cu has high volumetric heat capacity. Figure 3 illustrates the thermal diffusivity of the four samples.
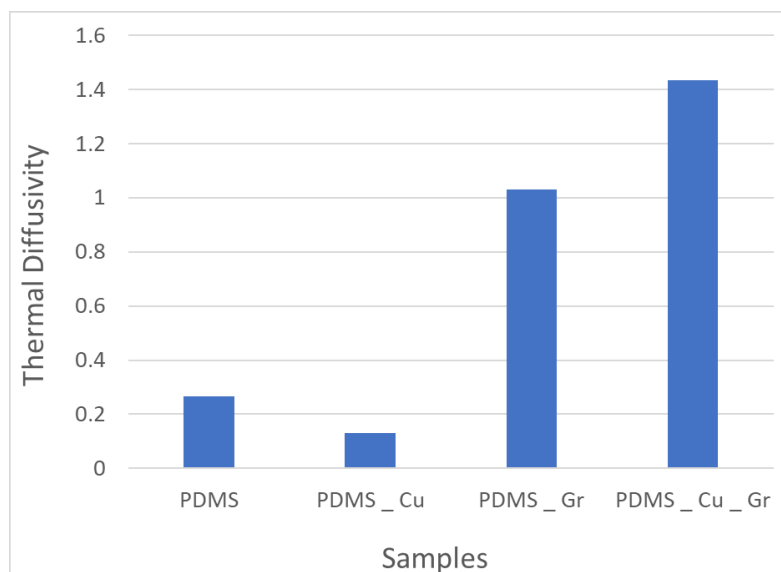
Figure 3: The thermal diffusivity of the samples

The thermal effusivity of the samples was obtained from the Hot Disk TPS 2500 S analysis. PDMS recorded a thermal effusivity of 398.8 $ws^{1/2}/m^2k$ while PDMS-Cu, PDMS-Gr, and PDMS-Cu-Gr exhibited a thermal effusivity of 1670, 2382, 2263 $ws^{1/2}/m^2k$ respectively. It was observed that despite the PDMS-Cu-Gr having high thermal conductivity, the thermal effusivity is lower. This owes to the fact that thermal effusivity is dependent on the volumetric heat capacity. Figure 4 illustrates the thermal effusivity of the four samples.
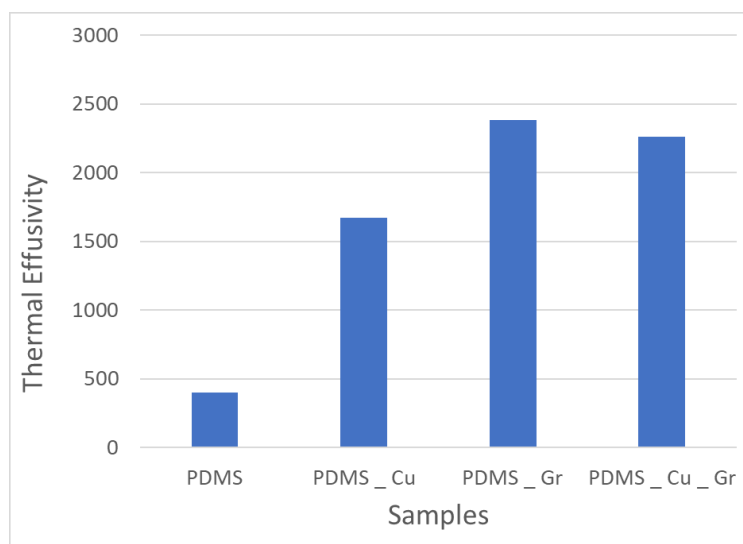
Figure 4: The thermal effusivity of the samples

The volumetric heat capacity for pure PDMS was determined as 0.77 MJ/m^3k while PDMS-Cu, PDMS-Gr, and PDMS-Cu-Gr exhibited a volumetric heat capacity of 4.49, 2.35, and 1.89 MJ/m^3k respectively. It was identified that PDMS-Cu showed the highest volumetric heat capacity as compared to the other samples. It was deduced that the high volumetric heat capacity of PDMS-Cu could be attributed to the high density of the copper filler particles. Figure 6 illustrates the volumetric heat capacity of the four samples.
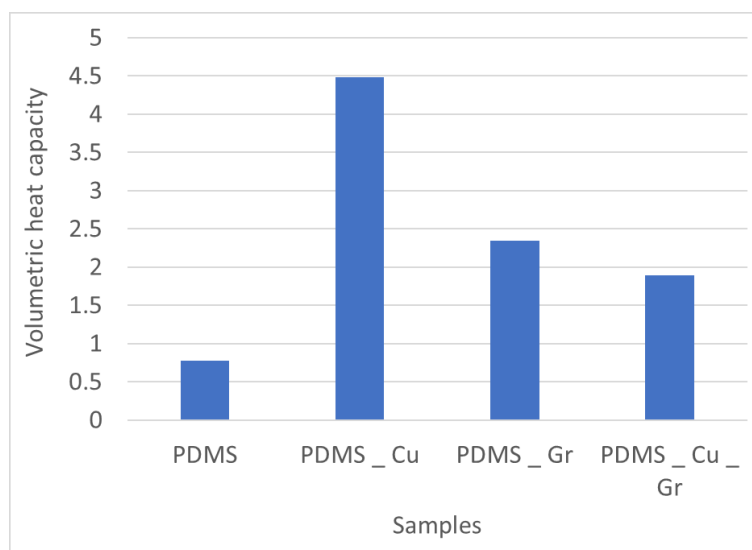
Figure 5: The volumetric heat capacity of the samples.

B. *Thermogravimetric analysis*

To test for the thermal stability of the fabricated PDMS samples, The TGA analysis showed that PDMS-Cu-Gr exhibited high thermal stability for up to 280 $^{\circ}$C which was identified as the maximum operational temperature beyond which the sample would undergo degradation. It was observed that the mean weight loss occurred at the initial stages of the test owing to the evaporation of the moisture content of the PDMS-Cu-Gr sample. Figure 6 illustrates the TGA results of the PDMS-Cu-Gr sample.
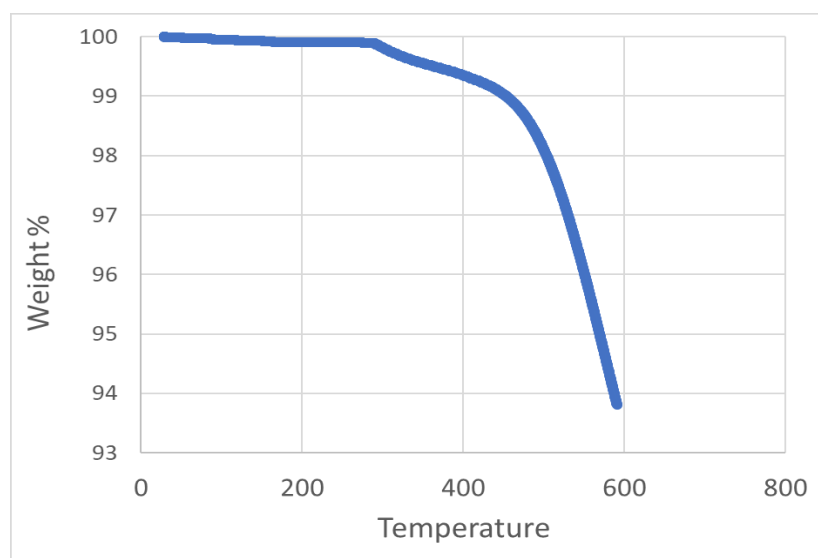
Figure 6: The TGA results for the PDMS-Cu-Gr sample.

V. CONCLUSIONS

To sum up, this research reports the analysis of four polymer-based composites including PDMS, PDMS-Cu, PDMS-Gr, and PDMS-Cu-Gr. The Hot Disk TPS 2500 S technique was utilized to evaluate the thermal conductivity, thermal diffusivity, thermal effusivity, and volumetric heat capacity. From this analysis, it was determined that Pure PDMS exhibited the lowest thermal conductivity of 0.20 wm^{-1}k^{-1}, while PDMS-Cu-Gr exhibited the highest thermal conductivity of 2.711 wm^{-1}k^{-1}. A similar trend was observed from the thermal diffusivity results whereby Pure PDMS recorded the lowest value of 0.26 mm^2/s while PDMS-Cu-Gr had the highest thermal diffusivity of 1.43 mm^2/s. However, the thermal effusivity results showed low values for PDMS recording 398.8 ws$^{1/2}$/m^{2}k while the PDMS-Gr exhibited the highest value of 2382 ws$^{1/2}$/m^{2}k. This was attributed to its low volumetric heat capacity since the thermal diffusivity is a ratio of thermal conductivity and volumetric heat capacity. From the volumetric heat capacity results, PDMS-Cu

exhibited the highest value of 4.48 MJ/m^{3}k while pure PDMS recorded the lowest value of 0.77 MJ/m^{3}k. The high volumetric heat capacity of PDMS-Cu was determined to be a result of the high density of copper. The study concluded that the thermal conductivity of the fabricated polymer-based TIM was improved from 0.20 wm^{-1}k^{-1} to 2.711 wm^{-1}k^{-1} with a 92% increment. The TGA results showed that PDMS-Cu-Gr exhibited excellent thermal stability with a maximum service temperature of 280 ^{o}C. Based on various analyses performed in this research it was concluded that polydimethylsiloxane and the hybrid filler (Cu-Gr) composite is the best option for thermal management as a thermal interface material.

VI. REFERENCES

1. Prasher, R.S., *Dependence of thermal conductivity and mechanical rigidity of particle-laden polymeric thermal interface material on particle volume fraction.* J. Electron. Packag., 2003. **125**(3): p. 386-391.
2. Sarvar, F., D.C. Whalley, and P.P. Conway. *Thermal interface materials-A review of the state of the art.* in *2006 1st Electronic Systemintegration Technology Conference.* 2006. IEEE.
3. Xu, J., *Silver nanowire array-polymer composite as thermal interface material.* Journal of Applied Physics, 2009. **106**(12): p. 124310.
4. Hansson, J., *Novel nanostructured thermal interface materials: a review.* International Materials Reviews, 2018. **63**(1): p. 22-45.
5. Razeeb, K.M., *Present and future thermal interface materials for electronic devices.* International Materials Reviews, 2018. **63**(1): p. 1-21.
6. Auciello, O. and A.V. Sumant, *Status review of the science and technology of ultrananocrystalline diamond (UNCD™) films and application to multifunctional devices.* Diamond and related materials, 2010. **19**(7-9): p. 699-718.
7. Hopkins, P.E., *Thermal transport across solid interfaces with nanoscale imperfections: effects of roughness, disorder, dislocations, and bonding on thermal boundary conductance.* International Scholarly Research Notices, 2013. **2013**.
8. Lin, Y., C.Y. Hui, and H. Conway, *A detailed elastic analysis of the flat punch (tack) test for pressure-sensitive adhesives.* Journal of Polymer Science Part B: Polymer Physics, 2000. **38**(21): p. 2769-2784.
9. Hamasaiid, A., *A predictive model for the thermal contact resistance at liquid–solid interfaces: analytical developments and validation.* International journal of thermal sciences, 2011. **50**(8): p. 1445-1459.
10. Cola, B.A., *Photoacoustic characterization of carbon nanotube array thermal interfaces.* Journal of applied physics, 2007. **101**(5): p. 054313.
11. Bejan, A. and A.D. Kraus, *Heat transfer handbook.* Vol. 1. 2003: John Wiley & Sons.
12. Grujicic, M., C. Zhao, and E. Dusel, *The effect of thermal contact resistance on heat management in the electronic packaging.* Applied Surface Science, 2005. **246**(1-3): p. 290-302.
13. Lee, H.J., *THERMAL DIFFUSIVITY IN LAYERED AND DISPERSED COMPOSITES.* 1975.
14. O'Keefe, M. and K. Bennion. *A comparison of hybrid electric vehicle power electronics cooling options.* in *2007 IEEE Vehicle Power and Propulsion Conference.* 2007. IEEE.

Production of White Cement by substituting Limestone with Waste Marble Powder

Ameer Ahmad Raza [A] and Muhammad Imran Ahmad [B]

[A, B]*University of Engineering and Technology Peshawar.*

Abstract- **The main purpose of this research is to investigate the possibility of replacing white limestone with waste marble powder for the production of white cement. Waste marble powder contains up to 95% of CaCO3 and white color of waste, produced around Peshawar area, generates a positive approach for its application in white cement production. For this purpose, experiments carried out by replacing 25%, 50%, 75% and 100% of white limestone with waste marble powder. Initial results shows that white limestone can be completely replaced with waste marble power with significant reduction in the power consumption per ton of cement produced without compromising the quality of final product. The possibility of utilizing waste marble powder will sustain the extraction of white limestone.**

Keywords— **Waste marble powder, white cement, sustainable production, energy effectiveness.**

I. INTRODUCTION

God has gifted Pakistan with large reserves of Marble and Granite. It is estimated to have about 300 billion tons of Marble and granite reserves in Pakistan of which about two third are located in KPK province. [1] Apart from the huge reserves, just the KP province has about 30 different types of marble and granite which has made it an attractive sector not just for the local businessman but the foreigners also shown keen interest in the industry. [2]

Pakistan has access to high quality marble reserves in KPK, FATA and Baluchistan but lacking the technology for its effective extraction, the law and order situation, and the energy crises in last few years resists the Marble industry from its growth. The development of Pakistan Stone and Development Corporation (PASDEC) has given strength to the marble industry in Pakistan especially the availability of mining machinery because it didn't have just reduced the extraction duration but reduced the marble waste generated by the traditional mining techniques. According to Alyamac, 30% of the total marble extracted is wasted during the quarrying by traditional means. [3]

The increased marble demand has created opportunity for the investors and skilled workers and over 2,000 marble processing units are just in operational in Peshawar district of KPK province. But on the other hand the handling of the waste generated during the processing of marble is problematic. The waste so generated is simply dumped by the processing units or disposed of in water streams which is polluting the environment in different ways.

On the other hand, the fast growing construction industry has increased the demand of cement and other construction material. Similarly, the demand of white cement has also increased but we have unfortunately just 2 white cement production units in Pakistan which is just because of the unavailability of high purity white limestone and we used to import white cement specially to cover up the need in the south of country. The marble processing waste is shown to be utilized by different studies including the utilization in the production of concrete, in the brick making industry, in the detergent industry and in the cement industry. Manpreet and his team has studied the partial replacement of cement with marble waste slurry in the concrete and concluded that the mechanical properties of the concrete has enhanced upto 15% replacement of the cement with waste marble slurry. [4]

On the other hand some Egyptians have studied the addition of waste marble powder in cement production during the finish grinding of clinker with gypsum. They concluded that marble waste powder can be added upto 15% without affecting the properties of cement although this ratio is quite questionable because the addition of marble dust can enhance the strength of concrete because of the its filler effect i.e. the fine particles of marble powder filled the pores of concrete and provides additional strength to the concrete but the addition of up to 15% marble powder may increase the LOI of cement and increases the expansion of

the cement and concrete as well. [5]

The purpose of this study is to investigate the possibility of replacing white limestone with waste marble powder generating during the processing of marble i.e. cutting and polishing in the marble processing unit for the production of white cement. Physical and chemical properties of the white cement produced by varying the percentage of white limestone with waste marble powder. Specimen were produced by replacing white limestone partially and completely with waste marble powder and result compared with the required standards and with the sample produced by pure white limestone in order to judge the difference due to the experimental process.

II. METHODOLOGY

For the experimental program, initially the samples were collected as per the availability from different locations of the province. The waste marble powder has taken from 3 different processing sites in Peshawar (Located at Warsak Road in Peshawar) The marble samples are first prepared and analyzed in order to check the acceptability of this waste for white cement and it has been observed that the waste marble powder has high percentage of CaCO3 upto 97%. The particle size analysis of the waste marble powder conducted and the results were satisfactory. White limestone was taken from Kohat Cement quarry, Silica sand, flint clay and white gypsum are taken from stocks of Kohat cement and analyzed each for samples preparation as per required composition for final calcination and clinker production.

Samples taken are more than 50 mm in size. Samples are then crushed and grinded in size reduction units i.e. roller crusher and rod mill in mining department at University of Engineering and Technology, Peshawar. Limestone or marble powder, Silica sand and flint clay are than mixed in rod mill in specified concentration so as to achieve proper mixing and fine grinding to prepare the meal for the burning stage.

Figure 1 Double roller crusher for sample crushing at Department of Mining engineering

Figure 2 Rod mill for sample preparation and finish grinding at Department of Mining Engineering, UET Peshawar

The sample prepared by mixing and grinding in the rod mill is then processed in lab scale rotary kiln at temperature of about $1600\,^{0}C$ for about an hour. The clinker so produced is then water sprayed the moment it dumbed from the rotary kiln in order to quench the clinker else the exposure to air promotes greenish color. Clinker is then grinded with 5% gypsum and 10% marble powder as a PI in rod mill.

Figure 3 Lab scale rotary kiln utilized for the production of cement clinker.

III. RESULTS AND DISCUSSION

The product samples are then analyzed to compare the physical and chemical properties of the cement. Samples are first analyzed for their chemical composition using XRF, available in Kohat Cement Company Limited. The chemical analysis of the samples are given below and it is found that there is slight variation in the results which is actually because of the slight variation in the raw material samples prepared for processing. The analysis however shows that there is no such difference in the results which gives an opportunity for the waste marble powder to be used completely as a replacement of white limestone however the physical properties including the strength could be decisive factor.

Table 1 Chemical Properties of the cement produced by varying ratio of limestone by waste marble powder

Component	100% LS	25% WMP	50% WMP	75% WMP	100% WMP
Si_2O	22.26	21.97	21.48	21.28	21.08
Al_2O_3	4.44	4.46	4.43	4.54	4.40
Fe_2O_3	0.25	0.28	0.31	0.32	0.35
CaO	62.38	62.96	63.32	63.63	63.81
MgO	1.04	1.09	1.10	1.12	1.16
SO_3	2.60	2.55	2.51	2.54	2.41
K_2O	0.50	0.55	0.54	0.57	0.54
Na_2O	0.12	0.12	0.11	0.11	0.11

After the successful chemical analysis of the cement samples produced by different compositions of the raw materials, the cement pastes are then analyzed in the physical laboratory of the Kohat Cement Company Limited. The samples are analyzed as per ASTM standards. The compressive strengths of the pastes are found satisfactory. The setting times of cement pastes measured by Vicat process is however found less although it is in the range of standards but could be adjusted by adjusting the ratio of gypsum during grinding. Soundness of cement pastes (Le-Chatlier) found little higher, the reason of higher soundness is possibly the processing mechanism of the experiment by lab scale rotary kiln which could be improved in further study

.

Table 2 Physical Properties of cement produced by varying ratio of limestone by waste marble powder.

	100% LS	**25% WMP**	**50% WMP**	**75% WMP**	**100% WMP**
Compressive strength, 3 day	17	18	18	18	19
Compressive strength, 7 day	23	24	24	26	27
Initial setting time, mins	100	110	115	120	118
Final setting time, mins	190	185	183	185	180
Soundness, mm	4.0	5.2	5.1	5.7	6.7

IV. CONCLUSION

In this research, the replacement of white limestone with waste marble powder for the production of white cement was studied and followings are the conclusions made from the study.

1. Waste marble powder from marble processing sites could be used for the production of white cement clinker or even gray cement clinker as per standards of ASTM.
2. Replacement of waste marble powder up to 100% in the feed results in no reduction of the cement strength and degree of whiteness.
3. The fineness of waste marble powder favors the reduction of 5% energy requirement per ton of cement for 100% replacement of waste marble powder.
4. Replacement of 100% waste marble powder eliminates the mining cost as compare to white limestone.
5. Waste marble powder can be use as additive in grinding with clinker and gypsum.

V. REFERENCES

[1] A.H. Kazmi and S.G. Abbas (2001) "Metallogeny and Mineral Deposits of Pakistan". *Orient Petroleum Ltd,* **Vol 2**.

[2] M.A. Pathan, R.A. Lashari, M. Maira, J.A. Pathan (2019) "Experimental study on the engineering properties of marble waste powder from Hyderabad marble market Sindh Pakistan for making concrete including recycled coarse aggregates". *Saudi Journel of Civil Engineering*, 3(3), 51-58.

[3] K.E.Alyamaç and R.İnce (2009). A preliminary concrete mix design for SCC with marble powders. *Construction and Building Materials*, 23, 1201–1210

[4] M. Singh, A. Srivastava and D. Bhunia (2016) "An investigation on effect of partial replacement of cement by waste marble slurry" *Construction and Building Materials,* 134, 471-488

[5] A.A. Aliabdo, M.A. Elmoaty, E.M. Auda (2014) "Re-use of waste marble dust in the production of cement and concrete" *Construction and Building Materials,* 50, 28-41

Experimental Investigation of Compressive Strength and Modulus of Elasticity of Cement Stabilized low-pressure-Compressed Earth Blocks Masonry. An approach towards the low cost-green building technology

Tariq Aziz [A], Mohammad Ashraf [B], Mohammad Adil [C], Khalid Khan [D] & Muhammad Ajmal [E]

[A] Department of Civil Engineering, University of Engineering and Technology, Peshawar Pakistan. Email: engrtareqazez@gmail.com

[B] Department of Civil Engineering, University of Engineering and Technology, Peshawar, Pakistan

[C] Department of Civil Engineering, University of Engineering and Technology, Peshawar, Pakistan

[D] US-Pakistan Centre for advanced studies in energy (US-PCASE), University of Engineering and Technology, Peshawar, Pakistan

[E] Department of Agricultural Engineering, University of Engineering and Technology, Peshawar, Pakistan

Abstract- **Earth is a well-known old construction material, which is both eco-friendly and energy-efficient. In comparison to the traditional construction materials like cement, steel, etc. which are not only energy-demanding, yet deteriorate the environment too. There is a significant need for alternative green building technologies. In the presented work an attempt is made to achieve this goal. Herein, the compressed earth blocks masonry is investigated for its compressive strength, as the compressive strength is the basic parameter that depicts the overall strength of the masonry. For this purpose, earth-blocks are made up of cement, sand, and soil in a ratio of 1:1:10. The mixture is compressed in a manual press machine having a very low compaction pressure of 0.123 MPa compared to the advanced available machines having compaction pressure greater than 2MPa. Therefore the blocks produced here are called Low-Pressure Cement-Stabilized Compressed Earth Blocks titled as SCEBs. The SCEBs prisms are then tested as per ASTM standards in Compression. The comparison of the results is brought out with the conventional burnt brick. In comparison, we found SCEB and its masonry very fragile. Yet its construction is possible following the recommendations of the presented work**

Keywords— **Compressed Earth Block, Green building Technology, Low-Pressure, Masonry, Mechanical Properties**

I. INTRODUCTION

Earth is used for a long for the construction of buildings in different forms like cob, adobe, rammed earth walls, and wattle and daub construction. It is cheap, easily available, and eco-friendly. It is used for 10,000 years and provides the basic shelter needs to the people [1]. On the other hand, the conventional construction material like fired clay bricks, cement, and steel is not only costly but are highly energy demanding and also deteriorates the environment [2].

Construction material costs almost 60% of the total building cost, and the cost of building from the earth is almost negligible comparatively [3]. The increase in the slum is one of the reasons for unaffordable housings. Besides, these conventional materials contribute to the degradation of the natural environment severely. Only cement emits 2070 tons of carbon dioxide per year globally which enhances global warming and climate changes [4]. Besides, they require a high amount of energy in production. The energy consumption during the production of fired bricks ranges from 0.54 to 3.14 Mega-joule of specific energy per kilogram of bricks [5]. It is also the source of solid waste generation. The production of ash and 20% of the sub-standard bricks is also a great challenge [6].

The aforementioned are some of the serious problems that have been aroused due to the use of traditional construction materials. An alternative approach is mandatory to be established, like using earth as a construction material, to cope with all these problems. As the earth is cheap and easily available, it drew

the attention of the people as a construction material and is being used for 1000 years [1].

But the earth as a construction material has several problems. The major ones are its low strength and less durability to wind and rain [7, 8]. That is why earth construction is left only for the people who cannot afford traditional construction materials. If solutions for these problems of earthen constructions are sought out, the people will be convinced and will adopt it. Thus it will prevent environmental degradation and will enable the lower economy class community to build low-cost houses. Moreover, it will stop the mass production of solid wastes from conventional building materials as the earth is degradable and recyclable and have low embodied energy [9].

Such efforts have been started since 1700BC. In 1950 a manual press machine was designed by an American engineer Raul Ramirez. He has given the idea of compressing the soil in the machine with the addition of optimum moisture contents, to give it a specific shape and density. These are termed "compressed earth blocks". Later on, the practice of addition of stabilizers like fly ash, cement, lime, etc. is also adopted. The bricks were then named Stabilized Compressed Earth Blocks [10, 11].

An attempt is made in this work towards the Sustainable-Green-Housing-Technology. A Manual press machine was used to construct the stabilized Compressed Earth Blocks (SCEBs). The basic mechanical properties were determined experimentally in the lab of the University of Engineering and Technology Peshawar. The properties were then compared with the traditional fired brick.

The SCEBs and its masonry are investigated by many researchers for its mechanical and physical properties with the addition of stabilizers and different natural and synthetic fibers. In all cases, compaction pressure higher than 2MPa has been used. In our case, we assumed that a man can apply vertical load on the lever equal to its weight. So for an average man of 55 kg, the compaction pressure is 0.123MPa. This compaction pressure is considerably lower and the blocks produced by it are therefore termed as low-pressure-stabilized compressed earth blocks. The compressive strength of SCEBs and its masonry at such a low production pressure is not reported in the literature so far. This research aims at enhancement of confidence about the SCEBs masonry building construction from blocks made at low compaction pressure (by the manual press), which will help the lower economy class community and will cast a positive impact on the environment.

II. METHODOLOGY

A. Manual Press Machine

A manual press machine is made locally shown in Figure 1. The lever arm is 168 cm, suitable for manual operation. The mold size is kept the same as the size of traditional burnt brick, i.e. 23 cm × 10 cm × 13.5 cm. The height of the mold is kept double of the required thickness of the SCEB.

(a)   3D View   (b)   Side View
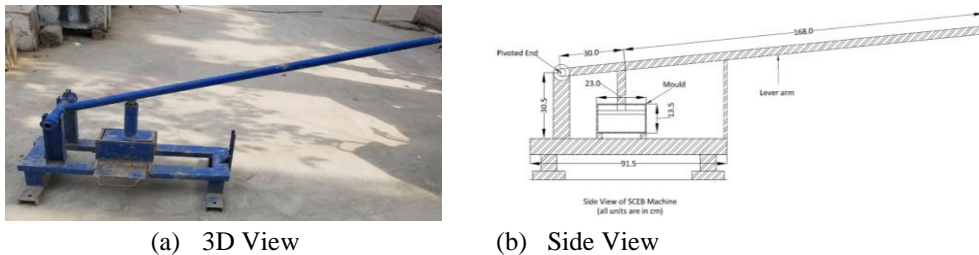
Figure 1. Manual Press Machine

B. Soil

Soil is selected from the locality of Peshawar. Sieve analysis and hydrometer analysis are carried out for particle size distribution as per ASTM-D6913 and ASTM-D7928-17 respectively. Liquid limit and plastic limit are determined as per ASTM-4318-00. The specific gravity of soil particles is calculated following ASTM-D854-14.

a) Hydrometer Analysis	b) Liquid Limit Test	c) Plastic Limit Test	d) Sieve Set
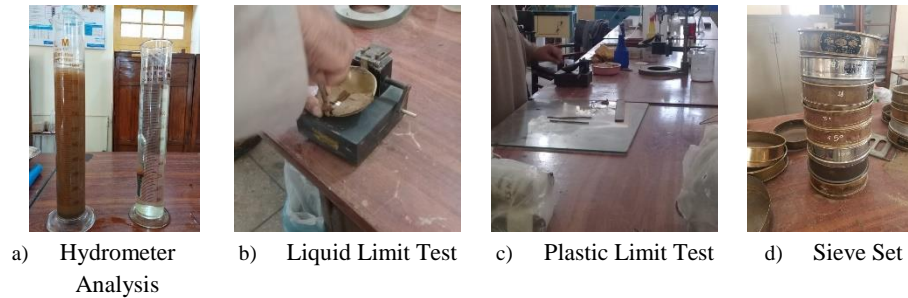
Fig. 2. Soil Tests

C. SCEB

The SCEBs are formed from the mixture of Cement, sand, and soil with a 1:1:10 ratio respectively. First, the soil is passed through a sieve having common size used conventionally to remove any debris and organic materials. Then 10% sand and 10% cement by weight are added and is mixed thoroughly. After complete mixing, water is added to dampen the soil and is mixed again to obtain a uniform mixture.

The mold of the press machine is then filled with the mixture. The compaction pressure is used to densify the soil to half of the mold, i.e. 6 cm, which is the required thickness of SCEB in our case. These blocks are placed in the shade to avoid direct sunlight, for 28 days. On the 28th day, they are tested in compression as per ASTM-C67-03a.

Figure 3. Stabilized Compressed Earth Blocks (SCEBs)

D. SCEB Prisms

Four prisms for compression test to evaluate compressive strength and modulus of elasticity are constructed in English bond. The width of the prism is equal to a full and a three-quarter brick which is almost 37.50 cm. The height of the prism is equal to 45.72 cm with a thickness equal to one full brick i.e. 22cm. there are kept in the shade for 28 days. They are constructed above a wooden board so that it could be easily shifted to the lab for the test. Jute fiber clothes are used to cover the specimen. They are used to be soaked in the water twice a day. After 28 days the prisms were tested in compression as per ASTM-C314-03a.

For the test, the specimen is shifted to the Universal Testing Machine (UTM). The specimen is kept under the center of the upper cylindrical head of the UTM. The wooden board is not removed under the specimen for not to damage it. The sand was spread over the top of the specimen and a steel plate is kept above it to distribute the load uniformly. Tow Linear Variable Differential Transducers (LVDTs) are installed.

One at the face of the specimen in the second row from the top and another was used to record the stroke of the UTM for cross-checking. The gauge length is noted. The load is then applied slowly to the specimen until it reached the maximum capacity. At a 20% drop in the capacity, the test was stopped. The test arrangements are shown in the figure.

The load and deformations are recorded. The load is divided on the cross-sectional area of the specimen to calculate the compressive stress. The deformations are divided on the gauge length to calculate the strain. Both are plotted on a graph to get the modulus of elasticity and compressive strength of the SCEB prisms.

E. Mortar

Three 50mm mortar cubes are taken from each batch of the mortar of the prisms. The composition of mortar is also the same as the SCEB, i.e. Cement, sand, and soil with the ratio of 1:1:10 termed as CSS mortar. A total of 12 samples are collected. They are kept in the same environment with parental prisms. They are tested on the same day as the compression test of the parental prisms as per ASTM-C109.

III. RESULTS AND DISCUSSION

A. Properties of Soil

The particle size distribution curve is given in Figure 4. The major portion of the curve is outside of the range recommended by [8] for manual compaction. The major portion of the soil is uniformly graded. 96.68% of the soil is silt and the remaining 2.32% is sand. No gravels and clay particles are found. We have added 10% sand to reduce the uniformity. Whereas the Plasticity Index is given in TABLE II is 12.12, within the range recommended by [8] for manual compaction.
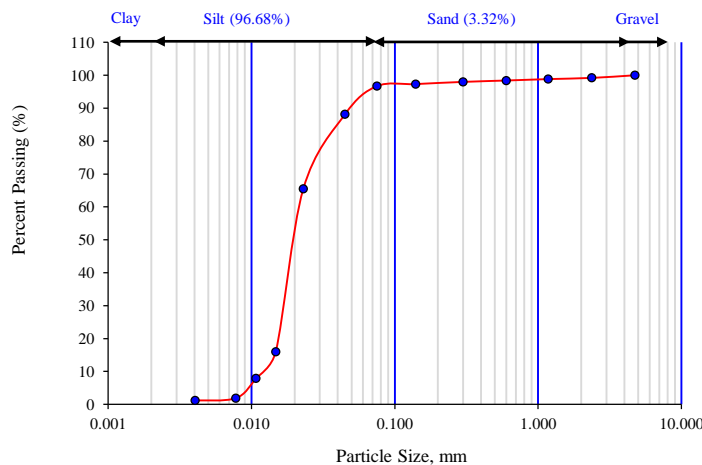
Figure 4. Particle Size Distribution Curve

TABLE II: Atterberg's Limits of Soil

Liquid Limit	35.80 %
Plastic Limit	23.43 %
Plasticity Index	12.12

B. *Compressive Strength of SCEB*

The mean compressive strength of the 12 SCEB samples is 3.084MPa. Data of seven researchers are presented in TABLE III, for burnt brick. The mean compressive strength of the seven values is 15.59 MPa. The percentage of the SCEB strength to the burnt brick is 19.78.

Figure 5. SCEB Compression test in Universal Testing Machine

TABLE III: Comparison of SCEB Compressive Strength with Burnt Brick

S.No	28-days Compressive Strength (MPa)	Reference
1	14.40	[12]
2	16.20	[13]
3	11.12	[14]
4	12.43	[15]
5	17.00	[16]
6	16.00	[17]
7	22.00	[18]
Mean	15.59	
Standard Deviation	3.536	
COV,%	22.67	
8	3.084	Presented Work
Percentage	19.78%	

C. Compressive Strength and Modulus of Elasticity of SCEB Prisms

1)Damage Pattern

Figure 6 shows the prisms after compression tests. The cracks initially started from the top diagonals and propagated slowly to the middle. The damage pattern is noted at the 20% decrease of the capacity and the test is stopped at this stage. The failure mode of all the specimen is conical breaking failure as per ASTM Standard C1314-03a
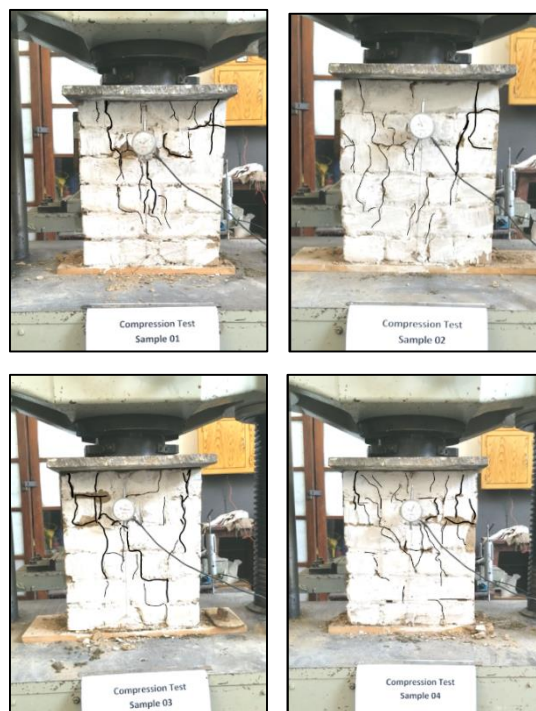
Figure 6. Damage Patterns of the Prisms after Compression Test
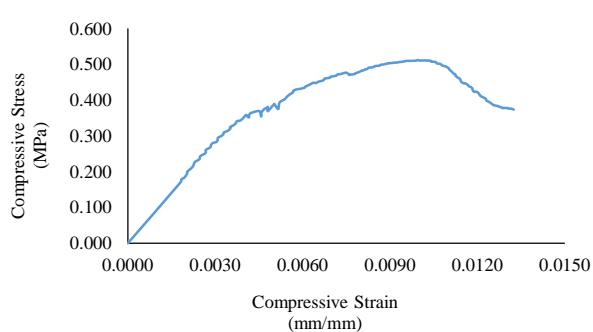
(a)Sample 01

(b)   Sample 02

(c)Sample 03   (d)   Sample 04
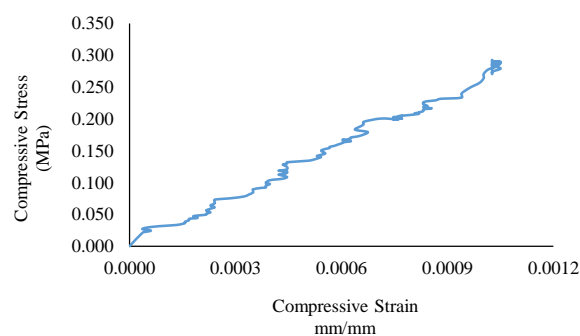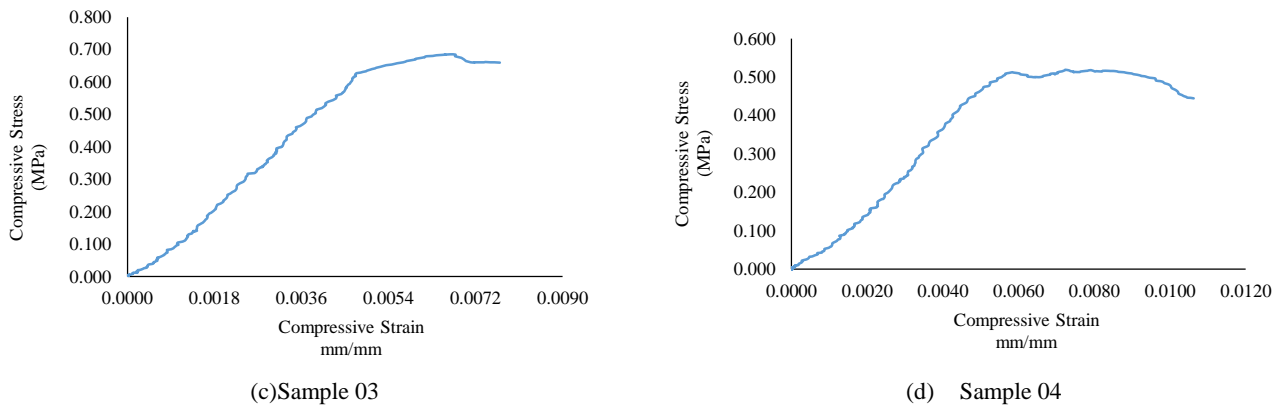
Figure 7. Stress-Strain Curves of the Compression Test Prisms

2)Graphical Representation

The stress-strain curves are presented for all the four prisms in Figure 7. The peak point of the curve is taken as the compressive strength. For sample 02, due to the ill-behavior of the instruments, the full data is not recorded. Only the initial straight portion is recorded. In the initial portion of the curves, a minor curvature is shown. This is the stage when the soft mortar is stiffening and achieved its maximum density. After the full compaction of the mortar, the whole response of the prism is started. The modulus of elasticity is calculated from the initial straight portion of the curve.

3)Results and Comparison

The mean value for the compressive strength of the prisms is 0.595 MPa, whereas the Modulus of Elasticity is 121.048 MPa. These values are compared with the burnt brick and presented in TABLE IV. The burnt brick masonry values are taken from the work of different researchers. The SCEB masonry compressive strength is 14.6% of the mean compressive strength of the burnt brick, whereas the Modulus of Elasticity of SCEB is 8.5% of the Modulus of Elasticity of Burnt Brick.

TABLE IV: Comparison of SCEB Compression Test Values with the Burnt Brick

S.No	28 days Compressive strength (MPa)	Modulus of Elasticity (MPa)	Reference
1	4.960	1407.221	[19]
2	4.540	1300.100	[18]
3	4.341	-	[13]
4	3.513	1227.422	[12]
5	3.024	1227.182	[15]
Mean	4.074	1428.800	
Standard Deviation	0.791	319.531	
COV, %	19	22	
4	0.595	121.414	Presented Work
Percentage of SCEB to Burnt Brick			
	14.6%	8.5%	

D. *Compressive Strength of Mortar*

The mean Compressive Strength of CSS mortar is 0.708 MPa. It is compared with the Cement-sand mortar (CS) and presented in the table. The percentage of the CSS is only 9.75% of the burnt brick. it has nothing with the compaction pressure.

TABLE V: Comparison of CSS mortar strength with CS mortar

S.No	28-days Compressive Strength (MPa)	Reference
	MPa	
1	7.951	[13]
2	5.054	[15]
3	8.333	[16]
4	6.900	[17]
Mean	7.064	
Standard Deviation	1.476	
COV,%	20.8	
8	0.687	Presented Work
Percentage of CSS to CS	9.75%	

IV. CONCLUSION

This work is aimed to enhance the confidence for self-help-based low-cost housing construction from the soil. In such a way, it will enable the lower economy class community to build engineered houses and also will prevent environmental degradation due to the conventional construction materials. Therefore the compression tests are carried out on the stabilized compressed earth blocks and its prisms, made by a manual machine having a low compaction pressure. As the compressive strength is the key parameter, which depicts most of the overall behavior of the element, therefore it was decided to investigate the compressive strength of SCEB and its masonry. The values are then compared with the conventional burnt/fired bricks. Based on the research work, the following important points are concluded.

The compressive strength of SCEB is 19.78% of the traditional burnt brick, almost one-fifth of the strength of the burnt brick. At such low pressure, this value seems encouraging. It could further be enhanced if the soil is well graded. The compaction pressure could also be increased by increasing the lever arm, or by decreasing the surface area of the block.The damage pattern of the compression prisms is conical breaking and not vertical splitting. This shows a satisfactory strength of the SCEB and ultimately its masonry.Excluding sample 02, which has insufficient data, the other graphs show good inelastic behavior. It shows SCEB masonry possesses good ductility properties.

The compressive strength of masonry is 14.6% of the traditional burnt brick masonry. Whereas the modulus of Elasticity of SCEB masonry is only 8.5% of the traditional burnt brick masonry. The values are although comparatively less yet encouraging at such a small compaction pressure

V. RECOMMENDATIONS FOR FUTURE WORK

Based on the presented work, the following are some recommended points

1)SCEB and its masonry should be investigated for compaction pressure greater than 0.123 MPa, and also for the lower cross-sectional area of the block.

2)Some inclusion of fibers should also be done to see the effect on the results with low compaction pressure.

3)SCEB and its masonry should be investigated at low compaction pressure for other basic mechanical properties too, like Shear strength parameters, flexure strength, principle tensile strength, and modulus of rigidity.

4)It should also be investigated at low compaction pressure for the lateral load parameters like lateral strength, stiffness, ductility, and energy dissipation. The overall behavior should be studied for gravity and lateral loads to reach a consensus about the construction of houses from low pressure compressed earth blocks.

VI. REFERENCES

[1]   H. Molla, "Study of stabilized mud brick as an alternative building material & development of models," *Addis Ababa University,* 2012.

[2]   M. C. N. Villamizar, V. S. Araque, C. A. R. Reyes, and R. S. Silva, "Effect of the addition of coal-ash and cassava peels on the engineering properties of compressed earth blocks," *Construction and Building Materials,* vol. 36, pp. 276-286, 2012.

[3]   A. G. Kerali, "Durability of compressed and cement-stabilised building blocks," University of Warwick Coventry, England, 2001.

[4]   B. Venkatarama Reddy, "Sustainable materials for low carbon buildings," *International Journal of Low-Carbon Technologies,* vol. 4, pp. 175-181, 2009.

[5]   E. Baum, "Black carbon from brick kilns," *Presentation for CleanAir Task Force,* 2010.

[6]   A. L. Murmu and A. Patel, "Towards sustainable bricks production: An overview," *Construction and Building Materials,* vol. 165, pp. 112-125, 2018.

[7]   A. Laborel-Preneron, J. E. Aubert, C. Magniont, and A. Bertron, "Influence of straw content on the mechanical and thermal properties of bio-based earth composites," in *First international conference on bio-based building materials*, 2015.

[8]   R. Bahar, M. Benazzoug, and S. Kenai, "Performance of compacted cement-stabilised soil," *Cement and Concrete Composites,* vol. 26, pp. 811-820, 2004.

[9]   S. H. Sameh, "Promoting earth architecture as a sustainable construction technique in Egypt," *Journal of cleaner production,* vol. 65, pp. 362-373, 2014.

[10]   RICS, "RICS Valuation Standards," ed: Royal Institution of Chartered Surveyors London, 2008.

[11]   V. Rigassi, "Compressed Earth Blocks: Volume I," *Manual of production,* vol. 1, 1985.

[12]   A. Ahmed, I. Ahmad, K. Shahzada, M. T. Naqash, B. Alam, M. Fahad, *et al.*, "Seismic Capacity Assessment of Confined Brick Masonry Building: An Experimental Approach," *Shock and Vibration,* vol. 2018, pp. 1-10, 2018.

[13]   H. U. Sajid, M. Ashraf, Q. Ali, and S. H. Sajid, "Effects of vertical stresses and flanges on seismic behavior of unreinforced brick masonry," *Engineering Structures,* vol. 155, pp. 394-409, 2018.

[14]   S. Phaiju and P. M. Pradhan, "Experimental work for mechanical properties of brick and masonry panel," *Journal of Science and Engineering,* vol. 5, pp. 51-57, 2018.

[15]   K. Shahzada, A. N. Khan, A. S. Elnashai, M. Ashraf, M. Javed, A. Naseer, *et al.*, "Experimental Seismic Performance Evaluation of Unreinforced Brick Masonry Buildings," *Earthquake Spectra,* vol. 28, pp. 1269-1290, 2012.

[16]   V. Alecci, M. Fagone, T. Rotunno, and M. De Stefano, "Shear strength of brick masonry walls assembled with different types of mortar," *Construction and Building Materials,* vol. 40, pp. 1038-1045, 2013.

[17]   A. Naseer, "Performance behavior of confined brick masonry buildings under seismic demand," NW. FP University of Engineering and Technology, Peshawar, Pakistan, 2009.

[18]   M. Javed, "Seismic risk assessment of unreinforced brick masonry buildings system of Northern Pakistan," NW. FP University of Engineering and Technology, Peshawar, Pakistan, 2009.

[19]   M. Ashraf, "Development of low-cost and efficient retrofitting technique for unreinforced masonry buildings," University of Engineering and Technology, Peshawar, Pakistan, 2010.

Effects of Cooling Techniques on the Secondary Hardening Behavior of 15CrMnMoV6 steel

Zahoor Ali [A], Prof. Dr. Afzal Khan [B]

[A] Postgraduate student, Department of Mechanical Engineering, University of Engineering and Technology, Peshawar. Phone +92-03315004884. Email. Zahoorali87@yahoo.com

[B] Professor, Department of Mechanical Engineering, University of Engineering and Technology, Peshawar. Phone +92-03449625242. Email. afzalkhan@uetpeshawar.edu.pk

Abstract— **15CrMnMoV6 is a low carbon alloy steel which combines high yield strength with good toughness. This high strength low alloy steel (HSLA) finds many applications in the aerospace and motorsports industries. This steel exhibits secondary hardening behavior which affects its mechanical properties. The secondary hardening behavior varies with the tempering temperature and needs to be investigated for optimal mechanical properties.In this research various cooling techniques such as water quenching, oil quenching and air cooling are used to study the secondary hardening behavior in the material. Optical Microscopy, Scanning Electron Microscope and X-ray Diffraction are used to study the alloy carbides along with mechanical characterization for determining the strength and hardness of the alloy.Results shows that the secondary hardening behavior is elevated in air cooled steel than the water quenched and oil quenched due to higher precipitates of Molybdenum carbide and Vanadium Carbide.**

Keywords— **Alloy carbides, Cooling techniques, 15CrMnMoV6 steel, Secondary hardening behavior, Tempering temperature.**

I. INTRODUCTION

15CrMnMoV6 steel is used in many critical applications in the aerospace and automotive industry. Various parts are manufactured in large numbers. The material is received in the annealed and forged condition. This material is then hardened for manufacturing of various parts. The material is heat treated by using Oil quenching technique. By this process the hardness is not achieved accurately. And the strength of the material varies from its desired value. The tempering temperature of the steel meets the secondary hardening behavior of the steel. So, it is essential to study the secondary hardening behavior of the steel.

The secondary hardening behavior of the material varies with heat treatment process. Heat treating process of Air cooled, Water quenched, and Oil quenched steel will be required to be studied. The hardening effect obtained in these processes will be compared and optimum process and temperature ranges will be recommended for the required mechanical properties.

The following are the main objectives in this regard.

I. To determine the optimum tempering temperature for required hardness and strength.

II. To study the secondary hardening behavior of15CrMnMoV6 by comparing the heat-treating processes.

III. To compare the strength and hardness at different tempering temperatures in Water quenched, Oil quenched and Air-cooled heat-treating processes.

Study on the effects of cooling methods on the microstructure and mechanical properties after heat treatment of High Strength Low Alloy Steel (HSLA) steel showed that the water-cooled specimens have ferritic matrix and tempered martensite. The air-cooled specimen had mix of ferritic matrix and tempered bainite. They reached at the conclusion that the air-cooled steel had good combination of strength and toughness as compared to water cooled [1].

The fraction of bainite and martensite can be increased by adding alloying elements which slows down the bainitic reaction. The carbide forming alloying elements greatly retard the ferrite-pearlite reaction, and chromium in particularly is very effective in the retardation of bainitic reaction. Increasing in the

carbon and chromium content will result in the increase of martensite content in the mix microstructure. The yield strength increases with decreasing the grain size of 15CrMnMoV6. The percent elongation and notch toughness also increase with the decreasing grain size [2].

15CrMnMoV6 contain bainitic structure and with the increase in temperature up to 650C the material undergoes a secondary hardening effect. In the beginning of the precipitation the size of the Mo_2C and VC is very small to keep coherent with the matrix, which results in increase in hardness and strength. But with the increase in tempering temperature the carbides coarsen and causes decrease in strength and hardness [5].

There are three strengthening mechanisms in modern microalloying (HSLA) steels that cause the final strength of the steel. In the first mechanism the precipitation takes place in the austenite and further precipitation takes place during the transformation from austenite to ferrite.

The second mechanism is the interphase transformation, in which the precipitates of the microalloying carbides takes place progressively as the interphase boundaries move through the steel.

The third type of strengthening mechanism occurs when the rate of cooling through the transformation is high, leading to the formation of super saturated plates of ferrite, the carbides will tend to precipitate within the grains, usually onto the dislocations, which numerous in this type of ferrite [6].

II. METHODOLOGY

In this study, different cooling techniques were used to study the 15CrMnMoV6. The steel was received in the form of forged rods. The material was analyzed by X-ray Spectroscopy for chemical composition. The chemical composition is C=0.18, Si=0.11, Mn=0.886, Mo=0.80, V=0.256, Cr=1.39, S= 0.012, P=0.011.

From the material lot, 21 rods were randomly selected. All this material was heated to a temperature of 925C for 1 hour and 30 minutes. Out of these 21 rods 07 rods were water quenched, 07 rods were oil quenched and 07 rods were air cooled. After this 07 lots consisting of 03 rods were made by selecting 01 rod from 03 quenched lots. The 07 lots were tempered at 300C, 400C, 500C, 550C, 600C, 625C and 650C independently for 2hours.

Samples for tensile testing, hardness testing and microstructure analysis were cut from the tempered lots. Microstructure was studied by Scanning Electron microscope (SEM) at different magnifications. The chemical composition after heat treatment was studied by Energy Dispersive Spectrometer (EDS), attached with SEM.
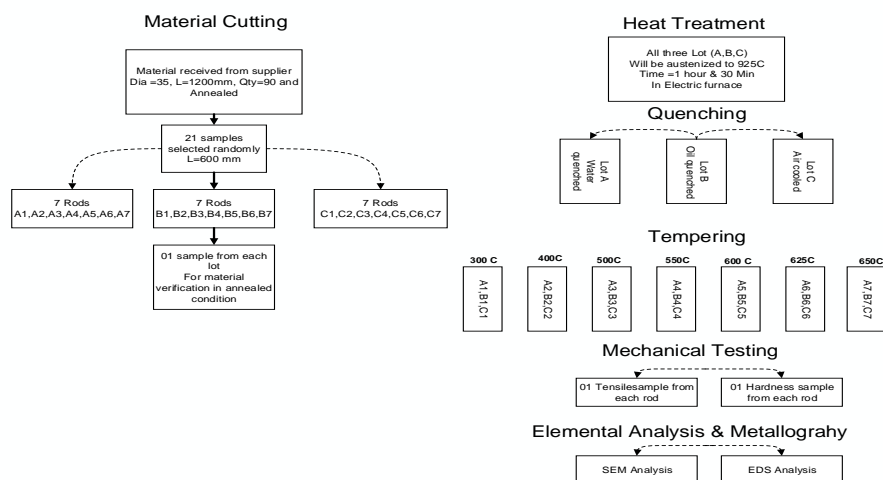
Fig. 1. Experimental Methodology

III. RESULTS AND DISCUSSION

A. Mechanical Properties

Fig 2 and 3 shows the hardness and tensile properties of the all the three quenching techniques applied to the material. These plots show increase in hardness and strength between 550C and 625C of tempering temperature. This behavior shows the secondary hardening behavior of the material. The hardness of the air-cooled steel is lower than water and oil quenched steels. But the rate of secondary hardening is higher than both oil quenched and water quenched steel. By examining the broken tensile specimens, all the three different quenched materials show nearly same area reduction and percent elongation with increase in temperature.
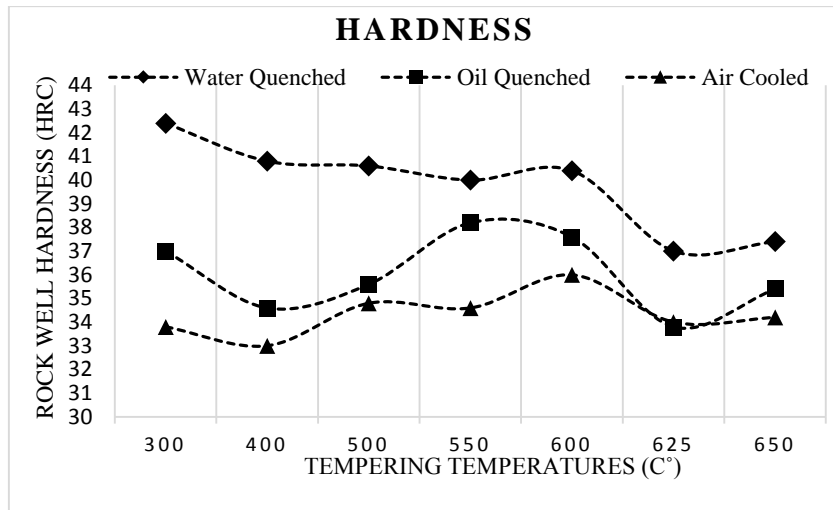
Fig. 2. Variation of Hardness with Tempering Temperatures of different Quenching Techniques
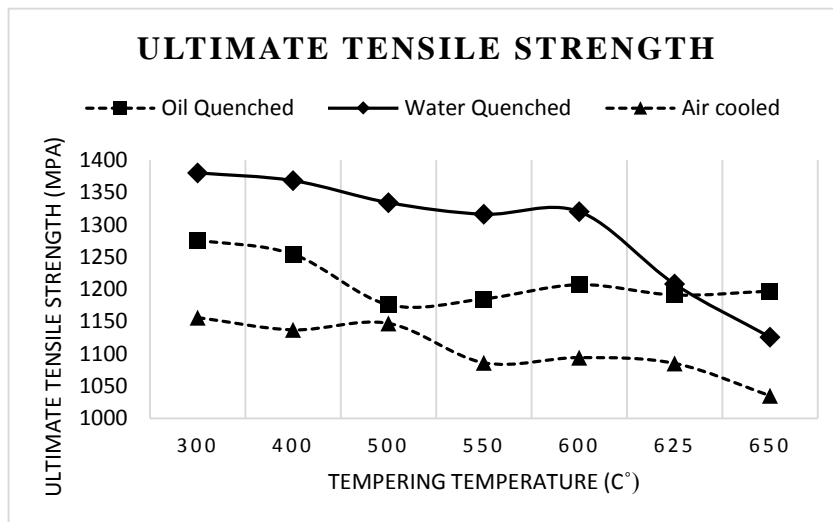
Fig. 3. Variation of Ultimate Tensile Strength (UTS) with Tempering Temperature of different Quenching Techniques

B. Metallurgical Structure

Fig. 4, 5 and 6 shows the metallurgical structures of water quenched, oil quenched and air-cooled specimens of heat-treated material at different magnifications on Scanning Electron Microscope. The water quenched and oil quenched specimens are tempered martensite and mixture of tempered martensite. The air-cooled specimens are tempered bainite.

| 4(a) | 4(b) | 4(c) |
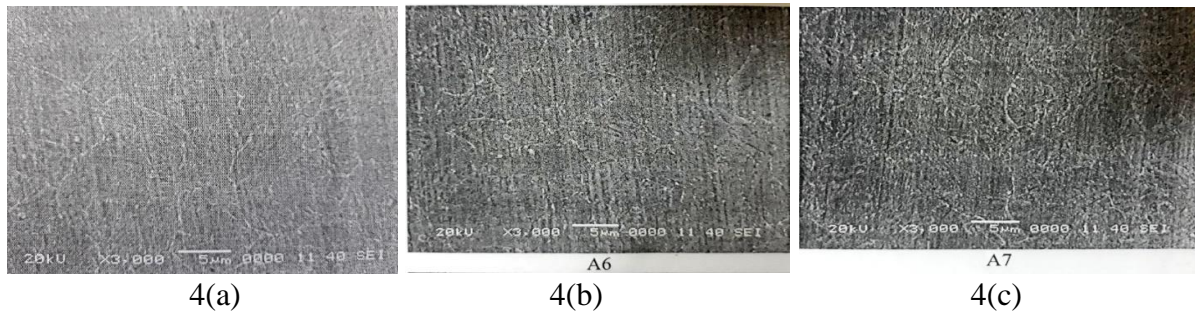
Fig. 4. SEM images of water quenched specimens

| 5(a) | 5(b) | 5(c) |
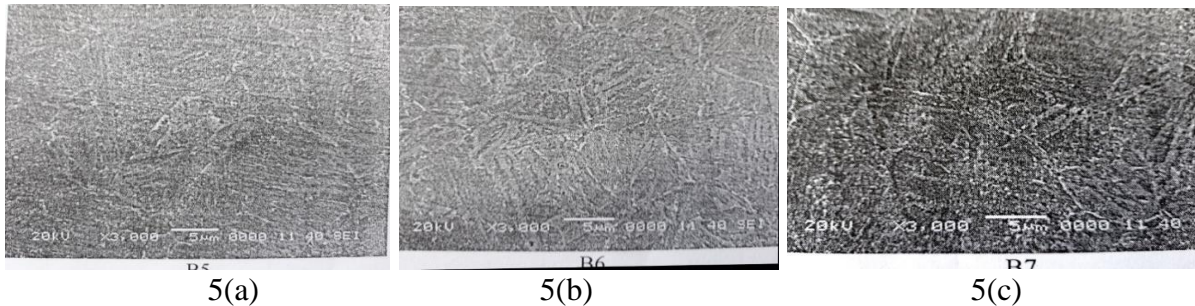
Fig. 5. SEM images of Oil quenched specimens

| 6(a) | 6(b) | 6(c) |
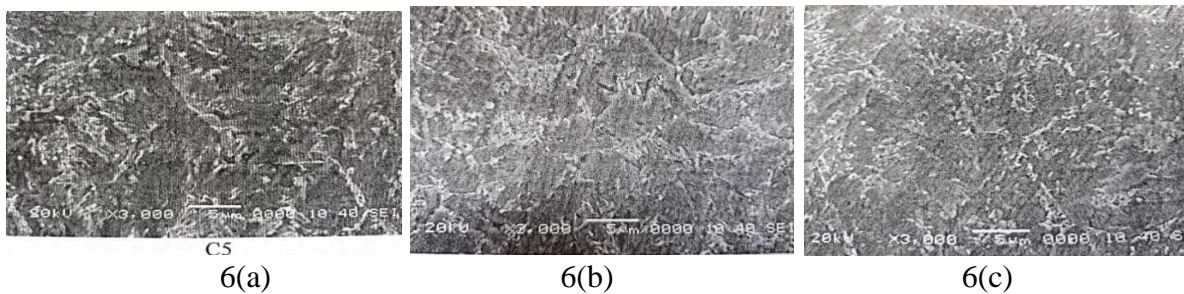
Fig. 6. SEM images of air-cooled specimens

If the cooling rate is high it will transform to martensitic structure and if the cooling rate is low, it will transform to bainitic structure.

After tempering the structure were converted into tempered martensite and tempered bainite in the region of 600 C to 650 C as shown in the above figures. From Fig. 4, it is obvious that the water quenched specimens has finer grain structure as compared to oil and air quenched. Therefore, their tensile properties are at higher side as compared to other two cooling techniques.

C. Carbide Analysis

EDS (Energy dispersive Spectrometer)

The metallographic samples were tested for carbide analysis on the Energy Dispersive spectrometer (EDS) which is attached with SEM. In this material the Vanadium and Molybdenum (Mo) are the main carbide former. Here we will take Mo as our focus element.

From the Fig.7 the carbide analysis of water quenched specimens shows that the Mo content in water quenched samples increases at 625C which means a decrease in the content of MoC and hence decrease in the hardness and ultimate tensile strength.

This change in Mo content in the oil quenched specimens as shown in Fig.8 is similar to the water quenched samples. The change in the Mo content in air-cooled specimen is not considerable as shown if Fig. 9. Hence the air-cooled specimens show stable values of hardness and ultimate tensile strength.
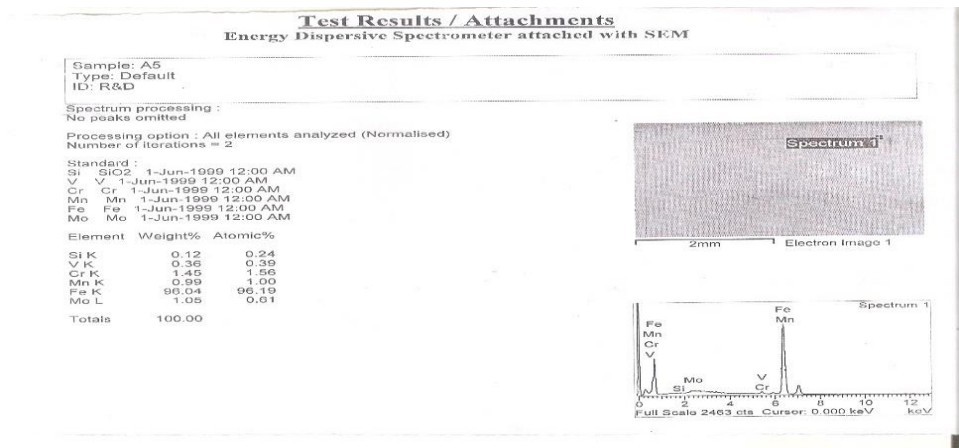
7 (a)
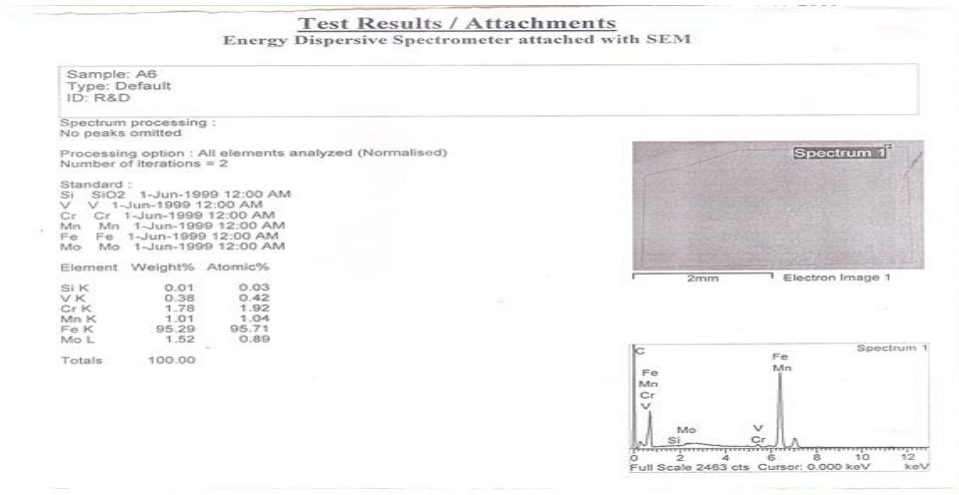
7 (b)
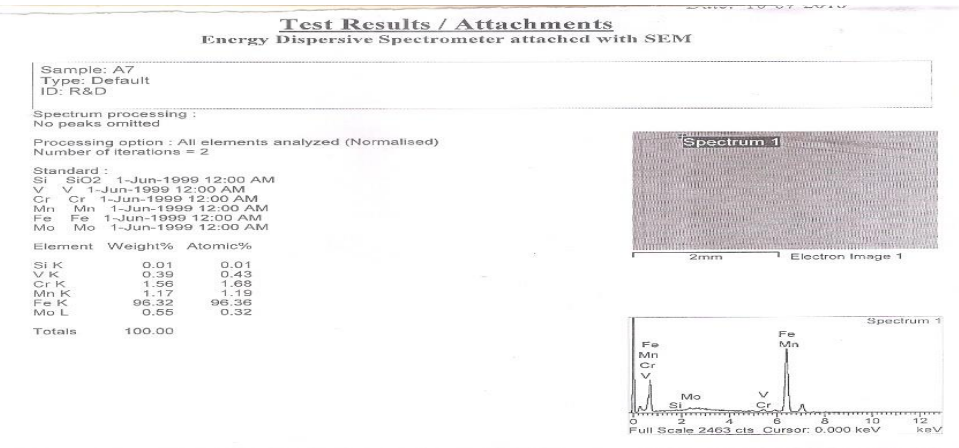
7 (c)

Fig. 7. EDS images of Water-Cooled Specimens
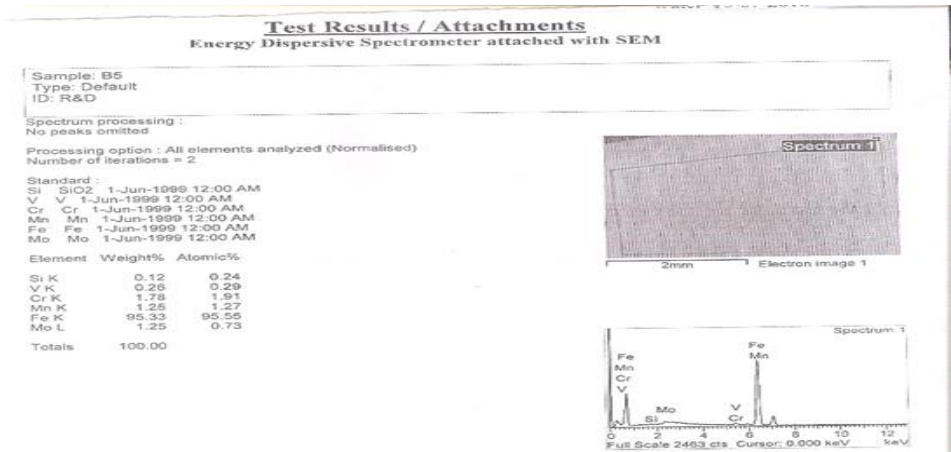
8 (a)
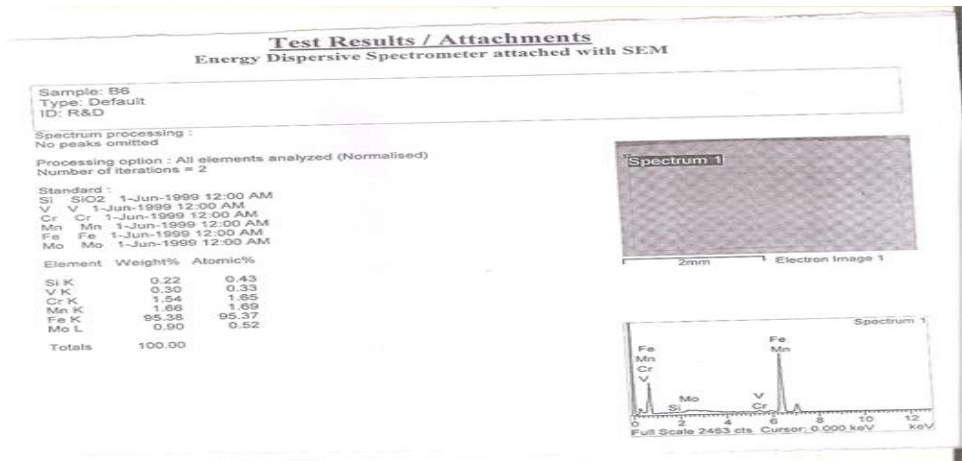
8 (b)
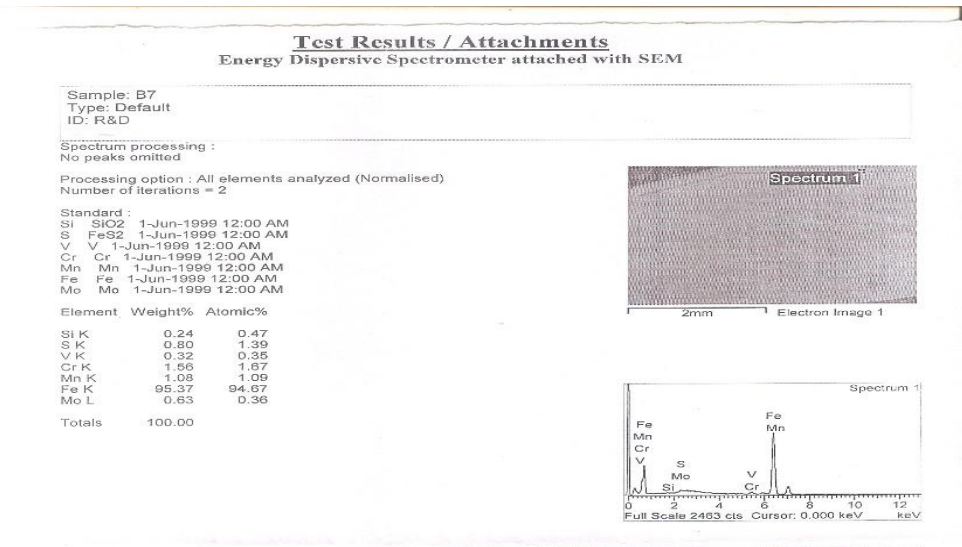
8 (c)

Fig. 8. EDS images of Oil Cooled Specimens
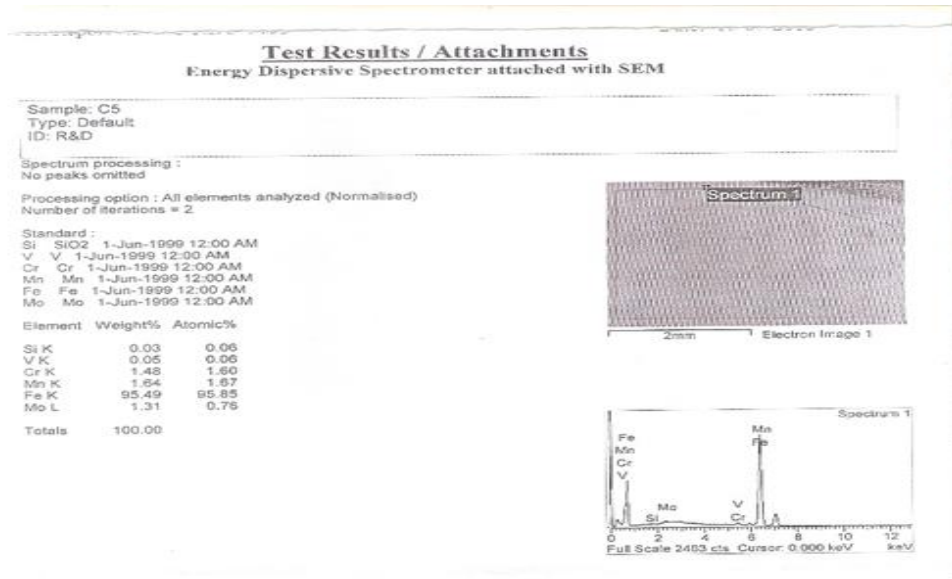
9 (a)
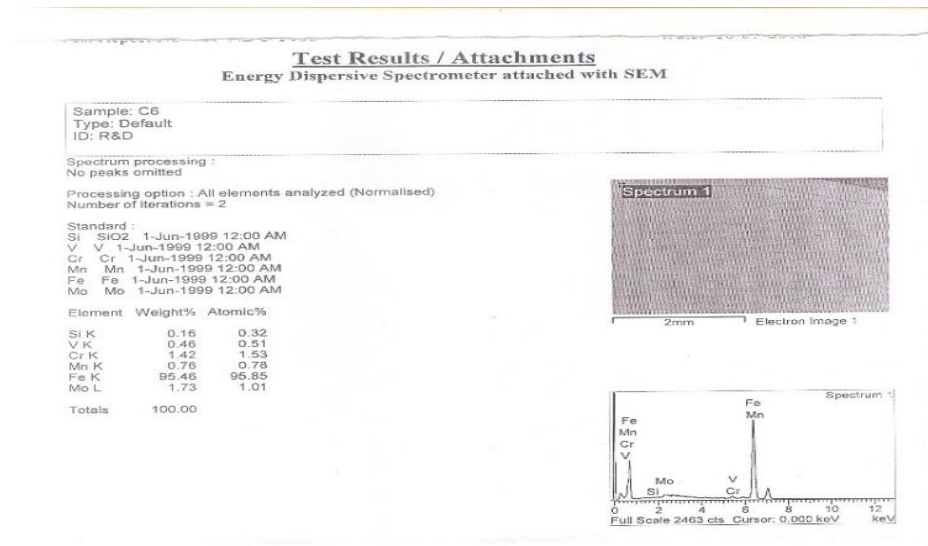
9 (b)
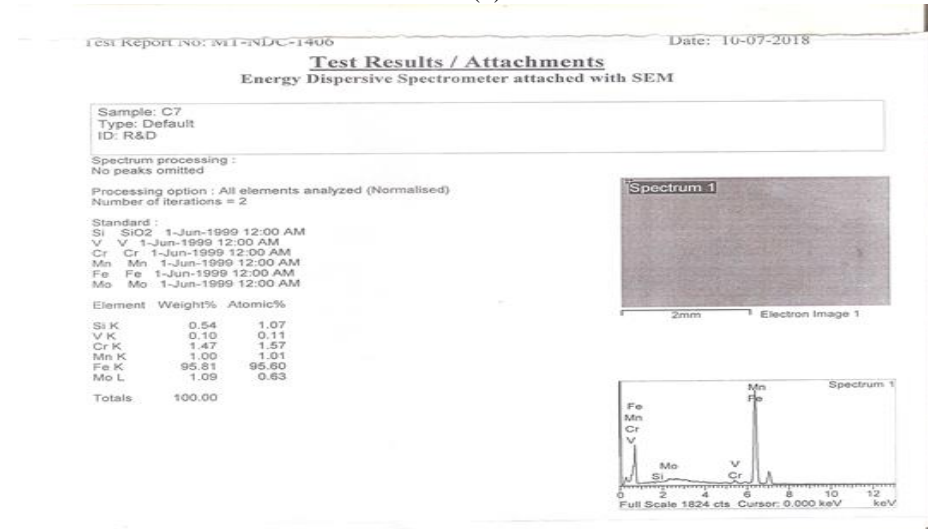
9 (c)

Fig. 9. EDS images of Air-Cooled Images

IV. CONCLUSION

The desired properties of the 15CrMnMoV6 is a result of the multiple mechanisms within the microstructure. The strength and hardness properties appear to be controlled primarily by the precipitation of the carbide formers i-e MoC and VC.

The secondary hardening effect in all the three types of samples lie between 500C to 600C. Although this response may be more prominent in the air-cooled steel. This response in the air-cooled steel is appeared to have due more precipitation of the carbide formers.

The strength and hardness of the water and oil quenched steel are high but not desirable for our requirement. The change in hardness and strength values of the water quenched samples is less with the change in tempering temperature. The oil quenched specimens also show little change in properties with the changing tempering temperature.

V. REFERENCES

[1] T.R. Bandyopadhyay, P. K. Rao and N. Prabhu. "Improvement in mechanical properties of standard 15CDV6 steel by increasing carbon and chromium content and inoculation with titanium during ESR". *ISRN Mater sci.*, pp.1-7, 2012.

[2] T. Cain. *Hardening, Tempering and Heat Treatment for Model Engineers.* Britain: Special Interest Model Books; 2003, ch 2. pp. 13-26.

[3] T.G. Diggies, S.J. Rosenberg, and G.W. Geil. *Heat treatment and properties of iron and steel*. National Bureau of Standards Monograph 88, November 1966.

[4] Ci. Ding, & W. HAN. "Secondary hardening behavior of 15CrMnMoV thin rolled tube*". Acta Mettal. Sin. (Engl. Lett.),* Vol.23, No. 4, pp. 261-266, August 2010.

[5] D. A. Skobir, M. Godec, M. Balcar & M. Jenko. "The influence of the microalloying elements of HSLA steel on the microstructure and mechanical properties". *MTAEC9.* Vol 44, Issue 6, pp. 343-347, 2010.

[6] J.L. Dosset, H.E. Boyer. *Practical heat treating*, 2nd ed. Materials park Ohio, ASM International, ch.7, pp.125-140, 2006.

[7] A. Kumar, A. Dhakad. "Effects of cooling techniques after heat treatment of reinforced HSLA steels on their structure, tensile and impact properties". *Int J Recent Sci Res*. Vol. 6, Issue, 5, pp. 4087-4097, 2015, May 2015.

[8] P.N. Kumar, Y. Bhaskar, P. Mastanaiah & CVS Murthy. "Study on dissimilar metal welding of 15CDV6 and SAE 4130 steels by Inter pulse gas tungsten arc welding". *Procedia Materials Science,* Vol 5, pp. 2382-2391, 2014.

[9] D.A. Skobir. "High strength low-alloy (HSLA) steels". *MTAEC9.* Vol 45, Issue 4, pp. 295-296, 2011.

[10] M.V.L. Ramesh, S.P. Rao, V.V. Rao. "Microstructure, and mechanical properties of laser beam welds of 15CDV6 steel,"*Defense Science Journal*, Vol. 65, Issue 5, pp. 339-342, 2015.

To Assess the Effect of Industrial Waste on The Quality of Ground Water. A Case Study of Hayatabad Industrial Estate, Peshawar, Pakistan.

Habib Ahmad Jan*[A], Nehar Ullah[B] and Rashid Rehan[A]

[A]*Department of Civil Engineering, National Institute of Urban Infrastructure Planning, University of Engineering & Technology, Peshawar, Pakistan*

[B]*Department of Chemical Engineering, University of Engineering & Technology, Peshawar, Pakistan*

Abstract— **Water is essential part of human life cycle. Pure water is used in several ways for domestic and industrial purposes. Many industrial and unformulated events make it polluted that consequently affect human health, aquatic life as well as ground water quality. Among other reasons, industrial pollution is one of the major sources and concern due to toxic substances and chemicals used as raw materials in various industrial applications. Residues in the form of heavy chemicals is continuously discharged from these industries into the water bodies without any proper treatment. In the Industrial Estate Peshawar, there is no arrangement for industrial wastewater management where different industrial unit directly release their wastewater into the receiving stream, which is passing through urban and rural parts of Peshawar and makes its way into the river Kabul apart 20 km away from HIE KPK Pakistan. Water from the river Kabul is widely used for irrigation purposes in this area which consequently affects human and marine life because of the untreated toxic effluents present. In this research work the effluent samples and tube well water was collected from pre-selected industry in Hayatabad industrial estate to investigate the quality of effluents and ground water at upstream points, downstream points and discharge points as well as main drain at a difference of 10 meters for each parameter to see if any contamination has accrued. Current study has investigated concentration of the selected heavy metals (Nickel and Lead) and water quality parameters (Electrical Conductivity and Turbidity) the industrial discharge into water bodies. The concentration of turbidity level in main drain were so high (1182 NTU) and minimum turbidity value of tube well water was recoded (8.44 NTU) near to ZRK industry, the maximum values of EC were recorded (1915 mg/l) which is also exceeding the permissible limits. Among heavy metals contamination the maximum values of Pd and Ni were (0.042 mg/l) and (0.013 mg/l) respectively in the specific industries in HIE. The variation of all these fore mentioned concentrations were investigated and represented through GIS. The effluents discharged by HIE adversely affect the ground water quality because the exceeding values in the fore mentioned water quality parameters and heavy metals are not in the acceptable limits of NEQS of Pakistan.**

Keywords— **Heavy metals, effluent, industrial waste water, impact, toxic**

I. INTRODUCTION

Industrialization has facilitated the human life in all aspects with some gifts in the form of pollution and exploitation of natural resources. Industrial wastes in the form of gases and chemicals has posed a serious threat to human life. The untreated wastes released from industries directly affects both surface and ground water sources making it unsuitable both for animals and plants. Serious attention is much needed to be paid to this issue otherwise the earth would become miserable for life [1] Moreover, the modern turn of events and safety of the environment can be made conceivable by applying the idea of industrial beneficial interaction. To lessen the effects on climate, center around environmental exhibitions is critical [2].

Grounder water is the main source of drinking water for plants and animals, being polluted by several means. The effluents released from industries is taken by surface and then reaches the ground water. The various effluents which makes the ground water polluted are heavy metals and raw materials which are discharged into the receiving stream during manufacturing of various industrial products [3] The heavy metals which are responsible for water contamination are arsenic, cadmium, chromium, copper, nickel, zinc, led etc. [4] To assess the water quality, PH, turbidity, total suspended solids, total dissolved solids, total nitrogen, total phosphorus and chlorides are needed to be checked.

The major contributors to the surface and ground water pollution are the byproducts of various industries such as textile, chemical, construction and others. High levels of pollutants in river water causes an increase in biological oxygen demand (BOD), chemical oxygen demand (COD), total dissolved solids (TDS), total suspended solids (TSS), toxic metals such as Cd, Cr, Ni and Pb and fecal coliform and hence make such water unsuitable for drinking, irrigation and aquatic life [5]; [6] It has been reported that 60 %

of population in developing countries has no access to pure drinking water [7]. Every year about 3.4 million peoples die due to water borne diseases and around 2.4 billion individuals need sufficient disinfection [8]

In Pakistan, the foundation of modern home began under the initial five years plan (1955-1960) and afterward quick improvements were recorded till 1990s [9] These days the modern area is confronting outrageous affliction in the nation by and large and Khyber Pakhtunkhwa (KPK) territory specifically. In KPK, there are 12 industrial areas having 1552 are open and 635 industrial estate are not functional. Subsequently, the territory has gotten a loss of Rs. 15.74 billion and a large number of gifted specialists got jobless [10]

The present study was therefore carried out to determine the important characteristics of various industrial effluents of Hayatabad Industrial Estate, Peshawar (KPK) and assess the impacts of such effluent on human health and environment. And also, to study and recommend most suitable process for effluent treatment which could improve the quality before these are disposed up into water body.

II. STUDY AREA

Peshawar Industrial Estate located in District Peshawar, Khyber Pakhtunkhwa (KPK), shown in Figure 1, was established in 1964 over 868 acres. A recent survey reveals that there are 196 medium and large industrial units in addition to 97 SIDB units in operation in the Industrial Estate. Different types of industries like Pulp and Paper, Ghee, Chemicals, Match Factories, Marble and Ceramics, Pharmaceuticals, Beverage & Food, Carpet, Textile, Steel Fabrication and Engineering Industries etc. have been established. The untreated waste of industries of Peshawar Industrial Estate are causing environmental problem in the area as the industrial waste is being drained out in the water bodies without treatment. The effluents discharged from industries are passing Peshawar and populated suburb areas of Peshawar. Several complaints have been received from the residents of locals regarding the pollution of Peshawar Industrial Estate.

In the Industrial Estate Peshawar, there is no arrangement for industrial wastewater management; where different industrial unit directly release their wastewater into the receiving stream. therefore, there is a need to monitor the industrial wastes for both physical and chemical parameters.
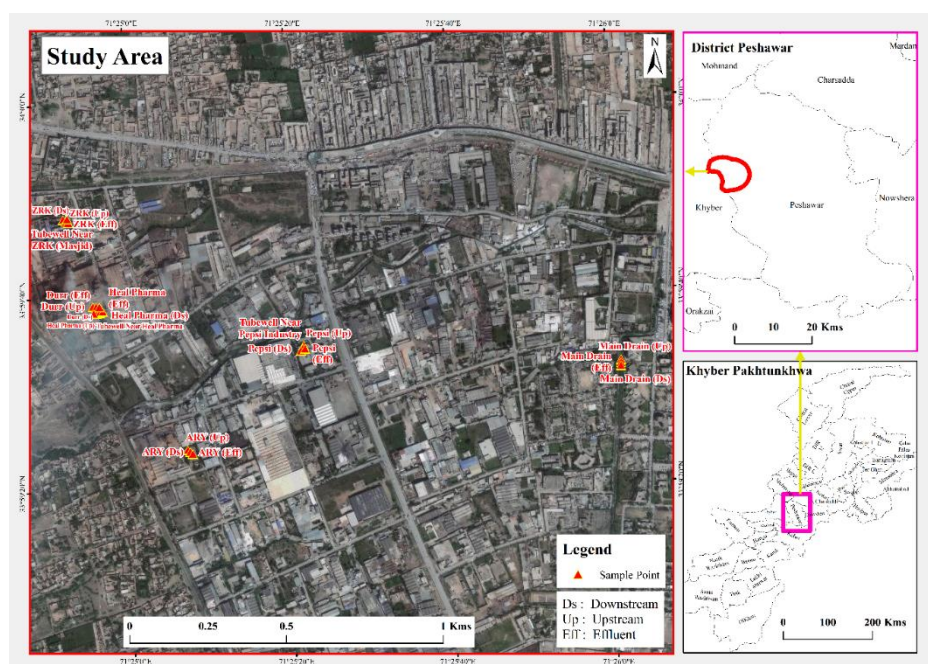
Figure 1: Study Area

III. METHODOLOGY

The water samples were collected from five different industrial units of Pepsi, ZRK Group of Industries, ARY Steel Mills, Durr Ceramic Industry and Heal Pharmaceutical Industry. The water samples were collected at upstream, downstream and discharge along with tube well at a difference of 10 meters between upstream and downstream. Simples were also collected form main drain. The samples were then tested for physiochemical characteristics, turbidity and electrical conductivity, some characteristics were determined in the sampling process while other were tested Palintest Photo Meter. Besides these, heavy metals like, nickel and led were also tested using Atomic Absorption Spectrometer in the Centralized Resources Laboratory at University of Peshawar, Pakistan. Figure 2 shows the sequence in which the samples were collected from different industrial units.
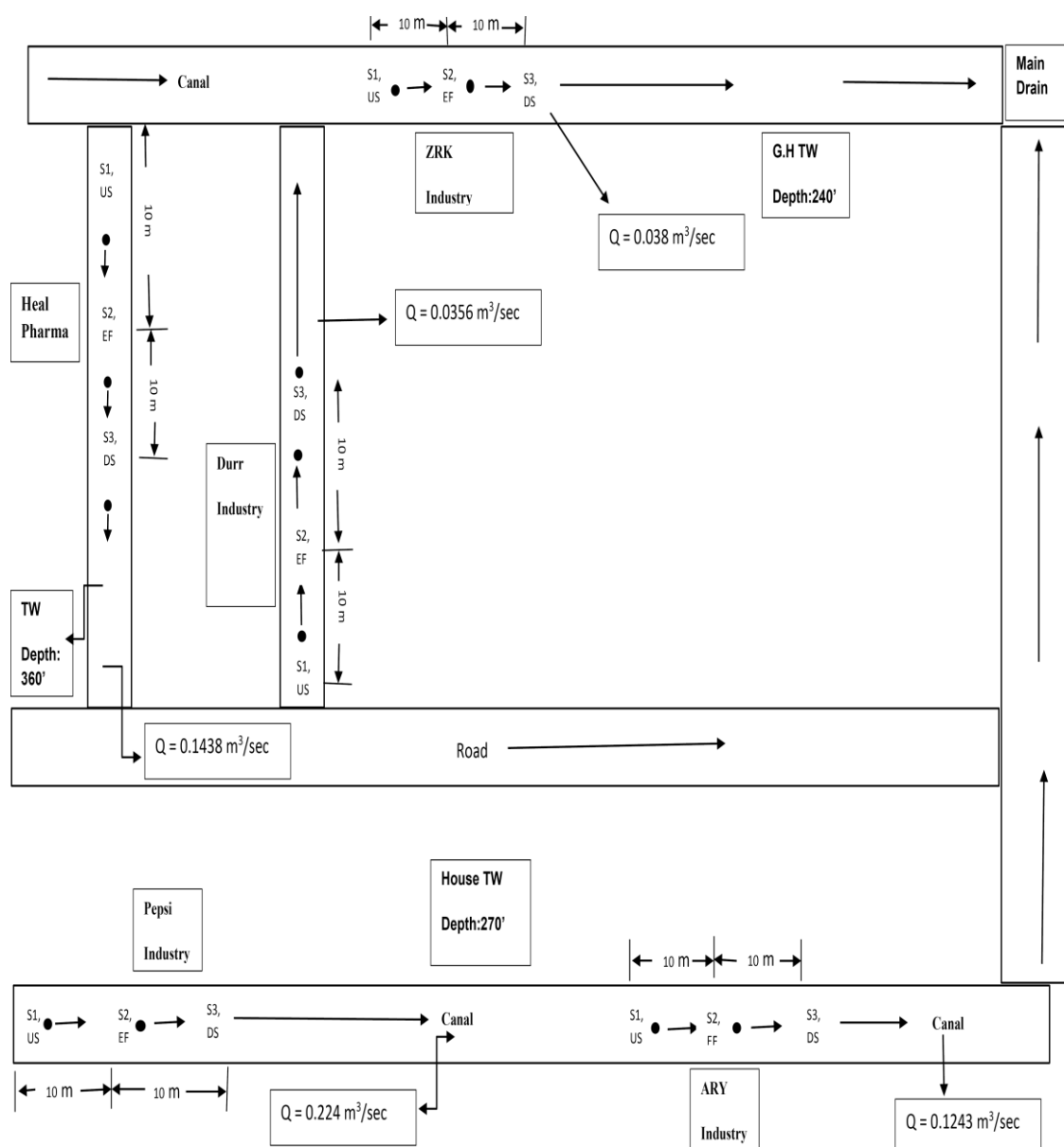
Figure 2: Review of methodology

IV. RESULTS AND DISCUSSION

1.1 Physiochemical Characteristics

1.1.1 Turbidity

The Figure: 3 shows turbidity values of different industries in Hayatabad industrial estate. The effluent values of turbidity change for each industry at upstream point, downstream point, discharge point and main drain in random way. The effluents value of turbidity is extremely high in almost all industries but maximum values for durr industry discharge point (801 NTU), ARY steel (796 NTU), heal pharma (746 NTU) and ZRK (736 NTU) respectively and the minimum effluents value of turbidity is for Pepsi industry (598 NTU) was recorded while main drain where all industrial effluents are fallen are was (179 NTU) values of turbidity in the ground water industries was within the permissible limit. The effluent value of turbidity inside all these specific industries become so high compared to permissible standard. Due to the very high turbidity of the above-mentioned industries is because using of high level of organic matter effluents from these industries is release. High turbidity levels influence fish sustaining and development. Light weakening by suspended particles in water has two principle kinds of ecological effect, decreased infiltration into water of light for photosynthesis and diminished visual scope of located creatures and individuals. High turbidity additionally because of all out suspended solids bolsters high quantities of outside microbiota in the water body, quickening microbial contamination.
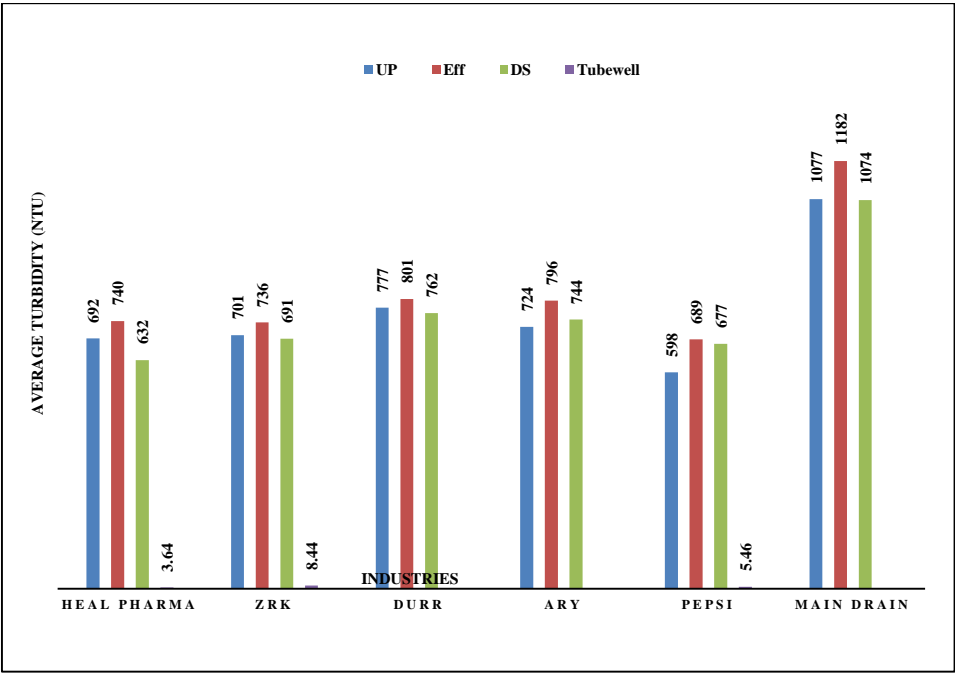
Figure 3: Turbidity Trend

1.1.2 Electrical Conductivity

The Figure: 4 is plotted between electrical conductivity values of different industries in Hayatabad industrial estate. The effluent values of EC change for each industry at upstream point, downstream point, discharge Point and main drain in random way. The maximum value of EC is for ZRK group was recorded at upstream point (1711.66 (uS/cm).) at downstream point of Pepsi industry the effluents value was recorded (1228 (uS/cm).), at downstream point at ZRK group the value was (1285 (uS/cm).) and minimum effluents values of the heal pharmaceutical industry was (546) respectively, while main drain values of EC was (1915 (uS/cm).). The effluent value of EC inside in all the mention industries was become so high compared to permissible WHO standard (400 (uS/cm). The exceeding limits of EC effluents of the above-mentioned industries was attributed very high level of contents of toxic chemical were used during manufacturing process. The effluent of waste water release from these industries not only causes corrosion in ground water but also have an adverse effect on aquatic life.
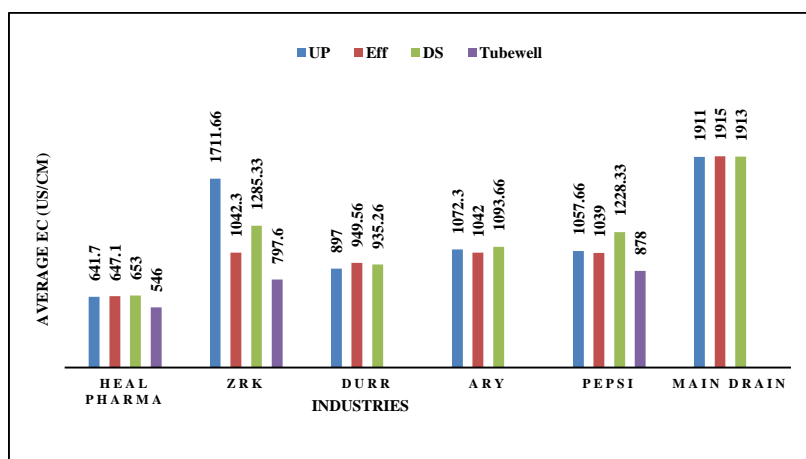
Figure 4: Electrical Conductivity Trend

1.2 Heavy Metals Concentration

1.2.1 Led

The Figure: 5 is plotted between Lead values of different industries in Hayatabad industrial estate. The effluent values of Pb change for each industry at upstream point, downstream point, discharge point and main drain in random way. The maximum value of Pb is for main drain was recorded (0.042 ppm) while the values of Pb is ARY Steel mills downstream point (0.035 ppm), Pepsi downstream (0.033 ppm) and durr downstream Point the effluents value was recorded (0.023 ppm) and the minimum values of lead heal pharmaceutical receptively. Compared to NEQS and WHO Standard (0.05). In the industrial area of Hayatabad, the lead value of most of the industries were below at specific sampling points. The outcomes show that the effluents discharged during manufacturing process into the streams have overwhelming metal fixations over those prescribed and this represents a hazard to the earth.

1.2.2   Nickel

The Figure: 6 is plotted between Ni values of different industries in Hayatabad industrial estate. The effluent values of Ni change for each industry at upstream point, downstream point, discharge point and main drain in random way. The values of Ni show High deviation in main drain compared to other industries. The maximum effluent value of Nickel for main drain (0.013 mg/l) at discharge point of ZRK group Pepsi and durr industry the effluents value of Ni was recorded (0.006 mg/l), At the downstream point of heal pharmaceutical the Ni effluents value were (0.004 mg/l) which is beyond the NEQS and WHO value. (0.02 mg/l). Significant levels of Ni were exceeding NEQS limits was recorded at above mentioned industries and main drain in (Fig 4.21) The most widely recognized utilization of Ni is the using of raw material during manufacturing process. The important sources of nickel infecting in the dirt are metallic coating enterprises, fiery of non-renewable energy sources, and nickel mining and electroplating. This can cause various sorts of dangerous development on different goals inside the arrays of animals, overwhelmingly of those that live near treatment offices.
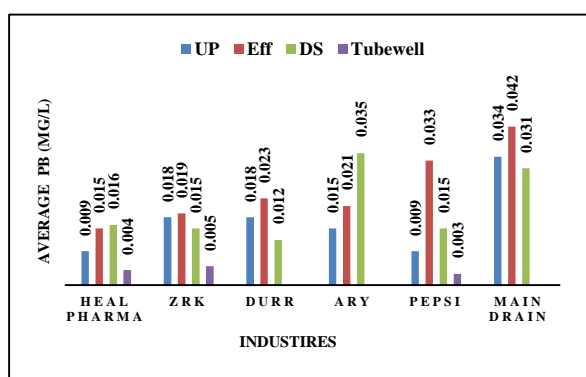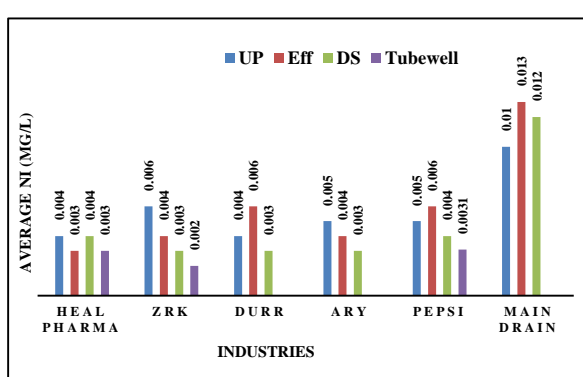
Figure 5: Lead Trend   *Figure 6: Nickle Trend*

V.   Conclusion

It is concluded that the selected industries in Hayatabad industrial Estate (HIE) discharge their untreated industrial waste wastewater into Kabul river through number of natural drains, and canals. Un-treated industrial waste results in discharge of pollutants and toxic waste into river that adversely affect humans as well as aquatic life. heavy metals concentration such as (Ni, Pb) and different water quality parameters (EC, turbidity) were tested. The concentration of turbidity level in main drain were so high (1182 NTU) and minimum turbidity value of tube well water was recoded (8.44 NTU) near to ZRK industry, the maximum values of EC were recorded (1915 mg/l) which is also exceeding the permissible limits. Among heavy metals contamination the maximum values of Pd and Ni were (0.042 mg/l) and (0.013 mg/l) respectively in the specific industries in HIE.The effluents discharged by HIE will drastically affect the ground water quality because the exceeding values in the mentioned water quality parameters and heavy metals are not in the acceptable limits of NEQS of Pakistan.The current study was carried out to assess groundwater quality of the area (District Peshawar industrial area) and to evaluate the impacts of different industrial effluents on the groundwater quality which is being used for various purposes including drinking, cooking etc.

Recommendation

- The discharge of untreated effluent in any of the natural water bodies, seepage drains or irrigation channels shall be prohibited.
- The government may ask each industry to allocate reasonable budget for environmental pollution control and accordingly may allow incentives in terms of tax rebate particularly for those units fulfilling pollution control measures.

VI. REFERENCES

[1]. Tariq and Shah, 2003: Characteristics of industrial effluents and their possible impacts on quality of underground water. Soil & Environ. 25(1): 64-69, 2006

[2]. IUCN. 2011: Sarhad Provincial Conservation Strategy Document: A report of IUCN.

[3]. Khan, S. and M. Noor. 2002: Investigation of pollutants in wastewater of Hayatabad Industrial Estate Peshawar. Pakistan Journal of Agriculture Sciences 2: 457-461.

[4]. Shivkumar, K. and G. Biksham. 1995: Statistical approach for the assessment of water pollution around industrial area. Environ Monitoring and Assessment 36: 229-249

[5]. Ali, A., H.N. Hashmi, I.A. Querashi and S. Athar, 2009: 'Treatment feasibility of NSSC pulping effluent using UASB reactor,' HYDRO Nepal: Journal of Water, Energy and Environment (Kathmandu) 5:57-60.

[6]. Muhammad Nafees, Asim Nawab and Wisal Shah, "Study on the performance of wastewater treatment plant designed for industrial effluents", J. Engg. and Appl. Sci., Vol. 34, January – June, 2015.

[7]. F.K. Bangash, M. Fida and Fazeelat, "Appraisal of effluents of some selected industries of Hayatabad industrial estate, Peshawar", Jour.Chem.Soc.Pak, Vol. 28, No.1, 2006.

[8]. Shah PB (2016). Chemical Parameter Analysis for Water, Waste Water and Ground Water. Intern. J. Innov. Res. in Sci. & Tech, 3(6): 43-49.

[9]. (Nasrullah et al., 2006): Pollution load in industrial effluent and ground water of gadoon amazai induatrial estate (gaie) swabi, NWFP.

[10]. (Nawaz et al., 2015): Causes of Sick Industrial Units and their Remedial Measures: A Case Study of Hayatabad Industrial Estate, Peshawar, Khyber Pukhtun Khwa

Technical Session 2-A (Google meet/Zoom)
Resource Recovery and Water Treatment Technologies

Session Chair: **Dr. Sofia Chaudry**
Session Co-Chair: **Dr. Naseer Ahmad Khan**

Mariam Mir Memon *(Dept. of Chem Eng., MUET Jamshoro)*	Removal of Fluoride from groundwater by using bone-char as a bio-adsorbent - A column study
Mian Imran ul Haq *(Dept. of Chem Eng., UET Peshawar)*	Carwash Wastewater Treatment
Qazi Iqra Shafi *(Dept. of Chem Eng., UET Peshawar)*	Removal of Electrolytes and E.coli from Groundwater Through Nanofiltration
Shebaz Ahmad *(Dept. of Chem Eng., UET Peshawar)*	Utilization of Marble Waste in Clay bricks and SO_2 Treatment

REMOVAL OF FLUORIDE FROM GROUNDWATER BY USING BONE-CHAR AS A BIO-ADSORBENT - A COLUMN STUDY

Mariam Mir Memon*, Murtaza Shah[A], Muhammad Idress[B] , Awais Ali[C], Sikandar Ali[D], Rakesh Kumar[E], Khadija Qureshi[F], Miraj Muhammad[G].
Department of Chemical Engineering, Mehran University of Engineering & Technology, Jamshoro, Sindh, Pakistan.

Abstract- Millions of people around the world are suffering from health issues because of high concentration of fluoride in drinking water. Pakistan is also affected severely by this contaminant; about 21.6 million inhabitants in Pakistan have no access to clean drinking water. A modest quantity of fluoride is significant for the improvement of teeth and bone. In any case, its overabundance substance may make a few infections in human as well animals. Islamkot and Tharparkar reported to have higher concentrations of Fluoride as compared to allowable limit reported in W.H.O, i.e. 1.5ppm. This study involves the removal of Fluoride from ground water. For this purpose, cow bone was synthesized as bone char and used in column study. The analysis was performed by using column study on both synthetic solution and ground water. Fluoride removal efficiency of synthesized bone char was analyzed by studying different parameters like flowrate, Empty bed contact time and initial fluoride concentrations. Fluoride removal efficiency was maximum i.e. 98.2% at flowrate 2.98 ml/min. This material is widely available and was found effective for fluoride removal, bone char water filters can be made to facilitate the people using fluoride contaminated water in this area.
Keywords- Fluoride, groundwater, bone char, adsorption, fluoride removal efficiency.

I. INTRODUCTION

Groundwater is key source of water supply in most rural societies of Pakistan. Unfortunately, groundwater is started to contaminate from time to time with naturally present chemicals. One such naturally occurring toxicant is fluoride [1]. Now a days Fluoride (F) presence in ground-water in has been renowned as one of the severe problem globally [2]. WHO also categorized fluoride as one of the dangerous contaminant of water for human health if it is present in excess amount likewise arsenic and nitrate and arsenic which are responsible for large scale health problems (W.H.O). The existence of fluoride in water is essential for human health if it is under defined limit, which ranges between 1.0-1.5 mg/L. However, if fluoride concentration is above the limits then it could be. Fluoride is necessary for human health when its concentration is 1.0- 1.5 mg/L. However, despite its significance, elevated concentrations of fluoride may result a dangerous conditions for Human health, animal and our environment [3, 4]. Fluoride concentration raising concentration in groundwater results in life threatening risk worldwide. Globally no of people have groundwater sources with elevated concentration of fluoride. The most recent assessments shows that approximately 0.2 billion people, among twenty-five countries of the overall globe are under terrible doom of fluorosis [5]. Greater than 260 million individuals globally drink drinking water with elevated level of fluoride concentrations [6]. Fluoride with small amount of concentration is valuable for human beings as it has good effect on the rate of occurrence in dental cavity, mostly for the children [7]. Differently, water with exceeding level of fluoride causes the different diseases like as brittle bones, Alzheimer syndrome, osteoporosis, cancer, arthritis, brain damage, thyroid disorder and infertility [8]. Fluorosis is a simple indication of high-level fluoride drinking showed by mottling of teeth in slight cases and neurological damage in severe cases and bones embrittlement [9].
Various technologies are available for the removal of fluoride contamination from drinking water including membrane process, filtration, precipitation, coagulation, adsorption methods and ion-exchange methods [10.11]. Most of the available de-fluoridation techniques are very complex which requires skilled labor, and have a high initial cost and maintenance cost and it is technically non-feasible in rural areas. Among those techniques used for defluoridation of water, adsorption is the favorable technique for de-fluoridation at industrial household and community levels in rural areas due to its very low cost, availability and easy to use, easy accessibility, high efficiency, environmental friendly, and no need of operational skill and electric power to run. In adsorption several adsorbents have been tested and applied for the removal of fluoride ions from aqueous solution, such as carbon-based sorbents, agricultural and

industrial wastes. The commercial adsorbents were more effective for fluoride removal from water are activated alumina and bone char [12].

This study involves the removal of Fluoride from ground water. For this purpose, cow bone synthesize as bone char and use in column study. The analysis performs by using column study on both synthetic solution and ground water. Fluoride removal efficiency of synthesize bone char analyze by studying different parameters like flowrate, Empty bed contact time and initial fluoride concentrations.

II.   MATERIALS AND METHODS

I.   COLLECTION OF SAMPLES AND PREPARATION OF ADSORBENT

a. Sample collection

Sample ground water was collected from the wells in Islamkot city, Tharparkar District. Three samples were collected from the depth of 10 to 16 meters of each well as shown in Figure1.
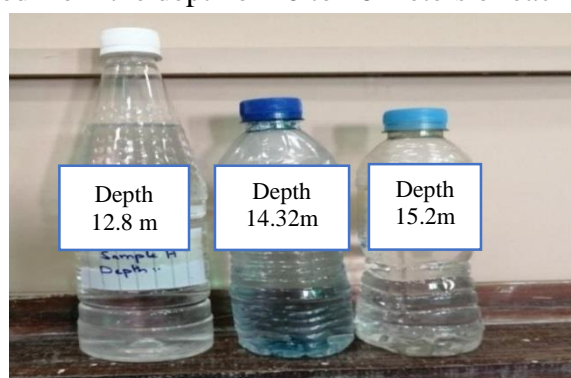
Figure1. Groundwater samples from Islamkot well

a. Bone char preparation

Cow Bones were collected from butcher shop in Hyderabad and then we removed unwanted materials. Firstly we simply washed the Bones with water. Hydrogen peroxide and Sodium Bi-carbonate mixture was used for bone cleaning of unwanted material and for removal of smell. Mixture was applied for One hour; then again bones were washed with water. After washing, bones kept in Sun light for about 15 days for complete drying to further proceed for crushing. Remaining moisture from bones will be removed using a Convective Oven. After removing moisture, the bones are crushed by using Jaw Crusher; this is done in order to provide a greater surface area for purpose of Pyrolysis. The size of Bones fed was average 12 inches and the reduced size obtained was 1-2 inches. The bones were undergone Pyrolysis process. The Pyrolysis process was performed to produce bone char for fluoride removal. This process was done by heating the bones for 2 hours at temperature of 550 ^{0}C in absence of air using closed container. After Pyrolysis the bone char temperature was decreased to ambient temperature and then grinding was performed using pestle and mortar to get average particle size. The bone char was sieved to get average particle size of 0.540mm.

Figure2. Bone char

A.

II.   ADSORPTION STUDIES

a.   *Theoretical Background*

The adsorption study was performed in adsorption column. The water is passed through the length of the column from top to bottom, which provided more contact time, which is needed for fluoride removal. In this study two types of adsorption were performed. First using stock solution and Secondly using Ground Water sample.

a.   *Preparation of Stock Solution*

In order to check the efficiency of synthesized bone char as adsorbent for the removal of fluoride ion, Sodium Fluoride powder in distill water was used for preparation of 5-ppm stock solution. We have taken 1.5 ml from 1000 ppm of stock solution and diluted with 298.5 ml of distilled water to make the 300 ml stock solution of 5 ppm.

Figure 3: (a) measurement of NaF powder (b): Stock Solution

b.   *Column flow experiments*

Fixed bed adsorption column was used in this experimental work. The bed was made by using bone-char synthesized in laboratory. Furthermore, bed was tightly packed, and supported by wool from the bottom of column to prevent the flow of absorbents along with water. Test solutions of 5-ppm concentration were passed through with support of peristaltic pump at the top of the column. Fluoride treated water samples were collected at the bottom of the column in a beaker, and stored in a plastic sample bottle for analysis.

c.   *Column parameters*

For adsorption capacity of column process parameters have great importance. Therefore, various parameters in adsorption column study such as pH, temperature; EBCT (Empty Bed Contact Time), Bed thickness etc. have great importance. However, we have selected some parameters such as flow rate, EBCT, and inlet fluoride concentration.

III. RESULT AND DISCUSSION

1. Characterization of stock solution

a. Effect of flow rate on fluoride removal efficiency:

The table shows that when stock solutions with initial fluoride concentration of 5ppmwere passed at three different flow rates of 2.98, 3.62 and 4.34 ml/mi resulted 98.2, 72.3 and 62.7 % respectively, fluoride removal efficiency. Results showed that as the sample flow rate through the adsorption column increased, the fluoride removal efficiency is decreased. It may be attributed by less contact time between adsorbent

and liquid sample. Similar findings were also reported by [13] for fluoride removal efficiency.

Table1. Summarizes the results of Fluoride removal efficiency at different flow rates.

S. No	Sample Stock	Flow rate	Initial Concentration	Final Concentration	Removal Efficiency
	Solution	(ml/min)	(ppm)	(ppm)	(%)
1.	Sample (A)	2.98	5	0.054	98.2
2.	Sample (B)	3.62	5	1.385	72.3
3.	Sample (C)	4.34	5	1.867	62.7
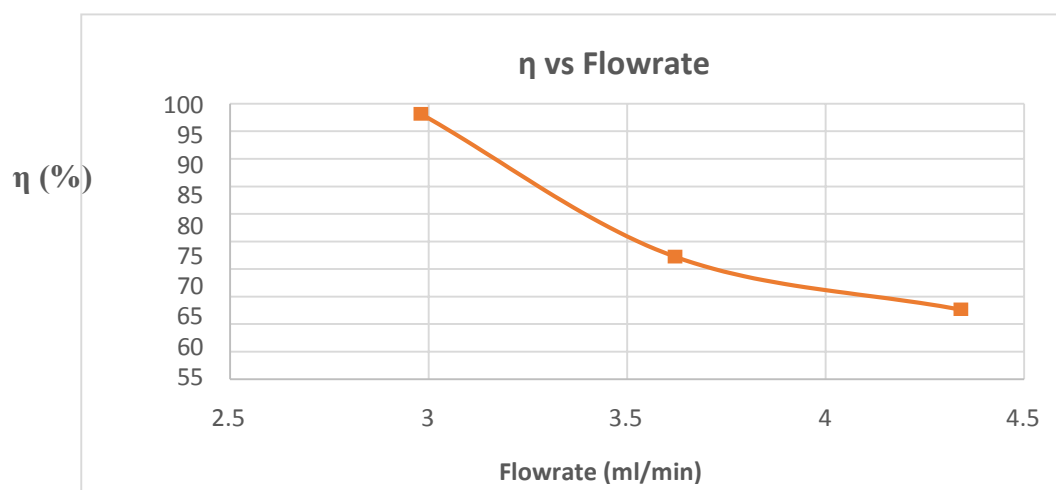
Figure 5: Graphical Representation of Fluoride removal efficiency at different Flowrates

b. Effect on empty bed contact time (EBCT) on removal efficiency:

The table shows that when water sample was passed through empty volume of column i.e. 2.513 ml at flow rates 2.98, 3.62 and 4.34 respectively, the Empty bed contact time was decreased, because increasing flow rates will result in reduction of time sample passes through column.

Table 2. Represents effect of flow rates on EBCT

S.no	Flow rate (ml/min)	Volume of Empty Bed (ml)	EBCT (min)
1.	2.98	2.513	0.84

2.	3.62	2.513	0.694
3.	4.34	2.513	0.579
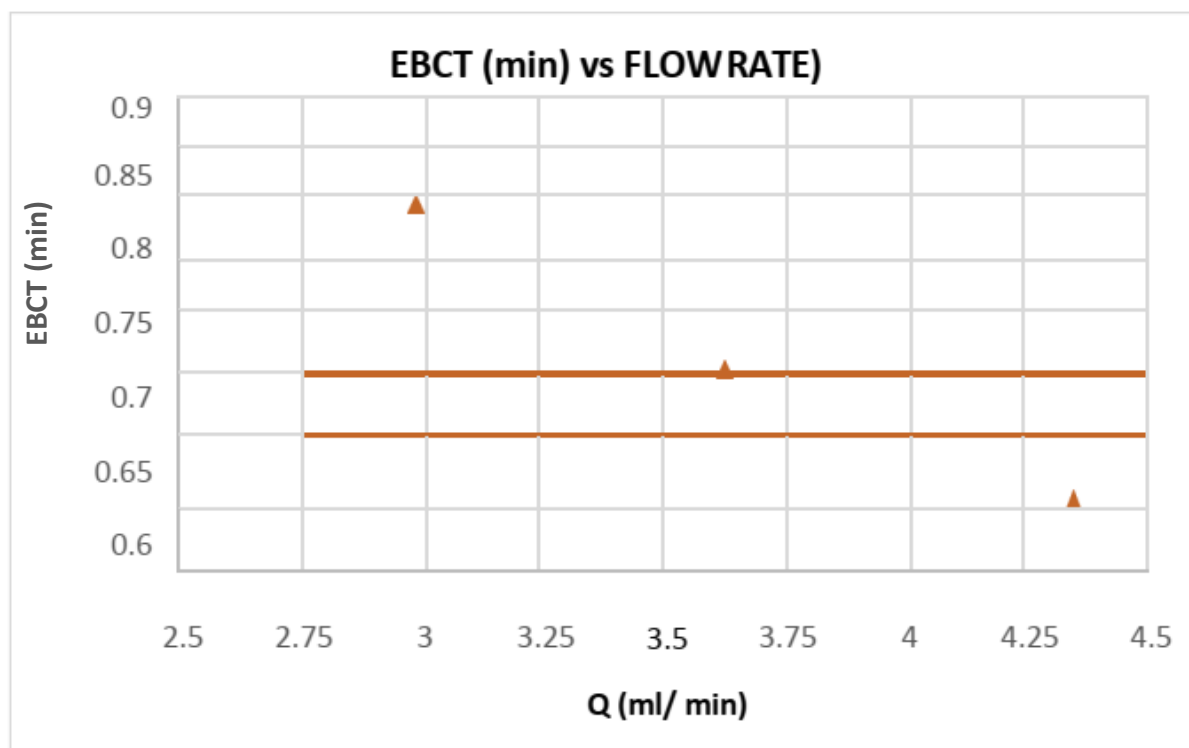
Figure6. Graphical Representation of EBCT at different Flow rates

III.   RESULTS OF FLUORIDE REMOVAL EFFICIENCY FROM GROUND WATER OF ISLAMKOT:

After testing fluoride removal efficiency of Stock Solution, Column Study was performed by optimized parameters for analyzing how much synthesized adsorbent would be effective, in ground water sample, which consists of higher initial concentrations of fluoride. The 3 different Ground Water samples from Islamkot were passed at optimized value of Flow rate (2.98ml/min) and bed height (8cm). The Results obtained from this analysis are shown in Table 4.4.

S. No	Sample Name Initial Name Concentration	Final Concentration	Removal Efficiency
	(ppm)	(ppm)	(%)

1.	Islamkot	6.25	2.30	97
2.	Islamkot	7.82	2.65	96.9
3.	Islamkot	8.09	2.47	95.7

Table 3: Represents effect of initial concentration on fluoride removal efficiency

From results presented in table, it is clear that Fluoride removal efficiency of BC decreased if the initial concentration of sample is increased. Graphical Representation is given in figure 7
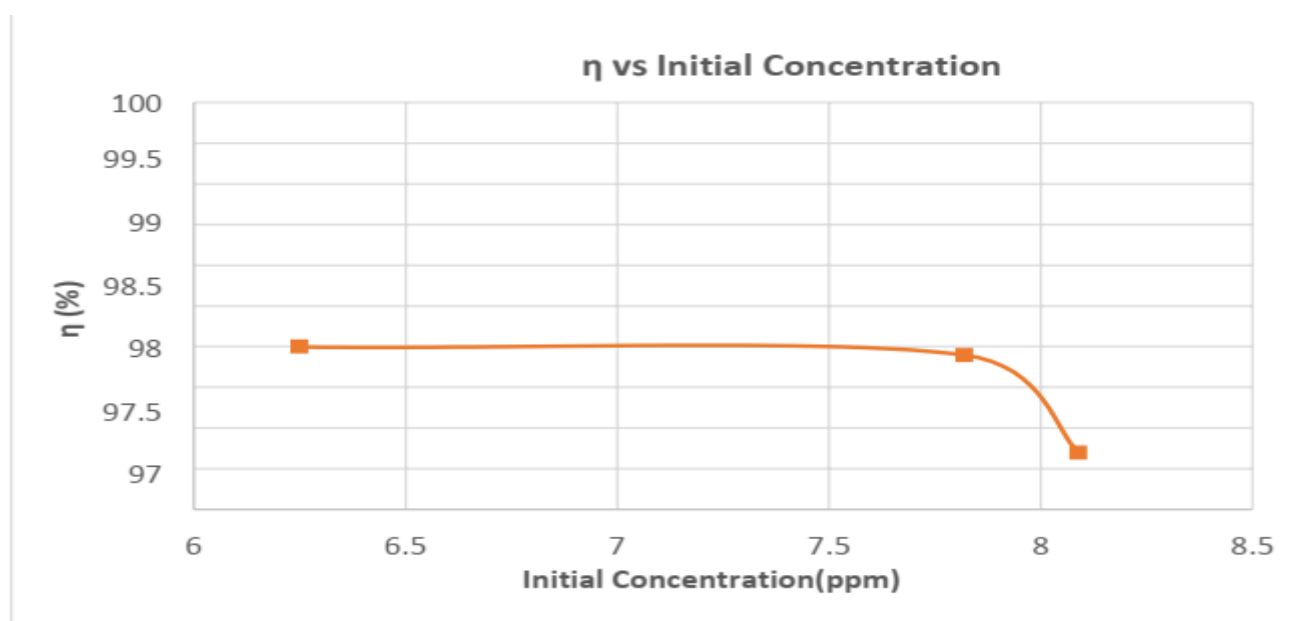
Figure 7: Graphical Representation of Fluoride removal efficiency at different initial concentrations.

1) **Abbreviations and acronyms**

GW: Ground Water, BC: Bone Char, NaF: Sodium Fluoride, ml/l: Milligrams per liter, ppm: Parts per million, EBCT: Empty Bed Contact Time.

2) **Equations**

For preparation of stock solution we have used equation (a) for find the volume of solution.

$$C1V1 = C2V2 \tag{a}$$

$$V1 = \underline{C_2 \times V_2}$$

$$C_1$$

Where, C1 = initial concentration of solution
V1 =initial volume of the solution.
C2 = desired/required concentration of the sample.
V2 = desired volume of sample.

3) Other Recommendations

From this study, it is drawn that bone char can be used as adsorbent because it showed excellent fluoride removal efficiency of ground water samples. More extensive work is required to examine the effectiveness of bone char for removal of fluoride with other contaminations such as arsenic by using a hybrid bed of bone char and other adsorbent materials. The present study can be used in providing potable water filters of bone char, in those areas where people are suffering as of fluoride contaminations.

IV. CONCLUSION

The health concerns associated with the high fluoride concentration in ground water sources were highlighted in this study. Due to the feasibility of bone char as a cheap and effective bio- adsorbent for fluoride removal. The bone char was synthesized from cow bones using pretreatment and pyrolysis at optimum temperature of 550^OC. The prepared bone char was grinded and sieved at average particle size of 0.540 mm. To analyze the effectiveness of synthesized bone char, column study was performed by varying different parameters i.e. Flow rate, bed height, EBCT and initial concentration. The samples for studying fluoride removal efficiency were stock solution and ground water of Islamkot, Tharparkar. Three different flow rates 2.98, 3.62 and 4.34ml/min were used respectively, the maximum fluoride removal efficiency about 98.2% of stock solution was observed at 2.98ml/min. While the efficiency was gradually decreased to from 98.2% to 62.7% at flow rate of 4.34 ml/min.

REFERENCE

[1]. Donkor, E. A.; Buamah, R. and Kwaye-Awuah, B. (2016) Defluoidation of Drinking Water Using Surfactant Modiefied Zeolite. Journal of Science & Technology Vol.36 No.1**,** 15-21.
[2]. Amini, M.; Abbaspour, K.; Berg, M.; Winkel, L.; Hug, S.; Hoehn, E.; Yang, H. and Johnson, C. (2008) Statistical Modeling of Global Geogenic Fluoride Contamination in Ground Water Environmental Science & Technology, 42(10)**,** 3662-3668.
[3]. Mohan, D.; Kumar, S. and Srivastava, A. (2014) Fluoride Removal from Drinking Water Using Magnetic and Nonmagnetic Corn Stover Biochar. Ecological Engineering 73**,** 798-808.
[4]. Avvannavar; Fawll, S. J.; Bailey, K.; Chilton, J.; Dahi, E.; Fewtrell, L. and Magara, Y. (2007) Fluoride in Drinking Water WHO IWA Publishers London.
[5]. Rasool, A.; Farooqi, A.; Xiao, T.; Ali, W.; Noor, S.; Abiola, O.; Ali, S. and Nasim, W. (2017) A Review of Global Outlook on Fluoride Contamination in Groundwater with Prominence on the Pakistan Current Situation. Environmental Geochemical Health.

[6]. Amin, F.; Talpur, F. N.; Balouch, A.; Surhio, M. A. and Bhutto, M. A. (2014) Biosorption of Fluoride from Aqueous Solution by White—Rot Funguspleurotus Eryngii Atcc 90888. Environmental Nanotechnology, Monitoring & Management

[7]. Mahramanlioglu, M.; Kizilcikli, I. and bicer, I. (2002) Adsorption of Fluoride from Aqueous Solution by Acid Treated Spent Bleaching Earth. journal of fluorine chemistry, 115(1), 41-47.

[8]. Harrison, P. T. (2005) Fluorine in Water a Uk Perspective. Journal of fluorine chemistry, 126(11-12), 1448-1456.

[9]. Zhou, Y.; Yu, C. and Shan, Y. (2003) Adsorption of Fluoride from Aqueous Solution on La3+-Impregnated Cross-Linked Gelatin. Separation & Purification technology 36, 89-94.

[10]. Chen L, Zhang K-S, He J-Y, Xu W-H, Huang X-J, Liu J-H (2016) Enhanced fluoride removal from water by sulfate-doped hydroxyapatite hierarchical hollow microspheres. Chem Eng J 285:616–624

[11]. Miretzky P, Cirelli AF (2011) Fluoride removal from water by chitosan derivatives and composites: a review. J Fluor Chem 132:231–240

[12]. Tovar-Gómez R, Moreno-Virgen MR, Dena-Aguilar JA, HernándezMontoya V, Bonilla-Petriciolet A, Montes-Morán MA (2013) Modeling of fixed-bed adsorption of fluoride on bone char using a hybrid neural network approach. Chem Eng J 228:1098–1109

[13]. Ma, W.; Ya, F.; Wang, R. and Zhao, Y. (2008) Fluoride Removal from Drinking Water by Adsorption Using Bone Char as a Biosorbent. International Journal of Environmental Technology and Management, 9, 59-69.

Carwash Wastewater Treatment

Imran ul Haq, Mian [A], Naveed ul Hasan, Syed [B], and Naseer Ahmad Khan [C]

[A, B, C]=*Chemical Engineering, University of Engineering and Technology Peshawar, Pakistan*

*Imran Ul Haq, Mian. [A]engr.miuh@gmail.com, [A]Department of Chemical Engineering University of Engineering and Technology Peshawar, Pakistan.
[B, C] Department of Chemical Engineering, University of Engineering and Technology Peshawar, Pakistan.

Abstract— **The focus of this research work was to treat wastewater from a carwash station and to make it suitable for reuse. Water scarcity is a worldwide issue and Pakistan is among one of the countries facing water shortage problems in most of its cities. Furthermore, carwash stations have emerged as an industry, and particularly speaking about Pakistan, these stations have massively increased in number during the last two decades, thus becoming a major source of consuming fresh water. In this study, wastewater samples from different carwash stations operating in the city of Peshawar were collected and analyzed. The selected samples were treated in a lab scale unit comprising sedimentation and a filtration unit. The filtration unit consisted of layers of gravel, coarse sand, fine sand and organoclay. To remove oil contents from the wastewater, organoclay was used in the filtration unit. It was found that the contaminants in the treated sample such as TSS reduced from 821 mg/l to 98, TDS reduced from 769 to 445, pH increased from 7 to 8, Turbidity reduced from 253 to 2.7, Hardness reduced from 321.6 to 120, alkalinity reduced from 250 to 220, and oil content reduced from 26 to zero. The water sample after treatment was found suitable to be reused for the carwash.**
Keywords—**Low Cost Treatment System, Filtration, Sedimentation, Organoclay, Carwash wastewater.**

I. INTRODUCTION

Water scarcity is a major global concern nowadays. It is estimated that 97% of world water is saltish and only 3% is fresh water available, of which 66% is in glaciers and only 33% is available on surface, underground and some part in air [1]. This limited water is used for drinking, cooking, cleaning, and other domestic usage of 7.8 billion people around the world.   The world population in 2050 is projected to be 10 billion people and there is no other fresh water source available in the world [2]. Statistic shows that 71% of the total world population (4.3 billon people) are living under severe to moderate water scarcity [3]. The number of people facing severe water scarcity for at least 4 to 6 months per year is 1.8 to 2.9 billion. Half a billion people face severe water scarcity all year round. Of those half-billion people, 180 million lives in India, 73 million in Pakistan, 27 million in Egypt, 20 million in Mexico, 20 million in Saudi Arabia, and 18 million in Yemen [4]. The quantity and quality of fresh water required for domestic, irrigation and industrial use has reduced to an alarming level in different parts of the world due to increased population and unprecedented industrial growth [5].

Pakistan is also facing water shortage problems in its different cities including the Capital city, Islamabad [6]. The issue of water scarcity is also recently addressed by the Supreme Court of Pakistan and stressed the need to build dams to save water for our future generations [7]. The need for water conservation at domestic and industrial level is the demand of today. Industries such as paper mills, marble and tiles manufacturing, refineries, fertilizer manufacturing and power plants use large amount of underground water that is drained without treatment or recycling.

Similarly, carwash stations have taken a shape of an industry as these stations have spread in a huge number in different cities of Pakistan [8]. This is due to the increase of production by car manufacturers and annual demand of consumers for cars put huge traffic on roads and car washing facilities [6]. This research work has addressed the need to treat the wastewater from carwash stations and make it suitable for car washing again. In this paper, the results of wastewater treatment have been shown. The wastewater was treated in a lab scale filtration unit.

II. METHODOLOGY

There is no actual data to report number of carwash station in Peshawar, however it is our hypothesis that the number is in thousands[9]. For our experiments we selected random carwash station and collected data based on our requirements. The wastewater samples were collected from ten carwash stations operating in Peshawar city. Each Batch of sample was 27 liters in capacity from each station. The water samples were first analyzed to examine the proportion of contaminants in it. The main contaminant to be removed from wastewater was oil and grease content in it, and this was to be removed by introducing organoclay in filtration unit. After the analysis, the wastewater was treated using an indigenously designed low cost wastewater treatment unit comprising of sedimentation and a filtration unit. Sedimentation was done before filtration to lower the amount of suspended particle and void blockage of filtration unit. Table 3.1 shows the analysis results of carwash stations sample before filtration. While table 3.2 shows the analysis results after filtration. The focus was to pass the wastewater from filtration unit and examine the oil content retention through it when it passes from the layer of organoclay.

2.1 Process Description

Wastewater from carwash station is feed to the sedimentation tank in feed inlet portion for water to retain for at least an hour. From there it was passed on to the designed filtration unit. The filtration unit was 1.2-meter-long consisting of nine layers of solid particle species as a filter media. At the top of the filtration unit a layer of 5cm of stone having 10 mm diameter was present, the purpose of which was to reduce the speed of water falling on filter media below this layer. The second 10cm layer was of gravel having 2mm diameter to retain small sediments from wastewater, then a 10cm third layer of coarse sand particles having 1mm diameter was used for retaining the non-visible particles present in wastewater. The fourth layer of 2cm was of organo-clay/activated clay 500-micron size for oil grease particle removal. The fifth and sixth 10cm layers were of fine sand 125-micron and 250-micron sizes for retaining the upper filter media. In the second last portion gravel having 2mm and 4mm diameter with 10cm layers are placed for holding the filter media and all small particles of filtration unit from entering the water tank. In the last 10mm stone are present for upholding the upper filter media. Collecting tank with the capacity of 33 liters is present just below the filtration unit for collecting the filtered water.

First portion of filtration unit is water retention space having the capacity of 14 liters of water where water is retained for some time while the water passes on from different beds of the filtration unit. Filtration unit is composed of different layers of filter media whose size and layer depths are already described. The filtered water is stored in the water tank fitted just below the filtration unit at a rate of 13.49min/liter. This rate of filtration was meant to change with time because of possible blockage factor of upper most filter media due to small particle in water. Figure 2.1 shows the complete filtration unit that was used for treatment of wastewater and removal of oil/grease content from carwash wastewater using organoclay as new item added to filtration unit.
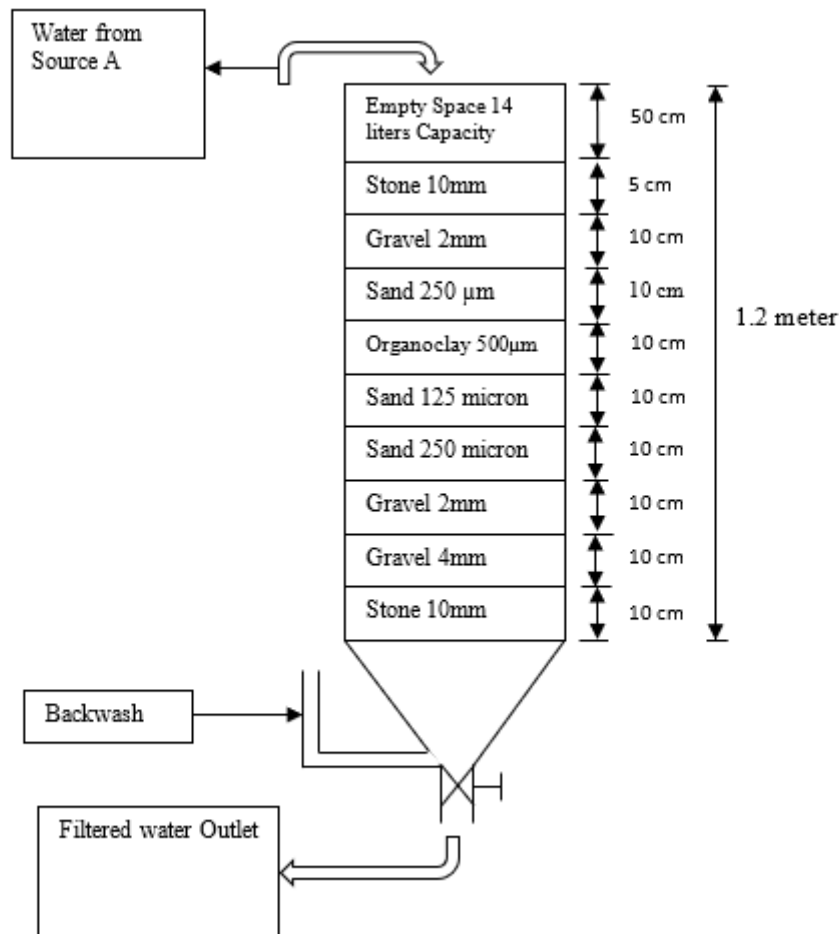
Figure 2.1 Complete Filtration Unit.

III.   RESULTS AND DISCUSSION

The quantity of wastewater collected from each station was 27 liters, 1000 milliliter samples was use for laboratory analysis and remaining was used for filtration purpose. Each sample was compared with the tape water standards. The results obtained are given below in Table 3.1. Where TS stands for Total Solids, TSS stands for Total Suspended Solids, TDS stands for Total Dissolved Solids and its values are given in Parts per millions, PPM. While Hardness, alkalinity and oil content is given in Milligram per liter (mg/l) and Turbidity in Nephelometric turbidity Unit, NTU. If we look at the results of tape water, TS of tape water is 505 ppm, TSS is 61 ppm, TDS is 444 ppm, Turbidity is 0.6 NTU, pH is 7, Hardness is 140.4mg/l, Alkalinity is 210 mg/l And oil Content is water is zero. All the other results are compared to this standard value of tape water in below table.

Table 3.1 Results of wastewater samples at collection points of carwash stations.

S.No	Station Name	TS (ppm)	TSS (ppm)	TDS (ppm)	Turbidity NTU	pH	Hardness (mg/l)	Alkalinity (mg/l)	Oil (mg/l)
1	Shinwari Service Station	1590	821	769	253	7	321.6	250	26
2	Liaqat Motors Services Station	2888	2017	871	1064.8	6	341	1120	18
3	Abaseen Service Station	2667	1967	700	697.97	7	315.6	297.5	20
4	Khan Car Wash Ring Road	888	211	677	907.5	8	192	245	12
5	Smart Car Wash	877	222	655	379	7	170	342	8
6	Gulf Car Wash	2234	1341	893	451	7	159	260	12
7	Muskan Car Wash	2134	1364	770	659	8	320	429	22
8	Shah Service Station	1321	567	754	983	7	259	346	13
9	Qazi Brothers Service Station	965	241	724	347	6	180	532	23
10	Zahid Jamal Car Wash	1200	453	747	756	7	223	317	32
11	Tape Water	505	61	444	0.6	7	140.4	210	0

The results obtained after filtration are given in table 3.2. where if we look at shinwair service station results the Total solids in wastewater reduced from 1590 mg/l to 543mg/l, Total suspended solids reduce from 821mg/l to 98mg/l, Total dissolved solids reduced from 769mg/l to 445mg/l, turbidity reduced from 253 NTU to 2.7 NTU, pH increased from 7 to 8, Hardness reduced from 321.6mg/l to 120mg/l, alkalinity reduced from 250mg/l to 220mg/l, while the oil content reduced from 26mg/l to 0.

Table 3.2 Results of wastewater after filtration process.

S.No	Station Name	TS (ppm)	TSS (ppm)	TDS (ppm)	Turbidity NTU	pH	Hardness (mg/l)	Alkalinity (mg/l)	Oil (mg/l)
1	Shinwari Service Station	543	98	445	2.7	8	120	220	0
2	Liaqat Motrs Services Station	536	87	449	2.1	8	133	231	0
3	Abaseen Service Station	534	80	454	2	9	135	243	0
4	Khan Car Wash Ring Road	545	78	467	1.8	9	140	245	0
5	Smart Car Wash	548	87	461	1.6	8	160	242	0
6	Gulf Car Wash	547	75	472	1.7	8	173	262	0
7	Muskan Car Wash	527	82	445	1.9	8	156	294	0
8	Shah Service Station	553	80	473	1.8	9	145	234	0
9	Qazi Brothers Service Station	518	70	448	1.2	8	153	232	0
10	Zahid Jamal Car Wash	521	72	449	1	9	167	231	0
11	Tape Water	505	61	444	0.6	7	140.4	210	0

IV. CONCLUSION

Analyzing the results show that the TS, TSS and TDS reduced at higher rates while pH slightly changed from 7 to 8, hardness and Alkalinity reduced at slightly lower rates while the oil content was completely removed, this was because of organoclay as filter media in filtration unit. The results obtained are almost the same as standard tape water. Hence the main purpose of our filtration was achieved by removing the oil content from wastewater using the organoclay as our filter media. Previously the oil content was not removed from same type of filtration unit where organoclay was not used as filter media.

As can be seen from the analysis the water will be perfectly safe for washing cars only because the resulted water quality is almost same as tape water. The main factors were turbidity, total suspended solids and oil content which have been reduced up to 98.93%, 88%., 100% respectively. The hardness decreases up to 120th mg/l which is equal to the standard value for tap water and according to WHO Standard the range of hardness is from 20-200 mg/l. Therefore, there will not be a problem in using soap during the car wash. The pH slightly increases but this will not be a problem as it is not to be used for drinking purpose. Since water cannot be recycled for indefinite times so this water must be at most changed with fresh water after 3 days.

If approved and applied to the service stations, it can reduce the water consumption up to great extent. As one of the major problem now a days is the scarcity of fresh water in major cities of Pakistan. Washing the cars with the ground water under such circumstances makes no sense. With the decrease in the consumption of water, more fresh water will be available to the humans rather than to cars. Hence lifeline of underground water table will last for future generations ahead.

If the government is willing to give any policy regarding the use of fresh water then most service stations will adopt this model of recycling the water in order to save fresh underground water as needs of human should be much more respected than needs of cars. Other areas where this recycling system can be proposed is paper making industry, PVC pipes manufacturing units, Tiles making plants, urban sanitation, and water management units.

References

[1]   Ahmad, B., 2011, "Water Management : A Solution to Water Scarcity in Pakistan," **9**(2), pp. 111–125.

[2]   Dillard, H. R., 2019, "Global Food and Nutrition Security: From Challenges to Solutions," Food Security, **11**(1), pp. 249–252.

[3]   M.Mekonnen, M., and Hoekstra, Y. A., 2016, "Four Billion People Facing Severe Water Scarcity," American Association for the Advancement of Science.

[4]   Mekonnen, M. M., and Hoekstra, A. Y., 2016, "Four Billion People Facing Severe Water Scarcity," (February), pp. 1–7.

[5]   Brown, C., 1999, "Water Conservation in the Professional Car Wash Industry," International Carwash Association, pp. 8–15.

[6]   Ahmad, B., 2019, "Water Management: A Solution to Water Scarcity in Pakistan," Journal of Independent Studies and Research-Management, Social Sciences and Economics, **9**(2), pp. 111–125.

[7]   Bhatti, Z. A., Mahmood, Q., Raja, I. A., Malik, A. H., Khan, M. S., and Wu, D., 2011, "Chemical Oxidation of Carwash Industry Wastewater as an Effort to Decrease Water Pollution," Physics and Chemistry of the Earth, **36**(9–11), pp. 465–469.

[8]   Ahmed, M., 2007, "Carwash Water Reclamation in Kuwait," **206**(May 2006), pp. 17–28.

[9]   Naveed, Jamil, Naseer, A. S. O. C. E. U. P., 2019, "A Low-Cost Wastewater Treatment Unit for Reducing the Usage of Fresh Water at Car Wash Stations in Pakistan," Pakistan journal of Science, (1), pp. 57–66.

[10]   Almeida, C. M. V. B., Jr, D. B., Bonilla, S. H., Giannetti, B. F., Ahmed, M., Naseer, E., Zaneti, R., Etchepare, R., Rubio, J., Guilbaud, J., Massé, A., Andrès, Y., Jaouen, P., Ma, K. S., Husain, S., Ferse, S. C. A., Ma, M., Zeng, Z., Liu, J., Savenije, H. H. G., Ahmad, I., Sattar, A., Vlasopoulos, N., Memon, F. A., Butler, D., Murphy, R., Khoso, S., Norton-brandão, D., Scherrenberg, S. M., Lier, J. B. Van, Flotation, D. A., Flotation, D. A., Parker, P. D. F., Csiro, C., Parker, J. B. F., Csiro, C., Parker, A. R. H. T. O., Csiro, C., Parker, T. V. N., Csiro, C., Parker, A. R. H. T. O., Csiro, C., Parker, D. W. S., Csiro, C., Ahmad, B., Zhang, H., Liang, Y., Yan, X., Wang, B., Wang, N., Mushtaq, M., Zaman, K., Irfan, D., Awan, U., Ahmad, J., El-dessouky, H., Mekonnen, M. M., Hoekstra, A. Y., Qureshi, M. E., Hanjra, M. A., Ward, J., Zaneti, R., Etchepare, R., Rubio, J., Sujo-nava, D., Scodari, L. A., Slater, C. S., Dahm, K., Savelski, M. J., Bibi, T., Khan, H., Khan, M. A., Cheema, M. J. M., Li, B., Stenstrom, M. K., Lau, W. J., Ismail, A. F., Firdaus, S., Radcliffe, J. C., Khan, S., Shahnaz, M., Jehan, N., Shah, M. T., Khair, S. M., Mushtaq, S., Culas, R. J., and Hafeez, M., 2013, "Drinking Water Quality and Human Health Risk in Charsadda District , Pakistan," Journal of Environmental Management, **107**(February), pp. 77–87.

[11]   Rehman, S., Din, I., Shahnaz, M., Khan, S., Jehan, N., and Shah, M. T., 2012, "Drinking Water Quality and Human Health Risk in Charsadda District, Pakistan," Journal of Cleaner Production.

Removal of Electrolytes and E.coli from Groundwater through Nanofiltration

Qazi Iqra Shafi [A], Muhammad Younas [B]

[A, B,] *Department of Chemical Engineering, University of Engineering and Technology, Peshawar, Pakistan*

Abstract— **This research experimentally studied the composite nanofiltration membrane and its application for the removal of electrolytes and *E. coli* from groundwater. A novel flat sheet PIP-CSP/TMC nanofiltration membrane was synthesized following the previous published work. The experiments were conducted at a lab-scale on cross-flow membrane and each experimental runs were carried out for 2.5 hrs under different operating parameters ranges: pressure (1-5 bar). The effects of pressure on rejection, recovery and flux were determined. An electrolyte solution of 0.25 wt. % KCl, was passed to test the membrane for pure water flux and solute rejection. Single binary solution shows rejection of K^{+1} (26%), and Cl^{-1} (95.5%), with a pure water flux upto 124 $L.m^{-2}.hr^{-1}$, permeance of 42.8 $L.m^{-2}.h^{-1}.bar^{-1}$ and feed recovery of 67.7%. The model solution of an *E.coli* after passing through membrane gives an e.*coli* rejection (97 %) with pure water flux up to 173 $L.m^{-2}.h^{-1}$, permeance of 45 $L.m^{-2}.h^{-1}.bar^{-1}$ and feed recovery of 67%. This percent of recovery ratio evaluates the antifouling property of membrane.**

Keywords— **electrolytes; e.coli; KCl; treatment of ground water; recovery.**

I. INTRODUCTION

Enlarged amount of water is needed to assist the industrial development and population density [1]. The 2.5% of earth's clean water is jeopardized due to rapid and continual increase in global demand for clean water in industrial, agricultural and domestic sectors [2-3]. WHO estimates that 1.1 billion people lack the availability of clean/drinking water [4]. From a report study of world water crises, by 2030 more than 3.9 billion people will live in "water scarcity" regions [5]. Beside this, groundwater gets contaminated when they pass through different channels. These contaminants have an adverse effect on human health [7]. To overcome the problems of water scarcity and availability of clean drinking water, treatment of mild salinity water resources can provide high quality water [4,6].

NF membranes have been used since long for wastewater treatment. Weng et al. studied the behavior of ESNA NF membrane at 25°C, 3 – 20 bar, 6.4 – 6.6 pH, in a cross flow mode for rejection of anions and cations from ground water [8]. L.Shao et al. used hollow fiber NF membrane and demonstrate rejection of different salts in order of $R(Na_2SO_4) > R(MgSO_4) > R(NaCl) > R(MgCl_2)$ with high resistance of pressure [9]. Jalanni et al. carried out experiments on polyester NF membrane and studied rejection of monovalence ions (NaCl) and divalence ions (Na_2SO_4). Because of electromigration effect and higher valence counter ion, rejection of NaCl is found to be lower than Na_2SO_4 [10]. Micah et al. considered a cross flow TFC-PEG20K NF membrane for desalination of water. He studied that membrane show separation efficiency for NaCl(35.7±3.1%) and Na_2SO_4 (91.1± 1.8%) at 6 bar with higher water flux (81.1±6.4 $L.m^{-2}.hr^{-1}$) [11]. Samee M.A, Harasek.M., Friedl.A., et al. study experimentally the separation of single and complex electrolyte mixtures by using NF(MPF-30) membrane in cross flow mode. From their study, a rejection of divalent SO_4^{-2} ion is from (96-99 %), Mg^{+2} (90-98%), Cl^{-1} (70-95%), and Na^{+1} (52-89%) under the operating pressure of 32 bar and 60°C temperature [12]. Alberto et al. mathematically investigate the function of FO-NF system for the treatment of waste water. The active NF membrane area was 700m². This design achieve water recovery up to 85% by using Na_2SO_4 and $MgCl_2$ as a draw solutes [13].

II. METHODOLOGY

Experiments were conducted at lab scale on membrane operating in a cross flow mode. Model solution of KCl and *E.coli* were prepared having a fixed initial concentration of 0.25 wt.%. all the experiments were conducted in a recirculation mode. The operating pressure ranges from 1-5 bar. Concentration of ions were analyzed using Spectrophotometer while the pathogens were detected using culture method.
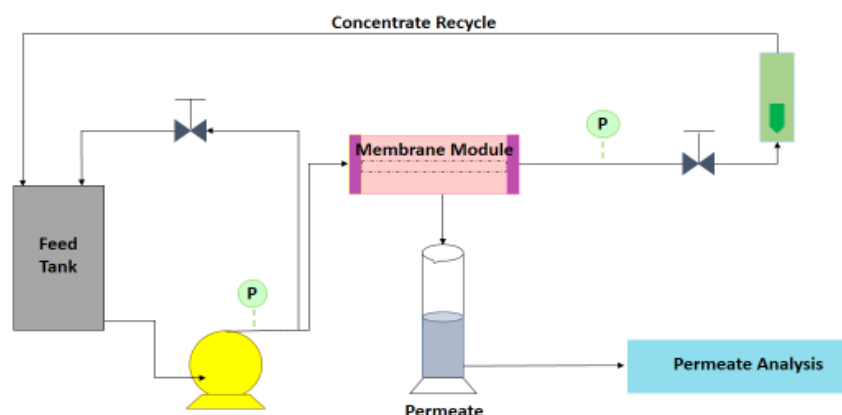
Figure 1: Experimental setup

III. RESULTS AND DISCUSSION

A. Rejection of KCl through nanofiltration membrane

With increase in applied pressure, the rejection and flux increases. The rejection of K^{+1} is found to be very low in range from $8 - 26\%$. From table:1, it can be observed that at pressure ≥ 3, the rejection of K^{+1} show very less change in rejection. Because of counter ion, K^{+1} show less rejection. The monovalent co-ion Cl^{-1} show high rejection from $53 - 95.5\%$ in response to maintain the electro neutrality condition. With an increase in pressure the feed recovery is also increasing which shows that membrane is more efficient to remove electrolytes at high recovery rate without decline in flux. This parameter highlights the antifouling property of membrane. From literature, the reduction or less retention of K^{+1} ion could be due to its less interaction with other ions, due to which it's chemical potential get reduces by electrostatic exclusion. At low salt concentration, the electrostatic exclusion influences the separation ability of membrane [14].

Table:1 Parametric study of KCl through nanofiltration

P_f (bar)	Flux, J (L.m^{-2}.hr^{-1})	R_k (%)	R_{Cl} (%)	Retentate Flow (L.hr^{-1})	Permeance, P ((L.m^{-2}.hr^{-1}.bar^{-1})	Feed Recovery (%)
1	32	8.510	52.5	41.408	50.37215745	29.4
2	51	18.085	71.4	37.77108434	44.6235892	41.4
3	80	24.978	80.57	35.97485542	43.744242	48.8
4	98.2	26.468	89.04	34.52207228	43.80187605	58.1
5	124	26.811	95.47	27.11443374	42.85719767	67.7

B. Rejection of E.coli through nanofiltration membrane

The PIP-NF membrane show high rejection of microbial contaminants from ground water than UF. The water sample containing *e.coli* was passed through NF membrane under the same operating condition as specified for the other experiment. The membrane show 97% rejection of an *e.coli* with a flux of 173.651 L.m^{-2}.h^{-1} and water recovery of 59.5%, as shown table: 2.This membrane shows a high antibacterial characteristics. The concentration of *e.coli* for the membrane permeate and retentate remains unchanged.

Table:2 Parametric study of *E.coli* through nanofiltration

P_f (bar)	Flux, J ($L.m^{-2}.hr^{-1}$)	$R_{E.coli}$ (%)	Retentate Flow ($L.hr^{-1}$)	Permeance, P (($L.m^{-2}.hr^{-1}.bar^{-1}$))	Feed Recovery (%)
1	88.8140	85.0	34.516	44.0	19.4
2	99.4187	88.0	27.104	45.0	27.6
3	128.581	92.0	23.360	45.7	41.4
4	148.465	93.0	22.665	46.0	49.2
5	173.651	97.0	21.902	45.3	59.5

IV. CONCLUSION

The rejection of monovalent K^{+1} is less than all the other ion because it possess a high diffusivity than Cl^{-1} ion. Another reason for the low rejection of K^{+1} ion is because it is counter ion. Membrane show a high rejection for microbial pollutants, but the presence of these contaminants can cause degradation to membrane surface. A proper cleaning process of membrane was adopted after each experimental run of individual samples.

The percent recovery and permeate flux increase with increase in applied pressure. However the flux of all the samples were found to be almost same upto 173.6 $L.m^{-2}.h^{-1}$. With an increase in pressure, the rejection of solute ions increases. The percent recovery offered by novel NF membrane increases from upto 67% of its feed.

V. REFERENCES

[1] N. García-Vaquero, E. Lee, R. Jiménez Castañeda, J. Cho, and J. A. López-Ramírez, "Comparison of drinking water pollutant removal using a nanofiltration pilot plant powered by renewable energy and a conventional treatment facility," *Desalination*, vol. 347, pp. 94–102, Aug. 2014, doi: 10.1016/j.desal.2014.05.036.

[2] B. A. Abdelkader, M. A. Antar, and Z. Khan, "Nanofiltration as a Pretreatment Step in Seawater Desalination: A Review," *Arabian Journal for Science and Engineering*, vol. 43, no. 9. Springer Verlag, pp. 4413–4432, Sep. 01, 2018, doi: 10.1007/s13369-018-3096-3.

[3] M. Raza, F. Hussain, J. Y. Lee, M. B. Shakoor, and K. D. Kwon, "Groundwater status in Pakistan: A review of contamination, health risks, and potential needs," *Crit. Rev. Environ. Sci. Technol.*, vol. 47, no. 18, pp. 1713–1762, 2017, doi: 10.1080/10643389.2017.1400852

[4] W. Ali, W. Ur Rehman, M. Younas, M. I. Ahmad, and S. Gul, "Reverse osmosis as one-step wastewater treatment: A case study on groundwater pollution," *Polish J. Chem. Technol.*, vol. 17, no. 4, pp. 42–48, Dec. 2015, doi: 10.1515/pjct-2015-0067.

[5] M. Zahid, A. Rashid, S. Akram, Z. A. Rehan, and W. Razzaq, "A Comprehensive Review on Polymeric Nano-Composite Membranes for Water Treatment," *J. Membr. Sci. Technol.*, vol. 08, no. 01, pp. 1–20, 2018, doi: 10.4172/2155-9589.1000179.

[6] Z. Wang *et al.*, "Nanoparticle-templated nanofiltration membranes for ultrahigh performance desalination," *Nat. Commun.*, vol. 9, no. 1, Dec. 2018, doi: 10.1038/s41467-018-04467-3

[7] M. Giagnorio, F. Ricceri, and A. Tiraferri, "Desalination of brackish groundwater and reuse of wastewater by forward osmosis coupled with nanofiltration for draw solution recovery," *Water Res.*, vol. 153, pp. 134–143, Apr. 2019, doi: 10.1016/j.watres.2019.01.014.

[8] N. Kasim and A. W. Mohammad, "Potential of nanofiltration membrane in groundwater treatment for drinking water resources," *J. Teknol. (Sciences Eng.*, vol. 65, no. 4, pp. 43–46, 2013, doi: 10.11113/jt.v65.2326.

[9] D. X. Wang, M. Su, Z. Y. Yu, X. L. Wang, M. Ando, and T. Shintani, "Separation performance of a nanofiltration membrane influenced by species and concentration of ions," *Desalination*, vol. 175, no. 2, pp. 219–225, 2005, doi: 10.1016/j.desal.2004.10.009.

[10] L. Shao *et al.*, "Newly developed nanofiltration (NF) composite membranes by interfacial polymerization for Safranin O and Aniline blue removal," *J. Memb. Sci.*, vol. 430, pp. 96–105, 2013, doi: 10.1016/j.memsci.2012.12.005.

[11] N. A. Jalanni, M. N. Abu Seman, and C. K. M. F. Che Ku Yahya, "New Polyester Nanofiltration (NF) Membrane for Humic Acid Removal," *Adv. Mater. Res.*, vol. 1107, pp. 383–388, 2015, doi: 10.4028/www.scientific.net/amr.1107.383.

[12] M. B. M. Y. Ang *et al.*, "Correlating PSf support physicochemical properties with the formation of piperazine-based polyamide and evaluating the resultant nanofiltration membrane performance," *Polymers (Basel).*, vol. 9, no. 10, pp. 1–17, 2017, doi: 10.3390/polym9100505.

[13] Y. Chiao *et al.*, "Membrane Modified by Fast Second Interfacial Polymerization.

[14] A. A. Hussain, M. E. E. Abashar, and I. S. Al-Mutaz, "Effect of Ion Sizes on Separation Characteristics of Nanofiltration Membrane Systems," *J. King Saud Univ. - Eng. Sci.*, vol. 19, no. 1, pp. 1–18, 2006, doi: 10.1016/S1018-3639(18)30844-4.

Utilization of Marble Waste in Clay bricks and SO_2 Treatment

Shehbaz Ahmad *[1] and Muhammad Imran Ahmad [1]

[1] Department of Chemical Engineering, University of Engineering and Technology, Peshawar;
*ashehbaz98@gmail.com

Abstract-Population growth is usually accompanied by growth in infrastructural development, casuing increase in demand for marble products for ornamental purposes such as flooring titles, décor products and kitchen toppings etc. Pakistani marble is known for its quality and availability to fulfill global demands. During the extraction and processing phase of marble ore, marble waste is generated in the form of slurry and aerosols casuing water contamination and air pollution. Hence, a symbiotic approach is needed to be adopted in order to reduce harmful impacts in short and longer time spans. The focus of this research is based on utilization of marble waste as an additive in fired clay bricks and treatment of flue gases (SO_x and NO_x) arising from chimnies as a flue gas. Marble wastes were collected and mixed with clay to study the compressive strength of fired clay bricks. The results revealed that, the uncalcined marble waste can be used as replacement of clay upto 30% and calcined marble waste can be used upto 40%. Marble waste used for treatment of flue gas shows 30-40% reduction in quantity of SO_x. Utilization of marble waste will not only help in control of pollution due to marble waste but will also help in reduction of soil erosion.

Keywords: Waste Marble, Calcination, Erosion, Flue Gas, Fired Clay Bricks, SO_x.

I. Introduction

Pakistan has large deposits of marble in the province of KPK, Balochistan and Sindh. According to Pakistan stone development company there are more than 300 billion tons of marble reserves in Pakistan. KPK is producing approximately 53,000 tons marble monthly [1]. Pakistan is developing country and we are still using old technologies for mining. During mining and processing (Cutting, polishing) 50% marble becomes waste. The waste marble is dumped on site or discharged with waste water. Due to this waste marble, porosity and permeability of agricultural lands are reduced and the alkalinity of soil is increased which affects fertility of agricultural lands [2].The uneven sized marble is dumped on site. Dust particles of dumped marble slowly spread out and are causing air borne diseases in nearby areas [3]. Marble slurry from processing plants is contaminating ground water reservoirs and is causing water borne diseases in nearby areas [1]. In Pakistan old kilns are used for brick manufacturing which is one of the most environmentally degrading processes. A huge amount of CO_2, SO_x and NO_x is released into the environment [4, 5]. Thus the marble dust waste needs to be utilized as an alternative material in preparation of bricks because this is economical and abundantly available locally. The objective of this study was to evaluate different properties of bricks and to determine the optimum replacement level of marble dust available locally. Marble waste utilization as replacement of clay in fired clay bricks is an economical solution to marble waste and soil erosion. In addition marble waste will reduce sulphur in flue gases from brick processing units (Kilns).

II.   Materials and Method

Clay and marble waste used for brick preparation was collected from brick kilns and marble processing units in Peshawar respectively. Composition of raw material was determined using X-ray fluorescence (XRF) and Energy-dispersive X-ray *spectroscopy. Chemical composition of marble waste and clay is shown in Table 1 and Table 2 respectively.* . Clay and marble waste was mixed until workable consistency was achieved. Specimens were dried in sun for 48hrs. After drying specimens were burned in kiln in three stages, 200-300^0 C followed by 500-800^0 C and finally 800-1100^0 C. Four tests were performed to find the properties of final fired clay bricks. Compressive strength was found by applying load with respect to brick area [6-9].

III.   Results and Discussion

i. CHEMICAL COMPOSITION OF RAW MATERIAL

It may be observed from Table 1 that Ca in marble waste is 43% and Mg is less than 2%. This shows that marble was rich in Ca and hence was calcite type. Table 2 shows composition of clay used for brick making. According to composition Si in clay is more than 20% (SiO_2 47%), hence making it feasible for fired clay bricks. Different percentages (10-40%) of marble wastes were used in clay bricks.

Table1 elemental composition (%) of Marble waste

Marble Waste Composition	C	O	Mg	Si	Ca	Fe	Sr	Cu	Ni
	9.61	42	0.66	0.34	47.38	0.331	0.076	0.060	0.048

Table2 Elemental composition (%) of Clay

	C	O	Na	Mg	Al	Si	K	Ca	Ti	Fe
Clay Composition	6.93	44.06	0.46	1.66	6.72	21.52	2.41	9.68	0.61	5.95

ii. COMPRESSIVE STRENGTH

It may be observed from Figure 1(a, b) that there is decrease in compressive strength of bricks with increase in marble waste proportion. The decrease in value is between 30 to 70% if compared to standard brick. The reason for decrease in compressive strength is increase in porosity of bricks with increase in proportion of marble waste.

(a)   (b)
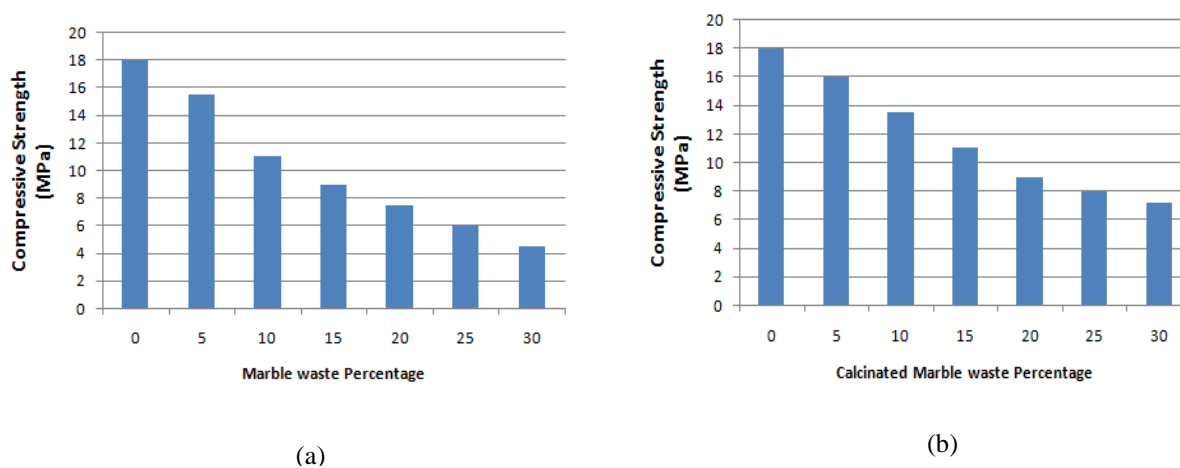
Figure 1 Effect of (a) marble waste and (b) calcined marble waste on compressive strength of clay bricks

iii. DESULPHURIZATION

There is decrease in value of SO_2 in flue gas after treatment with marble waste. Marble waste used for the desulphurizaton of flue gas shows 30-40% reduction in the SO_2 value. The reason for decrease in sulphur dioxide concentration is the reaction between calcium carbonate and sulphur dioxide.

$$CaCO_3(s) + SO_2(g) + \frac{1}{2}O_2(g) \rightleftharpoons CaSO_4(s) + CO_2(g)$$
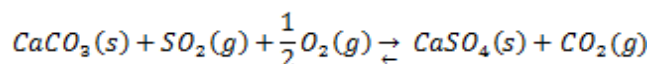
IV. Conclusions

According to studies and tests carried out it is found that compressive strength of brick decreases with addition of marble waste to clay. The decrease in strength is due to increase in porosity of clay bricks.The decrease in strength of clay bricks is less when calcinated marble waste is used as compared to uncalcinated marble waste. The reason for increase in strength is due to decrease in porosity. During calcinations CO_2 is removed from $CaCO_3$. As calcinatination has already taken place so during brick firing process very limited calcination takes place. Due to limited calcination porosity of brick doesnot increase as much as when uncalcinated waste was used. Flue gases from brick kiln can be used for calcination of marble waste. According to tests performed there is 20% heat recovery from flue gases and 40-50% reduction in SO_2. Calcinated marble waste in clay bricks is an economical solution to marble waste utilization, soil erosion and desulphurization of flue gases. The bricks can be used in areas where high strength is not required. The individual brick strength must be 7Mpa according to Turkish and corresponding European Standards. The calcinated marble waste upto 30% satisfies requirement of compressive strength.

References

1. Z. Khan, M. Umar, S. Khan, A. Ali, (2017). Utilization of marble dust in fired clay bricks. Journal of Environmental Monitoring.
2. Hisham Hussein, A. (2016). Properties of Fired Clay Bricks Mixed with Waste Glass.
3. Atilla, E., Bahri, E., & Hakan, C., (2019). Utilization of Marble and Boron Waste in Brick Products.
4. Tarun Naik and Giacomo Moriconi, Environmental-friendly durable concrete made with recycled materials for sustainable concrete construction, University of Wisconsin Milwaukee, 2006.
5. Abrar Awol, Using marble waste powder in cement and concrete production, M. Sc Thesis, Addis Ababa University School of Graduate Studies, March 2011.
6. ASTM C326-09. (2014). Standard Test Method for Drying and Firing Shrinkages of Ceramic Whiteware Clays.
7. ASTM Book of Standards, USA. ASTM C373-88. (2006). Standard Test Method for Water Absorption, Bulk Density, Apparent Porosity, and Apparent Specific Gravity of Fired Whiteware Products, Ceramic Tiles, and Glass Tiles.ASTM Book of Standards, USA.
8. ASTM C62-04. (2004). Standard Specification for Building Brick (Solid Masonry Units Made From Clay or Shale). ASTM Book of Standards, USA.
9. ASTM C67-03. (2003). Standard Test Methods for Sampling and Testing Brick and Structural Clay Tile. ASTM Book of Standards, USA.

Technical Session 2-B (Google meet/Zoom)
Wastewater Treatment and waste minimization

Session Chair: **Dr. Muhammad Zaman**
Session Co-Chair: **Dr. Irshad Ali**

Hamin Jaafar Mohammed *(Soran University-Kurdistan region-Iraq)*	Produced Water Treatment through an Integrated System; A Case Study
Ummar Khitab *(Dept. of Chem Eng., UET Peshawar)*	Boiler Feed Water Treatment Using Green Corrosion Inhibiter: An Alternative Approach
Muhammad Farhan *(Dept. of Chem Eng., UET Peshawar)*	A case study of commercial utilization of waste marble powder in conventional low cost concrete blocks.
Aizaz Ali Farman *(Dept. of Chem Eng., UET Peshawar)*	Investigation of reverse solute flux of binary and ternary draw solutions in forward osmosis

Produced Water Treatment through an Integrated System; A Case Study

Ihsan Ur Rahman [A], Hamin Jaafar Mohammed[B]

[A] *MS Research Scholar, Thermal System Engineering, U.S.-Pakistan Center for Advanced Studies in Energy (USPCAS-E), University of Engineering and Technology Peshawar, KPK, Pakistan*
(Email: ihsanrahman.uspcase@uetpeshawar.edu.pk)
[B] *MS Research Scholar, Department of Chemical Engineering, Soran University, Erbil Kurdistan region –Iraq*
(E-mail: hamin.mohammed@cheme.soran.edu.iq)

Abstract— **Amount of produced water generation is growing day by day due to recent advancements in oil and gas drilling and production techniques. At the same time world is suffering from water crisis. To incumbent the situation, purifying produced water is a better option to be used to fulfill the gap. As Majority of treatment plants are running with high operating/capital cost or producing low quality of water. The aim of current work is to take a step forward in purifying produced water by a cost effective operation process design. For this case study the detail of produced water constituents was obtained from a local crude oil Extraction Company in Pakistan. The separation processes were used in combination i.e. sedimentation process for macro particles removal, hydro cyclone for oil particles separation, electrocoagulation unit for metal particles removal and reverse osmosis unit for removal of salinity. The mass balance and energy balance calculations were also determined for the treatment of 22657 Kg/hour (3000 bbl/day) of produced water. The results are shown, the purified water was 18703.312 Kg/hour out of 22657 Kg/hour (3000 bbl/day) of produced water. The overall process energy consumed was 46.667 kW. Detailed cost analysis was conducted, the operational cost $80,148.7 and capital cost was $288,615. On the basis of $0.0014 per liter of purified water the total annual income was $179,156 with a payback period of less than 2 years.**

Keywords — **Electrocoagulation, Produced water, Purification, Sedimentation, Separation process.**

I. INTRODUCTION

Water shortages are experienced in many regions of the world and will be a major global consequence by 2025[1], [2]. As the surface water is only 1.5% of the total fresh water [3]. In other hand Produced water (PW) is the largest wastewater source by volume generated from oil and gas fields, around 60 % of produced water worldwide [4],[5],[6], close to 250 million barrels per day globally [7]. Hence putting forward a cost-effective solution for PW is vital to the sustainable exploitation of oil resources [8], [9]. It is estimated that by 2030, roughly a trillion dollars would be needed for the oil production, and a major part of this capital would be spent on PW treatment [10]. Despite that PW has characteristics that are the chemical and physical properties of it, and they affected by the geological location, life time of reservoir etc. [11],[12]. Produced water includes: dissolved organic compounds [13],[14], dispersed organic compounds [15], dissolved minerals [16], chemicals Solids, and dissolved gases [17]. By having a highly toxic, high salinity and containing naturally radioactive components hence the PW will be particular environmental concern [18]. At last discharge of such contaminated water, causes immense destruction to the aquatic environment [19].

The researchers are now trying to purify this produced water to become a potential resource rather than a waste outcome, moreover to meet produced water management under discharge regulations i.e. injection of produced water for Enhanced Oil Recovery (EOR) and consuming it in beneficial purposes such as irrigation [20], rangeland restoration, cattle and animal consumption, and drinkable water. As a solution the produced water will applied through an integrated treatment process considering cost effective process and high quality product plant design.

As demonstrated in [2], [21], [22] several methods are found in literature for the purification of PW, there are the numerous technologies exist for treating industrial wastewater. These technologies range from

simple treatment in a settling pond to a complex system of advanced technologies requiring sophisticated equipment and skilled operators [23] i.e. chemical operation, Oxidation and Chemical precipitation [24], electrochemical process, Photo-catalytic treatment [25], and Treatment with room temperature ionic liquids [26]. In some cases [23], [27], [2] for primary units of the treatment process the system of Coagulation and Flocculation were used, in which the suspended solids and colloidal particles could be removed. Merely this method due to its ineffectiveness for dissolved components and the increased concentration of metals in the sludge formed this method isn't always practicable and economical. Regarding to [27] stated that a multi-stage adsorption and separation system was developed to recover dispersed oil droplets in water, whose size is greater than 2 microns, with efficiency 85%. Also Cyclones mentioned in cases [28] for the same purpose unit but it's with low efficiency 50-70%. For metal removing unit, Sand filters were used with removal efficiency 90% [23] and what making this Process difficult to be applied, is it's requires series of pre-treatment steps such as pH adjustment, an aeration unit and a solid separation unit. Researcher interested toward finding the proper technology or combination of technologies adequate to treat a particular wastewater to meet federal and local requirements and yet still be cost-effective can be a challenging task.

In this case study an integrated system is designed which depends on technical, environmental, economic, and field-specific considerations. As horizontal Sedimentation tank type is preferred which do not need any pre chemical units, aiming to low plant capital cost with effective settling velocity, in contract with previous plants using chemicals (coagulants) that will cause increasing amount of impurities in the final product water (low quality) [24]. Afterwards the de-oiling hydro cyclone is being used. Due to its discharge levels can be below 10ppm, low pressure operation, high erosion resistance, and High capacity designs. Then a novel separation technique that is Electrocoagulation unit is used for the purpose of effective removing operation of those undesired components with lower capital and operation cost, compact in size, generally no chemical addition, low maintenance, instantaneous treatment, easy operation and high automation degree and at last treat multiple contaminants at a time In other hand it benefits the next unit which is reverse osmosis unit as a pre-treatment for its input. Finally desalination has been done through reverse osmosis membrane to get product of purified water.

II. METHODOLOGY

A. Process selection (flow chart),

The process flow diagram for this study integrated system is shown in the fig. 1. includes Sedimentation technique, which is an energy efficient methodology to remove the macro particles from the main stream of the produced water. Afterwards hydro cyclone is used to remove the oil particles from the coming stream from sedimentation tank. Hydro cyclone has some in built features i.e. exceptional removal efficiency of 99% and bulk oil removal -up to 20% free oil, and compact in size with no moving parts. From hydro cyclone the main streams further enters into electrocoagulation unit for the removal of metallic or inorganic particles including remaining oil particles, complex organics, pesticides and negatively charged salts. At last the main stream (having salts and negligible amount of other constituents) is then treated in reverse osmosis unit which works on the basis of pressure difference (ΔP) to remove the salinity. For RO, polyamide synthetic membrane in spiral wound configuration is used because it is robust and has high mechanical integrity. Considering the limitations imposed by the local factors.
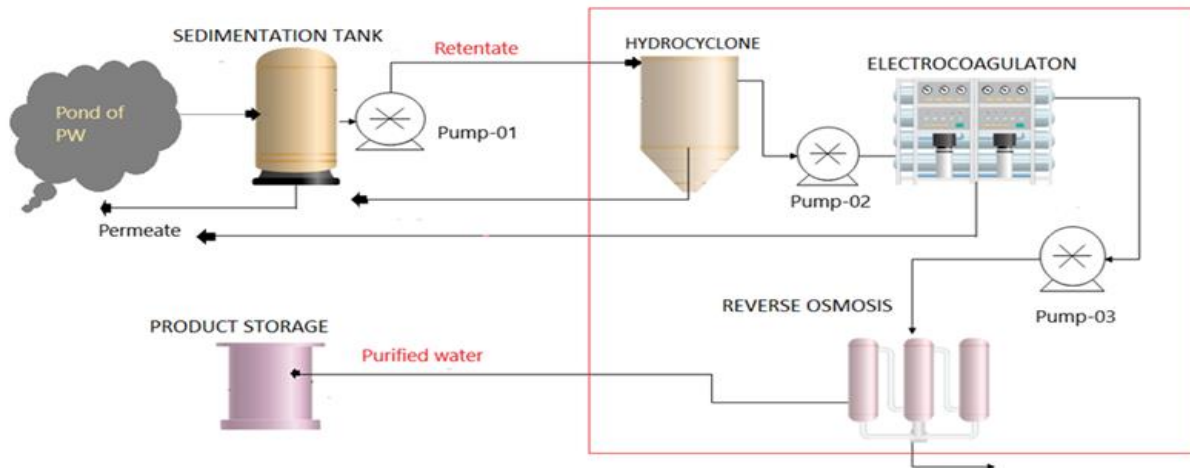
Fig. 1. Overall process flow diagram for produced water purification

B. Process Design

The first step for designing is estimating streams flow rate, each permeate (waste product) and retentate (main stream which is entering into next equipment) and energy consumption for equipment's through the plant using material and energy balance calculations. The constituents data that is present in the produced water provided by the local oil extraction company in Pakistan is shown in table 1 on the basis the produced water generated are 3000 bbl/day having density of 1140 kg/m^3 ($m°$ in = 22657 kg/hr).

TABLE I: MASS PERCENTAGE OF CONSTITUENTS IN REFERENCE TO TOTAL PW

Stream. No	Group 1	Percentage of mass (%) of total produced water Group
01	Macro Particles	3
02	Oil Particles (>5µm)	8.4
05	organic and Inorganics contaminants	5.1
07	Salt Particles	2.1

The important points considered during mass balance are the process is continuous, there is no chemical reaction involved, each equipment are working on its highest separation efficiency and at last the process is carried out at normal environmental conditions. The material balance was calculated by using (1), [29] :-

$$m° \ in + m° \ gen - m° \ out - m° \ con = m° \ acc \qquad (3)$$

Where $m°$ in is mass flowrate input into the each step process, $m°$ gen is the mass flowrate generated during each step, $m°$ out is mass flowrate going out of the system, $m°$ con mass flow rate that is consumed through each equipment and at last mass flow rate accumulated ($m°$ acc) in each step. By considering the explanation above equation (1) becomes

$$m° \ in - m° \ out \ = \ 0 \qquad (4)$$

As in each step there are two out flows 1st is retentate ($m°$ out 1) and 2nd one is permeate ($m°$ out 2), to find out these two we will use data from table 1.

$$Permeate \ (m° \ out \ 2) = Percentage \ of \ mass * m° \ in \qquad (5)$$

$$Retentate \ (m° \ out \ 1) = m° \ in - permeate \ (m° \ out \ 2) \qquad (6)$$

By utilizing all 4 equations the overall material balance is shown in the figure 2, the purified water is 18704 kg/hr. While all permeates are presented at each step.
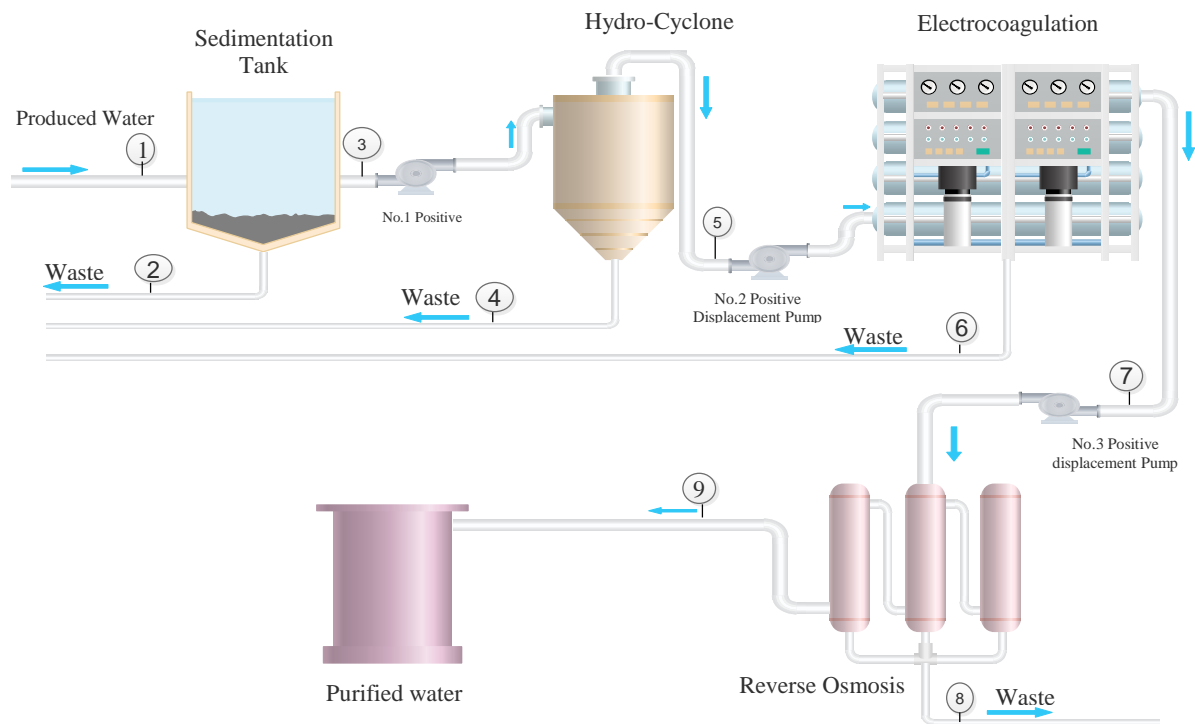
Line.No	1	2	3	4	5	6	7	8	9
Stream Component	Produced water	Wastes	Retentate	Wastes	Retentate	permeate	Retentate	wastes	Purified Water
Flow Rates (Kg/hr)	22657	679.71	21977.29	1846.0923	20131.189	1026.69108	19104.51	401.1946	18703.31202

Fig. 2. Overall material balance calculations

Energy Balance concerned with energy changes and energy flow in a chemical process. The general energy balance equation for a process is: -

Energy input +Energy generation= Energy output + Energy accumulation + (7)
Energy consumption

Here in this project energy required is for Pumps, Hydro cyclone and Electrocoagulation Unit. When there is no generation and accumulation of energy, so the above equation reduces to (7), for calculating each and every equipment energy balance calculation:

Energy in = Total Energy consumption (8)

First, the energy balance for each three pumps through the flow diagram, have been calculated by utilizing Bernoulli equation (8) [31]:

$$\Delta u_2 / 2gc + g\Delta z / gc + \Delta p / \rho + W = 0 \qquad (9)$$

Table 2 presents the result of energy consumption of pumps regarding to (7) and (8).

TABLE I<small>I</small>: ENERGY CONSUMPTION OF PUMPS

Pump	01	02	03
Energy required(kW)	3	3	5

Energy consumed by hydro cyclone for the duty of 3000 bbl/day of produced water = 7 kW
The power consumed by the Electrocoagulation unit is calculated by (9), [32]:-

$$P = M \; x \; N \; x \; I \; x \; Uc \qquad (10)$$

The result of power consumed using above equation is 28.666 kW. Hence finally the overall energy balance calculated by (7) and (11):-

> *Energy input = Energy consumed by pumps + Energy consumed by EC unit*   (11)
> *+ Energy consumed by Hydrocyclone*

Energy input = 3 kW + 3 kW + 5 kW + 7 kW + 28.666 kW = 46.666 kW

In this project three main process equipment's have been choose to evaluate design calculations, which are:- Sedimentation tank, Designing of RO membrane area, Designing of EC unit reactor and Designing of storage/sedimentation tank. First, As per the theory of sedimentation the settlement of a particle depend upon the velocity of flow[23] , the settling velocity of a spherical particle is expressed by Stoke's law [19]and calculated by using (11) :-

$$V_s = \frac{1}{18} \frac{g}{\upsilon} (SG_s - SG_F) * d^2 \qquad (12)$$

Where, V_s is the kinematic viscosity of fluid (m^2/s) , SG_s is the specific gravity of particle=1.5, SG_f is the specific gravity of fluid=1, and d = diameter of the particle= $5 * 10^{-5}$ m. The results analyzed by assuming data from [33] was $vs = 3.812 * 10^{-4} \ m/s$.

For designing of RO membrane, the area for salt rejection was calculated by (12) [34]):

$$\text{Area} = \frac{Feed\ Flow\ Rate}{Permeate\ Flux} \qquad (13)$$

When Feed rate is 3000 bbl/day= 476.962 m^3/day, and using (17) Permeate flux J_w (m/s) was estimated by [18]:

$$J_w = A_w (\Delta P - \Delta \pi) \qquad (14)$$

When, J_w is the permeate flux; A_w Permeability coefficient [35]; ΔP is Trans-membrane pressure difference; and $\Delta \pi$ is the osmotic pressure difference [36]. Hence the result is : -

$Jw = 0.043$ m^3 / (m^2.day.atm) * (61.3atm − 52atm) = 0.3999 m^3/m^2.day

Then

$$\text{Area} = \frac{476.962 \ m3/day}{0.3999 \ m3/m2.day} = 1192.703 \ m^2$$

For Electrocoagulation reactor Designing, the basis of calculations is treatment of 20131.198 Kg/hr = 141,192 m^3/year (8000 hours per year), produced water pre-treated through sedimentation and hydro cyclone, and assuming at Low Pressure, Continuous flow rate and PH from 6.5 to 7.5. The stream processing a minimal amount of dissolved iron estimated was 4.35 kg/hr and calculated by using (14) [37]:-

$$W = \frac{j * t * M}{n * F} \qquad (15)$$

when W is the mass of electrode material dissolved (kg/hr), j=200 the current density (Amperes per cm^2), t=75 sec; M=56 kg/kmol the relative molar mass of the electrode concerned, (n) the number of electrons in oxidation reaction, F the Faraday's constant, F=96,485 Coulombs per mole.

The current I flowing in a single cell (with a cathode and an anode) used for the production of iron ions by anodic dissolution was estimated by using (15) [38]:-

$$I = \frac{Z_{fer} * F * m_{fer}}{Mfer * \Phi} \qquad (16)$$

With Z_{fer} the number of electrons involved, F the Faraday number, Mfer the atomic weight of iron, Φ the columbic efficiency, m_{fer} the mass of dissolved iron. The application of relation leads to an extremely high current value 5265 A, it is not feasible to consider a single cell. We calculated the voltage of a cell by using (16) [39]:-

$$Uc=0.86+ei/k+0.20Ln \qquad (17)$$

When e is the electrode gap, set at 3 mm, i the current density in A m^{-2}, Ln logarithmic an the electrical conductivity of the effluent to be treated, here equal to 2 mS cm^{-1}. Elementary voltage Uc is estimated at 5.42 V.

The electric power consumed by the electrochemical installation regarding to equation 9 is approximately 28.667 kilowatts, Where M=20, N=50, given the hourly flow of effluent to be treated, this power corresponds to energy about P= 2.8 kWh m^{-3}.

Designing of storage /sedimentation tank there is Cylindrical tank with flat top and bottom, which Made from stainless steel, Working stress factor = 19580 psi = 1331.97 atm, Joint efficiency = 1, Density of water = 997 kg/m3 and its V = 20 m³. Hence the design calculations are showed in table 3:

TABLE III: STORAGE TANK PARAMETERS

Parameter	Volume (m³)	Inside diameter (m)	Height (m)	Pressure (atm)	Pabsolute (atm)	Thickness (m)	Outside diameter(m)
Equation	3	$(4 \times V/3\pi)$	D*3	$\rho.g.H$	$P_{atm} + P$	$\dfrac{P_{abs} \times D_i/2f_j - P_{abs}}{}$	$D_i + 2t$
Value	5.1	2.83	8.43	0.81	1.81	0.00191	2.81382

C. Instrumentation and process control

Control systems are used to maintain process conditions at their desired values by manipulating certain process variables to adjust the variables of interest [40]. In this case study the Control Process for the Overall process flow diagram of produced water purification is modified in for Figure 3.

is concerned. As For sedimentation unit, the parameter which is considered to be controlled is Level by low and high level control valves. Hydro-Cyclone temperature is controlled by sensors that can be connected to a temperature controller and Pressure control valves with high and low level control valves, as results in density parameter control also. For Electrocoagulation and Reverse osmosis Temperature, Pressure, and PH parameters are controlled.
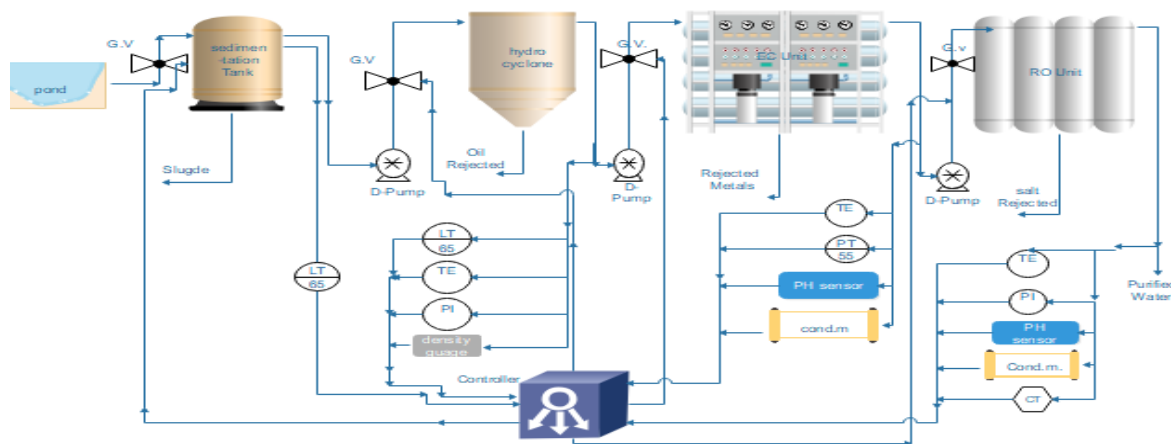
Fig. 3. Overall instrumentation diagrams

D. Process Economics

Process economics have three basic roles in process design: (i) Evaluation of design options: costs are required to evaluate process design options. (ii)Process optimization: some process variables have a major influence on the decision making in the development of the flow sheet and the overall profitability of the process. Optimization of these variables is necessary. (iii)Overall project profitability: the economics of the overall process should be evaluated at different stages during the design to access whether the project is economically viable.

There is two types of Cost estimation: Fixed and Operational Cost estimation, which the evaluations for equipment's in produced water purification process have been calculated and summarized in table 4 when the Fixed Cost For EC Unit is calculated by (17)[42] :

$$CF = \sum_i [(Fm.Fp.Ft)(1 + Fpip)]iCE, if + (Fer + Finst + Felect + \qquad (18)$$
$$Futil + Fos + Fsp + Fdec + Fcont + Fws) \sum_i CE, i$$

For calculating operating cost different types of equation were studied as well it includes the maintenance cost.

TABLE IV: COST ANALYSIS OF OVERALL PROJECT

Stream.No	Equipment name	Company equipment cost (CE) ($)	Capital cost/fixed cost (CF) ($)	Operating cost ($)/day
1	Sedimentation	1100	1100	
2	Hydro cyclone	14000	72380	20.16
3	Electrocoagulation	5500	28435	167
4	Reverse-Osmosis	120737+53000	120737+53000	47.6
5	Pump-01	136	788.8	8.64
6	Pump-02	136	788.8	8.64
7	Pump-03	250	1450	14.5

When the results of calculation estimated as follow:-

Total Capital Cost =$288,615

Total Operational Cost =$80,148.7

Total investment for first year =$368,763

Total annual income (325days, basis $0.0014 per liter of purified water) =$179,156

Simple Payback period = 2 Year

The breakthrough point can be seen from figure 6 which is less than 2 years a positive sign of carrying out this significant project.
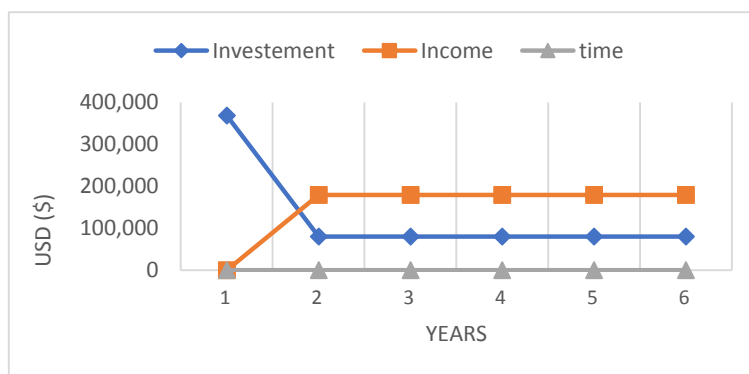
Fig.4. Breakthrough point for the overall project cost analysis

IV. CONCLUSION

As the world is going through water crisis, treatment of produced water can greatly help to counter control the current situation of drinkable water shortage and will also reduce the increasing water pollution. Treated produced water can be a saleable commodity which will greatly improve the economics of oil and gas extractions companies. Produced water treatment by integrated process was investigated in this current study. It is demonstrated that the integrated system of different purification techniques can efficiently remove particles from produced water. The benefits of this integrated system are higher permeate quality and flux, high rejection rates and no chemical cleaning needs. Water purified through

this process was 2477 bbl/day out of 3000 bbl/day. Total investment for the first year is $368,763 for both fixed and operational cost. While considering a very low base for selling the purified water $0.0014 per liter of purified water even not considering other raw permeates for selling, the annual income is $179,156. The calculated simple payback period is 2 years. The breakthrough points is find out which is less than two years a positive feedback at last for the conducted project.

ACKNOWLEDGMENT

V.   REFERENCES

[1]   Anon.(2017). "U.S. Municipal Wastewater...Where Is It Headed?" Empowering Pumps and Equipment. Retrieved October 31, 2020 .

[2]   C. C. Lee. *Water and Wastewater Calculations Manual*. McGraw-Hill Companies, Inc, 2007.pp.7.

[3]   R. C. Gaur. *Basic Environmental Engineering*. New Age International Pvt Ltd Publishers, 2009. *Pp.13.*

[4]   U.S. EPA. 2020 .*Summary of Input on Oil and Gas Extraction Wastewater Management Practices Under the Clean Water Act*. U.S. Environmental Protection Agency, Washington, DC, EPA 821-S19-001.pp.7

[5]   P. Ekins, R. Vanner, J. Firebrace, *Zero emissions of oil in water from offshore oil and gas installations: economic and environmental implications*, J. Clean. Prod. 15 (2007) 1302–1315.

[6]   J.K.Otton, *Environmental Aspects of Produced-water Salt Releases in Onshore and Coastal Petroleum-producing Areas of the Conterminous*, 2006.

[7]   B. Dal Ferro, M. Smith, Global Onshore and Offshore Water Production, http://www.touchoilandgas.com/global-onshore-offshore-water-a7137- 1.html, 2007.

[8]   Chen, L., Xu, Q., Gossage, J. L., & Lou, H. H. , *"Simulation and economic evaluation of a coupled thermal vapor compression desalination process for produced water management,"* Journal of Natural Gas Science and Engineering, vol. 36, pp. 442-453, 2016.

[9]   Sakineh Tavakkoli, Omkar R. Lokare, Radisav D. Vidic, Vikas Khanna, *"A techno-economic assessment of membrane distillation for treatment of Marcellus shale produced water," Desalination*, vol. 416, pp. 24-34, 2017.

[10] OSPAR Commission, *Report on Discharges Spills and Emissions from Offshore Oil and GasInstallations*,http://www.ospar.org/documents/dbase/publications/p00221 Offshore%20report%202003.pdf,2005.

[11] J. Veil, M.G. Puder, D. Elcock, R.J.J. Redweik, A White Paper Describing Produced Water from Production of Crude Oil, Natural Gas and Coal Bed Methane,2004

[12] Neff, J. M., Lee, K., & DeBlois, E. M. (2011, July). *Produced Water: Overview of Composition, Fates and Effects.*

[13] F. Ahmadun, A. Pendashteh, and L. Chuah, *Journal of Hazardous Materials*, **170**, pp.530–551, (2009).

[14] Daniel, A.J., Bruce, P.E., Langhus, G., Patel, C. (2005). Technical summary of oil and gas produced water treatment technologies. All Consulting. LLC, Tulsa, OK.

[15] Faksness, L.G., Per Gerhard, G., Daling, P.S. (2004). Partitioning of semi-soluble organic compounds between the water phase and oil droplets in produced water. *Marine Pollution Bulletin*, 48(7-8), pp. 731-742.

[16] Igunnu, E.T., Chen, G.Z. (2014). Produced water treatment technologies. International Journal of Low-Carbon Technologies, 9(3), pp. 157-177.

[17] Bretz, R.E., Martin F.D., Russell, C. (1994). Produced Water: Technological /Environmental Consquences and Solutions. *Journal of Environment Quality*, 23(2), p. 391.

[18] Plebon M., Saad M. and Fraser S. (2005) Further Advances in Produced Water De-oiling Utilizing a Technology that removes and Recovers Dispersed Oil in Produced Water 2 micron and Larger.

[19] Nelson L. Nemerow, et al. *Environmental Engineering: Water, Wastewater, Soil and Groundwater Treatment and Remediation*. John Wiley & Sons, 2009.

[20] Maximous,N.,Nakhla, G., Wan, W., 2009. Comparative assessment of hydrophobic and hydrophilic membrane fouling in wastewater applications, *J. Membrane. Sci.* **339,** 93-99

[21] David Hendricks ,*Fundamentals of Water Treatment Unit Processes Physical, Chemical, and Biological.*

[22] Mackenzie L. Davis. *Water and Wastewater Engineering: Design Principles and Practice*. McGraw-Hill, 2010. thuvienso.vanlanguni.edu.vn,pp.6

[23] G. Burke, B. Singh, and L. Theodore, *Handbook of Environmental Management and Technology*, 2nd edn, John Wiley & Sons, Hoboken, NJ, 2000.pp 30

[24] Maximous,N.,Nakhla, G., Wan, W., 2009. Comparative assessment of hydrophobic and hydrophilic membrane fouling in wastewater applications, *J. Membrane. Sci.* **339,** 93-99.

[25] Li G., An T., Nie X., Sheng G., Zeng X., Fu J., Lin Z. and Zeng E. (**2007**) Mutagenicity assessment of produced water during photo electro catalytic degradation. Environmental Toxicology and Chemistry. **26:** 416–463.

[26] McFarlane J., Ridenour W., Luo H., Hunt R., Paoli D. D. and Ren R. (2005) Room temperature ionic liquids for separating organics from produced water. Separation Science and Technology. **40:** 1245–1265.

[27] Bharat A. Bhanvase, Rajendra P. Ugwekar, Raju B. *Mankar, NOVEL WATER TREATMENT AND SEPARATION METHODS Simulation of Chemical Processes.pp.666*

[28] Broek W. V. d. and Zande M. V. d. (1998) Comparison of plate separator, centrifuge and hydro cyclone. SPE International Oil and Gas Conference and Exhibition, Beijing, 1998.

[29] Stephenson M.T. (1992). A Survey of Produced Water Studies. In: Ray J.P., Engelhardt F.R. (eds) Produced Water. Environmental Science Research, vol 46. Springer, Boston, MA.

[30] Himmelblau.D.M, Riggs.J. B. 2012. *Basic Principles and Calculations in Chemical Engineering.* 7th ed.

[31] Çengel, Yunus A., and John M. Cimbala. 2006. *Fluid Mechanics: Fundamentals and Applications.* McGraw-HillHigher Education 1st edn.

[32] Zongo, I., Leclerc, J. P., Maiga, H. A., Wethe, J., & Lapicque, F. (2009). *Removal of hexavalent chromium from industrial wastewater by electrocoagulation: A comprehensive comparison of aluminium and iron electrodes.* Separation and purification Technology, 66(1), 159-166.

[33] L.D. Hamilton, A.F. Mein hold, g. Nagy, *Health risk assessment for radium discharged in produced waters, in: J.P. Ray, F.R. Engelhard (Eds.), Produced Water: Technological/Environmental Consquences and Solutions,* Plenum Publishing Corp., New York, 1992, pp. 303–315.

[34] Atab, M. S., Smallbone, A. J., & Roskilly, A. P. (2016). *An operational and economic study of a reverse osmosis desalination system for potable water and land irrigation. Desalination,* 397, 174-184.

[35] Wijmans, J. G., & Baker, R. W. (1995). *The solution-diffusion model: a review.* Journal of membrane science, 107(1-2), 1-21.

[36] Bird, R. B., Stewart, W. E., & Lightfoot, E. N. (2002). *Interphase transport in nonisothermal mixtures.* Transport Phenomena, 2nd ed.(John Wiley & Sons, Inc., New York, United States of America, 2007), 679.

[37] Lee, C. H., Johnson, N., Drelich, J., & Yap, Y. K. (2011). *The performance of superhydrophobic and superoleophilic carbon nanotube meshes in water–oil filtration.* Carbon, 49(2), 669-676.

[38] Hamilton, L. D., Meinhold, A. F., & Nagy, J. (1992). Health risk assessment for radium discharged in produced waters In *Produced Water* (pp. 303-314). Springer, Boston,

[39] Chen, X., Chen, G., & Yue, P. L. (2002). *Investigation on the electrolysis voltage of electrocoagulation.* Chemical Engineering Science, *57*(13), 2449-2455.

[40] Coughanowr, D. R., & Koppel, L. B. (1965). *Process systems analysis and control ,*3rd edn,(Vol. 491). New York: McGraw-Hill.

[41] Smith, R. (2005). *Chemical Process: Design and Integration.* John Wiley & Sons.Smith, J. M., Van Ness, H. C., Abbott, M. M., & García, C. R.(1997*).Introduction to Chemical Engineering Thermodynamics.* 6th edn.Noakes, N., Chow, C. C. L., Ko, E., & McKay, G. (2011). *Safety education for chemical engineering students in Hong Kong: Development of HAZOP Study teaching module.* Education for Chemical Engineers, 6(2), e31-e55.

[42] L.G. Faksness, P.G. Grini, P.S. Daling, Partitioning of semi-soluble organic compounds between the water phase and oil droplets in produced water, Mar .Pollut. Bull. **48** (2004) 731–742.

Boiler Feed Water Treatment Using Green Corrosion Inhibiter: An Alternative Approach

Ummer Khitab[1], Hayat Khan[1]

[1] Department of Chemical Engineering, University of Engineering & Technology (UET),25120, Peshawar

Abstract—**Metallic pipe lines are subjected to corrosion due to its wide spread applications in process industries, a major means to transport fluids especially water. Consequently, the cost of the project increases due to frequent maintenance, pipe wall rupture and valuable product loss. Nevertheless, corrosion of the pipelines contaminates the discharge water, thus, leading to environmental and ecological concern. Corrosion inhibitors i.e. hydrazine and or sulfite salts are traditionally used in boiler metallic facilities to reduce the extent of corrosion as an economical and reliable approach. However, literature has revealed that hydrazine is a carcinogenic chemical and need to be replaced by an environmental friendly alternative. Two methods i.e. weight loss method, and Tafel test technique was used in the current study to investigate the effect of cyclohexylamine (green alternative) in evaluation of corrosion inhibition efficiency (CIE) as compared to hydrazine. The CIE of hydrazine at 0.5, 1.0 and 1.5 g/L of water sample was compared with the same concentration of cyclohexylamine. Results manifested that the CIE of cyclohexylamine was slightly higher as compared to hydrazine using weight loss method. Tafel test method also depicted the same trend. The highest CIE was observed for 1.5g/L of water sample in both the methods for cyclohexylamine which was recorded as 92 and 93.4% respectively. In conclusion, cyclohexylamine is not only a good replacement in term of CIE, but also provide toxic free working environment in boiler facilities.**

Keywords—**Green corrosion inhibitor, cyclohexylamine, boiler feed water, Hydrazine.**

I. INTRODUCTION

Metals and alloys such as; iron, stainless steel, mild steel, aluminum etc.are the commonly used material of construction for process equipments, which faces the problem of corrosion especially in dissolved oxygen rich atmosphere. Effective and good corrosion inhibitors extend the service life of the equipment and machinery [1].

Among the available corrosion inhibitors, sodium sulfite is widely used to scavenge oxygen in boiler water system specifically at low pressure due to its nontoxic nature and relatively easy to apply. However, in boiler water considerable solids (sulfate salts) is added with the usage of sodium sulfite limiting its application in system with high purity boiler feed water [2].

Hydrazine is also widely used to reduce corrosion rate in boilers despite of its geno-toxic carcinogenic quality. In 2006 the international conference on chemicals management decided to adopt a strategic approach to international chemicals management [3]-[4]. The European Union has to implement the new regulation and limitation of chemicals to acquire the world targets on sustainable development by 2020, in this regard hydrazine is among the controlled chemicals and it was recommended to find an alternative for its replacement[2]-[5].The development of "green" corrosion inhibitors are of interest, which requires the knowledge of the home country regulations, good corrosion protection for the inhibitor in the application area and the assessment of the environmental performance to which the product will be exposed.

In current work, cyclohexylamine (Amine-based compound) is evaluated as an alternative to hydrazine to scavenge oxygen in corrosive atmosphere for its advantage of forming a stable passive/protecting magnetite film on the metal/alloy surface such as; low carbon steel which lower its corrosion rate. In addition, other merits include its low toxicity and high volatility. Furthermore when used in boiler water feed systems, old deposits are removed without any damage and provide effective heat transfer and energy savings [6].

II. METHODOLOGY

Boiler feed water from Bestway Cement Farooqia Plant Taxila, Pakistan was investigated in this work for corrosion phenomenon. Experiments are repeated (3-4) times by varying the concentration of corrosion inhibitors. Two methods were used to compare the corrosion inhibition efficiency (CIE) of the corrosion inhibitors; Weight Loss method and Tafel Test method. First, we performed control experiments to measure the corrosion rate of boiler feed water (sample water), then in the following experiments   corrosion rate of sample water was measured adding different concentration (0.5, 1.0 and 1.5 g/L) of the Hydrazine, as corrosion inhibitor. The obtained results were compared with the suggested green alternative cyclohexylamine (in the same concentration; 0.5, 1.0 and 1.5 g/L) results.

Weight Loss Method:

A piece of corroded mild steel was taken from the stated industry (Bestway Cement Farooqia Plant Taxila, Pakistan), the rust is removed with the help of grinder pad (SiC emery paper). After measuring its dimensions and recorded its weight on weight balance, the mild steel pieces are dipped into sample water (controlled solution with no inhibitor), hydrazine solution and cyclohexylamine solution for 5 days (120 hr) as shown in Fig.1.Then, the samples were removed from their respective solution, the corroded part was removed with the help of a grinding pad and the sample weight was measured again. The measured data of sample dimensions (area), weight loss, sample density and exposure time was used to calculate the corrosion rate.

Tafel Test Method:

The same corroded mild steel piece was also evaluated by conducting Tafel Test and the rust is removed with the help of grinder pad. One surface of the mild steel piece (Working Electrode) was insulated by epoxy followed by dipping in hydrazine and cyclohexylamine solution of different concentration. During the experiments, the reference electrode (Calomel; Ag/AgCl) and counter electrode (Platinum Wire) was also dipped in the hydrazine and cyclohexylamine solution(Fig.2).The three electrodes in the electrochemical cell were connected with the Gamry instrument shown in Fig.3 (Reference 3000; Potentiostat/Galvanostat/ZRA)which give Tafel graph from which corrosion rate was calculated.

Fig. 1. Mild steel piece in solution for Weight Loss method
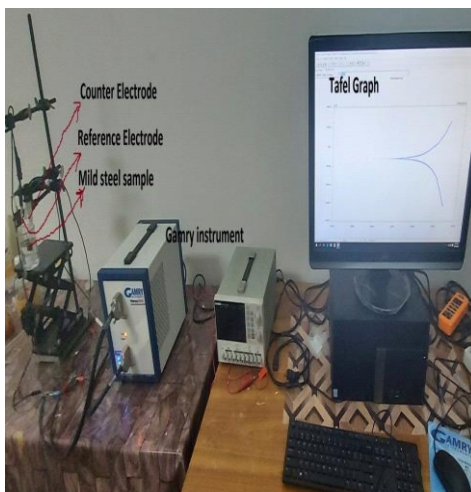
Fig. 2. Tafel Test setup

Fig. 3. Gamry Instrumnet

III. RESULTS AND DISCUSSION

(i) Weight Loss Method:

The following formula [7] was used for the corrosion rate determination

$$Corrosion\ Rate = \frac{534\Delta W}{\rho A t} \qquad (1)$$

Where, ΔW= Loss in weight (difference in initial and final weight, (mg))
ρ=Density of the mild steel sample (7.78 g/cm^3) [7]
A = Area of the mild steel (cm^2)
t= Exposure time of the mild steel sample in solution (120 hr)

Table I: The corrosion rate of different solution in the weight loss method

Solution	Control solution	Hydrazine (g/L)			Cyclohexylamine (g/L)		
		0.5	1.0	1.5	0.5	1.0	1.5
ΔW (g)	0.48	0.144	0.056	0.021	0.114	0.034	0.013
Area (cm^2)	0.013	0.013	0.01	0.006	0.013	0.007	0.005
Corrosion Rate (mpy)	21.6	6.3	3.05	2.0	5.2	2.8	1.53
% decrease in corrosion rate	-	71.0	86.0	91.0	76.0	87.0	93.0

Table I showed the corrosion inhibition efficiency of the control, hydrazine and cyclohexylamine solution. It reveals that the corrosion rate decreases as concentration of inhibitor increases. For the same concentration the cyclohexylamine have greater corrosion inhibition efficiency (CIE) as compared to hydrazine. The reason behind this trend is the pH control (pH of solution decreases from 9-12 in case of cyclohexylamie and 9-10.5 in case of hydrazine) of the solution and the passive nature of cyclohexylamine that form a passive magnetite film to retard the corrosion as nitrogen in the cyclohexylamine molecule makes coordinate covalent bond with the Fe^{2+} ion of metal (Chemisorption bonding Fe^{2+}—N—complex)[8]-[9]. As a result cyclohexylamine has both anodic and cathodic inhibition [10].

Tafel Test Method:

We used the following Tafel equation [11] to calculate the corrosion rate

$$Corrosion\ Rate = \frac{I_{corr}*K*EW}{\rho*A} \qquad (2)$$

Where, I_{corr}=corrosion current (Amps)
K = constant (3272 mm/(amp-cm-year))
EW= equivalent weight (g)
d= density of the sample (g/cm^3)
A= area of the sample (cm^2)
The corrosion current (I_{corr}) was calculated from the following equation [11]

$$I_{corr} = \frac{1}{2.303 * R_p\ [{(\beta_a \beta_c)}/{(\beta_a + \beta_c)}]}$$

Where, R_p= polarization resistance = 1.111*10^5 cm^2/A
β_a= Tafel constant (anodic β, volts/decade)

β_c= Tafel constant (cathodic β, volts/decade)

The Tafel graphfor each solution is given below;
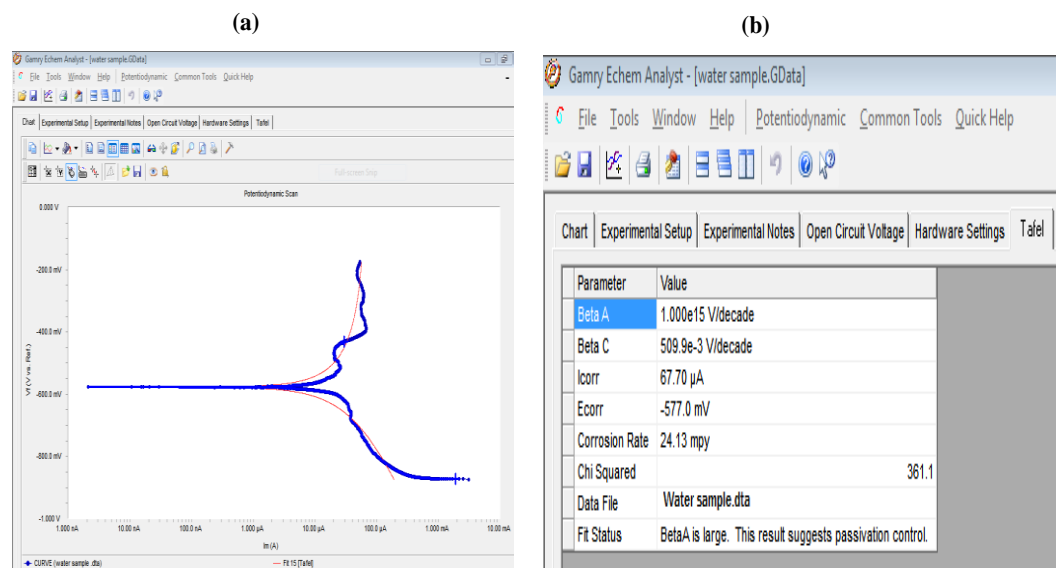
Fig 4. (a) Tafel graph of sample water, (b) corrosion rate of sample water

Fig.4 (a, b) illustrate the graph of water sample with both anodic and cathodic areas. The pH of water is 9 showing its basic nature. The calculated corrosion rate of sample water is 24.13 mpy.
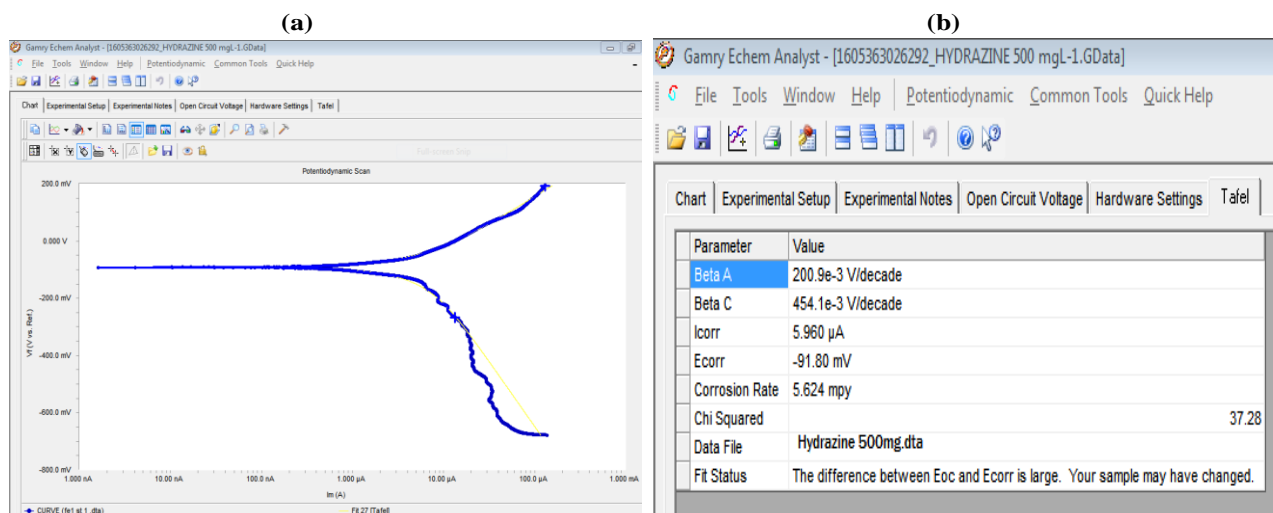
Fig. 5. (a) Tafel graph of Hydrazine (0.5g/L)in water sample, (b) Corrosion rate of Hydrazine (0.5g/L)

Fig.5 (a, b) showed the Tafel graph and corrosion rate of hydrazine (0.5 g/L in water sample). The pH of water sample increases from 9 to 10.5 on addition of Hydrazine, illustrating the basic nature of the solution. The measured corrosion rate of hydrazine was 5.62mpy, meaning the CIE of hydrazine 76.69%.

(a) **(b)**
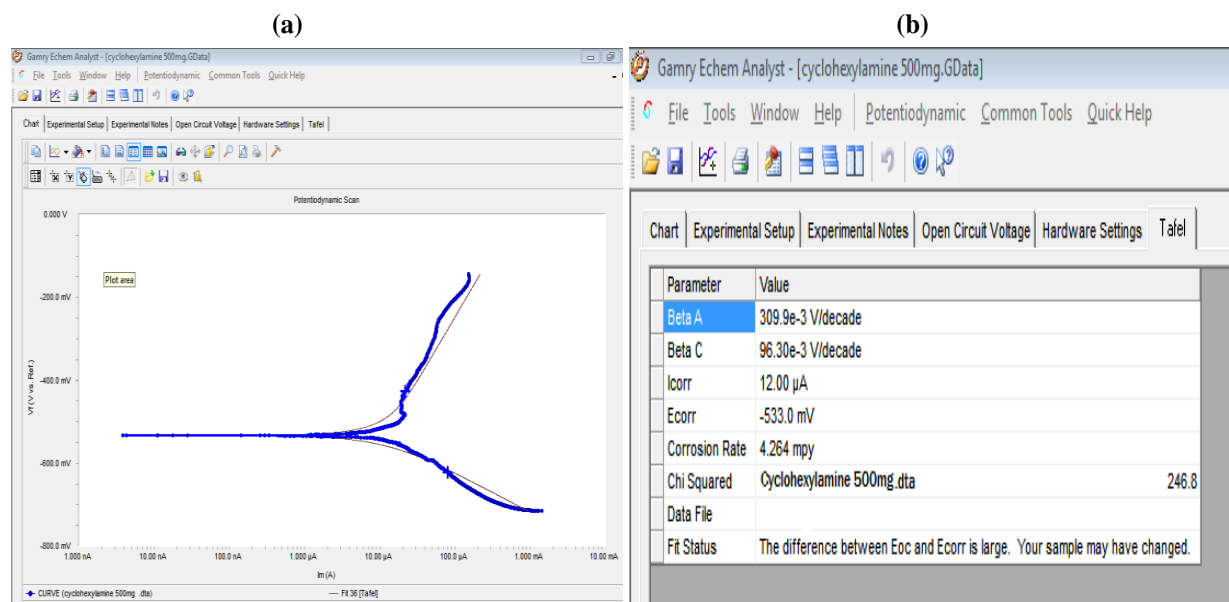
Fig. 6.(a)Tafel graph of Cyclohexylamine(0.5g/L) in sample water, (b) Corrosion rate of Cyclohexylamine.

Fig.6 (a, b) is the Tafel graph and corrosion rate ofcyclohexylamine solution (0.5g/L of water sample). The pH of the solution is 12 and corrosion rate is 4.264 mpy. The anodic portion showed some passiveness (potential is increased to more positive value) which is due to the protective magnetite film formation on the metal surface which inhibit corrosion rate[8].

(a) **(b)**
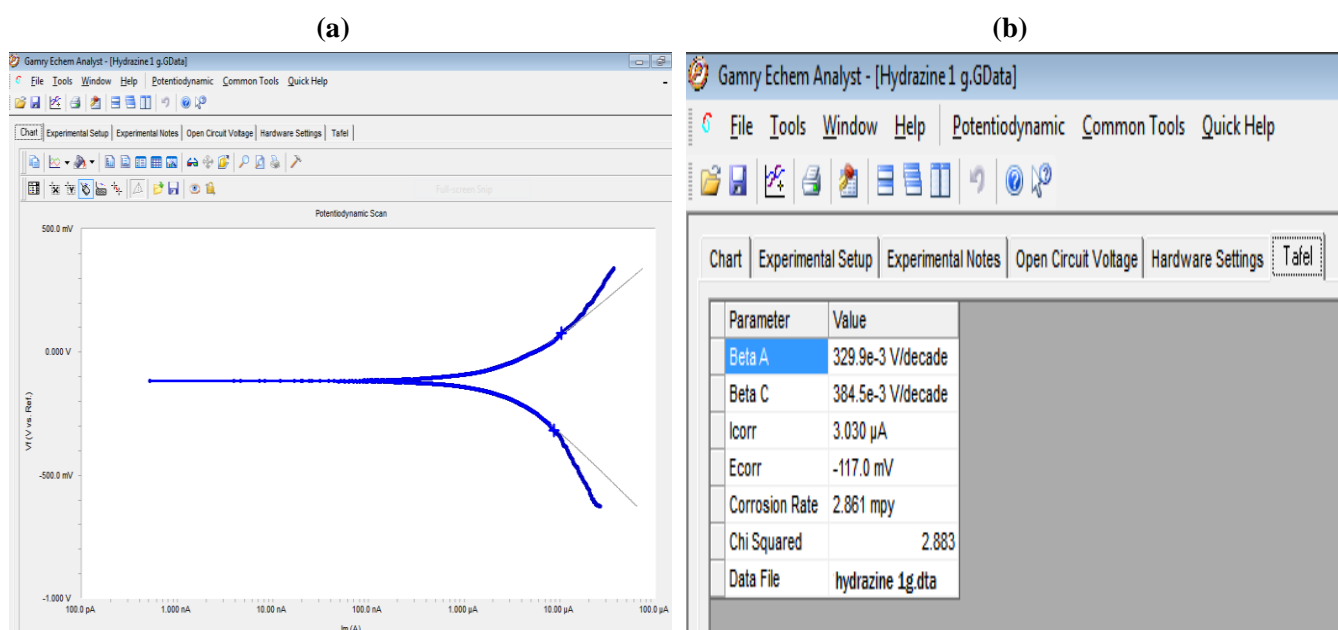
Fig. 7.(a)Tafel graph of Hydrazine (1.0 g/L) in sample water, (b)Corrosion rate of Hydrazine

Fig. 7 (a, b) demonstrate the Tafel graph and corrosion rate of hydrazine solution (1g/L in sample water). It showed a corrosion rate of 2.861 mpy (88% CIE), which is less compared to hydrazine solution of 0.5g/L in water sample. As concentration of hydrazine increases the pH of solution also increases due to the alkaline nature of hydrazine, which in turn decrease the corrosion rate [12].

(a) **(b)**
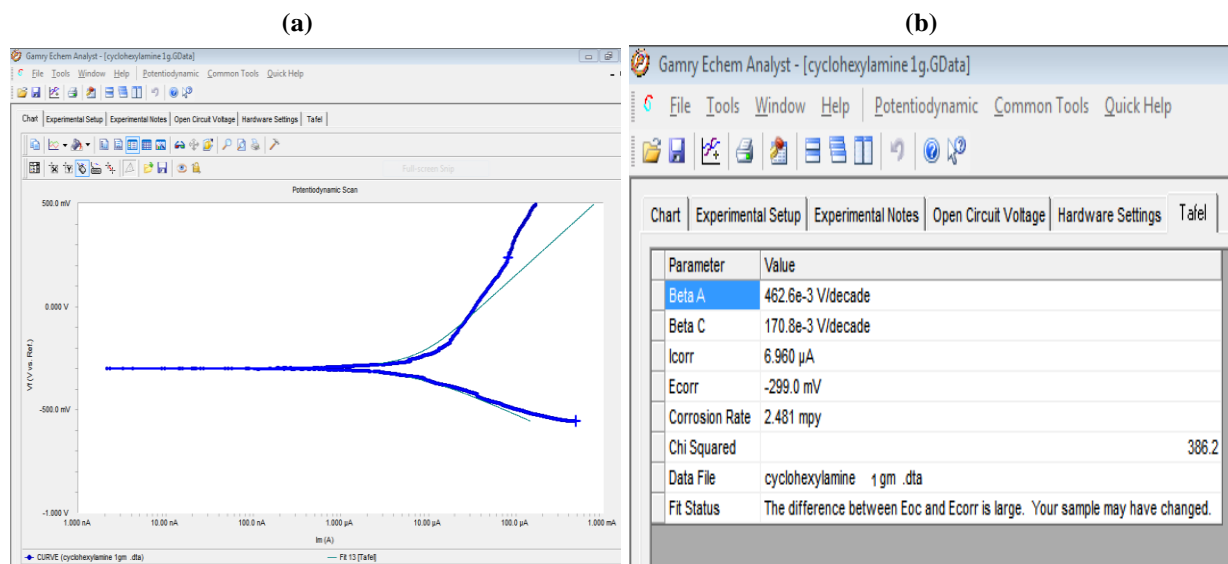
Fig. 8.(a)Tafel graph of Cyclohexylamine (1.0g/L) in sample water, (b) Corrosion rate of

Cyclohexylamine.

Fig. 8 (a, b) is the Tafel graph of cyclohexylamine (1.0 g/L in water sample). It showed that the corrosion rate is 2.481 (89.71% CIE) which is less than that of hydrazine solution (1.0 g/L of water sample). The passive region increases as concentration of cyclohexylamine solution increases because it increase the chance of coordinate covalent bonding of passive magnetite film (Fe^{2+}—N—complex) with metal surface retarding the oxidation of Fe^{2+} ion with oxygen[8].

(a) **(b)**
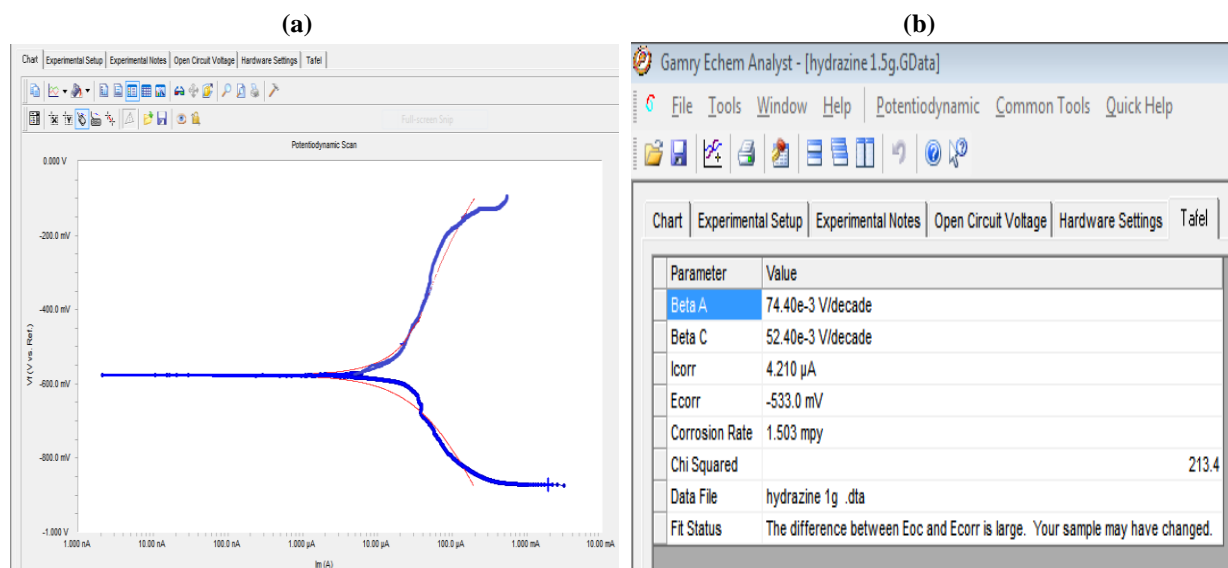
Fig. 9.(a)Tafel graph of Hydrazine (1.5g/L) in sample water, (b) Corrosion rate of Hydrazine

Fig. 9 (a, b) is the Tafel graph and corrosion rate of hydrazine (1.5 g/L in sample water). The corrosion rate of hydrazine solution is 1.503 mpy (93.78 % CIE).
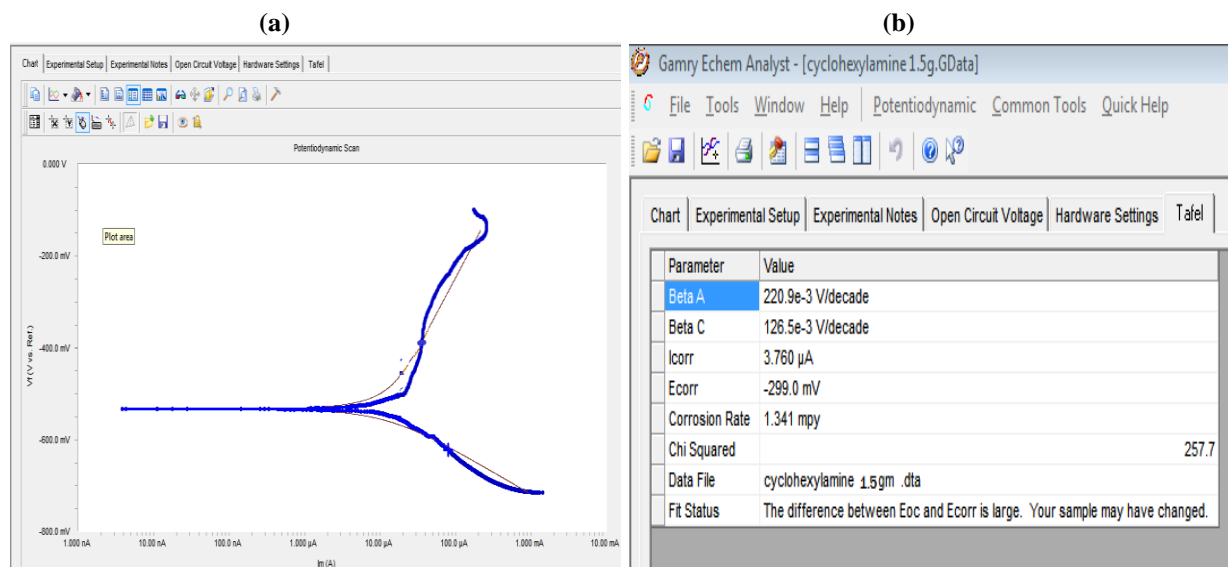
Fig. 10.(a)Tafel graph of Cyclohexylamine (1.5g/L) in sample water, (b) Corrosion rate of Cyclohexylamine

In Fig.10 (a, b) the Tafel graph showed the lowest corrosion rate which is 1.341 mpy (94.44 % CIE) for cyclohexylamine concentration of 1.5g/L in sample water. It is because of higher concentration of cyclohexylamine would largely inhibit both anodic and cathodic surface of metal making passive magnetite film[8].

TableII. The corrosion rate of different solution in Tafel Test Method

Sample No	Control solution	Hydrazine (g/L)			Cyclohexylamine(g/L)		
		0.5	1.0	1.5	0.5	1.0	1.5
Corrosion Rate (mpy)	24.13	5.62	2.86	1.50	4.26	2.48	1.34
% decrease in corrosion rate		76.7	88.2	93.8	82.3	89.7	94.5

Table II show CIE's of different solution shaving same trend as shown in weight loss method (Table I). It reveals that cyclohexylamine has CIE slightly greater than that of hydrazine. Cyclohexylamine solution (PH=12) is more basic than hydrazine solution (PH=10.5) and also form larger protective film compare to hydrazine making solution less corrosive.

Discussion:

The data illustrated that hydrazine showed its highest CIE at 1.5 g/L in water sample which is 93.8 % and cyclohexylamine has 94.44 % CIE at 1.5 g/L of sample water. As the concentration of both the solution increases the CIE also increases because of their well established passive film over the surface of mild steel. The concentration of film forming inhibitor must be as high as to cover the whole surface of mild steel otherwise pitting will be enhanced [8]. Mechanism of corrosion inhibition of Cyclohexylamine is mixed inhibition (both anodic and cathodic inhibition)and having larger passive film forming (chemisorptions) capability while hydrazine has only anodic inhibition[10]. The passive film formation in hydrazine is less compare to cyclohexylamine which make it slightly less effective than cyclohexylamine[8]-[12].

IV. Conclusion

In the study the proposed "green alternative" cyclohexyleamine showed highest CIE than Hydrazine, because, cyclohexyleamine generate larger passive magnetite film which helps in corrosion inhibition. Moreover, cyclohexylamine is less toxic, which made it a good and green alternative to hydrazine.

Acknowledgment

V. References

[1] B.A.Miksic, A.Y. Furman, M. A. Kharshan, "Biodegradable and renewable raw materialsin a new generation of water-treatment products", May 12, 2016.

[2] Behzad, Bavarian, Lisa Reiner, "Development of a new vapor phase corrosion inhibitorfor steam generating systems and boilers", March, 2017.

[3] "Human health perspective of environmental exposure to hydrazine" A review, Jan 05,2017.

[4] "International program on chemical safety—health and safety guide no. 56, hydrazine, "IPCS INCHEM. Geneva: WHO, 1991,Retrieved 24 Nov 2018.

[5] "Amine proves effective alternative to hydrazine - modern power systems", Jan 08, 2017.

[6] Cuisia, D.G., Rudolph, J.W., Hwa, C.M. and Tehle, Jr. T.E. "New oxygen scavenger forboiler systems", Corrosion, page -83, 1983.

[7]V. R. Rathi, bS. D. Nirmal and S. J. Kokate, "Corrosion study of mild steel, tor steel and CRS steel by weight loss method, J. Chem. Pharm, Res.2(2): 97-100,2010.

[8] Camila G. Dariva and Alexandre F. Galio, "Corrosion Inhibitors Principles, Mechanisms and Applications", Developments in Corrosion Protection, p 365-379, 2012.

[9] Rana S. N, Rana AfifMajed, Mohamed H. Hafiz, " Corrosion inhibition study of carbon steel A515 in sour water at 75 ∘C", 2013.

[10] GeethamaniPalanisamy, "Corrosion Inhibitors", Department of Chemistry, SNS College of Technology, Coimbatore, Tamil Nadu, India, 2019.

[11] J. R. Scully, "Polarization Resistance Method for Determination of Instantaneous Corrosion Rates", Corrosion,56-199, 2000.

[12] pranav s. Joshi, g. Venkateswaranand k. S. Venkateswarlu, "Passivation of carbon steel alloy in de-oxygenated alkaline PH media, The effect of various additives", corrosion science, vol. 34, no. 8, pp. 1367-1379, 1993.

A case study for commercial utilization of waste marble powder in conventional low cost concrete blocks.

Muhammad Farhan*[1] Shehbaz Ahmad [1] and Muhammad Imran Ahmad [1]

[1] Department of Chemical Engineering, University of Engineering and Technology, Peshawar;
*farhanshahzad36@gmail.com

Abstract-A number of studies have been carried out in order to utilize waste marble powder as partial replacement of sand in concrete blocks to increase strength and reduce cost. These studies concluded that 40 percent marble powder can be optimally used for maximum strength and workability. However Commercial scale application of waste marble powder incorporates a number of problems like transportation, mixing of hard lumps present in slurry, removal of plastics , marble stone scrap and other wastes from the slurry, workability problem in concrete block pressing machine. This study is aimed specifically to find suitable low cost methods and processes to make the commercial usage of waste marble slurry, or powder feasible. Types of mixers and sieves have been discussed for easy processing of marble waste.

Keywords: Waste Marble; proceesed waste marble powder, workability, and concrete mixing.

I. Introduction

Residence is the basic necessity of human beings for which entire human race is striving since stone ages. Construction is therefore one of the ever expanding industry. Marble stone is one of the most important raw material for this industry used for different purposes. in modern world marble is widely used as tile both in floor and walls although no specific data is available about the consumption of marble stone, however a very careful survey from Pakistan stone development corporation states that more than six thousands tonne of marble is excavated daily from Khyber Pakhtunkhwa province of Pakistan only. This huge amount of stone is processed in 8 marble industrial states of KPK, as well as is transported to other parts of the country and abroad also. The processing of marble stone is done in a very old fashion, with lot of flaws and deficiencies. About 25 to 40% of processed marble stone goes to waste. Two main types of wastes are produced:

Scrap or large aggregates: This type of scrap or waste is generated during the mining or blasting, they are smaller pieces of stone which can't be processed for tiles. This type of waste is also produced during resize of the tiles. Some grades of this waste are used as low cost alternative in construction while some grades are used in grinding, ball and impact mills for calcium powder.

Waste marble slurry: Approximately 85-95% of waste produced consists of waste marble slurry. This slurry produces during cutting, polishing, resize. A number of lab scale and pilot scale studies have been carried out in order to utilize and consume this waste, but none is successful for commercial scale. And millions of tonnes waste slurry is being dumped every year. The aim of our study is to address some of the reasons, why commercial scale application is unsuccessful.

Clay Waste marble powder is very sticky in nature with excellent adhesive properties. These adhesion properties sometimes create a lot of problems. And the other factor related to marble waste slurry is that it contains about 30 to 40 % water content. Following problems arises during the processing of waste marble powder commercially.

Transportation: It is not feasible to carry extra 30 to 40 % moisture with waste marble powder in bulk amounts. This moisture not only creates extra burden , but also causes wobbling in the container which damages the body of the container. Thus carriage of waste marble slurry is difficult to carry.

Improper mixing: Dried marble powder has large aggregates which make it nearly impossible to properly mix with gravel, sand, cement etc. The non-mixed lumps of marble powder are therefore weak points of the concrete blocks.

II.   Materials and Method

To overcome above mentioned issues we adapt the following strategy;

a) Slurry is pumped out of the sedimentation tank and left to dry for 3-4 days which will reduce the transportation cost.
b) For dry lumps sand muller mixer may be used followed by sieving.
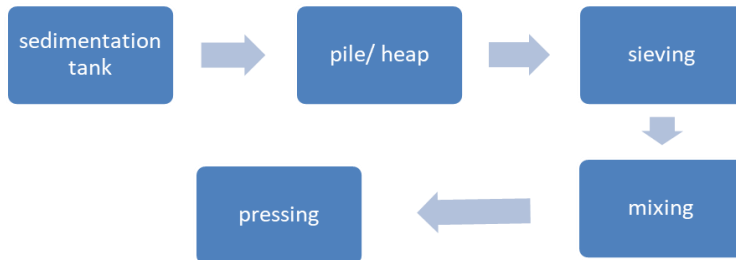
Fig. 1: Recommended processing plan.
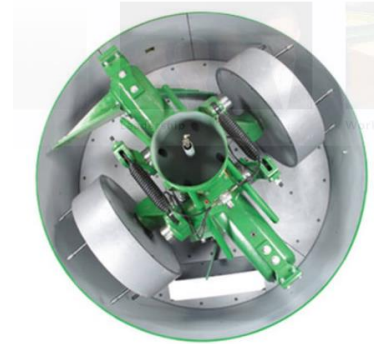
Fig. 2: Muller mixer used for WMP.

III.   Results and discussion

Following tables show composition of mixtures and their relative strengths.

Table 1: Mix 1 and its strength

component	volume (L)	strength (PSI)
Khaka	85	2371
Sand	15	2380
cement	10	
water	6.5	2374
WMP (grey)	20	

Table 2: Mix 2 and its strength

component	volume (L)	strength (PSI)
Khaka	85	2572
sand	15	2545
cement	10	
water	6.5	2562
WMP (grey)	20	

Table 3: Mix 3 and its strength

component	volume (L)	strength (PSI)
Khaka	85	1379
Sand	15	1390
cement	10	
water	6.5	1380
WMP (grey)	20	

Table 4: Mix 4 and its strength

component	volume (L)	strength (PSI)
Khaka	85	1379
sand	15	1390
cement	10	
water	6.5	1380
WMP (grey)	20	
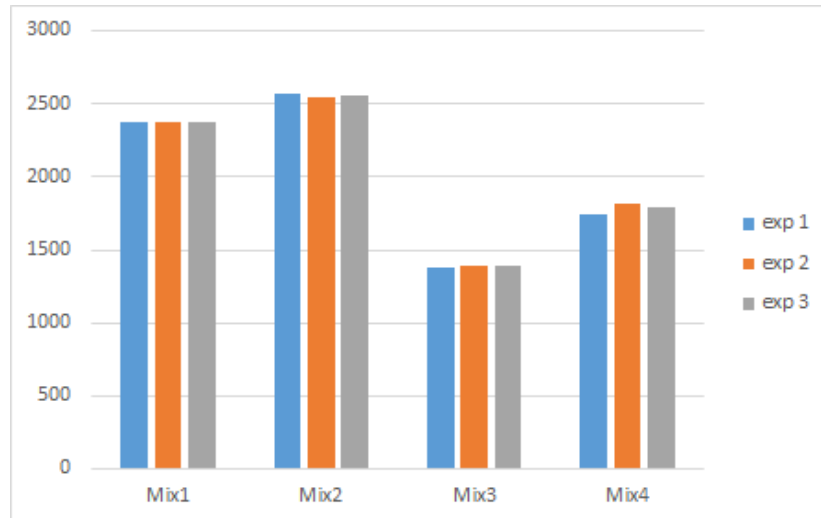
Fig 3: comparison of strengths for four mixtures.

Decrease in the strengths of non processed WMP mixtures is due to the fact that a non mixed lump creates weak spaces. As shown in the figures below.

Fig. 4: Concrete block with processed WMP.

Fig. 4: Concrete block with non processed WMP.

IV.   Conclusions

It is evident from the above discsussion that WMP can not be used as filler in the concrete blocks without processing. Processing includes on field drying for few days and then mixing with a specialized sand muller mixer followed by sieving with vibbrator sieve.

V.   Acknowledgement

VI. REFERENCES:

1. Arshad, A., Shahid, I., Anwar, U.H.C., Baig, M.N., Khan, S. and Shakir, K. (2014). The wastes utility in concrete. International Journal of Environmental Research, 8(4), 1323-1328.

2. BayramErcikdi, GökhanKülekci, TekinYılmaz (2015) Utilization of granulated marble wastes and waste bricks as mineral admixture in cemented paste backfill of sulphide- rich tailings. Construction and Building Materials, Volume 93, Pages 573-583

3. C. Vaidevi, 'Engineering study on marble dust as partial replacement of cement in concrete' Ind. J. Eng. (2013) (4), 9-11.

4. D. Eliche-Quesada, J. Leite-Costa. (2016). Use of bottom ash from olive pomace combustion in the production of eco-friendly fired clay bricks. Waste Management, Volume 48, Pages 323-333.

5. MucahitSutcu, HandeAlptekin, ErtugrulErdogmus, Yusuf Er, Osman Gencel (2015). Characteristics of fired clay bricks with waste marble powder addition as building materials.Construction and Building Materials, Volume 82, Pages 1-8

6. S. Dhanapandiana, M. Shanthib, (2009). Utilization of marble and granite wastes in brick products. Journal of Industrial Pollution Control, Volume 25, Pages 145-150

Investigation of reverse solute flux of binary and ternary draw solutions in forward osmosis

Aizaz Ali Farman [A], Malik Asim Zeb[A], Ahmad Sher Khan Marwat[A], Kashif khan[A], Saeed gul [A]

[A]Department of Chemical Engineering, University of Engineering and Technology
Peshawar 25000, Pakisatan

Abstract— **Reverse solute flux (RSF) is one of the most prominent issues concerned with forward osmosis. Inorganic salts like NaCl, $CaCl_2$ has been known to be one of the best solutes for draw solution in forward osmosis regarding their availability, performance, low price and nontoxic nature. Yet they exhibit high reverse solute flux. In this study, we have considered $CaCl_2$ as our test draw solution due to its high cross membrane flux. The issue of reverse solute flux has been addressed by addition of other salts (Sucrose and NaCl) in minor concentration with pure $CaCl_2$. It was concluded that in minor concentration, salts with higher molecular sizes like sucrose reduces the RSF significantly but at the cost of reduced flux; while the use of salts having mono-valent ions like NaCl increases the RSF due to small hydrated radius.**

Keywords—**Forward osmosis, Draw solute, Reverse salt flux, Solute diffusion, Desalination.**

I. INTRODUCTION

Forward osmosis is one of the most prominent technique among scientists and researchers in sight of its low pressure requirements and ambient conditions. Osmosis is the spontaneous exchange of water across a semi permeable membrane due to osmotic pressure difference [1]. Being an attractive alternative to the energy intensive pressure driven processes like reverse osmosis, forward osmosis still has its gray areas. The current challenges to forward osmosis includes Proper membrane design, better draw solution selection, and economic regeneration of draw solute from the diluted draw solution(DS). Draw solution is a specie that is used to induce water flux from a solution of low osmotic pressure. Scientists has been working far and wide to optimize the FO process by addressing one or all the challenges to it however a single draw solution cannot be considered the best [2]. For selection of a suitable draw solution, various criteria needs to be addressed, which includes high osmotic pressure(high water flux), low back diffusion(low reverse salt flux), economic regeneration, low viscosity, low toxicity and cost effective availability [3]. Draw solution are classified into various classes and in many contexts. The most common classification is given in Fig 1 [4]. The classification is based on the recovery methods of the draw solutions in terms of their response to certain external environmental conditions.
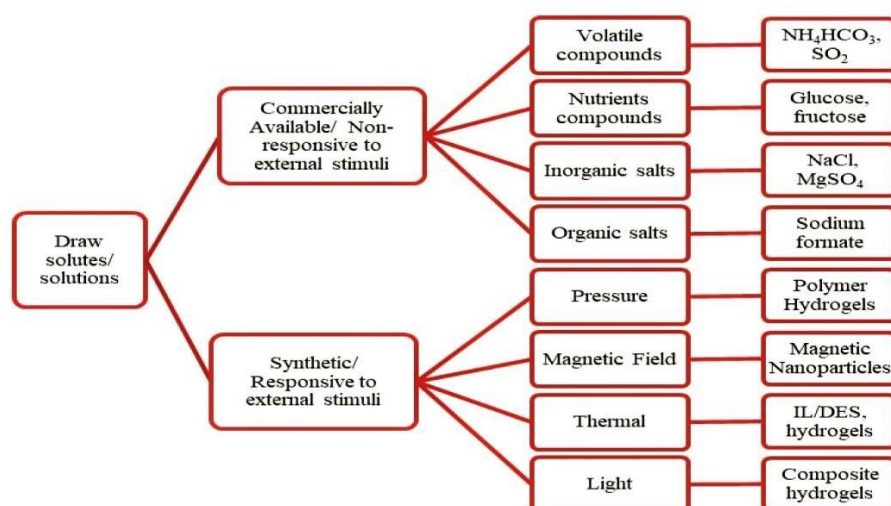
Before 2000's volatile compounds and various sugars were used as draw agents. Volatile draw agents like SO2 and thermolytic compounds could be separated using low grade heat[5]. Nutrient compounds including various sugars had the advantage of direct use after being diluted [6]. Magnetic nano particles has the advantage of recovery under magnetic field but has the problem of agglomeration after use [7]. Different kinds of polyelectrolytes were also investigated by Ge and his coworkers[8] due to their larger sizes and ability to produce good osmotic pressure. Wang and his team investigated stimuli responsive hydrogels[9] in an effort to optimize the regeneration of draw solute from the diluted draw solution.

Inorganic salts have been known to produce high water fluxes. This trait is associated with their ability to exhibit good osmotic pressure and high solubility in water. On the other hand they are also inexpensive and are easily available. However they have the problem of high RSF[10]. Organic and nutrient compounds have the capability of producing low RSF as compared with their inorganic counterparts[11]. The current investigation focuses on using combination of inorganic monovalent salt and sucrose with calcium chloride in an effort to reduce the RSF while keeping the osmotic pressure constant.

II. METHODOLOGY

A. Solutions

A number of experiments were performed on a bench scale equipment utilizing combination of Calcium Chloride ($CaCl_2.2H_2O$) as a major component and Sodium chloride (NaCl) and sucrose ($C_{12}H_{22}O_{11}$) as minor component. All the draw solution were designed to produce an osmotic pressure equivalent to 1 molar $CaCl_2$ solution. Osmotic pressure of the solution was evaluated using OLI stream analyzer.

TABLE 1 DRAW SOLUTIONS FOR EXPERIMENTS

Minor soule	Minor salt amount (10% of total osmotic pressure (grams)	Major salt ($CaCl_2$) amount (grams)	Total osmotic pressure (bar)
NaCl	5.9	135.1	77.54
Sucrose	107	135.1	77.54

B. Experimental setup

The bench scale equipment is given in Fig 2. It consists of two separate peristaltic pumps(Kamoer CK15) for feed and draw solution. An online conductivity meter was used to record the rise in concentration of the feed (de-ionized water) for evaluation of RSF and a digital balance(G&G Electronic scale) was used to monitor the mass/volume decline of the feed for evaluating water flux.

$$J_w = \frac{\Delta V}{A\Delta t} \tag{1}$$

Where J_w is water flux, ΔV is the change in volume, A is the effective membrane surface area, Δt is the time interval.

$$J_s = \frac{C_t V_t - C_o V_o}{A\Delta t} \tag{2}$$

Where Js is the reverse salt flux, A is the effective membrane surface area, Δt is the time interval, C_t and V_t are the concentration and volume of feed at any time respectively, while C_o and V_o are the initial concentration and volume of the feed respectively.

A cross flow cell having an effective area of 24 cm^2 was used. The osmosis process was carried out using PRO mode (Active layer facing the draw solution), temperature of 25^{0}C and a cross flow velocity of 0.20 m/sec was used. TFC polyamide membranes were utilized for all experiments. The minor salts were added to the major components such that only 10% of the total osmotic pressure was offered by them. Each experiment was carried out for 3 hours and concentration and mass decline was recorded with 10 minutes interval.

Fig 2 FO Bench scale equipment

III. RESULTS AND DISCUSSION

A. *Water flux and Reverse salt flux*

Water flux for single and combined draw solutions are summarized in Fig 3. The decreasing trend is due to the internal concentration polarization with time. A flux of 19.36 L/m^2.hr was recorded for the single 1 molar DS of CaCl$_2$ and a corresponding RSF of 14.32 g/m^2.hr was calculated. For combination with NaCl water flux of 19.15 L/m2.hr was observed and a corresponding RSF of 18.32 g/m^2.hr was recorded. This accounts for only 1% reduction in flux and a steep increase in RSF of about 21% as compared with single CaCl$_2$ solution. The increase in RSF can be associated with the addition of Na$^+$ cation which has higher diffusion coefficient and smaller size as compared with the Ca$^+$ cation. Cl$^-$ having the highest diffusion coefficient among the present candidates, accounts for most of the RSF [10], and because of the substitution of Ca$^+$ with Na$^+$ RSF has increases significantly as compared to pure CaCl$_2$ solution. Fig 4 indicates the average RSF of all the candidates.

Water flux of 6.02 L/m^2.hr and average RSF of 7.86 g/m^2.hr was recorded for combination of Sucrose with CaCl$_2$. This corresponds to a reduction of 69% and 45% in water flux and RSF respectively. The case here is a significant reduction in RSF as compared to single salt, at the cost of a significant reduction in water flux. This behavior can most probably be associated with the lower diffusion coefficient and larger molecular size of sucrose[12] . As most of the membrane would be sufficiently blocked by the larger and less diffusive molecules of sucrose which would not only hinder the back diffusion of Ca$^+$ and Cl$^-$ ions towards the feed solution but would also affect the water flux across the hydrophilic membrane. Fig 5 indicates the average water flux and RSF for all the candidates for the span of 3 hours.
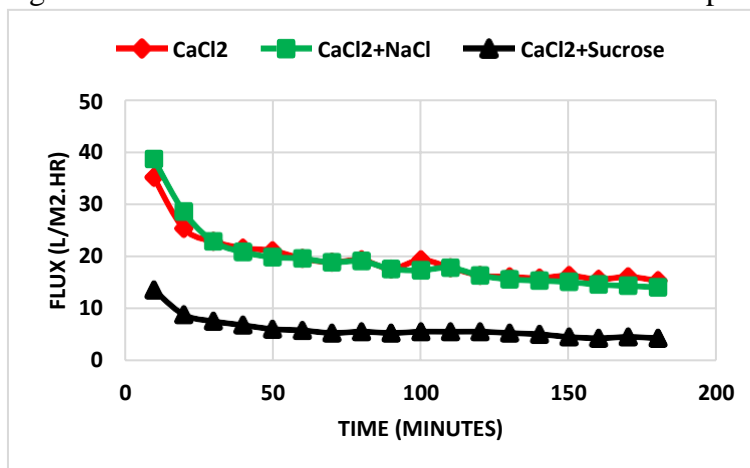
Fig 3 Cross membrane water flux for single salt and DS combinations
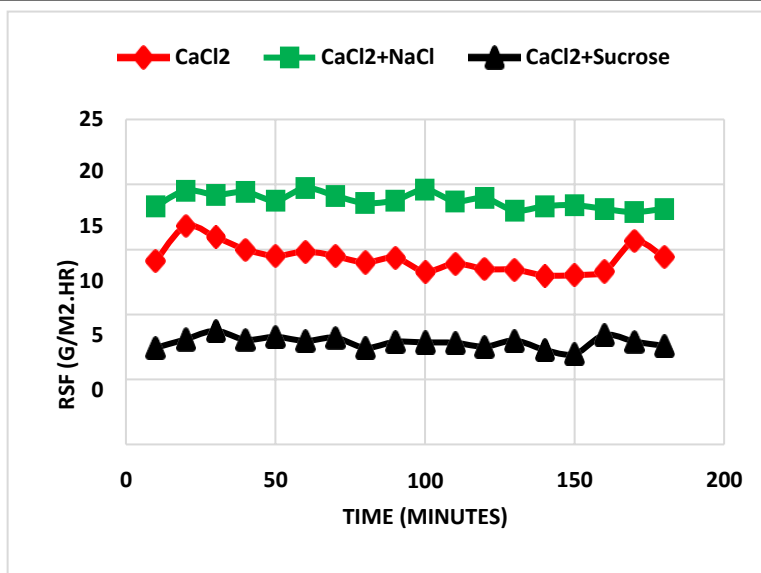
Fig 4 RSF of single salt and DS combinations
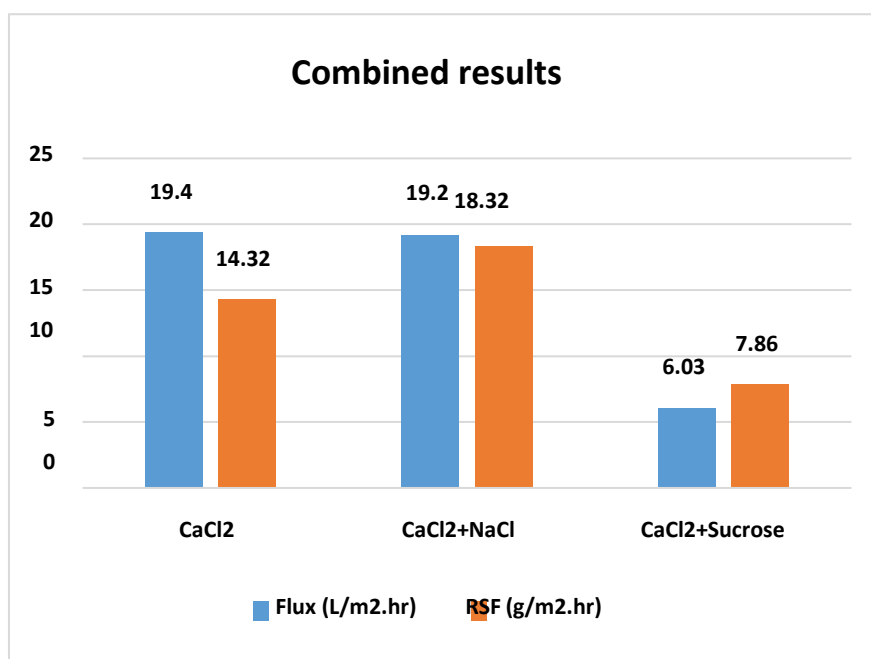
IV. CONCLUSION

Combination of Calcium Chloride with the monovalent NaCl and no electrolytic sucrose was investigated. It is concluded that adding NaCl to the CaCl2 DS increased the overall RSF without much affecting the water flux, whereas the addition of the low diffusing and larger sized sucrose component resulted in reducing both the flux and RSF to significant values.

V. REFERENCES

[1]   M. T. M. Pendergast, M. S. Nowosielski-Slepowron, and J. Tracy, "Going big with forward osmosis," *Desalin. Water Treat.*, vol. 57, no. 55, pp. 26529–26538, Nov. 2016, doi: 10.1080/19443994.2016.1168581.

[2]   D. L. Shaffer, J. R. Werber, H. Jaramillo, S. Lin, and M. Elimelech, "Forward osmosis: Where are we now?," *Desalination*, vol. 356, pp. 271–284, 2015, doi: 10.1016/j.desal.2014.10.031.

[3]   T. Alejo, M. Arruebo, V. Carcelen, V. M. Monsalvo, and V. Sebastian, "Advances in draw solutes for forward osmosis: Hybrid organic-inorganic nanoparticles and conventional solutes," *Chemical Engineering Journal*, vol. 309. Elsevier B.V., pp. 738–752, 01-Feb-2017, doi: 10.1016/j.cej.2016.10.079.

[4]   W. Y. Chia *et al.*, "Factors affecting the performance of membrane osmotic processes for bioenergy development," *Energies*, vol. 13, no. 2. MDPI AG, p. 481, 19-Jan-2020, doi: 10.3390/en13020481.

[5]   G. W. Batcheider and W. Ave, "United States Patent Office 3,171,799 PROCESS FOR THE DEMENERALIZATION OF WATER," Aug. 1962.

[6]   J. O. Kessler and C. D. Moody, "Drinking water from sea water by forward osmosis," *Desalination*, vol. 18, no. 3, pp. 297–306, Jun. 1976, doi: 10.1016/S0011-9164(00)84119-3.

[7]   Q. Ge, M. Ling, and T. S. Chung, "Draw solutions for forward osmosis processes: Developments, challenges, and prospects for the future," *J. Memb. Sci.*, vol. 442, no. October 2017, pp. 225–237, 2013, doi: 10.1016/j.memsci.2013.03.046.

[8]   Q. Ge, P. Wang, C. Wan, and T. S. Chung, "Polyelectrolyte-promoted Forward Osmosis-Membrane Distillation (FO-MD) hybrid process for dye wastewater treatment," *Environ. Sci. Technol.*, vol. 46, no. 11, pp. 6236–6243, Jun. 2012, doi: 10.1021/es300784h.

[9]   D. Li, X. Zhang, J. Yao, G. P. Simon, and H. Wang, "Stimuli-responsive polymer hydrogels as a new class of draw agent for forward osmosis desalination," *Chem. Commun.*, vol. 47, no. 6, pp. 1710–1712, Jan. 2011, doi: 10.1039/c0cc04701e.

[10]   A. Achilli, T. Y. Cath, and A. E. Childress, "Selection of inorganic-based draw solutions for forward osmosis applications," *J. Memb. Sci.*, vol. 364, no. 1–2, pp. 233–241, 2010, doi: 10.1016/j.memsci.2010.08.010.

[11]   R. W. Holloway, R. Maltos, J. Vanneste, and T. Y. Cath, "Mixed draw solutions for improved forward osmosis performance," *J. Memb. Sci.*, vol. 491, pp. 121–131, 2015, doi: 10.1016/j.memsci.2015.05.016.

[12]   K. S. Bowden, A. Achilli, and A. E. Childress, "Organic ionic salt draw solutions for osmotic membrane bioreactors," *Bioresour. Technol.*, vol. 122, pp. 207–216, Oct. 2012, doi: 10.1016/j.biortech.2012.06.026.

2nd Day, 16th December, 2020 **Technical Session 3-A (Google meet/Zoom)** **Membrane Separation and Water Treatment**	
Session Chair: **Prof. Dr. Khadija Qureshi** Session Co-Chair: **Prof. Dr. Muhammad Younas**	
Syed Ziaullah *(Dept. of Chem Eng., UET Peshawar)*	Computational fluid dynamics of hollow fibre membrane contactors for recovery of salts through osmotic membrane distillation
Saddam Hussain Dal *(Dept. of Chem Eng., MUET Jamshoro)*	Tea Bag Model Using Fe-Coated Chitosan as an Adsorbent for Dearsenification of Water
Misbah Ullah *(USPCAS-E UET Peshawar)*	Experimental investigation of vacuum membrane distillation for water desalination
Kashif Khan *(Dept. of Chem Eng., UET Peshawar)*	Synthesis of self-supported fly ash based geo-polymeric membrane by incorporating reduced graphene oxide
Muhammad Adnan *(Dept. of Chem Eng., MUET Jamshoro)*	Removal of Copper from Drinking Water Using Manganese Oxide Coated Adsorbent (MOCD)

Computational fluid dynamics of hollow fibre membrane contactors for recovery of salts through osmotic membrane distillation

Syed ziaullah [A], Muhammad Ayaz [B], and Mohammad younas[C]

A, 1 zia.syed1992@gmail.com, University of Engineering and Technology, Peshawar, Pakistan.

2 University of Engineering and Technology, Peshawar, Pakistan.

Abstract-The industrial waste water containing inorganic salts pose a great risk to aquatic life. To save aquatic life and utilize the inorganic salts these needs to be recovered from industrial waste water. Due to its easy scale up and low energy consumption, membrane distillation crystallization is one the best method for recovery of inorganic salts from water expelled by industries as waste. In the contemporary research, a membrane conactors whose fibres are hollow is used to simulate membrane distillation crystallization process. Numerical model is applied to recovery of inorganic soluble salts from aqueous solution with Sodium chloride as osmotic agent in (HFMC). To address the transfer of solute from fiber 's one side (aqueous phase) to fiber 's other side (osmotic phase), convection-diffusion based mass transfer Navier Stokes equations is implemented. The equations are solved numerically in the COMSOL Multiphysics™ software. The transmembrane flux increased with increase of osmotic concentration while increase or decrease of feed concentration and has no appreciable effect. The results were in good agreement with literature.
Keywords— CFD; Salt recovery; HFMC, membrane crystallization, numerical simulation

I. INTRODUCTION

Now-a-days clean technologies for removal of inorganic salts from waste water have attracted many researchers. These technologies use porous membrane contactors that achieve salts recovery through membrane distillation crystallization [1]. Membrane distillation crystallization in comparison to conventional crystallization processes use low energy have theoretical 100% rejection, low operating pressure and temperature. For the determination of position of interface between feed and solvent, the membrane feature of water attraction will be used [2]. Furthermore both phases can be selected without foaming and entrainment problems. [3, 4].

There are many membrane contractors available but most recognition is given to hollow fibre membrane contactors [1].On both sides of the HFMC i.e. Shell and lumen sides, two phases flow consistently which form an interface through pores of fiber wall [5]. High efficiency along with recovery of inorganic salts and removal of equilibrium limitations are achieved using membrane contractors [6].Osmotic membrane distillation is based on hollow fiber membrane contractor process which feed and osmotic streams runs counter currently in tube and shell sides respectively and the inorganic salts are obtained by the suction of water from feed side by osmotic stream through hydrophobic membrane as shown in Figure 1.
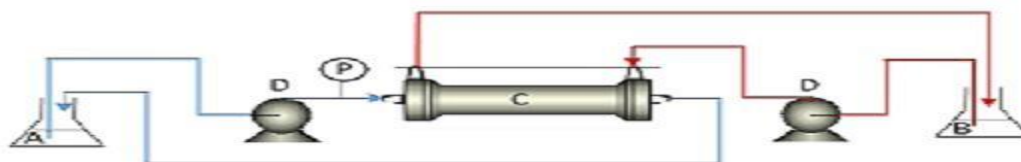
Figure 1. Osmotic membrane distillation-crystallization setup A inorganic salts laden industrial

waste water; B, Nacl solution; C, HFMC; D, pumps; P, System for controlling of pressure; E, pool

for crystal widening

On recovery of inorganic salts from wastewater based on membrane contactors (HFMC) with

hollow fibers, a great investigation has been done. However on the procedure of transport of mass and characterization of membrane contactors with hollow fibres, research is limited. Some researchers developed different mass transfer models across HFMC [6, 7].

Diffusion through a small hole and steady axisymmetric passage represented by numerical model was presented by Sushant et al [8] and verified it with Literature. The experimental data and simulation results were in good agreement. The outcome implied that the flux increased by increasing average temperature and rate of flow of feed while with increasing permeate pressure it decreased. When the concentration of salt of feed was in parts per million of forty thousands of sodium chloride, a removal of ninety nine percent was observed.

To probe in to the consequences of properties of membrane and variables of operation for sea-water desalination in modules by distillation through membrane by head-on exposure, Anas M. et al [9] applied computational fluid dynamics (CFD). For depiction of field of concentration, temperature and velocity, the laminar model was used while SST (shear stress turbulence) mathematical model was used for the modules containing spacers. The flow of volume through the membrane and concentration gradient at membrane interface was increased with a decrease in thickness and by increasing the rate of flow, it increased. The flux was increased more than 50% and polarization was reduced up to 50%.

II. MODEL DEVELOPMENT

A 2-D axial-radial mass transfer model will be developed for flow-cell shown in Figure 2 assuming diffusion in membrane and convection-diffusion transfer of solute in tube and shell.
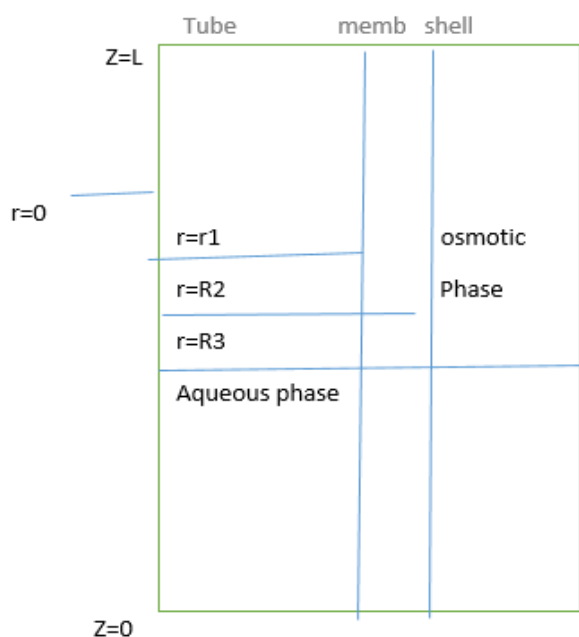
Figure 2. Speculative HFMC module flow cell

SIMULATION PARAMETERS

Table 1   Simulation Parameters

Tube side diffusion co-efficient	1.46e-9 m/s
membrane side diffusion co-efficient	2.51 e-5 m/s
shell side diffusion co-efficient	1.60 e-9
Scale factor	200

MODEL EQUATIONS

TUBE SIDE

Transfer of solute in tube side is due to conduction-convection and is given by:

$$D_{tube}\left[\frac{\partial^2 C_{tube}}{\partial r^2} + \frac{1}{r}\frac{\partial C_{tube}}{\partial r} + \frac{\partial^2 C_{tube}}{\partial z^2}\right] = u_{z-tube}\frac{\partial C_{tube}}{\partial z} \quad (1)$$

Whereas D_{tube} ($m^2 S^{-1}$), C_{tube} (mol m^3) and u_{z-tube} (m S^{-1}) represents diffusion coefficient, concentration of water solute and axial flow velocity of tube side, respectively
As laminar and fully developed flow is assumed in the tube side therefore the equation used for velocity distribution in this section is given as:

$$u_{z-tube} = 2u\left[1 - \left(\frac{r}{R1}\right)^2\right]$$

Whereas, u (m S^{-1}) represents tube's inside average velocity

MEMBRANE

Solute transfer through membrane is done by diffusion and is given by the following equation [1-2, 6]:

$$D_{mem}\left[\frac{\partial^2 C_{mem}}{\partial r^2} + \frac{1}{r}\frac{\partial C_{mem}}{\partial r} + \frac{\partial^2 C_{mem}}{\partial z^2}\right] = 0 \quad (3)$$

Whereas D_{mem} ($m^2 S^{-1}$) and C_{mem} (mol m^{-3}) and u_{z-tube} (m S^{-1}) represents diffusion coefficient and concentration of water's solute through membrane's pores, respectively.

SHELL SIDE

Transfer of water in the shell side is done through diffusion and convection and is given by the following equation:

$$D_{shell}\left[\frac{\partial^2 C_{shell}}{\partial r^2} + \frac{1}{r}\frac{\partial C_{shell}}{\partial r} + \frac{\partial^2 C_{shell}}{\partial z^2}\right] = u_{z-shell}\frac{\partial C_{shell}}{\partial z} \quad (4)$$

Whereas D_{shell} ($m^2 S^{-1}$) and C_{shell} (mol m^3) represents diffusion coefficient and concentration of water in shell side, respectively. While $u_{z-shell}$ (m S^{-1}) represents velocity of osmotic solution.
In the shell side for velocity distribution Navier-stoke equation is used as given below:

$$\rho u_{z-shell} \cdot \nabla u_{z-shell} - \nabla \cdot \mu \left(\nabla u_{z-shell} + (\nabla u_{z-shell})^T\right) + \nabla p = 0$$
$$\nabla u_{z-shell} = 0$$

Whereas ρ (kg m−3) represents density, u (m s−1) the velocity vector, μ (Pa s) the viscosity, and p (Pa) the pressure:
The mass and momentum balance equations were coupled for concentration profile.

Numerical simulation

The governing equations were solved using CFD technique in COMSOL Multiphysics version 5.5 software. COMSOL software uses finite element method (FEM) for solving the model equations in this research. The membrane structural parameters are shown in Table 2 below:

Table 2. Membrane contactor structural parameters

Parameters	Data from manufacturer
Module configuration	Hollow fibers
Membrane/Potting Material	Polypropylene/Polyethylene
Fiber i.d/o.d (µm)	240/300
Wall thickness (µm)	40
Effective pore size (µm)	0.04
Porosity (%)	40
Effective fiber length (m)	0.16
Effective membrane surface area (m²)	1.4
Number of fibers	10200

III. RESULTS AND DISCUSSION

To obtain results after model solving, we did post processing.

MODEL VALIDATION

The validation of the presented axisymmetric model was carried out with the experimentation of previous work in literature [10].Comparison of the experimental and simulation work is presented in figure 3.It is shown that there is good agreement between the experimental data and the results gained by the model.
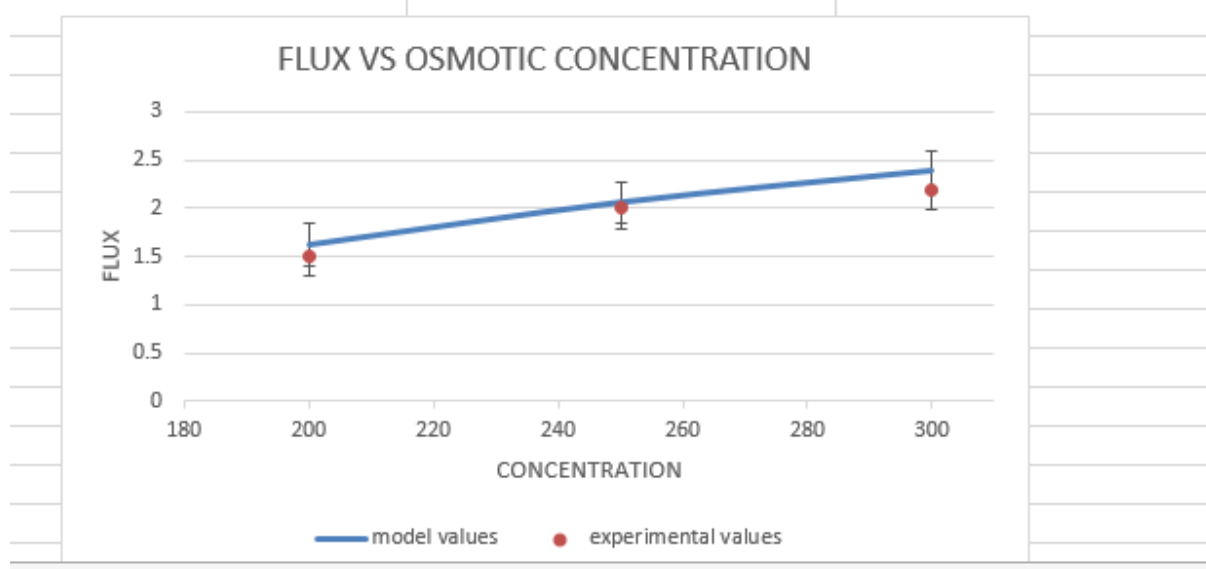
Figure 3. Comparison of model results with experimental data

In post processing the effect of concentration and flow rates of feed and osmotic solution on trans-membrane flux was studied.

A. **Concentration of feed**

With the increase or decrease of concentration of feed no effects on transmembrane flux was observed.

B   Concentration of osmotic solution

The transmembrane flux is affected by the change of osmotic concentration. It increases with increase of osmotic concentration while it decreases with decrease of osmotic concentration.The great transemembrane flux ensures more transport of water between tube and shell side and as a result maximum crystals are obtained.

C   flow rate of feed

There is no appreciable effect of increase or decrease of flow rate of feed on transmembrane flux.

D   Flow rate of osmotic solution

The transmembrane flux is not affected by change in flow rate of osmotic solution.

The surface concentration of water in tube, membrane and shell is shown in figure 4 while the graph of overall concentration is shown in figure 5.
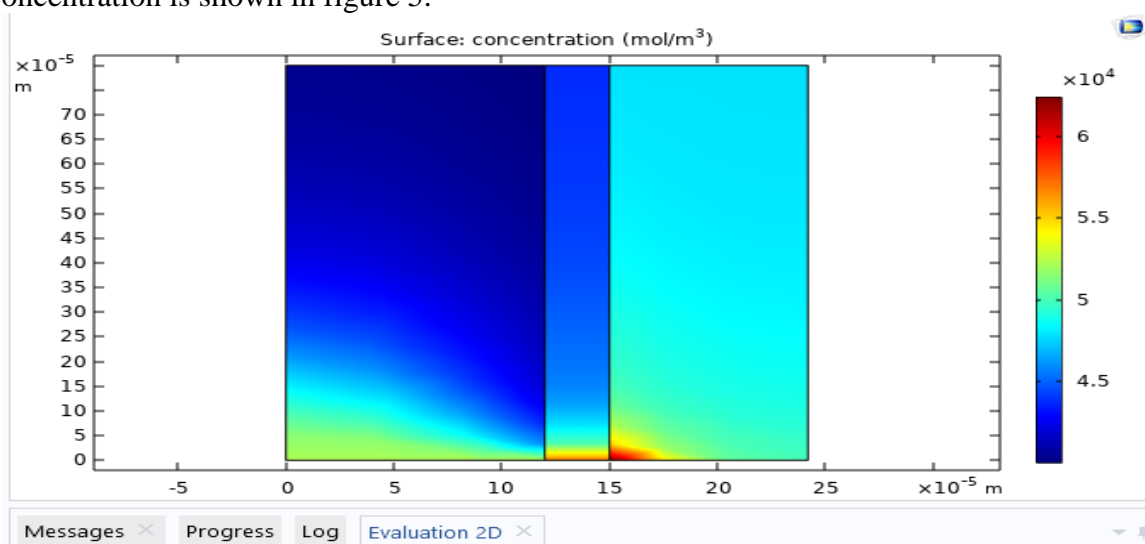
Figure 4. Surface concentration (Image from comsol multiphysics 5.5)
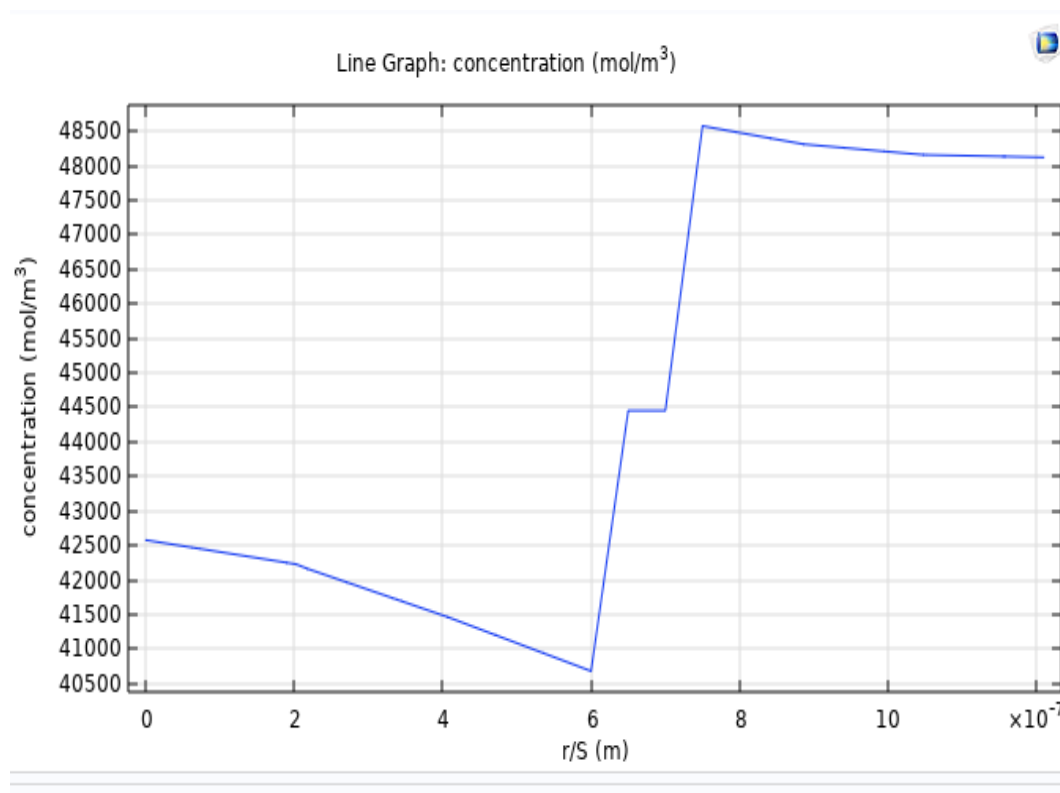
Figure 5. Overall concentration gradient

IV. CONCLUSION

A great threat   to aquatic life is possessed by industrial waste water containing inorganic salts. For the survival of aquatic life and utilization of inorganic salts, their recovery from industrial waste water is must. Due its easy scale up and low energy consumption, membrane distillation crystallization is one the best method for recovery of inorganic salts from water expelled by industries as waste. In the contemporary research, a membrane contactor whose fibres are hollow was used to simulate membrane distillation crystallization process. Numerical model is applied to recovery of inorganic soluble salts from aqueous solution with Sodium chloride as osmotic agent in (HFMC). To address the transfer of solute from fiber 's one side (aqueous phase) to   fiber 's other side (osmotic phase), convection-diffusion based mass transfer Navier Stokes equations is implemented. The equations are solved numerically in the COMSOL Multiphysics$_{TM}$ software. The transmembrane flux increased with increase of osmotic concentration while increase or decrease of feed concentration and has no appreciable effect. The result were in good agreement with literature

This study was used for recovery of sodium carbonate from waste water however it can also be used for other inorganic salts like potassium nitrate and sodium sulphate.

V. REFERENCES

1. Qin, L., Liu, Q., Meng, Q., Fan, Z., He, J., Liu, T., Shen, C., Zhang, G. Anoxic oscillating MBR for photosynthetic bacteria harvesting and high salinity wastewater treatment. *Bioresource technol.* **2017**, 224, 69-77

2. Smith, V. H., Tilman G. D., Nekola, J. C. Eutrophication: impacts of excess nutrient inputs on freshwater, marine, and terrestrial ecosystems.*Environ pollut*. **1999**, 100, 179-196.

3. G.C. Ionescu, G.L. Ionescu, Technologies for the removal of dissolved inorganic substances contained in wastewater, Int. J. Recent Dev. Eng. Technol. 3 (4) (2014) 2-6.

4. N.L. Nemerow, Industrial Waste Treatment:Contemporary Practice and Vision for the Future, Elsevier Science, 2010.

5. Marjani, A., Shirazian, S. Simulation of heavy metal extraction in membrane contactors using computational fluid dynamics. J. Desalination 281 (2011).

6. Younas, M., Druon-Bocquet, S., Sanchez, J. Kinetic and Dynamic Study of Liquid- Liquid Extraction of Copper in a HFMC: Experimentation, Modeling, and Simulation. AIChE J, 56 (2010) 1469–1480.

7. Gabelman, A., Hwang, S.T. Experimental results versus model predictions for dense gas extraction using a hollow fiber membrane contactor. J. Supercritical Fluids 35 (2005) 26–39

8. Sushant S, Kailash S, A., Rajeev K, Mathematical and CFD modelling of vaccum membrane distillation for desalination .. J. Desalination and water treatment.

9. Anas, M., Ahmed M, .,Umar F , Effect of membrane properties and operational parameters on systems for sea water desalination using computational fluid dynamics simulations J. Desalination and water treatment 161(2019) 92-107

10. Ruiz Salmon, K. Simon, C. Clérin, and P. Luis;salt recovery from waste water using membrane distillation crystallization 29 Oct 2018

Experimental investigation of vacuum membrane distillation system for water desalination

Misbah Ullah^{A}, Khurshid Ahmad^{A}, Muhammad Hassan^{A}, Ihsan Ur Rahman^{A}, Hurmat Khan^{A}.

^{A}US-Pakistan Center for Advanced Studies in Energy (USPCAS-E), University of Engineering and Technology Peshawar, Pakistan
misbah1110@yahoo.com, {khurshid, muhammad.hassan, ihsanrahman.uspcase }@uetpeshawar.edu.pk,
khanhurmat22@gmail.com

Abstract-Fresh and clean water shortage is one of the biggest problems in the world. Studies report that 70 percent area of the earth is covered by water but it is not suitable for drinking due to the high quantity of salt and other impurities. Only 3% is available as freshwater. Most countries in the world are using desalination technologies to make seawater fit for drinking by reducing the concentration of salt and other impurities. In this work, the performance of vacuum membrane distillation using hydrophobic microporous hollow fiber (HF) polypropylene membrane for the elimination of salt from salty water under various operating conditions such as different feed concentrations, feed flow rate, vacuum pressure, and temperatures of feed solution were investigated. Hot salt water was circulated over the shell side of the membrane while a vacuum was created on the tube side of the polypropylene hollow fiber (HF) membrane. A permeation flux of 6.15 kg/m^2.h was achieved for reverse osmosis (RO) water while 5.90 kg/m^2.h permeate flux was obtained for the salt concentration of 35 grams per liter at a 65 $^{\bullet}$C temperature, 1200 ml/min flow rate, and 11 kPa (abs) vacuum pressure. Moreover, the maximum flux for 50 grams per liter salt concentration turned out to be 5.60 kg/m^2.h. The results suggested that this technique works extremely well for salt removal from water. The results also suggested that the flux is more sensitive to the feed solution temperature than vacuum pressure created on the permeate side or flow rate of the feed and the salinity of the solution.

Keywords: Desalination, Hollow fiber membrane, Membrane performance, Vacuum membrane distillation.

I. INTRODUCTION

Researchers have found that more than one thousand million people are unable to get fresh potable water [1]. Potable water resources are depleting day by day which is a serious problem for the present as well as for future generations. Water covers 70 percent of the earth's area but most of it cannot be used for drinking purposes due to the high concentration of salt and other contaminations. Only a small portion is existing as freshwater which is in the form of glaciers, groundwater, ice caps, and surface water and a large amount of almost 97 percent is in the form of the ocean with a high concentration of salt [2, 3]. Since water can only be used for drinking purposes when the concentration of salt is less than 500 ppm, researchers [4, 5] have found various methods to remove salt and other minerals from the oceanic and brackish water. To overcome the problem of scarcity of water, purification and desalination techniques have been established which consume less energy and are environment friendly. Most countries produce drinking water by removing salt and other impurities from ocean water by using desalination and purification technologies. Around 80 counties in the world are facing a water scarcity problem [6]. Whereas Gulf countries like Kuwait, Saudi Arabia, and UAE entirely depend upon desalination for drinking water supply [7]. Seawater desalination is an encouraging substitute to fill the shortage of potable water [8]. There are many types of desalination technologies including Osmosis, capacitive deionization (CDI), multi-stage flash (MSF), humidification dehumidification (HD), multi-effect distillation (MED), and membrane distillation (MD) desalination. MD has four types a) vacuum membrane distillation desalination (VMD), b) Air gap membrane distillation (AGMD), c) Direct contact membrane distillation (DCMD) and d) Sweeping gas membrane distillation (SGMD) [3, 8]. The main significance of the membrane technology is due to its capability to gain a high permeate flux with a proper degree of separation. For this reason, vacuum membrane distillation is an appropriate arrangement for the desalination of seawater. The main advantages of this process are its high permeate flux and clean water under low feed temperature as compared to other technologies, insignificant conduction heat transfer due to small pressure on the permeation side, less conduction heat loss across the wall of the membrane, and no temperature polarization because of the reason that produced vapors are immediately removed from the permeate side during the process of vacuum membrane distillation [9-11].

II. Methodology

The sodium chloride crystals (Innovating science, the curated chemical collection) were dissolved in distilled water for making the feed solution of different concentrations. Experiments for vacuum membrane distillation desalination were performed by using hydrophobic HF microporous polypropylene (PP) membrane over a temperature range of 45-65 ^{o}C for saline water and flow rates changing between 700 ml/min and 1700 ml/min for the salt concentration of 35 g/L and 50 g/L over different vacuum pressures. The salt solution was first sent to the circulating water bath (Thermo Scientific DC10) ($\pm$ 0.1°C) for heating up to the required temperature with the help of Peristaltic pumps (Thermo Scientific Fh100 Peristaltic Pump) and then transferred to one side of the hollow fiber membrane. The peristaltic pump also maintained the feed solution flow rate at the desired rate. The other side (permeation side) of the membrane was exposed to a vacuum pump (Rocker 400). For distinct experimentations, various vacuum pressures were created. For increasing the temperature of the salt solution, the circulating water bath was set to the desired heating temperature. The temperature of feed solution both at the outlet and inlet of the HF membrane was measured by T-type Omega thermocouples connected to an NI data acquisition. The system of NI data attainment was connected to the computer for noticing the temperatures across the process. Condensate from the vacuum side of the membrane was collected in a cold trap which was immersed in an ice bath to condense the pure water vapors and the concentrated saline water was recycled to the salt solution tank. A laboratory-scale (B20002T) ($\pm$ 0.1g) was used for measuring the amount of purified water. The conductivity meter (HM DIGITAL EC Meter EC-3M) was used for measuring the conductivity of purified water. Distilled water was passed through the membrane at room temperature for some time to clean the membrane after every experiment. The flux was measured every 5 minutes across the entire experimental process, every process took 25 minutes. The mean value of the fluxes calculated at a steady-state process represents the permeation flux for each experimental run. The experimental setup is shown in Fig. 2.
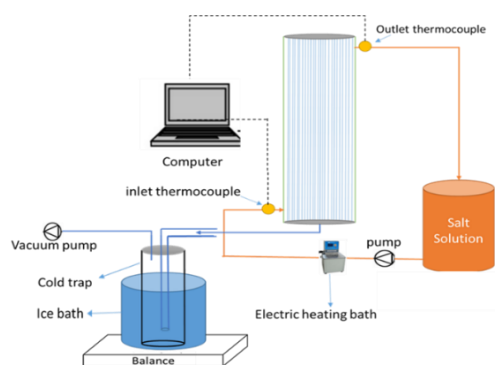
Fig. 1. Schematic diagram of Vacuum membrane distillation system
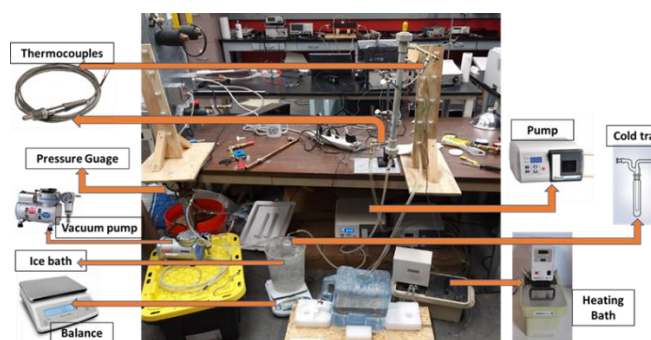
Fig. 2. Experimental setup of vacuum membrane distillation desalination system

TABLE I: Polypropylene membrane's Characteristics

Module Number	MD020CP2N	Number of fibers	40
Manufacturer	Microdyn	Shell Inner diameter (m)	0.021
Membrane Material	Polypropylene	Packing factor	0.7
Pore size (um)	0.2	Length (m)	0.45
Fiber's Outer diameter (mm)	2.8	Surface Area (m²)	0.1
Fiber's inner diameter (mm)	1.5	Porosity	0.7
The thickness of the membrane (mm)	0.65	Tortuosity	1.4

TABLE II: Equipment used in vacuum membrane distillation desalination system

Water heater	Circulating water bath (Thermo Scientific DC10) ($\pm$ 0.1°C).
Thermocouples	T-type Omega thermocouples connected to an NI data acquisition system.
Weight scale	B20002T, electronic balance laboratory scale ($\pm$ 0.1g)
Vacuum Pump	Rocker 400, Vacuum Pump
Conductivity meter	HM DIGITAL EC Meter EC-3M Electrical Conductivity

III. Results and Discussion

A. Effect of temperature on permeate flux

In Fig. 3, a plot of flux versus temperature is given. It shows that for a feed solution with a concentration of 35 g/L, the permeate flux increased directly with the temperature rise. The readings were recorded for temperature values of 45 °C, 55 °C, and 65 °C and feed flow rate of 1200 ml/min, and a vacuum pressure of 11 kPa. Fig. 4 shows the rise in flux was 2.35 times the original value when the temperature was changed from 45 to 55 °C and 3.95 times when the temperature was raised from 45 to 65 °C. The Permeation flux is

directly related to the vapor pressure because the real driving force for membrane distillation is the difference in vapor pressure across the hollow fiber membrane. The Vapor pressure increases directly as the feed temperature is raised, consequently escalating the permeation flux [12]. The flux increased at a very high rate with a temperature rise. The temperature cannot be raised beyond 65 °C as for higher values of temperature, the membrane may denature.
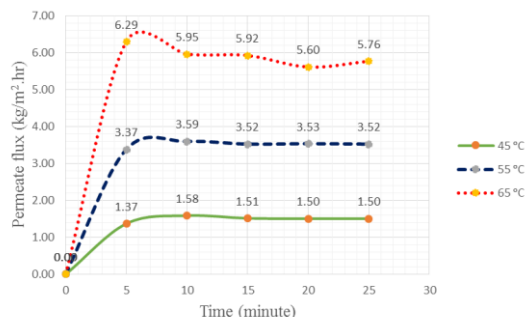
Fig. 3. Change in flux with time at various feed temperatures
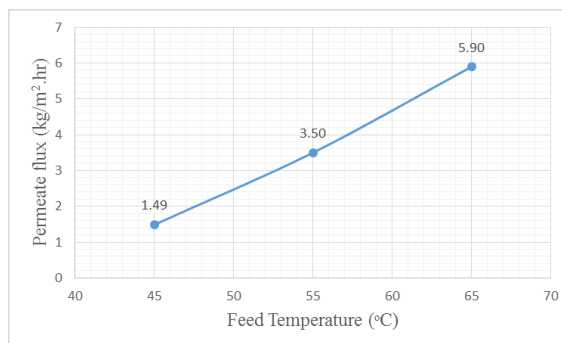
Fig. 4. Average flux as a function of various feed temperatures

B. Effect of vacuum pressure on permeate flux

The effect of vacuum pressure on the permeate flux is shown in Fig. 6. It depicts the relation of permeate flux to the vacuum pressure for the operating condition of 55 °C temperature, 1200 ml/min feed flow rate, and salt concentration of 35 g/L. The vacuum pressure ranged from 11 kPa to 16 kPa. From the results, it is clear that there was an inverse relationship between the vacuum pressure and flux. The flux decreased as a result of the increase in vacuum pressure on the permeate side. The permeated flux reduced by 54 % for a rise of vacuum pressure from 11 kPa to 13.5 kPa, and it further declined by 81 % when the vacuum pressure was raised from 11 kPa to 16 kPa which indicates a high impact of vacuum pressure on the flux, Fig. 5 shows the results. The flux increased as the vacuum pressure was reduced on the permeate side, this is because the reduction in pressure prevents the development of the boundary layer on the permeate side as it becomes a nearly insulated region and produces a high evacuation rate at the permeate side. Salt rejection in these experiments was 99.99 percent approving that the performance of VMD was outstanding.
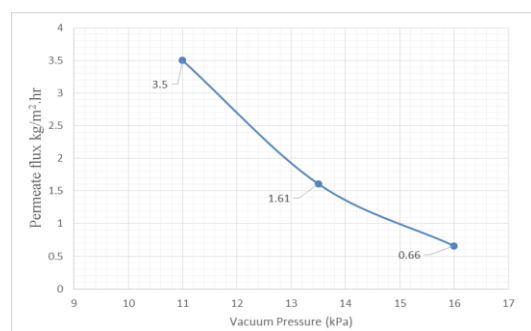
Fig. 5. Average flux as a function of various vacuum pressures
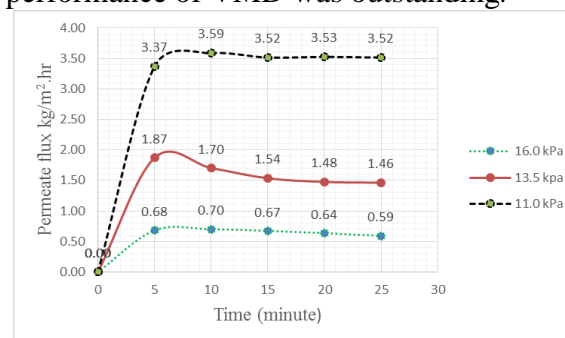
Fig. 6. Flux variation with time at various vacuum pressures

C. Effect of feed flow rate on permeate flux

In Fig. 8, a plot of flux versus feed flow rate is given. A change of feed flow rate from 700 ml/min to 1700 ml/ min in the vacuum membrane distillation process was recorded. The figure shows the flux increases with the increase in flow rate. Fig. 7 shows the increase in flux by 40 % for the change in flow rate from 700 ml/min to 1200 ml/min and 45 % for the change in flow rate from 700 ml/min to 1700 ml/min. This increase in permeation flux is due to the decrease in the width of the boundary layer at the feed side with the rise in the feed solution flow rate, which in turn increases the mass transfer coefficient as the flux of the HF membrane side increases [13]. The improvement in flux when the flow rate increased from 1200 to 1700 ml/min was insignificant. This is because the boundary layers have already been reduced at 1200 ml/min and no further reduction can be achieved with increasing flow rates.
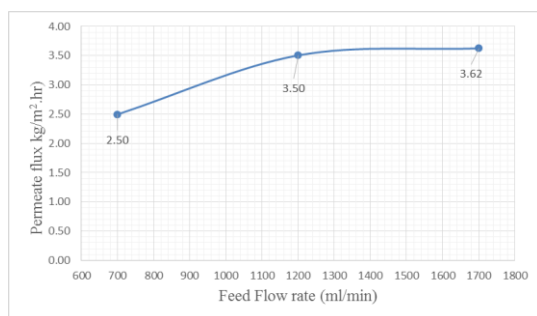
Fig. 7. Average flux as a function of various flow rates
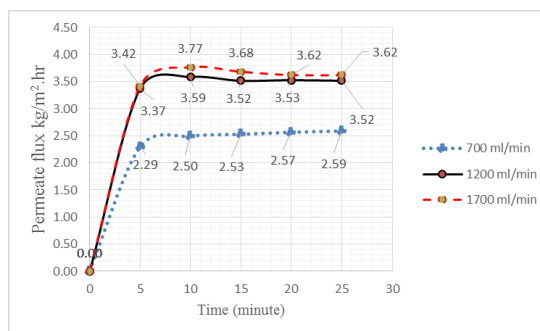
Fig. 8. Flux variation with time at different flow rates

D. Effect of concentration on permeate flux

The effect of concentration (0 g/L, 35 g/L, and 50 g/L) on the permeate flux at different feed solution temperatures, 11 kPa vacuum pressure, and 1200ml/L flow is shown in Fig. 9. It indicates that the permeate flux decreased as a result of the increase in the concentration of salt in the feed. An increase in salt concentration from 0 to 35 g/L resulted in a decrease in permeate flux by 13 %. At high salt concentration, the concentration boundary layer is created parallel to the thermal boundary layer, which when combined with the thermal boundary layer offers resistance to the transfer of vapor, thus reducing the required driving force which is needed for evaporation, which leads to a reduction in flux [14]. With the change in concentration from 0 g/L to 50 g/L, a reduction in flux by 22 % was recorded. This is due to the reality that the dissolved salt (compounds) reduces the vapor pressure of the solution [15]. Moreover, an increase in the salt concentration results in a reduction in the water activity coefficient which leads to a reduction in water partial pressure. Consequently, it will result in decreasing the driving force through the membrane interface. 6.15 $(kg/m^2.h)$, 5.90 $(kg/m^2.h)$ and 5.60 $(kg/m^2.h)$ were the maximum fluxes which were observed for RO water, 35 g/L and 50 g/L salt concentration at 65 °C temperature, 1200 ml/min flow rate, and 11 kPa (abs) vacuum pressure respectively.
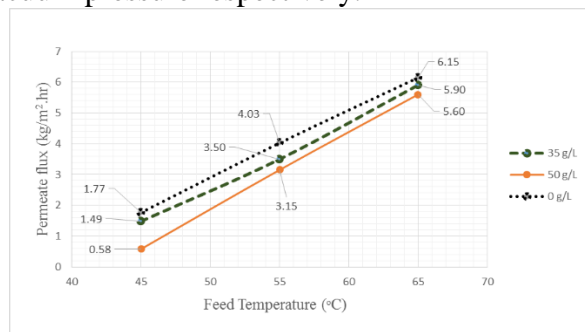
Fig. 9. Flux variation with different temperatures at different concentrations
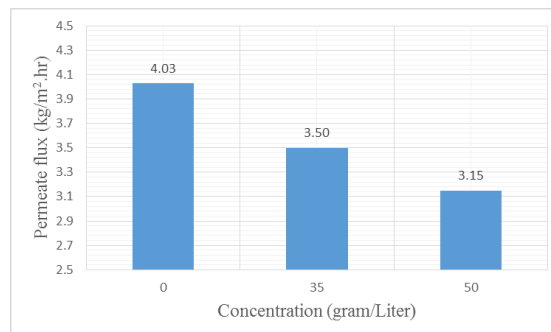
Fig. 10. Average flux as function of various concentrations

TABLE III: Net Permeate flux at different concentrations, different temperatures, constant flow rate, and vacuum pressure

Run	Temperature (°C)	Concentration (gram/Liter)	Flow rate (ml/min)	Vacuum pressure (kPa)	Permeate flux $(kg/m^2.h)$
1	55	35	700	10	2.50
2	55	35	1200	10	3.50
3	55	35	1700	10	3.62
4	55	0	1200	10	4.03
5	55	35	1200	10	3.50
6	55	50	1200	10	3.15
7	55	35	1200	10	3.50
8	55	35	1200	12.5	1.61
9	55	35	1200	15	0.67

TABLE IV: Net permeates flux at different concentrations, different pressure, different flow rates, and constant temperature

Run	Temperature (°C)	Concentration (gram/Liter)	Flow rate (ml/min)	Vacuum pressure (kPa)	Permeate flux $(kg/m^2.h)$
1	45	0	1200	10	1.77
2	55	0	1200	10	4.03
3	65	0	1200	10	6.15
4	45	35	1200	10	1.50
5	55	35	1200	10	3.50
6	65	35	1200	10	5.90
7	45	50	1200	10	0.58
8	55	50	1200	10	3.15
9	65	50	1200	10	5.60

IV. CONCLUSION

The effect on polypropylene hollow fiber membrane performance of different operating parameters such as feed solution concentration, feed flow rate, vacuum pressure, and feed solution temperature was investigated. The results indicate that the flux is directly related to the temperature and feed flow rate and inversely related to feeding concentration and vacuum pressure. The least influence of feed concentration on the efficiency of the system is one of the main advantages of the vacuum membrane distillation process for seawater desalination. The most prominent factor which affects the permeate flux is the feed temperature, while the least significant one is the concentration of the feed solution which influences the permeate flux.

V. REFERENCES

[1]   N. A. Eckardt, E. Cominelli, M. Galbiati, and C. Tonelli, "The future of science: food and water for life," vol. 21, ed: Am Soc Plant Biol, 2009, pp. 368–372.

[2]   P. H. Gleick, "Water in crisis," *Pacific Institute for Studies in Dev., Environment & Security. Stockholm Env. Institute, Oxford Univ. Press. 473p,* vol. 9, 1993.

[3]   M. M. A. Shirazi, A. Kargari, and M. J. A. Shirazi, "Direct contact membrane distillation for seawater desalination," *Desalination and Water Treatment,* vol. 49, pp. 368-375, 2012.

[4]   R. Einav, K. Harussi, and D. Perry, "The footprint of the desalination processes on the environment," *Desalination,* vol. 152, pp. 141-154, 2003.

[5]   M. K. Wittholz, B. K. O'Neill, C. B. Colby, and D. Lewis, "Estimating the cost of desalination plants using a cost database," *Desalination,* vol. 229, pp. 10-20, 2008.

[6]   I. C. Karagiannis and P. G. Soldatos, "Water desalination cost literature: review and assessment," *Desalination,* vol. 223, pp. 448-456, 2008.

[7]   A. D. Khawaji, I. K. Kutubkhanah, and J.-M. Wie, "A 13.3 MGD seawater RO desalination plant for Yanbu Industrial City," *Desalination,* vol. 203, pp. 176-188, 2007.

[8]   S. Parekh, M. Farid, J. Selman, and S. Al-Hallaj, "Solar desalination with a humidification-dehumidification technique—a comprehensive technical review," *Desalination,* vol. 160, pp. 167-186, 2004.

[9]   J. Mengual, M. Khayet, and M. Godino, "Heat and mass transfer in vacuum membrane distillation," *International Journal of Heat and Mass Transfer,* vol. 47, pp. 865-875, 2004.

[10]   M. Safavi and T. Mohammadi, "High-salinity water desalination using VMD," *Chemical Engineering Journal,* vol. 149, pp. 191-195, 2009.

[11]   A. C. Sun, W. Kosar, Y. Zhang, and X. Feng, "Vacuum membrane distillation for desalination of water using hollow fiber membranes," *Journal of membrane science,* vol. 455, pp. 131-142, 2014.

[12]   S. Devi, P. Ray, K. Singh, and P. S. Singh, "Preparation and characterization of highly micro-porous PVDF membranes for desalination of saline water through vacuum membrane distillation," *Desalination,* vol. 346, pp. 9-18, 2014.

[13]   H. Abdallah, A. Moustafa, A. A. AlAnezi, and H. El-Sayed, "Performance of a newly developed titanium oxide nanotubes/polyethersulfone blend membrane for water desalination using vacuum membrane distillation," *Desalination,* vol. 346, pp. 30-36, 2014.

[14]   T. Mohammadi and M. A. Safavi, "Application of Taguchi method in optimization of desalination by vacuum membrane distillation," *Desalination,* vol. 249, pp. 83-89, 2009.

[15]   A. Criscuoli, M. C. Carnevale, and E. Drioli, "Evaluation of energy requirements in membrane distillation," *Chemical Engineering and Processing: Process Intensification,* vol. 47, pp. 1098-1105, 2008.

Synthesis of self-supported fly ash-based hybrid geopolymeric membrane by incorporating porous reduced graphene oxide

[1]*Kashif khan, [1]Saeed Gul

[1] Department of Chemical engineering University of Engineering and Technology, Peshawar, 25000 Pakistan

Abstract— **Inorganic membrane has attracted great attention in the recent years because of its high mechanical strength, good chemical resistance and long life but its application is limited due to the heat intensive steps involved in its synthesis and the source material are expensive. Geopolymeric membrane synthesis is a low-cost sintering free technique and uses waste fly ash as raw material. In this research work we report sintering free, eco-friendly and economical synthesis of geopolymeric membrane. Geopolymer slurry was obtained by mixing fly ash, porous reduced graphene oxide (PRGO) and alkaline activator, the viscus paste was then expanded with hydrogen peroxide and egg albumen. Geopolymer paste was then molded and cured at 60°C in a closed environment. Compressive strength of the hybrid geopolymeric membrane were investigated. The study revealed that mechanical strength could be controlled by adding different amount of PRGO.**

Keywords— **Geopolymeric membrane, Porous reduced graphene oxide, egg albumen, hydrogen peroxide, compressive strength.**

I. INTRODUCTION

Ceramic membranes are well devolved, have controlled porous structure and good compressive strength. Inorganic membranes have been widely used for different membrane processes and had delivered good results. However, the synthesis of ceramic membrane is an energy intensive process due to high sintering temperature i.e. above 1000 ^{0} C. Further, the source materials are also very expensive which increase the overall cost of the process[1]. Geopolymerization is sustainable, cost effective and sintering free novel technique for synthesis of inorganic binding materials[2]. Geopolymerization is a heterogenous reaction between high alkali and aluminum silicate which form a semi crystalline compound known as geopolymer. The source material is alkaline activator ($NaOH.Na_2SiO_3$) and fly ash. Coal fly ash is rich in pozzolanic materials (alumina and silica) is obtained from a coal power plant. Geopolymerization is also an ecofriendly process because it is also utilizing waste fly ash as a source material which is an environmental threat[3]. Currently geopolymeric membrane has been widely recognized because of its easy synthesis, low cost, free sintering, alkali resistive and environmental friendly[4]. A metakaolin based geopolymeric membrane has been prepared using hydrogen peroxide as foaming agents for the purification of paper pulp green liquid. The study was done to find the effect of foaming agents on the morphology of the membrane. The porosity enhanced with hydrogen peroxide but the mechanical strength drastically reduced from 14 MPa to 4 MPa[5]. Chengyang bai-Paolo columbo synthesized metakaolin based geopolymeric membrane using hydrogen peroxide and egg albumen as surfactant. Porosity of the membrane was 74 % with the compressive strength of 4 MPa [6]. Graphene and its derivatives have been emerged as prominent reinforcing for composite materials. Graphene sheets have been used to upgrade the mechanical properties of different organic polymers[7]. GO has been used to enhance the compressive strength and electrical conductivity of fly ash geopolymers[8] this can be due to the excellent mechanical properties of GO(40 GPa tensile strength and 307 GPa young's modules) and the strong interaction between the wrinkled GO sheets and the matrix[9].

In the previous studies the graphene geopolymer composite was studied for concrete or electrical purposes in the current work we portray such a method to synthesis a hybrid geopolymeric composite membrane and to characterize the effect of PRGO on the mechanical properties and morphology of the membrane.

II. METHODOLOGY

A. Porous reduced GO synthesis

GO was synthesized in the laboratory with the help of modified hummer`s method. In this technique, graphite was oxidized with sulfuric acid and potassium permanganate which is very good oxidizing agent for GO [10]. 2 grams of graphite was added to sulfuric acid and stirred in a beaker on magnetic stirred for 2 h until a dark solution was obtained. The solution was then put on an ice bath to maintain its temperature below 20 ºC and KMnO4 was slowly added to the solution to obtain dark green colure solution. Then solution was then removed from ice bath and 100 ml of water was added and then the reaction was neutralized with hydrogen peroxide. The solution was then filtered and washed with hydrochloric acid and deionized water. The obtained paste was then dried in muffle furnace at 70 ºC to get. The obtained GO was the converted into PRGO by combustion method described by Q.Y. Yang in the paper.

B.Synthesis of Flat Geopolymeric membrane

Lakhra power plant (Sindh, Pakistan) provided the class F fly ash was used in the process which has an optimum silica alumina ratio of (2.8). The mechanical properties and pore size depend on the silica alumina ratio. 10 M NaOH solution and sodium silicate were used to chemically activate the fly ash. Basic activator arrangement was set up by dissolving sodium hydroxide in distilled water and stir for 30 mins at 125 rpm on a magnetic stirrer. Then sodium silicate was added in the ratio of 2.5 to sodium hydroxide. The mixture was then stirred at 60 rpm for 24 hrs.' to obtain a uniform solution. Chemicals (NaOH, Na_2SiO_3) was provided by sigma Aldrich. PRGO in different weight percent (0.3,0.7,1wt%) was then added to 50 ml deionized water and stirred for 3 hrs, a uniform suspension was formed. Alkaline activator solution, graphene oxide suspension and surfactant (H_2O_2 1 wt.%, egg albumen 5 wt. %) is mixed and stirred for 30 mins to form a uniform suspension. Fly ash (2.5 weight ratio Fly ash/AA) is mixed with the alkaline activator in a mixer for 1 hr to form a uniform paste. Paste was then molded in (4cm*2cm) molds and cure at 60 ℃ in muffle furnace for 24 hrs. Fig I summarizes the method carried out for the synthesis of membrane.
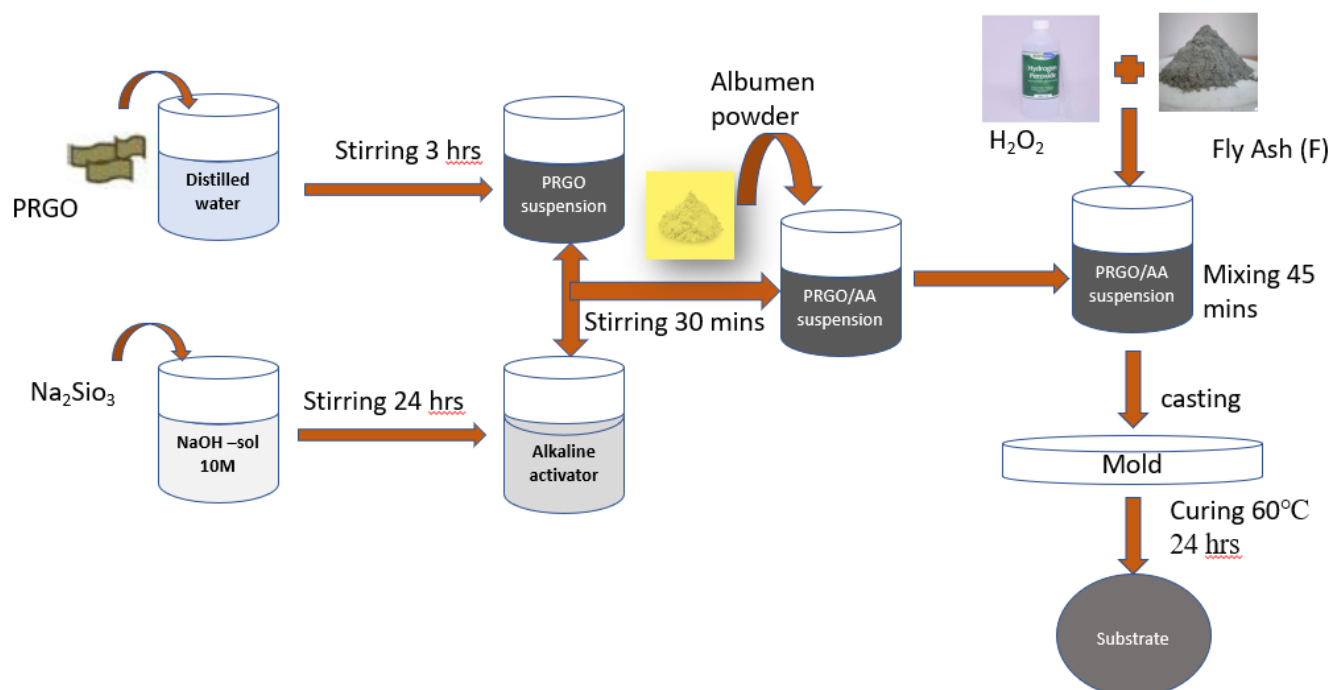
Figure 2 GP Membrane preparation method

III. RESULTS AND DISCUSSION

A. XRF Analysis

XRF analysis of the fly ash received from the Lakhra power plant shows that it contains suitable amount of silica and alumina for geopolymerization reaction. The power plant Fly ash contain 85% of silica and alumina oxides which is perfect for geopolymerization as shown in the Table 1. XRF analysis constitute that fly ash have 63% silica and 22 % alumina. The results show that fly ash does not requires any additive for the silica alumina ratio adjustment. The ratio of silica to alumina were 2.8 from the XRF analysis Silica and alumina percent composition plays an important role in the compressive strength of geopolymer material[11].

Table 1 **XRF analysis of fly ash**

Oxides	Composition %
Al_2O_3	23
Si_2O_3	61
CaO	4
MgO	8.2
K_2O	0.7
Na_2O	1.7
TiO_2	1.3

B. Compressive strength Analysis

Generally, geopolymers are extremely porous it is due to the aqua pore solution evaporation and incomplete reaction of the materials. As a result, the compressive strength of the geopolymer reduce due to the un reacted fly ash and the resulted geopolymer are highly porous. The Graphene based geopolymers are on the other hand less porous because of the good chemical bonding between the graphene and geopolymer thus results in dense micro structure[12]. The compressive strength of geopolymer with different amount of PRGO was measured through UTM. It is concluded that the compressive strength and stiffness of the PRGO geopolymer composite improved with increasing amount of PRGO as shown in FIG 2. Ranjbar used low calcium fly ash in their research but the difference was that they used graphene in the form of graphene nano pellets (GNP). Because of toughening enhancer mechanisms and uniform stress distribution by increasing GNP material, the incorporation of GNP showed an increase in the compressive and flexural strength, toughness and stiffness of the composites. The presence of overlapping GNPs, however, caused defects, leading to the elimination of the extra resistance from the drag by GNP sheets and stress concentration, respectively [13].
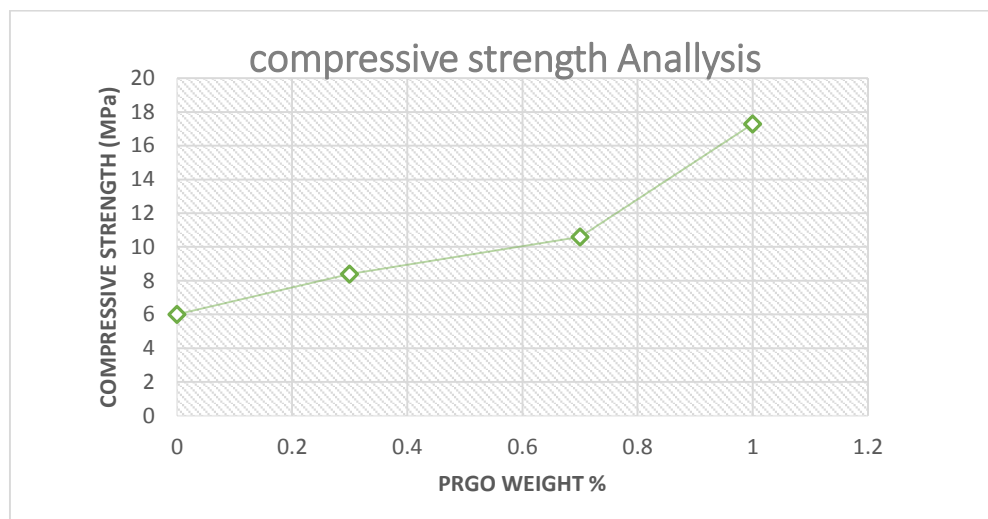
Figure 3 Effect of PRGO content on the compressive strength of geopolymer

IV. CONCLUSION

Incorporating PRGO in the fly ash based geopolymer offer great potential to enhance the compressive strength and Longevity of the fly ash based geopolymer. This study will help to improve the use of geopolymer as membrane which is eco-friendly and economical because it uses fly ash as raw material which is an environmental threat. The results of this study show that the compressive strength of the geopolymers were increased from 6 MPa to 17 MPa by incorporating 1% (by weight of fly ash) of PRGO. The PRGO not only increased the geopolymers polymerization but also surface quality of the geopolymers.

V. REFERENCES

[1]   A. Naveed, S. Gul, N. U. Amin, M. Khraisheh, and R. Gul, "Graphene Oxide (GO) Based Coated Geopolymeric Membrane for Concentrating Orange Juice through Forward Osmosis," *Int. J. Fruit Sci.*, vol. 00, no. 00, pp. 1–14, 2020, doi: 10.1080/15538362.2020.1753140.

[2]   M. F. Zawrah, R. A. Gado, and R. M. Khattab, "Optimization of Slag Content and Properties Improvement of Abstract :," pp. 40–57, 2018, doi: 10.2174/1874088X01812010040.

[3]   S. F. Azzahran Abdullah, L. Yun-Ming, M. M. Al Bakri, H. Cheng-Yong, K. Zulkifly, and K. Hussin, "Effect of Alkali Concentration on Fly Ash Geopolymers," *IOP Conf. Ser. Mater. Sci. Eng.*, vol. 343, no. 1, 2018, doi: 10.1088/1757-899X/343/1/012013.

[4]   M. xue Xu, Y. He, Z. han Liu, Z. fa Tong, and X. min Cui, "Preparation of geopolymer inorganic membrane and purification of pulp-papermaking green liquor," *Appl. Clay Sci.*, vol. 168, no. November 2018, pp. 269–275, 2019, doi: 10.1016/j.clay.2018.11.024.

[5]   "Sci-Hub | Preparation of geopolymer inorganic membrane and purification of pulp-papermaking green liquor. Applied Clay Science, 168, 269–275 | 10.1016/j.clay.2018.11.024." https://scihub.wikicn.top/10.1016/j.clay.2018.11.024 (accessed Sep. 18, 2020).

[6]   C. Bai and P. Colombo, "High-porosity geopolymer membrane supports by peroxide route with the addition of egg white as surfactant," *Ceram. Int.*, vol. 43, no. 2, pp. 2267–2273, 2017, doi: 10.1016/j.ceramint.2016.10.205.

[7]   S. Yan *et al.*, "Effects of graphene oxide on the geopolymerization mechanism determined by quenching the reaction at intermediate states," *RSC Adv.*, vol. 7, no. 22, pp. 13498–13508, Feb. 2017, doi: 10.1039/c6ra26340b.

[8]   M. Saafi *et al.*, "Graphene/fly ash geopolymeric composites as self-sensing structural materials," *Smart Mater. Struct.*, vol. 23, no. 6, 2014, doi: 10.1088/0964-1726/23/6/065006.

[9]   H. Kim, A. A. Abdala, and C. W. MacOsko, "Graphene/polymer nanocomposites," *Macromolecules*, vol. 43, no. 16, pp. 6515–6530, 2010, doi: 10.1021/ma100572e.

[10]   D. A. Dikin *et al.*, "Preparation and characterization of graphene oxide paper," *Nature*, vol. 448, no. 7152, pp. 457–460, 2007, doi: 10.1038/nature06016.

[11]   A. Naveed, Noor-Ul-Amin, F. Saeed, M. Khraisheh, M. Al Bakri, and S. Gul, "Synthesis and characterization of fly ash based geopolymeric membrane for produced water treatment," *Desalin. Water Treat.*, vol. 161, pp. 126–131, 2019, doi: 10.5004/dwt.2019.24283.

[12]   N. S. Danial *et al.*, "Graphene geopolymer hybrid: A review on mechanical properties and piezoelectric effect," *IOP Conf. Ser. Mater. Sci. Eng.*, vol. 572, no. 1, 2019, doi: 10.1088/1757-899X/572/1/012038.

[13]   G. Xu, J. Zhong, and X. Shi, "Influence of graphene oxide in a chemically activated fly ash," *Fuel*, vol. 226, pp. 644–657, 2018, doi: 10.1016/j.fuel.2018.04.033.

Removal of Copper from Drinking Water Using Manganese Oxide Coated Adsorbent (MOCD)

Muhammad Adnan[A], Khadija Qureshi[B], Khan Muhammad[C] Muzamil Hussain Memon[D]

[A, B, C, D] = *Department of Chemical Engineering Mehran University of Engineering Sciences and Technology Jamshoro Pakistan.*

Abstract— **In this study, manganese-oxide coated adsorbent (M.O.C.D) was synthesized and characterized and then manganese oxide coated adsorbent (M.O.C.D) employed for the removal of the copper from drinking water in laboratory scale. F.T.I.R and Scanning electron microscopy (S.E.M) analysis were performed to determine structure, morphology, and crystallinity or amorphous phase of adsorbent properties. The batch study was carried out on adsorbent concentration, shaking time and adsorption dose. Further, the removal efficiency of copper increases with increasing the adsorbent dose and shaking time but it decreases with ionic strength. When M.O.C.D dose increase greater than 1g/l the copper absorptivity obtained from shaking time minute is less.**

Keywords— **batch studies, cationic pollutants, characterization, drinking water, manganese coated adsorbent.**

I. INTRODUCTION

Drinking-water impurity with several synthetic concoctions and intense metals, discharged from the various anthro-pogenic source has overturned into a global interest [1]. Drinking-water impurity is a commonly new issuance and spread out the pressure emergent because of phenomenal people development, industrialization, and urbanization ever since 1990s. The defilement water resources have vital impacts on the earth and human health [2]. For the most part, drinking water contains Copper (Cu) and other diverse light and substantial metals include Cr, Co, Cd, Pb, Ni, Hg, Zn and so on., has critical antagonistic impacts on human wellbeing either through lack or lethality because of over the top admission and furthermore cause cancer-causing impacts . In any case, an excess amount Copper (Cu) can cause adverse well-being impacts, including heaving, stomach spasms looseness of the bowels, and queasiness. It has alike been related with kidney ailment and liver harm [3]. Copper (Cu) focuses on water can be credited to both geo-genic and anthropogenic sources. The most noteworthy geo-genic and soil wellsprings of metals are weathering of rocks, mineral and vulcanization exercises from which the discharged metals discover their way into the water bodies. As per Pakistan Environmental Protection Agency (E.P.A) and World Health Organization (W.H.O) has suggested an incentive for Copper (Cu) present in drinking water esteem is 2 (mg/L) if esteem is surpassed to this isn't considered as standard one [4].

Various methods are accessible for water cleaning and metal recuperation activities from water. Huge numbers of these are built up techniques, while others are still in the trial organize. Frequently, just a blend of different treatment procedures can give the pro-fluent quality wanted. Inorganic substantial metals are typically expelled from fluid waste streams by synthetic precipitation, electro-deposition, and cementation [5]. Different techniques, including enacted carbon, particle trade, and turn around osmosis, can be utilized to think to squander streams and expel the overwhelming metals. Initiated carbon is viable in lessening hexavalent chromium, mercury, what's more, numerous metals are complexes by natural ligands. Likewise, different particle trade tars have been observed to be successful in diminishing metal particles from arrangement. Intrigue has risen and manganese oxide covered as of late in expelling overwhelming metals from arrangement by authoritative or covered with sand, biomass and other material to produce a low-cost adsorbent. Precipitation is common water purification technique, it's taken after by purification has a tendency to stay best well-known strategy utilized because of its straightforwardness [6-7]. Basically, precipitation includes changing the broke down metal particles into unsolvable durable state kinds by a synthetic response with precipitation, for example, a salt or sulfide. Usually, the unsolvable solids are evacuated by purification, which includes completely immersed filter media in water. A mixing of two phases i.e. precipitation response and purification, in single-phase appears favorable [8]. In the end, this can be accomplished by purification on responsive media and such system is named as an enacted un-saturated

filter, it's major contemplated aside Parramatta et al. For the evacuation of manganeses & iron. Essentially, it is initiated granulated filter media (e.g. sand) working in un-saturated circumstances (i.e. H_2O didn't completely possess all the sieve holes). The enactment of the media should be possible through $KMnO_4$ arrangements and past examinations have demonstrated that this method prompts speedier response rates of metals evacuation [9-10]. In addition, the nearness of sans water openings in the sieve circulates air through the H_2O which likewise advances the substance responses in the arrangement. Strong metal species shaped because of the precipitation response encourage and are expelled on the same filter media.

II. METHODOLOGY

The material was collected from Kotri Barrage District Jamshoro. All the chemicals used were of analytical reagent grade. Copper sulfite was used for the preparation of stock solutions. Hydrochloric acid and Sodium hydroxide were used to adjust the solution pH. Distilled water was used throughout the experimental studies. The preliminary procedure started by screening using sieve size is 200μm to take particle uniform using Russel sieve and weighing 450g material. then washing that sieved material and drying it at 105 °C for 12 hr in electro oven, after drying sand mixed with $KMnO_4$ (0.01N) for 2 hr. Now mixed material was washing server time with distilled water then again drying 105 °C at 12 hr and activated sand stored in plastics bottle for further process. Activated sand coated with manganese dioxide to synthesis M.O.C.A For preparation 350g sand (200 mm) add to 350 ml of a (0.2 M) potassium per magnet solution. Then add sodium hydroxide 350 ml of a (0.4M) solution in sand magnet were add to neutralize acid. Thereafter 350 ml of 0.3 M manganese chloride dropwise and mixed magnet stirrer. Sand manganese drying in oven for 24 h at 105 °C. Then wash dried overnight 105 °C, and stored in plastic bottles for further batch study. Then manganese's oxide coated adsorbent M.O.C.A were Characterized using FT-IR spectroscopic and S.E.M technique. Describe the methodology adopted to carry out the experimental/simulation work.

III. RESULTS AND DISCUSSIONS

A. Manganese's Oxide Coated Adsorbent (M.O.C.A) Scanning Electron Microscopy (S.E.M) Analyze

The Structure and morphology of Manganese's Oxide Coated Adsorbent (M.O.C.A) analyze using Scanning Electron Microscopy. The Fig.1 signifies the structure and morphology of the particulates constituents of adsorbent properties. The width and length of the constituent were measured on the amplifications of Photo-micrograph with a clear millimeter (mm) scale.
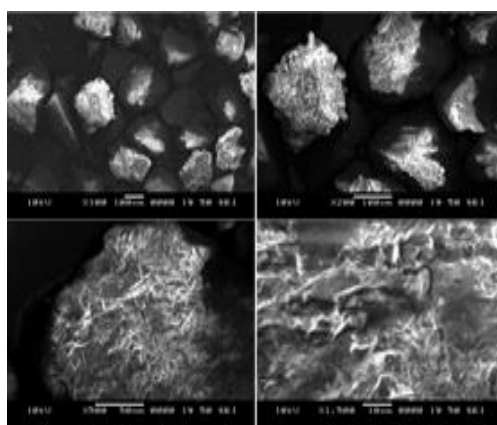
Fig.1. Manganese's Oxide Coated Adsorbent S.E.M Results

The width peak was recorded for a constituent with ordered surfaces. The microscope conditions used in the study were as follows: The accelerating voltage was 10 kV, the working distance was 19–50 mm, magnification x100, x200, x550, x1500 and resolution was 10, 20 & 100 μm when magnification and resolution rise adsorbents crystals showed clear. M.O.C.A scanning electron microscopy result shows the roughness, porous and MnO_2 particles attached with crystal particles of sand it is shown Fig.1.

B. FT-IR Spectroscopic Analysis of Manganese's Oxide Coated Adsorbent (M.O.C.A)

The FT-IR Spectroscopic analysis is commonly used to detect functional groups in compound organic combinations and to associate the resemblances between substances. In this study, FT-IR Spectroscopic was used to validate the functional groups and physical structure of the organic constituents. The FT-IR spectra of the constituents of the M.O.C.A are shown in Fig.2. Most of the bands are similar to those detected FT-IR spectra (Bodir et al. 2008, Xui et al. 2013). Frequently, the band in the highest-energy region is due to a huge quantity of OH.
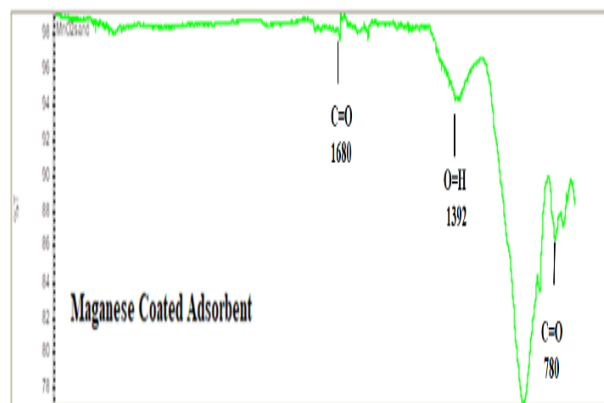
Fig. 2. FTIR Result Manganese's Oxide Coated Adsorbent (M.O.C.A)

The peaks of MOCA sample at 900.00 cm^{-1} resemble the C–H vibration to asymmetrical stretching of aliphatic structures, while other bands in the pattern region (1800 to 900 cm^{-1}) are compound; this is an outcome of numerous vibration modes in 1,2,4-trisubstituted (Bodirlau et al. 2008). The indications at, 1043.04 cm^{-1} can be recognized to C-O-R or C-O-H (esters or alcohols) vibrations (Cham and Li 2008; Zapate et al. 2009). In conclusion, FTIR spectroscopy was used to inspect the variations in the structure of the suggested wastes treatment. While all adsorbent spectra were alike (Fig.2 and Table.1), slight variations were detected from spectrum to spectrum, perhaps it representative that comparable strategy.

TABLE I: FUNCTIONAL GROUPS OF MANGANESE'S OXIDE COATED ADSORBENT (M.O.C.A)

S#	Functional group	M.O.C.A
1.	O=H Stretching	1392.00
2.	C-H Stretching	900.00
3.	C=O Stretching	780.42
4.	C-O Stretching	1275.20
5.	C=H Stretching	810.00
6.	CH2 and CH3 Stretching	1383.70
7.	C-O-H and C-O-R Stretching	1043.04

C. Effect of the Adsorbent Dose on Removal Efficiency of Copper

It is observed that's the effect of the adsorbent dose on the removal efficiency of copper, where a copper stock solution has been prepared as shown in Fig.3. The stock solution of copper and another sample of removal of copper analyzed on Atomic Absorption Spectroscopy (A.A.S) where stock solution results show copper is 5.852 ppm present. Another sample S2, S3, and S4 in which time is 60 min, R.P.M is 150 and pH is 6 parameters remain constant but adsorption dose change where S2 is 0.25g, S3 is 0.5g, and S4 is 1g. Their adsorption dose outcome shown in Table.2 and Fig.3 where S2 copper removal is 2.399ppm (57%), S3 is 1.780ppm (68%), and S4 is 0.846ppm (86%). The highest removal gets on 1g adsorbent dose and lowest 0.25g.
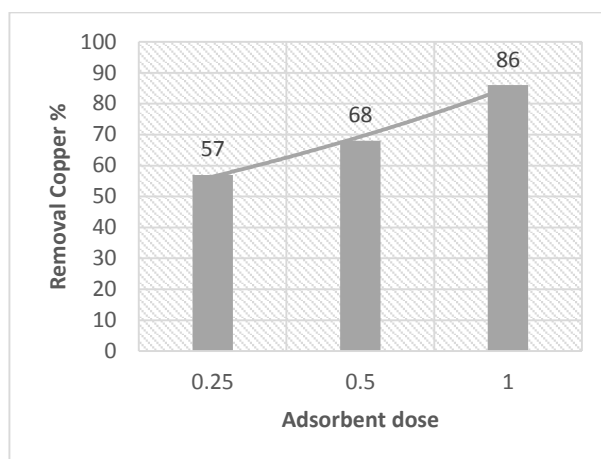
Fig. 3. The removal efficiency of absorbent dose.

TABLE II: EFFECT OF THE ADSORBENT DOSE ON THE REMOVAL EFFICIENCY OF COPPER

Samples	D	P	R	T	R	%
S2	0.25	6	150	60	2.399	57
S3	0.5	6	150	60	1.780	68
S4	1	6	150	60	0.846	86

D=Dosage (g), P=pH, R=RPM, T=Time (min), r=Removal Copper ppm, %=Percentage Removal Copper

D. Effect of the Content Time on Removal Efficiency of Copper

In this study effect of the content time on the removal efficiency of copper in which remain constant variables setup where pH is 6, RPM is 150 and adsorbent dose is 0.5g but changing variable is time which is 30, 60, and 90 min and the sample is S5, S3, and S6 as shown Fig.4 and Table.3.
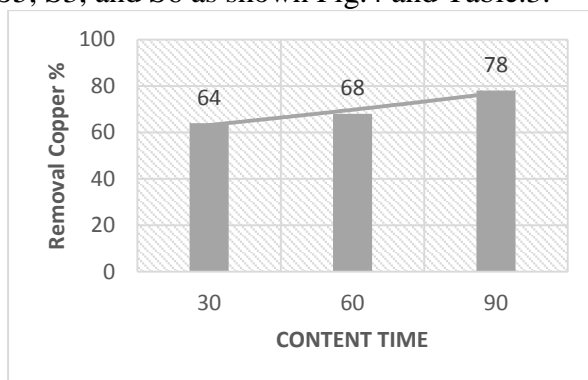
Fig. 4. Removal of efficiency of content time.

The result are S5 is 1.750ppm (64%), S4 is 1.780ppm (68%), and S6 is 1.256ppm (78%). The removal of copper is shown in S5 to S3 is less where time is less increase but S3 to S3 high where content is 90min.

TABLE III: EFFECT OF THE CONTENT TIME ON THE REMOVAL EFFICIENCY OF COPPER

Samples	D	P	R	T	R	%
S5	0.5	6	150	30	1.750	64
S3	0.5	6	150	60	1.780	68
S6	0.5	6	150	90	1.256	78

D=Dosage (g), P=pH, R=RPM, T=Time (min), r=Removal Copper ppm, %=Percentage Removal Copper

E. *Effect of the RPM on the Removal Efficiency of Copper*

It is investigated that effect of the R.P.M on the removal efficiency of copper when some constant variables where the dose is 0.5, pH is 6 and time is 60 min and another change variable RPM is 100,150 and 200. The result is shown in Fig.5 and Table.4 where S7 copper removal is 3.232 ppm (45%), S3 is 1.780ppm (68%), and S1 is 1.156ppm (76%). The maximum removal is shown sample is S1.
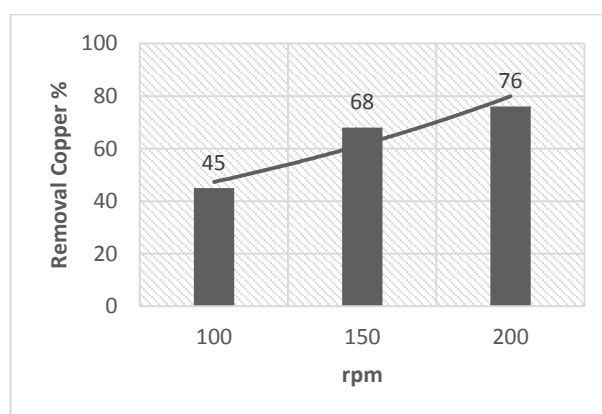
Fig.5. The removal efficiency of R.P.M.

TABLE IV: EFFECT OF THE RPM ON THE REMOVAL EFFICIENCY OF COPPER

Samples	D	P	R	T	R	%
S7	0.5	6	100	60	3.232	45
S3	0.5	6	150	60	1.780	68
S1	0.5	6	200	60	1.156	76

D=Dosage (g), P=pH, R=RPM, T=Time (min), r=Removal Copper ppm, %=Percentage Removal Copper

IV. CONCLUSION

The main objective of this research was to utilize native residue material for the formation of Manganese's Oxide Coated Adsorbent (M.O.C.A) which has been discovered that it is ideal for the preparation of high-quality adsorbent. The M.O.C.A formed in this work has been determined and found amorphous in nature and does not show any crystalline nature which is again ideal for preparation of high-quality adsorbent. The M.O.C.A formed at pH 5 value has a high specific surface area which is 370.2 m^2/g. The obtained silica gel characteristics show that it has high porous texture and great adsorption capacity. Also obtained product is not amorphous in nature and crystalline which is suitable for the preparation of adsorbent.

V. REFERENCES

[43] S. Chen, B. Mulgrew, and P. M. Grant, "A clustering technique for digital communications channel equalization using radial basis function networks," *IEEE Trans. on Neural Networks*, vol. 4, July 1993, pp. 570-578.

[44] S. Bajpai and M. Chaudhuri, "Removal of Arsenic from Ground Water by Manganese Dioxide–Coated Sand," Journal of Environmental Engineering, vol. 125, no. 8, 1999, pp. 782–784.

[45] N. Boujelben, J. Bouzid, and Z. Elouear, "Adsorption of nickel and copper onto natural iron oxide-coated sand from aqueous solutions: Study in single and binary systems," Journal of Hazardous Materials, vol. 163, no. 1, 2009, pp. 376–382.

[46] D. Filip, V. Thomaspeters, E. Deanadams, and J. Middlebrooks, "Residual heavy metal removal by an algae-intermittent sand filtration system," Water Research, vol. 13, no. 3, 1979, pp. 305–313.

[47] A. Rauf ,M. Javed, "Copper-toxicity to water and plankton in the river Ravi, Pakistan," International Journal of Agriculture and Biology (Pakistan), 2007.

[48] S. Lu and S. W. Gibb, "Copper removal from wastewater using spent-grain as biosorbent," Bioresource Technology, vol. 99, no. 6, 2008, pp. 1509–1517.

[49] S. Mehmood,A. Ahmad,A. Ahmed,N. Khalid, and T. Javed, , "Drinking water quality in capital city of Pakistan", Science Rep,vol 2, 2013, p.637.

[50] P. E. Lim, T. F. Wong, and D. V. Lim, , "Oxygen demand, nitrogen and copper removal by free-water-surface and subsurface-flow constructed wetlands under tropical conditions," Environment International, vol. 26, no. 5-6, 2001, pp.425-431.

[51] S. R. Taffarel and J. Rubio, "Removal of Mn2 from aqueous solution by manganese oxide coated zeolite," Minerals Engineering, vol. 23, no. 14, 2010, pp. 1131–1138.

[52] W. Zou, R. Han, Z. Chen, J. Shi, and Liu, "Characterization and Properties of Manganese Oxide Coated Zeolite as Adsorbent for Removal of Copper(II) and Lead(II) Ions from Solution," Journal of Chemical & Engineering Data, vol. 51, no. 2, 2006, pp. 534–541.

[53] 'Impact of chromium toxicity on water, plankton and bed sediments of River Ravi, Pakistan," International Journal of Biosciences (IJB), vol. 11, no. 5, 2013 pp. 294–300.

Technical Session 3-B (Google meet/Zoom)
Waste Utilization and Water Treatment

Session Chair: **Dr. Tanveer Iqbal**
Session Co-Chair: **Prof. Dr. Saeed Gul**

Presenter	Paper Title
Imran Ahmad *(Dept. of Chem Eng., UET Peshawar)*	Selection of task specific ionic liquids for Calcium-based batteries
M.Suleman *(Dept. of Chem Eng., MUET Jamshoro)*	Adsorption Of Arsenic (V) From Ground Water Using Zero Valent Iron Coated Beads As Adsorbent
Syed Nasir Shah *(UET Taxila)*	Removal of Methylene Blue using Biobased Activated Carbon Alginate Membrane
M. Aftab Khan *(Dept. of Chem Eng., UET Peshawar)*	Mixing of Coal and Solid Olive Waste to Enhance the Properties of Hybrid Fuel
Ihsanullah Qureshi *(MUET Jamshoro)*	Adsorption of Arsenite From Aqueous Solution Using Graphene Oxide / Fe_2O_3 Coated Indus Sand

Utilization of ionic liquids in Calcium-based batteries

Muhammad Imran Ahmad [A], Muhammad Noman[A], Mansoor ul Hassan Shah[B], and Huma Warsi Khan[C]

[A]*Centre for Advanced Studies in Energy, UET Peshawar*

[B]*Department of Chemical Engineering, UET Peshawar*

[C]*University Teknologi PETRONAS, Malaysia*

Abstract—**This paper aims to investigate the choice of electrolytes for calcium-based batteries. Carbonate solvent based electrolytes such as ethylene carbonate and propylene carbonate have been widely investigated for reversible plating and stripping in calcium-based systems. Such electrolytes are economically more viable, however are highly flammable and toxic. In this work a screening of ionic liquids was carried out using conductor-like screening model for real solvents (COSMO-RS) tool. Based on activity coefficient at infinite dilution, capacity, selectivity, and performance index ionic liquids suitable for application as electrolytes in calcium-based batteries were shortlisted. Overall, tetramethylammonium-sulphate [TMAm-SO4] was found to be a suitable ionic liquid as solvent for electrolytes in multivalent ion batteries. Experimental investigation is needed for validation and performance evaluation.**

Keywords— **Calcium-based batteries, COSMO-RS prediction, electrolytes, ionic liquids.**

I. INTRODUCTION

Increasing energy demands in Pakistan due to population and economic growth as well as desire to generate electricity through renewable energy technologies serve as a motivation behind increasing interest in energy storage devices. Lithium-ion batteries are commercially available, however, there is still need for exploration of materials that may be relatively widely available economically and are safer for use [1]. One of the preferred materials being investigated as an alternative for Lithium is Calcium being the fifth most abundant element in the Earth's crust [2-3]. Sources of Calcium are abundantly available in Pakistan [4]. The standard reduction potential of Calcium is -2.87 vs. NHE and has a charge capacity of 1.34 Ah/g which renders it to perform better than graphite employed in commercially available Lithium-ion batteries [5]. Although magnesium based energy storage systems have more advanced technology, nevertheless Calcium-based batteries may offer faster reaction kinetics [6]. However, demonstration of a stable electrolyte for multivalent-ion batteries such as Calcium-based batteries is considered to be a challenge [6]. This work aims to screen ionic liquids as suitable electrolytes for reversible plating and stripping in Calcium metal systems.

II. METHODOLOGY

The methodology followed primarily consisted of screening of ionic liquids using the conductor-like screening model for real solvents (COSMO-RS) as shown in Fig 1. However, a literature review was first carried out for identifying the properties of electrolytes based on which the COSMO-RS screening was performed.
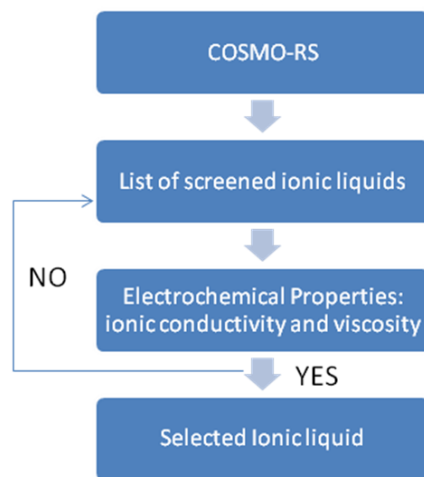
Fig. 1. Research methodology

Performance evaluation of screened electrolytes would be conducted subsequently for validation of the results.

III. RESULTS AND DISCUSSION

In this work six cations were screened in combination with nineteen anions resulting in a screening to 114 ionic liquids using COSMO-RS. The cations screened are shown in Table. 1.

TABLE I: CATIONS SELECTED FOR COSMO-RS SCREENING

S.No	Abbreviation	Cation
1	BMIm	1 butyl-3-methyl-imidazolium
2	BMPyrro	1-butyl-1-methyl-pyrrolidinium
3	BMPyri	1-butyl-3-methyl-pyridinium
4	BMPip	1-butyl-1-methyl-piperidinium
5	TBMPh	Tributylmethyphosphonium
6	TMAm	Tetramethylammonium

The method followed in COSMO-RS screening is based on activity coefficients at infinite dilution, and capacity wherein less ionic liquid is required corresponding to high capacity [7]. Capacity of ionic liquids predicted using COSMO-RS is presented in Fig. 2.
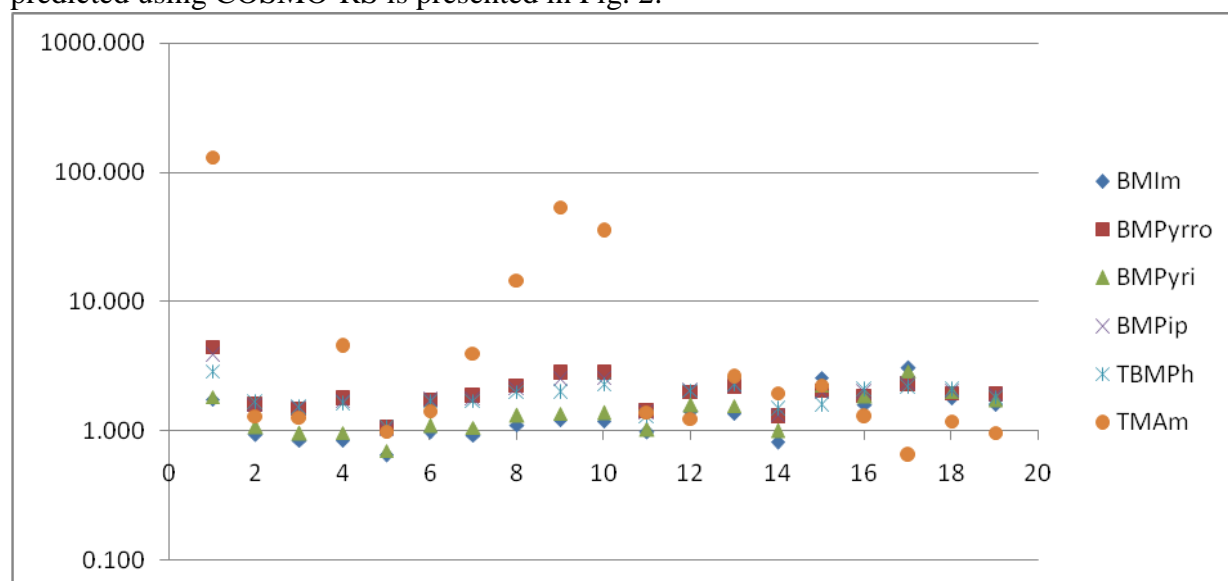
Fig. 2. Capacities of selected ionic liquids for propylene carbonate at 298.15 K

It may be observed from Fig. 2 that the highest capacities are predicted for the tetramethylammonium cation. Three anions for which highest capacities are predicted in combination with tetramethylammonium ion are SO_4^-, Cl^-, and Br^- respectively. Therefore, the most suitable ionic liquid for propylene carbonate is tetramethylammonium-sulphate.

IV. CONCLUSION

In this work screening of 114 ionic liquids was performed using COSMO-RS to predict the capacities of ionic liquids as solvents for propylene carbonate. Ionic liquids offer promising prospects for application as solvents for electrolytes in multivalent batteries such as calcium batteries. Tetramethylammonium cation was found to be suitable in combination with SO_4^-, Cl^-, and Br^- anions. Tetramethylammonium-sulphate was predicted to have highest capacity for propylene carbonate.

ACKNOWLEDGMENT

V. REFERENCES

[1] S. Engelke, "Current and Future Sodium-Ion Battery Research" *Storage4*.
[2] P. Canepa, G.S. Gautam, D.C. Hannah, R. Malik, M. Liu, K.G. Gallagher, K.A. Persson, and G. Ceder, "Odyssey of Multivalent Cathode Materials: Open Questions and Future Challenges" *Chem. Rev,* 117: 4287-4341, 2017.
[3] R.J. Gummow, G. Vamvounis, M.B. Kannan, and Y. He, "Calcium-ion Batteries: Current State-of-the-art and Future Perspectives" *Adv. Mater,*30: 1801702, 2018.
[4] G.S. Abbas, and A.H. Kazmi, *Metallogeny and Mineral Deposits of Pakistan,* Orient Petroleum Inc.: Islamabad, 2001.
[5] M.E. Arroyo-de Dompablo, A. Ponrouch, P. Johansson, and M.R. Palacin, "Achievements, Challenges, and Prospects of Calcium Batteries. In Press.
[6] S. Biria, S. Pathreeker, F.S. Genier, H. Li, and I.D. Hosein, "Plating and Stripping Calcium at Room Temperature in an Ionic Liquid Electrolyte"*ACS Applied Energy Materials*, 3: 2310-2314, 2020.
[7] H.W. Khan, A.V.B. Reddy, M.M.E. Nasef, M.A. Bustam, M. Goto, and M. Moniruzzaman, "Screening of ionic liquids for the extraction of biologically active compounds using emulsion liquid membrane: COSMO-RS prediction and experiments" *Journal of Molecular Liquids*, 309: 113122, 2020.

Adsorption of arsenic (V) from ground water using zero valent iron coated beads as adsorbent

M.Suleman[A*], Zafar ali[A], Mohsin ali[A] Khadija Qureshi[B], Zulfiqar bhatti[C]

Department of Chemical Engineering Department, Mehran University of Engineering and Technology, Jamshoro, Pakistan

[* A] **Corresponding Author**
E-mail: mohammadsulemanmemon@gmail.com

Abstract-Arsenic (V) removal from ground water has been accomplished for many years in relative to the health harms, bestowing to World Health Organization arsenic is one of most hazardous element for human health and adsorption limits of this contaminant are hardly reached in drinking water. To remove this toxic metal, the adsorption method has been studied and synthesis of nZVI (nano scale zero valent iron) is developed for target metal. Batch study was undertaken to evaluate the proficiency of zero valent iron coated beads as an adsorbent for arsenic removal from ground water under the effects of various parameters like pH, retention time and adsorbent dosage. The results show that higher adsorbent efficiency of 93% was attained at pH-6. The maximum arsenic removal efficiency of 90% was achieved with 150rpm. Whereas,91% efficiency was achieved with 90 min contact time. The prepared adsorbent showed good results and its low cost making it more suitable and feasible option for commercial use.
Keywords: Contaminated water, Arsenic, adsorbent, zero valent iron coated beads

I. INTRODUCTION

Shortage of water and safe drinking water are the two major challenges are alive in the world in the area of water supply. It is predicted that more than 663 million people around the world does not have approach to pure drinking water [1]. Water is a fundamental constituent for human growth, and water nature affects the survival of human life. Elements of different naturally exist in apparent and drinking water such as fluoride, nitrate, sulfate, iron, manganese, chloride, selenium, arsenic, and other dense metals [2] . The nature of drinking water is of extraordinary people requirements these days. Many years ago, natural filters use in incumbent soil layers for protected ground waters. Though, drinking water impurities can exist in different forms, in inclusion to natural (geochemical) pollution such as by infiltration of contaminated surface water, by leaks in pipelines, from landfill leachates, etc[3]. Arsenic is one of the poisonous elements having most different effect on the people life and in around the world his effects are increasing day by day. mostly rocks occur in mixture type below earth that on dissolution contaminates H2O [4]. It is one among the foremost toxic chemicals found within the surroundings this one poisonous element occur and give as countless compound forms or types in the water environment. Arsenite (AsO3 3−) and arsenate (AsO4 3−), referred to as As (III) and As (V), respectively, are common in natural waters[5]. As mostly occur in Organic and Inorganic form in ground water, Organic Arsenic form exist due to usage of organo-arsenic pesticide and micro-organism bio methylation and Inorganic Arsenic form occur due to a result of the dissolution of minerals such as arsenolite, arsenic oxide and realgar [6].Most areas of Pakistan such as Sindh province As occur in ground water in 24 district such as both on the left and right bank of RI (River Indus) were evaluate from it some districts such as Sakrand, district Shaheed Benazirabad followed by Hala, Matiari , TMK (Tando Mohammad Khan) and Nasarpur regions where As concentration was detected as two hundred(200) ppb (parts per billion),where WHO (World Health Organization) limit is (10 ppb) [7]. Rice is found in rich quantity, the husk obtained is the upper covering of the rice after processing or polishing[8]. for removal of As from poisonous water many treatment technologies have been practiced such as these are coagulation/filtration, ion exchange, lime softening, adsorption on iron oxides or activated alumina, and reverse osmosis.[3] for Ground water and soil remediation Nanoscale zero-valent iron (nZVI) mostly used as engineered nanoparticles [9]. Adsorption is a cost advantage and technological method use for removal of arsenic from drinking water. Due to high affinity for arsenite (As(III)) and arsenate (As(V)), elemental iron and iron hydroxides are broadly used as the adsorbents for arsenic removal [10]. In now days, removal of different drinking water contaminated nano scale zero-valent iron (nZVI) has been used. The benefits of nZVI over zero-valent iron (ZVI) contain higher reactive surface area, faster and more complete reactions, and better inject ability into aquifers [11]. under flow conditions nZVI cannot be used for water treatment due to a porous reactive barrier or a filter consisting of a permeable reactive bed. bentonite, kaolinite, chitosan

and ion exchange resins they are also include for tested as supporting matrices for different synthesis and natural minerals [12].

II. MATERIALS AND METHODOLOGY

A. Preparation of pottery granules (PG):

The raw material China clay was collected from Thar, Sindh, White flour from Memon Mill Dadu, Rice Husk from Kotri Mill. Distilled water is produced in water quality laboratory of chemical engineering department Mehran university Jamshoro. 50 gram of each China Clay, White Flour, Rice husk were mixed with 100ml of distilled water and well agitated in the Agitator/Stirrer (Midget Stirrer, MZ-800H) for the time of 10 minutes with speed of 170rpm. After the mixing slurry dried in Oven temperature at 110 0C for 2 hours then we have reduced the size of paste in Mortar with Pastle after size reduction grinded pottery granules are heated in the Muffle Furnace 500 0C for 3 hours.

B. Synthesis of nano zero valent iron coated :

For the solution of synthesis of nano-zero-valent iron (nZVI) we take 0.5406 g of FeCl3.6H2O which dissolved in a ratio of $\frac{4}{1}$ V/V ethanol /H2O mixture (24 mili liter ethanol + 06 milliliter deionized water) and stirred well. And for the grow up iron nanoparticles we take 0.1 M sodium boro hydride solution mixture which was prepared by mixing 0.3783 g of NaBH4 in 100 ml of deionized water, an excess of boro hydride is required after it boro hydride solution was prepared by discharge into a burette and dropped drop wise $\frac{1}{2}\frac{drop}{second}$ into the ferric chloride solution with vigorous stirring. After putting first drop of NaBH4 directly in solution the black solid particles will appeared and remaining borohydride solution it use as to accelerate the reduction of reaction by mixing it. After mixing all of the borohydride solution, the mixture was stirred for another 10 minutes. Removal of Black Iron Nano particles from liquid phase mixture a vacuum filtration technique used. What man filter papers was use as filter for remove solid particles by washing 3 times with 25 ml of absolute ethanol to remove all water after it the solid particles as synthesized nanoparticles was dried overnight in a 323 K oven. For storage, a layer of ethanol is added to prevent the nano-iron particles from being oxidized.

C. Coating of nZVI on pottery granules:

For the coating we have agitated of pottery granules with nZVI (30/70), after agitation iron coated pottery granules ICPG heated at 80 c and 500 c for 1 hour.

D. Preparation of stock solution:

Stock solutions of Arsenate (V) were prepared in the maximum acceptable concentration set by EPA i.e. 50 ppb. Firstly, the stock solution of 100ppm and 100 (ml) volume was prepared from which the stock solution with 50 ppb was derived. For the preparation of 100 ppm stock solution, 0.2402 grams of Potassium Arsenate Monobasic (H2AsKO4) were weighed using measuring balance and completely diluted in 100 ml distilled water along with 1 drop of Nitric Acid (HNO3) in round bottom flask. For the derivation of 50 ppb stock solution dilution formula was used;

C1V1=C2V2.

Here, C1 and C2 are the concentration of first and second concentrations of stock solution and V1 and V2 are the volumes of first and second solution respectively.

Here in our case,

Let C1=100 ppm, C2=1, V2= 100ml ppm then V1 will be calculated as,

$$V1 = \frac{C2 \times V2}{C1} = \frac{1ppm \times 100ml}{100ppm} = 1ml$$

That means we'll take 1ml from the 100 ppm stock solution and dilute it with 99ml of Distilled water to make the 100ml stock solution of 1ppm. Now for 50 ppb we'll again use same formula.

Let C1=1 ppm=100 ppb, C2= 50 ppb, V2=100 ml, V1=?

$$V1 = \frac{C2 \times V2}{C1} = \frac{50ppb \times 100ml}{1000ppb} = 5 ml$$

That means we'll take 5 ml from the 1 ppm stock solution and dilute it with the 95 ml of Distilled water to make the 100 ml stock solution of 50 ppb. Here our step 1 is completed and we proceed towards next step.

E. Batch adsorption study

Batch technology was used to study the adsorption of As (V). At room temperature (20 ± 1 ° C) zero valent iron coated beads mixture is used for adsorption capacity by adsorption isotherm in aqueous solution. In some glass flasks, 50 ml of each of the As(V) (0.25, 0.5, 1.0, 1.2, 1.5) g solutions was contained per 50 ml of adsorbent. The vial was located in a water bath at 20 ° C and shaken at (90, 120, 150) rpm for nearly (60, 90, 120) min to ensure equilibrium was achieved. The effect of pH and contact time was performed.

The extracted data are used to calculate specific parameters for technology effectiveness and cost, when possible. To standardize the data on effectiveness, the following formula is used to calculate the arsenic removal efficiency of each technology, where n is the removal efficiency of adsorbent, C_0 is the influent arsenic concentration of the water sample, and Ce is the effluent arsenic concentration.

$$n \% = \frac{C_0 - Ce}{C_0} \times 100$$

III. RESULTS AND DISCUSSION

1. Effect of pH

For all water and waste water treatment process the pH of the solution is an essential factor that we perform an experiment which was conducted to study the influence of the early pH of the solution to be preserved on As (V). At pH = 2.0 to 9.0, the percentage of removal of As (V) varies with pH. The % of arsenic As (V) removed powerfully cleaned it depend on the pH of the medium. In addition, it can be noted that the maximum adsorption capacity of the zero-valent iron coated adsorbent for As(V) occurs at pH 6-6.8, at pH 6.0 (93.27%) highest removal efficiency was achieved, which was selected as the best condition of PH for further experiments.

As(V) having a pH higher than 2.0 exists in an anion form and thus can be efficiently removed by iron hydroxide which exists in the form of a cationic monomer (Fe(OH)2+) in this pH range. At pH 9.0 or higher, the removal rate of As (V) is lowered.

Fig. 1 represents the percentage removal efficiency of arsenic at different pH. From this study it is clearly observed that the percentage efficiency of arsenic removal was improved from 77 to 93 as the pH value increased from 2 to 6 due to Acidic state to neutral state).

However, the percentage removal of arsenic was decreased gradually from 93 to 84 as the pH value increased, it may be attributed by disturbing the neutral state to basic state
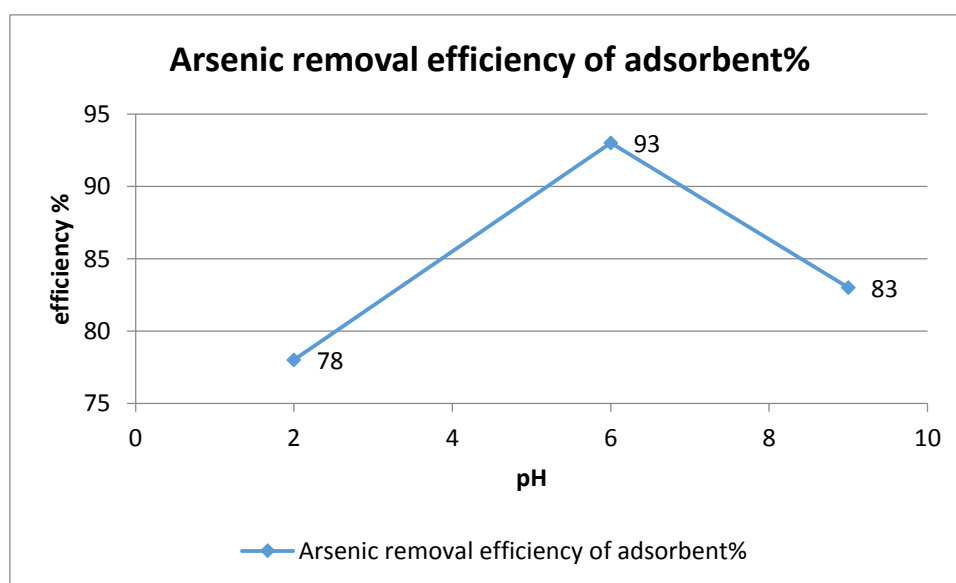
Fig.1. Effect of pH

2. Effect of time

For the reaction the time has been investigated for different parameters as it influence Contact time is one of the real factors in the intermittent adsorption process. As adsorption efficiency time variation has shown in Figure 2.
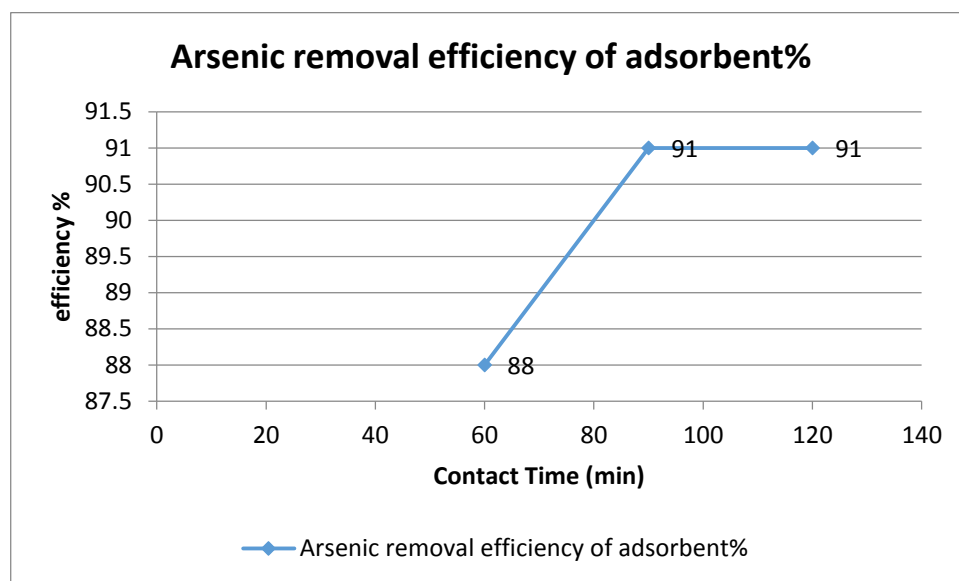
Fig.2. Effect of Contact Time

During the initial adsorption phase, the removal efficiency of As(V) by the zero-valent iron-coated adsorbent is significantly increased (0–90 minutes) and then continues to increase at a comparatively slow rate with increasing contact time until 90 minutes. After reaching equilibrium. After 90 minutes, the As (V) removal rate did not change significantly. On behalf of these results, 90 minutes was taken as the time of the adsorption experiment. Typically, the rate of removal of the adsorbate is initially very fast, but gradually decreases over time until equilibrium is reached. This phenomenon can be recognized to the point that in the early stage, a large number of vacant surfaces are available for adsorption, and over time, it is hard to occupy the remaining free surface due to the repulsive force among the solute molecules.

3. Effect of adsorbent dosage

The effect of the amount of adsorbent on the As(V) adsorption percentage is shown in Figure 3, As in figure we can see that As(V) removal efficiency increase greatly by increase in the amount of adsorbent. The sorbent dose increased from 0.25 mg / 50 ml to 1.0 mg / 50 ml, resulting in an increase in As (V) adsorption from 79% to 92%. It will happen by the higher obtainability of exchangeable places or surface areas at higher concentrations of adsorbent. On the other side, the increase in removal efficiency can be recognized to the fact that as the adsorbent dose increases, more adsorbent surface or more adsorption points can be used for the adsorbed solutes. A further increase in sorbent dose (> 1.0 mg / 50 ml) does not cause a important improvement in As(V) adsorption. It will happen due to the statistic that nearly all of As(V) is adsorbed onto the adsorbent and a balance is established between As(V) adsorbed onto the adsorbent and As(V) not adsorbed in the solution. Therefore, 1.0 mg / 50 ml of zero-valent iron-coated adsorbent was selected for further study.
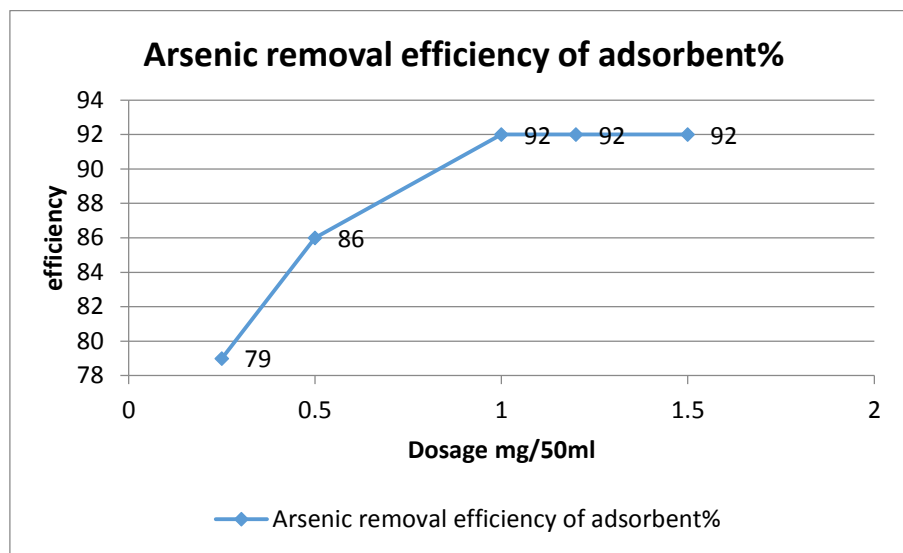
Fig.3. Effect of Adsorbent Dosage

4. **Effect of rpm**

The effect of the rotational speed (rpm) is one of the effective causes in the intermittent adsorption process. Obviously, the adsorption rate increases with increasing agitation speed (90, 120, 150, 180) rpm because the thickness of the boundary layer around the adsorbent particles decreases as the turbulence increases. As can be seen from the figure, the adsorption capacity of the adsorbent was the largest at 150 rpm. In addition, as shown in Fig. 4, the adsorption capacity of the adsorbent is not further increased, and the equilibrium time is also increased. This means that for the adsorption process, there is an optimum speed and will be studied for each adsorbent.
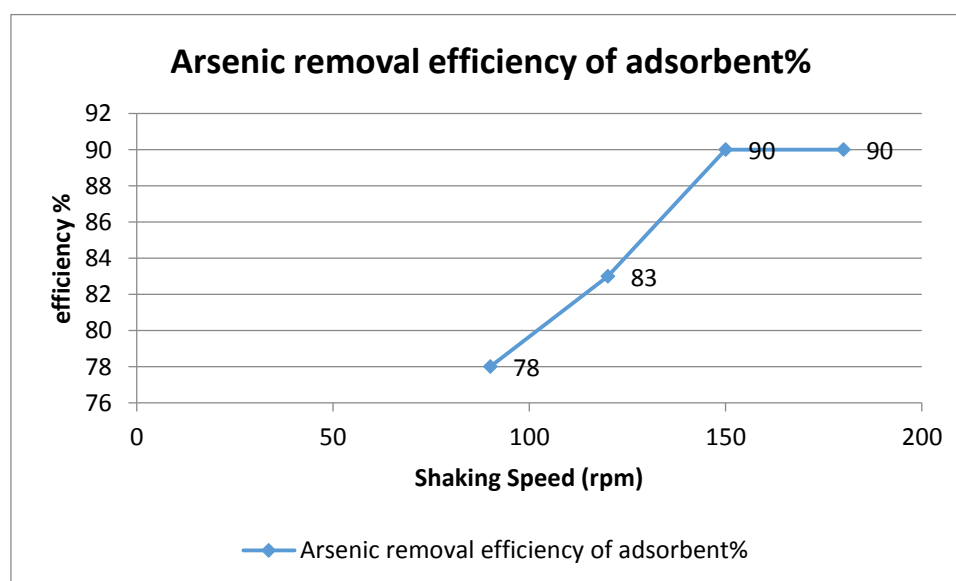
Fig.4. Effect of rpm

IV. IV. CONCLUSION AND RECOMMENDATION

For removal efficiency of arsenic from ground water by zero valent iron coated beads has been studied and investigated as new effective adsorbent. Numerous benefits of ICPG media are (a) cost effective process makes ICPG media a greatly competent adsorbent for removing As at ordinary pH. (b) its As adsorption competency by means of F(0) coated on the sample. From this research, it is evidently concluded that ICPG sample can be appropriately used for As expulsion from portable water. Batch adsorption study was used to remove As(v) by isotherm in aqueous solution at room temperature (20± 1 ^{0}C) determine the adsorption strength of zero valent iron coated beads complex by taking different parameters as pH=6 give highest

adsorbent efficiency of 93%, furthermore by taking 90mint contact time 91% efficiency was achieved , highest adsorbent capacity of 92% was achieved at dosage of 1.0 mg/50ml and at 150rpm 90% As removal efficiency was achieved .after optimization of all four parameters the overall average percentage removal efficiency was achieved as 91.5%.

V.   REFERENCES

1.   Nidheesh, P. and T.A. Singh, Arsenic removal by electrocoagulation process: recent trends and removal mechanism. Chemosphere, 2017. 181: p. 418-432.
2.   Bhatti, Z.A., et al., Study of PAN Fiber and Iron ore Adsorbents for Arsenic Removal. Civil Engineering Journal, 2020. 6(3): p. 548-562.
3.   Zouboulis, A.I. and I.A. Katsoyiannis, Recent advances in the bioremediation of arsenic-contaminated groundwaters. Environment international, 2005. 31(2): p. 213-219.
4.   Siddiqui, S.I. and S.A. Chaudhry, Iron oxide and its modified forms as an adsorbent for arsenic removal: A comprehensive recent advancement. Process safety and environmental Protection, 2017. 111: p. 592-626.
5.   Qureshi, K., et al., Surface adsorption study of saponified orange waste gel for arsenic (III) removal. Engineering, Science & Technology, 2014. 13(2): p. 54-58.
6.   Adio, S.O., et al., Arsenic and selenium removal from water using biosynthesized nanoscale zero-valent iron: a factorial design analysis. Process Safety and Environmental Protection, 2017. 107: p. 518-527.
7.   Bhatti, Z., et al., Determination of Arsenic and Health Risk Assessment in the Ground Water of Sindh, Pakistan. 2017.
8.   QURESHI, K., et al., PREPARATION OF INSULATING MATERIAL FROM RICE HUSK AND SAW DUST.
9.   Han, Y., et al., Optimizing synthesis conditions of nanoscale zero-valent iron (nZVI) through aqueous reactivity assessment. Frontiers of Environmental Science & Engineering, 2015. 9(5): p. 813-822.
10.   Zhu, H., et al., Removal of arsenic from water by supported nano zero-valent iron on activated carbon. Journal of Hazardous Materials, 2009. 172(2-3): p. 1591-1596.
11.   Shi, L.-n., X. Zhang, and Z.-l. Chen, Removal of chromium (VI) from wastewater using bentonite-supported nanoscale zero-valent iron. Water research, 2011. 45(2): p. 886-892.
12.   Toli, A., et al., Incorporation of zero valent iron nanoparticles in the matrix of cationic resin beads for the remediation of Cr (VI) contaminated waters. Environmental Pollution, 2016. 214: p. 419-429.

Removal of Methylene Blue using Hydrophobic Ionic Liquids

Syed Nasir Shah[a,*], Muddassir Ali[a], Ouahid Ben Ghanem[b], Zahoor Ullah[c]

[a]Department of Energy Engineering, Faculty of Mechanical and Aeronautical Engineering, University of Engineering and Technology Taxila, Pakistan

[b]Department of Process Plant Operations, Qatar Technical, Doha, Qatar.

[c]Department of Chemistry, Balochistan University of IT, Engineering and Management Sciences (BUITEMS), Pakistan

Abstract-The coloring of various products such as paper, leather, and textile products is one of the critical processes in different industries. The wastewater from these industries contains a significant concentration of these dyes, contributing significantly to the water treatment problems. A large concentration of these dyes is present in wastewater, thus increasing the chemical oxygen demand and decreasing the light penetration capability, which has a negative effect on the photosynthesis phenomenon. In the current study Trihexyltetradecylphosphonium [P6,6,6,14] based hydrophobic ionic liquids along with different anions are used to extract methylene blue from wastewater. The anions used are Cl- and BF4-. The effect of various parameters such as pH, the concentration of ionic liquids, and the temperature is investigated. It is found that with the increase in the concentration of ionic liquids the extraction efficiency enhances. The pH of the solution is varied from 4.5-8.0, and it is found that with the increase in pH, the extraction efficiency further improves. The recyclability of ionic liquids is also studied, and it is found that the efficiency of the ionic liquid decreases for each. The regeneration of ionic liquids is studied as well.

Corresponding Author:

Email: nasir.shah@uettaxila.edu.pk, nasir876@gmail.com

To confirm the mixidness of coal and solid olive waste

Muhammad Aftab khan [1,*] and Muddasar Habib [1] , Amad Ullah Khan[1]

[1]Department of Chemical Engineering, University of Engineering and Technology, Peshawar;

maftab.che@uetpeshawar.edu.pk

Abstract-The naturally available hydrocarbon matter, coal is available in exceptionally high quantity on the planet. The current coal reserve estimates stand at 1.1 trillion tons (1,139,471 million tons). The current proven reserves can be used for estimated 150 years at the current rate of utilization. Pakistan holds 3377 million tons of demonstrated coal reserves positioning 20th on the planet. It still looks imperative that the coal use will see its utilization for comming decades as an energy source with the disadvantage of greenhouse gas emissions causing environmental pollution. Various efforts have been reported to overcome this environmental isues. Pakistan is an agrarian country and produces a lot of agricultural waste with limited utilization. Recently there has been a surge in the cultivation of Olive trees which also result in produing waste of high Calorific Value (C.V) which often is of no use after oil has been extracted from its fruit. Capitilizing on the opportunity this work will look into the improved mixing characteristics of solid olive waste (SOW) and low rank coal to improve the calorific value of the hybrid fuel. Different type of coal samples and solid olive waste were collected, grinded, sieved and mixed with different ratio to confirm the mixedness of coal and solid olive waste by sieving analysis and Photographic Information Technique (PGI). 95% mixedness values were confirmed by the image analysis. Various tests such as compressive strength caloric value, ignition point was carried out to test the suitability of the hybrid fuel. The experimental results showed that, the solid olive waste can be used up to 50 mass% with coal to reduce the consumption of primary fuel coal which reduces the emission of (SO_2) to half of the initial value in comparision to when coal is used alone. It increase the calorific value of hybrid fuel and improves the ignition point. Usage of solid olive waste with coal will help in reduction of soil pollution and reduce (SO_2) emission to the environment.

Keywords: Solid olive Waste; photo graphic information, mixing, hybrid fuel.

I. Introduction

The buring of hydrocarbons resulting in CO_2 discharge to air has caused a worldwide temperature alteration, scientist say that the temperature of earth has increased to $2C^o$ because of CO_2 emissions. The result is an environmental change, manifestations of which incorporate dissolving of the polar ice covers, ascending of ocean levels, and aggravation of creature's regular living spaces, extraordinary climate change, thus a lot more negative results that are hazardous and exponentially increasing day by day. The significant danger from expanded CO_2 is the greenhouse impact. As an ozone harming substance, extreme CO_2 makes a spread that traps the sun's warmth energy in the air bubble, warming the planet and the seas. An expansion in CO_2 plays devastation with the Earth's atmospheres by causing changes in climate designs.

The grouping of carbon dioxide in Earth's climate is presently at almost 412 Parts per million (ppm) and rising. This speaks to a 47 percent expansion since the start of the Industrial Age, when the focus was almost 280 ppm, and an 11 percent increment since 2000, when it was close to 370 ppm.

Many decades will see the coal utilization as an energy source and hence the emission of greenhouse gases is eminent. Inovative ways to tackle this problem are necessary and hence there has been an interest in this field exporing different options. One such option is the use of solid waste with coal to make hybrid fuel. Olive wate is of high calorific value and can be combined with low rank coal to give a stable domestic fuel. Hence we have chosen it to form a near to perfect hybrid fuel by looking into the mixedness, strength, stability, C.V and other parameters to suggest its suitability [1].

The mixing of particle and powder is an old unit operation (nearly 4000 years) but due to complex nature a very limited information is known about the mechanism of mixing [2]. The combined combustion of coal and solid olive waste was done by Armesto et al. showing that mixing of solid olive waste and coal is possible [3]. In the past 50 years, the blending and segregation have been viewed as two contending systems to control the particle dispersion, Rowe et al., [4]. The early research has looked into the blending and isolation with a focus on density contrasts, Nienow et al., [5].

II.   Materials and Method

Solid olive waste (SOW) and coal were collected for mixing from olive oil extraction unit Ternab form and daara respectively. Composition of raw material was determind by proximate and ultimate analysis. Chemical composition of solid olive waste and coal is shown in Table 1.

Solid olive waste and coal were taken for grinding, vibratory seieving to obtain a particle size of 250 and 500 µm. Mixing of SOW and coal were then performed in different concentrations as shown in Table 2. Samples were taken from top, bottom and middle of the resulting mixture and then passed from vibratory sieve shaker to find the mixidness of SOW and coal as shown in Table 3.

Different light effects were created to find the distribution of particle and mixidness of mixtures. A 15mega pixel camera was used to record the pictures which were then examined by diving into equal ares to find the mixedness of the sample.

III.   Results and Discussion

3.1 Chemical Composition of Raw Material

It may be observed from Table 1 that sulpher content of solid olive waste is 0.10 and of coal where its value is 1.78 which is very high as compared to solid olive waste.The calorific value (sow 12500-21000kj/kg) and volatile matter of SOW is comparatively to coal (coal calorif value 17000-23000kj/kg) .Hence SOD can be mixed to controle sulpher emission, reduce the consumption of primary fuel coal and utilization of SOW as usefull rather to pollute the environment.

Table 1
Proximate and Ulitmate anylisis of SOW coal (by wt %)

Proximate analysis (by wt %)

	FC (wt %)	VM (wt %)	Ash (wt %)	Moisture (wt %)	HHV (kj/kg)	LHV (kj/kg)
SOW	16.30	69.20	9.20	6.60	19,805	19,595
Coal	41.10	27.35	23.55	7.30	23,208	22,045

Ultimate analysis (dry basis, wt %)

	C	H	N	O	S	Ash
SOW	46.60	6.01	0.70	36.63	0.10	9.50
Coal	59.20	4.53	2.08	11.50	1.78	20.59

Table 2 mixing proportion of coal (500 micrometer) and SOD (250 micrometer)

Sample	Coal (mass %)	SOD (mass %)
1	100	0
2	90	10
3	80	20
4	70	30
5	60	40
6	50	50
7	40	60
8	30	70
9	20	80

Table 3 Confirmation of mixidness of coal and solid olive waste

Sample	SOD (mass %)	Mixture proportion (mass %)
1	0	0
2	10	8
3	20	18.5
4	30	27
5	40	35
6	50	46
7	60	58
8	70	65
9	80	77

3.2 Solid olive waste (SOW)

3.2.1Pre treatment of SOW

The moisture content is a significant factor that lessens the SOW energy quality during the burning measure. In fact, the contained water in SOW material devours its fundamental dissipation energy from the SOW entire energy. Moreover, numerous unfortunate responses happen because of the water presence in the solid olive waste material. In request to expand the burning energy proficiency and limit the unsafe ensuing discharges, a drying pre-treatment of SOW pre-treatment is a suitable arrangement.

3.2.2 Density and ash analysis

The density of SOW is 1.0674gm/cm^3. The X-ray fluorescence (XRF) of the ash of SOW has shown the main elements to be Si, Al, Fe, Ca, S, Mg, K, Ti, Na, P, Mn, and Cl [12]. The big proportion elements in SOD ash are potassium (K) (15990-27744mg/kg) followed by calcium (Ca) (1702-3205mg/kg). The sodium (Na), magnesium (Mg) and iron (Fe) are also present in considerable quantities (104-214mg/kg, 511-808 mg/kg and 87.4-302mg/kg, respectively).

3.2.3 Confirmation of mixidness

The mixidness of coal and Solid olive waste was confirmed by sieve analysis and Photograpgic Technique (PGI). The mixing proportion of solid olive waste in different samples is shown in Table 3. The 16 Mega Pixel digital camera taking 15 images per second was set on conveyer belt. Different lights effect were created on the mono layer and images were recorded. The images were divide into equal nine parts and counting of the distinct number of particles in each squre showed that it had 95 % equal distribution of particle. The image 1 and image 2 given below shows the confirm degree of mixidness.

Table 3 Confirmation of mixidness of coal and solid olive waste

Sample	SOD (mass %)	After sieving Mixture proportion (mass %)
1	0	0
2	10	8
3	20	18.5
4	30	27
5	40	35
6	50	46
7	60	58
8	70	65
9	80	77

Image 1

Image 2

4. Conclusions

The above study shows that the coal and solid olive waste mixedness can be accessed from the monolayer distribution by image analysis as also confirmed by the sieve analysis. The mixedness values of 95 % were obtained in this work. Hence the mixing of coal and solid olive waste were confirmed in this work for better utilization of the mixture for producing high quality hybrid fuels.

References

1. L. Armesto *et al.*, "Co-combustion of coal and olive oil industry residues in fluidised bed," *Fuel*, vol. 82, no. 8, pp. 993–1000, 2003, doi: 10.1016/S0016-2361(02)00397-6.

2. M. Alonso and F. J. Alguacil, "Dry mixing and coating of powders," *Rev. Metal.*, vol. 35, no. 5, pp. 315–328, 1999, doi: 10.3989/revmetalm.1999.v35.i5.640.

3. A. T. Atimtay and H. Topal, "Co-combustion of olive cake with lignite coal in a circulating fluidized bed," *Fuel*, vol. 83, no. 7–8, pp. 859–867, 2004, doi: 10.1016/j.fuel.2003.09.015.

4. G. Wu, B. Yu, Y. Guan, X. Wu, K. Zhang, and Y. Li, "Mixing characteristics of binary mixture with biomass in a gas-solid rectangular fluidized bed," *Energies*, vol. 12, no. 10, pp. 1–8, 2019, doi: 10.3390/en12102011.

5. Y. Zhang, B. Jin, and W. Zhong, "Experimental investigation on mixing and segregation behavior of biomass particle in fluidized bed," *Chem. Eng. Process. Process Intensif.*, vol. 48, no. 3, pp. 745–754, 2009, doi: 10.1016/j.cep.2008.09.004.

ADSORPTION OF ARSENITE FROM AQUEOUS SOLUTION USING GRAPHENE OXIDE / Fe₂ O₃ COATED INDUS SAND

Ihsanullah Qureshi [A], Prof. Dr. Khadija Qureshi [B], and Dr. Zulfiqar Ali Bhatti[C]

Abstract— **Arsenic is a broadly appropriated component of the Earth's hull at a normal of around 5 g ton $^{-1}$[1]. Arsenic is a persevering, accumulating, poisonous substance. The U.S Environmental Protection Agency (EPA) has used 10 μg L^{-1} arsenic as the highest acceptable level of groundwater[2]. It is very important to remove heavy metals from the aqueous solution. In recent decades, many strategies have been developed to eliminate arsenic from contaminated water, including chemical rainfall, adsorption and ion exchange, membrane and biological processes, and so on. Due to its high arsenic performance and low cost, adsorption is the most popular method[3].**
This analysis was carried out by means of an adsorption method to eliminate Arsenic (III) from aqueous solution using Graphene oxide / iron oxide coated indus sand as adsorbent. Indus sand was amended by treating it with HCl and then covered with Graphene oxide / iron oxide.Study were conducted batchwise for experimental parameter. Arsenic (III) exclusion efficiency of Graphene oxide / iron oxide coated Indus sand from aqueous solution was determined. The ideal conditions for the expulsion of Arsenic (III) from aqueous solution utilizing Graphene oxide / iron oxide coated indus sand as adsorbent were noticed as; pH: 6, adsorbent dose: 1g, stirring speed: 200 rpm and contact time: 90 min. The highest evacuation efficiency accomplished on these ideal conditions was 98%. The maximum efficiency along with cheap and easy to manufacture makes iron oxide-Graphene oxide coated Indus sand promising for removal for Arsenic (III) from aqueous solution.

Keywords— Arsenic (III) expulsion, Iron oxide (Fe₂O₃), Indus sand , Graphene oxide(GO), Arsenic adsorption .

I. INTRODUCTION

From both the characteristic and the toxicological points of view, arsenic can be portrayed into three significant groups: inorganic; natural and arsine gas. The most notable is arsenic trioxide, sodium arsenite and arsenic trichloride . Arsenic trioxide is simply imperceptibly water soluble also in sodium hydroxide it structures arsenite and with concentrated hydrochloric corrosive it shapes arsenic trichloride [4]. Naturally exist in food, water and air. Known for a considerable length of time to be a powerful toxin; however, some animal studies recommend that arsenic might be a fundamental supplement at low concentrations. It is pervasive in nature and involves roughly 0.00005% of the earth's crust. People exposed to water contaminated with arsenic generally show arsenical skin sores, which are a late appearance of arsenic toxicity. Long term exposure to arsenic debased water may prompt different illnesses, for example, hyperkeratosis, cardiovascular diseases, skin cancer and lung diseases[5].

GO is a single atomic layered material containing carbon, hydrogen, and oxygen atoms by the oxidation of graphite crystals, which are cheap and bottomless .

Graphene oxide (GO)/iron oxide nanocomposites have been proposed to guarantee adsorbents. GO is produced by oxidative shedding of graphite, viewed as the most commonly utilized graphene forerunner due to its minimium cost and abundance[6].

II. Methodology

1. Preparation of HCl treated Indus Sand :
a. Collection and sieving of sand/silt

For the readiness of mud, sediment was gathered from Indus River close Almanzar jamshoro. After the gathering of residue it was sieved to acquire a similar size of the sediment, required size is 90 micro meter engineering department MUET jamshoro.

b. Leaching of silt/sand

Leaching of the silt was because of extraction of undesirable substance from the silt, for that reason silt was leached by the including of 0.5 molar concentration of hydrochloric acid in the silt to separate undesirable substance from silt.

c. Washing and drying of silt/sand

After leaching washing was done to keep up the pH of the silt for that washing of silt with deionized water was done for 5 to 8 time to get the pH level 7.

Due to some amount of water present in the silt it is dried to vanish water from sand to get dried sand.

2. Preparation of GO / Fe_2O_3 Coated Indus sand

GO (3 g) were spread on water (100 ml) through ultra-sonication for half hour, Fe_2O_3 (30 g) was added along with leached sand. Mixture were stimulate for 24 h at normal conditions. During this procedure, H_2O_2 was added four times according to the ratio of $Fe_2O_3/ H_2O_2 = 1$ g/10Ml for approximately 6 h . After one day slight amount of ammonium hydroxide added until the pH became 8. During it the mixture became a deep red color because of ferric hydroxide formation. Then mixture was dried to evaporate water in the oven at 105 degree centigrade to yield 300 g of GO/Fe_2O_3 coated Indus sand.

III. RESULTS AND DISCUSSION

1. To characterize Fe_2O_3 / GO coated indus sand:

Determination of Surface morphology by SEM and FTIR

a. Scanning Electron Micrograph Analysis :

An analysis of the adsorbent surface was performed using SEM. Figures 1 and 2 show the surface morphology of uncoated Indus sand (before) and Graphene oxide / Fe_2O_3 coated indus sand (after) used in this study. SEM work on 10 kV accelerating voltage, magnification (100x 1000x) and resolution (10-100 μm) was performed by both materials.
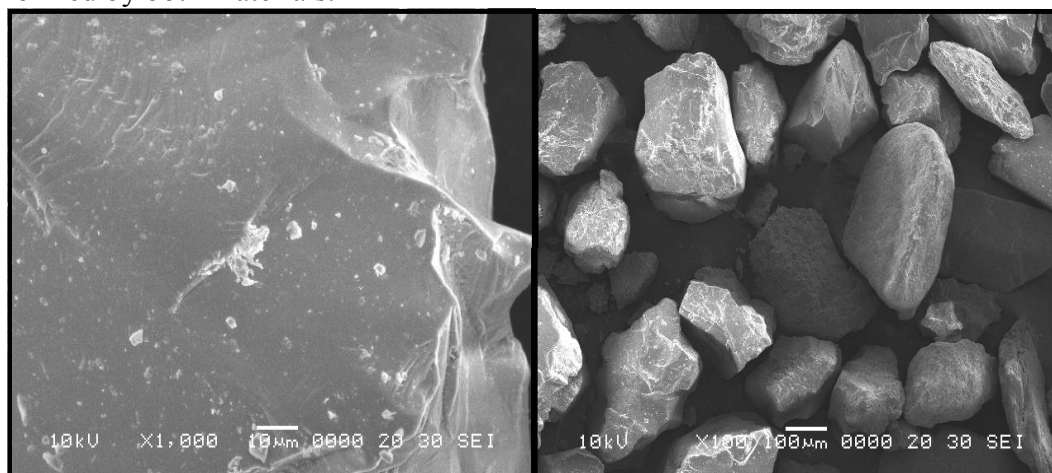
Fig 1 : SEM result before coating sand with GO / Fe_2O_3

It is observed that the graphene oxide / Fe_2O_3 coated indus sand adsorbent surface roughness was high, which is one of the desirable parameters for efficient adsorption but has less roughness and less adsorption-

efficient pores compared to uncoated material. The surface roughness and porousness of the structure were also higher in the Graphene oxide / Fe_2O_3 coated indus sand .
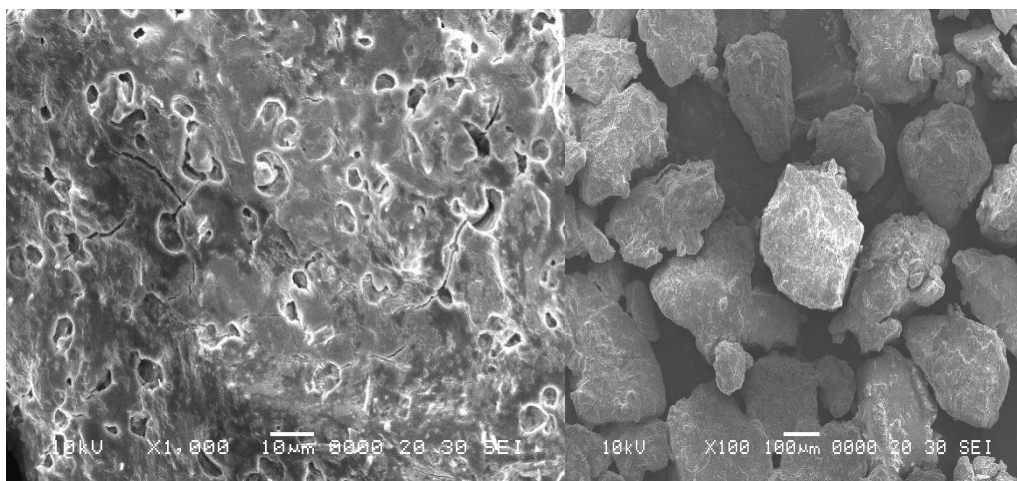
Fig 2: SEM result after coating sand with GO / Fe₂O₃

b. Fourier Transform Infrared Spectroscopy (FTIR) :

FTIR studies were conducted to determine the functional group development and structure of modified GO / Fe_2O_3 coated indus sand. Figures 3 and 4 display the GO / Fe_2O_3 coated sand FTIR spectra before and after the As (III) adsorption. According to the $Si - O$ party occupancy, the less extreme sharp peak at 1047.49 and 924.49 cm-1might was. The 826.50 cm-1 height reflects the $Fe - O$ bond .
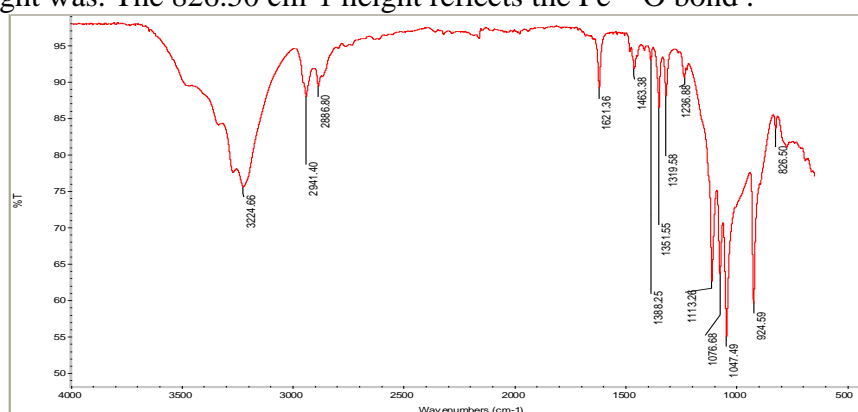
Fig. 3 FTIR result of GO / Fe₂ O₃ coated indus sand

The transfer of functional groups from 98.35 and 776.98 to 1047.49 and 924.59 cm-1 , respectively, shows the graphene oxide / iron oxide-coated indus sand as (III) adsorption.
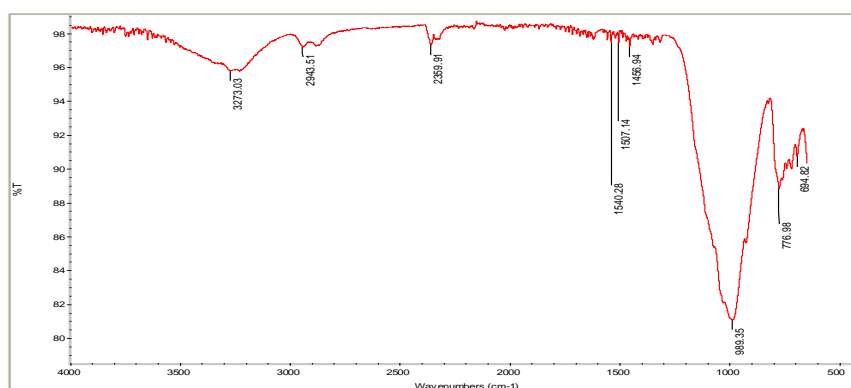
Fig. 4 FTIR result of GO / Fe₂ O₃ coated indus sand after arsenic test

2. BATCH EXPERIMENTS ANALYSIS :

Batch experiment carried out for analyzing parameters such as pH effect, effect of interaction time, effect of adsorbent dose and effect of stirring speed .

a. Effect of pH :

In adsorption, pH is important, therefore exclusion efficiency varies as of pH . The maximum efficiency for the removal of As (III) using GO / Fe_2O_3 coated Indus sand adsorbents has been studied by varying the pH from 2 to 10 of even numbers. The experiments were conducted with 100 ml of 50 ppm of As (III) aqueous solution, 0.5 g of adsorbents at 120 min, respectively.

The maximum removal of As (III) was 98.00% at pH 7 for GO / Fe_2O_3 coated indus sand . Therefore, pH 7 gives best results.
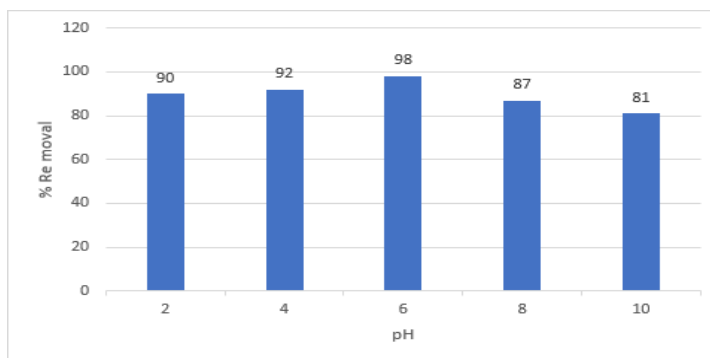
b. Effect of Adsorbent Dose :

The effect of adsorbent dosage was investigated at pH 7, 120 min contact time, and 50 mgl^{-1} initial concentration of As(III). The adsorbent dosage was varied from 0.25 to 1.5 g/100 ml of solution. The maximum Arsenic removal was attained at 1 g of GO/Fe_2O_3 coated indus sand respectively.
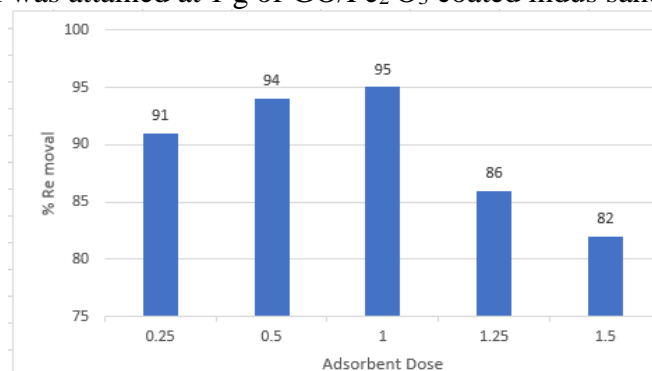
c. Effect of Contact Time :

The contact time studies were performed by varying the time from 30 to 150 min and the variation in the percentage of removal with contact time is shown in graph .

The equilibrium was attained at 90 min for GO/Fe_2O_3 coated indus sand , and the removal of As (III) was found to be 96%.
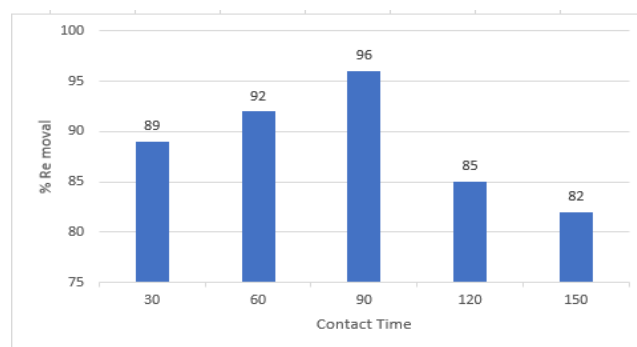
d. Effect of Stirring Speed :

The contact time studies were performed by varying the time from 30 to 150 min and the variation in the percentage of removal with contact time is shown in graph .

The equilibrium was attained at 90 min for GO/Fe$_2$O$_3$ coated indus sand , and the removal of As (III) was found to be 97%.
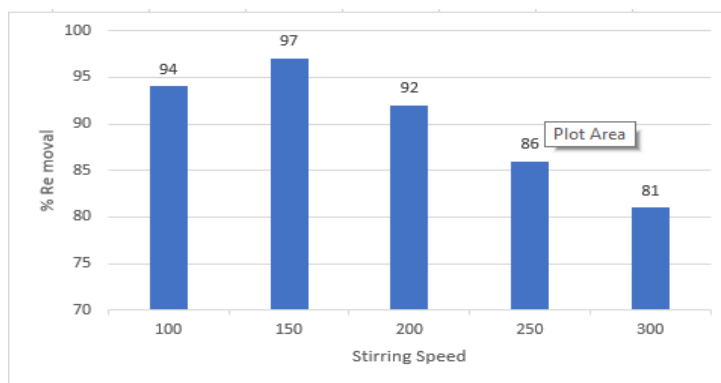
1)Abbreviations and Acronyms

ppm: Parts per million , SEM: Scanning Electron Microscope , rpm : Rotations per minute , FTIR: Fourier Transform Infrared Spectroscopy , GO : Graphene oxide

2)Equations

The amount of adsorption, Quantity and the percentage removal were calculated using Equations (3.1) and (3.2).

$$Q= \{(C_o - C_e)\ V\}/M \qquad (3.1)$$

Where Q is the adsorption capacity, C_o and C_e are the concentrations of metal ion in the initial and final solutions, respectively, and M is the mass of adsorbent (g) used. Percentage of adsorption was determined by the following equation:

$$\% \text{Arsenic removal} = \frac{\text{Total As}_{in} - \text{Total As}_{out}}{\text{As}_{in}} \times 100$$

$$\text{Percentage of removal} = C_o - C_e/C_o \times 100 \qquad (3.2)$$

Where C_o denotes the concentration of metal ion initially and Ce represent concentration of metal ion in final solution.

3)Other Recommendations

Based on the outcomes obtained for the expulsion of arsenic (III), the graphene oxide / iron oxide coated indus sand can likewise be utilized for the end of other harmful metals, for example lead, mercury, copper etc. Tests can be conducted for afore mentioned toxic metals.

IV. CONCLUSION

In this study, Graphene oxide/Fe$_2$O$_3$ coated Indus sand is best adsorbent for dismissal of Arsenic (III) present in drinking water. From all experimental results the removal percentage is 76% to 98%.

Indus sand coated with graphene oxide / iron oxide, has been recognized as competent adsorbent that has capability to eliminate Arsenic (III) from contaminated solution even when its concentration is as low as 5 ppm.

V. REFERENCES

1. Langsch, J.E., Costa, M., Moore, L., Morais, P., Bellezza, A. and Falcão, S., 2012. New technology for arsenic removal from mining effluents. *Journal of Materials Research and Technology*, *1*(3), pp.178-181.
2. Tavakoli, H., Azari, A., Ashrafi, K., Salimian, M. and Momeni, M., 2020. Human health risk assessment of arsenic downstream of a steel plant in Isfahan, Iran: a case study. *International Journal of Environmental Science and Technology*, *17*(1), pp.81-92.
3. Barakat, M.A., 2011. New trends in removing heavy metals from industrial wastewater. *Arabian journal of chemistry*, *4*(4), pp.361-377.
4. Bissen, M. and Frimmel, F.H., 2003. Arsenic—a review. Part I: occurrence, toxicity, speciation, mobility. *Acta hydrochimica et hydrobiologica*, *31*(1), pp.9-18.
5. Mandal, B.K. and Suzuki, K.T., 2002. Arsenic round the world: a review. *Talanta*, *58*(1), pp.201-235.
6. Chen, X., Zhao, J. and Zhang, L., 2019. Graphene- Based Fiber Optic Label- Free Biosensor. *Handbook of Graphene, Volume 6: Biosensors and Advanced Sensors*, p.371.

Technical Session 3-C (Google meet/Zoom) Petroleum and Renewable Energy	
Session Chair: **Dr. Muhammad Shehzad Kamal** Session Co-Chair: **Dr. Muhammad Daud**	
Al-Faran *(Dept. of Chem Eng., UET Peshawar)*	Performance Evaluation of Compression Station Facility to Cater for Modification to Extend Production till Tail End Suction Pressure
Muhammad Saad Rehan *(USPCAS-E UET Peshawar)*	Peroxide Crosslinking of Ultra High Molecular Weight Polyethylene using Tea-Polyphenols as Antioxidants
Syed Mustafa Shah *(Dept. of Chem Eng., UET Peshawar)*	Comparative Analysis Of Soxhlet And Microwave Assisted Extraction Techniques For The Pomace Olive Oil Extr.
Hurmat Khan *(USPCAS-E UET Peshawar)*	Solar Thermal Water and Space Heating: Comparative Analysis of Charging and Discharging Behavior of Phase Change Materials.
Muhammad Farooq Siddique *(USPCAS-E UET Peshawar)*	Analysis of dual booster mirrors box type solar cooker integrated with thermal storage.
Naveed ullah *(USPCAS-E UET Peshawar)*	Smart Monitoring of the Solar Energy Power

Performance Evaluation of Compression Station Facility Modification

Al-Faran Javaid [A], Muddasar Habib [A]

[A] =*Department of Chemical Engineering, University of Engineering and Technology Peshawar*.

Abstract— Sui Gas Field since its discovery has been continuously producing gas, SML (Sui Main Limestone) being its main reservoir. Production of gas since 1956 gradually reduced reservoir pressure and made installation of a gas compression station a necessity to accommodate for dropping gas pressure. Sui Field Gas Compression Station (SFGCS) was inaugurated in 1987 to provide sufficient gas supply pressure, however, because of unceasing gas production the main reservoir of Sui is diminishing and as per estimation, by the year 2022 gas suction pressure will drop to its lowest design i.e. ~7barg. To increase production life of the reservoir till year 2040 when the lowest possible gas suction pressure i.e. ~1.5barg is expected, a modification is required for which booster compressor system is proposed. To accommodate modification, analysis of present equipment and facility to evaluate performance in reduced pressure scenarios to recognize mandatory changes in existing system was compulsory. For which, detailed Aspen HYSYS simulation was modelled along with compressors' performance curves, which was used to evaluate hydraulics as per compressors performance. Rating of Condensate handling system at different future scenarios was also carried out. Hydraulic checks for some pipeline headers showed velocities higher than recommended for H2S service i.e. > 100 ft/s, therefore, changing some pipelines diameter to bigger sizes is proposed. Capability check of Slug Catcher determines high velocity in gas risers i.e. 4 - 4.75 m/s causing higher micron size carryover i.e. 2000- 5000 micron and also 10- 15% liquid entrainment, meaning inadequate performance of the slug catcher and transferring the load to Gas scrubbers which are evaluated to be capable of handling high liquid levels in all scenarios.

Keywords—**Compression, Performance, Hydraulic, Simulation, Rating.**

I. INTRODUCTION

Pakistan Petroleum Limited (PPL) is the discoverer and producer of Sui Gas Field which is unceasingly producing since 1956. Sui Gas Field has four gas reservoirs SML (Sui Main Limestone), SUL (Sui Upper Limestone), HRL (Habib Rahi Limestone), Pab which are in production.

Sui Main Limestone is the main producing reservoir of Sui Gas Field. Because of unceasing gas production, the main reservoir of Sui is diminishing. To provide contractual gas supply pressure to customers, Sui Field Gas Compression Station (SFGCS) was inaugurated in 1987. The present SML gas treatment facilities include Condensate Handling System; Slug Catcher & Raw Gas Scrubbers, and Seven Gas Turbine Driven Compression Trains which comprise Knockout Drums, inter- stage Air Coolers with Compressors.

As Sui reservoir is in declining trend and it is expected that the production will go to lowest design pressure i.e. ~7 barg by year 2022.[1] To increase production life of the reservoir till year 2040 when the lowest possible gas suction pressure i.e. ~1.5barg is expected, a modification is required for which booster compressor system is proposed.[2]

To accommodate modification, analysis and evaluation of Sui SML Compression System for the Low-Pressure scenarios along with hydraulics and equipment rating was necessary.
Gas turbines are made up three components; mostly common shaft air compressor, expander with a combustion chamber in-between.[3] Brayton cycle is used generally for analyzing gas turbine systems.
The Ratio of the energy output to the energy input is the turbine thermal efficiency. Lower heating value of fuel is taken while calculating thermal efficiency.[4]
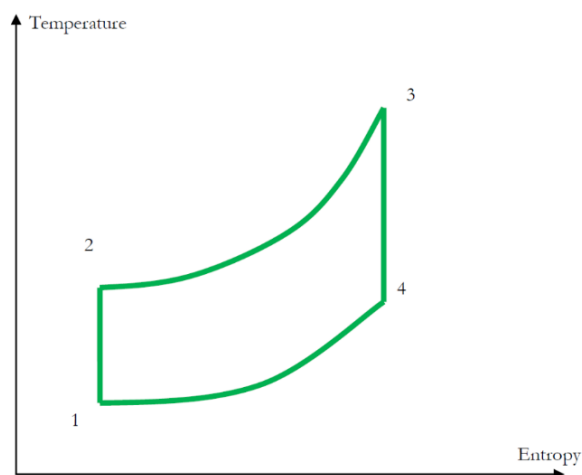
Figure 4: TS Diagram for Closed Gas Turbine Cycle

The efficiency of gas turbine is given as; η = Net Work Output / Heat Supplied.[5]

A process simulation model is a representation of a process plant to facilitate design, rating, monitoring of the plant. Basic simulation steps using Aspentech Hysys were reviewed as described by Nishabth et.al. [6] Centrifugal Compressor Operations in Aspen HYSYS for typical solution methods, efficiency equations, Performance curves, rating and performance were studied.[7, 8]

A schematic of a pipe-type slug catcher is shown in Figure-2.

Ideal separation of liquid droplets of <600 micron shall occur.[9]

Slug catcher bottle velocity upto 2m/s with 650 – 1000 micron separation is recommended as per SHELL recommended practice.[10, 11]

SFGCS scrubbers can handle entrained liquid upto 0.5m3/hr.[12]

As per API-14E, for combined header high H2S service gas pipeline velocities higher than 100ft/s are not recommended, moreover, vibration and noise can be caused by velocity greater than 60ft/s.[13]

Norsok Standard suggests that velocities should be typically, V= 175 (1/ρ)0.43 or 60m/s, whichever is lowest.[14]

Figure 5: Pipe-type Slug Catcher

ASME-B31.8 recommends gas velocities lower than 100ft/s to avoid excess of turbulence, noise, and pressure drop which may cause internal pipe erosion.[15]

Key process conditions for pipeline design suggest ti minimize noise and corrosion inhabitance by keeping gas piping velocity between 60 – 80 ft/s and not exceed. For corrosives in gas, such as CO_2, lower velocity of 50ft/s is recommended.[16]

II. METHODOLOGY

A detailed process simulation model is developed using Aspentech HYSYS software to evaluate hydraulics of inlet and outlet lines of slug catchers and raw gas scrubbers along with compressors performance in different cases of production profile.

Existing compressors curve are fed into HYSYS model and adjusted to meet current performance.

Table 6: Cases for Simulation

Case	Year	SML Rate	SML Suction
		MMSCFD	Barg
Case-1	2021-22	302.2	7.8
Case-2	2026-27	208.1	4.5
Case-3	2032-33	135.1	2.6
Case-4	2036-37	105.3	1.8
Case-5	2026-27	86.2	1.5

Booster (1st stage) compressors curve as provided by vendor after modification are also fed into model to have real- time simulation.

Table 7: Design Parameters of Compressors

Parameter	Unit	LP Compressor	HP Compressor
Suction Pressure	barg	8.0	18.5
Discharge Pressure	barg	19.3	70.0
Suction Temperature	C	60	60
Discharge Temperature	C	150	214
Flowrate	MMSCFD	40.31	48.37
Compression Ratio		2.41	3.78
Polytropic Efficiency	%	77.1	68.4
Power	kW	2024	4379

Further, for evaluation of current performance of compressors, operating data from site has been collected. Based on operating data, compressor efficiencies are estimated via HYSYS Model as shown in figure-3.
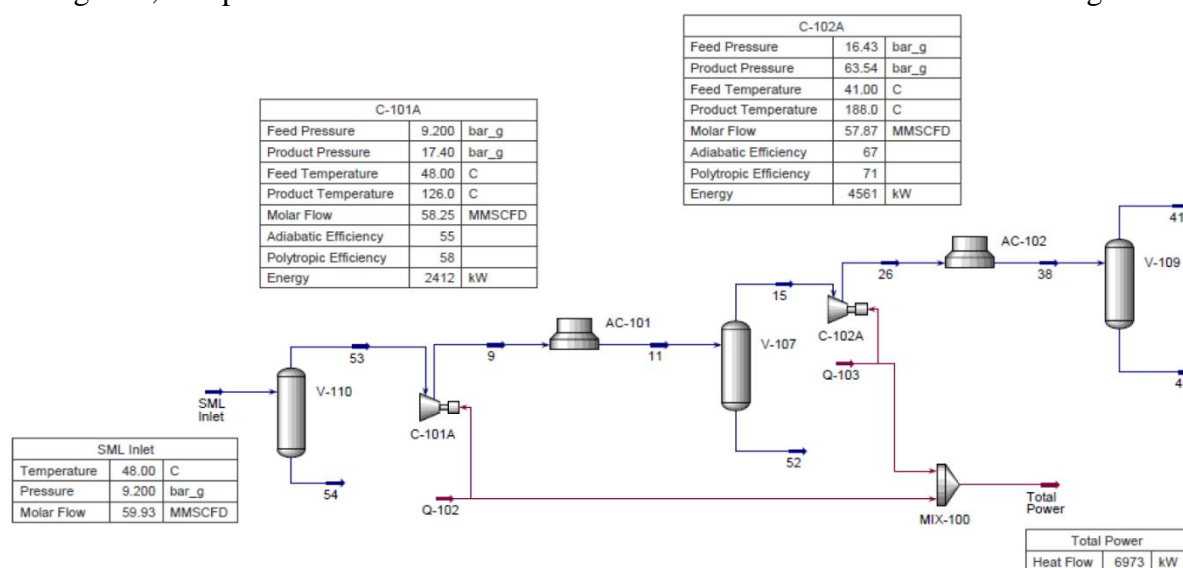
Figure 6:HYSYS model for Compressors' Efficiency Estimation

Table 8: Compressors' Simulation Result Data

Parameter	Unit	LP Compressor	HP Compressor
Suction Pressure	barg	9.2	16.4
Discharge Pressure	Barg	17.4	63.5
Suction Temperature	C	48	41
Discharge Temperature	C	126	188
Flowrate	MMSCFD	58.25	57.87
Compression Ratio		1.89	3.87
Polytropic Efficiency	%	58	71

Power	kW	2412	4561

LP Compressor (C- 101A) efficiency decrease to 58% from the design efficiency of 77%.
Based on current fuel consumption and compressor work load, turbine efficiency is calculated as follows:

Table 9: Current Turbine Efficiency Calculation

Parameter	Unit	Value
Total Compressor Power	kW	6973
Fuel (per Turbine)	MMSCFD	3.306
Treated SML LHV	Btu/scf	858.8
Turbine Fuel Heating	MMBtu/hr	118.3
Turbine Efficiency (incl. Combustion Efficiency)	%	20.1

If the performance of LP Compressor intact same as design value as per datasheet and performance curve i.e. efficiency ~77%, then compressor power consumption lowered which will result in fuel saving.

Table 10: Current Turbine Efficiency vs Design Efficiency

Parameter	Unit	Current Efficiency	Design Efficiency
Polytropic Efficiency	Barg	58	77
Total Compressor Power	Barg	6973	6037
Fuel (per Turbine)	C	3.306	2.86
Treated SML LHV	C	858.8	858.8
Turbine Fuel Heating	MMSCFD	118.3	102.4
Turbine Efficiency (incl. Combustion Efficiency)	%	20.1	20.1

If LP compressor work as per its design efficiency then fuel consumption would be ~2.86 MMSCFD (Fuel saving ~0.45 MMSCFD per turbine; overall ~2.68 MMSCFD fuel saving from six turbines).

Total seven (07) number of compressor trains are installed in the Sui Gas Field named as Sui Field Gas Compression Station (SFGCS) to boost the pressure from ~8.0 Barg to ~70.0 Barg. Each train consists of a LP and HP compressor driven by Gas Turbine (GT) via a speed increasing gearbox. Currently, all trains are installed in parallel (six operating and one standby).
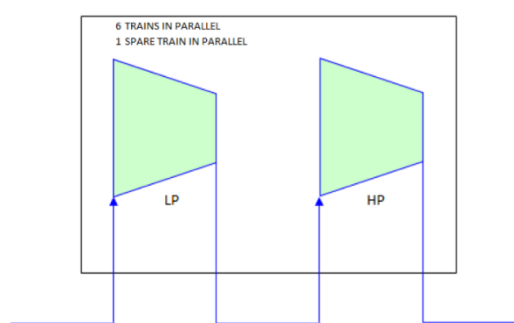
Figure 7: Existing LP-HP Compressor Train

Vendor proposed future configuration based on the production profile which contains three (03) Booster Compressors (First Stage Compression) and four (04) Export Compressors (Second Stage Compression).
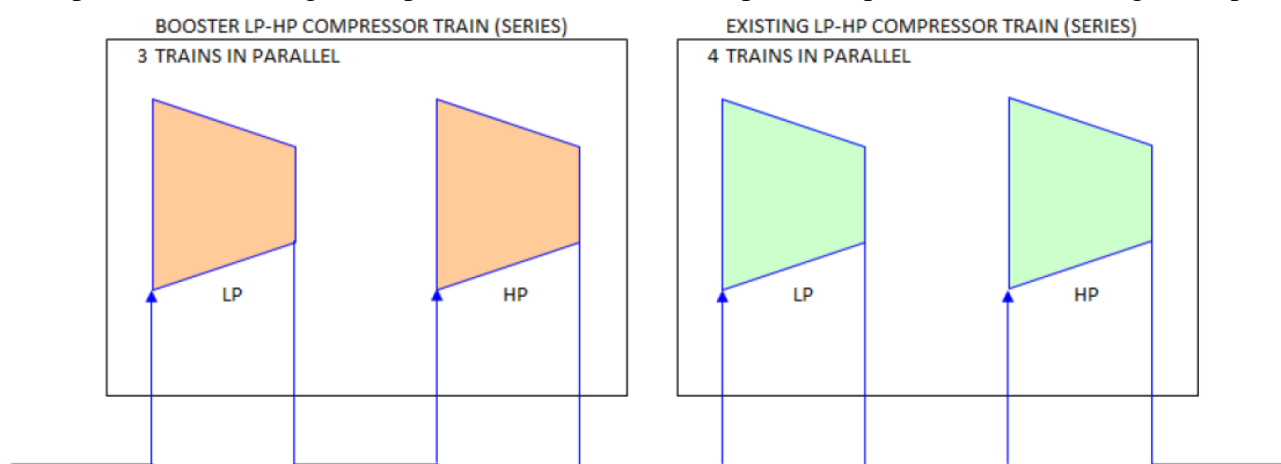
Figure 8: Vendor Proposed Compressors Configuration

III. RESULTS AND DISCUSSION

A. *Compressors' Performance*

Proposed compressors configuration by vendor is simulated by feeding Performance Curves provided by vendor for all cases into HYSYS Simulation to evaluate performance and following limitations were derived and applied.

Based on the Case- 1 i.e. 302.2 MMSCFD at 7.8 Barg suction pressure as per Production Profile, all four (04) compressors will be in operation. Booster Compressor speed limited to 80% i.e. 10,496 rpm, 2nd stage Compressor speed limited to 80.7% (10,500 rpm) to limit power requirement below 6.5 MW (site rated power of turbines).

Based on the Case- 2 i.e. 208.1 MMSCFD at 4.5 Barg suction pressure as per Production Profile,
three (03) compressors will be used instead of four (04) compressors to avoid surge flow. Booster Compressor speed limited to 90% i.e. 11,808 rpm, 2nd Stage Compressor speed limited to 80.7% (10,500 rpm) to avoid surge flow.

Based on the Case- 3 i.e. 135.1 MMSCFD at 2.6 BarG suction pressure as per Production Profile, two (02) compressors will be used instead of four (04) compressors to avoid surge flow.
Booster Compressor speed limited to 95% i.e. 12,464 rpm, 2nd Stage Compressor speed limited to 87.7% (11,400 rpm) and 86% (11,180 rpm) of LP/HP compressors respectively to limit power requirement below 6.5 MW (site rated power of turbines).

Based on the Case- 4 i.e. 105.3 MMSCFD at 1.8 BarG suction pressure as per Production Profile, two (02) compressors will be used instead of four (04) compressors to avoid surge flow.
Booster Compressor speed limited to 95% i.e. 12,464 rpm, 2nd Stage Compressor speed limited to 92.5% (12,025 rpm) to keep HP Casing discharge temperature below 200degC.

Based on the Case- 5 (worst case) i.e. 86.2 MMSCFD at 1.5 BarG suction pressure as per Production Profile, two (02) compressors will be used instead of four (04) compressors to avoid surge flow, Booster compressor speed limited to 95% i.e. 12,464 rpm, 2nd Stage Compressor speed limited to 90% (11,700 rpm) to keep HP Casing discharge temperature below 200degC.

B. *Pipeline Hydraulics*

Velocities at different cases have been checked at upstream and downstream of slug catcher and raw gas separator.

Table 11: Pipelines Hydraulic Evaluation

Parameter	Line Size (inch)	Velocity (ft/s)				
		Case-1	Case-2	Case-3	Case-4	Case-5
Northern/Southern Inlet Header	20	104	113.9	112.5	113.7	104.4
Northern/Southern Slug Catcher Gas Outlet	20	103.1	114.2	114.1	114.9	105.6
Northern/Southern Raw Gas Separator Outlet Header	20	103.2	114.6	114.6	115.3	105.8
Booster Compressor Suction Header	30	91	101.2	101.1	101.7	93.4
Booster Compressor Inlet	16	110.3	122.6	121.3	122.1	112

Velocity in combined line are higher which requires special attention.

C. Slug Catcher Evaluation

For slug catcher and raw gas scrubber, equipment rating has been carried out separately to check adequacy of nozzles and equipment itself. In- house excel based program is used for slug catcher rating. However, vendor data is used for Raw Gas Scrubber evaluation.

The SFGCS facility consists of two (02) Finger Type Slug Catchers.

- Northern Slug Catcher (A- 501)
- Southern Slug Catcher (A- 502)

All production profile cases have been evaluated for worst case scenario i.e. 60 C Temperature. The velocity limitation in the bottles of the slug catcher as per FW highlighted is 1.5 m/s whereas the shell standard allows velocities up till 2 m/s. However, the velocities for cases evaluated are in the range of 4.09 to 4.75 m/s. Velocities summary is presented below.

Table 12: Slug Catchers' Evaluation

Cases	Year	Suction Pressure Barg	Temperature degC	Flowrate MMSCFD	Velocity m/s	Entrained Liquid	
						Micron	m3/hr
Case-1A	2021-22	7.8	60	302.2	4.09	302.2	4.09
Case-2A	2026-27	4.5	60	208.1	4.56	208.1	4.56
Case-3A	2032-33	2.6	60	135.1	4.61	135.1	4.61
Case-4A	2036-37	1.8	60	105.3	4.75	105.3	4.75
Case-5A	2039-40	1.5	60	86.2	4.40	86.2	4.40

All evaluation is carried out considering maximum ambient temperature as 60 C.

Slug catcher evaluation results show that due to high velocities in the bottles of slug catcher, the separation is not occurring up to the level as recommended by the shell standard (i.e. 650 micron to 1000 micron) of liquid entrained in gas whereas the cases evaluated show that the liquid droplets entrained shall be in the range of 5250 micron to 1700 micron.

D. Scrubbers' Rating

The SFGCS facility includes six (06) feed gas scrubbers; three (03) in the northern header, and the other three (03) in the southern header.The rating conditions of the SGFCS raw gas scrubber grade data provided by the supplier have been used.

The scrubber A/B on the two headers is produced by one supplier, and the scrubber C is produced by another supplier.

Table 13: Scrubbers' Rating

Cases	Entrained Liquid		Per Sock Gas Handling (SCFH)		Total Gas Handling
	Micron	m³/hr	A/B	C	MMSCFD
Case-1A	5250	0.52	160000	110000	647
Case-2A	4000	0.48	140000	100000	574
Case-3A	2800	0.47	120000	82000	484
Case-4A	2200	0.45	110000	78000	450
Case-5A	1700	0.51	100000	72000	411

According to the manufacturer's data, D-501 A/B and D-502 A/B can handle 0.5 cubic meters of entrained liquid per hour. Therefore, in all cases, the feed gas scrubber is sufficient to handle gas and liquid flows.

IV. CONCLUSION

Hydraulic simulation has been carried out on the pipelines within the battery limit and it is found that the speed is very high, that is, the speed in different combined headers is >100ft/s. Due to the higher H2S service, it is not recommended. In addition, per API-14E, speeds higher than 60ft/s may cause noise and vibration problems, requiring special attention. Therefore, for speeds less than 90ft/s, it is recommended to increase the pipeline size from 20 inches to 24 inches, and for speeds less than 60ft/s, it is recommended to increase the pipeline size to 28 inches. The slug catcher was rated under different circumstances and found that the flow rate in the gas riser was higher, that is 4-4.75 m/s, while the recommended flow rate in the standard was 2 m/s. This will result in a higher micron size residue, namely 2000-5000 microns and 10-15% liquid entrainment. This will result in insufficient operation, and the load will be transferred to the downstream raw gas scrubbers. The adequacy of the feed gas scrubber has been considered, and the higher liquid entrainment from the slug catcher has been considered. Based on available supplier data, the raw gas scrubbers were found to be suitable for the new conditions in all cases. A compressor package based on three (03) first-stage (booster) compressors and four (04) second-stage (outlet) compressors has been evaluated. It has been found that the recommended supplier's modified compressor, namely three (03) compressor sets, can provide approximately 60-63 Barg of discharge pressure under maximum environmental conditions (i.e 60°C). Initially four (04) second stage (outlet) compressors will be required by 2026, after which three (03) compressors will be required to keep the flow above the surge limit. Starting in 2032, two (02) compressors will be in operation.

V. REFERENCES

[1].   *Sui Gas Field Production Profile*. 2018.

[2].   *Vendor Proposed Data for Compressor Station Modification*.

[3].   Chmielniak, T.J.W., Warsaw, *Energy technologies.* 2008.

[4].   Std, A.J.C. and G.I. Services, *616 Gas Turbines for the Petroleum.*

[5].   Brooks, F.J.J.G.P.S., Schenectady, NY, *GE gas turbine performance characteristics.* 2000.

[6].   Chemmangattuvalappil, N. and S.J.C.E.P.S. Chong, *Basics of Process Simulation With Aspen HYSYS.* 2017: p. 233.

[7].   Haydary, J., *Chemical process design and simulation: Aspen Plus and Aspen Hysys applications*. 2019: John Wiley & Sons.

[8].   Aspentech, *Aspen HYSYS Unit Operations Reference Guide*.

[9].   Mokhatab, S. and W.A. Poe, *Handbook of natural gas transmission and processing*. 2012: Gulf professional publishing.

[10].   Circulars, D.J.D., *Gas/Liquid Separators–Type Selection and Design Rules.* 2007. **31**.

[11].   Circulars, D., *Design Of Multiple-Pipe Slug Catchers* 2010.

[12].   FWEL, *Design Manual for Gas Compression Station.* 1987. **04**.

[13].   API, R.J.R.P.f.D. and Installation of offshore Production Platform Piping Systems, *14E.* 1991.

[14].   Standard, N., *Process Design P-001*. 2006, Edition.

[15].   ANSI, A., *B31. 3, ASME ANSI B31. 8*. 2009, ASME PRESS.

[16].   al., S.e., *Key Process Considerations for Pipeline Design Basis*. 2019.

Peroxide Crosslinking of Ultra High Molecular Weight Polyethylene using Tea-Polyphenols as Antioxidants

M. Aaqib Ishaq [A], Rizwan M. Gul[A], Muhammad Saad Rehan[B,*], Nouman Ali Shah[C] and Jiazhuag Xu[C]

[A] Department of Mechanical Engineering, University of Engineering and Technology Peshawar, Pakistan
[B] U.S.-Pakistan Center for Advance Studies in Energy (USPCAS-E), University of Engineering and Technology Peshawar, Pakistan
[C] College of Polymer Science and Engineering, Sichuan University, China
*Corresponding Author
Email: saad.rehan@uetpeshawar.edu.pk

Abstract— **Surface crosslinking of ultra-high molecular weight polyethylene (UHMWPE) is successfully used to increase the wear resistance of orthopaedic implants. Long term stability of UHMWPE is a major concern and it is addressed by crosslinking in the presence of Vitamin-E. However, it reduces the crosslink density and wear resistance of UHMWPE. In this context, tea polyphenols represent an interesting alternate antioxidants to Vitamin-E. This paper presents an approach to surface-crosslinked UHMWPE by diffusion in the dicumyl peroxide (DCP) in the presence of tea polyphenols including epigallocatechin gallate (EGCG) and lipid soluble epigallocatechin gallate (lsEGCG) as antioxidants. A comparison has been made in the crosslink density and oxidative stability of UHMWPE using these tea-polyphenols and Vitamin-E. The results show that in comparison to Vitamin-E, the crosslink density was 8.8% and 15.7% higher for EGCG and lsEGCG blends respectively and hence an improved wear resistance. However, lesser oxidation induction time (OIT) has been reported for both the tea-polyphenols based blends.**

Keywords— antioxidants, crosslinking, crosslink density, diffusion, wear resistance.

I. INTRODUCTION

Ultra-high molecular weight polyethylene (UHMWPE) belongs to the polyethylene family having extremely long chains and molecular weights up to millions of g/mol [1]. It has a proven record in the replacement of total joints as the bearing surface material and has dramatically improved the life of patients with joint disabilities [2]. It is widely used as acetabular cup in total hip replacement (THR) and tibial component in total knee replacement (TKR). The long-term durability and performance of the implants of UHMWPE is dependent on three crucial aspects including the wear resistance, oxidative stability and mechanical properties; where as the leading failure cause is wear debris-induced osteolysis and loosening of implant [3]. The wear in the implants of UHMWPE can be minimized by crosslinking which generates a network structure on the surface that resists the plastic deformation and ultimately results in prolonging the wear time [4]–[7]. One method of achieving the cross-linking is by radiation, however, this deteriorates the mechanical performance since the radiation dose generates free radicals which serve as the precursors for oxidation embrittlement through a cascade of reactions with oxygen [8]. These radicals can be fully eliminated if the radiation dose is followed by melting, however, fatigue and other mechanical properties are reduced as a result of this process because of degraded crystalline structure [9]. This increases the risk of early failure of an implant especially when exposed to excessively high stresses. An alternate method of addressing this issue is stabilizing the radiation induced radicals by using antioxidant such as Vitamin-E. The antioxidant hinders the cascaded oxidation reactions by donating a hydrogen atom [10]. The drawback of this method is that during the cross-linking, Vitamin-E reacts with the radicals leading to a reduced cross-link density. Hence, low concentrations of Vitamin-E (< 0.2 wt %) are recommended to minimize the adverse effects on cross-linking, however, sufficient amount of antioxidant is also required for effective stabilization [11].

Though Vitamin-E has emerged as a successful candidate for enhanced oxidative stability of UHMPWE [12]–[17] but the reduced crosslink density is still a major concern and thus the research on more competitive antioxidants is required. Several studies have been conducted on the use of tea polyphenols including epigallocatechin gallate (EGCG), lipid soluble epigallocatechin gallate (lsEGCG) and lipid soluble tea polyphenols (lsTPP) as antioxidants using radiation cross-linking which resulted in improved wear resistance and oxidative stability of UHMWPE, however, crosslinking of UHMWPE using peroxides in the presence of tea polyphenols has not been explored. This study investigates the performance of tea polyphenols based
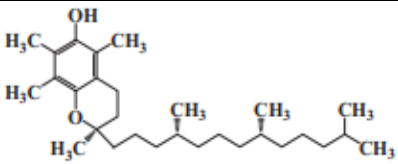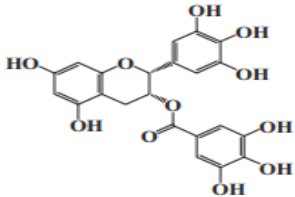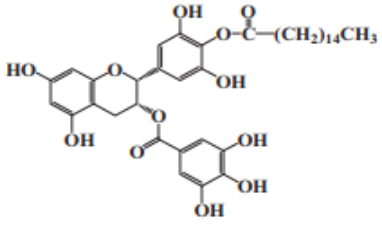
UHMWPE blends using organic peroxide cross-linking with improved wear resistance. The study also demonstrates the impact of peroxide crosslinking on the oxidative stability.

II. METHODOLOGY

A. Materials

UHMWPE was blended with 0.2wt% Vitamin-E, 0.2wt% EGCG, and 0.2wt% lsEGCG in 120 ml Isopropanol. The chemical formulae and structure of these antioxidants are presented in Table 1. The resulting blends were then dehydrated for a week at 60oC under vacuum. The dehydration was followed by consolidation into pucks through compression molding at a temperature of $200°C$ and pressure of 10 MPa. A total of five cubes, each of 1cm3, were machined from each of these consolidated blends.

TABLE I. ANTIOXIDANTS USED IN THIS STUDY; THEIR MOLECULAR FORMULAE, CHEMICAL STRUCTURE AND NUMBER OF PHENOLIC HYDROXYL GROUPS [18]

Antioxidant	Molecular Formula	Chemical structure	Numbers of Phenolic hydroxyl groups
Vitamin-E	$C_{29}H_{50}O_2$		01
EGCG	$C_{22}H_{18}O_{11}$		08
lsEGCG	$C_{38}H_{48}O_{12}$		07

B. Diffusion of Peroxide

The peroxide used was dicumyl peroxide $C_{18}H_{22}O_2$ (Alpha Aesar, Massachusetts, USA). The cubes were doped in DCP under nitrogen gas at $80°C$ for 4 hours and then heated at $150°C$ for 4 hours to decompose the peroxide. The samples were weighed at each step.

C. Characterization Techniques

Crosslink density: To measure the surface crosslink density, (3×3×1mm) samples were cut from surface and to measure the bulk crosslink density, cubes (3x3x3mm) were cut from bulk from each of the 5 cubes and then were swollen in Xylene for 2 hours at $130°C$. The xylene swollen weights at initial and final stages were measured for determining the crosslink density and swell ratio as prescribed in ASTM D2765-16.
Volume swelling ratio can be calculated from (1) [8].

$$q_{eq}=[T_{eq}-\alpha\Delta T-(\rho_s/\rho_m -1)] \qquad (1)$$

where ρ_s is the machining cubes cross-link density at ambient temperature , ρ_m is the hypothetical density

of the fluid phase,α is the volumetric coefficient of expansion and ΔT is the difference of temperature between ambient and experimental temperature. The equivalent temperature Teq, can be calculated from (2) [8].

$$Teq=(h_f/h_i\ )^3 \hspace{3cm} (2)$$

where hi and hf are initial and final height of machining cubes once it reaches equilibrium. The cross-link density in mole per unit volume, υc was calculated using Equation (3) [8].

$$v_c=-(\ln(1-q^{-1}\ )+ q^{-1}+\chi q^{-2})/((V_1)\overline{q}^{-1/s}) \hspace{1cm} (3)$$

Here q is the swell ratio, V_1 is the xylene partial volume and $\chi= 0.33 + 0.55/q$ also known as the interaction parameter of Flory–Huggins.

OIT: Differential Scanning Calorimeter (QA 2000; TA Instruments, USA) was used to measure the OIT. Samples (n=3) were cut from the surface and bulk. For the sake of comparison, un-cross-linked samples were also cut. Samples weighing ~ 5 mg were placed in aluminum pans. An empty aluminum pan was used as a reference. Both the pans were left uncovered for OIT testing. Heating rate of 10°C/min was used for heating the samples from 40 °C to 200 °C under nitrogen atmosphere with the flow rate of 50ml/min. At 200°C, the sample was held isothermal for 3 mins. After equilibrating, the purge gas was toggled to oxygen at the flow rate of 50 ml/min. The sample was then held isothermally under oxygen till the appearance of an exothermic peak. The time measured from the switching of purge gas to the onset of oxidation, known as OIT, was measured in TA Universal Analysis software by extending the recorded baseline beyond the exothermic peak and extrapolating the steepest linear slope of this peak to intersect the extended baseline, as prescribed in ASTM D3895-98.

III. RESULTS AND DISCUSSION

A. *Weight change after doping and decomposition*

The weight of cubes after doping with DCP increased by 1.6±0.02, 1.8±0.05, 1.6±0.03 and 1.5±0.02g for control (UHMWPE without antioxidant), VE, EGCG and lsEGCG, respectively as shown in fig.1. Similarly, after heating at 150°C, a drop of 0.9±0.01, 1.1±0.02, 1.0±0.02 and 0.9±0.04 g, respectively was recorded in the weight of the cubes. The weight change, after doping and decomposition processes, was highest for 0.2 wt% VE as compared to other samples.
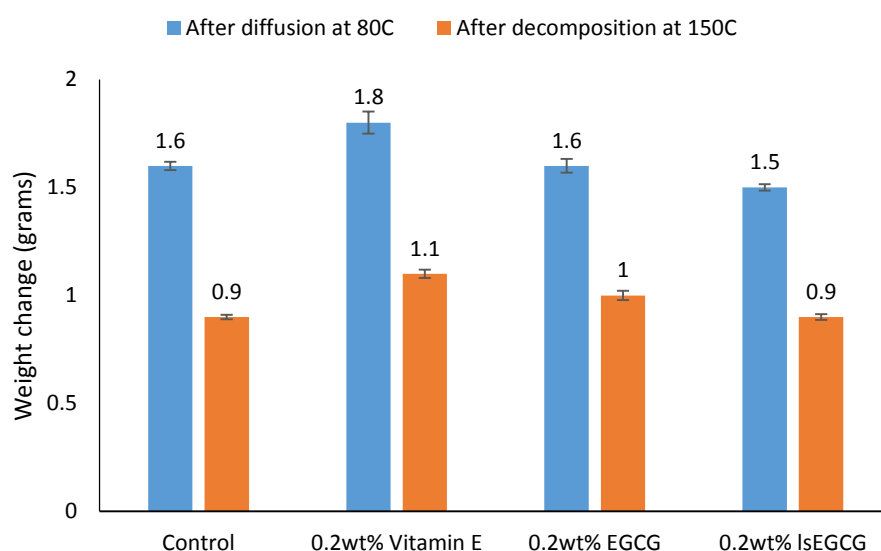
Fig. 8. Weight change in UHMWPE blends after diffusion and decomposition

B. *Impact on crosslink density*

The mean crosslink density of samples (n=5) cut from the surface was found to be 338±0.82, 288.5±0.95, 313.9±0.94 and 333.9±0.35 moles/m3 for control, VE, EGCG and lsEGCG, respectively as shown in fig.2. In comparison to the control, the crosslink density decreased by 14.6%, 7.3% and 1.2% for Vitamin-E, EGCG and lsEGCG respectively. The use of tea polyphenols resulted in a lesser drop in the crosslink density.

Similarly, samples cut from the bulk also depicted a similar trend with the mean crosslink density of 67±0.90, 58±0.50, 62.5±0.70 and 63.5±0.55moles/m3for control, VE, EGCG and lsEGCG, respectively. As expected, the crosslink density of surface cut samples was higher than that of bulk for all the samples, and the lowest crosslink density was observed for VE both at surface and bulk.

The reduced crosslink density in the case of Vitamin-E can be attributed to the fact that during crosslinking, VE reacts with the free radicals which leads to a reduced crosslink density. In comparison to this, the tea polyphenols having more phenolic groups can donate more hydrogen atoms during crosslinking. The increased number of hydrogen atoms can easily scavenge more free radicals. This is why tea polyphenols have shown a lesser inhibitive effect on crosslink density.
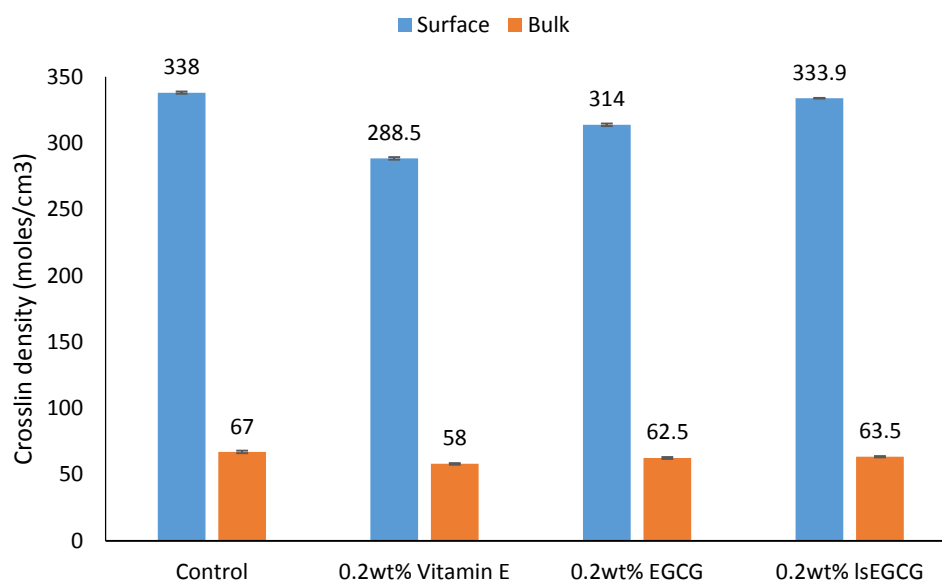
Fig. 9. Crosslink density of UHMWPE blends cut from surface and bulk

C. *Impact on oxidative stability*

The mean oxidation induction time recorded for samples cut from surface were 0.3, 40.6, 3.9 and 1 min for control, VE, EGCG and lsEGCG, respectively as depicted in fig. 3. Similarly, the mean oxidation induction time recorded for samples cut from bulk was 0.3, 55.3, 5.9 and 1 min for control, VE, EGCG and lsEGCG respectively. Control showed the lowest OIT and was rapidly oxidized in a few seconds. VE blends had the highest OIT as compared to all other samples. The addition of EGCG and lsEGCG increased OIT up to 3.9 min and 1 min, respectively.

The oxidative stability of the blends was also compared in terms of the measured OIT. For control, this was a few seconds which is not reliable and can be considered negligible. Though previous studies have reported higher OIT for tea polyphenols based UHMWPE blends using radiation crosslinking here, opposite to our expectations, the OIT for both tea polyphenols was lesser than Vitamin-E. One possible reason for this might be the use of different mechanism of crosslinking. Another reason might be the low concentration of antioxidant. Similarly, the samples have to kept under high vacuum at a temperature ranging from -4°C to 0 ℃ in an empty bottle before the OIT testing [18]. Had these conditions been achieved, higher OIT can be expected. More detailed investigations are intended to investigate the impact of tea polyphenols on the OIT of UHMWPE. The OIT of surface cross-linked samples was lesser than that of bulk cross-linked. This is because of the fact that crosslinking reduces the value of OIT. Since the crosslinking is higher at the surface, lower OIT are recorded for surface than bulk.
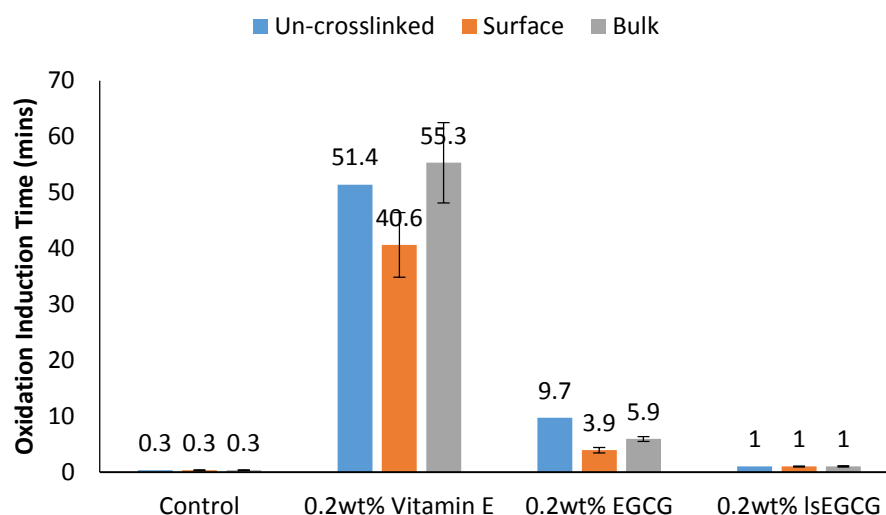
Fig.10. OIT of UHMWPE blends

IV. CONCLUSION

The study concludes that peroxide crosslinking of UHMWPE in the presence of antioxidants decreases its crosslink density. This reduction is lesser for tea polyphenols as compared to Vitamin-E. Thus, peroxide crosslinking in the presence of tea polyphenols can result in an improved wear resistance of UHMWPE. As far as the oxidative stability is concerned, the oxidation induction time of tea polyphenols based blends did not improve. This was quite opposite to the results of previous studies in which the radiation cross-linking approach was used. Hence it is concluded that the type of crosslinking mechanism is one of the factors which determine the oxidative stability of UHMWPE and the radiation crosslinking should be explored for effective oxidation resistance. Since peroxide crosslinking is an easier and an economically viable method as compared to the radiation crosslinking, it can be used for improving the wear resistance of UHMWPE using tea polyphenols as antioxidants.

ACKNOWLEDGMENT

V. REFERENCES

[1] S. M. Kurtz, The UHMWPE Handbook Ultra-High Molecular Weight Polyethylene in Total Joint Replacement, vol. 11, no. 3. Elsevier, 2004.

[2] S. M. Kurtz, O. Muratoglu, M. Evans, and A. A. Edidin, "Advances in the processing, sterilization, and crosslinking of ultra-high molecular weight polyethylene for total joint arthroplasty," Biomaterials, vol. 20, no. 18, pp. 1659–1688, Sep. 1999, doi: 10.1016/S0142-9612(99)00053-8.

[3] J. Fu, B. N. Doshi, E. Oral, and O. K. Muratoglu, "High temperature melted, radiation cross-linked, vitamin e stabilized oxidation resistant UHMWPE with low wear and high impact strength," Polymer, vol. 54, no. 1, pp. 199–209, 2013, doi: 10.1016/j.polymer.2012.11.017.

[4] D. Pokorný, A. Sosna, M. Šlouf, P. Fulín, J. Štefan, and I. Landor, "UHMWPE- polyethylene for articulating surfaces of joint replacements," Casopis lekaru ceskych, vol. 155, no. 8, Czech Republic, pp. 433–437, 2016.

[5] A. M. Crugnola, E. L. Radin, R. M. Rose, I. L. Paul, S. R. Simon, and M. B. Berry, "Ultrahigh molecular weight polyethylene as used in articular prostheses (a molecular weight distribution study)," J. Appl. Polym. Sci., vol. 20, no. 3, pp. 809–812, 1976, doi: 10.1002/app.1976.070200321.

[6] T. M. McGloughlin and A. G. Kavanagh, "Wear of ultra-high molecular weight polyethylene (UHMWPE) in total knee prostheses: A review of key influences," Proc. Inst. Mech. Eng. Part H J. Eng. Med., vol. 214, no. 4, pp. 349–359, 2000, doi: 10.1243/0954411001535390.

[7]   G. Blunn, E. M. B. Preva, L. Costa, J. Fisher, and M. A. R. Freeman, "Ultra high molecular-weight polyethylene (uhmwpe) in total knee replacement: fabrication, sterilisation and wear," J. Bone Jt. Surg., pp. 946–949, 2002.

[8]   O. K. Muratoglu et al., "Unified wear model for highly crosslinked ultra-high molecular weight polyethylenes (UHMWPE)," Biomaterials, vol. 20, no. 16, pp. 1463–1470, 1999, doi: 10.1016/S0142-9612(99)00039-3.

[9]   O. K. Muratoglu, C. R. Bragdon, D. O. O'Connor, M. Jasty, and W. H. Harris, "A novel method of cross-linking ultra-high-molecular-weight polyethylene to improve wear, reduce oxidation, and retain mechanical properties: Recipient of the 1999 HAP Paul award," J. Arthroplasty, vol. 16, no. 2, pp. 149–160, 2001, doi: 10.1054/arth.2001.20540.

[10] E. Oral, S. L. Rowell, and O. K. Muratoglu, "The effect of α-tocopherol on the oxidation and free radical decay in irradiated UHMWPE," Biomaterials, vol. 27, no. 32, pp. 5580–5587, 2006, doi: 10.1016/j.biomaterials.2006.07.017.

[11] E. Oral and O. K. Muratoglu, "Vitamin E diffused, highly crosslinked UHMWPE: A review," Int. Orthop., vol. 35, no. 2, pp. 215–223, 2011, doi: 10.1007/s00264-010-1161-y.

[12] R. M. Gul, E. Oral, and O. K. Muratoglu, "Oxidation resistant peroxide cross-linked UHMWPE produced by blending and surface diffusion," IOP Conf. Ser. Mater. Sci. Eng., vol. 60, no. 1, 2014, doi: 10.1088/1757-899X/60/1/012015.

[13] R. M. Gul, "The effects of peroxide content on the wear behavior, microstructure and mechanical properties of peroxide crosslinked ultra-high molecular weight polyethylene used in total hip replacement," J. Mater. Sci. Mater. Med., vol. 19, no. 6, pp. 2427–2435, 2008, doi: 10.1007/s10856-008-3368-7.

[14] E. M. Brach del Prever, A. Bistolfi, P. Bracco, and L. Costa, "UHMWPE for arthroplasty: Past or future?," J. Orthop. Traumatol., vol. 10, no. 1, pp. 1–8, 2009, doi: 10.1007/s10195-008-0038-y.

[15] R. M. Gul, K. Fung, B. N. Doshi, E. Oral, and O. K. Muratoglu, "Surface cross-linked UHMWPE using peroxides," J. Orthop. Res., vol. 35, no. 11, pp. 2551–2556, 2017, doi: 10.1002/jor.23569.

[16] F. Addiego, O. Buchheit, D. Ruch, S. Ahzi, and A. Dahoun, "Does texturing of UHMWPE increase strength and toughness? A pilot study," Clin. Orthop. Relat. Res., vol. 469, no. 8, pp. 2318–2326, 2011, doi: 10.1007/s11999-010-1716-7.

[17] J. Z. Xu, K. K. Wannomae, O. K. Muratoglu, and E. Oral, "Increased oxidative protection by high active vitamin E content and partial radiation crosslinking of UHMWPE," J. Orthop. Res., vol. 36, no. 7, pp. 1860–1867, 2018, doi: 10.1002/jor.23835.

[18] Y. Ren et al., "Enhanced oxidation stability of highly cross-linked ultrahigh molecular weight polyethylene by tea polyphenols for total joint implants," Mater. Sci. Eng. C, vol. 94, no. September 2018, pp. 211–219, 2019, doi: 10.1016/j.msec.2018.09.036.

Comparative Analysis for Extraction of Pomace Olive Oil Using Microwave Assisted Extraction Solvent Extraction.

Syed Mustafa Shah [A], Yahya Gul [A], Uzair Tariq [A,] Muddasar Habib [A]

[A] =*University of Engineering and Technology Peshawar*

Abstract— **Olive pomace is a waste produced every year in huge quantities by the oil industry. The elimination of olive pomace is problematic due to the high concentration of phenolic compounds, which is a environmental problem. However, phenolic blends are used in the health industry. Therefore, the recovery of olive pomace is essential for ecological and economic sustainability without neglecting the challenges. This current study describes the exaction of pomace oil extraction by microwave extraction (ME). Percent yield, total phenol content, DPPH and phenol compounds were studied. The results of MASE and those of the traditional extraction (Soxhlet extraction) were compared. The results showed that the extraction conditions had a significant impact on the extraction of the TPC, %yield, DPPH and the phenol content in the short time of MASE use. However, it was also found that the ratio of solid-to-solvent are the variables to influence extraction yield. The highest result values for pomace oil in MASE and Soxhlet separately in TPC was 0.204 mg GA / g oil and 0.148 mg GA / g oil, DPPH was 33.12% and 26.37% and the extraction yield it was 8.04% and 6.34% individually. The phenolic compound result was found (9.87%) in ME and (6.46%) in SE. Antioxidant found to be more active radical scavenger in Microwave extraction than the Soxhlet extractor. The highest extraction conditions for the extraction of MASE pomace oil with high TPC, DPPH, low energy consumption and low CO_2 production were for the high power 1: 05 ratio of 500W power in 05 min. In the SE they were 70 minutes, 75 ° C and containing 1:05 ratio. These results suggest that MASE was a more efficient separation technique than Soxhlet extraction.**

Keywords— **Olive oil, Pomace Oil, Microwave Assisted Solvent Extraction, Soxhlet Extraction, Total Phenolic Content, Antioxidant, Phenolic Compound**

I. INTRODUCTION

Olive oil is of great importance in this world and has been used by humans for centuries in medicine, cosmetics, textiles and illumination [1]. Today, it is also arguably one of the richest sources of fat and is associated with many important health benefits of the Mediterranean diet. As the rapid global demand for olive oil, pollution from olive mills waste (OMW) is becoming increasingly acute, especially in the Mediterranean region. Olive-growing places face the difficult task of finding environmentally friendly and economically viable solutions for the management and disposal of OMW. When waste enters the environment, it also produces foul smell. The deterioration of natural water quality in refinery waste is a serious problem, manifested by coloration, greasy appearance and increased oxygen demand. It also affects the quality of the soil, is harmful to the life of plants, and produces a stench when thrown on the ground. Waste residual oil (about 8%) usually recovered by solvent extraction is of significant economic interest [3-4]. Hexane is the main solvent used in solid-liquid extraction step [5]. The most widely used procedure for oil removing from the solid matrix remains conventional Soxhlet extraction which is straight forward and inexpensive., whereby the solid material is placed in a cellulose thimble within an extraction chamber, which is situated on top of a collecting flask and under a reflux condenser [5–7]. This method has the advantage that the extraction is a continuous process but has several disadvantages such as high consumption of solvent, long extraction time, and risk of thermal decomposition of the bioactive compounds. In recent years, the demand for new extraction techniques has been an increasing calling for automation with shorter extraction times and less consumption of organic solvent. Microwave heating is increasingly used for promoting solvent extraction of various compounds from solid wastes. The absorption of microwave energy in mixtures depends both on the nature of the solvent and the solids to be treated. When the solid phase does not absorb microwave radiation (because of a low dielectric constant) then a solvent is needed which effectively absorbs microwave energy (a high dielectric constant solvent). The past decade has seen reports emerging on the successful use of MASE for oil extraction from vegetable biomass as an alternative to the conventional solvent extraction [6-8]. MASE is driven by several advantages including energy savings, reduced solvent consumption, more selective extraction, better yields and more homogeneous treatment. Addition of acetic acid in hexane is also known to improve efficiency of oil extraction from solids [9-15]. The aim is to optimize the operating conditions,

including the amount and ratio of solvent, and the time and temperature of the extractions, to achieve better extraction yields. In addition, we have used another conventional extraction technique, i.e. Soxhlet extraction, to compare the effectiveness of the two extraction methods with respect to the total extract yielded and other phenolic properties.

II. METHODOLOGY

A. Materia and Chemical

Olive cake was obtained by a local mill of cold press system, Pirsabak Nowshera, Pakistan. The olive cake was dried by an oven at 1050C for 3 hours, to reduce the moisture content. The moisture content was found to be 3.12% (w/w). The olive cake shown in the figure 1. Hexane, Methanol, Foline Ciocalteu's reagent, Gallic acid, Sodium carbonate 1,1 diphenyl-2picrylhydrazyl (DPPH), were purchased of Sigma Aldrich Chemical Co.

Figure 1 Olive cake before and after drying

B. Method

C. Soxhlet Extraction (SE)

50 g of the dry cake was set on a filter paper which was doubled up and tightly wrap utilizing a cotton wire. Each prepared sample was put in vital chamber of Soxhlet extractor. The n-hexane was utilized as a solvent with a proportion of 1 :3 and 1:5 at various temperatures of 50 ^{0}C, 60 ^{0}C and 70 ^{0}C with about refluxes (ration of solvent circulates each time, to extract the desired compound to the round bottom flask, through the solid material). Different interval of time period including of 30 mins, 45 mins, 60 mins and 75 mins was the total length of program. The mixture was separated by filtration through Whatman No. 42 filter paper, at the end of each experiment.

D. Microwave assisted solvent extraction (MASE)

The dry pomace samples were subjected to microwave as shown in figure 2, in round bottom flask by adding distinctive volume of n- hexane (1 :03) and (1 :05) solid-to-solvent ratio at power irradiation of 200, 350 and 500 W for extraction of oil. In the vial, the mass of dry pomace 50 g was kept constant for each analysis. after each sample experimentation and then extracted oil was further refine from n-hexane through a rotatory evaporator at 50 ° C, reduced pressure to obtain pomace oil. The EO was calculated from the following equation expression.
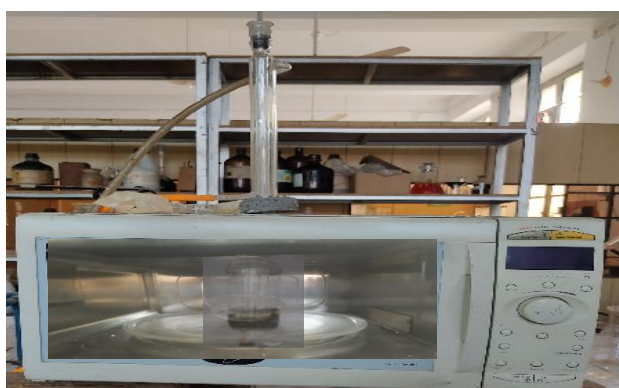
Figure 2 Microwave Assisted Solvent Extraction Unit

Extraction Yield of Oil% = (mass of extracted oil/ mass of dried material) x 100   (1)

E.   Qualitative analysis of EO:

F.   Determination of total phenolic content (TPC):

The total phenols (TP) content of the oil extracts was determined calorimetrically at 760 nm using the Folin-Ciocalteu reagent according to a modified method of the **Gutfinger (1981)** [15]. The total phenolic content was evaluated calorimetrically using the spectrophotometer UV (Agricultural Chemistry, University of Agricultural, Peshawar). Total phenolic content of n-Hexane extract of Pomace Olive oil was determined employing the method involving Folin-Ciocalteau reagent agent and Gallic acid as standard.

D. Determination of antioxidant activity, DPPH (2,2-Diphenyl-1-Picrylhydrazyl) Assay:

Free radical scavenging activity of samples was determined using the 2,2-diphenyl-2-picrylhydrazyl (DPPH) calorimetrically at 517 nm according to a modification method of **Bandoniene et al. (2002)** [16]. The DPPH was evaluated calorimetrically using the spectrophotometer UV. The percentage (%) inhibition activity was calculated from the following equation. (A_0 is the absorbance of the control and A_1 is the absorbance of the extract/ standard)

$$\% \ I = \{(A_0 - A_1)/ A_0\} \ x \ 100 \qquad (2)$$

III.   Results and Discussion

A.   Comparative analysis (Comparison of Microwave and Conventional extraction)

Combined analysis shows that overall performance of MASE is better than SE in terms of power consumption, TPC, Antioxidant and % yield wise as well.

Extraction yield results are illustrated in figure 3 and figure 4. Both figures demonstrate that oil yield increased with extraction time and power. Figure 3 and figure 4 shows the result of % yield of sample to solvent ratio of 1:03 and 1:05 of SE and MASE, when conventional extraction highest %yield achieved was 5.83 at 70 ^{0}C in 75 mins, the MASE at same ratio attains maximum %yield was 6.89 at 500W in 5 minutes shown in figure 3 both achieved in same ratio of 1:03, as radiation power had more positive influence on the oil yield. While increasing the sample to solvent ratio to 1:05, the % yield increased, and results obtained are better than 1: 03 ratio. The highest %yield achieved in conventional and ME was 6.38 and 8.04 at different time of 70 mins and 5 mins as shown in figure 4, all due to the 3-dimensional heating mechanism of microwave. Which properly rupture the cell and get more % yield from it.
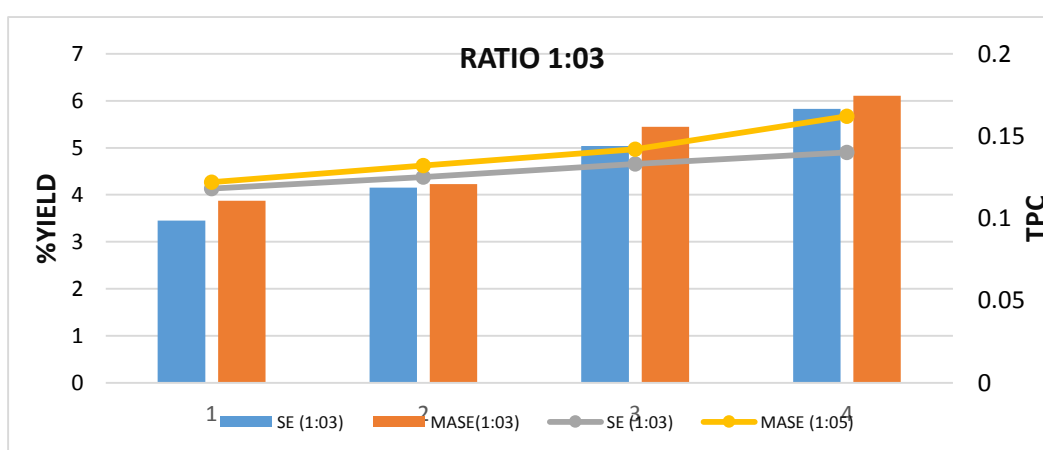
Figure 3 Comparative analysis of %Yield and TPC for Both techniques (ratio 1:03)
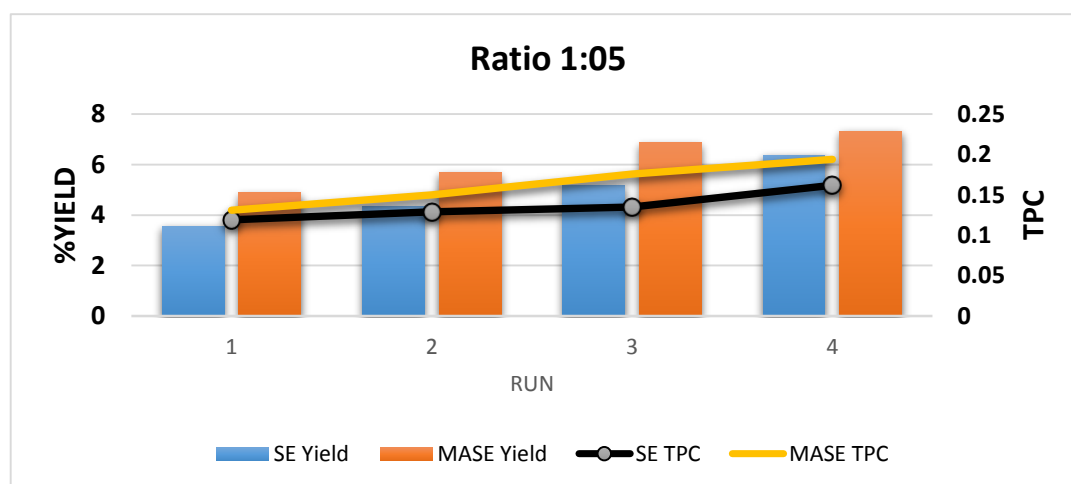
Figure 4 Comparative analysis of %Yield and TPC for Both techniques (ratio 1:05)

In the total phenolic content vs time, the microwave assisted solvent extraction experiments on different ratio of 1:03 and 1:05 solid to solvent ratio was used and compared with the Soxhlet extraction method. Since the total phenolic content was the highest in the solid to solvent ratio of 1:05 as compared to solid to solvent ratio 1:03. Total phenolic contents of S: L= 1:03 which were extracted by using SE were found to be between *0.095 - 0.137* mg GAE/g oil and MASE were found to be between *0.118 and 0.183* mg GAE/g oil shown in figure 3. While for 1:05 (solid to solvent ratio) the SE found at its' maximum was *0.184 mg* GAE/g oil and MASE found to be highest *as 0.204 mg* GAE/g oil shown in figure 4**.** As the results of both figures 5 and 4.33 showed that highest value extract in MASE is 9.89% more than SE in 1:05 while in ratio of 1:03 the MASE is 13% increased in value than SE. Total phenolic content increased with time and power but achieved the highest value when solid to solvent
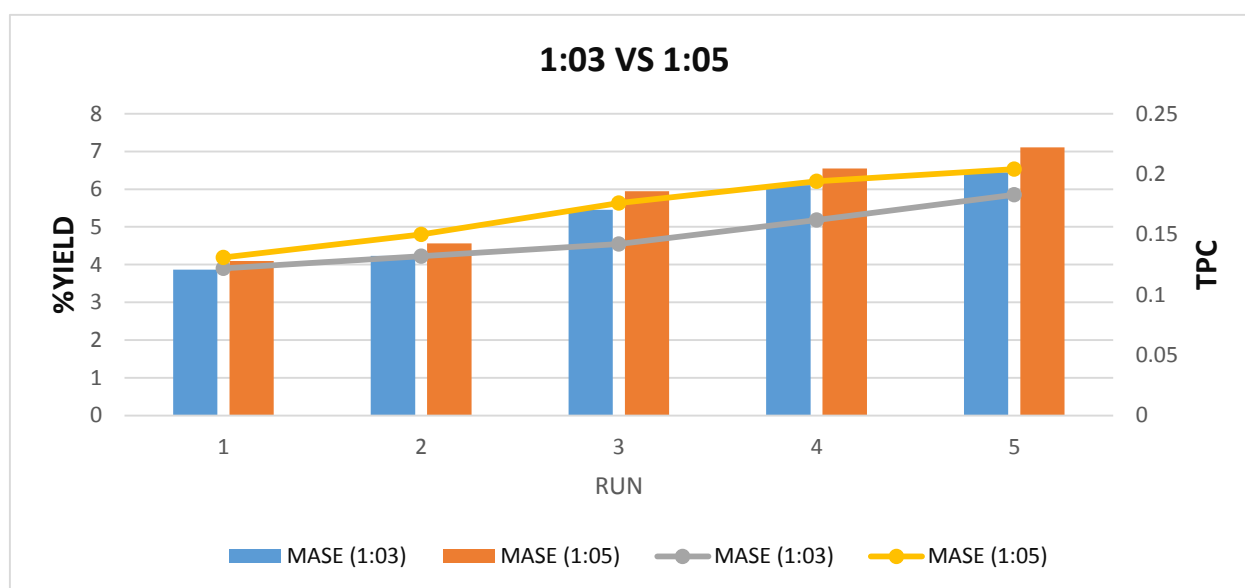
Figure 5 Comparative analysis on solvent ratio of %Yield and TPC for Both techniques   ratio

increased

The graphs of Figure 6 show the antioxidant activities of pomace oil extracted with 500 W microwave irradiation power – 5 minutes and 70 °C temperature for Soxhlet. Antioxidant activities with respect to time- 70 mins for different ratio of 1:03 and 1:05. The highest antioxidant activity was found in MASE was 31.23% scavenging in 5 minutes, ratio of 1:03 while SE achieved was 26.37% scavenging in 75 mins. Whereas the maximum value for the ratio of 1:05 was 33.12 in MASE at 5 minutes and 28.70% in SE at 75 minutes. The 13% increase can clearly be observed in 1:03 and 15% in 1:05. The better result shown in MASE is the evidence of the rupture cells and more phenolic compounds from microwave extracts. In addition, power and time as well as sample to solvent ratio, in the tested ranges, had a significant interactive effect on DPPH scavenging capacity
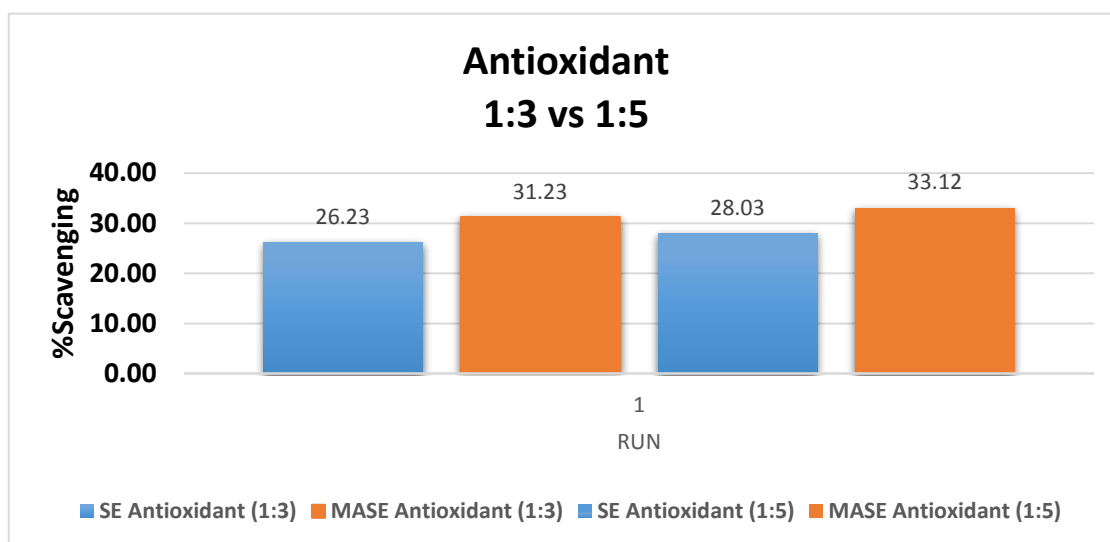
Figure 6 Comparative analysis of Antioxidant for both techniques

The comparison of power consumed per gm between the SE and MASE shown in figure 7 and figure 8 with both ratio of S: L= 1:03 and S: L= 1:05 for different techniques. The power consumed per gm for highest % yield in SE (1:03) was 0.0212 (kW/gm E.O) (Time= 70 mins, %yield= 5.83) while in MASE the power consumed was 0.0121 (kW/gm E.O) (Time= 05 mins, %yield= 6.89) shown in figure 7. The low power consumption and high % yield also had less effect on environment in term of CO_2 emission, more the power consumption will have adverse effect one environment. But increasing the sample-to-solvent ratio save more power consumption and increase %yield. As S: L= 1:05 the power consumed per gm in SE was 0.0194 (kW/gm E.O) (Time= 70 mins, %yield= 6.38) whereas 0.00996 (kW/gm E.O) (Time= 05 mins, %yield= 8.04) in MASE as shown in figure 8. The environmental effect will be more less in 1:05 then 1:03.
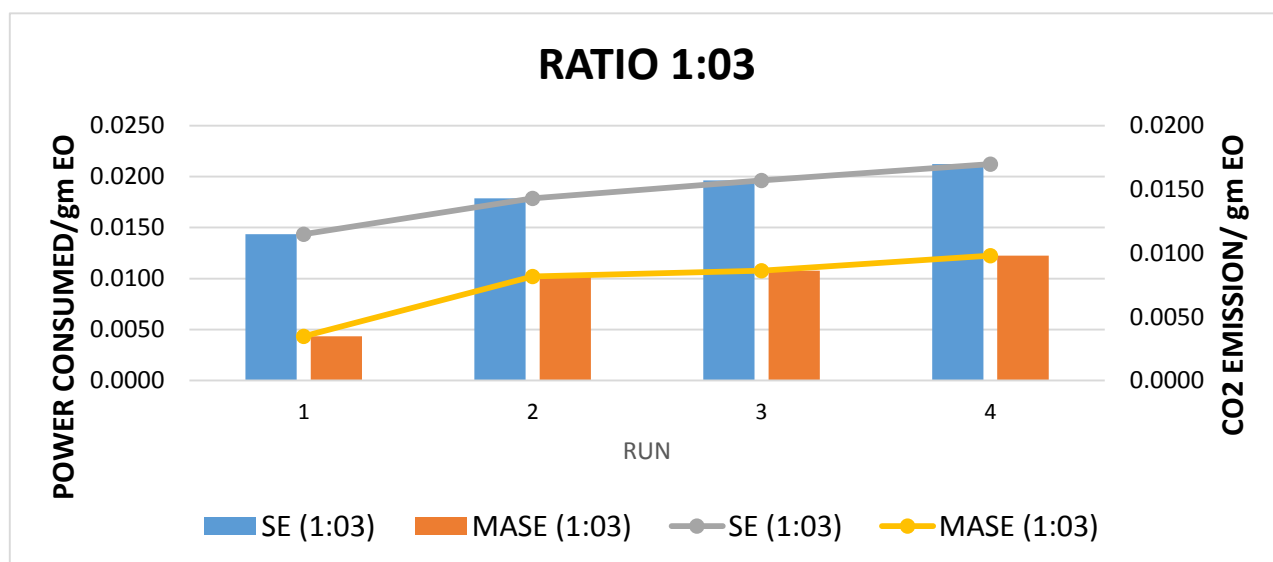
Figure 7 Comparative analysis on ratio of 1:03 of Power consumption/gm and CO2 emission/gm for both SE and MASE
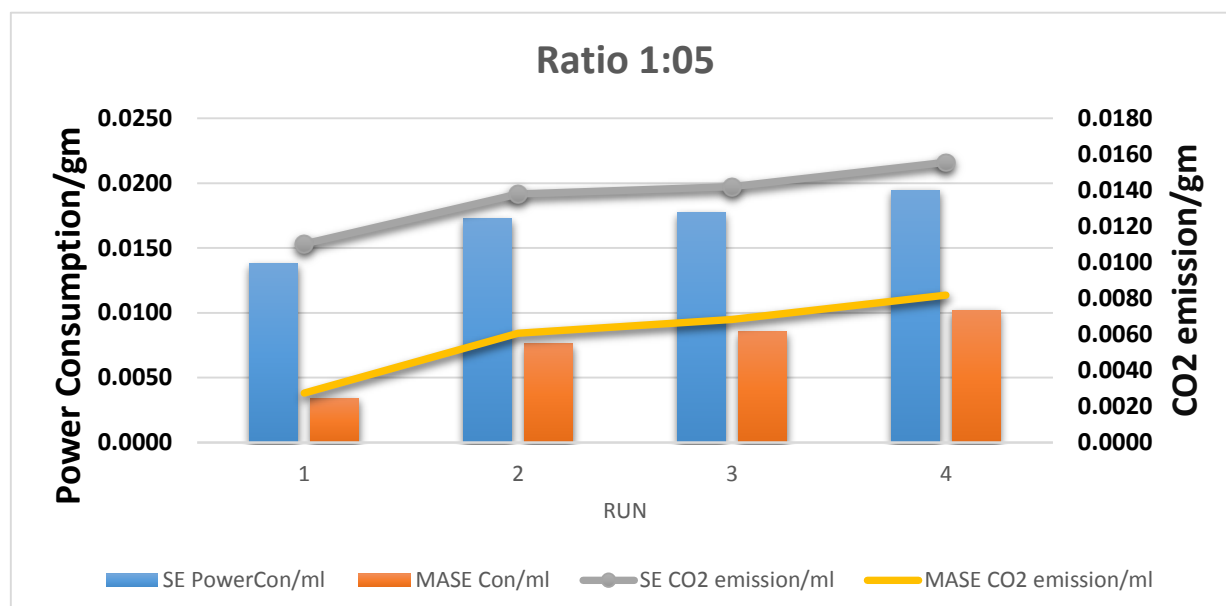
Figure 8 Comparative analysis on ratio of 1:05 of Power consumption/gm and CO2 emission/gm for both SE and MASE

IV.   Conclusion

In this study, extraction of pomace oil obtained through microwave assisted solvent extraction and Soxhlet extraction. Both techniques were analyzed and tested for percentage yield, total phenolic content and antioxidant activity. The conventional method (Soxhlet extraction) been used for long period but is very time consuming and usually requires large amounts of solvents. Our results showed that microwave-assisted soluble extraction is a more effective method than the traditional technique (Soxhlet). The heating mechanism of microwave-assisted soluble extraction is to disrupt cell pant cells and increase the mass transfer of intracellular in extraction. The Microwave assisted solvent extraction result was validated to assess its efficiency in comparison with Soxhlet extraction (conventional technique). The use of microwave-assisted extraction, %yield could be achieved in minutes instead of hours with high reproducibility, reducing the consumption of solvent, energy and time due to its shorter time extraction. The minimum CO_2 emission was also observed in MASE, which will have least adverse effect on environment. The highest %yield, total phenolic content and antioxidant activity values were obtained when 1:05 solid to solvent ratio, time period of 5 minutes and 500 W microwave power were used. As showed in results the different solvents ratios of 1:03 and 1:05, the ratio of 1:05 was more effective in term of %yield and extraction of phenolic compounds from the olive cake. So, increasing the solid -to-solvent can simply increase the extraction from olive cake. However, it does have impact on phenolic compound and antioxidant activity. But regarding the phenolic compounds and the DPPH, the extraction time has a significant influence and tends to increase as the extraction time increases. Overall, MASE has proven to be a preferred extraction technique for olive pomace oil over the conventional methods of olive pomace oil production. This simple and inexpensive technique could quickly be extended to provide some sort of income to olive oil producers and processors, a wise use of this agricultural by-product.

V.   REFERENCES

[1]   J. Mataix and J. F. Barbancho, "Olive Oil in Mediterranean Food," in CAB International, CAB International, 2006, pp. 1–36.

[2]   M. El Riachy, F. Priego-Capote, L. León, L. Rallo, and M. D. Luque de Castro, "Hydrophilic antioxidants of virgin olive oil. Part 1: Hydrophilic phenols: A key factor for virgin olive oil quality," Eur. J. Lipid Sci. Technol., vol. 113, no. 6, pp. 678–691, Jun. 2011, doi: 10.1002/ejlt.201000400.

[3]   Kiritsakis and A. K, Olive Oil: From the tree to the table. Food and Nutrition Press, 1998.

[4]   A. Montaño, A. H. Sánchez, A. López-López, A. De Castro, and L. Rejano, "Chemical Composition of Fermented Green Olives: Acidity, Salt, Moisture, Fat, Protein, Ash, Fiber, Sugar, and Polyphenol," in Olives and Olive Oil in Health and Disease Prevention, Elsevier Inc., 2010, pp. 291–297.

[5]   J. C. G. Esteves Da Silva, "Chemometric Classification of Cultivars of Olives: Perspectives on Portuguese Olives," in Olives and Olive Oil in Health and Disease Prevention, Elsevier Inc., 2010, pp. 33–42.

[6]   M. H. Ahmad-Qasem, J. Cánovas, E. Barrajón-Catalán, V. Micol, J. A. Cárcel, and J. V. García-Pérez, "Kinetic and compositional study of phenolic extraction from olive leaves (var. Serrana) by using power ultrasound," Innov. Food Sci. Emerg. Technol., vol. 17, pp. 120–129, Jan. 2013, doi: 10.1016/j.ifset.2012.11.008.

[7]   A. F. Vinha et al., "Phenolic profiles of Portuguese olive fruits (Olea europaea L.): Influences of cultivar and geographical origin," Food Chem., vol. 89, no. 4, pp. 561–568, Mar. 2005, doi: 10.1016/j.foodchem.2004.03.012.

[8]   R. Malheiro, A. Sousa, S. Casal, A. Bento, and J. A. Pereira, "Cultivar effect on the phenolic composition and antioxidant potential of stoned table olives," Food Chem. Toxicol., vol. 49, no. 2, pp. 450–457, Feb. 2011, doi: 10.1016/j.fct.2010.11.023.

[9]   M. Pinelo, M. Rubilar, M. Jerez, J. Sineiro, and M. J. Núñez, "Effect of solvent, temperature, and solvent-to-solid ratio on the total phenolic content and antiradical activity of extracts from different components of grape pomace," J. Agric. Food Chem., vol. 53, no. 6, pp. 2111–2117, Mar. 2005, doi: 10.1021/jf0488110.

[10]   A. Liazid, M. Palma, J. Brigui, and C. G. Barroso, "Investigation on phenolic compounds stability during microwave-assisted extraction," J. Chromatogr. A, vol. 1140, no. 1–2, pp. 69 9–34, Jan. 2007, doi: 10.1016/j.chroma.2006.11.040.

[11]   B. Lanza, M. G. Di Serio, E. Iannucci, F. Russi, and P. Marfisi, "Nutritional, textural and sensorial characterisation of Italian table olives (Olea europaea L. cv. 'Intosso d'Abruzzo')," Int. J. Food Sci. Technol., vol. 45, no. 1, pp. 67–74, Dec. 2009, doi: 10.1111/j.1365-2621.2009.02104.x.

[12]   B. Bayramoglu, S. Sahin, and G. Sumnu, "Solvent-free microwave extraction of essential oil from oregano," J. Food Eng., vol. 88, no. 4, pp. 535–540, Oct. 2008, doi: 10.1016/j.jfoodeng.2008.03.015.

[13]   M. R. González-Centeno, K. Knoerzer, H. Sabarez, S. Simal, C. Rosselló, and A. Femenia, "Effect of acoustic frequency and power density on the aqueous ultrasonic-assisted extraction of grape pomace (Vitis vinifera L.) - A response surface approach," in Ultrasonics Sonochemistry, 2014, vol. 21, no. 6, pp. 2176–2184, doi: 10.1016/j.ultsonch.2014.01.021.

[14]   M. L. Chávez-González et al., "Conventional and emerging extraction processes of flavonoids," Processes, vol. 8, no. 4. MDPI AG, p. 434, Apr. 01, 2020, doi: 10.3390/PR8040434.

[15]   Gutfinger, T., O. Vatario, M. Alter and A. Letan, Grasas Aceites (Seville) 26:8 ... J Am Oil Chem Soc 58, 966–968 (1981)

[16]   Bandoniene D, Murkovic M, Pfannhauser W, Venskutonis PR, Gruzdiene D. Detection and activity evaluation of radical scavenging compounds by using DPPH free radical and on-line HPLC– DPPH methods. Euro Food Res Technol. 2002;214(2):143–147. doi: 10.1007/s00217-001-0430-9.

Solar Thermal Water and Space Heating: Comparative Analysis of Charging and Discharging Behavior of Phase Change Materials

VI. Hurmat Khan[A], Khurshid Ahmad[A], Muhammad Hassan[A], Misbah Ullah[A], Muhammad Farooq Siddique[A].

[A]US-Pakistan Center for Advanced Studies in Energy (USPCAS-E), University of Engineering and Technology Peshawar, Pakistan
{khanhurmat22, farooqsiddique.mech}@gmail.com ,{ khurshid, muhammad.hassan, }@uetpeshawar.edu.pk,
misbah1110@yahoo.com,

*Abstract-*According to the renewable energy global status report (GRS) 2018, around 48% of the total global energy consumed is used for heating and cooling purposes. This energy is obtained mainly, from the burning of fossil fuels resulting in CO2 emissions, which is the largest contributor to global warming. To use solar energy for heating purposes during both, the sunshine and off sunshine hours, phase change material (PCM) could be one of the best choices. Phase change material stores solar thermal energy during sunshine hours and the stored energy is extracted back by the circulation of heat transferring fluid (HTF) through conductive conduits inside the PCM, for heating purposes during off sunshine hours. In this research solar thermal water and space heating system (STWSHS) integrated with PCM was used to investigate the charging (energy stored) and discharging (energy recovered) behavior of PCMs. Two PCMs stearic acid palmitic acid (SAPA) and puretemp 68 (PT68) were used during experiments. During the daytime, PCM absorbed heat energy from HTF, heated in solar thermal collectors by absorbing solar energy. The results showed that SAPA outperformed PT68 by storing 31.7% more heat. Moreover, during discharging experiments 36.7% more energy was recovered from SAPA as compared to PT68. The maximum energy recovery ratio (ERR) was 0.88 for SAPA and 0.79 for PT68. The results suggested that SAPA can be a better choice for solar thermal water and space heating applications.

Keywords: PCM, Charging, Discharging, Energy Recovery Ratio.

I. INTRODUCTION

According to the renewable energy global status report (GSR) 2018, almost 48% of the total global energy consumed is used for heating and cooling purposes [1]. This energy is obtained mainly from the burning of fossil fuels resulting in CO_2 emissions causing global warming. By 2050 CO_2 emissions due to the burning of fossil fuels for energy will be approximately doubled [2]. Solar energy can be a very good source to meet the increasing demand of the heating sector compared to fossil fuels which upon burning releases CO2 [3]. Solar thermal water and space heating (STWSH) systems can be used for domestic water and space heating applications. There are two main problems associated with using solar thermal water and space heating system for heating purposes, (i) STWSH technologies completely depends on the weather conditions for energy storage (availability of solar irradiance) [4], and (ii) lack of availability of high energy storage materials [5]. To use PCM for thermal energy storage for water and space heating in buildings, it is needed to design and develop a technically feasible, and compact STWSH system integrated with PCM) [6]. The efficiency of solar thermal water and space heating systems can be increased by integrating PCM in STWSH systems [7].

Energy storage has a great role in energy conservation, reduces the energy supply-demand gap, and improves energy systems performance [8]. For thermal energy storage, the PCM should have desirable charging and discharging properties. PCMs are classified as solid-liquid, liquid-gas, solid-gas [9]. Solid-liquid PCMs are preferred over liquid-gas PCMs due to their low volumetric changes during phase transition, high energy storage density, and wide range of operating temperatures [10]. Solid- liquid organic PCMs and their eutectics have advantages like non-toxic, bio-based in nature, low vapor pressure, smooth melting, and abundant availability [11]. Solid-Liquid PCMs are classified as inorganic (salts, hydrates, and hydroxides) and organic (paraffin, fatty acids, esters, and many others) [12]. Joseph et al. [13] performed the experiments on PCM dodecanoic acid. The dodecanoic acid latent heat energy storage (LHES) system absorbed 20% more thermal energy than the equivalent water storage system. Canbazoglu et al. [14] experimentally investigated solar thermal energy storage performance for the PCM (sodium thiosulfate

pentahydrate) and found that solar thermal energy storage performance has improved as compared to the solar thermal energy storage without PCM. Sharma, Tyagi, et al. [15, 16] performed experiments on fatty acids, eutectic PCMs for thermal and chemical stability. Myristic acid and palmitic acid were found to be thermally and chemically stable after performing 1500 melting and freezing cycles. Robaidi et al. [17] found that latent heat thermal energy storage (LHTES) systems integrated with PCM can store almost 5 to 14 times more heat energy per unit volume as compared to sensible heat storage materials.

II. MATERIALS AND METHODOLOGY

A. Materials

The materials which are used in solar thermal water and space heating (STWSH) system integrated with PCM are water-glycol mixture as Heat transferring fluid (HTF), stearic acid palmitic acid (SA/PA), puretemp 68 (PT68) as phase change materials, and water.
Details of the materials used are given in the tables.

TABLE I: Properties of water-ethylene glycol mixture (50:50 volume ratio)

Temperature Range	0-150 °C
Density	1050 kg/m^3
Heat Capacity	3470 J/ kg.K

TABLE II: Properties of Phase Change Materials

PCM	Total Quantity	Melting Temperature Range	Cp (liquid)	Cp (solid)	Latent Heat of Fusion
Stearic acid palmitic acid (SAPA)	2 kg	55.1-59.5 °C	2.65 J/g.K	1.83 J/g.K	181 kJ/kg
Puretemp 68 (PT68)	2 kg	68-73.8 °C	1.91 J/g.K	1.85 J/g.K	198 kJ/kg

TABLE III: Equipments used in solar thermal water and space heating system

Thermally insulated containers (cylindrical shape)	Digital Arduino circuit	Charging battery
Copper coil	12 V DC pumps	Omega thermocouple data logger
Wooden chamber (2ft^3)	Solar charger	Flowmeter
Evacuated tube solar thermal collectors	Thermocouples	Pyranometer

B. Methodology

In Fig. 1, red dash lines represent thermocouple feedback system to the thermocouple data logger, the direction of the solid black lines represent the direction of HTF in copper coil, dash green lines represent temperature feedback to pump controller and solid green lines represent ON/OFF signal from the controller to pumps. The experimental setup of the solar thermal water and space heating (STWSH) system operates in such a way that, HTF circulating through copper coil absorbs solar energy through STC and transfer its energy to PCM to get PCM charged. The HTF in the discharging copper coil takes heat energy from PCM and is utilized for water and space heating. The thermal comfort of the controlled environment (CE) was kept from 17-27 °C. The HTF circulating in the copper coil through water storage container and CE absorbs heat energy from PCM during discharging and transfer heat energy to CE for space heating and water heating. When the temperature of CE drops below 17 °C, pump 3 will operate and HTF circulation starts to CE and HTF transfer its heat to CE for space heating. When the temperature in CE reaches 27 °C, pump 3 will automatically be turned OFF and HTF circulation through CE stops.

A: PCM storage container B: Water storage container C: CE (wooden chamber) D: Not CE (wooden chamber) E: Evacuated tube STC
F: Pump controller G: PV panel
H: Battery
I: Thermocouple data logger J: Computer
K: Flow meter
P1-P3: HTF circulation Pumps V1-V6: Valves
T1-T18: Thermocouples
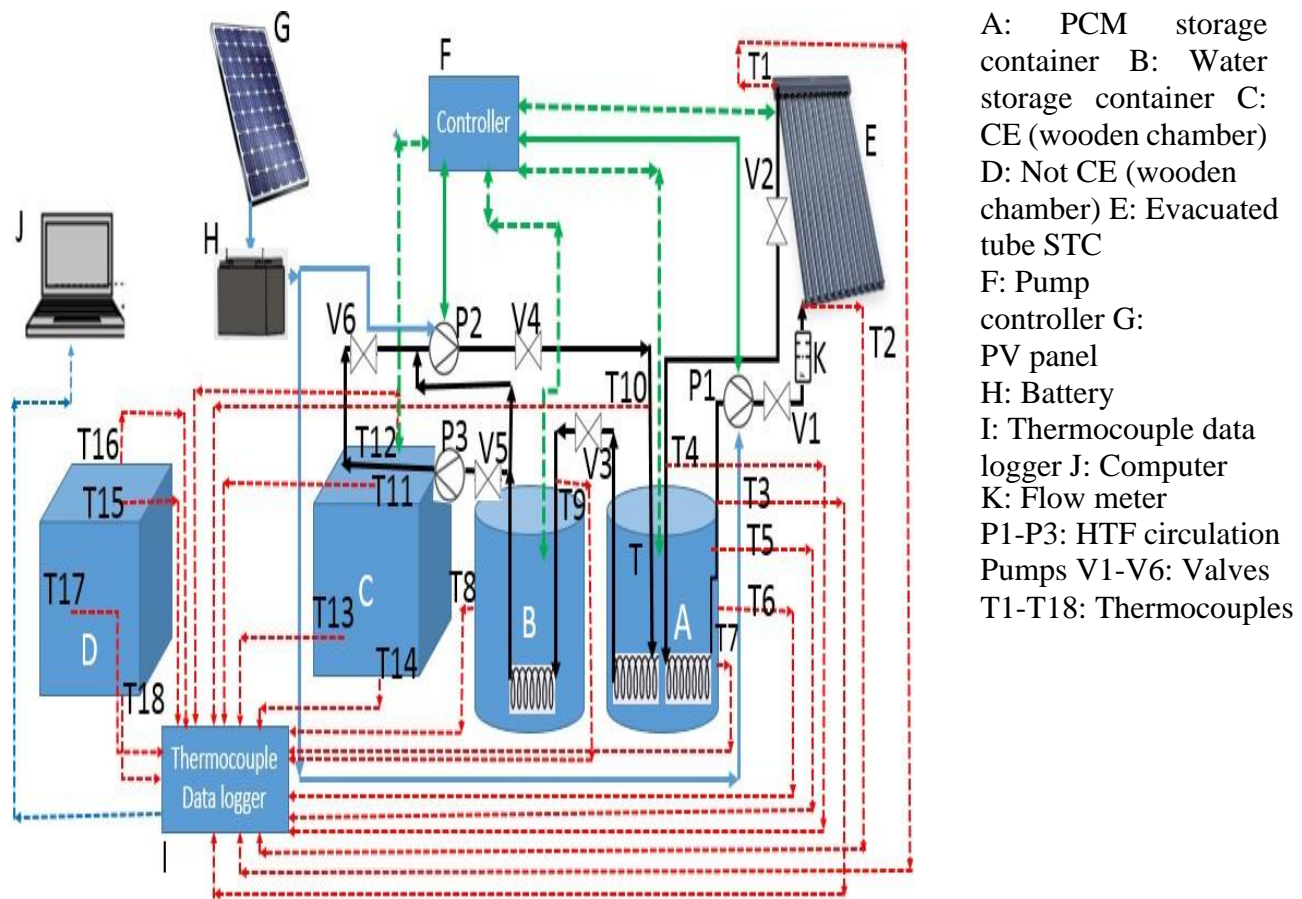
Fig. 1. Schematic of solar thermal water and space heating system.

C. Heat Transfer Equations

The equation for the charging of phase change material (PCM) is given by.

$$Q_{stored} = m[C_{p,s}(T_s - T_i) + X\Delta h + C_{p,l}(T_f - T_l)] \tag{1}$$

Where $C_{p,s}$, and $C_{p,l}$ are the specific heat of PCM in solid and liquid phase respectively, T_i and T_f are the PCM temperatures at the initial and final state of charging respectively (T varies from initial state i to final state f).

The equation for discharging of PCM is given by.

$$Q_{recovered} = m[C_{p,s}(T_s - T_{final}) + X\Delta h + C_{p,l}(T_{initial} - T_l)] \tag{2}$$

$T_{initial}$ and T_{final} the temperatures of PCM temperature at the initial and final state of the discharging. Energy Recovery Ratio equation is given by.

$$ERR = \frac{Q_{max-recovered}/t_{complete\ discharge}}{Q_{max-stored}/t} \tag{3}$$

complete charge

III. RESULTS AND DISCUSSION

The results of the charging (heat energy stored) and discharging (heat energy recovered) experiments of phase change materials (PCMs) are discussed below.

A. Charging Experiments of Phase Change Materials (PCMs)
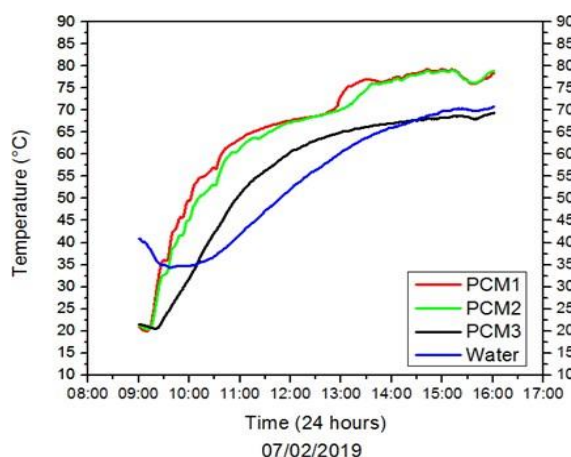
(a) Charging of PT68 and water heating
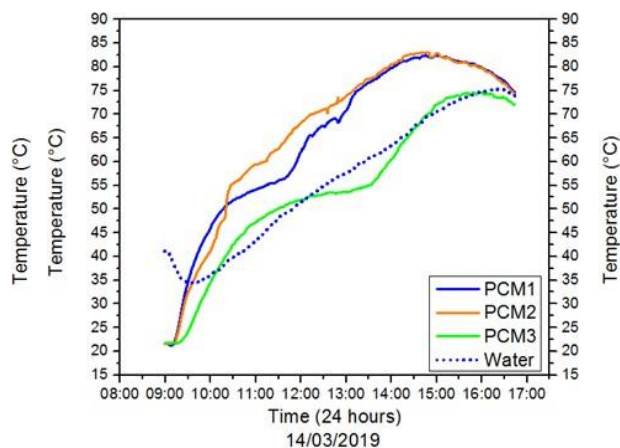
(b) Charging of SA/PA and water heating

Fig. 2. The temperature profile of PCM at three different positions PCM 1, PCM 2, PCM 3 (bottom, center, top surface respectively) and water heating during charging of PCM using (a) PCM PT68 on 7 February 2019, (b) PCM SA/PA on 14 March 2019

.
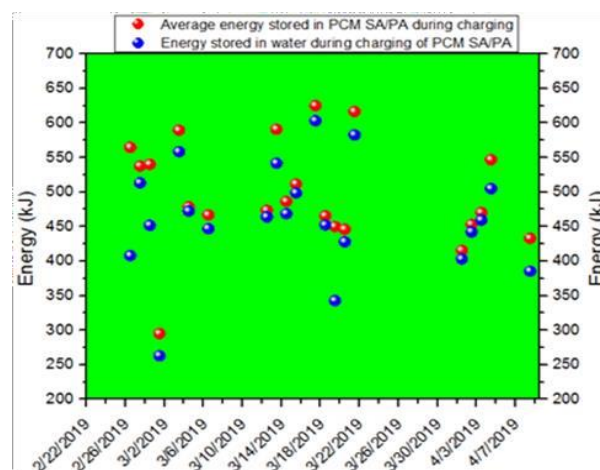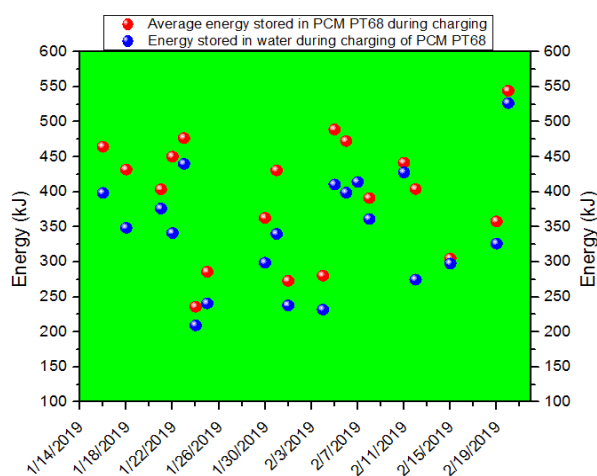
Fig. 3. Average energy stored in PCM and energy stored in water during all charging experiments using (a) PCM PT68 and
(a) PCM SA/PA.

Fig. *2* represents the temperature profile of the charging of PCM PT68, SA/PA, and water heating. The water heating started above 40 °C in both cases. This is because the same water which was heated at nighttime during discharging of PCM was used at daytime during charging of PCM for water heating. PCM was cooled down before charging experiments, to lower its temperature (to increase the temperature

difference between PCM and HTF so that heat flow is efficient, and more heat is absorbed by PCM). At the start of the charging experiments in both the cases water heating started above 40 °C, loses some heat first to come in thermal equilibrium with PCM which is at a lower temperature than water. In Fig. 2 (b) the temperature at position PCM 3 (solid green curve) behaves differently than the other two curves between 12:00 to 14:00 due to convection heat transfer from the top surface of PCM (thermocouple placed at position PCM 3 just immersed in PCM) because the lid of the PCM storage tank was kept open to observed whether the PCM is completely melted.

B. Discharging of Phase Change Materials

The temperature profile of HTF at the inlet-outlet of the PCM storage tank, water heating, and PCM discharging is shown in Fig. *4*. From Fig. 4 (a) for PCM PT68 at positions PCM 1 and PCM 2 from point B to C is phase transition stage and at position PCM 3 from point A to point C is the phase transition stage, because at position PCM 3 the PCM has not melted completely during charging experiment and its temperature is in phase transition temperature range. In Fig. 4 (b) from point A to B is the phase transition

range for SA/PA during discharging, as during the phase transition stage there is latent heat transfer so there is no temperature change from point A to B.
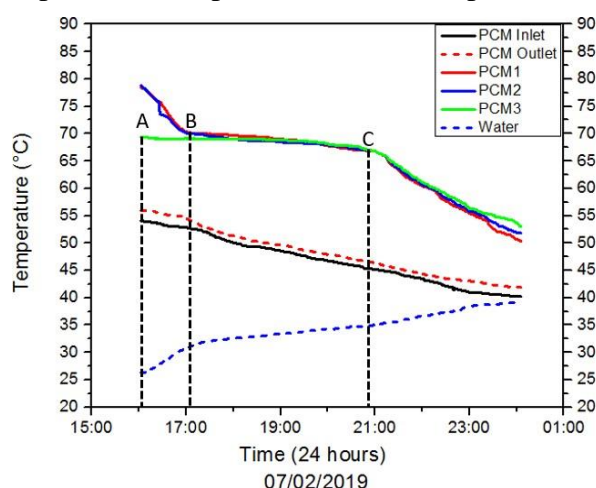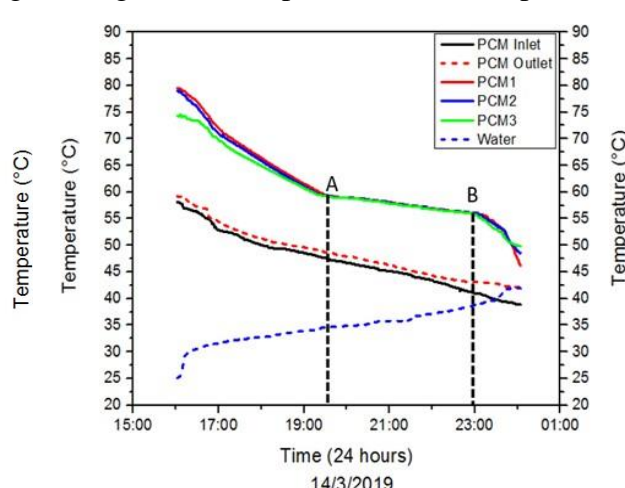
(a) Discharging of PT68   (b) Discharging of SA/PA

Fig. 4. The temperature profile of HTF inlet-outlet to the PCM storage tank, water heating and discharging of PCM at three different positions PCM 1, PCM 2, PCM 3 (bottom, center, top surface respectively) during discharging of PCM using (a) PCM PT68 on 7 February 2019 and (b) PCM SA/PA on 14 March 2019.
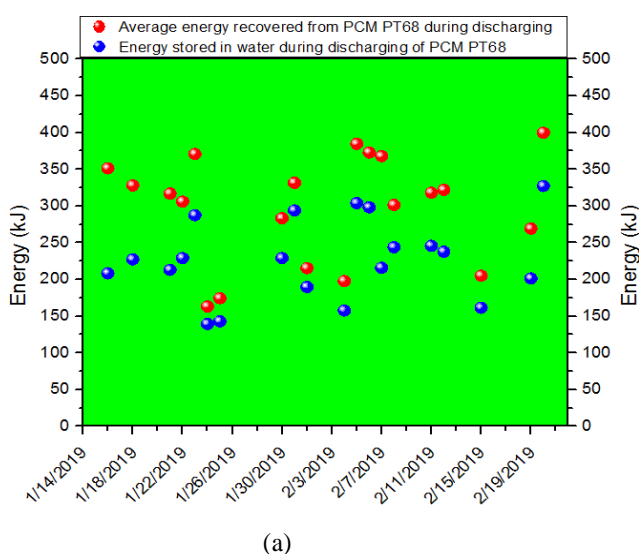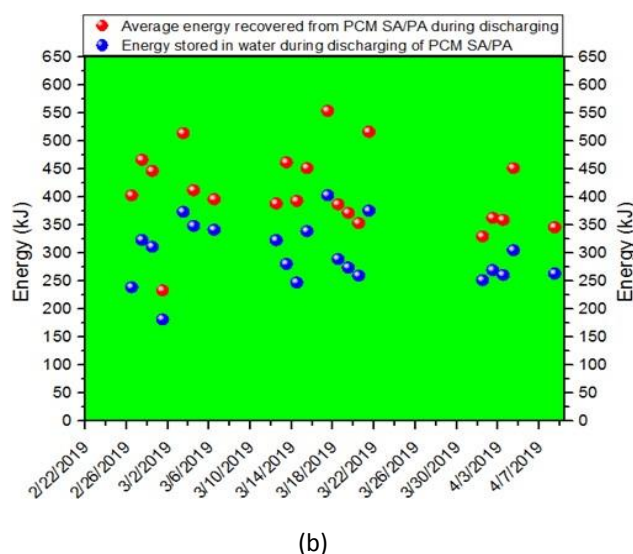
(a)   (b)

Fig. 5. Average energy recovered from PCM and energy stored in water during discharging of PCM, using (a) PCM PT68,
(b) PCM SA/PA.
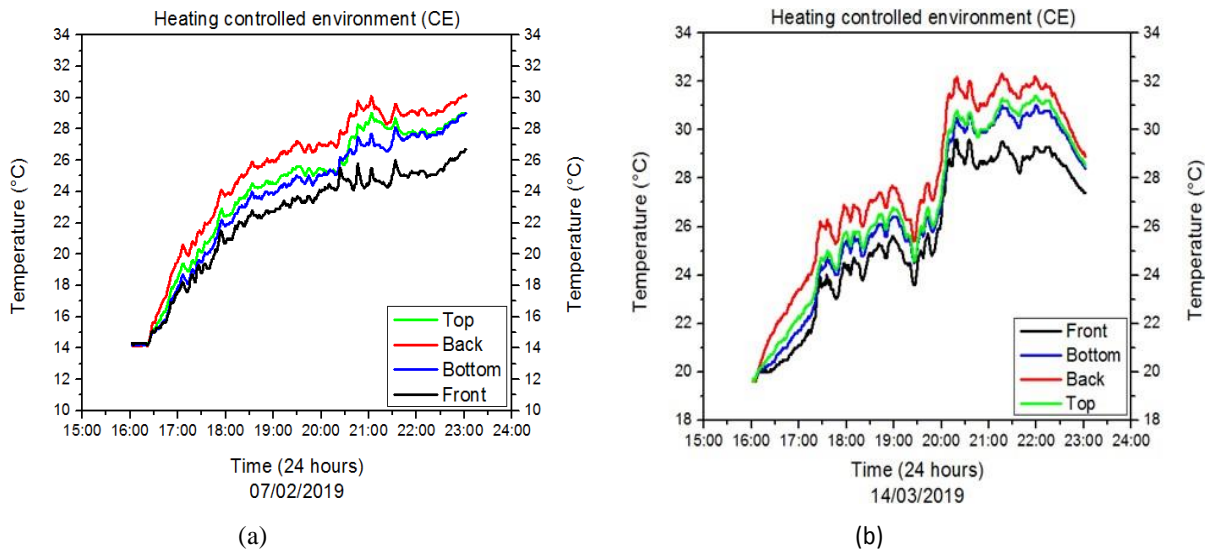
Fig. 6. Heating of the controlled environment (CE) during discharging of PCM using (a) PCM PT68 on 7 February 2019, and

(b) PCM SA/PA on 14 March 2019.

Inside the controlled environment (CE) the temperature profiles of the top, back, bottom, and front walls are shown in Fig. 6. The thermal comfort in CE was kept from 17°C to 27°C. When the temperature in CE reaches 27 °C, HTF circulation through CE stops. In Fig. 6, the temperature is above
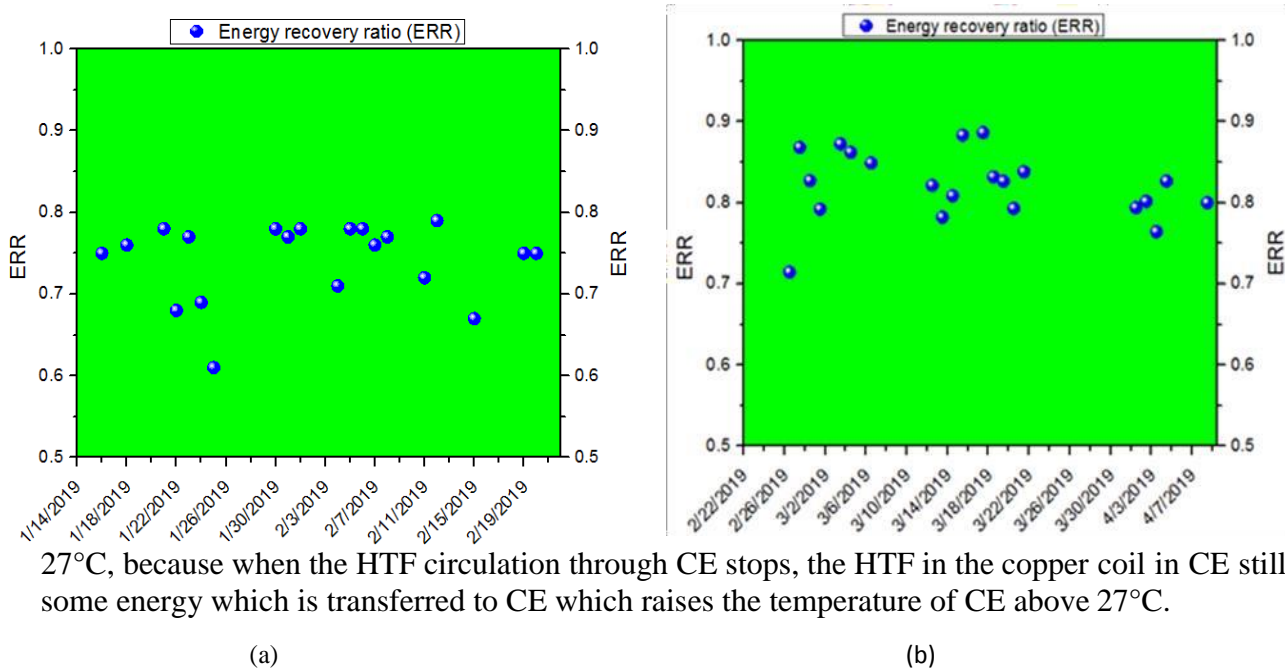
27°C, because when the HTF circulation through CE stops, the HTF in the copper coil in CE still has some energy which is transferred to CE which raises the temperature of CE above 27°C.

Fig. 7. Energy recovery ratio (ERR) for all the experiments performed using (a) PCM PT68 and (b) PCM SA/PA

A comparison of the energy recovery ratio (ERR) is shown in Fig. 7. The energy recovery ratio of PCM SA/PA is higher as compared to the energy recovery ratio of PT68, which shows better heat storage and heat recovery capacity of SA/PA.

IV. CONCLUSION

The total energy stored during all charging experiments in PT68 was 7.94 MJ and in SAPA total energy stored was 10.46 MJ. It shows that during charging experiments 31.73% more energy is stored in SAPA as compared to PT68. The total energy recovered from PT68 was 6.29 MJ and from SAPA was

8.60 MJ during all discharging experiments. Energy recovered during all discharging experiments using SAPA was 36.72 % more than PT68. The maximum energy recovery ratio (ERR) for one day was 0.79 using PT68 and 0.88 using SAPA. The average ERR using PT68 was 0.75 and using SAPA was 0.82. The average ERR for SAPA is 9.33% more than PT68. So, overall SAPA has good charging and discharging capabilities as compared to PT68. Therefore using SAPA as a PCM in solar thermal water and space heating systems can be a practical solution for the harvesting of solar energy, which can solve concerns related to STWSH systems usage in off sunshine hours.

V. REFERENCES

[1] J. L. Sawin, F. Sverrisson, J. Rutovitz, S. Dwyer, S. Teske, H. E. Murdock, *et al.*, "Renewables 2018-Global status report. A comprehensive annual overview of the state of renewable energy. Advancing the global renewable energy transition-Highlights of the REN21 Renewables 2018 Global Status Report in perspective," 2018.

[2] S. P. Energy, "Technology Roadmap," 2014.

[3] E. Kabir, P. Kumar, S. Kumar, A. A. Adelodun, and K.-H. Kim, "Solar energy: Potential and future prospects," *Renewable and Sustainable Energy Reviews,* vol. 82, pp. 894-900, 2018.

[4] N. Gill, P. Osman, L. Head, M. Voyer, T. Harada, G. Waitt, *et al.*, "Looking beyond installation: Why households struggle to make the most of solar hot water systems," *Energy Policy,* vol. 87, pp. 83-94, 2015.

[5] G. Alva, L. Liu, X. Huang, and G. Fang, "Thermal energy storage materials and systems for solar energy applications," *Renewable and Sustainable Energy Reviews,* vol. 68, pp. 693-706, 2017.

[6] H. Shabgard, L. Song, and W. Zhu, "Heat transfer and exergy analysis of a novel solar-powered integrated heating, cooling, and hot water system with latent heat thermal energy storage," *Energy Conversion and Management,* vol. 175, pp. 121-131, 2018.

[7] Y. Tian and C.-Y. Zhao, "A review of solar collectors and thermal energy storage in solar thermal applications," *Applied energy,* vol. 104, pp. 538-553, 2013.

[8] H. Garg, S. Mullick, and V. K. Bhargava, *Solar thermal energy storage*: Springer Science & Business Media, 2012.

[9] K. Pielichowska and K. Pielichowski, "Phase change materials for thermal energy storage," *Progress in materials science,* vol. 65, pp. 67-123, 2014.

[10] R. Sharma, P. Ganesan, V. Tyagi, H. Metselaar, and S. Sandaran, "Developments in organic solid–liquid phase change materials and their applications in thermal energy storage," *Energy Conversion and Management,* vol. 95, pp. 193- 228, 2015.

[11] B. Zalba, J. M. Marın, L. F. Cabeza, and H. Mehling, "Review on thermal energy storage with phase change: materials, heat transfer analysis and applications," *Applied thermal engineering,* vol. 23, pp. 251-283, 2003.

[12] A. Sharma, V. V. Tyagi, C. Chen, and D. Buddhi, "Review on thermal energy storage with phase change materials and applications," *Renewable and Sustainable energy reviews,* vol. 13, pp. 318-345, 2009.

[13] A. Joseph, M. Kabbara, D. Groulx, P. Allred, and M. A. White, "Characterization and real- time testing of phase-change materials for solar thermal energy storage," *International Journal of Energy Research,* vol. 40, pp. 61-70, 2016.

[14] S. Canbazoğlu, A. Şahinaslan, A. Ekmekyapar, Ý. G. Aksoy, and F. Akarsu, "Enhancement of solar thermal energy storage performance using sodium thiosulfate pentahydrate of a conventional solar water-heating system," *Energy and buildings,* vol. 37, pp. 235-242, 2005.

[15] H. Ke, "Phase diagrams, eutectic mass ratios and thermal energy storage properties of multiple fatty acid eutectics as novel solid-liquid phase change materials for storage and retrieval of thermal energy," *Applied Thermal Engineering,* vol. 113, pp. 1319-1331, 2017.

[16] R. Sharma, P. Ganesan, and V. Tyagi, "Long-term thermal and chemical reliability study of different organic phase change materials for thermal energy storage applications," *Journal of Thermal Analysis and Calorimetry,* vol. 124, pp. 1357-1366, 2016.

[17] A. Al Robaidi, "Development of novel polymer phase change material for heat storage application," *Int J Mater Sci Appl,* vol. 2, pp. 168-172, 2013.

Analysis of Dual Booster Mirrors Box Type Solar Cooker Integrated With Thermal Storage

MUHAMMAD FAROOQ SIDDIQUE [A,*], KHURSHID AHMAD [A], MUHAMMAD ARIF KHATTAK [A]

Ihsan Ur Rahman [A] and Hurmat Khan [A]

[A] = US-Pakistan Center for Advanced Studies in Energy (USPCAS-E), University of Engineering and Technology (UET) Peshawar, Pakistan

[A,*] Email: farooqsiddique.mech@gmail.com

Abstract— **Domestic sector is one of the major consumers of energy in many countries. Among the various household energy consumers, cooking and baking consumes significant energy. Use of solar energy for cooking is an interesting approach that has been widely studied. In this research, the effect of use of heat storage material on the cooking capacity was studied under various design conditions. Oxalic acid di-hydrated was used as a heat storage material. The performance parameters like first and second number of figures, cooking power, exergy input and output, exergy efficiency and quality factor were analyzed. The results showed a significant improvement in these parameters and increase in the cooking capacity and availability of the cooker.**

Keywords—**, Aspect ratio of solar cookers, Box type solar cookers, Solar box cooker, Tracking free conditions, Storage material (PCM)**

I. INTRODUCTION

The rapid depletion of Conventional Energy Resources and the alarming environmental Problems arising because of the use of those resources are igniting the needs to dig for alternate greener technologies that can ensure sustainable development and environmental preservation. Cooking is one such activity that is responsible for around 33% of total energy consumption in many countries[1]. Developing countries (DCs) are mainly dependent on traditional biomass and open fire stoves to meet their cooking needs because of lack of access to clean and modern cooking facilities. However, by incomplete combustion of solid fuels, flue gases are produced causes more than 4 million deaths each year especially among children and women, due to certain diseases like lung cancer and pneumonia etc.[2]. Moreover, the due to large use of biomass for cooking enhances rate of deforestations and all related soil degradation in many DCs. Diverting attentions to renewable energy resources at local level through suitable designs of energy technologies are considered as sustainable solutions [3].Solar energy is, among other sources, a potential substitute of wood in a large portion of the DCs: For Solar energy exploitation, Solar Cooker is considered as one of the best possible option. Until now different types of solar cookers have been developed. However they can be broadly classified into three different categories [4]i.e.

1) Indirect type
2) Concentrator type
3) Box type

Our main concern of the research topic is the Box type solar cookers. The box type solar cookers are further subdivided into two categories which are Box type solar cookers with mirrors and Box type solar cookers without mirrors. The number of mirrors used in box type solar cookers could range from one to four mirrors [5].Among the above mentioned types of Solar Cookers, the most popular and well known solar cookers are the box type owing to its ease of manufacture and lower cost [6].The box type solar cooker operates on the principle of greenhouse effect and thus it harnesses the diffused component of solar radiation. The simple box type solar cooker can reach a maximum temperature of 120°C. Thus water based cooking was possible with box type solar cookers [6].The addition of the booster mirrors is a design improvement that makes the solar cooker able to utilize the direct radiation as well and thus making it a viable option for water and oil based solar cooking. The two booster mirrors are oriented at an optimal angle that varies for a specific day of the year and thus making sure that most of the direct radiations falling on the booster mirrors in utilized to serve the cooking job. The use of the box type solar cooker with booster mirrors is so far tested for water based cooking and there is a room to improve it with using appropriate storage material, not only to increase cooking duration but making it possible to have effective use i-e use only whenever required when there is no solar energy directly available. Different storage materials have been used in different researches, the one preferred here is Oxalic acid di-hydrated[7]. The whole setup is shown in Fig. 1.
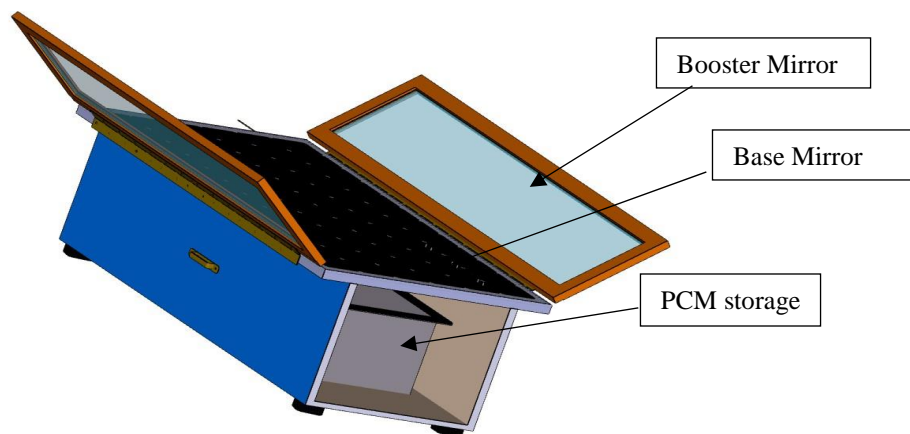
Fig.1. CAD model of solar cooker with PCM

II. METHODOLOGY

The experimental work of the research was performed at 33.9893° N, 71.4356° E location (US- Pakistan Centre for Advance Studies in Energy, Peshawar KPK Pakistan). The booster mirrors of the said solar cooker had the length of 120cm, a width of 45 cm and a height of 30 cm. The aperture area of the cooker was calculated to be $0.44 m^2$. The absorber plate of the cooker was painted matt black to have maximize the absorptivity. In between the wooden box and the absorber plate cotton was filled for insulation. The cooker was placed at the rooftop of the building. Both the booster mirrors were inclined at their specific optimized angles calculated by the computer simulations. The primary booster mirror B-1 and the secondary booster mirror B-2 faced south and north respectively. Wooden protractors were fixed to the cooker to help incline the booster mirrors at their optimal angles. Oxalic acid di-hydrated is used as PCM and is placed inside the box of the said type cooker. To increase the absorptivity, the cooking vessels used for experimentation were also painted black with non-reflective (Matt black) paint from the outside. The cooking vessels were covered with lids which were also painted Matt Black on the outer surface. To make the solar cooker airtight a rubber strip was fixed, on which the top lid of the cooker would rest when the cooker was closed. The top glazing had two transparent plain glass sheets with a separation of 2 mm in between them. Based on the $0.44 m^2$ aperture area, the total load of the cooker was calculated to be 3200 gm. For standard performance calculations a total of four experiments were conducted.

A total of four standard tests were conducted on different days. The first test was conducted under un-loaded conditions and the rest three were conducted under fully loaded conditions. It was confirmed that the booster

mirrors are oriented at optimal angles calculated for specific days. The first unloaded test was carried out on 7th May, 2020. For the unloaded conditions two temperatures were noted i.e. the cooker base temperature and the ambient temperature. The experiment was continued until the base of the cooker reached the maximum temperature, i.e. the stagnation temperature. The stagnation temperature stayed the same for about 30 minutes. After experiencing no change in the stagnation temperature for about thirty minutes. It was observed that the maximum (stagnation) temperature achieved by the solar cooker under unloaded conditions for the particular solar radiation intensity. After the stagnation test, three more experiments were conducted under fully loaded conditions with 3200 gm of water evenly filled in three vessels. The first, second and third test under fully loaded conditions were carried out on 14th, 20th, and 21st May respectively. During all the four tests, the booster mirrors were inclined at their optimal angles for the respective days. For the fully loaded conditions, temperature was measured for two containers i.e. the middle one and one on the side. The solar irradiance, cooker base temperature and ambient temperature were measured during all the three experiments. It was noted that the middle container reach the boiling point earlier than the other containers as it is receiving thermal energy from either side as well as directly.

III. RESULTS AND DISCUSSIONS

To calculate the results of the said solar cooker, different experiments are performed. In the start, the solar cooker is loaded with tap water and all the values are calculated. Then two sets of experiments on solar cooker were conducted. The first one was without thermal storage and readings were carried out for 6 hrs. i-e from 9 am to 3 pm. This set comprises the following stated experiments;

1) Unloaded without PCM
2) Loaded without PCM

The second set of experiments was conducted with thermal storage (PCM) and that too in the following stated experiments;

1) Unloaded with PCM
2) Three set of loaded experiments with PCM. These experiments are named as A, B and C. Mean values are calculated to get appropriate result.

In the end, separate two experiments are done for cooking of different food items and their time and level of cooking are noted. The whole set of experiments and there are results are shown.

Before starting experiment, optimal values of required angles of both mirrors are calculated by running the program of MATLAB. The value of N (number of day starting from January 01) is inserted after defining the location for the given programing. The mirrors are tilted accordingly. The our location of research experiment, the values found by the computer simulation for the mirrors as optimum angles are given;
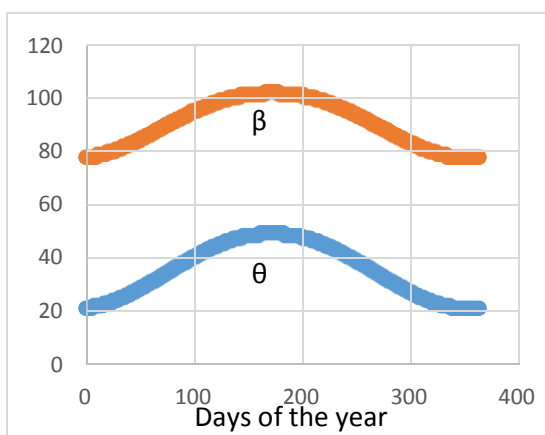
Fig. 1. Plot of the optimum angles of the mirrors for any day of the year from 9:00 to 15:00 (β for Booster mirrors B-1 curve and θ for booster mirror B-2 bottom curve)[8]
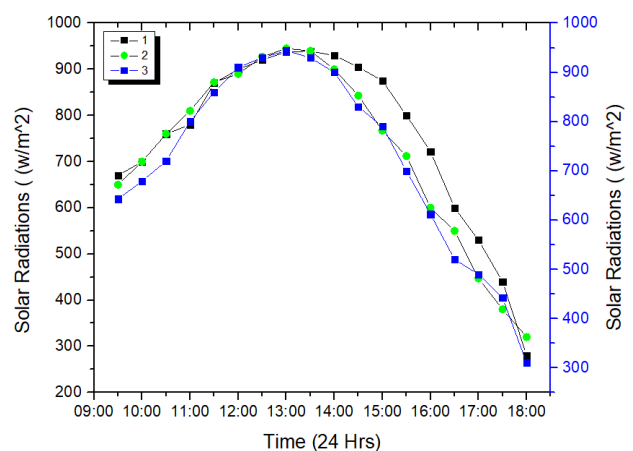
Fig.2. Solar radiations intensity vs time plot
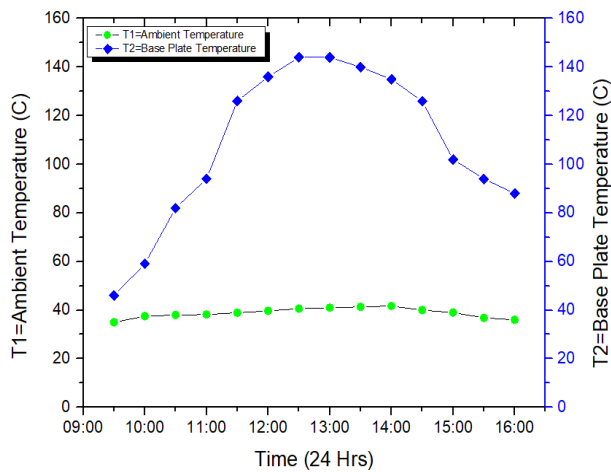
Fig.3. Temperature and time plot for the unloaded condition
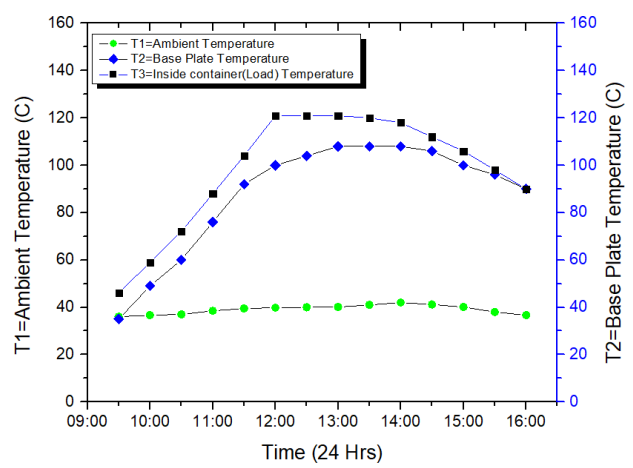
Fig. 4. Temperature and time plot for 1st test under loaded conditions
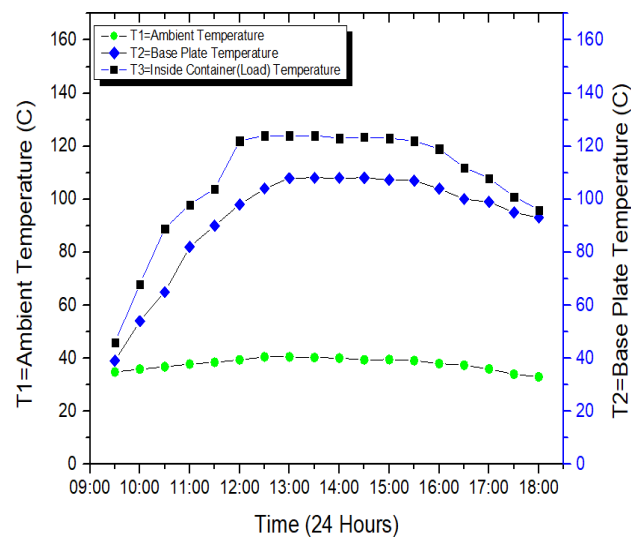
Fig. 5. Temperature and time plot for mean of the 3 tests under loaded conditions with PCM

TABLE **1**: CALCULATION OF THE FIRST FIGURE OF MERIT (F_1)

T_b (°C)	T_{amb} (°C)	H_s (W/m²)	F_1
142	35	918	0.120

TABLE 4.1: CALCULATION OF THE SECOND FIGURE OF MERIT F_2 AND THE COOKING POWER

Exp. No	Aperture Area(m^2)	T_{wi} (°C)	T_{wf} (°C)	T_{av} (°C)	H_{av} (W/m^2)	Duration (seconds)	(M.C) (j/k)	F_2
1	0.44	33	100	37.5	911	14200	13440	0.2276
2	0.44	35	100	38	902	14200	13440	0.2242
3	0.44	35	100	37.8	919	14200	13440	0.2241
							Average	0.2243

TABLE 4.2: CALCULATION OF THE COEFFICIENT OF OVERALL HEAT LOSS

IV. CONCLUSION

This paper reports the effective use of solar energy in cooker is main objective of the research. The performance parameters of the Box type cooker evaluated under tracking free conditions are satisfactory and suggest that the angular optimization technique is an excellent replacement for the labor involved in adjusting the solar cooker after every 15-30 minutes. The maximum time required to cook a dish is 2.5 to 3 hours, which implies that the same cooker can be used for cooking twice a day, making it possible to cook 6.4 kg of six different dishes in one day with no need for continuous attention thus making the cooking activity easy and less time consuming. With the thermal storage, it is experienced to cook till 6 PM and can keep it warm till 7 PM within the cooker. Hence, an extra cooking was made possible with the storage (PCM), making it possible to cook 9.6 kg of different dishes in a single sunny day. The value of F_1 calculated for the box type dual booster mirror solar cooker is in the range of the optimum values for F_1 and the cooker is a "Grade-A Solar Box Cooker" based on its calculated value of F_1. The value of F_2 is found to be 0.23. The overall heat loss co-efficient is the average of the heat loss co-efficient for all the three experiments conducted under fully loaded conditions. The overall heat loss co-efficient for the cooker is 0.54 W/K.m^2. The quality factor is the average of the quality factor for all the three loaded experiments which is found to be 0.04. The peak exergy power of the cooker is found to be 15.01 watts. All the values of the performance parameters are in a close proximity with the suggested values of these performance indicators.

The presence of thermal storage (PCM) enhances its importance by adding more time to cook food i-e the solar cooker gets potential of cooking food in three phases. In general as evident from the experimental data, the cooking takes 3 hrs. to cook the food properly, with enhancing the time up to 6 PM in sunny days, the solar cooker can cook 9 dishes in three phases.

V. REFERENCES

1. Muthusivagami, R., R. Velraj, and R. Sethumadhavan, *Solar cookers with and without thermal storage—a review.* Renewable and Sustainable Energy Reviews, 2010. **14**(2): p. 691-701.

2. Wentzel, M. and A. Pouris, *The development impact of solar cookers: a review of solar cooking impact research in South Africa.* Energy policy, 2007. **35**(3): p. 1909-1919.

3. Otte, P.P., *Solar cookers in developing countries—What is their key to success?* Energy Policy, 2013. **63**: p. 375-381.

4. Cuce, E. and P.M. Cuce, *A comprehensive review on solar cookers.* Applied Energy, 2013. **102**: p. 1399-1421.

5. Farooqui, S.Z., *A gravity based tracking system for box type solar cookers.* Solar Energy, 2013. **92**: p. 62-68.

6. Saxena, A., S. Pandey, and G. Srivastav, *A thermodynamic review on solar box type cookers.* Renewable and Sustainable Energy Reviews, 2011. **15**(6): p. 3301-3318.

7. Vigneswaran, V., et al. *Performance evaluation of solar box cooker assisted with latent heat energy storage system for cooking application.* in *IOP Conference Series: Earth and Environmental Science.* 2017. IOP Publishing.

8. Nkhonjera, L., et al., *A review of thermal energy storage designs, heat storage materials and cooking performance of solar cookers with heat storage.* Renewable and Sustainable Energy Reviews, 2017. **75**: p. 157-167.

Smart Monitoring of the Solar Energy Power

Dr. Arif Khattak [A], and Naveed Ullah [B]

[A] Department of Renewable Energy, USPCAS-E, UET Peshawar, KPK

Abstract— **This research paper addresses the issues regarding the monitoring of the generated power via the smart monitoring of the PV solar arrays. Monitoring of the generated power has always been a challenging issue in solar energy technologies, many times the generation is halt but we don't get notice of it and thus we get prone to energy wastage. For this issue to be addressed, properly, this research paper presents a comprehensive approach for the monitoring of energy generated particularly and solar energy specifically. There are a couple of important parameters, which have to be monitored for checking the performance of installed PV arrays. These chosen parameters are solely based on the objectives of that specific research, but in our case, for the monitoring of the system, the selected parameters are temperature and shadow the effect, irradiance, and power. Different sensors have been used, like LM335, GO2Y1010AUOP, an LDR Sensor, voltage, and ACS712. These have been fixed on the installed system, after getting their real-time data, and transferring to the cloud: thingSpeak web-server with the help of the ESP8266 module. Their performance can be monitored via the ThingSpeak android Application on the cell phone. Their results show that if we nicely monitor the shadow effect only, after its removal it increases the generated power by 20-30%. Likewise, when we monitor the temperature effect, after reducing the temperature effect augments the power generation by 3-5% further. It's also shown that by monitoring the irradiance, which can be removed via changing the orientation of the panels here comes further increase ranging from 20-30%, to sum up, we can easily say that this smart monitoring: monitoring via an android application, helps in getting the real-time monitoring, which helps in resolving the issues at the required time and thus helps in generating the power more efficiently than normal.**

Keywords— **ACS712: Sensor uses for measuring the current, GO2Y1010AUOP: Sensor used for measuring the Irradiance, LM335: Temperature sensor, ThingSpeak: Web-server uses for saving data in the cloud.**

I. INTRODUCTION

The demands of energy across the globe are increasing dramatically owing to continuous expansion in industries, uncontrolled population growth, and per capita continuous increase. It's worth notable that the major consumption is in the form of electrical energy. There are a couple of energy harvesting techniques that are suitable but they accompany some environmental issues which make them not some preferable choices. These things made the gap between supply and demand the worst, and is expected to go more awry than the recent one down the road. Renewable energy resources can play a positive role in coping the supply with the demand in the future. In this regard, Renewable energy resources: Solar, biomass, Wind, Micro-Hydro, geothermal and nuclear, are converted into Electrical energies and feed into the demand sector or grid stations [1]-[4]. The other sole factor behind rushing towards Renewable energies are the clean environment and energy. Countries in tropical regions are considered to be the most proficient for solar energy harvesting than otherwise renewable energy resources [5]. In the past few decades, Photovoltaic (PV) technologies developed more than expected owing to the investment by the governments and other private bodies to expedite the generation of electrical energy production using PV technologies. This whole effort tipped the overall energy production of PV technologies from 103MW in 1992 to a total of 139795.2MW in the year 2014, this whole data is based on International Energy Agency-photovoltaic Power Systems Program (IEA-PVPS) [6].

Other than this, Industrialists and the urban population are taking a keen interest in using PV technologies for their electricity production, this will make PV technologies reign over the deficiencies of energy demands or gaps, and a dramatic rise in its usage is expected in the following years. To be the usage and implementation in the verge it's quite important to have a design which may keep track of the energy production and keep its production up in every possible aspect. The sole factor for smart monitoring is to predict the faults which can ruin the PV production under a specific irradiance [7]. The issues, which need to be tackle are for getting the specified and desired response are avoiding shadow effect, temperature effect, etc. according to a paper 10-20% loss occurs due to shadow effect annually [8]. There is some other inevitable and production sort of losses, which solely depends on the meteorological data, affecting

the PV energy production, of the area where the Photovoltaic system is installed [9]. Thus, it's mandatory to have a paradigm, which can address the issues altogether and figure out the ones hampering the desired response [10]. A competent solution for all the said issues is termed as a "Smart monitoring System", which can boost the performance with minimal cost. Monitoring System provides information about energy production, extraction, and different faults to be detected. This system can also be used for future predictions. There is a huge interest shown by the researchers in this field for developing a comprehensive monitoring system for small, medium, and large enterprises. There are a couple of models in the market, their selection mostly happens based on the climate conditions of that specific area.

II. METHODOLOGY

In this proposed method the system is always monitored. It detects the errors via selected parameters when these parameters undergo some changes. It shows and makes the user informed and speculated about certain errors and reasons, the user after implementing that gets the system flawless and thus augments the ratio of the generated power.

The diagram shown below depicts that the generated power of the solar panels is checked with the help of two sensors, which are the current sensor and the voltage sensor, their values are then fed to the microcontroller or Arduino here. There are a couple of sensors, too, fed to the micro-controller it then processes the information and then forwards them up to the cloud with the help of the ESP8266 module which can then be accessed via smartphone or laptop/PC anywhere.
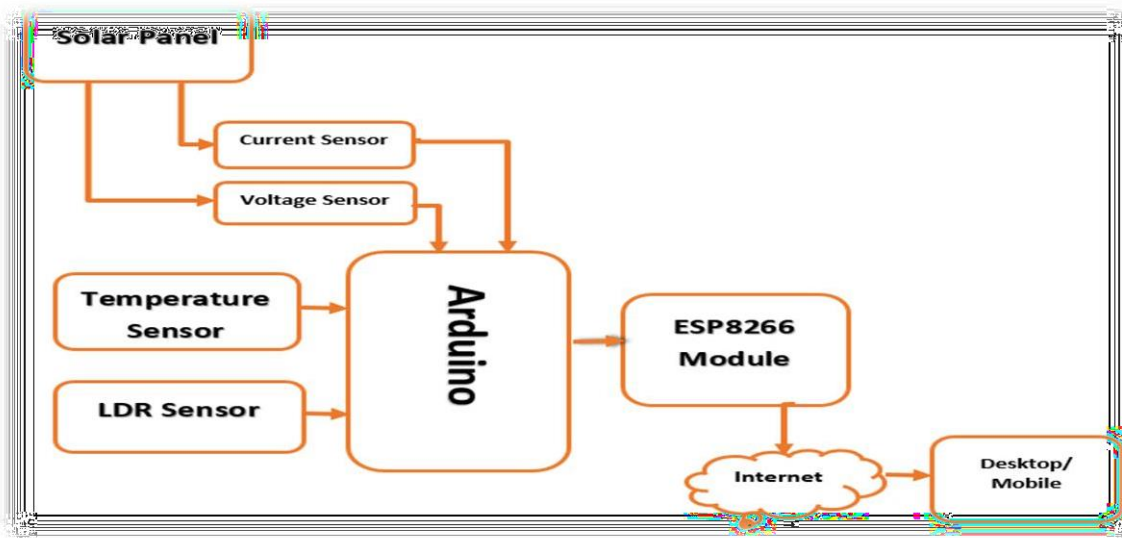
The following sensors are used in the research paper and used for doing the experiments and the results.
1. Current Sensor
2. Voltage Sensor
3. Temperature Sensor
4. LDR Sensor
5. Dust Sensor

III. RESULTS AND DISCUSSION

Based on the adopted approach, here are a couple of results, which are parts of the project to monitor them up as good as possible. These graphs are based on metrological and other operational parameters selected at the start. Here are the results of the monitoring of the solar PV system. These results are explained below.

A. CURRENT GRAPH

The graph of the current sensor identifies the real-time values of the current of the PV based solar system. This is a real-time graph, in a ThingSpeak webserver. The Y-axis shows the values of the current that generates from the solar panel. It shows the values current comes from the solar panel in Amperes in centimeters (cA) and the X-axis shows the time in which these values have been recorded. This current has relations with different parameters like light intensity, it varies and changes drastically in variation with the intensity of light. The shadow over the panels affects this current as well. This current has maximum value according to the panel(s) selected.

The current here according to our scenario, the trend is dependent upon a couple of parameters like, temperature, shadow effect, soiling effect, humidity, and the hovering clouds. Here is the effect overcurrent of those erstwhile parameters in a bit of detail.

The current increases with the decrease in temperature of the solar panel, also as a reverse relation with the shadow effect and soiling effect. In case of humidity, it indirectly affects the current, humidity affects the radiation over the panel, which further affects the current generation of the solar panel. Here below is the graph, which shows everything that came from the real-time monitoring of the solar panel(s).
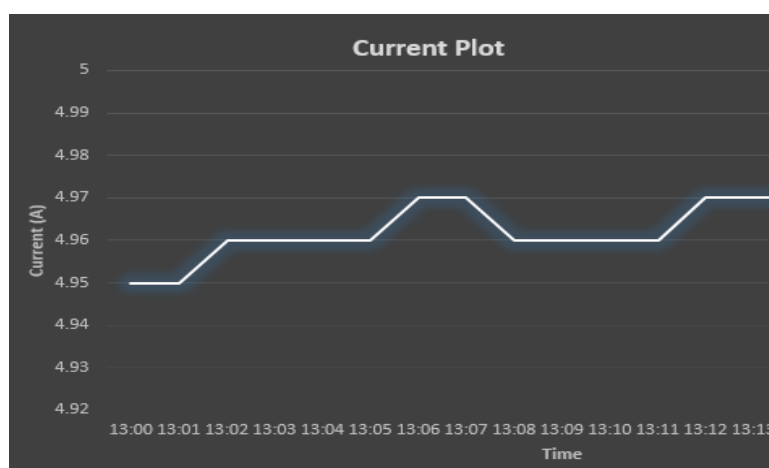
Fig 2 The real-time current graph
drawn over ThingSpeak

B. Voltage Graph

The voltage graph is the data of the voltage comes from the solar panel (s), this tells about the production of the installed system, whether that is a full setup of panels or a single panel. The voltage values much tell about the performance of the system. Voltage is much dependent upon the countless as erstwhile mentioned for the current, which are the temperature, shadow effect, the soiling effect, the weathering effect like clouding humidity, etc. Voltage has been found directly linked with the parameters mentioned above.

The trend can't be easily described through those said parameters. The trend of voltage with time is dependent on many parameters, but the graph often remains constant if there is no disturbance like there is mentioned in the above about shadow, soiling, etc. This feature helps in monitoring better performance, etc., like if there comes an issue in a sense of monitoring this voltage graph, and thus the linearity will vanish with time. This will be a clue that something has happened thus the better performance has not been achieved. The graph is drawn for the best can and exemplifies the ideal case, where there will be some issues regarding the performance, which will jeopardize its shape. Here is the graph below in the figure, which had been explained earlier.
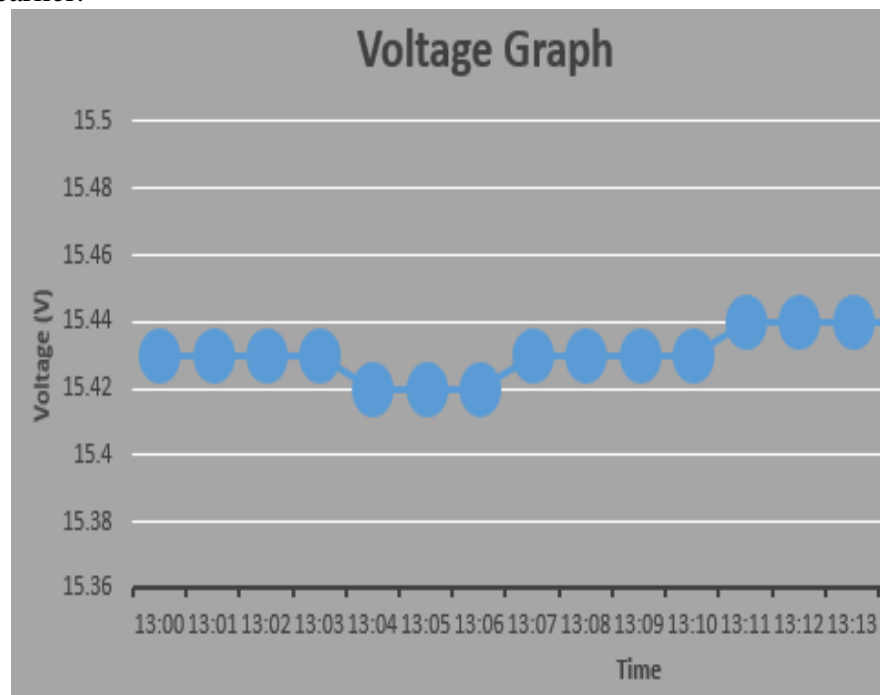
Fig 3 Voltage curve of real-time data of solar panel.

C. POWER GRAPH

The power graph shows the performance of the solar panel, here it depicts the performance based on the environment of solar panels. As power is the product of the generated current and voltage of the solar panel. The greater the power means either the current is drawn more, means the solar panel is connected to the full load of the voltage is high, which depicts that the solar panel is getting the best intensity of the light or both the current and voltage are in average which means that the load and the intensity of the sun are average.

The trend in the graphs explains different scenarios, in this case, it's most important to know whether the season is winter or summer. In the former case, the efficiency at the noontime will be better than in the latter case. The reason is owing to the effect of the temperature on the solar panels. While in the case of summer the power generation of the panels in the evening and the mooring will be much better than the power generation of the same panel in the winter.

This graph has taken for less duration, that's why there aren't things encountered wholly, these graphs are roughly linear. Here it shows that the power generated is almost constant, while variation can be seen via variation in load and the intensity of light or creating the shadow over the panel. Here in the graph, the values of the generated power are drawn over the Y-axis, which shows the actual power, while over the X-axis time/date, etc. has drawn, which shows the variation of the power over time. Here these erstwhile things are shown in the graph below.
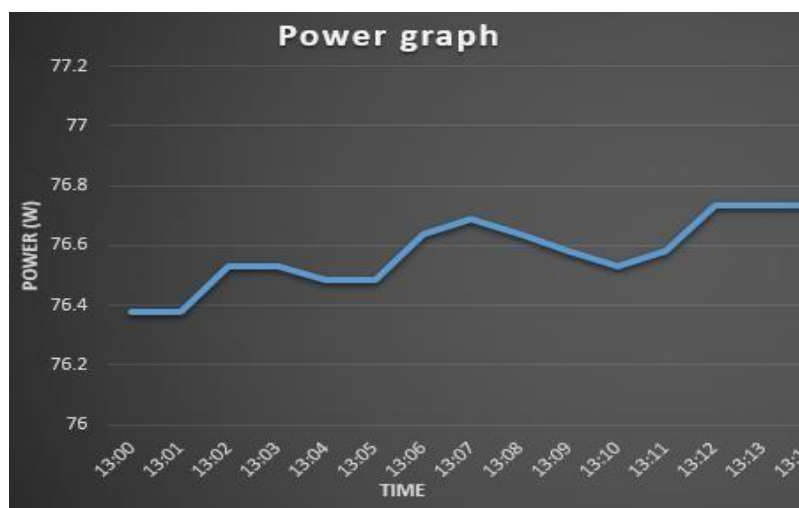
Fig. 4 The real-time graph of Power over ThingSpeak

IV. CONCLUSION

This paper proposes a concise and comprehensive approach for monitoring the solar system and sheds light on a different aspect of smart monitoring. The sensors discussed in the paper are the basics ones, which are temperature, current, voltage, and solar irradiation sensors. The reason for selecting only these sensors is that these are almost prerequisites to every monitoring.

This approach takes the real-time data, feeds it to the could due to an interfacing module, and then makes it accessible all over. The graphs are shown based on real-time data. For future recommendation, this can be assembled into a single unit having all in one assembly with a good packing for commercializing it.

REFERENCES

[1] Canale M, FagianoI, Milanese M.Kite Gen. Are volution in wind energy generation. Energy 2009; 34: 355–61.

[2] Kalogirou SA.The potential of solar industrial process heat applications. ApplEnergy 2003; 76:337–61.

[3]Tien W, KuoK-C. An analysis of power generation from municipal solid waste(MSW) incineration plants in Taiwan. Energy 2010; 35:4824–30.

[4] Mercure J-F, Salas P. An assessment of global energy resource economic potential. Energy2012; 46:322–36.

[5] Singh GK. Solar power generation by PV(photovoltaic) technology: are view. Energy 2013;53:1–13.

[6]IEAPVPS, International Energy Agency – Photovoltaic Power Systems Programme, 2014. Trends in photovoltaic applications. Report availableat⟨http://www.iea-pvps.org/fileadmin/dam/public/report /national /IEA-PVPS Trends_ 2014_-_MedRes.pdf⟩.

[7] Benghanem M. Low-cost management for photovoltaic system in isolated site with new IVcharacterization model proposed. Energy Convers Manag 2009; 50:748–55.

[8] Hanson AJ, Deline CA, MacAlpine SM, Stauth JT, Sullivan CR. Partial-shading assessment of photovoltaic installations via module-level monitoring. IEEE J Photovolt 2014; 4(6):1618–24.

[9] Sánchez-Pacheco FJ Sotorrio-Ruiz PJ Heredia- Larrubia JR Pérez-Hidalg oF Sidrach-de Cardona M. Low cost DC lines PLC based photovoltaic plants parameters smart monitoring communications and control module. In: Power Engineering, Energy and Electrical Drives (POWERING) International Conference on2011; pp.1–6; 2011.

[10] Davarifar M Rabhi AEL-Hajjaji A Dahmane M. Real-time model-based fault diagnosis of PV panels using statistical signal

processing. In: Renewable Energy Research and Applications (ICRERA) International Conference on 2013; pp. 599–604; 2013.

[11]Sumathi S, Kumar LA, Surekha P. Solar PV, and wind energy conversion systems: an introduction to the theory, modeling with MATLAB / SIMULINK, and the role of soft computing techniques. Switzerland: Springer International Publishing; 2015.

[12] Hansen AD Sørensen PE Hansen LH Bindner HW. Models for a stand-alone PVsystem ;2001.

[13] Bechtel Nationale. Handbook for battery energy storage in photovoltaic power systems. J Power Sources 1980; 5(4):3401. 14] Borowy BS, Salameh ZM. Methodology for optimally sizing the combination of a battery bank and PV array in a wind∕

PV hybrid system. IEEE Trans Energy Convers 1996; 11(2):367–75.

[15] ISC Committee. IEEE standard for interconnecting distributed resources with electric power systems. NewYork, NY: Institute of Electrical and Electronics Engineers; 2003.

[16]International Electrotechnical Commission. IEC 61724, photovoltaic system performance monitoring guidelines for measurement, data exchange, and analysis. 1sted. Geneva, IEC: International Electrotechnical Commission; 1998.

[17] Ziegler S, Woodward RC, Iu HH, Borle LJ. Current sensing techniques: are-view. IEEE Sens J2009; 9(4): 35476.

[18] Spaziani L. Using copper PC Betch for low value resistance. Unit rode Design Note DN-71; 1997.

[19]Ray WF Hewson CR. High-performance Rogowski current transducers. In: Conference Record of the IEEE Industry Applications Conference; Vol.5 ,pp .3083–3090; 2000.

Technical Session 4-A (Google meet/Zoom) Computational Modelling and Mineral Processing	
Session Chair: **Dr. Thi Bang Tuyen Nguyen** Session Co-Chair: **Dr. S. Naveed ul Hasan**	
Ahmad Khan *(USPCAS-E UET Peshawar)*	Computational Fluid Dynamics of The Impact of Embedded Tubes in A Twin Chamber Fluidized Bed.
Sohail Khan *(USPCAS-E UET Peshawar)*	Numerical Simulations of condensation heat transfer of refrigerant R134a in a smooth horizontal tube.
Raza Ullah *(PIEAS Islamabad)*	Preliminary Evaluation of Bajawar Chromite Ore for Up-Gradation Purpose
Faizan Ullah *(Dept. of Mining Eng., UET Peshawar)*	Characterization of Kohistan Chromite Ore For The Selection of A Beneficiation Technique

Computational fluid dynamics of the impact of embedded tubes in a twin chamber fluidized bed

Ahmad Khan [A], Muhammad Hassan [B], Khurshid Ahmad [C], Fahad Ullah Zafar [D], Muhammad Ali Durrani [E]

[A, B, C, D, E] *=U.S.-Pakistan Center for Advanced Studies in Energy, University of Engineering and Technology, Peshawar, Pakistan*

Abstract— **A numerical simulation of twin chamber internally circulating fluidized bed reactor (ICFB) with tubes inserted in reaction chamber (RC) and then in heat exchanger chamber (HEC) was done using Eulerian-Eulerian model (EEM). The model equations are solved through ANSYS Fluent, a computational fluid dynamics (CFD) tool. A two dimensional geometry is analyzed to explore the impact of tubes on the gas and solid phases flow in the bed. As the solid particles are continuously circulating from RC to HEC above the central baffle and from HEC back to RC through the slot below baffle, so a complete understanding of solids and gas circulation behavior is necessary. Based on gas and solids flow behavior achieved through simulation, both phases circulation fluxes through the slot have been investigated. It has been seen that the inserted tubes lower the velocity of both the solids and gas phases in the middle region of the chambers but enhances it near the walls and baffle. A time averaged values of parameters like bed pressures and its difference, solids circulation flux, gas circulation flux is calculated through simulations. All the three parameters of the cases in which tubes are installed in RC and then in HEC are compared to the tubeless ICFB. It has been noted that due to hindrance created by tubes, pressure gradient between the two chambers and both phases circulation fluxes are affected.**

Keywords— **Eulerian-Eulerian model, Gas phase circulation flux, Heat exchanger chamber, Internally circulating fluidized bed, Reaction chamber, Solid phase circulation flux.**

I. INTRODUCTION

Fluidized bed technology is broadly used in several applications for instance in chemical and process industries, coal or biomass combustion and gasification and power generation etc. A phenomena of fluidization is a process in which granular particles of solid phase behave like a fluid when air or gas is blown upward over the bottom of reactor filled with solid coal particles [1]. The passage of gases or air through the solid particles in the bed causes the fluidization. A bed filled with solid particles that act like a fluid when gas or air is passed uphill over the lower section of the bed is known as Fluidized bed. A prototypical fluidized bed consists of cylinder-shaped column that comprises coal fragment and through which flow of gas or liquid phase occurs. The time a gas/air flow through the base of a bed filled with solid phase coal fragments, the voids or space between the solid particles allows the gas to move upward. The fluid like behavior occurs due to unbalancing of drag forces of individual solid particles with the gravity. Friction between the particles become so small that the integral constituents act as a fluid.

Factors that affects fluidization caliber are gas to solid ratio, arrangements of gas inlet, kind of solid particles used, fluidization vessel geometry and the size of dense phase and its distribution [2]. For bed behavior the rate upon which the gaseous or uninterrupted phase flows straight upward through the solid or particulate matter is significant. The velocity of the gaseous phase varies throughout the bed. At sufficiently low superficial gas rate, u_g which is the volumetric gas flow rate over the bed divided by bed cross-sectional area [3], the gas leaks through the porous surface or voids between particles of the bed, which is called fixed bed. However, the system changes to fluidized bed as u_g increases. The state of minimum fluidization occurs when the drag between rising gas and individual particles counterbalance the gravity. At this stage the minimum fluidization rate or velocity, u_{mf} is attained by superficial gas rate [4]. As u_g increases, the particles motion also

increases which results into two kinds of fluidization: 1) Homogeneous and 2) Heterogeneous.

Particles circulation in fluidized bed combustion systems are mainly categorized as externally circulated and internally circulated fluidized Bed. Externally Circulated Fluidized Bed (ECFB) consist of large central column as a riser and particle restoring container known as down comer or cyclone. The pipes circulation system connects two fluidized bed i.e. main column and cyclone. During fluidization, the riser particles are accumulated in cyclone and returns it back to riser. The pipes are controlled by valve and gas velocity in which the particles flow [5]. In Internally Circulated Fluidized Bed (ICFB), the solid circulation takes place in a single vessel. There are several chamber or compartments in one vessel which are divided by internal walls. The compartments are named as reaction chamber (RC) and heat exchanger chamber (HEC). The walls contain orifices through which solid particles can flow easily by applying uneven fluidizing flow rates between different compartments. The internally circulated fluidized bed system has low investment cost, reduced height, simple structure, compact size and low energy consumption and small heat loss as compared to externally fluidized bed system.

Several researchers worked on bypassing of gas and circulation rates of solid in CFB reactors. For circulation of solid particles based upon difference between density of fluidized and stirring bed in ICFB LaNauze [6] developed a model with gap-height sort of draft tube. The opening ratio as well as velocity of gas in ICFB controls the solid circulations [7]. To determine bypassing of gas and circulation of solids in an ICFB, three distinct categories of distributors of gas was used by Song, Y. Kim and S. Kim [8] and found that best circulation of solid was provided by conical plate type distributor. In an ICFB using draft tube with an orifice, the orifice diameter influence bypassing of gas commencing the annulus region to the draft tube [9]. The influence of temperature on circulation of solids and gas bypassing was examined by Namkung, Guy, Boiseelle and Legros [10]. The impact of gas velocity to draft tube as well as particle on circulation of solids was studied by Done Kim, Han Kim, Roh and H. Lee [11]. A mathematical model were established by Toyoda *et al*. [12] to predict based upon pressure stability surrounding an opening the solid mass flow rate in an ICFB. The influence of relative humidity, solid circulation rate, particle diameter and velocity of gas on rate of attrition in an ICFB was studied by Chu and Hwang [13]. To quantify the flow dynamics properties in ICFB, several models have been proposed [14]-[15]-[16]-[17].

In Industrial Fluidized Bed Combustion System there could be a bundle of in-bed or immersed tubes or pipes installed in the combustion chamber carrying water or other chemicals to increase the amount of mass or heat transfer and also chemical transformation method. These tubes decrease the rise velocity of the bubbles due to which good mixing of the mixture, homogeneous distribution and smooth fluidization of the particles occur. It also greatly affects the hydrodynamics of the bed, the gas movement shape over the bed and dispersal of air bubbles inside the bed [18]-[19]. Which subsequently affects the total mixing of solid particles and as a result the chemical conversion process and heat transfer rates. In order to set a proper tube arrangement in the bed and study its impact on gas-solid hydro dynamic in fluidized bed is a challenging task. The Computational fluid dynamics can prove a good mean to carry out such analysis.

The core aim of this study is to examine the hydrodynamics of twin chamber fluidized with in-bed pipes or tubes and their arrangements, in order to advance the performance of the bed flow dynamics and rate of heat transfer. Such improvements can enhance proper chemical reactions, dryness, rate of heat transfer, mass transfer rate also combustion efficiency. The emphasis is to explore the bed tube geometry and arrangement, particle size, bubble shape and size and rise velocity.

II. METHODOLOGY

A. Mathematical modeling using Eulerian-Eulerian model

The Eulerian-Eulerian model also notorious as Two Fluid model (TFM) solves separate mass and momentum conservation equations for all phases and treats both phases as continuous and interacting media. Some appropriate interaction terms between the phases are also solved during simulations. These conservation equations are generalized form of Navier-Stokes equations that define the mean position and velocity of the gas and solid phase system.

The hydrodynamic modeling of fluidized bed with multiphase gas and solid flow practice the laws of mass and momentum conservations. Anderson and Jackson [20] uses the averaging techniques and Ding and Gidaspow [21]-[22] describes KTGF to derives governing equations. Detail description of these governing equations are given in the above references. Our model includes separate continuity and momentum equations for all phase of two phase flow.

The equations of continuity for both phases of solid and gas without any transfer of mass are given as:

$$\frac{\partial(\alpha_g \rho_g)}{\partial t} + \nabla.(\alpha_g \rho_g \boldsymbol{u_g}) = 0 \tag{1}$$

$$\frac{\partial(\alpha_s \rho_s)}{\partial t} + \nabla.(\alpha_s \rho_s \boldsymbol{u_s}) = 0 \tag{2}$$

The conservation of momentum equations for both phases of solid and gas are related as:

$$\frac{\partial(\alpha_g \rho_g)}{\partial t} + \nabla.(\alpha_g \rho_g \boldsymbol{u_g u_g}) = \nabla.\bar{\bar{\tau}}_g - \alpha_g \nabla P - \beta(u_g - u_s) + \alpha_g \rho_g g \tag{3}$$

$$\frac{\partial(\alpha_s \rho_s)}{\partial t} + \nabla.(\alpha_s \rho_s \boldsymbol{u_s u_s}) = \nabla.\bar{\bar{\tau}}_s - \alpha_s \nabla P - \nabla P_s + \beta(u_s - u_g) + \alpha_s \rho_s g \tag{4}$$

The transfer coefficient of interphase momentum relation by Wen and Yu [23] is:

$$\beta = \frac{3}{4} C_d \frac{\alpha_g(1-\alpha_g)}{d_p} \rho_g |u_g - u_s| \alpha_g^{-2.65} \tag{5}$$

Where

$$C_d = \begin{cases} \dfrac{24}{\alpha_g \operatorname{Re}_p}\left[1+0.15(\alpha_g \operatorname{Re}_p)^{0.687}\right] & \operatorname{Re}_p \leq 1000 \text{ and } \operatorname{Re}_p = \dfrac{\rho_g |u_g - u_s| d_p}{\mu_g} \\ 0.44 & \operatorname{Re}_p > 1000 \end{cases} \tag{6}$$

Gidaspow [22] relation for β is:

$$\beta = 150 \frac{(1-\alpha_g)^2}{\alpha_g} \frac{\mu_g}{(d_p)^2} + 1.75(1-\alpha_g)\frac{\rho_g}{d_p}|u_g - u_s| \qquad \alpha_g < 0.8 \tag{7}$$

$$\beta = \frac{3}{4} C_d \frac{\alpha_g(1-\alpha_g)}{d_p} \rho_g |u_g - u_s| \alpha_g^{-2.65} \qquad \alpha_g \geq 0.8 \tag{8}$$

Syamlal and O'Brien [24] relation for β is:

$$\beta = \frac{3}{4} C_d \frac{\alpha_g(1-\alpha_g)}{u_t^2 d_p} \rho_g |u_g - u_s| \tag{9}$$

Where,

$$C_d = \left(0.63 + \frac{4.8}{\sqrt{\text{Re}_p \big/ u_t}} \right)^2 \tag{10}$$

$$u_t = 0.5 \left(A - 0.06\,\text{Re}_p + \sqrt{(0.06\,\text{Re}_p)^2 + 0.12\,\text{Re}_p(2B-A) + A^2} \right) \tag{11}$$

$$A = \alpha_g^{4.14}, B = 0.8\alpha_g^{1.28}, \qquad \alpha_g \le 0.85 \tag{12}$$

$$A = \alpha_g^{4.14}, B = \alpha_g^{2.65}, \qquad \alpha_g > 0.85 \tag{13}$$

According to KTGF, the granular temperature relation which defines the gradient of particle velocity fluctuations is calculated by:

$$\frac{3}{2}\left(\frac{\partial \alpha_s \rho_s \Theta}{\partial t} + \nabla.(\alpha_s \rho_s \Theta u_s) \right) = \left(-P_s \overline{\overline{I}} + \overline{\overline{\tau}}_S \right) : \nabla u_s - \nabla.q - \gamma_s + J_s \tag{14}$$

Where,

$$\Theta = \frac{1}{3} u'^2 \text{ and } q = k\nabla\Theta \tag{15}$$

$$k = k_{dilute} + k_{dense} \tag{16}$$

The gas phase stress tensor using Newton law of viscosity stress-strain relation is given by:

$$\overline{\overline{\tau}}_g = -\alpha_g \left[(\xi_g - \frac{2}{3}\mu_g)(\nabla.u_g)\overline{\overline{I}} + \mu_g(\nabla u_g + (\nabla u_g)^T) \right] \tag{17}$$

As the solid phase is behaving like fluid, so the solid phase stress tensor can also be derived using Newton law of viscosity and is given by:

$$\overline{\overline{\tau}}_s = -\alpha_s \left[(\xi_s - \frac{2}{3}\mu_s)(\nabla.u_s)\overline{\overline{I}} + \mu_s(\nabla u_s + (\nabla u_s)^T) \right] \tag{18}$$

Solid bulk viscosity [25] is specified by:

$$\xi_s = \frac{4}{3}\alpha_s \rho_s d_p g_0 (1+e)\sqrt{\Theta\big/\pi} \tag{19}$$

Solid shear viscosity is given by:

$$\mu_{s,KTGF} = \mu_{s,collision} + \mu_{s,frictional} + \mu_{s,kinetic} \tag{20}$$

Where,

$$\mu_{s,collision} = \frac{4}{5}\alpha_s \rho_s d_p g_0 (1+e)\sqrt{\Theta\big/\pi} \tag{21}$$

$$\mu_{s,frictional} = \frac{P_{s,frictional}\sin\varphi}{2\sqrt{I_{2D}}} \tag{22}$$

$$\mu_{s,kinetic} = \frac{1}{15}\sqrt{\pi\Theta}\frac{\rho_s d_p g_0 \alpha_s^2 (1+e)(3/2e-1/2)}{(3/2-1/2e)} + \frac{1}{12}\sqrt{\pi\Theta}\frac{\rho_s d_p \alpha_s}{(3/2-1/2e)} \tag{23}$$

Radial distribution function [26]:

$$g_0 = \left[1 - \sqrt[3]{\frac{\alpha_s}{\alpha_{s,max}}} \right]^{-1} \tag{24}$$

Frictional shear viscosity [27]:

$$\mu_{s,f} = \frac{P_s \sin \vartheta}{2\sqrt{\overline{\overline{I}}_{2D}}}$$ (25)

Frictional solid pressure [28]:

$$P_{s,f} = F_r \frac{(\alpha_s - \alpha_{s,\min})^n}{(\alpha_{s,\max} - \alpha_s)^p}$$ (26)

The circulation fluxes of solid and gas phases are calculated as:

$$SCF = \rho_s \alpha_s u_s$$ (27)

$$GCF = \rho_g \alpha_g u_g$$ (28)
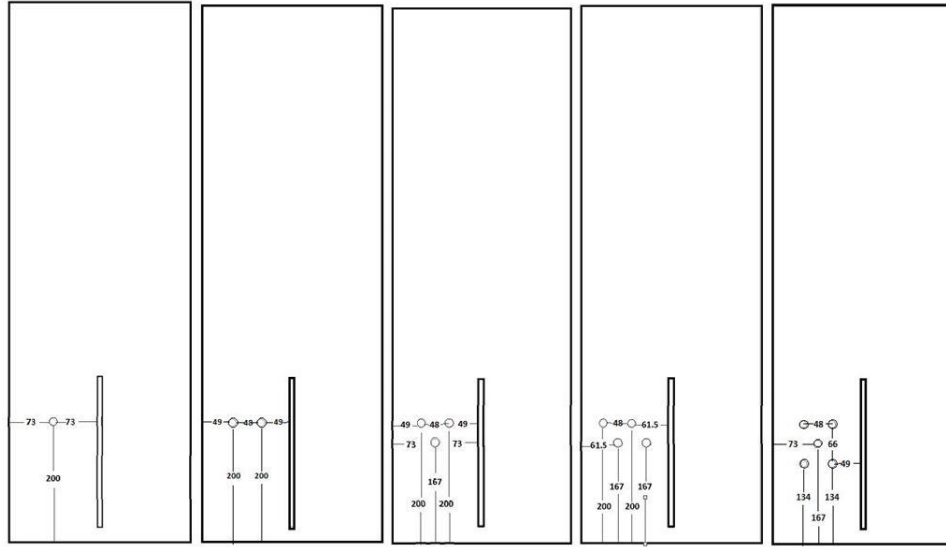
Fig. 11: Graphic design of twin chamber ICFB with different tubes configuration and arrangement.

B. Geometry description

In our study to investigate internally circulated fluidized bed (ICFB), the structural layout are based upon the work of Feng *et al*. [29] with modifications to include tubes in it. The geometry represents part of Fluidized bed reactor which has two interconnected chambers namely reaction chamber (RC) and heat exchanger chamber (HEC). The 2D geometry are created in ANSYS Design Modeler in order to reduce the computational effort. The ICFB has length of 900 mm and width of 300 mm. The baffle in the center between RC and HEC has length 250 mm and width 8 mm and also there is a slot of length 25 mm below the baffle which enables the solids coming back from HEC to RC. To see impact of tubes on the gas and solid phase flow dynamics in the bed, tubes have been added first in RC and then in HEC. Initially there is only one tube in RC and then it is incremented up to five tubes. The geometry design and arrangements of tubes in both RC and HEC is same, but for tubes in HEC only the inlet velocities condition are reversed. The diameter of all the tubes is taken as 12.7 mm. Schematic diagram of ICFB with tubes in left hand chamber (RC) is presented in **Fig. 1**.

C. Grid size

In numerical simulation grid sensitivity analysis play an important role to check the effect of grid size on the outcomes. In order for grid to be independent a common rule for gas and solid flow system is that the mesh size ought to be about ten times the diameter of particle. The grid sensitivity analysis has been done in the literature [30] for three different grid sizes termed as coarse (4 mm × 4 mm), medium (3 mm × 3 mm) and fine (2.5 mm × 2.5 mm) in which there is a little difference in simulation results when medium and fine sized grid strategy is applied. Also the results turn

out to be grid independent when the mesh size are 3 mm × 3 mm or finer. So following the grid sensitivity analysis of this literature, medium sized (3 mm × 3 mm) uniform quadratic mesh strategy is applied for all geometries in our work to save the computational cost.

D. Initial and boundary conditions

The simulation conditions, gas and solid phase properties are abridged in **Table I**. At inlet the gaseous phase is uniformly applied at the base of ICFB through two distributors namely u_r and u_h, both the inlet velocities are constant and specified. The solid volume fraction at the inlet is zero i.e. there is no solid phase flow at the inlet. There is a single outlet of both chambers with boundary condition as atmospheric pressure set for the mixture phase. For solid phase in multiphase flow no-slip, free-slip and partial-slip are wall boundary conditions that can be applied. For gas phase with very dilute flows the no-slip boundary conditions is used at the walls [31]. At the wall no-slip condition can also be assumed for the solid phase when there is a little impact on bed hydrodynamics. But when the mesh is fine the effects of wall boundary conditions

Table XIV: Simulation conditions, gas and solid properties [29]

RC inlet velocity, u_r	0.24 [m/s]	HEX inlet velocity, u_h	0.12 [m/s]
Density of solid, ρ_s	2760 [kg/m^3]	Density of gas, ρ_g	0.585 [kg/m^3]
Viscosity of gas, μ_g	5.12×10^{-5} [Pa.s]	Solid particle diameter, d_p	0.0003 [m]
Initial volume fraction of solid, α_s	0.60	Maximum limit of solid phase packing, $\alpha_{s,max}$	0.62
Initial solid packing height	275 [mm]	Specularity coefficient,	0.05
Restitution coefficient, e	0.9	Minimum fluidization velocity, u_{mf}	0.028 [m/s]

are visible near the walls. Johnson and Jackson [32] introduces a model for solid phase which takes partial-slip wall boundary conditions. In this model 'specularity coefficient' is defined for wall frictional effects. Specularity coefficient measures the fraction of collisions that transport momentum to the walls and fluctuates from zero (free-slip) to one (no-slip). Different values of this coefficient has been used in the literature. In our case a value of 0.05 were used. The value of restitution coefficient is set 0.9 (For perfectly elastic collision its value is equal to one). Initially, the reactor vessel is packed with solid particles up to the height 275 mm (baffle height). The volume fraction of solid is taken as 0.60.

E. Solution procedure

For the solution purpose commercial CFD coded software package ANSYS Fluent 19.2 [33] are used to solve model equations. This state of the art software is used for modeling of fluid flow, chemical reactions, heat transfer rate etc. in different types of complicated geometries. For modeling of interacting multiphase model, the Eulerian multiphase model is selected in Fluent. To handle pressure-velocity and phase coupling, the phase-coupled SIMPLE algorithm is used. For turbulent flow modeling, k-ε dispersed turbulence model with standard wall function is used. The pressure-based second order implicit unsteady solver are used to solve coupled phase momentum, volume fractions and shared pressure equations. A first order upwind discretization scheme is used to transform general scalar transport equations to algebraic one in control volume. The resulting algebraic equations are solved by ANSYS solver through Gauss-Seidel linear equation technique accompanied by algebraic multigrid (AMG) method. Interested readers can study details about ANSYS solver and solution method in ANSYS Fluent 19.2 Theory and User Guides.

The calculation activities include time step size of 0.001 s, total number of time steps 15000 and with maximum 50 iterations per time step. So all simulations are executed for a total of 15 s time period. The desired values of variables across the slot below the baffle is obtained by taking average of the data of last 10 s.

III. RESULTS AND DISCUSSION

A. Gas and solid flow behavior

The instantaneous snapshots of tubeless twin chambers fluidized bed with different specified cases of solid volume fraction, solid and gas velocities and bed pressure at a time instant of 8.5 s are shown in **Fig. 2** respectively. The initial packing height is 275 mm and inlet velocities for both chambers are $u_h = 0.12$ m/s and $u_r = 0.24$ m/s.

These figures illustrate the solid phase flow behavior in both chambers of the bed with left compartment named as RC and right one as HEC chamber. The vigorously induced gas in RC forms bubbles in the bottom region due to which wake is produced. The solid particles tend to occupy empty wake region and then it is dragged to upward region by the rising bubbles. The bubbles during upward motion merge to form bigger bubbles. After reaching of the big formed bubbles to bed surface, it explodes in to the free domain of the bed. Due to this eruption of the bubbles
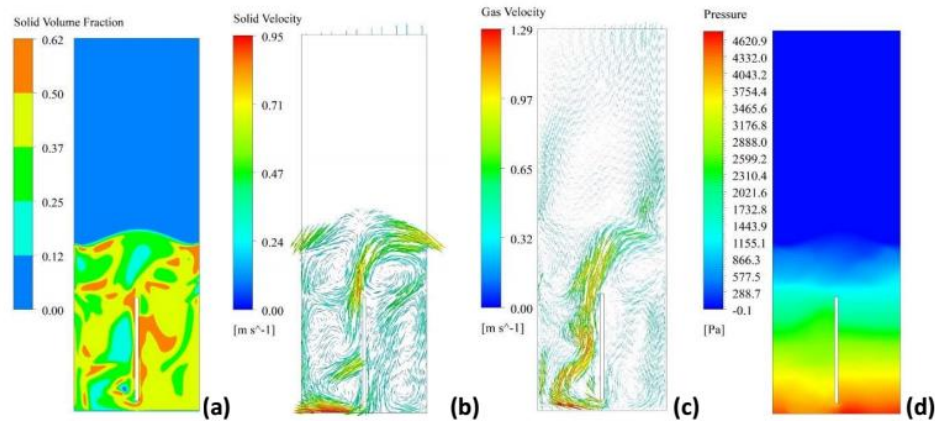
Fig. 12: Contours plots of different parameters when simulation time is 8.5 s: (a) solid volume fraction; (b) solid velocity; (c) gas velocity; (d) bed pressure.

sufficient amount of particles drop alongside the wall of RC and others are dispersed into HEC from RC above the baffle. In HEC as the gas phase inlet velocity is half of the introduced velocity of gas in RC, so in almost packed bed majority of the particles advances slowly downward. As the bottom region of HEC is reached the particles in the right bottom are circulated back to RC through slot beneath the baffle as presented in **Fig. 2(a)**. Due to unequal gas velocities aroused at the inlets of both the chambers internal solid circulation continues to develop below and above the baffle. Vector plot of solid velocity showing circulation pattern of solid phase amid two compartments is displayed in **Fig. 2(b)**. The bypassing of gas in the slot below the baffle from HEC to RC which nourishes the lateral solid circulation is shown in **Fig. 2(c)**. The gas divergence from RC to HEC over head the baffle stimulates solid circulation in the upper region. A density difference in the bed system is caused by expanded gas holdup in RC and due to which pressure gradient is generated between the two chambers of ICFB and as a result gas-solid flow bypassing become achievable as shown in **Fig. 2(d)**. So the key component for circulation process in the above phenomena is the central baffle which separates the two chambers.

B. Impact of insertion of tube bundle in RC and HEC

The installation of tube bundle in ICFB reestablish the gas and solid phases flow in the bed. In our study the influence of tubes on pressure, solid and gas circulation flux through the slot, bubble rise velocity and bubble properties were investigated.

1) Pressure gradient variation

The pressure gradient between the two chamber which is developed due to uneven inlet velocities introduced at the base of the bed is responsible for solid circulation through slot. The results of time averaged pressure in RC and HEC are obtained from simulation. The comparison of variation of time averaged pressure gradient due to addition of tubes in RC and HEC is shown quantitatively through bar chart in **Fig. 3** and **4** respectively. The pressure difference among two chambers represent interaction intensity which drives solid particles motion through slot below the baffle. A variation tendency of pressure gradient can be observed from bar charts when tubes are inserted separately in RC and HEC. The increase or decrease in pressure gradient might be mainly due to different configuration and arrangement of tubes.

2) Solid circulation flux variation

The time averaged results of solid circulation flux through slot of both cases are obtained through simulation and comparison of solid circulation flux parameter with different configurations of tube separately in RC and HEC are represented through bar charts in **Fig. 5** and **6** respectively. With the addition of tubes separately in both RC or HEC of the bed a decreasing tendency in SCF can be seen through the slot. This is due to the fact that insertion of tubes produces an obstacle for solid particles motion in vertical direction. The flow decreases in central region but increases near the walls and baffle.
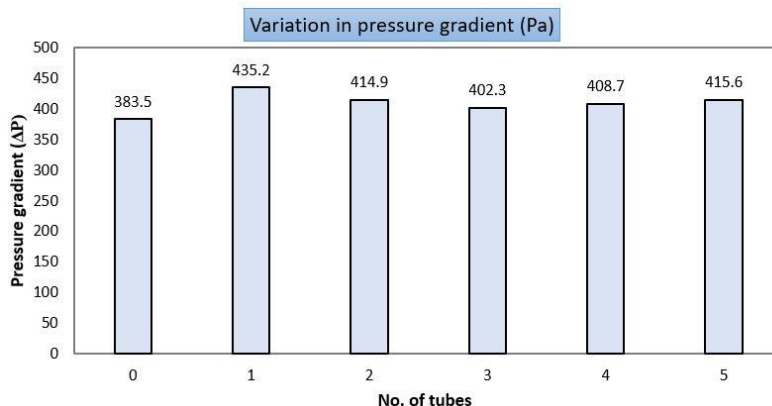
Fig. 13: Variation in pressure difference for different number of tubes in RC.
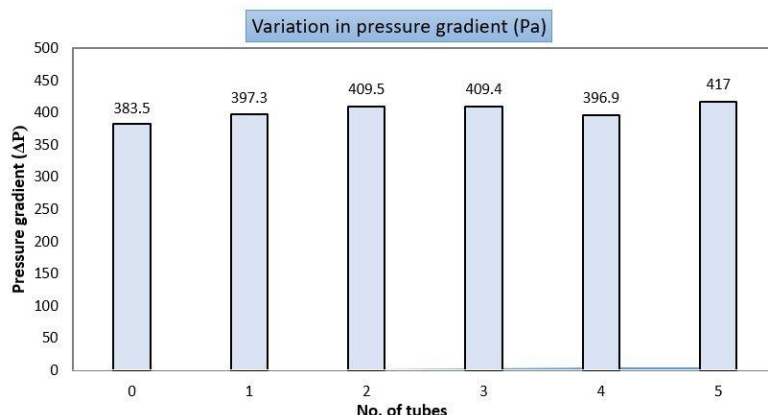
Fig. 14: Variation in pressure difference for different number of tubes in HEC.

The increase or decrease in SCF with tubes installed in different cases might be due to tube configurations.

3)Gas circulation flux variation

The time averaged values of gas circulation flux of both cases are calculated through simulation and comparison of GCF parameter with different tubes arrangement in RC and HEC separately are shown through bar charts in **Fig. 7** and **8** respectively. As explained above insertion of tubes in RC or HEC of an ICFB block the vertical movement of solid particles, so along with this gas phase motion is also interrupted. Due to this blockage GCF is affected through the slot beneath the baffle. The volumetric gas flow decreases in the central region but enhances in the vicinity of the walls and baffle.

4)Variation in bubble properties

During fluidization of solid particles in fluidized bed the cluster formed by bubbles grows continuously when there is no hindrance in its path i.e. when there are no tubes present in the bed. The rise velocity also enlarges with the bed height as it is proportional to bubble size. On contrast with insertion of immersed tubes the bubbling behavior changes significantly. **Fig. 9** compares the changes in bubble characteristics of tubeless ICFB with bed in which tubes are present. For brevity only the tubes in RC is considered here. The snapshot is taken at a time instant of 8.5 s. During simulation it was observed that rise velocity, shape and size of bubbles, bubble diameter etc. changes intensely when it interacts with tubes. The installed tubes increased bubbles bursting rate when it is collided by bubble coalescence. When the fluidizing gas enters the inlet of the two chambers, small bubbles are formed initially which grew up as it moves towards the tubes. After reaching the first queue of tubes it splits up again into small bubbles and this continues until it passes through the tubes bundle. The first contour of **Fig. 9** shows the bed without tube in which it can be observed that the solid volume fraction in the central region of RC is lower as related to other cases. This indicates that bubble concentration is high
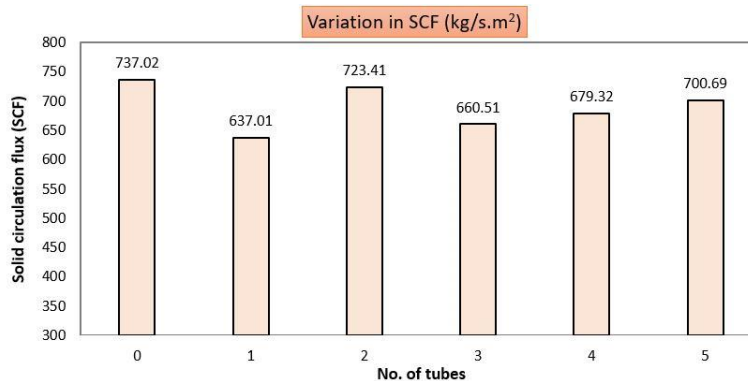
Fig. 15: Variation in solid circulation flux for different number of tubes in RC.
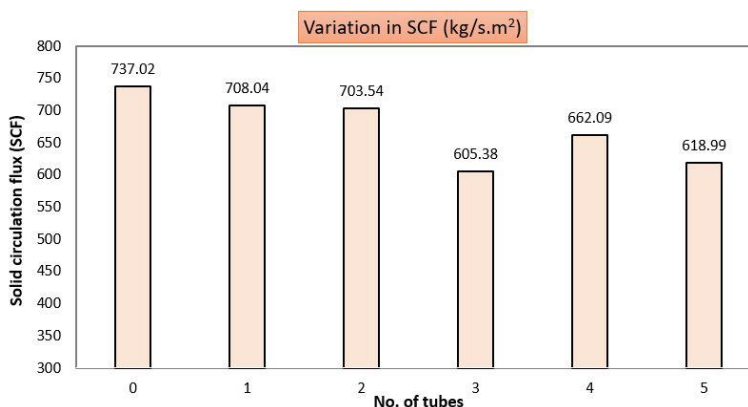
Fig. 16: Variation in solid circulation flux for different number of tubes in HEC.

in this region due to which size or diameter of the bubbles grows fast. The increasing mechanism in bubble diameter is proportional to rising velocity of the bubbles.

While in immersed tubes case volume fraction of solid in the middle installed tubes region is high and rising velocity is low so consequently good mixing is achieved.

C. Different stages of solid and gas phase mixing during fluidization

When reaction take place between different groups of solid particles then mixing of solid phases in the bed affects interaction of particles and quality of the product. To analyze visually the impact of dipped tubes bundle on the gas/solid and particles mixing in the bed, **Fig. 10** represents mixing practices of solid particles in the bed during different stages of fluidization without tubes, with five tubes in RC and five tubes in HEC. The geometry of fluidized bed with five tubes in HEC is same with tubes in RC, but only inlet velocities are reversed. Other cases of tubes in ICFB are exempted for brevity.

When inlet gases are blown through the bottom of ICFB, the solid particles of different groups disperse and mix with each other during fluidization. It can be understood from the **Fig. 10** that homogeneous mixing of solids is obtained through introduction of tubes bundles in RC and HEC as compared to tubeless ICFB system. Quantitative estimation of impact of bundle of tubes on mixing of solids is carried out in the literature [34]. Diffusion of particles into each other and solid mixing is attained due to disturbance of local agglomeration of particles by tube bundle which can be seen at time interval of 0.01 to 4 s. Thus it can be concluded that faster and better mixing and mixing quality can be obtained by inserting tubes in ICFB as it intensifies the disordered and turbulent flow of solid phase. The above phenomena are useful in situation when chemical reaction is involved between different phases of the bed.
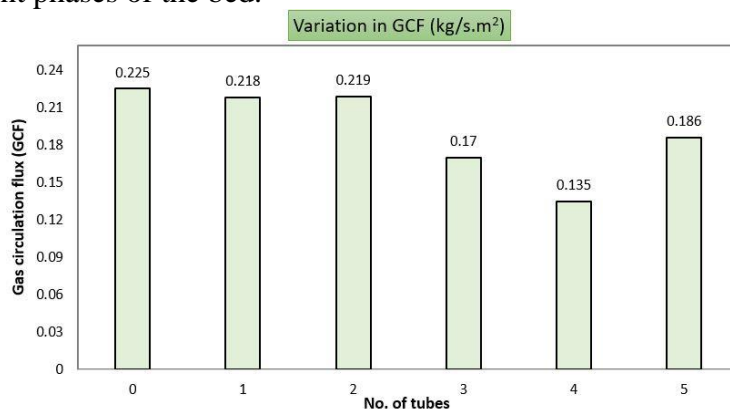
Fig. 17: Variation in gas circulation flux for different number of tubes in RC.
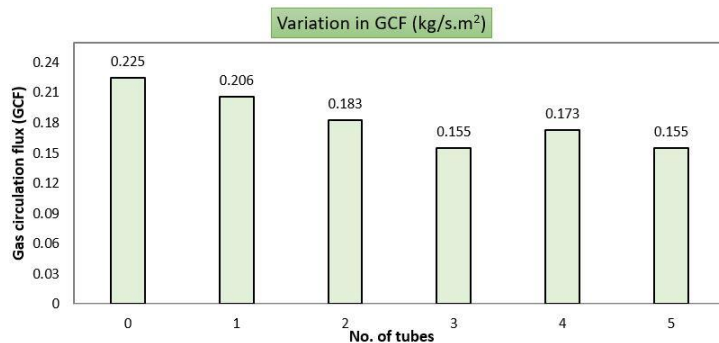
Fig. 18: Variation in gas circulation flux for different number of tubes in HEC.

IV. CONCLUSION

The key aim of this study were to explore the impact of immersed tubes on gas and solid phase motion in twin chamber ICFB system. The Eulerian-Eulerian model incorporating the kinetic theory of granular flow (KTGF) approach were employed for numerical simulation purpose.

A commercial CFD coded software ANSYS Fluent 19.2 were used to solve the model equations. The results obtained through simulation concluded the following points:

1. In twin chamber fluidized internal solid circulation can be achieved by the use of central baffle. The addition of tubes in RC or HEC disturbs the gas and solid phase flow in the central region. The vertical velocity decreases in the center due to presence of tubes and increases near the walls and baffle.

2. The simulation results of gas and solid flow dynamics in an ICFB well explained the solid circulation below the baffle through its contour plots and animations. Results shows that the driving force responsible for the circulation of solids through the slot and above the baffle is basically the pressure gradient among RC and HEC which arises due to uneven inlet velocities induced through the bottom of both chambers.

3. As the presence of tubes enhances gas velocity near the baffle, it produces pressure gradient between the two chambers and consequently SCF and GCF through the slot is affected. The solid and gas circulation fluxes decrease as more tubes are added to the chambers.

4. Better mixing of solid particles can be achieved by the addition of tubes. This situation is helpful when chemical reactions are involved in fluidized bed reactor.

5. The presence of tubes bundles also affect bubble properties like shape, size and diameter of bubble, rise velocity etc. When there is no tube present in the chamber then the solid volume fraction in the middle region is low and high nearby the walls and baffle. The concentration of bubble is high and grows toward the upper portion of the bed. But when tubes are installed the solid volume fraction is not low now and accordingly the rise velocity of bubbles is reduced in the center.
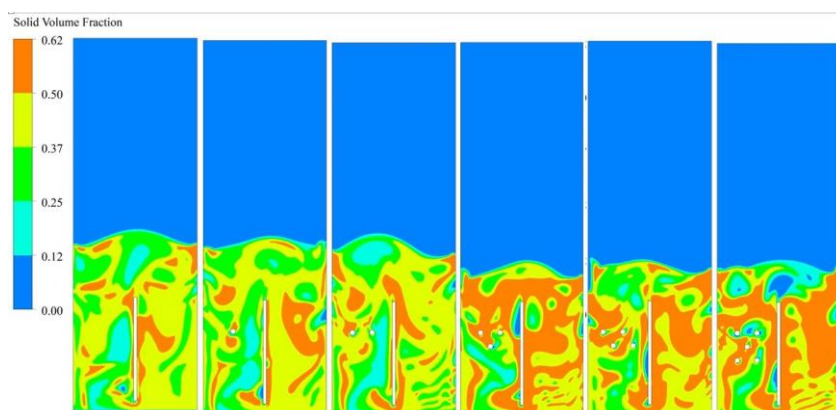
Fig. 19: Visual comparison of bubble properties of without tube bed with different tube arrangements in the bed.
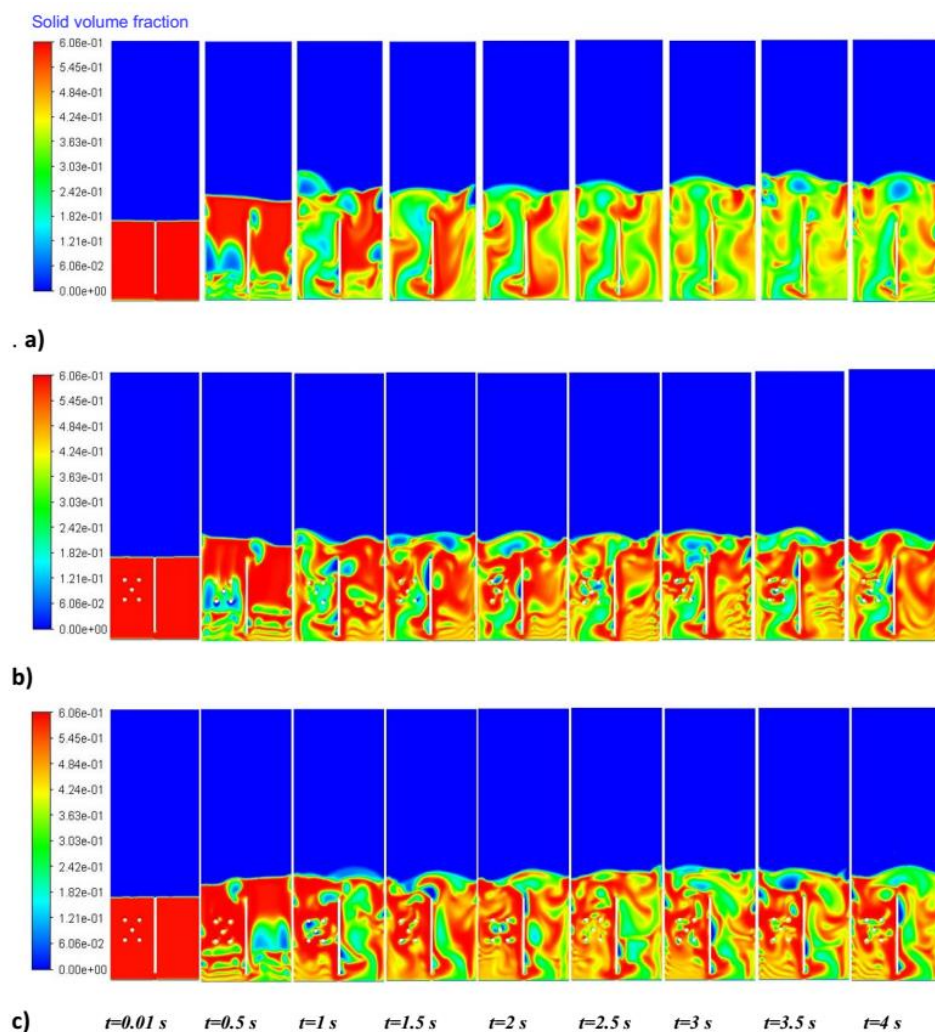
Fig. 20: Different stages of solid and gas phase mixing in fluidization process during time interval t = 0.01 s to 4 s: (a) without tubes; (b) five tubes in RC; (c) five tubes in HEC.

APPENDIX

List of Acronyms

2D	Two dimensional
3D	Three dimensional
CFD	Computational fluid dynamics
EEM	Eulerian-Eulerian model
TFM	Two fluid model
DPM	Discrete particle model
DEM	Discrete element method
AMG	Algebraic multi grid
KTGF	Kinetic theory of granular flow
CFB	Circulating fluidized bed
BFB	Bubbling fluidized bed
AFBC	Atmospheric fluidized bed combustion
PFBC	Pressurized fluidized bed combustion
ICFB	Internally circulating fluidized bed
ECFB	Externally circulating fluidized be
RC	Reaction chamber
HEC	Heat exchanger chamber
SCF	Solid circulation flux
GCF	Gas circulation flux
P_{RC}	Reaction chamber pressure
P_{HEC}	Heat exchanger chamber pressure
ΔP	Pressure difference
FCC	Fluid catalytic cracking
u	Velocity vector
u_h	Heat exchanger chamber inlet velocity
u_r	Reaction chamber inlet velocity
u_{mf}	Minimum fluidizing velocity
u_{trans}	Transition velocity
u_{mb}	Minimum bubbling velocity
ρ	Density
d_p	Particle diameter
t	Time
α	Volume fraction
$\alpha_{s,max}$	Maximum volume fraction of solid phase
β	Coefficient of interphase momentum exchange
g	Gravity
C_d	Drag coefficient
Re_p	Particle Reynold number
μ	Shear viscosity
$\mu_{s,f}$	Frictional shear viscosity
Θ	Granular temperature
P_s	Solid pressure
$P_{s,f}$	Frictional solid pressure
ϕ	Internal pressure angle
γ	Collisional energy dissipation

ξ	Bulk viscosity
q	Heat
k	Diffusion coefficient
e	Restitution coefficient
g_o	Radial distribution function
$\bar{I}$	Unit tensor
I_{2D}	Deviatoric stress tensor second invariant
τ	Stress tensor

Subscripts

s	Solid phase
g	Gas phase

V. REFERENCES

1. Latif, A., *A study of the design of fluidized bed reactors for biomass gasification*. 1999, University of London.
2. Kunii, D. and O. Levenspiel, *Fluidization engineering*. 2013: Elsevier.
3. Krishna, R., J. Van Baten, and J.J.P.T. Ellenberger, *Scale effects in fluidized multiphase reactors.* 1998. **100**(2-3): p. 137-146.
4. Brown, R.J.C.N.f.M.C., Iowa State University, Ames, IA, *ME 539: fluidized bed processes.* 1997.
5. Rudolph, V. and M. Judd, *Circulation and slugging in a fluid bed gasifier fitted with a draft tube*, in *Circulating Fluidized Bed Technology*. 1986, Elsevier. p. 437-442.
6. LaNauze, R.J.P.T., *A circulating fluidised bed.* 1976. **15**(1): p. 117-127.
7. Kuramoto, M., D. Kunii, and T.J.P.T. Furusawa, *Flow of dense fluidized particles through an opening in a circulation system.* 1986. **47**(2): p. 141-149.
8. Song, B.H., Y.T. Kim, and S.D.J.C.E.J. Kim, *Circulation of solids and gas bypassing in an internally circulating fluidized bed with a draft tube.* 1997. **68**(2-3): p. 115-122.
9. Ahn, H.-S., et al., *Solid circulation and gas bypassing in an internally circulating fluidized bed with an orifice-type draft tube.* 1999. **16**(5): p. 618-623.
10. Namkung, W., et al., *Effect of temperature on gas bypassing and solids circulation rate in an internally circulating fluidized bed.* 2000. **78**(6): p. 1025-1031.
11. Kim, S.D., et al., *Solid circulation characteristics in an internally circulating fluidized bed with orifice-type draft tube.* 2002. **19**(5): p. 911-916.
12. Toyoda, S., et al., *Analysis of particle flow in an internally circulating fluidized bed having several chambers.* 2002. **28**(4): p. 424-434.
13. Chu, C.Y. and S.J.J.P.T. Hwang, *Attrition and sulfation of calcium sorbent and solids circulation rate in an internally circulating fluidized bed.* 2002. **127**(3): p. 185-195.
14. Marschall, K.-J. and L.J.C.E.S. Mleczko, *CFD modeling of an internally circulating fluidized-bed reactor.* 1999. **54**(13-14): p. 2085-2093.
15. Bin, Y., et al., *Discrete particle simulation and visualized research of the gas− solid flow in an internally circulating fluidized bed.* 2003. **42**(1): p. 214-221.
16. Zhang, K., S. Brandani, and J.J.P.i.N.S. Bi, *Computational fluid dynamics for dense gas-solid fluidized beds.* 2005. **15**(S1): p. 42-51.

17. Wei, X., et al., *Characterizing particle dispersion by image analysis in ICFB.* 2006. **49**(19-20): p. 3338-3342.
18. Jeon, J.H., et al., *Solid circulation and gas bypassing characteristics in a square internally circulating fluidized bed with draft tube.* 2008. **47**(12): p. 2351-2360.

19.   Fang, M., et al., *Experimental research on solid circulation in a twin fluidized bed system.* 2003. **94**(3): p. 171-178.
20.   Anderson, T.B., R.J.I. Jackson, and E.C. Fundamentals, *Fluid mechanical description of fluidized beds. Equations of motion.* 1967. **6**(4): p. 527-539.
21.   Ding, J. and D.J.A.j. Gidaspow, *A bubbling fluidization model using kinetic theory of granular flow.* 1990. **36**(4): p. 523-538.
22.   Gidaspow, D., *Multiphase flow and fluidization: continuum and kinetic theory descriptions*. 1994: Academic press.
23.   Wen, C. *YH Yu. Mechanics of fluidization*. in *Chemical Engineering Progress Symposium Series*. 1966.
24.   Syamlal, M. and T.J. O'Brien. *Computer simulation of bubbles in a fluidized bed*. in *AIChE Symp. Ser*. 1989. Publ by AIChE.
25.   Lun, C., et al., *Kinetic theories for granular flow: inelastic particles in Couette flow and slightly inelastic particles in a general flowfield.* 1984. **140**: p. 223-256.
26.   Lun, C. and S.J.A.M. Savage, *The effects of an impact velocity dependent coefficient of restitution on stresses developed by sheared granular materials.* 1986. **63**(1-4): p. 15-44.
27.   Schaeffer, D.G.J.J.o.d.e., *Instability in the evolution equations describing incompressible granular flow.* 1987. **66**(1): p. 19-50.
28.   Johnson, P.C., P. Nott, and R.J.J.o.f.m. Jackson, *Frictional–collisional equations of motion for participate flows and their application to chutes.* 1990. **210**: p. 501-535.
29.   Feng, Y., et al., *CFD modeling of gas–solid flow in an internally circulating fluidized bed.* 2012. **219**: p. 78-85.
30.   Hassan, M., et al., *Numerical simulations of solid circulation characteristics in an internally circulating elevated fluidized bed.* 2017. **40**(4): p. 769-777.
31.   Hiltunen, K., et al., *Multiphase flow dynamics.* 2009. **722**.
32.   Jackson, R.J.T.I.C.E., *The mechanics of fluidized beds. I. The stability of the state of uniform fluidization.* 1963. **41**: p. 13-21.
33.   Fluent, A.J.A., Canonsburg, PA, *ANSYS fluent theory guide 15.0.* 2013.
34.   Fang, M., et al., *Computational fluid dynamics-discrete element method investigation of solid mixing characteristics in an internally circulating fluidized bed.* 2013. **52**(22): p. 7556-7568.

Numerical Simulations of condensation heat transfer of refrigerant R134a in a smooth horizontal tube using Mixture model.

Sohail Khan [A], Muhammad Ali Kamran [B]

USPCAS-E UET Peshawar [A], UET Peshawar [B]

Abstract— **Multiphase flow occurs in almost all HVAC and refrigeration systems. In this research study, numerical simulations of condensation heat transfer phenomenon of R134a refrigerant inside smooth horizontal tube is carried out in order to better visualize the flow behavior and analyze heat transfer characteristics of R134a refrigerant. For multiphase flow analysis of R134a refrigerant, k-omega shear stress transport (SST) turbulence model is used which is well suited for simulating flows in the viscous sub-layer. For predicting and analyzing the heat transfer characteristics, Heat and mass transfer model (Lee Evaporation-Condensation Model) is used for internal flow condensation to occur. Convective heat transfer coefficient is determined throughout the tube using surface integral method which matched with the convective heat transfer coefficient obtained using experimental data. Volume fractions of both the liquid and vapor phases are obtained at both the symmetrical and cross-sectional planes which indicated that homogeneous condensation occurred resulting in mist flow which later on changed to stratified and stratified wavy flow. The temperature distribution obtained for the two phase flow (liquid and vapor) showed that the refrigerant was initially in dry saturated state which then condensed into two phase mixture (liquid and vapor) as the condensation process proceeds downstream. The results indicate that the k-omega (shear stress transport) turbulence model predicts the multiphase flow characteristics better than the k-epsilon turbulence model.**

Keywords—**Computational fluid dynamics, Convective heat transfer coefficient, Multiphase flow, Shear stress transport.**

I. INTRODUCTION

Efforts are in progress in the field of HVAC & refrigeration systems to increase the efficiency of refrigeration systems and to minimize the system footprints [1]. For this purpose, researchers are working in the field of refrigeration to discover new refrigerants and refrigerant blends which not only minimize the adverse effects on atmosphere but also are more efficient and environment friendly [2]. Due to this importance and need, worldwide researchers are busy in conducting experimental and numerical studies of different multiphase condensation flow of refrigerants using different flow geometries like micro-channels, shell and tube heat exchangers, circular tubes, dimpled tubes [3]. Condensation plays a major role in both domestic and industrial applications like power generations, HVAC & R, petrochemical industries, farm preserves, cooling of heat emitting appliances [4], [5]. Different types of condensation flows are observed in refrigeration systems like direct contact, film-wise, external film, internal flow condensation etc. Internal flow condensation is mostly observed in refrigeration system due to which major research is done on internal flow condensation. Rabiee et al conducted heat transfer analysis of two phase flow of R134a refrigerant to investigate the dependence of heat transfer coefficient on heat flux and tube dimensions [6]. Juggurnath et al performed 3D numerical simulations of R134a condensing flow and analyzed heat transfer characteristics using constant mass flux, vapor quality (0.25-0.75). The results showed stratified wavy flow pattern which were in good agreement with experimental data [7]. Internal flow condensation is different from dropwise and film condensation because of the involvement of volume fractions of vapor and liquid phases. Consider initially dry saturated vapors enter the tube. As the vapor proceeds downstream, they condense on the inner surface of condenser tube resulting in the increased quality of the flow [8] giving different localized flow structures like annular, stratified, stratified wavy, intermittent, dispersed as shown in Fig. 1 [9], [10].
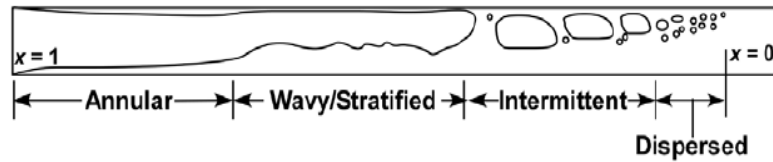
Fig. 1. Two phase flow regimes (Flow from left to right)

Volume fraction of both the vapor and liquid phases depends on the inlet boundary conditions and numerical models specified during simulations. Heat transfer and pressure drop characteristics of two phase flow are strongly dependent on the flow regimes obtained as the film thickness increases downstream. Researchers have developed different models like void fraction, pressure drop, empirical, semi-empirical for different fluid flows, design and operating conditions [11] in an effort to improve the reliability of predictions of multiphase flows. Since two phase flow occurs in majority of refrigeration and cooling system which may be aerospace applications, electronics cooling systems [12], rockets and jet propulsion systems etc. therefore there is a need to understand the dynamics of two phase flow of R134a refrigerant.

This research study is conducted in order to better visualize, understand and compare the numerical results with the experimental and two phase flow behavior inside a smooth tube using mixture multiphase model. Contrary to most of the available literature where a constant heat flux on the tube surface was defined, variable heat flux has been defined on the tube surface at different sections in an effort to obtain accurate results [13], [14].

The paper is organized into five sections. Section 2 explains the heat exchanger model (geometry and meshing). Numerical models selected for analysis are explained in section 3. Numerical results obtained from simulations are explained in section 4. Section 5 gives conclusions of the current research work.

II. METHODOLOGY

A. Geometry Design

Tube geometry is designed using ANSYS workbench R19.2. The copper tube has length and diameter of 202.7 mm and 4.7 mm respectively. The tube is divided into eight (8) segments and different surface heat flux is defined on each segment using experimentally available boundary conditions. The wall thickness of tube is taken as zero for radial convection only. The 3D isometric view of tube geometry is shown below in Fig. 2.
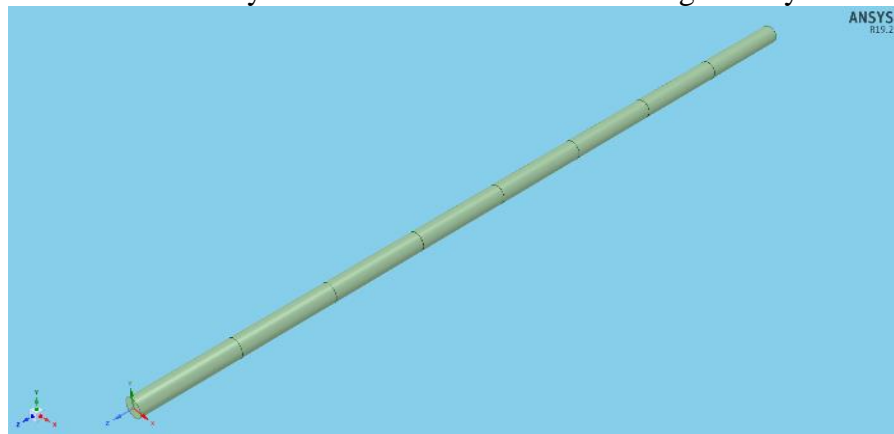
Fig. 2. 3D model of circular tube

B. Mesh generation

ICEM CFD ANSYS 19.2 meshing tool is used for geometry meshing. An O-grid consisting of 698390 hexahedral elements was generated for the geometry as recommended by different authors for circular geometries [15]. The near wall region has inflation layer with number of refined grid rows equal to 20. The SST k-ω turbulence model used in this study requires the wall to be discretized with near wall region Y plus

(y^+) value close to one [1] . The first row of boundary layer grid near the wall is having cell height of 1e-5 m with growth ratio of 1.2. Fig. 3 shows cross section of the meshed circular tube.

1)Mesh Independence

Mesh independence study was conducted using three different grid sizes having different grid elements in a 3D smooth tube. The condensation heat transfer coefficient obtained using different grid sizes is plotted as a function of tube length. The results indicated that grid size with 698390 grid elements gave improved results with given convergence criteria after which the dependence of mesh size on the results was negligible as shown in Fig. 4.
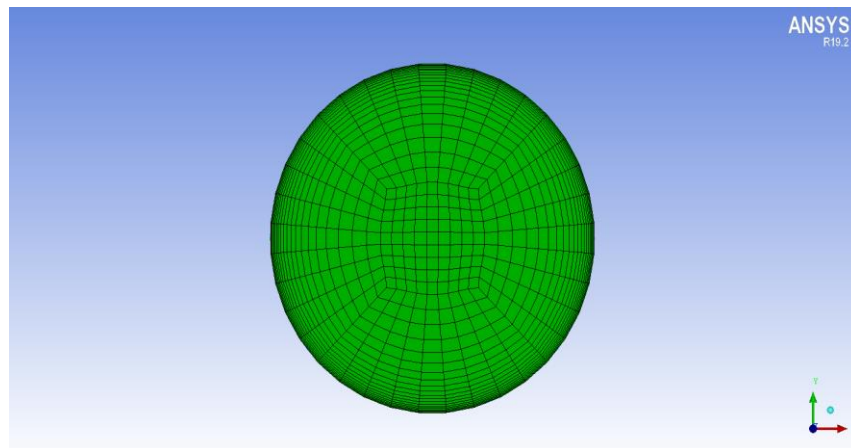
Fig. 3. Cross sectional view of the computational domain
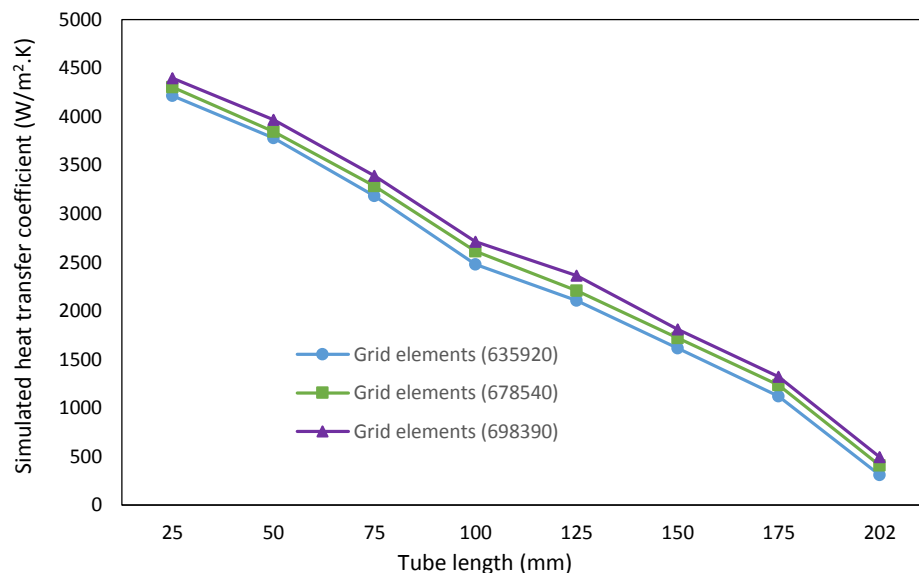
Fig. 4. Mesh sensitivity analysis

III. NUMERICAL MODELS

Use of various numerical models for modeling turbulence, multiphase flow, and heat and mass transfer has been reported in the literature, with varying accuracies. In the numerical investigation conducted, the condensation problem for R134a refrigerant was solved using the k-ω SST turbulence model, Mixture multiphase model and Lee model.

A. Turbulence model

The CFD community is still in pursuit of a turbulence model which is able to predict all types of turbulent flows. In general, the factors considered while identifying the turbulence model are the physical phenomenon of a given problem, simulation accuracy time, and available computational resources. The most frequently used turbulence models are the k-ω and k-ε models in which k-ω SST turbulence model is used here [16];

1) k-ω (SST) turbulence model

The SST k-ω turbulence model was developed by menter to efficiently blend the robust and accurate formulation of the k-ω model in the near wall region with the free stream independence of the k-ε model in the far field. [17] To achieve this, k-ε model is transformed into k-ω model with the refinements like incorporation of different modeling constants, damped cross diffusion derivative and modified turbulent viscosity for turbulent shear stress. Transport equations for SST k-ω model are as follows [16]:

$$\frac{\partial}{\partial t}(\rho k)+\frac{\partial}{\partial x_i}(\rho k u_i)=\frac{\partial}{\partial x_j}\left(\Gamma_k \frac{\partial k}{\partial x_j}\right)+G_k-Y_k+S_k \tag{1}$$

$$\frac{\partial}{\partial t}(\rho \omega)+\frac{\partial}{\partial x_j}\left(\rho \omega u_j\right)=\frac{\partial}{\partial x_j}\left(\Gamma_\omega \frac{\partial \omega}{\partial x_j}\right)+G_\omega-Y_\omega+D_\omega+S_\omega \tag{2}$$

Where G_K represents the generation of turbulence kinetic energy due to mean velocity gradients, G_ω represents the generation of ω, Γ_K and Γ_ω represents the effective diffusivity of K and ω respectively, Y_K and Y_ω represents the dissipation of K and ω due to turbulence, S_K and S_ω are user-defined source terms.

B. Heat and mass transfer model

Lee model is a mechanistic model with a physical basis. It is used with both VOF and mixture multiphase models as well as with the Eulerian multiphase model if one of the overall interfacial heat transfer coefficient models are used [18]. In the Lee model, the liquid-vapor mass transfer mechanism (evaporation and condensation) is governed by the following vapor transport equation:

$$\frac{\partial}{\partial t}(\alpha_v \rho_v)+\nabla \cdot (\alpha_v \rho_v \overline{V}_v)=\dot{m}_{lv}-\dot{m}_{vl} \tag{3}$$

Where
v = vapor phase
α_v = vapor volume fraction
ρ_v = vapor phase density
V_v = vapor phase velocity
$\dot{m}_{lv}$, $\dot{m}_{vl}$ = the rates of mass transfer due to evaporation and condensation respectively
Based on the following temperature regimes, the mass transfer can be described as follows [19];

If $T_v < T_{sat}$ (condensation)

$$\dot{m}_{vl}=coeff * \alpha_v \rho_v \frac{(T_{sat}-T_v)}{T_{sat}} \tag{4}$$

From the above equation, coefficient known as accommodation coefficient which is the inverse of the relaxation time (1/s) is defined as:

$$coeff = \frac{6}{d_b}\beta\sqrt{\frac{M}{2\pi RT_{sat}}}L\left(\frac{\alpha_v\rho_v}{\rho_l-\rho_v}\right)$$

(5)

This expression for the condensation process treats the source terms in implicit way in the phase conservation equation. The accommodation coefficient and the bubble diameter are not usually well known. Accommodation coefficient need to be tuned according to the experimental data and by default 0.1 is the value for both evaporation and condensation [16].

For current study, accommodation coefficient (condensation frequency) was set as 0.90 using experimental data values for saturation temperature of 319 K and condensation pressure of 1.193 N/mm^2.

C. Multiphase model

The mixture model is used for modeling multiphase flows having different phase velocities and assuming equilibrium condition over short length span. The mixture model is used to model flows with n-different phases by solving the continuity, momentum, and energy equations for the mixture, volume fractions equations for all secondary phases, and algebraic expressions for the phase's relative velocities.

The continuity equation for the mixture of the phases is;

$$\frac{\partial \rho_m}{\partial t} + \nabla.(\rho_m v_m) = 0$$

(6)

Where v_m is the mass is averaged velocity of the phase and is given by;

$$v_m = \sum_{k=1}^{n}\frac{\alpha_k\rho_k v_k}{\rho_m}$$

(7)

Where ρ_m is the mixture density and is defined as;

$$\rho_m = \sum_{k=1}^{n}\alpha_k\rho_k$$

(8)

Where α_k is the volume fraction of the phase, k.

The equation of momentum for the mixture model is given by;

$$\frac{\partial(\rho_m v_m)}{\partial t} + \nabla.(\rho_m v_m v_m) = -\nabla p + \nabla.[\mu_m(\nabla v_m + \nabla v_m^T)] + \rho_m g + F + \nabla.\{\sum_{k=1}^{n}\rho_k\alpha_k v_{dr,k}v_{dr,k}\}$$

(9)

Where n represents the phases involved, F is the body force and μ_m is the viscosity of mixture.

$$\mu_m = \sum_{k=1}^{n}\alpha_k\mu_k$$

(10)

$v_{dr,k}$ is the secondary phase drift velocity and is given by;

$$v_{dr,k} = v_k - v_m$$

(11)

The energy equation in case of mixture model is given by;

$$\frac{\partial \sum_{k=1}^{n}(\alpha_k\rho_k E_k)}{\partial t} + \nabla.\sum_{k=1}^{n}(\alpha_k v_k(\rho_k E_k + p)) = \nabla.(k_{eff}\nabla T) + S_E$$

(12)

Where k_{eff} represents the effective thermal conductivity and S_E is the volumetric heat source term.

IV. RESULTS AND DISCUSSION

The numerical results obtained from simulations for internal flow condensation of R134a refrigerant are discussed in terms of volume fraction, temperature distribution, velocity distribution, flow regimes transition, convective heat transfer coefficient of the two phases (vapor-liquid phases) are displayed and explained below;

A. Vapor volume fraction

Numerical simulation results for the vapor phase fraction are shown at the cross sectional planes. The copper tube representative length is 202.7 mm and the cross-sectional planes are defined at different axial locations (50, 150 mm) from the tube inlet as given below;

1)Cross sectional planes

Contours of vapor fraction at cross sectional planes defined at two different axial locations of 5 mm and 150 mm from the tube inlet are shown in Fig. 5. High quality vapor enters the tube which condenses as the flow advances downstream. Homogeneous condensation takes place due to low inlet vapor phase velocity resulting in formation of fog (droplets) which settles at the base in the form of condensate due to gravity.
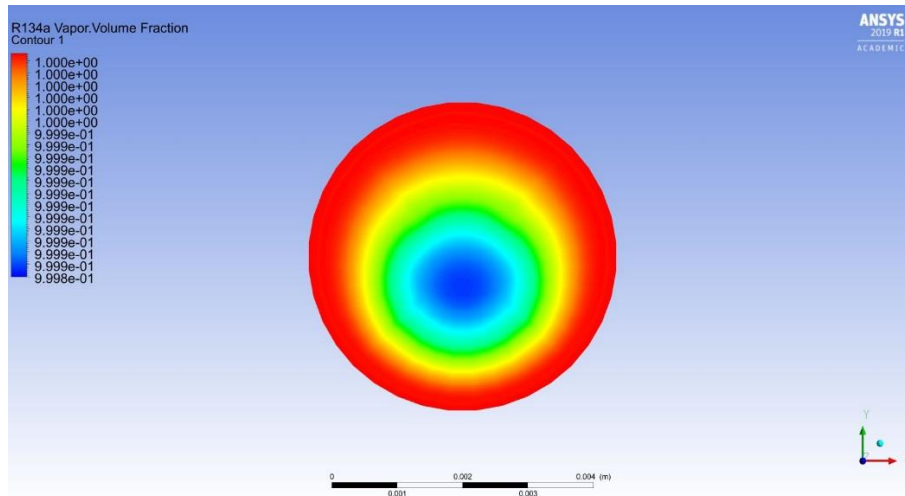
(a) 5 mm
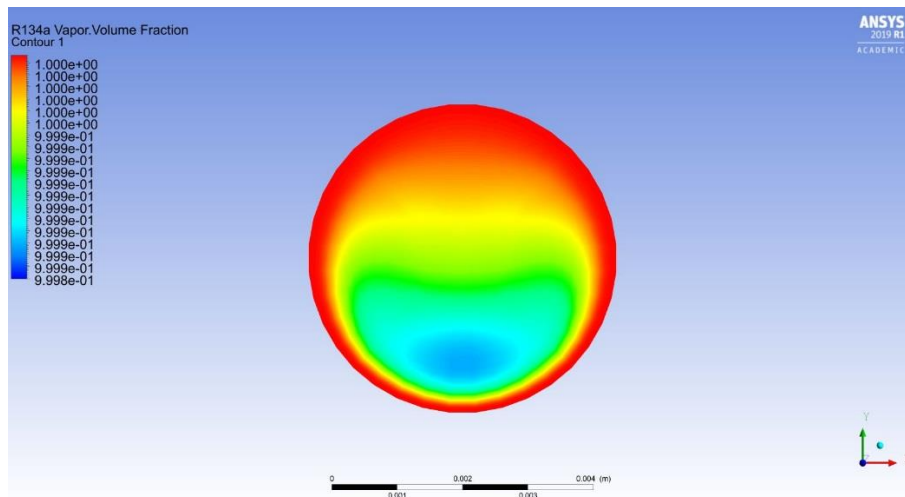
(b) 150 mm
Fig. 5. Vapor volume fraction at different cross-sectional planes

B. *Liquid volume fraction*

Contours of the liquid volume fraction are shown at both the symmetrical as well as the cross sectional planes as explained below;

1)Cross sectional planes

The cross sectional planes are defined at distances (5, 50, 150, 200 mm) from the tube inlet. The R134a liquid (condensate) formed inside the tube as a result of homogeneous condensation drains down to the base of the tube due to high density, gravity and also flow shear stresses as shown in Fig 6 (a, b, c, d).

2)Symmetrical plane

The liquid volume fraction contour at the symmetrical plane is shown in Fig 7. Initially liquid volume fraction is zero up to some length (approximately 2-3 mm) as the vapors are dry saturated but after that condensation of R134a takes place due to radial heat flux defined at the tube surface. The liquid condensate begins to form as a result of internal surface condensation at low mass flow rate. The condensate formed flows to the base of the tube as a result of high density and gravity effects.
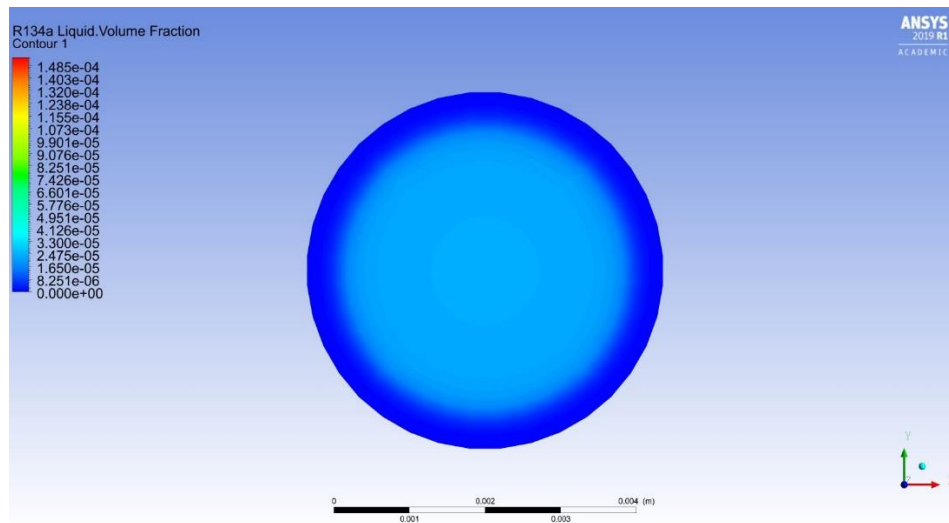
(a) 5 mm
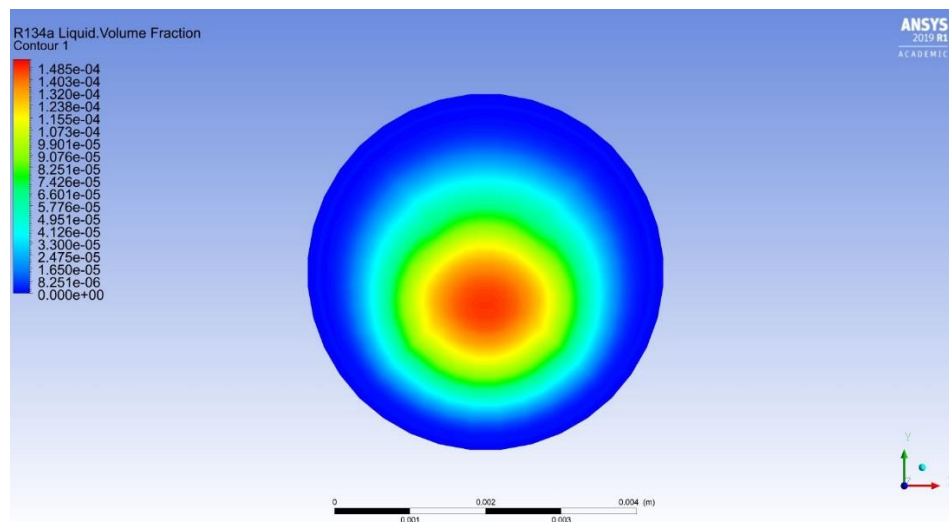
(b) 50 mm
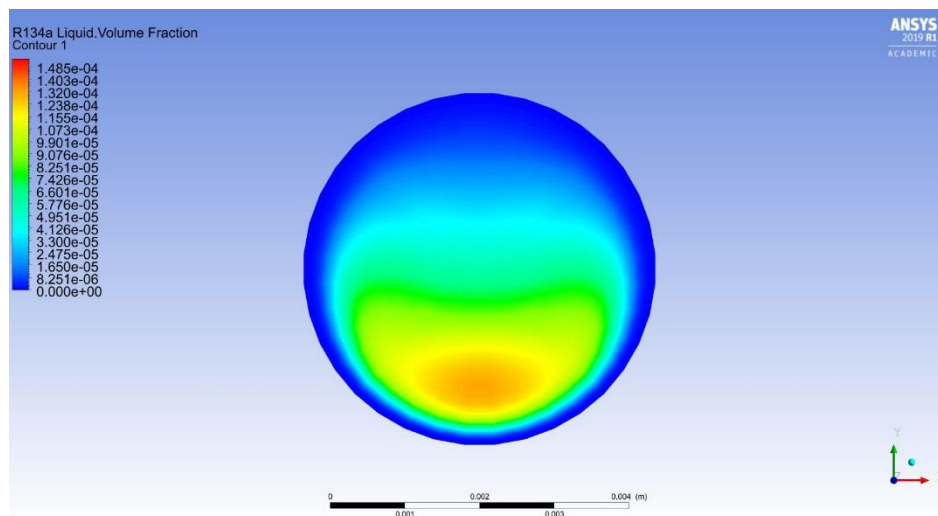
(c) 150 mm
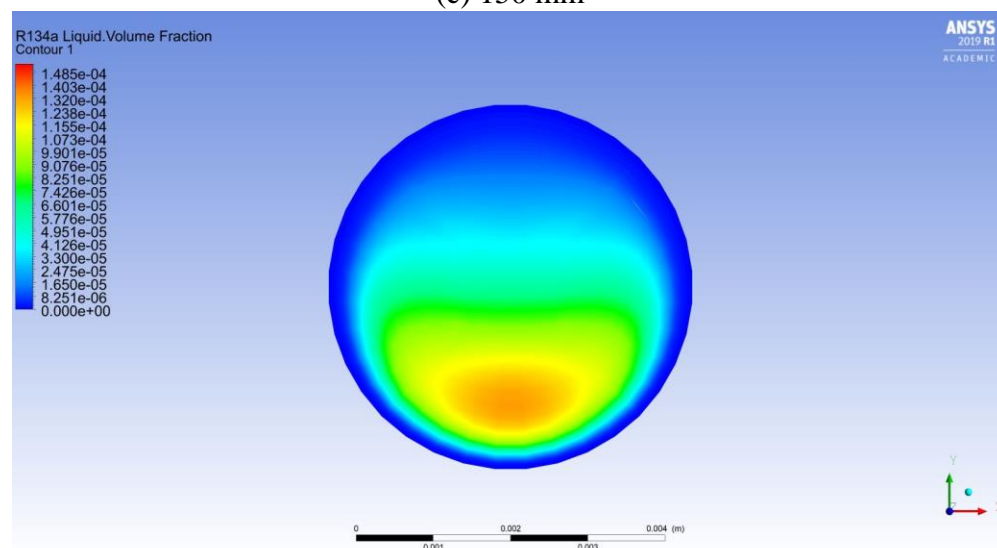
(d) 200 mm
Fig. 6. Liquid volume fraction at different cross-sectional planes
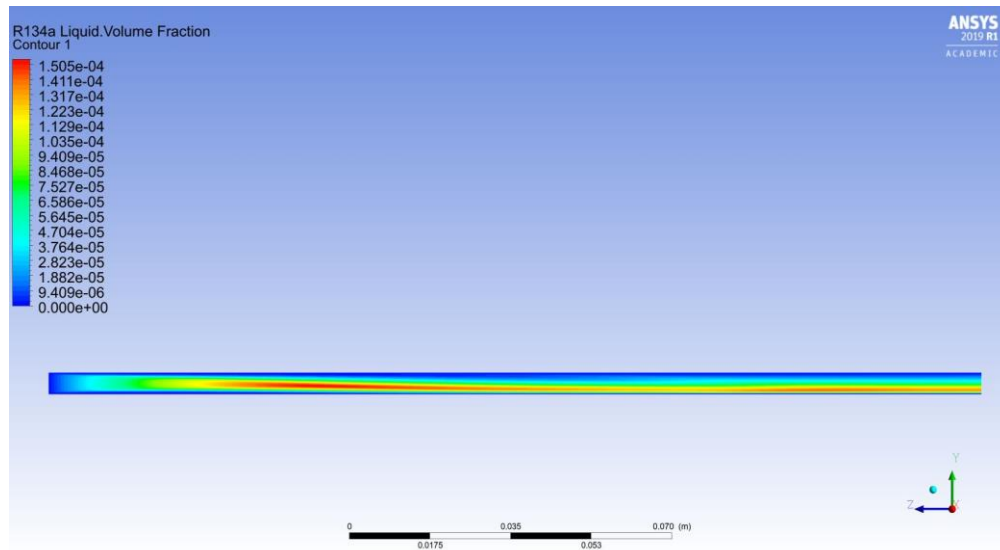
Fig. 7. Liquid volume fraction at the symmetrical plane

C. Temperature distribution

Temperature distribution contours for both the cross sectional planes and symmetrical plane are shown in Figs. 8 (a, b, c, d) and 9 respectively. The temperature distribution corresponds to the vapor-liquid two phase distribution cloud images showing liquid phase temperature lower than the vapor phase temperature. Initially all the mass exists is vapor phase dominant, so the temperature is high at the tube inlet but as the flow advances downstream liquid condensate is generated which produces certain degree of sub cooling resulting in the decreased heat transfer and temperature downstream. From the symmetrical plane, it is clear that vapor phase is dominant in the tube central region due to which temperature is high unlike near wall region where temperature is low because of the sub cooling caused due to condensation phenomenon.
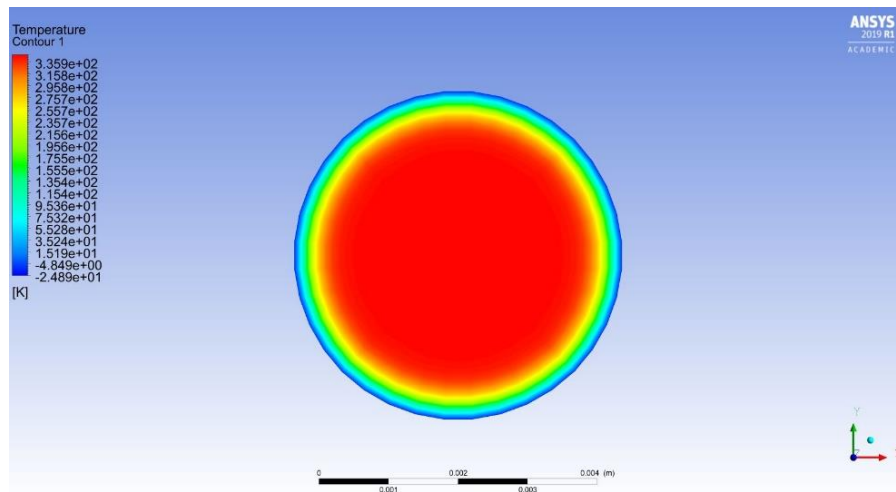
(a) 5 mm
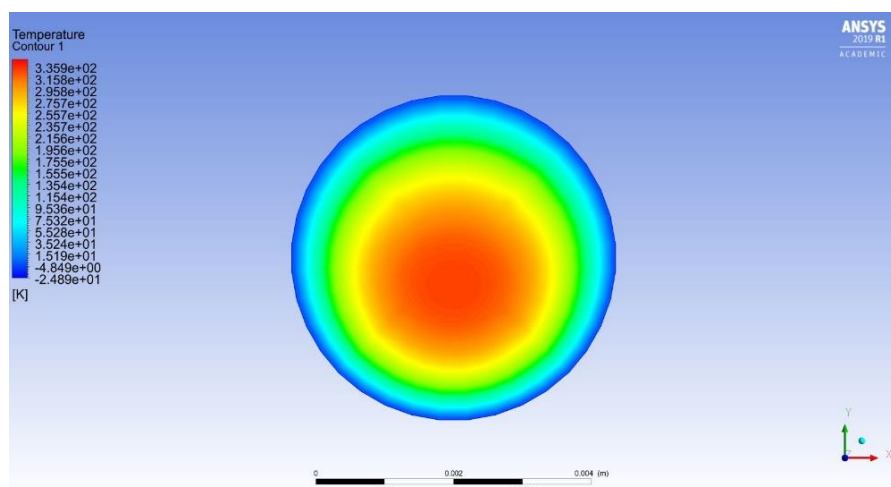
(b) 50 mm
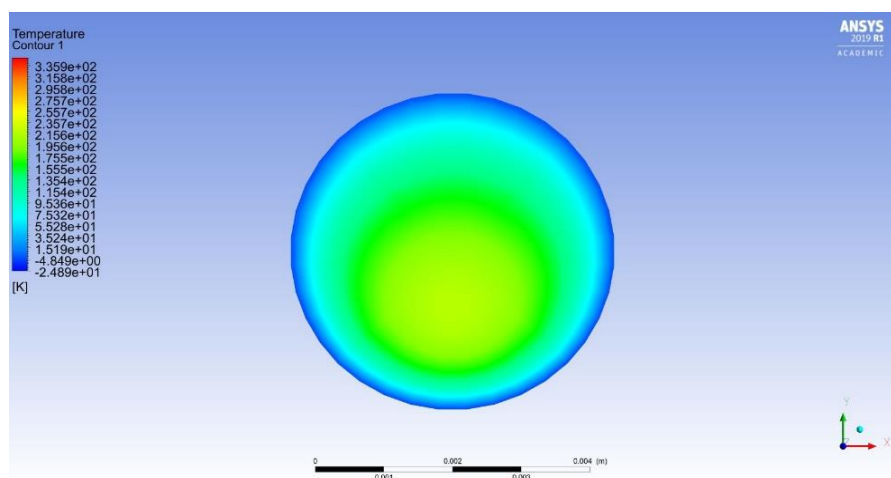
(c) 150 mm

Fig. 8. Temperature distribution at different cross-sectional planes
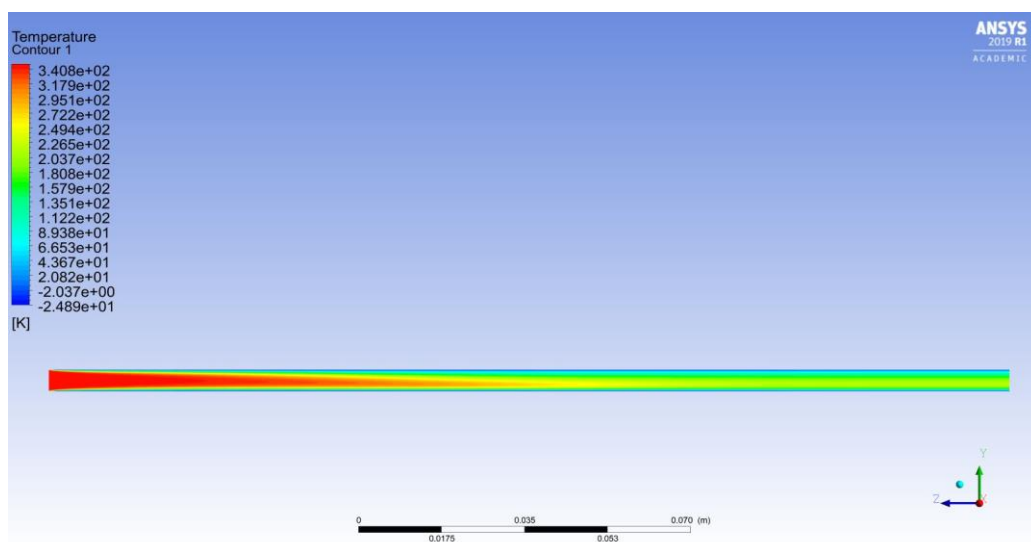
Fig. 9. Temperature distribution at the symmetrical plane

D. Two phase flow regimes

Different flow regimes were observed in case of mixture multiphase model during the two phase condensing flow of refrigerant R134a inside a smooth horizontal tube. As vapors flow downstream inside the tube, vapors starts condensing and condensate is formed that results in different flow patterns. Initially all the mass exists is vapor which starts condensing as the flow advances downstream. From Fig. 10 it is clear that mist flow occurs initially in the first tube section (approximately 76 mm) as the flow velocity is low (0.08 m/s) and the vapors are dispersed in the whole volume of first tube section. When the liquid volume fraction (condensate) reaches certain value then the gravity effects are dominated due to which the condensate is collected at the base causing stratified flow as flow proceeds downstream.
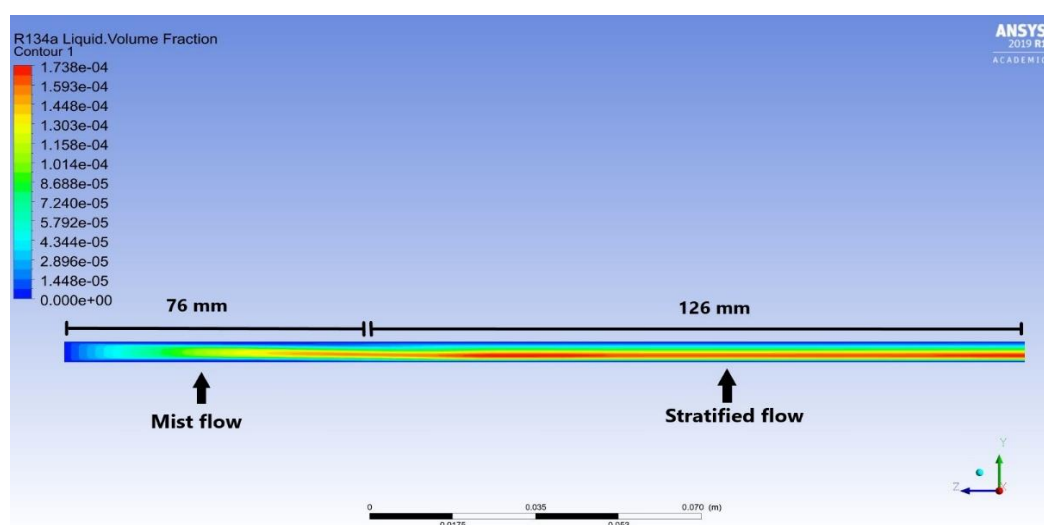
Fig. 10. Flow regimes transition

E. Heat transfer coefficient

Simulated heat transfer coefficient distribution as a function of axial location is plotted in Fig. 11. The heat transfer coefficient decreases along the length of the tube as the temperature gradient decreases along the flow direction due to sub cooling caused because of condensate formation at the inner wall surface. The heat transfer coefficient as a function of length and dryness fraction (vapor quality) is shown below in Fig. 11 and Fig. 12. The high quality vapors enter the tube at low inlet flow velocity having Re<35000 making the flow laminar. As the flow proceeds downstream, the condensate film thickness increases causing the thermal resistance to increase due to which rate of convective heat transfer decreases. The simulated heat transfer coefficient obtained from numerical simulations was compared with the experimental heat transfer coefficient as shown in Fig. 13. The results indicate that simulated heat transfer coefficient shows good agreement with the experimental results.
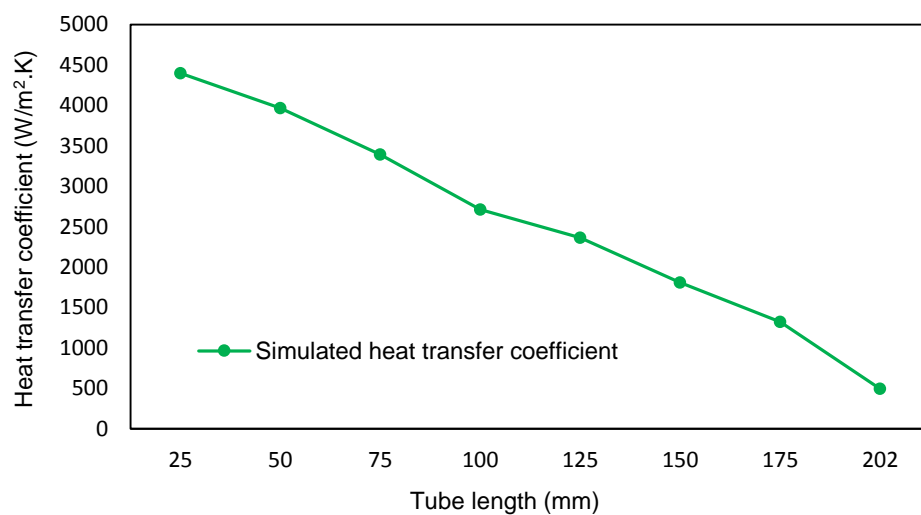
Fig. 11. Simulated heat transfer coefficient v/s tube length
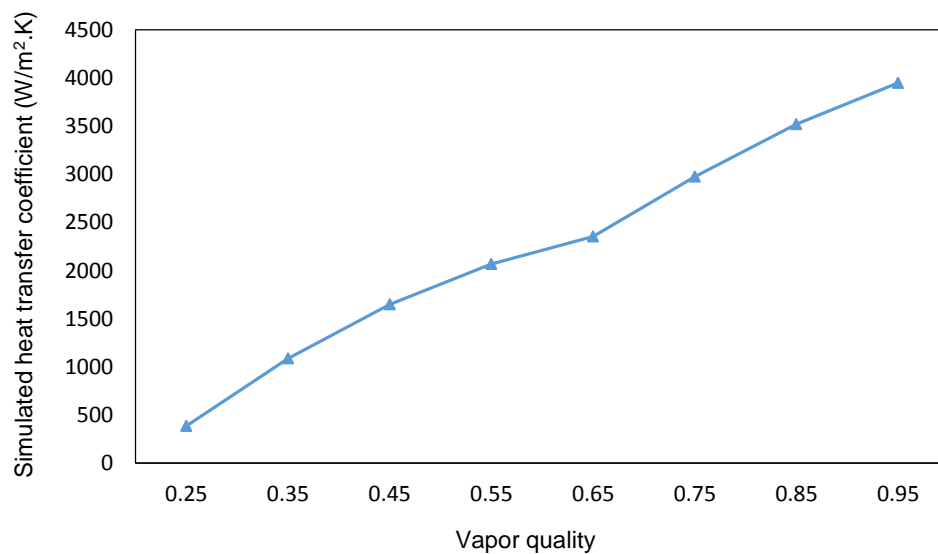
Fig.12. Simulated heat transfer coefficient v/s vapor quality
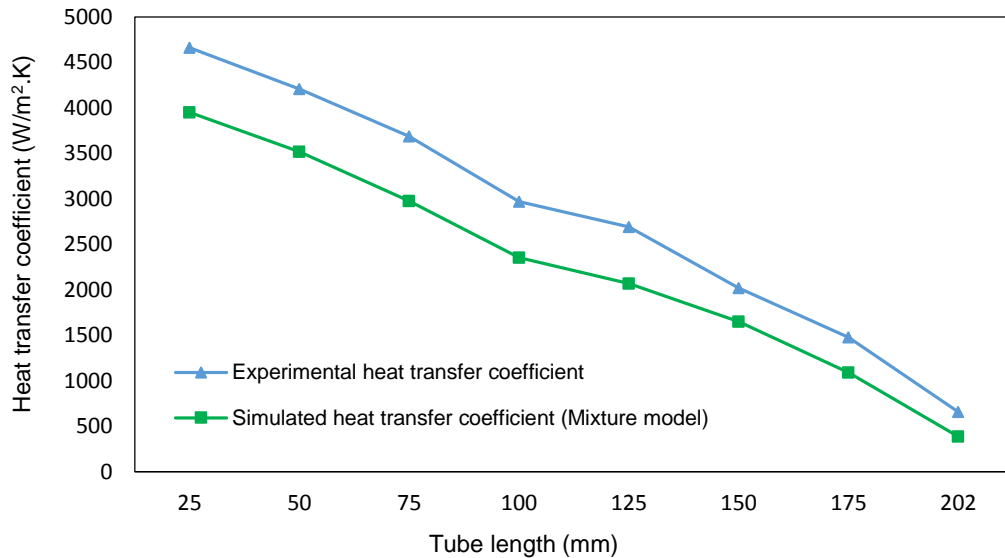
Fig. 13. Comparison of simulated and experimental heat transfer coefficient

V. CONCLUSIONS

In this paper, two phase condensation heat transfer of refrigerant R134a is simulated using mixture multiphase model, k-ω (SST) turbulence model, and Lee (evaporation-condensation) mass transfer model with variable surface heat flux defined on the tube surface. The simulation results for heat transfer coefficient, volume fraction of liquid and vapor phases, temperature, and velocity distribution are obtained which showed good agreement with the experimental data available, due to implementation of variable surface heat flux boundary conditions unlike literature available where constant surface heat flux is considered at the tube surface. The results for simulated and experimental heat transfer coefficient were compared and analyzed which indicated that mixture model better predicted the two phase in tube condensation flow of refrigerant R134a. It was also noted that heat transfer coefficient gets decreased along the length of the tube as the vapor quality decreased due to increase of condensate film thickness downstream causing increased thermal resistance. Flow velocity and surface tension effects both effected the simulated heat transfer coefficient results due to increased turbulence and interface shear stresses between the vapor-liquid phases which caused the condensate layer to become thinner along the flow direction thereby resulted in increased convection downstream.

VI. REFERENCES

[1]   D. Zhang, G. Li, Y. Liu, and X. Tian, "Simulation and experimental studies of R134a flow condensation characteristics in a pump-assisted separate heat pipe," *Int. J. Heat Mass Transf.*, vol. 126, pp. 1020–1030, 2018.

[2]   S. M. Sami and J. Grell, "Prediction of two-phase condensation characteristics of some alternatives to R-22 inside air/refrigerant enhanced surface tubing," *Int. J. Energy Res.*, vol. 24, no. 14, pp. 1277–1290, Nov. 2000.

[3]   J. López, H. Pineda, D. Bello, and N. Ratkovich, "Study of liquid-gas two-phase flow in horizontal pipes using high speed filming and computational fluid dynamics," *Exp. Therm. Fluid Sci.*, vol. 76, pp. 126–134, 2016.

[4]   H. Lee, I. Mudawar, and M. M. Hasan, "Flow condensation in horizontal tubes," *Int. J. Heat Mass Transf.*, vol. 66, pp. 31–45, 2013.

[5]   J. P. Meyer, J. Dirker, and A. O. Adelaja, "Condensation heat transfer in smooth inclined tubes for R134a at different saturation temperatures," *Int. J. Heat Mass Transf.*, vol. 70, pp. 515–525, 2014.

[6]   R. Rabiee, B. Rajabloo, M. Désilets, and P. Proulx, "Heat transfer analysis of boiling and condensation inside a horizontal heat pipe," *Int. J. Heat Mass Transf.*, vol. 139, pp. 526–536, 2019.

[7]   D. Juggurnath *et al.*, "NUMERICAL SIMULATIONS OF CONDENSING R134a FLOWS IN HORIZONTAL PIPES," in *4th Thermal and Fluids Engineering Conference*, 2019, pp. 413–422.

[8]   E. Da Riva and D. Del Col, "Numerical simulation of laminar liquid film condensation in a horizontal circular minichannel," *J. Heat Transfer*, vol. 134, no. 5, pp. 1–8, 2012.

[9]   G. Fronk Brian, *Encyclopedia of Two-Phase Heat Transfer and Flow I*, vol. 2. WORLD SCIENTIFIC, 2015.

[10]   R. Suliman, L. Liebenberg, and J. P. Meyer, "Improved flow pattern map for accurate prediction of the heat transfer coefficients during condensation of R-134a in smooth horizontal tubes and within the low-mass flux range," *Int. J. Heat Mass Transf.*, vol. 52, no. 25–26, pp. 5701–5711, 2009.

[11]   G. Fronk Brian, *Encyclopedia of Two-Phase Heat Transfer and Flow I*, vol. 2. WORLD SCIENTIFIC, 2015.

[12]   J. B. Campbell *et al.*, "Two-Phase Cooling Method Using the R134a Refrigerant to Cool Power Electronic Devices," vol. 43, no. 3, pp. 648–656, 2007.

[13]   S. M. A. N. R. Abadi, J. P. Meyer, and J. Dirker, "Numerical simulation of condensation inside an inclined smooth tube," *Chem. Eng. Sci.*, vol. 182, pp. 132–145, 2018.

[14]   S. M. A. Noori Rahim Abadi, J. P. Meyer, and J. Dirker, "Effect of inclination angle on the condensation of R134a inside an inclined smooth tube," *Chem. Eng. Res. Des.*, vol. 132, pp. 346–357, 2018.

[15]   "Computational Fluid Dynamics a Practical Approach Jiyuan Tu pdf - Books Free." [Online]. Available: https://www.booksfree.org/computational-fluid-dynamics-a-practical-approach-jiyuan-tu-pdf/. [Accessed: 20-Nov-2020].

[16]   ANSYS Fluent Theory Guide, "ANSYS Fluent Theory Guide," *ANSYS Inc., USA*, vol. 15317, no. November, pp. 724–746, 2013.

[17]   "ANSYS Fluent Theory Guide," vol. 15317, no. November, pp. 724–746, 2013.

[18]   F. Toapanta-ramos, P. D. C. Nieto-londoño, and W. Quitiaquez, "Ansys CFD Analysis of the Thermal Behavior of Coolant 134a in a Condenser within a Refrigeration Cycle," no. May 2020, 2018.

[19]   "Ansys fluent 18 tutorial guide.pdf | Trademark | Computing." [Online]. Available: https://www.scribd.com/document/408997965/ansys-fluent-18-tutorial-guide-pdf. [Accessed: 19-Sep-2020].

Preliminary Evaluation of Bajawar Chromite Ore for Up-Gradation Purpose

Engr. Raza Ullah [A], Engr. Khaleeq Ahmed [B], and Dawar Abbass [C]

[A, B, C]=*Department of Chemical Engineering, Pakistan Institute of Engineering & Applied Sciences, Islamabad, Pakistan*

Abstract— **Chromium has significant economic and industrial importance because of its refractory and alloying properties. Almost all potential chromite deposits are associated with ultramafic-mafic igneous rocks but there are alluvial placer deposits of the sedimentary environment with low-grade as well. In Pakistan, chromite deposits are known from the ophiolitic sequence and are being targeted for potential mineral exploration. Several mineral resources could be transformed into economic-mineral deposits with the careful characterization of mineral resources. Therefore, it is very important to carry out detailed characterization before the application of any processing technique.**

The prime focus of the research is the characterization of Bajawar chromite ore Khyber Pakhtunkhwa (KP), Pakistan. Five tools that include Thin-section study, Energy Dispersive X-ray analysis, X-ray Diffraction (XRD), Scanning Electron Microscopy (SEM), and X-ray Fluorescence (XRF) were utilized in research to evaluate the precise characterization of Bajawar chromite. Characterization study identifies the ore body as a low-grade mineral deposit (Refractory grade) as the ore body shows the Cr_2O_3 content 35.6% and chemical grade based on Cr/Fe is 2.1. High concentrations of silica and iron oxide have been observed from the Bajawar chromite ore body. Crystal system, hardness, porosity, and average grain size combined with the results obtained from the tools used for characterization suggest the usage of shaking-table separation technique followed by a magnetic separator to upgrade Bajawar chromite ore and to make it marketable.
.

Keywords— **Characterization; Magnetic Separator; Ophiolitic Sequence; Shaking Table.**

I. INTRODUCTION

Pakistan contains Precambrian to recent rock and has a high potential of metallic and non-metallic mineral resources deposits such as copper, gold, silver, iron, radioactive minerals, lead-zinc, chromite, while low potential deposits are antimony, magnesite, Sulphur, mica, feldspar, etc [1]. In our country, Pakistan, people just searching for the deposit, observing that the deposit is of some economic value, mine it and sold to higher international companies at low prices. High-grade ore deposits are depleted day by day. Most of the Pakistani ore deposits are low-grade which does not fulfil the demands of the marketable end product. Several low-grade mineral resource deposits could be transformed into economic-mineral deposits with careful characterization. The achievement of high-grade ore directly depends on the accurate and precise characterization study. Poor characterization of ore leads to failure in the production of marketable products. Therefore, it is very important to carry out detailed characterization before the application of any processing technique [2]. The rapid advancement in micro-analytical technology has made it easy and possible to characterize the ore/mineral. Now Industries are awarded about pre-processing studies and beneficiation. Minerals processing sometimes also called ore dressing is based on these characterization studies. Based on the knowledge obtained after characterization, the owner satisfying and compel to take practical steps towards the up gradation of low-grade deposits.

Characterization of ore is the most important step before going to perform mineral processing. In the characterization of mineral deposits may involve the determination of both quantitative and qualitative

analyses such as the grade of ore, impurity content, chemical composition, crystal habit, grain size, shape, density, porosity, and other features. These characterizations of the mineral deposits give proper guidelines for the selection of mining methods, beneficiation techniques, the feasibility of the deposits, and economical evaluation of the mineral deposit [3-5].

The primary objective of this research was to provide comprehensive data on the chemical composition of the deposit. These may include general engineering, metallurgical properties, the mineralogical and elementary composition of the local chromite ore from Bajawar (Ex-FATA) area. All these investigations are only possible by characterization. Five tools are used for this characterization. Detail of each tool is discussed in the subsequence section of the paper.

Chromite is the only ore of chromium that is used commercially in the metallurgical industries [6]. The metallurgical usability of the chromite ore depends upon the chromium (Cr) and iron (Fe) ratio rather than Cr percentage. Almost all potential chromite deposits are associated with ultramafic-mafic igneous rocks but there are alluvial placer deposits of the sedimentary environment with low-grade as well [7]. Chromium is the most important element of modern industries and it is a raw material for the production of stainless steel and ferrochrome alloy. About 80% of the chromium ores are used in the stainless steel industry [8]. Chromites are classified into three classes based on Cr and Fe element ratio. Metallurgical grade (high-grade) contains 46-48% chromium oxide and the ratio of Cr to Fe is 3:1. Chemical grade of chromite contains 40-46% chromium oxide and 1.5-2.1 is Cr and Fe ratio. Refractory grade of chromite contains 30-40% chromium oxide [9].

II. MATERIALS AND METHODOLOGY

A. SAMPLE COLLECTION AND PREPARATION

Samples were collected from "Charmang" area located near Durand Line, Bajawar Agency, KP, Pakistan. Samples were taken from the top surface of the deposit at some distance apart from each other so that they are not biased. The collected chromite ore samples were then subjected to sample preparation process i.e. cutting and breaking, crushing, grinding, and sieve analysis. Crushing and grinding were performed in the "Mineral Processing Laboratory" Department of Mining Engineering, UET Peshawar. The required samples for XRD and XRF were prepared after coning and quartering. Chips samples for SEM, EDX and Thin section were prepared in "Rock Cutting Lab" Department of Geology, University of Peshawar.

For detailed characterization of Bajwara chromite ore to determine the average grade, shape, and tonnage of the total deposit. It is necessary to take ore samples with a regular interval at 10m distance along the strick and dip with some depth. The geological and value continuity of the deposit can change with depth [10].

B. CHARACTERIZATION TECHNIQUE

1)Thin section study

Thin section slide is studied to determine the texture of the chromite and mineral identification of ore in the samples. This study is carried out in "sedimentology lab" of 'National Center of Excellence in Geology' of University of Peshawar by using Optical Microscope with 5x lenses.

2)Scanning Electron Microscope (SEM) Analysis

Scanning Electron Microscope is used for morphological and mineralogical characterization of ore samples to determine crystal size, shape, position, and cry form of the minerals [11]. Here SEM is used to find porosity of ore, shape, and form of the chromite crystals in samples. Attaching of Energy Dispersive X-Ray Analyzer (EDX or EDA) device with SEM is used for the element's identification and quantitative compositional information. It is a non-distractive and bulk analysis method of minerals [12]. The EDX technique for the current research is used to determine the elemental composition of the ore sample.

3)X-Rays Flourances Analysis

X-ray fluorescence (XRF) is the non-destructive elemental analysis technique used for minerals and solid material to determine the presence or absence of the elements whose atomic number is greater than 3 and their

relative percentage in the samples [13]. In the current research, XRF is used to determine the elemental composition of the chromite ore.

4)X-Rays diffraction

X-Rays diffraction (XRD) is a quantitative calculation of the minerals in the sample. It is most suitable when studying small scale variations in the mineralogy. It is one of the standard methods and techniques used for the investigations of industrial mineral and products [32]. For the same purpose, XRD is used in this research.

III. RESULTS AND DISCUSSIONS

A. THIN SECTION STUDY

Thin section study revealed that the black and brownish grains in Fig. 1 -A, B, C, & D are chromite which is opaque in both plan and cross light. The white grains in Fig. 1- A, B, C, & D is quartz, while the greenish grain is serpentine i.e. serpentinization has been done by the reaction of olivine with water [14]. The lowest grain size is 0.31mm, the largest grain size is 3.15 mm and the average grain size 1.15mm. The grain shape of this chromite is mostly tabular i.e. plate-like having one shorter and one longer dimension. Some of them are almost equant but they are rare. The Bajawar chromite is hypo crystalline i.e. it includes both crystals and glass.
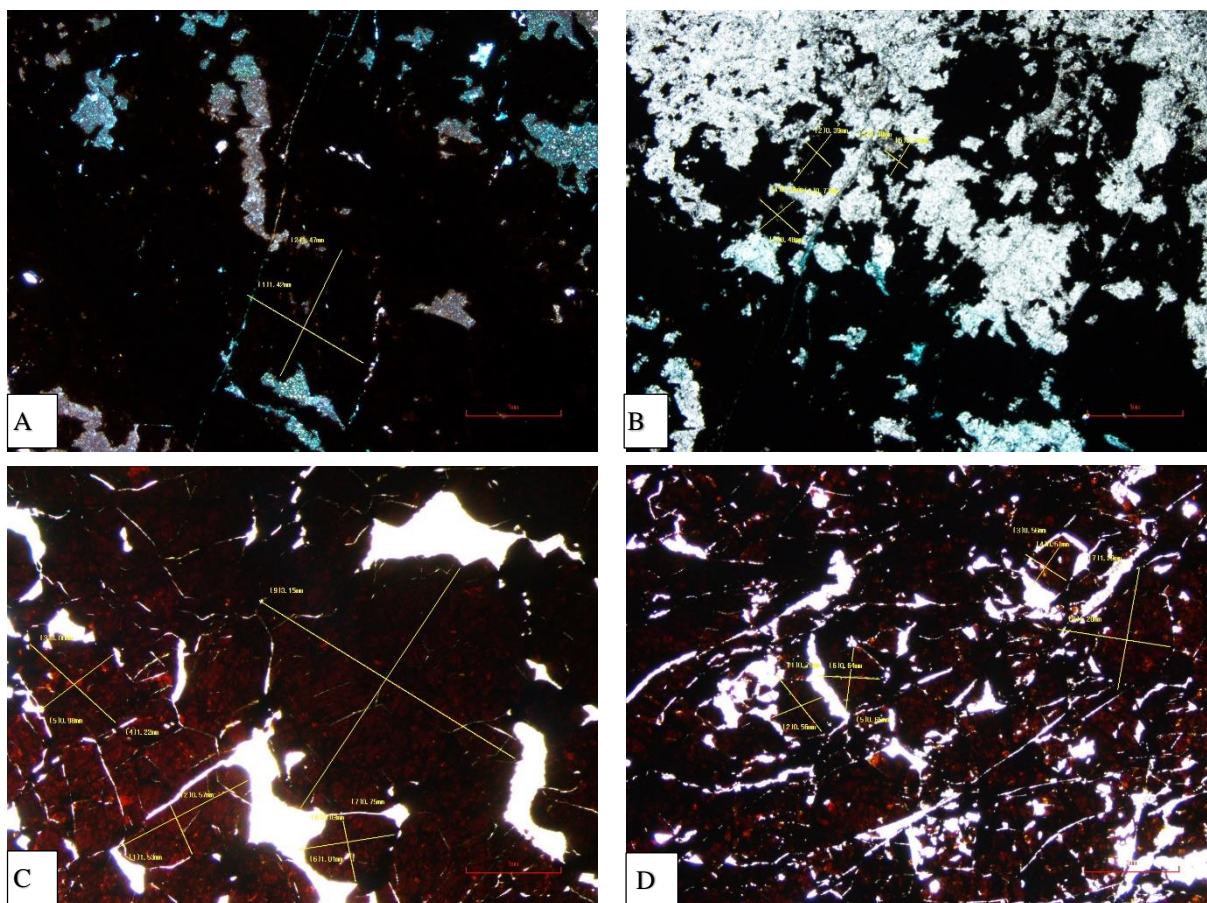
Fig. 1 Thin sections under Optical microscope

B. SEM-EDX analysis

SEM is used to determine the morphology and porosity of the Bajawr chromite ore. Microphotographs Bajawar chromite ore is taken by SEM which revealed that the crystal perfection is not well developed as shown in Fig. 2-B so it is in between euhedral and anhedral. The porosity of representative samples is determined from the image of the SEM by "Average Area method" i.e. Porosity = Area of Pores in the image/ Area of total solid

crystals in Fig. 2 SEM images for porosity and morphology. A. Porosity = No of pore block 450 / No of total block 3588 = 0.125, 0.125 * 100 = 12.5 %.

RESULT OF FIVE SPECTRA OF EDX IS SUMMARIZED IN

Element	Spectra 1		Spectra 2		Spectra 3		Spectra 4		Spectra 5		Overage %	
	Wt%	At%	Wt%	At%	Wt%	At%	Wt%	At%	Wt%	At%	Wt%	At%
C K	2.08	4.12	1.60	3.13	1.82	3.57	2.55	4.79	0.0	0.0	1.61	3.122
O K	39.60	58.78	40.97	60.02	40.15	59.07	42.52	60.00	40.32	61.30	40.712	59.834
Mg K	10.76	10.51	11.09	10.69	11.23	10.88	12.09	11.23	10.35	10.36	11.104	10.734
Al K	5.11	4.50	5.59	4.85	5.33	4.65	5.93	4.96	5.61	5.06	5.514	4.806
Si K	6.65	5.62	7.35	6.14	7.54	6.32	7.95	6.39	6.68	5.79	7.234	6.048
Ca K	2.85	1.69	2.83	1.66	3.00	1.76	2.10	1.18	3.13	1.90	2.782	1.638
Ti K	0.32	0.16	0.0	0.0	0.31	0.15	0.0	0.0	0.41	0.21	0.208	0.104
Cr K	23.69	10.82	21.99	9.91	22.44	10.16	19.54	8.48	24.76	11.58	22.484	10.19
Fe K	8.94	3.80	8.57	3.60	8.18	3.45	7.32	2.96	8.74	3.81	8.35	3.524
Total	100	100	100	100	100	100	100	100	100	100	100	100

TABLE. II. BAJAWAR CHROMITE ORE CONTAINS CARBON, POTASSIUM, MAGNESIUM, ALUMINUM, SILICON, CALCIUM, TITANIUM, CHROMIUM, AND IRON. WEIGHT (WT) % AND ATOMIC (AT) % OF EACH ELEMENT IN FIVE SPECTRA ARE SHOWN IN

C.   TABLE. II. Elemental composition of Bajawar chromite ore by SEM-EDX EDX gives the elemental composition of the chromite ore sample and to convert this elemental result into their oxide form, some basic formulas in the Excel are used e.g. (Elemental per cent/ Conversion Number = Oxide Percent). The conversion number is a standard value given for each element.   X-RAYS FLOURANCES ANALYSIS

X-RAY FLUORESCENCE (XRF) IS THE NON-DESTRUCTIVE ELEMENTAL ANALYSIS TECHNIQUE USED FOR MINERALS AND SOLID MATERIAL TO DETERMINE THE PRESENCE OR ABSENCE OF THE ELEMENTS WHOSE ATOMIC NUMBER IS GREATER THAN 3 AND THEIR RELATIVE PERCENTAGE IN THE SAMPLES [13]. THE ELEMENTAL COMPOSITION

TABLE. III ELEMENTAL COMPOSITION OF BAJAWAR CHROMITE ORE (XRF)

TABLE. IV MINERALOGICAL COMPOSITION OF BAJAWAR CHROMITE ORE.

Elemental composition of Bajawar chromite ore (XRF) of the Bajawar chromite ore shown in Table 3. Percentage of chromium is less than 27 which is low-grade chromite ore. The ratio of chromium to iron is 1.5 so Bajawar chromite ore is in the range of refractor grade.

S.NO	Analyte	Result	int.(cps/uA)	oxides	Conversion	% of mineral in
1	Cr	25.422 %	3062.8570	Cr_2O_3	1.4615	37.154253
2	Fe	16.099%	706.8174	Fe_2O_3	1.4297	23.0167403
3	Al	18.115%	1.3735	Al_2O_3	1.8895	34.2282925
4	Si	14.232%	3.9581	SiO_2	2.1392	30.4450944
5	Ca	5.766%	35.8657	CaO	1.3992	8.0677872
6	Ni	3.476%	19.1908	NiO	1.2725	4.42321
7	K	2.250%	2.8519	K_2O	1.2046	2.71035
8	Ti	2.203%	8.9626	TiO_2	1.6681	3.6748243
9	V	1.179%	7.9796	V_2O_5	1.7852	2.1047508
10	Zn	1.090%	5.1126	ZnO	1.2448	1.356832
11	Ir	1.073%	1.8456	IrO	1.0832	1.1622736
12	Bi	1.065%	2.4702	Bi_2O_5	1.1914	1.268841
13	Cu	0.031%	1.5097	CuO	1.2518	0.0388058

(Overlaid table)

Oxide	MgO	Al_2O_3	SiO_2	CaO	TiO_2	Cr_2O_3	FeO
Percentage	19.9702	11.30542	16.80565	4.22467	0.375603	35.66122	11.6573

TABLE. I SHOWS THE OXIDE COMPOSITION OF THE BAJAWAR CHROMITE ORE. THIS ORE IS IN THE RANGE OF REFRACTORY GRADE CHROMITE (Cr_2O_3, 35.66%) [9]. WHERE K IN THE FIRST COLUMN OF

TABLE. II represent the shell from which characteristic rays emitted. Four spectral graphs of the EDX are shown in Fig. 3.
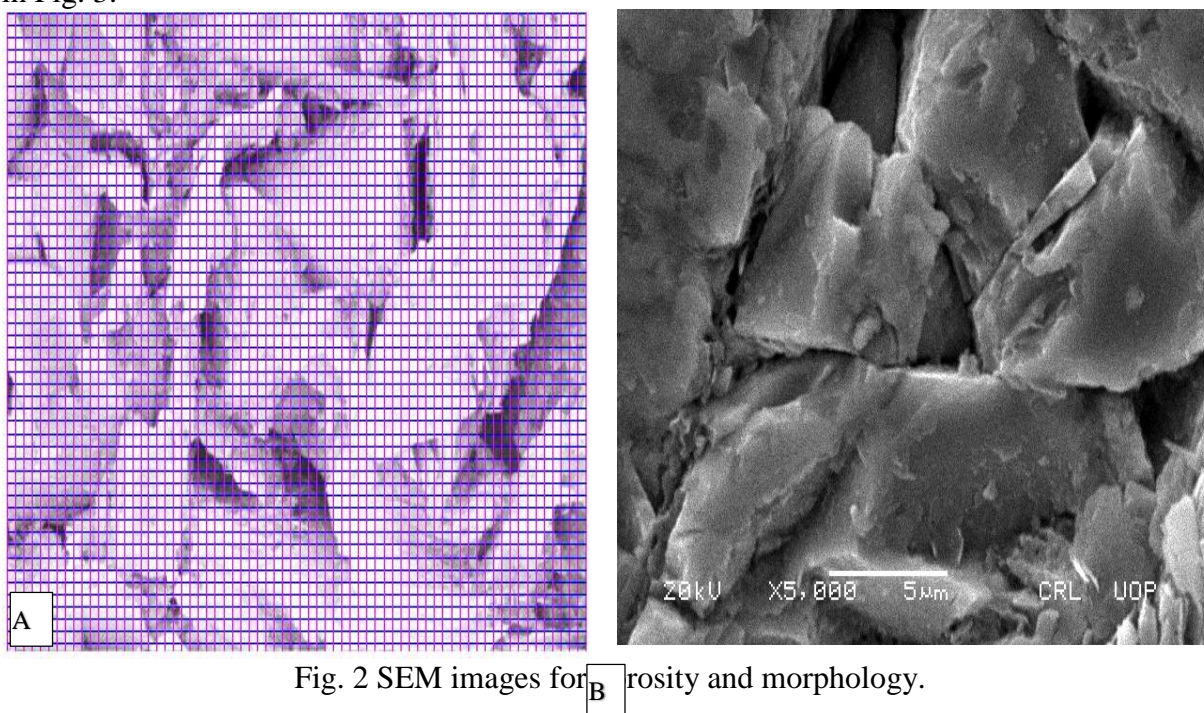
Fig. 2 SEM images for porosity and morphology.
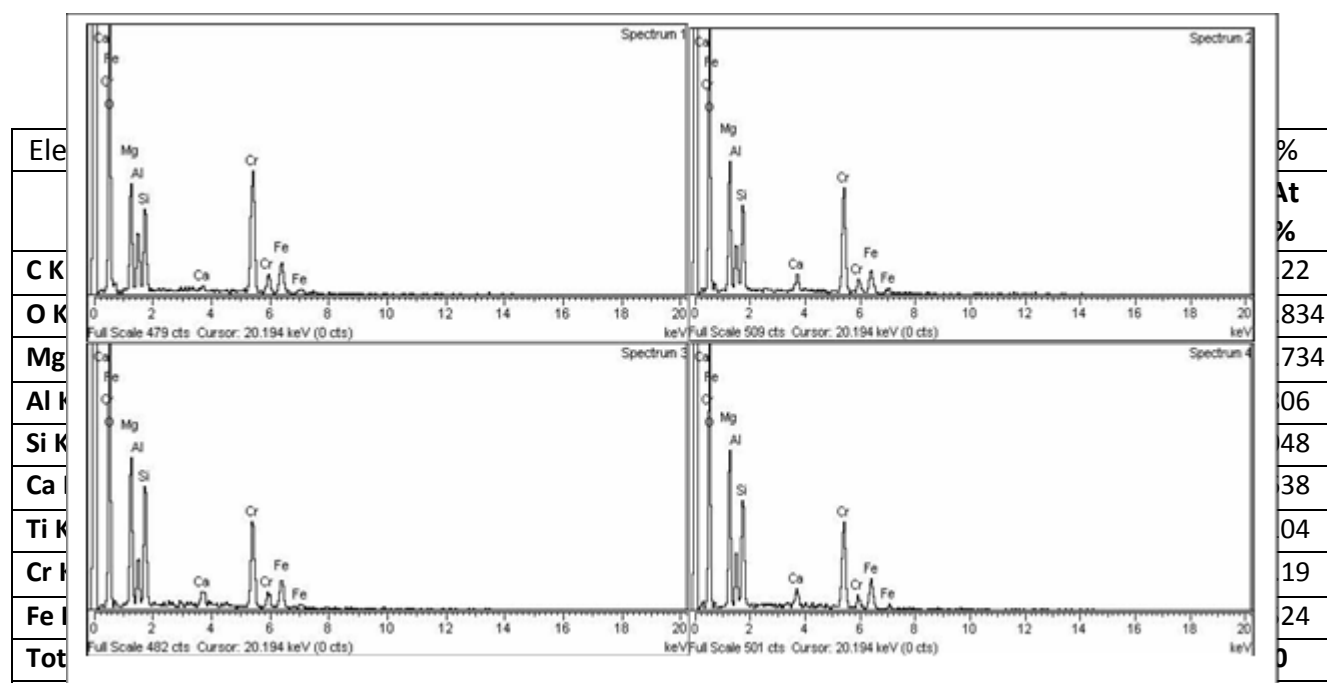
Fig. 3 Four spectra of EDX

D. X-RAYS FLOURANCES ANALYSIS

X-RAY FLUORESCENCE (XRF) IS THE NON-DESTRUCTIVE ELEMENTAL ANALYSIS TECHNIQUE USED FOR MINERALS AND SOLID MATERIAL TO DETERMINE THE PRESENCE OR ABSENCE OF THE ELEMENTS WHOSE ATOMIC NUMBER IS GREATER THAN 3 AND THEIR RELATIVE PERCENTAGE IN THE SAMPLES [13]. THE ELEMENTAL COMPOSITION

TABLE. III ELEMENTAL COMPOSITION OF BAJAWAR CHROMITE ORE (XRF)

TABLE. IV MINERALOGICAL COMPOSITION OF BAJAWAR CHROMITE ORE.

Elemental composition of Bajawar chromite ore (XRF) of the Bajawar chromite ore shown in Table 3. Percentage of chromium is less than 27 which is low-grade chromite ore. The ratio of chromium to iron is 1.5 so Bajawar chromite ore is in the range of refractor grade.

TABLE. I OXIDE COMPOSITION OF BAJAWAR CHROMITE ORE

Oxide	MgO	Al_2O_3	SiO_2	CaO	TiO_2	Cr_2O_3	FeO

TABLE. II ELEMENTAL COMPOSITION OF BAJAWAR CHROMITE ORE BY SEM-EDX

S.NO	Analyte	Result	int.(cps/uA)	oxides	Conversion	% of mineral
1	Cr	25.422 %	3062.8570	Cr2O3	1.4615	37.154253
2	Fe	16.099%	706.8174	Fe2O3	1.4297	23.0167403
3	Al	18.1..	..735	Al2O3		
4	Si	14.23%	..81	SiO2		
5	Ca	5.766 %	35.8657	CaO	1.3992	8.0677872
6	Ni	3.476 %	19.1908	NiO	1.2725	4.42321
7	K	2.250 %	2.8519	K2O	1.2046	2.71085
8	Mg	2.203 %	8.9626		1.6681	3.6748243
9	V	1.179 %	7.9796	V2O5	1.7852	2.1047508
10	Zn	1.090 %	5.1126	ZnO	1.2448	1.356832
11	Ir	1.073 %	1.8456	IrO	1.0832	1.1622736
12	Bi	1.065 %	2.4702	Bi2O3	1.1914	1.268841
13	Cu	0.031 %	1.5097	CuO	1.2518	0.0388058

Element	Spectra 1		Spectra 2		Spectra 3		Spectra 4		Spectra 5		Average %	
	Wt%	At%	Wt%	At%	Wt%	At%	Wt%	At%	Wt%	At%	Wt %	At %
C K	2.08	4.12	1.60	3.13	1.82	3.57	2.55	4.79	0.0	0.0	1.61	3.122
O K	39.60	58.78	40.97	60.02	40.15	59.07	42.52	60.00	40.32	61.30	40.712	59.834
Mg K	10.76	10.51	11.09	10.69	11.23	10.88	12.09	11.23	10.35	10.36	11.104	10.734
Al K	5.11	4.50	5.59	4.85	5.33	4.65	5.93	4.96	5.61	5.06	5.514	4.806
Si K	6.65	5.62	7.35	6.14	7.54	6.32	7.95	6.39	6.68	5.79	7.234	6.048
Ca K	2.85	1.69	2.83	1.66	3.00	1.76	2.10	1.18	3.13	1.90	2.782	1.638
Ti K	0.32	0.16	0.0	0.0	0.31	0.15	0.0	0.0	0.41	0.21	0.208	0.104
Cr K	23.69	10.82	21.99	9.91	22.44	10.16	19.54	8.48	24.76	11.58	22.484	10.19
Fe K	8.94	3.80	8.57	3.60	8.18	3.45	7.32	2.96	8.74	3.81	8.35	3.524
Total	100	100	100	100	100	100	100	100	100	100	100	100

E.   X-RAY DIFFRACTION

X-Rays diffraction (XRD) is the determination of the minerals in the ore sample. It is the most suitable technique used for studying small scale variations in the mineralogy of the ore. It is one of the standard methods and techniques used for the investigations of mineral [15]. Result of XRD of the Bajawar ore is summarized in TABLE. IV. This result of XRD revealed that the Percentage of the chromite ore is less than 40 so it occurs in the range of refractory grade [9]. Minerals in the Bajawar chromite ore in the pie charts form are shown in Fig. 4 (B).

TABLE. III Elemental composition of Bajawar chromite ore (XRF)

TABLE. IV Mineralogical composition of Bajawar chromite ore.

S.NO	Analyte	Result	int.(cps/uA)	oxides	Conversion	% of mineral in
1	Cr	25.422 °/°	3062.8570	Cr_2O_3	1.4615	37.154253
2	Fe	16.099°/°	706.8174	Fe_2O_3	1.4297	23.0167403
3	Al	18.115°/°	1.3735	Al_2O_3	1.8895	34.2282925
4	Si	14.232 °/°	3.9581	SiO_2	2.1392	30.4450944
5	Ca	5.766 °/°	35.8657	CaO	1.3992	8.0677872
6	Ni	3.476 °/°	19.1908	NiO	1.2725	4.42321
7	K	2.250 °/°	2.8519	K_2O	1.2046	2.71035
8	Ti	2.203 °/°	8.9626	TiO_2	1.6681	3.6748243
9	V	1.179 °/°	7.9796	V_2O_5	1.7852	2.1047508
10	Zn	1.090 °/°	5.1126	ZnO	1.2448	1.356832
11	Ir	1.073 °/°	1.8456	IrO	1.0832	1.1622736
12	Bi	1.065 °/°	2.4702	Bi_2O_5	1.1914	1.268841
13	Cu	0.031 °/°	1.5097	CuO	1.2518	0.0388058

Index	Constituents	Formula sum	Amount (%)	Crystal System	Calculated density(g/cm³)
A	Chromite	Al0.723 Cr1.125 Fe0.687 Mg0.444 Ni0.002 O4 Ti0.014 Zn0.005	39.5	cubic	4.494
B	$Al_2(H_2P\,O_4)_3$ $(H_2O)_6(P\,O_4)$	$Al_2\,H_{18}\,O_{22}\,P_4$	30.3	Trigonal (hexagonal axes)	2.125
C	Wroewolfeite	$Cu_4\,H_{10}\,O_{12}\,S$	19.5	Monoclinic	3.320
D	$As_2(Fe(CO)_3)_3$	$C_9\,As_2\,Fe_3\,O_9$	10.7	orthorhombic	2.400
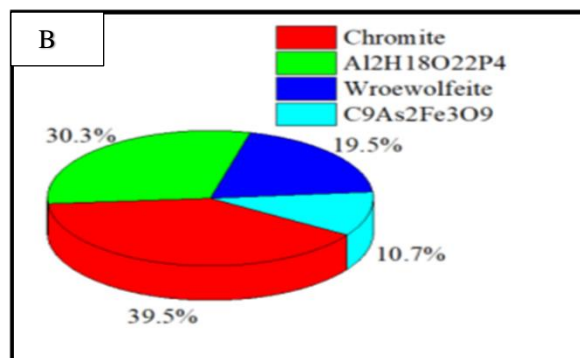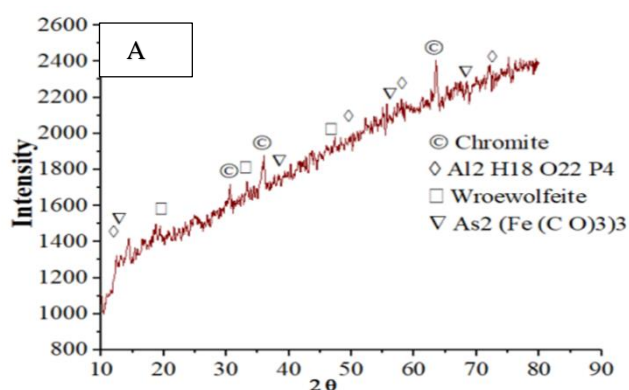
Fig. 4 (A) XRD graph of chromite ore (B) Pei chart of mineral in Bajawar chromite ore

IV. CONCLUSIONS

Following conclusions were drawn for all the characterization techniques carried out for chromite ore:

1. Thin section study reveals that there are chromite grains associated with traces of serpentine and olivine.
2. From SEM analysis, it has been concluded that the porosity of Bajawar chromite is 12.5% and the crystal system is isometric
3. The EDX analysis shows that it has 22.5% chromium with maximum content of iron and Magnesium i.e. 8.35% and 11.1%.
4. The conversion of EDX results to oxides form confirms that ore has SiO_2 -16.8%, Cr_2O_3 -35.6%, FeO - 11.6% which is low-grade chromite ore.
5. The XRD analysis display that the ore contains four major minerals i.e. $Al_2(H_2PO_4)_3(H_2O)_6(PO_4)$ – 30.3%, Chromite – 39.5%, $As_2(Fe\,(CO)_3)_3$ – 10.7%, and Wroewolfeite – 19.5%.
6. The XRF analysis shows the chromium content in Bajawar chromite ore is 25.4% along with impurities of iron, silicon, and aluminum.

A. Bajawar Chromite Grade

According to Cr/Fe which is almost 2.1/1, chromite ore can be classified into chemical-grade chromite but according to the percentage of chromium oxide in the ore which is almost 36%, it can be categorized to low-grade chromite ore.

V. RECOMMENDATIONS

1. The chromite ore of Bajawar area may be characterized using some other methods like Electron Probe Microanalysis (EPMA), Laser ablation–inductively coupled plasma–mass spectrometry (LA-ICP-MS) etc.
2. The chromite ore of Bajawar is low grade according to Cr_2O_3 and type of chemical grade according to Cr/Fe. It can be upgraded to a high grade (marketable end product) by using various up-gradation techniques.
3. The proposed up-gradation techniques for Bajawar chromite ore are Shaking table followed by Magnetic Separation to produce the marketable end product.

References

[1] M. S. Malkani, A. M. K. MH, S. Tariq, F. S. Buzdar, G. Khan, and J. Faiz, "Mineral Resources of Pakistan-an update," Lasbela University Journal of Science & Technology, vol. 5, pp. 90–114, 2016.

[2] S. K. Tripathy, Y. R. Murthy, V. Singh, and N. Suresh, "Processing of ferruginous chromite ore by dry high-intensity magnetic separation," Mineral Processing and Extractive Metallurgy Review, vol. 37, no. 3, pp. 196–210, 2016.

[3] O. J. Kolawole, A. A. Akanni, B. S. Ameenullahi, and A. A. Adediran, "Preliminary Characterisation of Iron Ores for Steel Making Processes," Procedia Manufacturing, vol. 35, pp. 1123–1128, Jan. 2019, doi: 10.1016/j.promfg.2019.07.020.

[4] N. J. Cook, "Mineral characterisation of industrial mineral deposits at the Geological Survey of Norway: a short introduction," NORGES GEOLOGISKE UNDERSOKELSE, vol. 436, pp. 189–192, 2000.

[5] J. J. Kiptarus, A. M. Muumbo, A. B. Makokha, and S. K. Kimutai, "Characterization of selected mineral ores in the Eastern Zone of Kenya: Case study of Mwingi North Constituency in Kitui County," International Journal of Mining Engineering and Mineral Processing, vol. 4, no. 1, pp. 8–17, 2015.

[6] S. Subandrio, W. Dahani, M. Alghifar, and T. T. Purwiyono, "Enrichment Chromite Sand Grade Using Magnetic Separator," in IOP Conference Series: Materials Science and Engineering, 2019, vol. 588, no. 1, p. 012033.

[7] S. K. Tripathy, V. Singh, and Y. Ramamurthy, "Improvement in Cr: Fe ratio of Indian chromite ore for ferro chrome production," International Journal of Mining Engineering and Mineral Processing, vol. 1, no. 3, pp. 101–106, 2012.

[8]   Y. R. Murthy, S. K. Tripathy, and C. R. Kumar, "Chrome ore beneficiation challenges & opportunities–A review," Minerals Engineering, vol. 24, no. 5, pp. 375–380, 2011.

[9]   A. K. Bhandary, P. Gupta, S. Mukherjee, M. G. Chaudhuri, and R. Dey, "Beneficiation of Low Grade Chromite Ore and Its Characterization for the Formation of Magnesia-Chromite Refractory by Economically Viable Process," International Journal of Chemical and Molecular Engineering, vol. 10, no. 8, pp. 1096–1104, 2016.

[10]   S. K. Haldar, Mineral exploration: principles and applications. Elsevier, 2018.

[11]   P. Gottlieb et al., "Using quantitative electron microscopy for process mineralogy applications," JOM, vol. 52, no. 4, pp. 24–25, Apr. 2000, doi: 10.1007/s11837-000-0126-9.

[12]   D. E. Newbury* and N. W. Ritchie, "Is scanning electron microscopy/energy dispersive X-ray spectrometry (SEM/EDS) quantitative?," Scanning, vol. 35, no. 3, pp. 141–168, 2013.

[13]   Z. W. Chen, W. M. Gibson, and H. Huang, "High Definition X-Ray Fluorescence: Principles and Techniques," X-Ray Optics and Instrumentation, vol. 2008, p. 318171, May 2008, doi: 10.1155/2008/318171.

[14]   A. R. Philpotts, Petrography of igneous and metamorphic rocks. USA: Pearson College Division, 1989.

[15]   K. Macchiarola, U. Koenig, L. Gobbo, I. Campbell, A. M. McDonald, and J. Cirelli, "Modern x-ray diffraction techniques for exploration and analysis of ore bodies," in 5th. Decen. Int. Conf. Miner. Explo., 2007, pp. 1007–1018.

CHARACTERIZATION OF KOHISTAN CHROMITE ORE FOR THE SELECTION OF A BENEFICIATION TECHNIQUE

1'Faizan Ullah', 2'Ishaq Ahmad, 3'Rashid Minhas

1, 2, 3 Mining Engineering Department UET

Peshawar, Email:1faizanullah631@gmail.com

Abstract-Chromite is metallic mineral based on chromium and is the only available source of chromium metal. Chromium is largely used as alloying elements for the production of stainless steels. In the present study, Chromite samples collected from Kohistan of Khyber Pakhtunkhwa (KPK) Pakistan were investigated using thin section studies by polarizing microscope, X-ray florescence (XRF), X-ray diffraction (XRD), scanning electron microscope (SEM) and energy dispersive spectroscopy (EDS).In thin section studies it was confirm that chromite occur at a range of (+200-400)µm. The major phases identified in these samples by XRD are of Iron Magnesium Chromium Oxide with Silicon Oxide and Magnesium Silicate. The chemical analysis through XRF confirmed that the samples comprise 51.41% Cr_2O_3 along with 26.21% Fe_2O_3 and 25.45% SiO2. It was concluded that the chromite can be treated by gravity separation techniques (Shaking Table). Furthermore, it is recommended that the detail characterization of the area may be investigated with effective laboratory investigation of chemical analysis, mineralogy, morphology etc.

Keywords: characterization, chromite, thin section, XRD, XRF, EDS.

I. INTRODUCTION

Chromite is the primary producer of chromium metal and additives for use in refractory applications. The mineral is categorized by various users on the basis of its physical and chemical characteristics. Chromite is an iron chromium oxide: FeCr2O4. Magnesium can be replace iron in variable concentrations whenever it forms a solid solution with megnesium chromite (MgCr2O4)[1]. Aluminum replacement occurs leading to hercynite (FeAl2O4)[2]. Chromite, a dark - brown cubic mineral belongs to the spinel group, has been the only mineral through which metal chromium and chromium products are formed. Chromium is the primary raw material used in the manufacture of specialized steel and ferrochrome alloys. About 90 percent of the chromite ore extracted is converted by the metallurgical industry to various grades of ferrochrome. The steel industry consuming about80 per cent of ferrochrome produced (typically high-carbon/charge grade) [3]. Chromite also has theoretical composition of 32.0 percent of FeO and 68.0 percent of Cr2O3. In its natural state, it appears in solid state with other minerals in the spinel group, so that the chromite proportion would be less than the theoretical 68%.[4] The most important application of chromite is in the manufacture of high-strength alloys and alloys that are heat, abrasion, corrosion and oxidation resistant. About half of all chromite production goes to the manufacturing of stainless steel. Chromium chemicals are used for various purposes; pigments, photography and plating are but a limited. Chromite can be used as a refractory in the manufacturing of steel, zinc, glass and cement [5].

I.I CHROMITE DEPOSITS OF PAKISTAN

Chromite is an oxide mineral that contains Iron, Oxygen and Chromium [(Fe, Mg) Cr2O4]. It occurs in mafic and ultramafic rock deposits produced by concentrations of igneous rocks, such as norite, called stratiform deposits, while the podiform deposits comprise metamorphic rocks. Due to the weathering of laterite soil, i.e. formed over peridotite and chromite-bearing rocks, chromite can also be present in beach sands[6]. Coulson (1940) referred to chromite in Pakistan as first mentioned by Vredenburg (1901)[7] and its mining began in 1903 in the Khanozai region and was spread to Muslimbagh in 1915 and began in the early twenties in the Ms Salwat area, 29 km south of Muslimbagh. It is now mainly being mined in Balochistan and Khyber Pakhtunkhwa. It occurs mainly in the belt of the Indus Suture. Kohistan's Sapat mafic-ultramafic complex can contain many chromite. Chromite Deposits are found in Chilas Complex, Sapat Complex, Jijal Complex, Shangle- Mingora, Malakand Agency-Sakhakot (Dargai), Waziristan, Zhob Valley Igneous Complex, Bela and Muslimbagh.

Chilas chromite (Chilas District) is located in the Chilas complex consisting of norites, ultramafics, anorthosites, gabbros and diorites, pyroxene granulite facies. Ultramaphics are dunites with subordinate peridotites, pyroxenites and unusual amphiboles. Jan et al. (1984) represents a systematic similarity to stratiform instead of alpine or concentric complexes, and reported thin chromite layers show Cr2 O3 26 percent, Al2 O3 26 percent, FeO 37 percent and MgO 9 percent.

Besham Jijal chromite, Kohistan is located on the Karakoram highway near Jijal (Kohistan District). The Jijal complex is composed of granet granules and ultramafic rocks. Ultramaphics are dunite, peridotite, diopsidite, vebsterite and chromitite. Numerous numbers of chromite pods and lenses were reported in ultramafic rocks in the northwest region of the Jijal complex.. The Sarhad Development Authority (SDA) reported 0.6mt of ore reserves with Cr2O3 at 40-50 percent, Fe2O3 at 12-18 percent and Cr:Fe at 2.8:1 to 3.6:1. Significant deposits are produced in the vicinity of Jijal, Shungial, Kokial, Taghtai, Gabar, Mani Dara, Khairabad, Jag, Tangai, Chinari, Serai, Lomoto and Kot. Also Identified deposition of nickel in Swat ophiolitic rocks.

Dargai chromite (Malakand District) comprises of ultramafic cumulates composed of harzburgite (80 per cent) and dunite (20 per cent) and mafic cumulates comprising of gabbro with few sheets of serpentine and ultramafic tectonites made up of harzburgite (90 per cent +) and dunite (<10 per cent). Chromite exists as horizontally broad sheets (3-4.5m deep, up to 2km long) confined to the higher part of the complex (Qila deposits), irregularly formed small bodies (< 1m square) uncovered in the western part of the complex and podiform, large and slightly curved deposits with sharp contact (Hiro Shah deposits). (Hiru Shah deposits). The major deposits are in Hiro Shah, Barjo Kanri, Landi Kand, Badasar, and Qila and have been continuously mined. Dargai chromite is higher in iron and poor in chromite oxide and low in Cr:Fe ratio, but some of the ore contains Cr2O3 45 per cent and the lower quality ore has been upgraded Cr2O3 to 45 per cent. The reserves are estimated about 0.67mt. Reserves are calculated to be around 0.67mt. It was commercially feasible to mine 20,000 tonnes of ore to produce 8,000 tonnes of basic chromite sulphate and 1,500 tonnes of sodium dichromate and 300 tonnes of sodium sulphate per year [8].

II.   MATERIAL AND METHODOLOGY

30 kg of representative sample were collected from Kohistan Khyber Pakhtunkhwa having coordinates of (35º02'47.6"N, 72º55'09.6"E). The chromite ore were mostly 15cm*10cm, 14cm*14cm etc. in size and in hard form. The color of ore is from gray to light black. The streak of the chromite ore were found at a Geology laboratory of Mining Engineering Department University of Engineering and Technology Peshawar by streak plate and is dark brown in color.

III.   EXPERIMENTAL WORK/RESULTS AND DISCUSSION

A. Characterization

Characterization studies have been conducted to understand the physical and chemical properties and model their separation efficiency. Results obtained from each characterization analysis are also discussed.

B. Thin Section Study

Six representative thin sections has been made from the chromite sample shown in figure.1

Fig. 1. Six representative thin sections of Kohistan chromite ore.

The thin section has been studied under polarizing microscope at National Center of Excellence in Geology Peshawar (Nikon LV 100 ND transmitted-cum-reflected microscope with standalone 5 megapixels camera attached with 42 inches Screen). Pictures shown in figures.2, 3 confirm the presence of chromite with the olivine and serpentine as gangue mineral. Valuable Mineral Chromite (Cr_2O3 *FeO Impure) Gangue Minerals: Serpentine [$Mg_3 Si_2O_5$ (OH) $_4$], Olivine [$(Mg,Fe)_2 SiO_4$], Calcite ($CaCO_3$). During the above examination it was noticed that the individual crystal of chromite were fairly pure and could be easily distinguished from the gangue minerals by their color and isotropic

characteristics which is typical of all chromite minerals. The gangue minerals seemed to occur as separate unite and sometimes had intruded in the chromite crystals. Serpentine is the most predominant gangue mineral followed by olivine and small amount of calcite. Also the size has been identified by taking the average of the chromite ore in the polarizing microscope as shown in figures 4, 5 which has been between (+250-400)μm[9].
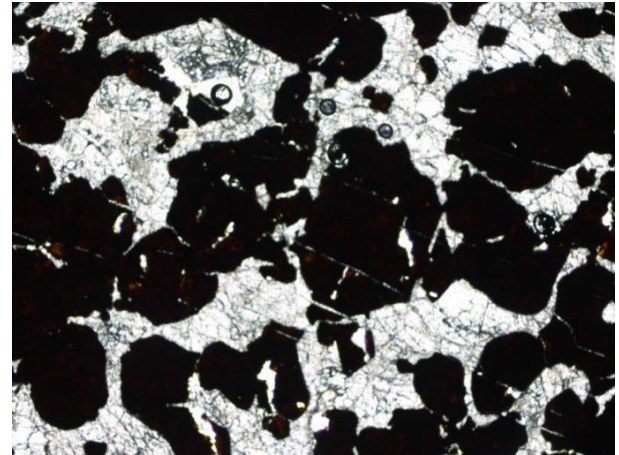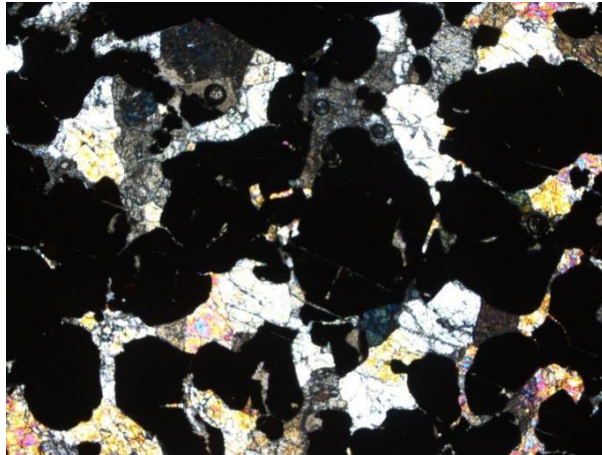
Figs. (2, 3). Kohistan chromite ore thin sections by polarizing computers
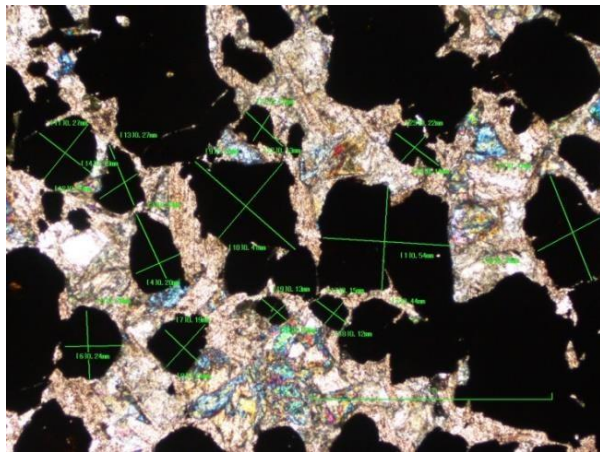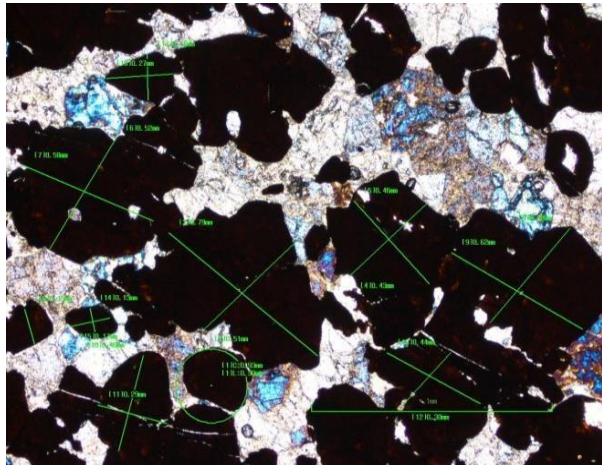
Figs. (4, 5). Kohistan chromite ore thin sections by polarizing computers with lines.

C. X-Ray Fluorescence (XRF) Analysis

Chromite ore has been characterized by X-ray fluorescence (XRF) and the finding is given in Table 1. Chromite ore has been shown to contain mostly Cr_2O_3 with Fe_2O_3 MgO Al_2O_3 etc

Table.1 chemical analysis of Kohistan chromite ore by XRF.

Compound	CR_2O_3	Fe_2O_3	SiO_2	CaO	NiO
percentage	46.6	26.21	25.45	0.69	0.58

D. X-Ray Diffraction (XRD) Analysis

XRD study was conducted to classify the various mineral phases of the sample and their trends as displayed in Figure 6. The phases concerned were studied using JEOL 3532, an X-ray diffractometer with Cu k5-007 (1.54Ao) working at 40 kV and 30 mA. The main phases found in the sample are Iron Magnesium Chromium Aluminum Oxide [Fe, MG, Cr] 2O3, Silicon Oxide SiO2, Magnesium Silicate MgSiO2, Iron Oxide FeO, and Aluminum Oxide ALO. The XRD characteristics installed at CRL are Model: JDX-3532, Make: JEOL, Japan, Voltage: 20-40kV, Current: 2.5-30mA, X-Rays: CuKa (Wavelength = 1.5418Å), 2Theta-Range: 0 to 160°, Required Physical State: 20-40kV, Current: 2.5-30mA, X-Rays: (Powder or bulk).
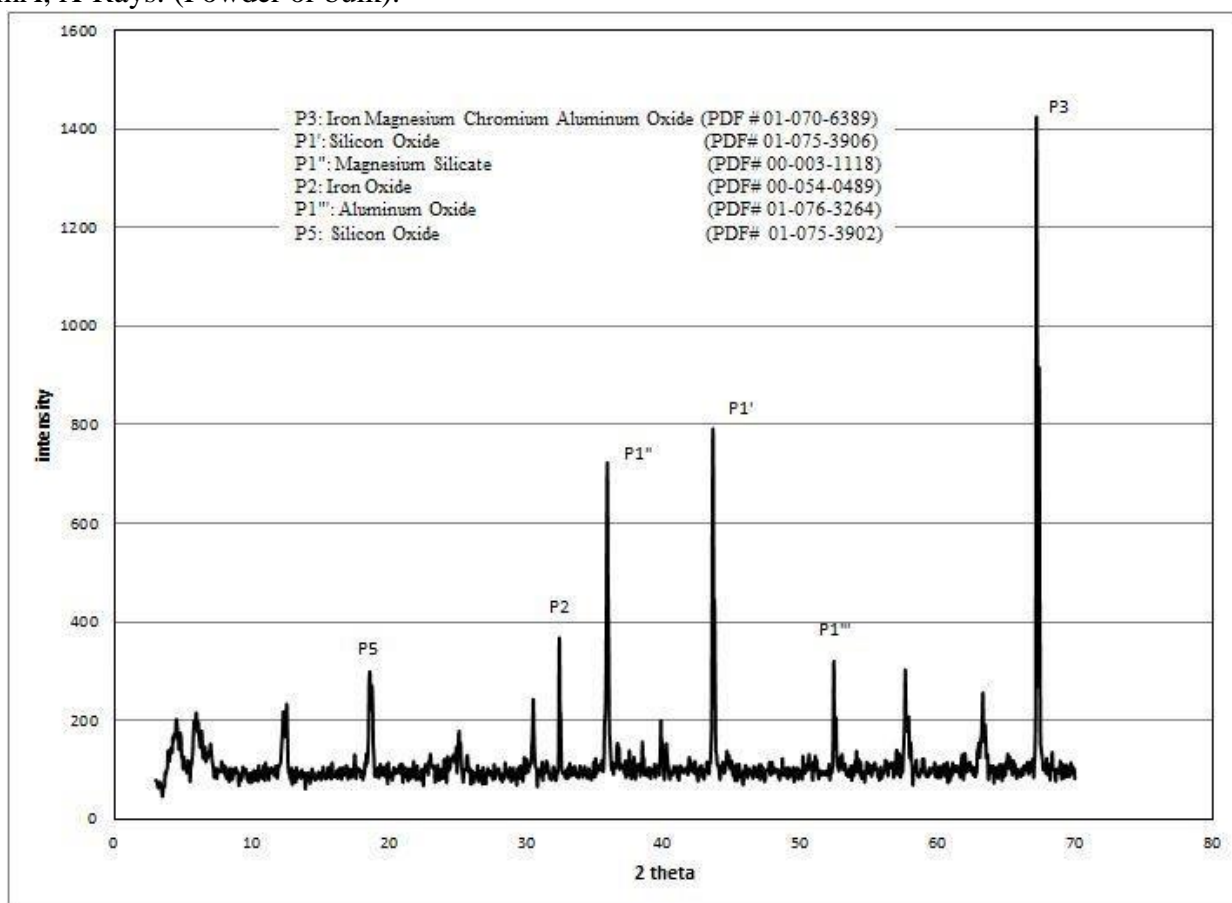
Fig. 6. XRD pattern of Kohistan chromite ore.

E. Scanning Electronic Microscopy (SEM) Analysis

The surface morphology of chromite has been observed using a scanning electronic electron microscope SEM (JEOL JSM 5910 SEM) and the SEM images are shown in figs. 7 and 8 with different resolutions. Dissimilarities in shapes and sizes are observed from the imagesThe specifications of the scanning electron microscope mounted in the CRL are as follows Model: JSM5910 Manufacturer: JEOL, Japan, Energy: 30KV, Magnification (Max): 300,000X, Resolving Power (Max): 2.3nm, Required Physical State of Sample is solid (Powder or bulk).
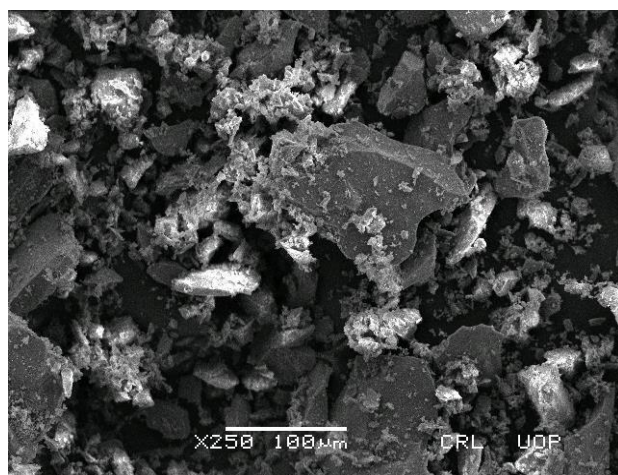
Fig.7 SEM image of ore sample at 250X   Fig.8 SEM image of ore sample at 2500X
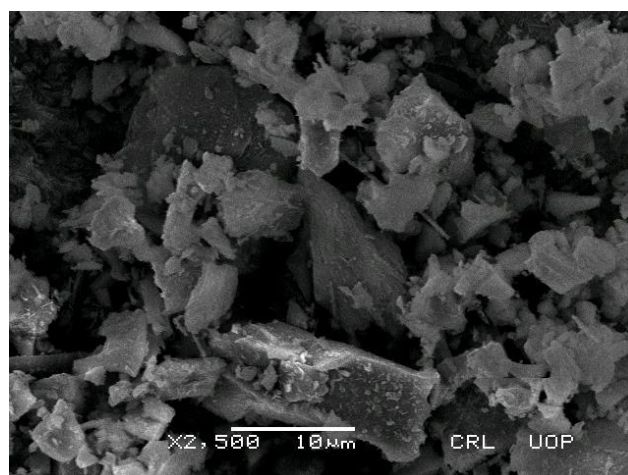
F. Elementary Dispersive X-ray Spectrometry EDX

Sample of chromite ore was analyzed by EDX compound present in maximum percentage are chromium, iron, silicon and calcium etc. shown in table.2. EDX with SEM (JSM5910)INCA200/ Oxford instruments, U.K.

Table.2 EDX Analysis of Kohistan chromite ore.

Element	C	O	Mg	Al	Si	Ca	Cr	Fe
Weight %	2.41	10.56	17.37	1.95	7.94	1.46	40.32	17.99

IV.   CONCLUSION

This study presents preliminary findings of Chromite in Kohistan (Jijal) KPK the conclusions regarding the characterization of the Kohistan chromite ore under investigation are:
The XRF analysis shown that the ore contain Cr_2O_3 with Fe_2O_3 , MgO, and Al_2O_3.
The mineralogical study through XRD confirm the presence of Iron Magnesium Chromium Aluminum Oxide $[Fe,MG,Cr]_2O_3$, Silicon Oxide SiO_2, Magnesium Silicate $MgSiO_2$, Iron Oxide FeO, and Aluminum Oxide ALO.The thin section studies show that the chromite exist and from the area cover by the chromite has been determine and occur in range of $(+250\text{-}400)\mu m$.
From the characterization of the Kohistan chromite it is been concluded and recommended that Gravity separation may be used for the beneficiation of ore concerned.
This paper cannot cover the detail characterization of the Kohistan chromite ore Therefore neither these findings are conclusive regarding the entire chromite reserve studied nor could the findings be generalized in the larger context.

ACKNOWLEDGMENT

REFERENCES

1. Atalay, U., Ozbayolu, G., Beneficiation and agglomeration of chromite and its application in Turkey. Miner. Process. Extr. Metall. Rev. 1992, 9, 185–194.

2. Guney, A., Onal, G., Atmaca, T., New aspect of chromite gravity tailing reprocessing. Miner. Eng. 2001, 14, 1527– 1530.

3. http://www.mindat.org/min-8675.html Mindat

4. R K Sahoo, Chromite and Nickel Ore, Geology and Mineral Resources of Orissa, Society Of Geoscientists and Allied Technologists (SGAT), 1995, p108.

5. Y. Rama Murthy , Sunil Kumar Tripathy , C. Raghu Kumar , Chrome ore beneficiation challenges & opportunities – A review, Journal of Minerals Engineering,2011, 24, 375-380

6. Shah et al, chromite deposits of Pakistan: a short review, International journal of research – granthaalayah, 2019, 7.

7. Coulson A.L. Mineral resources of NWFP. GSI, Rec. 75, Prof. paper 2, 1940.

8. Malkani et al, Mineral Deposits of Khyber Pakhtunkhwa and FATA (Pakistan), U. J.Sci. Techl, 2017, 8, 23-46.

9. F.GU and B.A. Wills., Chromite- Mineralogy and Processing, Mineral engineering, 1988, 2, 235-240.

Technical Session 4-B (Google meet/Zoom) Modelling and Simulations	
Session Chair: **Dr. Iftikhar Ahmad** Session Co-Chair: **Dr. Mansoor ul Hassan**	
Mah Noor Saeed *(GIKI, Topi)*	Modification of Soave-Redlich-Kwong Equation of State and Peng-Robinson Equation of State using parameter b as the function of temperature and pressure.
Abdul Aziz *(USPCAS-E UET Peshawar)*	Computational Fluid Dynamics Analysis of Air Flow Distribution in Forced Draft Tobacco Barn
Ali Ahmed Durrani *(Dept. of Chemical Engineering, UET Peshawar)*	Analysis of Nuclear Energy Growth in Pakistan. Part 1: Falling into the Vicious Cycle of Coal.
Izaz Ahsan *(USPCAS-E UET Peshawar)*	Gasification of sugarcane bagasse and woodchips in a downdraft biomass gasifier.

Modification of Soave-Redlich-Kwong equation of state and Peng-Robinson equation of state for better prediction of volumetric properties for water

Mah Noor Saeed [A], Aqeel Ahmad Taimoor [B], Khurram Imran Khan[C]

[A, B, C]=*GIK Institute, Topi, Distt Swabi, 23640, KPK*

Abstract— **Cubic equation of states has been an essential practical model to describe phase equilibrium and has been modified several times since its introduction in 1873. However, it still lacks in its ability to accurately predict some of the thermodynamic properties especially for polar compounds and for near critical region. The two parameters: parameter *a* and parameter *b* has been a part of almost all of the major equation of states including Soave Redlich Kwong equation of state and Peng Robinson equation of state. New modified equations for parameter *b* are developed for water using compressibility factor as the dependent variable. The equations are then compared with original equation of state values and experimental values for molar volume and the difference is then evaluated. The newly developed equations show promising results as compared to Soave Redlich Kwong equation of state and Peng Robinson equation of state.**

*Keywords—***Cubic Equation of States, Modeling, Peng Robinson Equation of State, Phase Equilibrium, Soave Redlich Kwong Equation of State.**

I. INTRODUCTION

Phase equilibrium is a science which is based on the summarization of thermodynamic properties for different phases within a phase diagram [1]. Cubic equation of state (EoS) is a model that can describe the molecular interactions using its two important parameters introduced by van der Waal [2]. These two parameters are the attractive parameter *a* and the repulsive parameter *b* [3]. Van der Waals equation (1873) was the first ever mathematical model introduced for real gas thermodynamic properties prediction, which was followed by Redlich-Kwong (1949). Van der Waals model was discarded for practical use because of its inaccuracies, but his idea of molecular interaction became the basis for many other cubic equations of states [4]. In 1949 Redlich and Kwong introduced a temperature dependent term in their model for parameter *a*. Despite being a much better model for the prediction of volumetric and thermal properties as compared to the previous models, this model was discarded for its inaccuracies in predictions, which were attributed to its inaccurate temperature dependent term [5][6]. Soave introduced another temperature dependent term for parameter *a* for Redlich-Kwong equation of state which could accurately predict volumetric and thermal properties for many compounds and their mixtures. This equation is also known as Soave-Redlich-Kwong equation of state (SRK EoS) and is mostly used in simulation programs for different process industries till date [7]. However, SRK equation of state lacks in its ability to predict accurately the liquid densities, especially for heavy hydrocarbons [8]. Peng Robinson equation of state (PR EoS) was introduced in 1976 when two scientists Ding-Yu Peng from China and Donald B. Robinson from Canada started worked together for a project in University of Alberta to modify SRK equation of state for better prediction of different properties [9]. They modified the *α*-function with a different temperature dependent expression which resulted in the improvement of prediction for liquid density [10][11]. In both SRK EoS and PR EoS the attractive term or parameter *a* is the temperature dependent term and the repulsive term or parameter *b* is a constant whose value is dependent on the critical temperature and critical pressure. In both the equations parameter *b* is referred as the rigid sphere molecular volume and the repulsive term [12]. Both the SRK EoS and PR EoS gives satisfying values for liquid molar volumes at the subcritical region but values get inaccurate at the near critical region [13].

Four types of amendments in EoS are generally used: 1) Amendment by changing parameter *a*, or parameter *b*, or the *α*-function. 2) Proposing different functions e.g volume translation. 3) Proposing new

terms or parameters. 4) Altering mixing rules [9]. Some of the scientists that contributed in the modification of EoS are pressure by Mathias & Copeman (1983) [14], Stryjek & Vera (1986) [15], Gasem (2001) [16], and Peneloux who introduced the concept of volume translation [17] [18]

This work is based on the development of modified SRK EoS and PR EoS by introducing a different parameter b to reduce the inaccuracies in the prediction of thermodynamic properties, especially for the region closer to the critical point.

II. METHODOLOGY

Experimental data is taken from NIST database for various thermodynamic properties and their compressibility is calculated using equation of states. Generalized Reduced Gradient (GRG) algorithm is applied to the results to calculate values for the same thermodynamic properties closest to the experimental data. The resultant values are then regressed. The equations developed are then compared with the original equation of state for volumetric properties.

III. RESULTS AND DISCUSSION

Equations are developed for parameter b for a specific EoS i.e SRK EoS and PR EoS using regression analysis. These equations are then inserted in the original EoS and referred to as the newly developed equation in this work. Now molar volume is calculated for water using this newly developed equation as well as using the original SRK EoS and PR EoS. The calculated molar volumes are then compared with the experimental values at the respected thermodynamic conditions. Percentage error is calculated for values of molar volumes using both the equations i.e original EoS and newly developed EoS. These percentage errors are then compared.

Fig.1 shows the percentage error of original SRK EoS for volume calculation as error SRK and the percentage error of the newly developed equation for volume calculation as error new. This figure shows that the percentage error for newly developed EoS is much less than the original SRK EoS. The error especially decreases with the increase of temperature and pressure. From Fig.1 (b) it can be seen that for the region closer to the critical point the error in volumetric calculation for original SRK EoS is very large and is not justifiable. The newly developed model overcomes this problem and especially gives a very low error.

Unlike the percentage error of newly developed SRK EoS, the percentage error of newly developed PR EoS is inconsistent but small as comparison to the original PR EoS as seen in Fig.2. It especially decreases as the value reaches the near critical region.
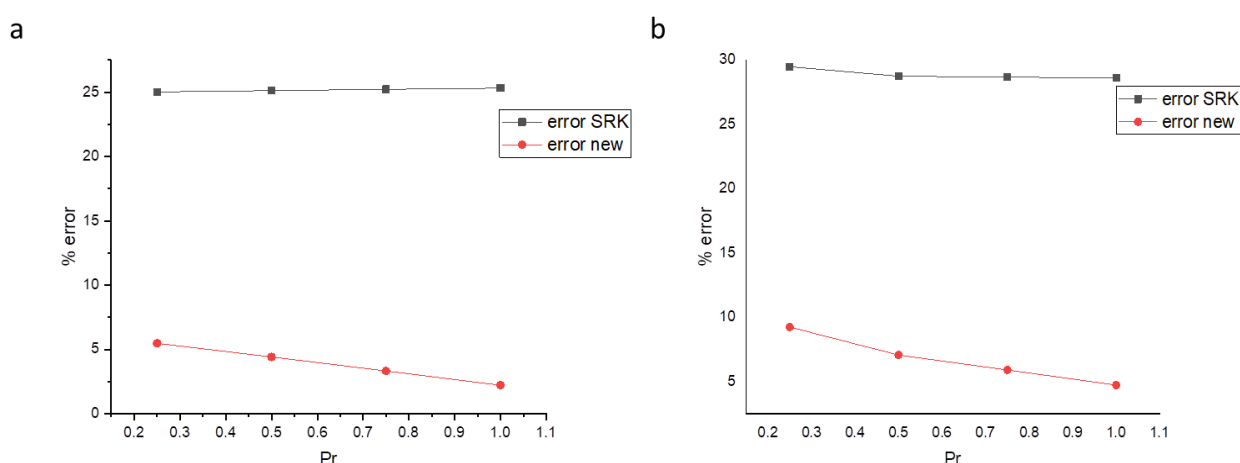
Fig. 1. Percentage error of original SRK EoS and newly developed SRK EoS at (a) Tr=0.5 and (b) Tr=0.8

a

b
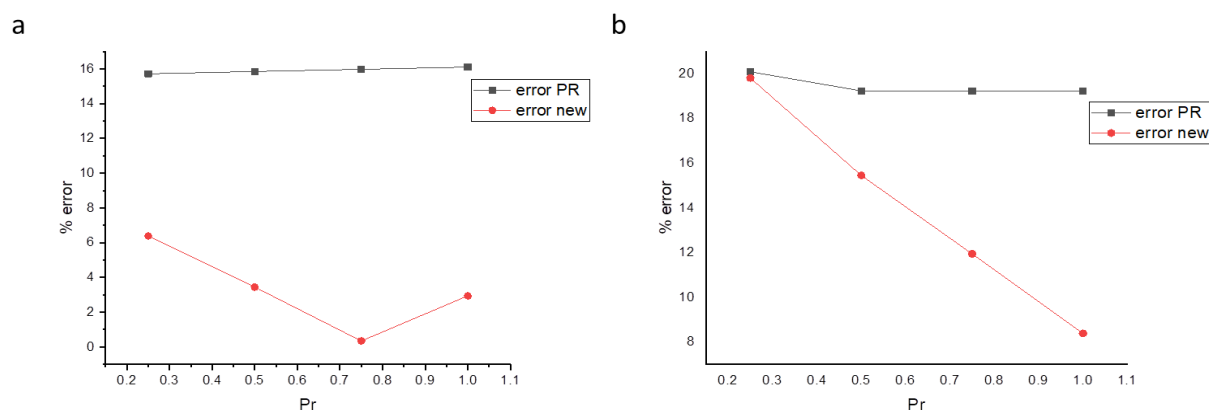
Fig. 2. Percentage error of original PR EoS and newly developed PR EoS at (a) Tr=0.5 and (b) Tr=0.8

IV. CONCLUSION

The results for the newly developed equations show a high degree of accuracy as compared to the originally used popular equation of states. It also overcomes the flaw of original SRK EoS and original PR EoS by giving predicting the values of near critical region with high accuracy.

V. REFERENCES

[1] J. D. S. Arons, "The systematic study of phase behaviour and the emerging coherence of phenomena," Fluid Phase Equilibria J., vol. 104, pp. 97–118, 1995.

[2] G. M. Kontogeorgis and I. G. Economou, "Equations of state : From the ideas of van der Waals to association theories," J. Supercrit. Fluids, vol. 55, pp. 421–437, 2010.

[3] J. O. Valderrama, "The legacy of Johannes Diderik van der Waals , a hundred years after his Nobel Prize for physics," J. Supercrit. Fluids, vol. 55, pp. 415–420, 2010.

[4] T. Y. Kwak and G. A. Mansoori, "Van der waals mixing rules for cubic equations of state. Applications for supercritical fluid extraction modelling," Chem. Eng. Sci., vol. 41, no. 5, pp. 1303–1309, 1986.

[5] G. G. Fuller, "A Modified Redlich-Kwong-Soave Equation of State Capable of Representing the Liquid State," Ind. Eng. Chem, vol. 15, no. 4, pp. 3–6, 1976.

[6] G. Soave, "Equilibrium constants from a modified Redkh-Kwong equation of state," Chem. Eng. Sci., vol. 27, no. 6, pp. 1197–1203, 1972.

[7] Zakia NASRI and Housam BINOUS, "Applications of the Soave–Redlich–Kwong Equation of State Using Mathematica," J. Chem. Eng. Japan, vol. 40, no. 6, pp. 534–538, 2007.

[8] L. S. Wang and J. Gmehling, "Improvement of the SRK equation of state for representing volumetric properties of petroleum fluids using Dortmund Data Bank," Chem. Eng. Sci., vol. 54, no. 17, pp. 3885–3892, 1999.

[9] J. S. Lopez-Echeverry, S. Reif-Acherman, and E. Araujo-Lopez, "Peng-Robinson equation of state: 40 years through cubics," Fluid Phase Equilib., vol. 447, pp. 39–71, 2017, [Online]. Available: http://dx.doi.org/10.1016/j.fluid.2017.05.007.

[10] C. H. Twu, J. E. Coon, and J. R. Cunningham, "A new generalized alpha function for a cubic equation of state Part 1. Peng-Robinson equation," Fluid Phase Equilib., vol. 105, no. 1, pp. 49–59, 1995.

[11] B. Schmid and J. Gmehling, "From van der Waals to VTPR: The systematic improvement of the van der Waals equation of state Bastian," J. Supercrit. Fluids J., vol. 55, pp. 438–447, 2010.

[12] K. Liu, Y. Wu, M. A. Mchugh, H. Baled, R. M. Enick, and B. D. Morreale, "Equation of state modeling of high-pressure, high-temperature hydrocarbon density data," J. Supercrit. Fluids, vol. 55, pp. 701–711, 2010.

[13] H. Baled et al., "Fluid Phase Equilibria Prediction of hydrocarbon densities at extreme conditions using volume-translated SRK and PR equations of state fit to high temperature , high pressure PVT data," Fluid Phase Equilib., vol. 317, pp. 65–76, 2012, [Online]. Available: http://dx.doi.org/10.1016/j.fluid.2011.12.027.

[14] P. M. Mathias and T. W. Copeman, "Extension of the Peng-Robinson equation of state to complex mixtures: Evaluation of the various forms of the local composition concept," Fluid Phase Equilib., vol. 13, no. C, pp. 91–108, 1983.

[15] R. STRYJEK and J. H. VERA, "PRSV : An Improved Peng- Robinson Equation of State for Pure Compounds and Mixtures," Can. J. Chem. Eng., vol. 64, no. 2, pp. 223–233, 1986.

[16] K. A. M. Gasem, W. Gao, Z. Pan, and R. L. R. Jr, "A modified temperature dependence for the Peng–Robinson equation of state," Fluid Phase Equilib., vol. 181, pp. 113–125, 2001.

[17] B. S. Jhaveri and G. K. Youngren, "Three-parameter modification of the Peng-Robinson equation of state to improve volumetric predictions," SPE Reserv. Eng., vol. 3, no. 3, pp. 1033–1040, 1988.

Computational Fluid Dynamics Analysis of Air Flow Distribution in Forced Draft Tobacco Barn

Abdul Aziz [A], Khurshid Ahmad [A], and Muhammad Hassan[A]

[A] US-Pakistan Center for Advanced Studies in Energy (USPCAS-E), University of Engineering and Technology Peshawar, Pakistan

Abstract— **Tobacco barns are widely used to cure tobacco leaves. The tobacco drying process consumes large amount of fuel. In order to obtain sustainable and cost-effective tobacco curing process, understanding the dynamics of tobacco curing process e.g., air flow distribution, temperature distribution, is important. In this research, a forced draft tobacco barn was selected, modeled, and simulated. The k-ε turbulence model was used for the analysis. It was found that the existing rack design in forced draft tobacco barn significantly hinders the air movement. The modified design not only improved the air movement, but also helped in temperature uniformity inside the barn.**

Keywords— **Forced draft tobacco barn, Temperature distribution, Tobacco racks, Velocity distribution.**

I. INTRODUCTION

Tobacco is produced from the fully ripened and fresh leaves of tobacco plant which belongs to genus Nicotiana. It is widely used as an organic pesticide and in cigarette making. There exists various types of tobacco e.g., Virginia [1]. Curing of tobacco is an important stage when making processed tobacco. Yellowing, leaf drying, and stem drying are the main three stages in curing tobacco [2]. Enzymatic reactions and water evaporation from tobacco govern flue curing process [3]. Air flow, temperature and humidity distribution highly influence the quality of curing tobacco.

For the first time in 1960, bulk curing at farm-scale started in North Carolina [4]. Forced ventilation for curing tobacco replaced traditional natural ventilation in the bulk tobacco curing barns. Forced draft curing process utilized hot air circulation system and automated control systems, which saved both energy and labor cost. With the introduction of forced draft curing technology, different structure of curing barns with various air flow directions is gaining a lot of interest, especially air rising in the curing barns [5] [6].

Computational tools are gaining a lot of interest in simulating flow field, heat and mass transfer processes. CFD modeling for the prediction of temperature and relative humidity distribution has been widely used in thermosiphon [7] and cool store [8]. Recently artificial neural network has been used to study temperature and relative humidity distribution in tobacco bulk curing barns [9]. Numerical studies focusing tobacco curing process were rarely considered.

II. METHODOLOGY

A. *k-ε Turbulence Model*

Launder and Spalding proposed this model for fully turbulent flows [10]. The effects of viscosity are not taken into account and fully turbulent flow is assumed while deriving this equation [11] [12]. Until now, its two variants RNG and realizable models are available inside fluid component of ANSYS.

Equations for k- ε are obtained from following equations:

$$\frac{\partial}{\partial t}[\rho k] + \frac{\partial}{\partial x_i}[\rho k \mu_i] = \frac{\partial}{\partial x_j}\left[\left(\mu + \frac{\mu_t}{\sigma_k}\right)\frac{\partial k}{\partial x_j}\right] + G_k + G_b - \rho \varepsilon - Y_M + S_k \qquad (1)$$

and

$$\frac{\partial}{\partial t}[\rho \mathcal{E}] + \frac{\partial}{\partial x_i}[\rho \mathcal{E} \mu_i] = \frac{\partial}{\partial x_j}\left[\left(\mu + \frac{\mu_t}{\sigma_\mathcal{E}}\right)\frac{\partial \mathcal{E}}{\partial x_j}\right] + C_{1\mathcal{E}}\frac{\mathcal{E}}{k}(G_k + C_{3\mathcal{E}}G_b) - C_{2\mathcal{E}}\rho\frac{\mathcal{E}^2}{k} + S_\mathcal{E} \quad (2)$$

The time derivatives are put zero for steady state assumption.

Model constants have following values which have been determined experimentally:
$C_{1\mathcal{E}}$=1.44, $C_{2\,\mathcal{E}}$=1.92, C_μ=0.09, σ_k=1.0, σ_E=1.3

B. Governing Equations

1)Energy Equation

Energy equation solved by fluent is written as:

$$\frac{\partial}{\partial t}(\rho E) + \nabla.\left(\vec{v}(\rho E + p)\right) = \nabla.\left(k_{eff}\nabla T - \sum_j h_j \vec{J}_j + (\overline{\overline{\mathcal{T}_{eff}}}.\vec{v})\right) + S_h \tag{3}$$

The time derivatives are put zero for steady state assumption.

Here k_{eff} is the effective conductivity. In the energy equation last three terms correspond to energy transfer terms for conduction, specie diffusion and viscous dissipation respectively.

2)Continuity Equation

Equation of continuity solved by fluent is as follow:

$$\frac{\partial}{\partial t}(\rho) + \frac{\partial(\rho u)}{\partial x} + \frac{\partial(\rho v)}{\partial y} + \frac{\partial(\rho w)}{\partial z} = 0 \tag{4}$$

The time derivatives are put zero for steady state assumption.

3)Momentum Equation

The vector form of momentum equation is as follow:

$$\frac{\partial(\rho u)}{\partial t} + \nabla(\rho u u) = -\frac{\partial p}{\partial x} + \frac{\partial \mathcal{T}_{xx}}{\partial x} + \frac{\partial \mathcal{T}_{xy}}{\partial y} + \frac{\partial \mathcal{T}_{xz}}{\partial z} + \rho g_x + S_x \tag{5}$$

$$\frac{\partial(\rho v)}{\partial t} + \nabla(\rho v u) = -\frac{\partial p}{\partial x} + \frac{\partial \mathcal{T}_{xy}}{\partial x} + \frac{\partial \mathcal{T}_{yy}}{\partial y} + \frac{\partial \mathcal{T}_{zy}}{\partial z} + \rho g_y + S_y \tag{6}$$

Where $\mathcal{T}_{ij}$ are the viscous stress components. The time derivatives are put zero for steady state assumption.

C. Geometry of Tobacco Barns

A 2D geometry of forced draft tobacco barn (both existing and modified) using space claim ANSYS was created. Air enters the barn through a 2.12 ft hole at speed of 3.5 m/s in both the barns. The air then enters from the heat exchanger room into the tobacco loading area through a hole of 1 ft. There are three wooden racks in the existing forced draft tobacco barn, while the number of racks in modified barn is four with the introduction of modification of a space of 0.5 ft. The dimensions of both the barns are specified in the fig. 1 and 2.
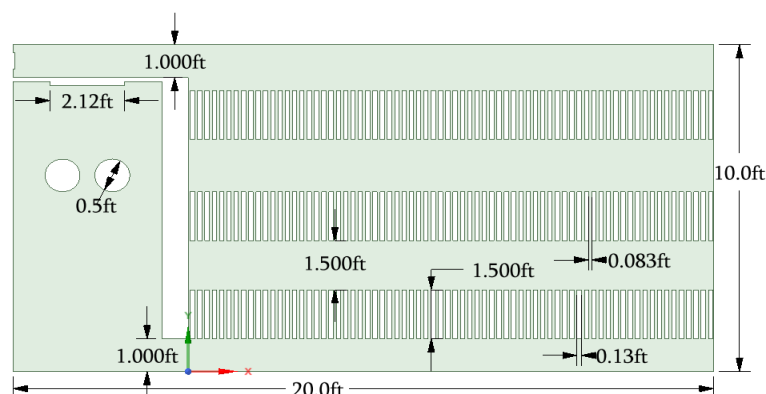
Fig. 1. Graphic design of existing forced draft tobacco barn.
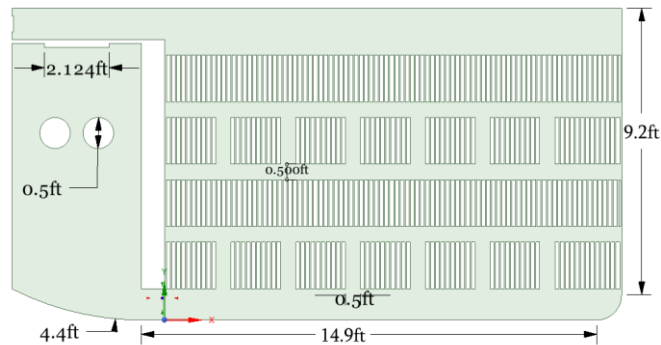
Fig. 2. Graphic design of modified forced draft tobacco barn.

D. Initial Conditions for Simulation

The initial conditions provided for the simulation are provided in the table.

TABLE I: Values of initial conditions for simulation in fluent.

Air Inlet Velocity	3.5 [m/s]
Temperature of Inlet Air	313 [K]
Density of Tobacco	1600 [kg/m^3]
Specific Heat of tobacco	3800 [J/kg.K]
Thermal Conductivity of Tobacco	0.086 [W/m.K]
Thermal Conductivity of Tobacco	0.086 [W/m.K]

III. RESULTS AND DISCUSSION

A. Behavior of Air Flow and Temperature Distribution

Velocity and temperature distribution inside the barn are shown in fig. 3 and fig. 4. The inlet velocity for the both the barn is 3.5 m/s.

(a)   (b)
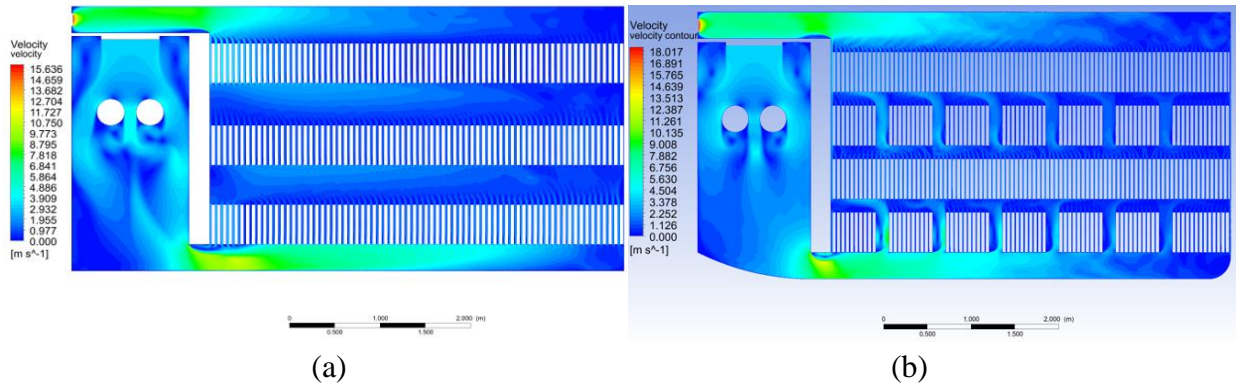
Fig. 3. Velocity contour in: (a) existing forced draft tobacco barn, (b) modified forced draft tobacco barn.

(a)   (b)
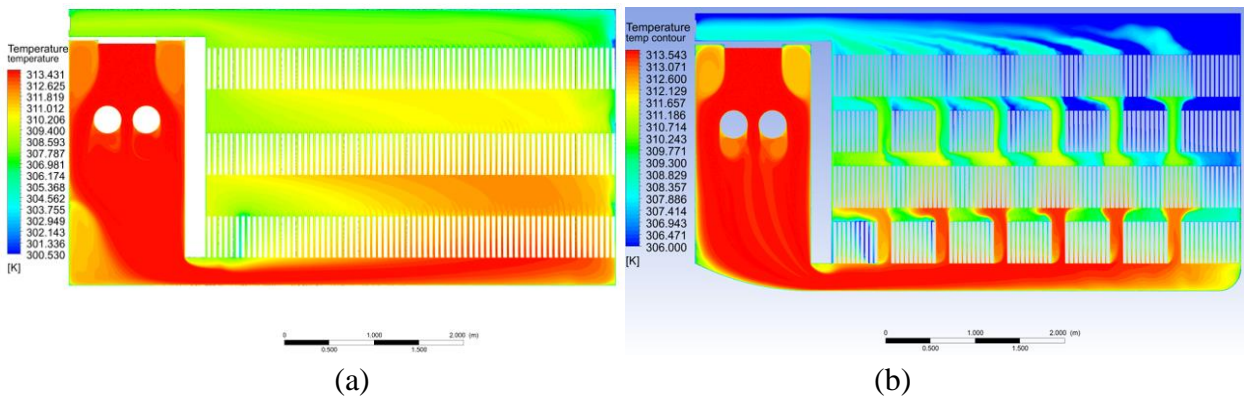
Fig. 4. Temperature distribution in: (a) existing forced draft tobacco barn, (b) modified forced draft tobacco barn.

The air introduced into the conventional forced barn finds little space to channelize through the leaves of tobacco which results in non-uniform distribution of air and temperature. This leads to poor quality of processed tobacco. In modified barn a 0.5 ft gap in bottom and middle-top rack distributes the air uniformly. This results in uniform curing of tobacco leaves which in turn improves the quality of processed tobacco leaves.

B. Air Flow Behavior Inside Tobacco Racks

Fig. 5 indicates the distribution of velocity in top rack of both conventional and modified forced draft tobacco barns. Air in the top rack of conventional modified barn is below the baseline of 0.9 m/s, which affects the channelization of air through the leaves of tobacco. In contrast, the velocity in the top rack of modified barn is well above the threshold of 0.9 m/s.

(a)   (b)
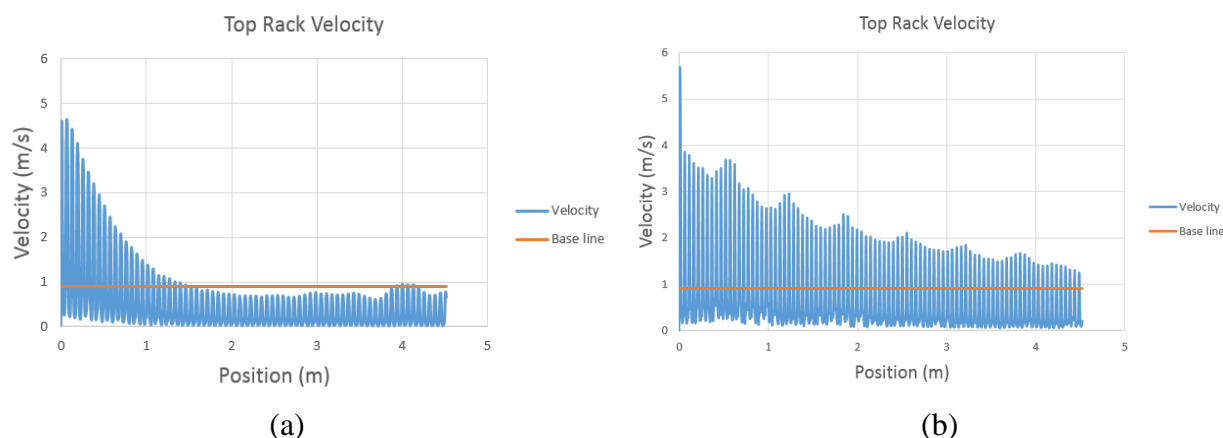
Fig. 5. Velocity distribution in top rack of : (a) existing tobacco barn, (b) modified tobacco barn.
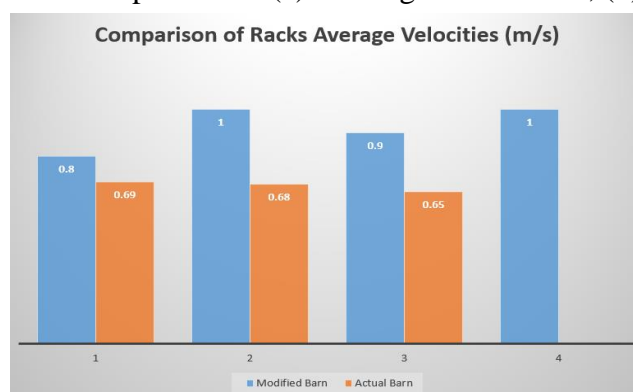
Fig. 6. Average air velocities in racks of existing and modified tobacco barns.

IV. CONCLUSION

In order to distribute the air properly inside the racks of forced draft tobacco barn, modifications were made to the racks of forced draft tobacco barn. The k-ε turbulent model with standard wall function was employed. ANSYS fluent was used for the solution of the geometry. We concluded:

1. Air speed decreases significantly as it passes through the racks as evident from the velocity contour in conventional forced draft tobacco barn. Upon modification in the racks in modified forced draft tobacco barn, air channelizes and velocity distribution improves.
2. As evident from the temperature contour of conventional forced draft tobacco barn that the temperature distribution is not uniform. With the inclusion of modification, the overall distribution inside the tobacco barn improved.
3. Keeping the same process parameters i.e., quantity of fuel, air speed, large quantity of tobacco leaves can be cured in the modified forced draft tobacco barn.
4. With improved air and temperature distribution, higher quality of cured tobacco will be obtained.

References

[1] T. yaia, Tobacco, [Online]. Available: http://www.tobacco.yaia.com/types.html. [Accessed 20 November 2020].

[2] Y. Abubakar, J. Young, W. Johnson and W. Weeks, "Modeling moisture and chemical changes during bulk curing of flue-cured tobacco.," *ASAE,* no. 46, pp. 1123-1134, 2003.

[3] B. Wisniowska-Kielian and A. Kielian, "Dynamics of chemical composition of flue-cured tobacco leaves during the yellowing process.," *Acta Physiologiae Plantarum,* no. 120, 2007.

[4] W. Johnson, " Influence of harvesting and process variables on bulk curing of bright leaf tobacco," *ASAE,* no. 8, pp. 354-357, 1965.

[5] N. Tippayawong, C. Tantakitti and S. Thavornun, " Use of rice husk and corncob as renewable energy sources for tobacco-curing.," *Energy Sustain. Dev. ,* no. 10, p. 68–73, 2006.

[6] K. Siddiqui, "Analysis of a malakisi barn used for tobacco curing in East and Southern Africa.," *Energy Convers. Manag,* no. 42, p. 483–490., 2001.

[7] A. Alizadehdakhel, M. Rahimi and A. Alsairafi, " CFD modeling of flow and heat transfer in a thermosyphon.," *Int. Commun. Heat Mass Transfer,* no. 37,, p. 312–318., 2010.

[8] H. Nahor, M. Hoang, P. Verboven, M. Baelmans and B. Nicolaï, "CFD model of the airflow, heat and mass transfer in cool stores.," *Int. J. Refrig,* no. 28, p. 368–380, 2005.

[9] V. Martínezmartínez, C. Baladrón, J. Gomezgil, G. Ruizruiz, L. Navasgracia, J. Aguiar and B. Carro, "Temperature and relative humidity estimation and prediction in the tobacco drying process using artificial neural networks.," *Sensors,* no. 12, p. 14004–14021, 2012.

[10] B. E. L. a. D. B. Spalding., " Lectures in Mathematical Models of Turbulence," Academic Press, London, England, 1972.

[11] W. W. L. A. S. Z. Y. J. Z. T.-H. Shih, "A New - Eddy-Viscosity Model for High Reynolds Number Turbulent Flows - Model Development and Validation," *Computers Fluids,* vol. 2, no. 24, pp. 227-238, 1995.

[12] S. A. O. V. Yakhot, "Renormalization Group Analysis of Turbulence I Basic Theory," *Journal of Scientific Computing,* vol. 1, no. 1, p. 1–51, 1986.

[13] A. C. P. Fluent, *ANSYS fluent theory guide 15,* Canonsburg, 2013.

Analysis of Nuclear Energy Growth in Pakistan. Part 1: Falling into the Vicious Cycle of Coal

Ali Ahmed Durrani*A, Muhammad Imran Ahmad A, and Irfan Ahmed Khan B

A Department of Chemical Engineering, University of Engineering and Technology, Peshawar, Pakistan
B Department of National Institute of Urban Infrastructure Planning (NIUIP), University of Engineering and Technology, Peshawar, Pakistan

Abstract— **National policies regarding energy sector specifically nuclear, hydro and coal while keeping in consideration multilateral agreements and international obligations are investigated. Energy crisis has been prevailing since long in Pakistan and is further increasing. Policy making in energy sector is a complex issue as the energy demand and its generation depends upon many other factors, which are constantly changing over the time and due to other factors, such as population growth and economic growth. Solving such issues using old fashioned linear thinking approaches may solve the problem in short term but in long term face 'unintended consequences', which further aggravates the problem that was addressed at the first instance. A non-linear feedback-based system thinking approach is adopted using causal loop diagram (CLD) eliciting the interconnected components and subcomponents that are playing key role in energy sector policy making in Pakistan. The underlying structure that governs the behavior of the overall energy system in Pakistan is captured by using system archetypes to study causal loop diagrams. The qualitative model explicitly shows various high and low leverage points that are present in the energy system. The results are helpful for policy makers to intervene in the system effectively and efficiently.**

Keywords— **Energy Policy, Systems Thinking, Casual Loop Diagram (CLD), Nuclear Energy, System Archetypes**

I. INTRODUCTION

A. Pakistan Energy Context

Pakistan is having annual per capita energy consumption of 457kWh which lies way below the world average of 2892kWh [1]. Whereas, Pakistan has an untapped potential of electricity generation of 100,000MW (Thar coal) for 20 years, 56,000MW (hydro), 150,000MW (wind), ~50,000MW (solar) [2]. The electricity generation mix of Pakistan is shown in Figure 1 for 2018 [3].
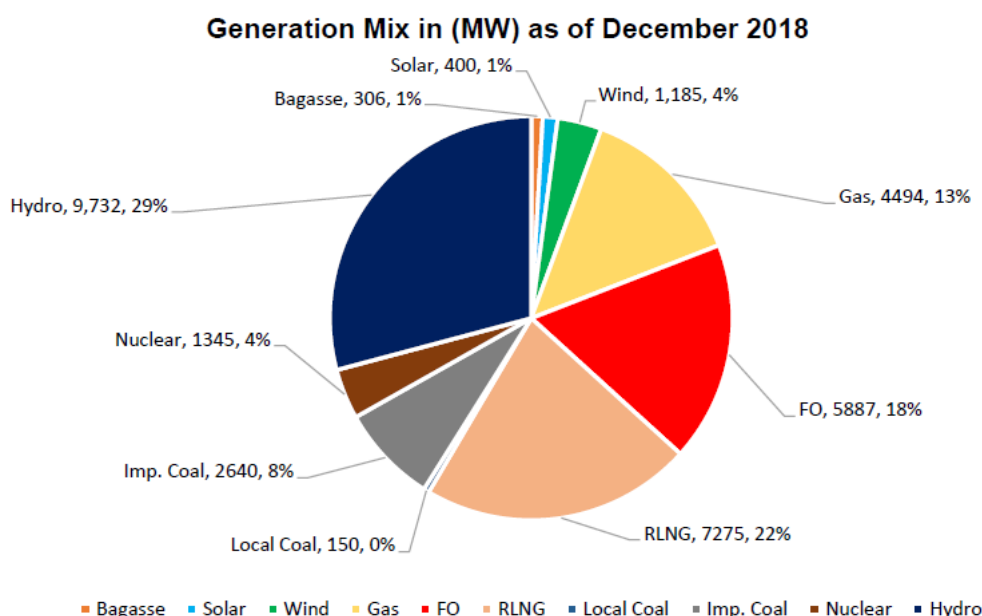
Fig.1. Energy mix of Pakistan in 2018 [3]

The overall energy mix of Pakistan consists of 4% nuclear, 29% hydro, 61% fossil-based fuels and 6% others [3]. Future projection of electricity generation in Pakistan using Hydro, local coal, and nuclear are shown in Figure 2.

NTDC (IGCEP, 2019-2040)

	2020	2025	2030	2035	2040
Nuclear	1232	4278	4278	4278	4278
Hydro	9991	16155	28890	35240	38790
Local Coal	630	3333	3303	9914	24939
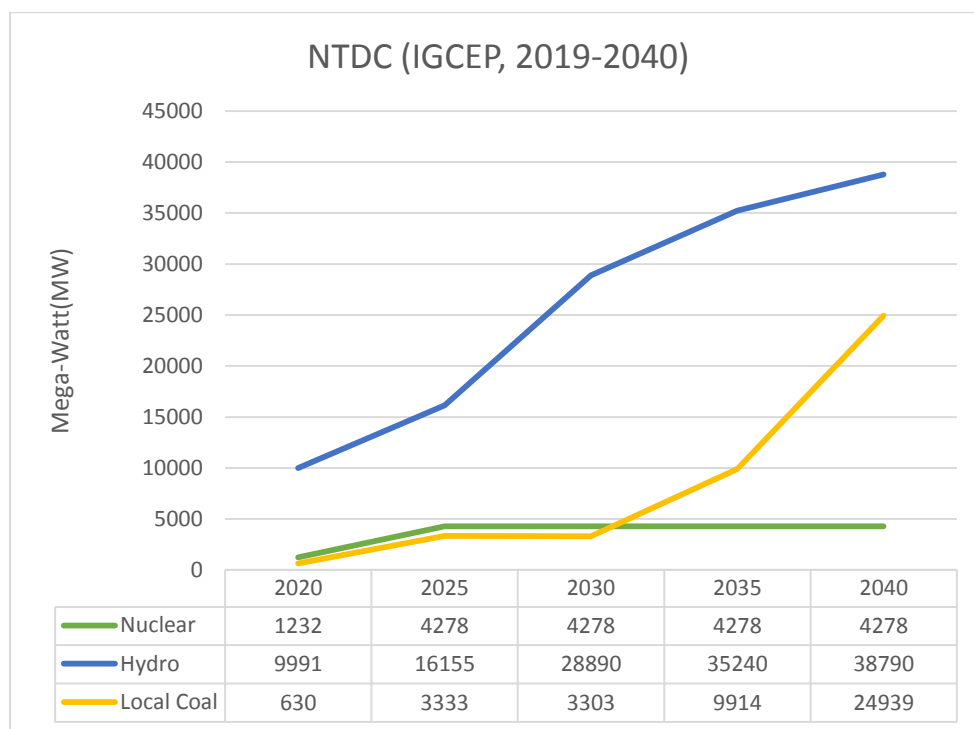
Fig.2. Future projections of energy generation [3]

A significant increase in the share of hydro power and local coal are projected with minimal growth in nuclear sector. Hydro power share is expected to increase from 29% in 2018 to 40% in 2040. Local coal share is negligible in 2018, which will be increased to 25% by 2040. Whereas, share of nuclear is expected to increase during 2020-2025 and may remain the same till 2040 [3].

B. Multilateral Agreements

Pakistan has been a signatory to Kyoto Protocol adopted in Conference of Parties (COP3) in 1997 with targets to reduce 5.2% of their Greenhouse gas (GHG) emissions of 1990's level by 2012 [4]. Then Paris agreement was adopted in 2015, to limit the average global temperature rise between 1.5-2 degree Centigrade by 2100 [5]. Along with these Protocols and agreements Pakistan also strives to remain compliant with the sustainable development goals (SGDs) [6].

II. METHODOLOGY

The methodology of systems thinking is elaborated in Figure 3 [7], wherein a Bull's Eye diagram identifies key variables of the system that are being mapped in casual loop diagram (CLD) to develop understanding of the energy system as well as apply systems thinking tools such as system archetypes to develop insights. The archetypal lens was applied to the CLD to investigate the systemic problems in energy sector of Pakistan and leverage points were identified [8] .
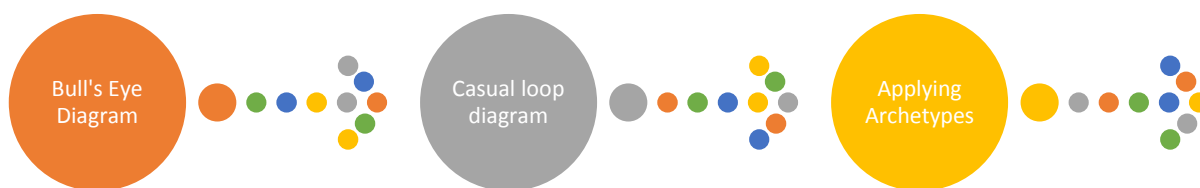
Fig.3. Methodology adopted

III. RESULTS AND DISCUSSION

A. Causal Loop Diagram of Energy Mix of Pakistan
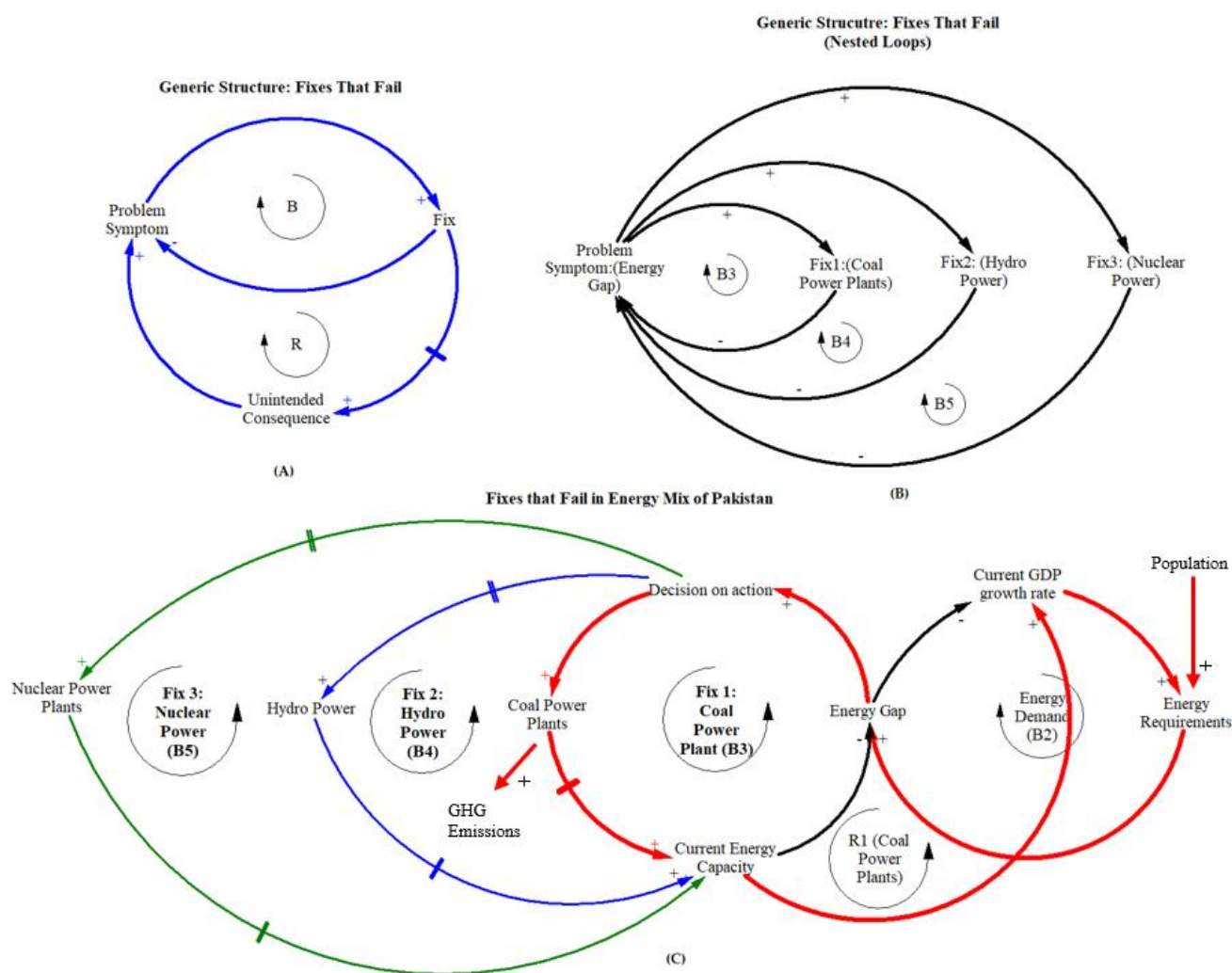
Fig.4. **(a)** Generic Casual loop Diagram of Fixes that Fail. **(b)** Nested Casual loop Diagram of Fixes that Fail. **(c)** Casual loop Diagram of (Fixes that Fail) in Energy Mix of Pakistan.

Figure 4 (c) shows a causal loop diagram of alternate energy solutions for growing energy demand in Pakistan. Loop B2, reflects on the energy demand of the system. The variables involved are *current GDP growth rate*, *energy requirements* and *energy gap*. In order to increase *current GDP growth rate*, the *energy requirements* caused by the *current GDP growth rate* and *population* need to be fulfilled. Otherwise, the *energy requirement* will annually increase the *energy gap*, causing an overall negative impact. The trend in GDP growth rate in 2017 (5.3%), 2018 (5.6%), and in 2019 (3.9%) [9]. Employing

the rule of 70 [10] the energy requirements would be expected to double in approximately 20 years. However, as envisioned in vision 2025; 7% GDP growth rate will require approximately the same amount of energy in about 10 years.

loop B3, shows the vicious cycle of coal. The variables involved are *energy gap*, *decision on action*, *coal power plants*, *current energy capacity*. Due to the increased energy demand in loop B2, the *energy gap* intensifies, causing severe energy crisis, resulting in thousands of factories, industries and organizations to shutdown affecting the livelihood of thousands of families [11]. Energy crisis has adversely affected the economy with estimated 7% loss to the overall GDP [12]. As *energy gap* increases more *decision on actions* are taken in the form of establishment of *coal power plants*. Pakistan is believed to have huge potential of energy sources, if properly utilized it can fulfill the current and future requirements, providing energy security, environmental protection and sustainable economic growth [13]. Pakistan possesses huge local coal reserves but unluckily its importing coal due to relatively high content of ash and Sulphur. Hence to deal with the energy crises and increasing population it is vital to discover new local coalfields in order to meet the energy requirements [14] and also understand the limitations of the coal resource in Pakistan i.e. environmental. These coal reserves of Pakistan have the potential to produce as much as 100,000MW electricity for a lifetime of 30years [15] but at the cost of environment. The production of local coal in Pakistan has been significantly very low but gradually picking up with peak production year to be in 2080 with an estimated production of 134.06 million tonnes [16]. As number of *coal power plants* increase the power generated, is added into the *current energy capacity* which in-turn reduce the *energy gap*. The share of local coal in energy mix is projected to increase to 2% in 2020, 7% in 2025, 6% in 2030, 13% in 2035 and 25% in 2040 [5]. Taking into account the following parameters coal power plants based on local coal are projected to contribute about 25% in energy mix fulfilling the *energy gap*. Such a growth in coal fired plants will furthermore, result in increase in *current GHG emissions* and require large quantities of water mainly contradicting to at least three SDG's which seek to A) reduce water scarcity B) increase the incorporation of renewable energy sources and C) address climate change [17].But as it is shown in Figure 4(c) that the gap is reduced for moment however, after some years the gap increase again due to the economic growth. Hence the cycle of energy requirements and their fulfillments continues, forcing the system into an unintended spiral. Loops B4 and B5 are the alternates, which are greener and act as fundamental solutions to the energy crisis. But once a quick fix such as coal in B3 is applied the chance of fundamental solution fades away. This behavior imitates the system archetype known as quick fix as depicted in Figure 4(a) and 4(b).
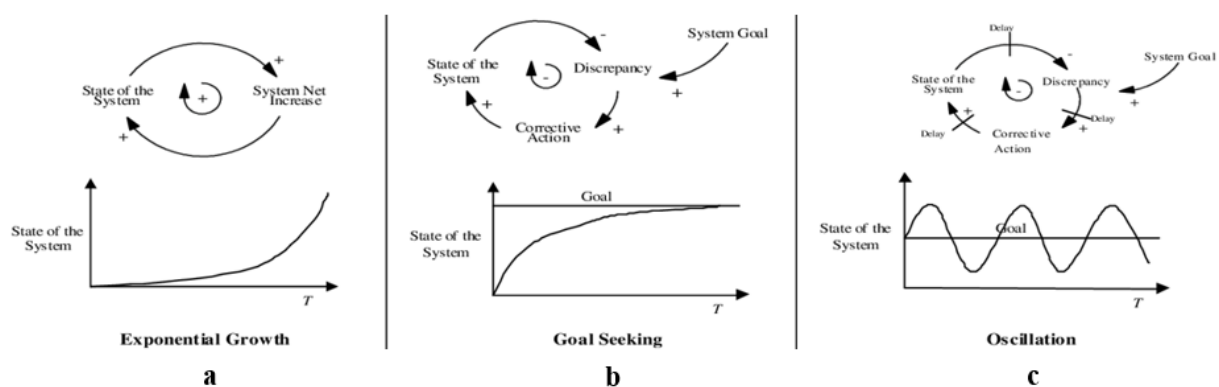
Fig.5. Behaviors in dynamic systems [18]

In Figure 5 it may be seen in part (a) the system is a reinforcing loop causing the system to exponentially grow. Part (b) it is shown that the loop is a balancing loop in which the system changes its self until the goal is achieved. In Part (c) there is a goal seeking loop to improve the state of the system accompanied by various delays causing the system to oscillate.

It may be seen that loop B2 is a balancing or goal seeking loop in which the desire is to increase the *current GDP growth rate* and reduce the *energy gap*. Similarly, in loop B3 to fulfill the *energy gap* energy is added from *coal power plants,* as it increases the *current energy capacity* increase, it provides the energy required for *current GDP growth rate* to flourish as the growth kicks off it in-turn increases the *energy requirement* which in-turn increase the *energy gap.* Hence the system is locked into the vicious cycle of coal and to break this vicious cycle, focus on identifying the root cause of the problem symptom is essential and develop a two-tier approach i.e. while the quick fix is applied in parallel planning on fundamental solutions such as hydro and nuclear is worked out.

IV. CONCLUSION

It may be concluded that energy systems are complex in nature. The actions taken on short term planning usually work for the moment and lessens the energy crisis situation, but in longer term reverts back in an aggravated form reducing time for planning. Hence, as short-term fixes are applied proper parallel planning should be carried out by incorporating fundamental solutions such as hydro and nuclear.

V. REFERENCES

[1]   A. Mahmood, N. Javaid, A. Zafar, R. A. Riaz, S. Ahmed, and S. Razzaq, "Pakistan's overall energy potential assessment, comparison of LNG, TAPI and IPI gas projects," *Renew. Sustain. energy Rev.*, vol. 31, pp. 182–193, 2014.
[2]   J. Akhtar, M. I. Yaqub, J. Iqbal, N. Sheikh, and T. Saba, "Way forward in meeting energy challenges in Pakistan," *Int. J. Ambient Energy*, vol. 39, no. 8, pp. 904–908, 2018, doi: 10.1080/01430750.2017.1341430.
[3]   NTDC, "Indicative Generation Capacity Expansion Plan," no. February, 2019.
[4]   E.-R. Korhola, *The Rise and Fall of the Kyoto Protocol: Climate Change as a Political Process*. University of Helsinki, 2014.
[5]   Pak-INDC, "Pakistan's Intended Nationally Determined Contribution," vol. 7, no. 2, pp. 1–16, 2016.
[6]   Government of Pakistan, "Pakistan Vision 2025," 2017, [Online]. Available: https://fics.seecs.edu.pk/Vision/Vision-2025/Pakistan-Vision-2025.pdf.
[7]   A. Ford and F. A. Ford, *Modeling the environment: an introduction to system dynamics models of environmental systems*. Island press, 1999.
[8]   W. Braun, "The system archetypes," *System*, vol. 2002, p. 27, 2002.
[9]   A. D. Bank, "Asian Development Outlook," 2018.
[10]   C. B. MURPHY, "The rule of 70." https://www.investopedia.com/terms/r/rule-of-70.asp.
[11]   P. NEPRA, "NEPRA State of Industry Report," *NEPRA Islam.*, 2015.
[12]   S. S. Ashley Feng, "China's Power Move Reading between the (transmission) lines on Beijing's global infrastructure project," 2018. https://blogs.scientificamerican.com/observations/chinas-power-move/?fbclid=IwAR3NpyuoVAgdqHqNYXUIdl0GbL8Ny7i_FX9Ok8wmWUqZFKj_uOTWZVi8UPs.
[13]   M. A. Sheikh, "Renewable energy resource potential in Pakistan," *Renew. Sustain. Energy Rev.*, vol. 13, no. 9, pp. 2696–2702, 2009.
[14]   M. S. Malkani and Z. Mahmood, "Coal Resources of Pakistan: entry of new coalfields," *Geol. Surv. Pakistan, Inf. Release*, no. 981, pp. 1–28, 2016.
[15]   M. A. Javaid, S. Hussain, A. Maqsood, Z. Arshad, A. Arshad, and M. Idrees, "Electrical energy crisis in Pakistan and their possible solutions," *Int. J. Basic Appl. Sci. IJBAS-IJENS*, vol. 11, no. 05, p. 38, 2011.
[16]   S. A. U. Rehman, Y. Cai, N. H. Mirjat, G. Das Walasai, I. A. Shah, and S. Ali, "The future of sustainable energy production in Pakistan: A system dynamics-based approach for estimating hubbert peaks," *Energies*, vol. 10, no. 11, p. 1858, 2017.
[17]   J. Macknick, R. Newmark, G. Heath, and K. C. Hallett, "Review of operational water consumption and withdrawal factors for electricity generating technologies," National Renewable Energy Lab.(NREL), Golden, CO (United States), 2011.
[18]   P. Monga, "A system dynamics model of the development of new technologies for ship systems." Virginia Tech, 2001.

Gasification of sugarcane bagasse and woodchips in a downdraft biomass gasifier

Izaz Ahsan [A], Muhammad Hassan [A], Abid Ullah[B,C], Khurshid Ahmad [A]

[A] *Department of Thermal System Engineering, U.S.-Pakistan Center for Advanced Studies in Energy, UET Peshawar,, Pakistan*
[B] *Department of Energy Engineering, University of Science and Technology China, Heife, China*
[C] *Department of Material Science and Engineering, Arizona State University, Phoenix, Arizona*

Abstract— **Most of the people in Pakistan has no access to clean cooking food source. Around 55% of the population of Pakistan still burns wood and dung cake for cooking food. Pakistan has a huge potential of biomass including sugarcane bagasse and woody biomass. Direct burning of these biomass results into waste of energy, along with harmful emissions. One of the best options is the conversion of solid biomass into gaseous form known as syngas which is efficient and environmentally friendly. For this purpose, a small-scale downdraft biomass gasification system was fabricated and simulated for wood chips and sugar cane bagasse. The system converts solid fuel into useful flammable syngas. In this study proximate and ultimate analysis of biomass was also performed. The moisture content and ash content for wood chips and bagasse was recorded as well. Moisture Content and Ash content for wood chips are 6.2% and 6.90% and for sugar cane bagasse is 5.14% and 1.53%. The H and C content for wood chips and bagasse was recorded as 6.34%, 4.7% and 45.3%, 43% respectively. The moisture content, Ash content, %H and %C are the factors effecting the performance of gasification process mainly. The calculated calorific value of wood chips/woody biomass is 19.89 MJ/Kg; while the calorific value of sugar cane bagasse is 15.33MJ/Kg. From the results we concluded that such a gasifier can be used for cooking and heating purposes in biomass rich rural areas of Pakistan.**

Keywords— Biomass gasification, Calorific value, Syngas, Ultimate analysis, Proximate analysis
.

I. INTRODUCTION

The traditional type of energy used by human beings since earlier times is biomass. All biologically produced matters are termed as biomass [1]. The energy of biomass comes through the process of photosynthesis from sun [2]. There a is dare need of renewable energy due to depletion of fossil fuels and climate change [3]. Scientists and governments worldwide; are in search of locally available renewable energy sources [4]. One of the adoptable, integrated and easily available energy source is the energy obtained from the biomass [5]. Further, the energy obtained from biomass is sustainable and environment friendly.

After three major energy sources i.e. coal, petroleum and natural gas; biomass is the fourth imperative renewable energy source. It is easily available locally and can provide energy on urgency basis [6]. In addition to, one of the considerable benefits of biomass is; its available in plenty and emit low magnitude of GHG, S [7]. 4500 EJ of biomass is produced annually.[8]. Worldwide the capacity of energy obtained from biomass is considered as sustainable source of energy. Right now, the world 50% energy demand can sustainably be fulfilled by provision of approximately 270EJ of energy obtained from biomass [9]. Furthermore, 270EJ of energy is obtained from about 6.5% of the total production of biomass annually. Land availability is directly related to the production of biomass.

Right now, the predicted agro and agro-industrial waste are; 20,494 and 25,271 million tons, respectively [10]. 1,121 million tons of wood chips is also produced right now in the world. [11] 50,000 GW h/year is the predicted biomass prepatent of Pakistan [12], that accounts for approximately 36% of the total Pakistan energy demand [13]. Conventional ways of burning of biomass is still adopted in Pakistan. Traditional methods of burning of biomass results in loss of energy along with harmful emissions. The energy shortage in Pakistan is due to high price and unavailability of fossil fuel [14]. Pakistan is an agricultural country, about 60% of the total population of Pakistan is directly or indirectly related with agrobusinesses. 62% of the peoples residing in rural area of Pakistan are relying on biomass to fulfill their needs, primarily cooking and heating purpose [15, 16, 17]. In these areas the primary biomass energy source is wood and animal waste; and they had little access to fossil fuel energy [18]. Energy crisis can

be controlled by focusing on local energy resources. Conventional burning of biomass result in wastage of energy and high greenhouse emission. CO2 emissions is mainly produced from combustion of wood and other biomass, depending upon the composition of the specific biomass. About 2.8% of Carbon dioxide is released from the combustion of wood globally [19]. Gasification of biomass is an energy efficient and economical technology that can tend toward adoption of renewable energy. The technique of transforming of any solid fuel or biomass into gaseous fuel i.e. syngas at higher temperature is known as gasification [20, 21]. The gasification reactions are conserved through heat produced from the oxidant [22].

In context of environmental point of view, energy obtained from biomass through gasification process has many advantages [23]. Conversion of biomass through gasification leads to valuable products i.e. combustible syngas, chemicals and synthetics [24]. Syngas can be then used as fuel for cooking purpose and driving mechanical engine. The fire tube/reaction tube in which gasification process occur is called gasifier. There are many types of gasifier depending upon the direction of flow of air and fuel. Compare to others types of gasification process; the downdraft biomass gasifier is cheap method of gasification and result in generation of low tar content [25]. Tar is the term used to describe the unreacted carbon and its content in gasification product and is undesirable. The optimum design of gasifier depends upon various factor such as dimensions of fire tube and system for limited supply of air. Although there are several types of biomass available in Pakistan. But the biomass focus herein are the agricultural waste of sugar cane known as sugar cane bagasse and forest wood residues; because of its availability and suitability for gasification process.

II. METHODOLOGY

A. Research activities

Literature data of downdraft biomass gasifier and selection of biomass that are available plenty in Pakistan were studied. During study few designs of downdraft gasifier comes out and that design was selected that can produce a syngas with low tar content, but the size has been reduced to lab scaled [1]. Each part of the downdraft biomass gasifier such as cyclone separator, Filter unit, grate height and angle, Dimension and specification of reaction tube inlet position of air, exit point of syngas were studied, analyzed and then fabricated; with the aim to make all part air tight, so that the gasification process may not be disturb by the external factors.

B. Simulation of Downdraft Biomass Gasifier

For simulation of downdraft biomass gasifier different articles and recent research work was study in technical and academic journal. ASPEN plus software was selected; because ASPEN is a software package that deliver a complete solution to a chemical process and reactor. For modelling each zone of gasifier various ASPEN built in gasifier should be selected; and hence ASPEN simulator don't have built in gasifier. The reactors used in the simulation of downdraft biomass gasifier are RStoic, RYield and RGibbs respectively.

C. Experimental set-up

Small-scale downdraft gasifier was designed and fabricated with a 1.0kg capacity of Biomass. The biomass used are the pieces of wood and sugar cane bagasse having size ranging from 25mm to 30mm. The gasifier was run separately for both biomasses such as wood chips and SCB. Small amount of biomass such as wood chips/SCB was added into the gasifier before fulfilling the fire tube with wood chips/SCB. The small combustion is done to attain the temperature necessary for the initiation of gasification process. When the temperature was achieved; then the fire tube is filled with full capacity of biomass used and along with controlling the supply of air/O_2 or limited supply of air/O_2.

D. Fabrication of Downdraft Biomass Gasifier

The fabrication of downdraft biomass gasifier is easy; when steps are followed strictly. Only dimensions of the fire tube should be strictly followed with the standard; The dimensions of other components like casing of firetube, Piping system, dimensions and specifications of filter unit and cyclone can be fixed any; until and unless airtightness of these components must be maintained.
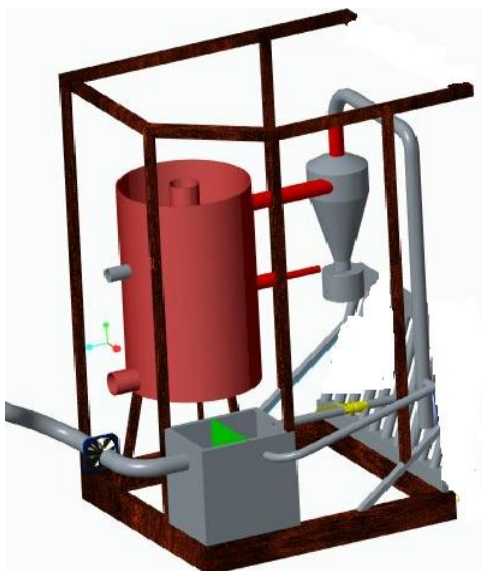
A. Creo model of downdraft biomass gasification system   B. Fabricated downdraft biomass gasification system

E. Gas Chromatographic Analysis of syngas

In order to observe the different components in the syngas precisely and closely; The GC selected for the project is Agilent 490 Micro with four columns. These four columns were attached to a Chemstation. However, in this thesis project only column one and two are used. Column one is a MS5 mol sieve whereas column two is a Pora PLOT U (PPU) column. Column one gives the peak of gaseous that contributes to higher percentage of syngas; such as He, H_2, O_2, N_2, CH_4, and CO, whereas column two measures CO_2, C_2H_4, C_2H_6 concentration in syngas. The downdraft biomass gasifier was run separately for both biomasses i.e. wood chips & SCB. The sample of the syngas were taken in airtight syringes with marking as syringes A & B respectively. The very airtight syringe A represent the syngas produced from wood chips & syringes B represent the syngas produced from SCB. Then the syngas is injected to column of GC for analysis. The interior of gas chromatograph is shown in the figure C below.
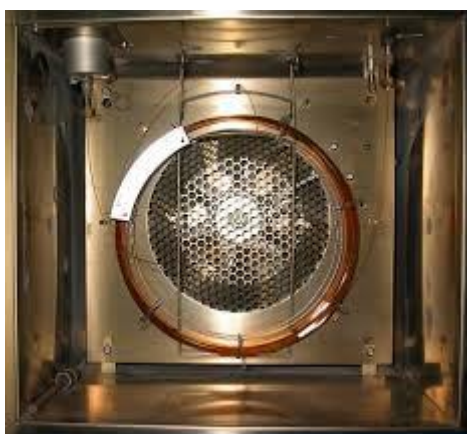
C. Interior of gas chromatograph

F. Pre-treatment of feed stocks (Wood chips/Sugar cane bagasse)

The pre-treatment of feedstock is necessary before the simulation of the downdraft gasifier. The pre-treatment of feedstock means the proximate and ultimate analysis of wood chips and sugar cane bagasse. Proximate analysis measures sulfur, moisture, volatile matter, ash, and fixed carbon in the feedstock. Proximate analysis of the desired feed stock was performed using TGA analysis. Ultimate analysis investigates the different components present in feed stock such as carbon, hydrogen, Sulphur, oxygen, and nitrogen. The ultimate analysis of woody biomass and sugar cane bagasse is performed using CNHS analyzer.

III. RESULTS AND DISCUSSION

The results of the simulation study are shown graphically in Figures 1-4. According to the literature survey the hot gas efficiency range of 85-90% for down-draft gasifies. Figure. 2 shows the conversion efficiency decreasing as particle diameter increases. According to the research larger the particle size, the higher the reactor length required to obtain the same conversion efficiency. Although a smaller particle size results in a higher conversion, very small particles may cause bridging and channeling problems, and reduce the residence time in the Gasifier.

Figure. 3 show that conversion efficiency increases as the capacity of the Gasifier decreases. A higher reactor load tends to reduce the residence time as the particle move faster. To obtain the same conversion efficiency, the reactor length has to be longer. Thus, for the same rector length the efficiency decreases for higher reactor loads. In Figure 4.6 the moisture content of wood has a significant effect on conversion efficiency Conversion efficiency reduces from 73% to 57% as moisture content increases from 0 to 40%. To obtain the same conversion, the reactor length has to be increased for fuel with higher moisture contents. Although a low moisture content results in higher conversion efficiency, for large scale gasification plants, the practical difficulties and economic factors involved in reducing the moisture content have to be considered.

In Figure 4 .7the variation of capacity and feed rate is linear as expected. In figure. 1 & 2, the efficiency of Gasifier at higher temperatures is better, and produced more CO and H_2 gases and low quantity of CH_4 and CO_2 gases as compared to low temperature process. The optimum temperature of gasification of sugar cane bagasse is 690 C whereas the optimum temperature for gasification of woody biomass/wood chips is 750 C in case of our result. The gas chromatography result is comparable with the literature result. From the calculation of energy conversion efficiency, we can conclude that about same amount of energy is generated from the gasification and direct combustion of sugar cane bagasse, but gasification is preferable; because gasification process is environmentally friendly.

The energy conversion efficiency of syn gas produced from the gasification of wood chips is higher having value of 90%. While the energy obtained from the same amount of wood chips through direct combustion is 60%. Thus, by burning same amount of wood directly through combustion is energy inefficient compare to burning of syn gas produced from the gasification of same amount of wood chips. Looking to the results one can conclude that biomass gasification can be used as alternative of direct combustion in rural area of Pakistan, where biomass is available plenty. This will decrease the dependent on fossil fuel and harmful emissions associated with direct combustion of biomass. So, we can use biomass gasification system as an alternative of combustion in rural area of Pakistan, where biomass is available plenty

TABLE I: RESULT OF PROXIMATE ANALYSIS WOOD CHIPS & SCB

%	Wood Chips	SCB		Standard
Moisture Content	6.2	5.14		ASTM E1358-97
Volatile Content	75.70	67.99		ASTM E872
Ash Content	6.90	4.53		ASTM E1534-93(2019)
Fixed Carbon	11.20	15.19		*ASTM* E870

TABLE I I: RESULT OF ULTIMATE ANALYSIS WOOD CHIPS & SCB

%	Wood Chips	SCB		Standard
C	45.3	43		ASTM D5375-02
H	6.36	4.7		ASTM D5375-02, (E 777)
O	4.145	43		The Oxygen is calculated value
N	0.12	0.2		ASTM D53/3--02, (E 778)
S	0.14	0.04		ASTM D5375-02, (E 775)

TABLE III: Simulation result of sugar cane bagasse at different temperature

Simulation	1	2	3
Temperature (C°)	690	730	750
Gas Comp Vol (%)			
CO	59.42	56.82	53.57
H_2	15.30	18.32	23.21
CO_2	35.32	25.37	21.00
CH_4	0.1	0.4	2.40

TABLE III: Simulation result of wood chips at different temperature

Simulation	1	2		3
Temperature (C°)	700	800		900
Gas Comp Vol (%)				
CO	56.83	55.32		53.23
H2	25.2	26.32		27.24
CO2	8.43	10.50		14.32
CH4	6.32	5.32		1.86

TABLE III: GC result of syngas produced from SGC & Wood Chips

Percent Comp	SGC Syn gas	Wood Chips Syn gas		
H2	18.35	14.32		
N2	38.33	47.32		
CO	23.25	22.42		
CO2	8.30	7.52		
CH4	2.53	1.30		
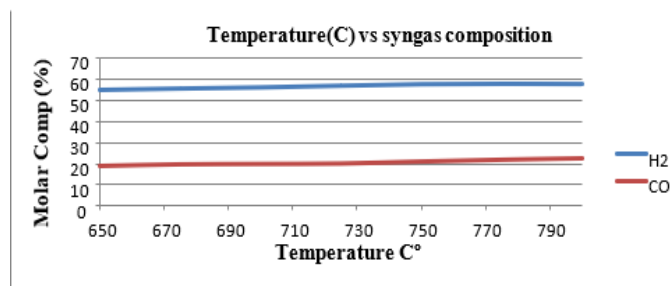
Fig. 1. Percent mole comp (H_2 & CO) versus Temp C°
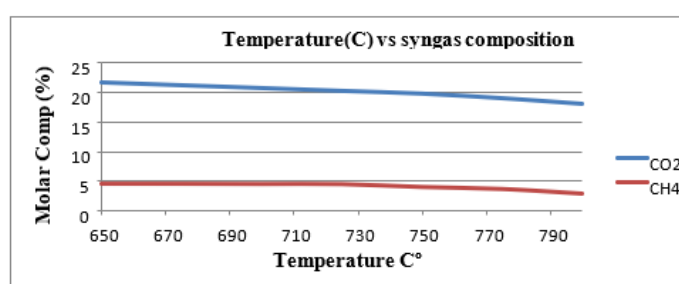
Fig. 2. Percent mole comp (CO_2 & CH_4) versus Temp C°
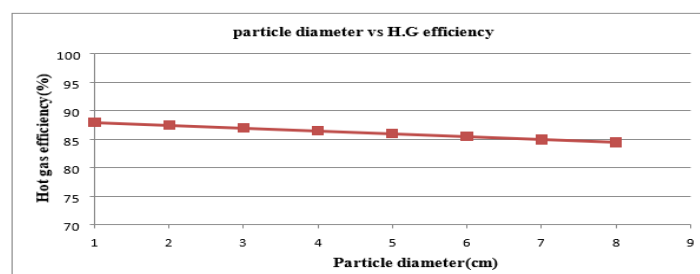
Fig. 3. Particle diameter vs hot gas efficiency of Downdraft Gasifier
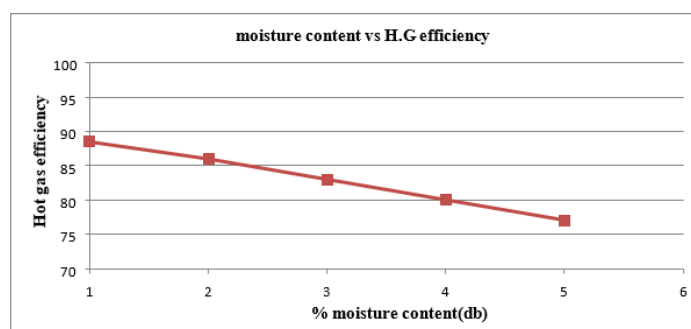
Fig. 4. Moisture vs HGE of Downdraft Gasifier

IV. CONCLUSION

Using downdraft biomass gasifier not only convert solid biomass into syngas, but is energy efficient and environmentally friendly. According to the experimental analysis the calculated calorific value of wood chips/woody biomass is 19.89 MJ/Kg; while the calorific value of sugar cane bagasse is 15.33MJ/Kg. The results suggest that such a gasifier can be used for cooking and heating purposes in biomass rich rural areas of Pakistan.

V. REFERENCES

[1] Mehedintu, A.; Sterpu, M.; Soava, G. Estimation and forecasts for the share of renewable energy consumption in final energy consumption by 2020 in the European union. Sustainability 2018, 10, 1515.

[2] Contescu, C.I.; Adhikari, S.P.; Gallego, N.C.; Evans, N.D.; Biss, B.E. Activated Carbons Derived from High Temperature Pyrolysis of Lignocellulosic Biomass. C, Journal of carbon research 2018, 4, 51.

[3] Abbasi, T., Premalatha, M., & Abbasi, S. (2011). The return to renewables: Will it help in global warming control? Renewable and Sustainable Energy Reviews, 15, 891–894

[4] Lu, Y., Nakicenovic, N., Visbeck, M., & Stevance, A.-S. (2015). Policy: Five priorities for the UN sustainable development goals. Nature, 520, 432–433. http://dx.doi.org/10.1038/520432a

[5] Twidell, J., & Weir, T. (2015). Renewable energy resources. Routledge.

[6] Rehman M Saif Ur, Rashid Naim, Saif Ameena, Mahmood Tariq, Han Jong-In. Potential of bio energy production from industrial hemp (cannabis sativa): Pakistan perspective. Renew Sustain Energy Rev 2013; 18:154–64.

[7] Roberts D. 2007. Globalization and Its Implications for the Indian Forest Sector. TIFAC/IIASA Joint Workshop "Economic, Societal and Environmental Benefits Provided by the Indian Forests", New Delhi, India, April.

[8] Sims R.H. 2004. Bioenergy Options for a Cleaner Environment: In Developed and Developing Countries. Elsevier Ltd., Oxford, UK, 184 pp.

[9] Hall D.O. & Rosillo-Calle F. 1998. Biomass - other than wood. World Energy Council 1998, Survey of Energy Resources, 18th Edition, London, pp.227-241.

[10] Anwar, Z., Gulfraz, M., and Irshad, M. (2014). Agro-industrial lignocellulosic biomass a key to unlock the future bio-energy: a brief review. J. Radiat. Res. Appl. Sci. 7, 163–173. doi: 10.1016/j.jrras.2014.02.003

[11] Farooqui, S. Z. (2014). Prospects of renewables penetration in the energy mix of Pakistan. Renew. Sustain. Energy Rev. 29, 693–700. doi: 10.1016/j.rser.2013.08.083

[12] Asif, M. (2009). Sustainable energy options for Pakistan. Renew. Sustain. Energy Rev. 13, 903–909. doi: 10.1016/j.rser.2008.04.001

[13] Raheem, A., Abbasi, S. A., Memon, A., Samo, S. R., Taufiq-Yap, Y. H., Danquah, M. K., & Harun, R. (2016). Renewable energy deployment to combat energy crisis in Pakistan. Energy, Sustainability and Society, 6(1), 16.

[14] Kakar, Z. K., Khilji, B. A., & Khan, M. J. (2011). Relationship between education and economic growth in Pakistan: A time series analysis. Journal of International Academic Research, 11(1), 27-32.

[15] Sahir, M. H., & Qureshi, A. H. (2008). Assessment of new and renewable energy resources potential and identification of barriers to their significant utilization in Pakistan. Renewable and Sustainable Energy Reviews, 12(1), 290-298.

[16] Jan, I. (2012). What makes people adopt improved cook stoves? Empirical evidence from rural northwest Pakistan. Renewable and sustainable energy reviews, 16(5), 3200-3205.

[17] Shaikh, F., Ji, Q., & Fan, Y. (2015). The diagnosis of an electricity crisis and alternative energy development in Pakistan. Renewable and Sustainable Energy Reviews, 52, 1172-1185.

[18] Tam, C. K., & Ahuja, K. K. (1990). Theoretical model of discrete tone generation by impinging jets. Journal of Fluid Mechanics, 214, 67-87.

[19] Xu, D., Tree, D. R., & Lewis, R. S. (2011). The effects of syngas impurities on syngas fermentation to liquid fuels. biomass and bio energy, 35(7), 2690-2696.

[20] Richardson, Y., Blin, J., & Julbe, A. (2012). A short overview on purification and conditioning of syngas produced by biomass gasification: catalytic strategies, process intensification and new concepts. Progress in Energy and Combustion Science, 38(6), 765-781.

[21] Babu, B. V., & Chaurasia, A. S. (2003). Modelling, simulation and estimation of optimum parameters in pyrolysis of biomass. Energy Conversion and Management, 44(13), 2135-2158.

[22] Ahuja, D. R. (1990, May). Research needs for improving bio fuel burning cook stove technologies: incorporating environmental concerns. In Natural Resources Forum (Vol. 14, No. 2, pp. 125-134). Oxford, UK: Blackwell Publishing Ltd.
[23] Tate, K. R., Scott, N. A., Saggars, S., Gilt rap, D. J., Baisden, W. T., Newsome, P. F., ... & Wilde, R. H. (2003). Land-use change alters New Zealand's terrestrial carbon budget: uncertainties associated with estimates of soil carbon change between 1990–2000. Tellus B: Chemical and Physical Meteorology, 55(2), 364-377.
[24] Rodríguez-Labajos, B. (2015). Patterns of global biomass trade.
[25] Malkani, M. S., Mahmood, Z., Somro, N., & Shaikh, S. I. (2017). Revised Stratigraphy and Mineral Resources of Kirthar Basin, Pakistan. GSP, IR, (1010), 1-59.

Abbreviations and Acronyms

ASPEN	Advanced System for Process Engineering
EJ	Exa Joule
LPG	Liquified Petroleum Gas
C	Carbon
GHG, S	Green House Gases
MSW	Municipal Solid Waste
SCB	Sugar Cane Bagasse
TCD	Tons of Cane Per Day
GDP	Gross Domestic Product
ASPEN	Advanced System for Process Engineering
F_C	Centripetal Force
CGE	Cold Gas Efficiency
HGE	Hot Gas Efficiency
ASTM	American society for testing and materials
CV	Calorific Value
GCV	Gross Calorific Value
NCV	Net Calorific Value
KW	Kilowatt

.

Technical Session 5-A (Google meet/Zoom) Quality, Optimization and Performance analysis	
Session Chair: **Prof. Dr. Nadia Tahir** Session Co-Chair: **Dr. Imran Ahmad**	
Hassan Sardar *(USPCAS-E UET Peshawar)*	Optimization of Inventory Management in Frontier Foundation Foundry Pvt. Ltd. (FF Steel)
M. Adnan *(PIEAS Islamabad)*	Performance comparison of Shell and General Electric Gasifiers for low quality Pakistani coal
Kashif Ismail *(USPCAS-E UET Peshawar)*	Thermal Energy Efficiency Assessment of Small and Medium Industries: A Case Study.
M.Yahya *(Dept. of Chem Eng., UET Peshawar)*	Comparative study of Conventional and microwave assisted pyrolysis of corncob.
Zaeem Ahmed *(USPCAS-E UET Peshawar)*	Energy Efficiency Resource Assessment for Marble Industry of Peshawar City

Optimization of Inventory Management in Frontier Foundry Pvt Ltd (FF Steel)

Hassan Sardar [a], Misbah Ullah [a, *], Shafi Ur Rehman [b], Zarak khan

[a] University of Engineering and Technology Peshawar, Pakistan

[b] U.S.-Pakistan Center for Advanced Studies in Energy (USPCAS-E), UET Peshawar,

Pakistan

hsuet2940@gmail.com [a], engr.shafi2962@gmail.com [b], zk@ff.com.pk

Abstract-Inventory management is a technique of controlling, storing, and keeping track of the inventory items. Inventory management regulates all the operations that are involved from the moment an item enters the store until it has been used. In this research, real inventory problem in FF Steel has discussed, industry managed the inventory of 1450 store items by ordinary method of replenishment and not considering the inventory ordering and holding costs and not defining the safety stock which obviously affect the service level. The objective of our inventory management to make decision regarding the appropriate level of inventory. We have categorised the inventory by ABC analysis on the basis of annual cost. We focus our research on managing the inventory level for spare parts, class A and B which commonly known as important classes. We have focused on economic order quantity method to determine the ordering quantity and reorder point for the inventory. The result from the research indicates that the economic order quantity method gives a significant amount of saving compared to an existing policy used by the company. The proposed policy gives average saving 41% of 30 category A items and 73% of 30 category B items. Safety Stock levels are decided by considering 95% service level and decided the Re order point for inventory.

Keywords: Economic order quantity (EOQ), Re-order point, Safety stock, Service level.

I. INTRODUCTION

Frontier Foundry (FF Steel) is one of the fastest and largest re-rolling mill in Pakistan. FF Steel is the only manufacturer intrusively produce Grade-60 and Grade-75 deform steel bars of different sizes (3mm to 36mm) according to the standards of ASTM-615 and ASTM-706 [1, 2] Since its foundation in 1986, the company has excellent in manufacturing steel products by meeting the international standard. The company has superiority over other re-rolling mills also in the quality assurance procedure and process.

FF Steel recently launched two software that is SAP Business and SCADA System. SAP is used to smoothen the business operations and SCADA is used for the Optimal Quality Production. Automatic Cutting Machine also play its roll to attain the accurate steel bars length. To achieve fine grain size of quality steel bars, 120 feet long cooling bed allows the hot steel bars to cool down at room temperature. Automatic bar bundling machine also play its function to make best steel bundles of required weight in best finished shape. CNC machine is used for ribs and steel bar fins size accuracy purpose. Finished products of different sizes are tested by UTM machines.

Inventory is nothing but a stock of goods that we maintain to facilitate the continuous production of goods and services [3]. According to the Monks, inventory as an idle resources that possess economic value [4]. According to the Sundaresan inventory is defined as the sum of raw materials, fuels, lubricant, spare parts, maintenance consumable, semi processed material and finished stock at any point of time [5]. According to the ARTB the term inventory means the aggregate of those items of tangible personal property which are held for ordinary course of business and to process the smooth production [6].

Inventories are held basically to smoothen the operations of the firm. Shortage of inventory at any point would disrupt operations resulting in either idle time for men and machines or lost sales. A manufacturing firm may have inventories of different

stages in the production process. Generally, the inventory can be classified into four major types. Such as raw materials inventory, work in process inventory, finished goods inventory and MRO.

A. Literature Review and Data Collection

The spare parts inventory system is extensively studied by many researchers. First inventory model was introduced by J. D. Croston [10] forecasting and stock control of intermitted demand. Aris A Syntetos and Jon E Boylan Studied the Accuracy of intermitted demand estimates by collecting four forecasting methods. Simple Moving Average, Single Exponential Smoothing (SES), Croston's method, and a new method (based on Croston's approach) recently developed by the authors, are compared on 3000 real intermittent demand data series from the automotive industry [11].
Aris A Syntetos and Jon E Boylan studied on the stock control performance of intermittent demand estimators [12]. Aris A Syntetos and Jon E Boylan [10-12] proposed the deterministic inventory model for spare parts which is considering some forecasting methods. The demand for consumable spare parts is forecasted and then the optimal inventory level had determined by some formula and calculation.
Mehdizadeh, M. (2019) studied the Integrating ABC analysis and rough set theory to control the inventories of distributor in the supply chain of auto spare parts [13].
ABC classification system is a method that classifies the spare parts based on how critical the spare parts for the company. This method, segments the spare parts into three categories, that is A, B and C. A items make up roughly 20 percent of the total number of items and represent 80 percent of the dollar sales volume. B items comprise roughly 30 percent of the items and represent 15 percent of the dollar volume. C items comprise roughly 50 percent of the items and represent only 5 percent of dollar volume. The A items must receive more attention from manager. The B items are of secondary importance in relation to class A items and the class C items are relatively unimportant items, hence, the manager can manage them as simple as possible [13,14].
Chu, C. W, Liang, & Liao research Controlling inventory by ABC analysis and fuzzy classification combining both [14].
Teunter and Sani gave their research attention on the lumpy demand. They used order-up-to policy to determine the inventory level, which previously used the method by Croston method to forecast the demand. Result from this work is that the combination of Croston method and order up-to-level policy result in optimal service level [15].
Parras and Dekker determine spare parts inventory level at oil refinery it compares different re-order point methods for effective spare parts inventory control, motivated by a case study at a large oil refinery. Different demand modelling techniques and inventory policies using the oil and refinery inventory data [16].
Van Jaarsveld, W., Dollevoet, T., & Dekker, R. worked on improving spare parts inventory control at a repair shop spare parts are allocated on a first come first served basis to repairs, and their inventory is controlled using (s, S) policies [17].
De Smidt-Destombes, K. S., van der Heijden, M. C., & van Harten, worked on Joint optimization of spare part inventory, maintenance frequency and repair capacity for k-out-of-N systems. To achieve a high system availability at minimal costs, relevant decisions include the choice of preventive maintenance frequency, spare part inventory levels and spare part repair capacity. We develop heuristics for the joint optimization of these variables for (a) a single k-out-of-N system under condition-based maintenance and (b) an installed base of multiple identical k-out-of-N systems under block replacement [18].
Kilpi J., Toyli J., & Vepsalainen, A. Develop Cooperative strategies for the availability service of repairable aircraft components and determined the factor that give the contribution to the cooperative strategy [19].
Wong, H., Van Oudheusden, D., & Cattrysse investigated the Cost allocation problem in the context of repairable pooling with game theoretical model [20]. The results of this research showed that the cost allocation policy affect the company's policy in making the decision in the inventory management. Even many methods have been implemented in the determining spare parts inventory level, lack of

them considering the utilization of continuous review model and periodic review model in the reducing the total inventory cost.

In this research we will determine the spare parts inventory level in order to minimize the total inventory cost. We will focus both periodic review model and continuous review model and safety stock. The research from many studies showed that the periodic review policy and continuous review policy are more easily than other inventory policies. The focus on determining the optimal inventory policy for category A and B. There are four types of inventory policies which are Periodic review policy, order up-to-r policy, continuous review policy and EOQ model.

An economic order quantity system is the arrangement in which the inventory level is continuously monitored and replenishment stock is ordered in previously-fixed quantities whenever at-hand stock falls to the established re-order point [27].

Before starting to calculate the EOQ model important assumption are fixed. Ordering cost is constant, the rate of demand is also constant, the lead time (LT) is fixed, the purchase price of an item is constant, the replenishment is made instantaneously and the whole batch is receiving at once.

Let x be the lot size of the company

Ordering cost is denoted by S

Holding cost is denoted by H

Annual demand is denoted by D

Total cost is denoted by T.C

Optimum lot size is x_{opt}

Ordering cost per year = No of order/year * Ordering cost /order

Ordering cost per year = $\frac{D \times S}{x}$ ……………………….…… eq (1)

Carrying cost per year = Average inventory $\times$ Carrying cost

Let min inventory = 0 Max inventory = x

Av inventory = $\frac{(0+x)}{2} = \frac{(x)}{2}$

Carrying cost per year = $\frac{(x)}{2} H$ …………………………. eq (2)

Material cost or purchasing cost = Total demand $\times$ Cost per unit

Material cost or purchasing cost = $D \times C_p$……………………. eq (3)

Equation 1 and 2 is a function of x and equation 3 is not a function of x

$\frac{D \times S}{x} = F(x)$ and $\frac{(x)}{2}H = F(x)$ but $D \times C_p \neq F(x)$

Total inventory cost = O. cost/year + H cost/year + Purchasing cost

Total inventory cost (T.C) = $\frac{D \times S}{x} + \frac{(x)}{2} H + D \times C_p$ ……………… eq (4)

T.C /year = $F(x)$

Tacking $\frac{dy}{dx}$ both side $\frac{d(\text{T.C})}{dx} = \frac{d}{dx}\frac{DS}{x} + \frac{d}{dx}\frac{x}{2}H + \frac{d}{dx}DC_p$

We want to minimize the total cost so that we put $\frac{d(\text{T.C})}{dx} = 0$

$0 = -\frac{D}{x^2}s + \frac{H}{2} + 0$

$\frac{D}{x^2}s = \frac{H}{2}$ the $x_{opt} = \sqrt{\frac{2DS}{H}}$ ………… eq (5)

It is the best lot size on which total cost will be minimum it is also called economic order quantity [28, 36]. In this model purchasing cost excluded because the $D \times C_p \neq F(x)$

Total cost per year at x_{opt}, using equation 4

Total inventory cost (T.C) = $\frac{D \times S}{\sqrt{\frac{2DS}{H}}} + \frac{\sqrt{\frac{2DS}{H}}}{2} H = \sqrt{2DSH}$………… eq (6)

In inventory management, two primary questions are related. How much should be ordered? and when to ordered? [27]. The determination of when to order in a continuous inventory system is the reorder point, the inventory level at which a new order is placed. The concept of lead time is illustrated, it is

the combination of procurement administrative lead time, production lead time and procurement lead time [32].
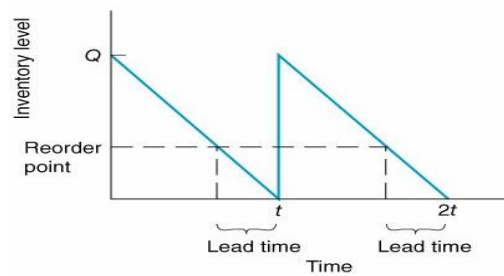
Fig. 1. Lead time and re-order point

The reorder point in basic economic order quantity calculated by multiplication of lead time with consumption rate.

ROP = TL × r, While TL is lead time and r is the consumption rate per unit time.
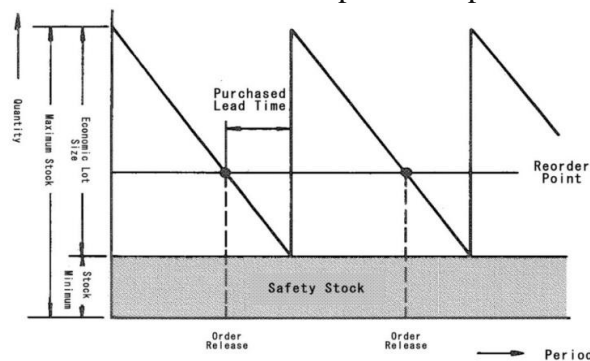
Fig. 2. Safety stock.

II. METHODOLOGY

In the first stage of our research we have collected 1450 different spare parts and classify it on the basis of ABC analysis. ABC analysis carried on the basis of annual consumption value and selected 30 category A and 30 category B items for detail analysis. Determining ordering cost, holding cost and number of orders per year of each selected item and then determined the inventory cost of the existing company policy. Determining the ordering quantity, re-order point and inventory cost by considering EOQ. Determining safety stock by inducting 95% service level.

```
┌─────────────────────────────────────────┐
│  Data Collection of 1450 inventory items │
└─────────────────────────────────────────┘
                    │
                    ▼
┌─────────────────────────────────────────┐
│  Classification of inv. items by ABC     │
│  Analysis                                │
└─────────────────────────────────────────┘
                    │
                    ▼
┌─────────────────────────────────────────┐
│  Selection of 30 Category A and 30       │
│  Category B items for further analysis   │
└─────────────────────────────────────────┘
                    │
                    ▼
┌─────────────────────────────────────────┐
│  Determining ordering cost, Holding cost │
│  and number of order per year            │
└─────────────────────────────────────────┘
                    │
                    ▼
┌─────────────────────────────────────────┐
│  Determining the inventory cost of       │
│  existing company policy                 │
└─────────────────────────────────────────┘
                    │
                    ▼
┌─────────────────────────────────────────┐
│  Determining the ordering quantity, re-  │
│  order point and inventory Cost by       │
│  considering EOQ                         │
└─────────────────────────────────────────┘
                    │
                    ▼
┌─────────────────────────────────────────┐
│  Determining Safety stock by inducting   │
│  95% service level                       │
└─────────────────────────────────────────┘
```
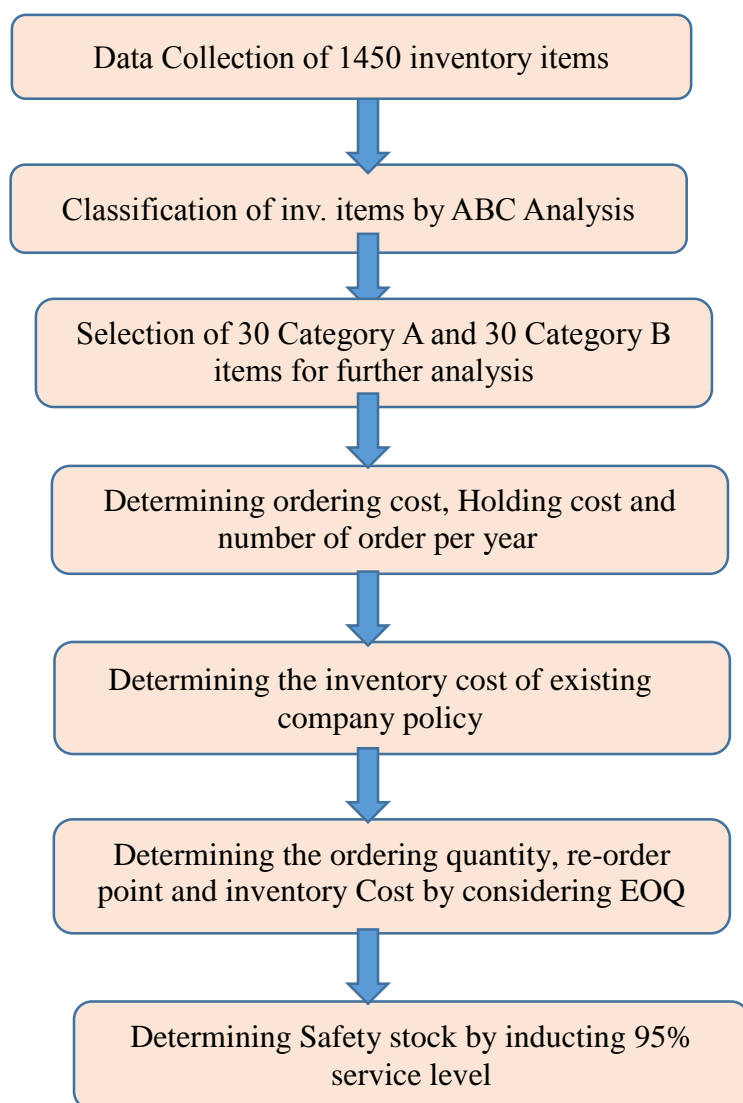
The actual data of inventory spare parts provided by FF Steel, is the one-year data from 30th September 2018 to 30th September 2019. It consists of 1450 different items. This data generated by SAP Business 1 software.

Table I. Format of data collected from FF Steel Mill.

Item Code	Item Name	Unit	Purchased Qty per Year	Issued Qty per year	Unit Price	Total Cost (Rs)
SS00003203	Breaker 2 amp 2/pole	Each	20.00	13.00	1,000	20000
SS00003479	Nut for pneomatic Jack	Each	44.00	16.00	453	19960
SS00000040	Grinder Baby 4"	Each	5.00	11.00	3,980	19900
SS00000191	Belt B-110	Each	40.00	33.00	495	19800
SS00001567	Grease Gun Hydraulic (Big)	Each	1.00	1.00	19,800	19800
SS00002488	Gun Metal Bush (Casting)	KGs	24.60	24.60	800	19680

ABC analysis is the technique of inventory optimization in which items divide in three different category A, B, C on the basis of annual Consumption values.

Table II: ABC Analysis results table

Categories	Values	Number of items	%age of items	%age of values
Category A ≥70000	28905800	122	8%	69%
Category 20000≤ B< 70000	7731449	206	14%	18%
Category C<20000	5443935	1123	77%	13%
Total	42081184	1451	100%	100%
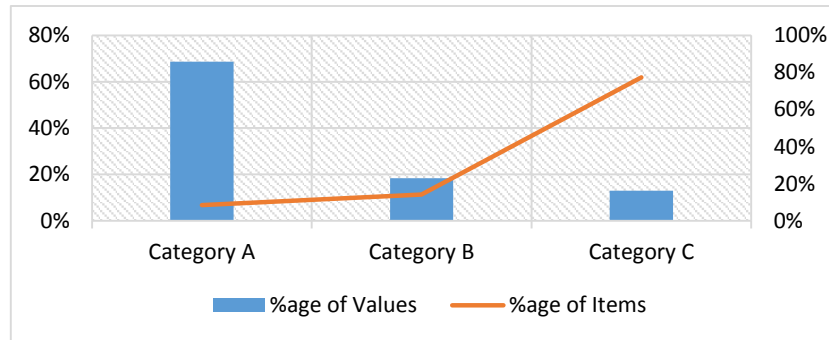
Fig. 3. ABC Analysis of Store inventory

III. RESULTS AND DISCUSSION

Economic Order Quantity policy is proposed for the FF steel inventory system, in which fixed quantity or optimum quantity (Q*) replenishment order place considering lead time. Number of orders considerably decreased and percentage saving will help us to understand the new policy.

Table III. Annual total cost the company policy and proposed policy and % savings category A.

Item Code	Purchased Qty per year (D)	Existing Policy Order Quantity per order X	No of order D/X	Annual total cost without purchasing cost =(X/2)*H + (D/X)*S	Economic Order Quantity Q*	No of order of EOQ D/Q*	Annual total cost without purchasing cost =(Q*/2)*H + (D/Q*)*S	Percentage saving (ECP-EOQ)/EOQ*100
SS00002543	7,200	1200	6	112620	2394	3.0	90240	24.8
SS00000496	379	15	25	11478	21	18.1	10872	5.6
SS00003695	4	1	4	23602	1	4.0	23602	0.0
SS00000322	12,765	700	18.2	24990	1858	6.9	16491	51.5
SS00002748	3,280	1200	2.73	46631	1987	1.7	41273	13.0
SS00000495	474	20	23.70	29776	92	5.1	12328	141.5
SS00000036	6,002	800	7.50	15240	1344	4.5	13397	13.8
SS00000959	840	200	4.20	16170	231	3.6	16002	1.0
SS00000734	1,325	60	22.0	12338	175	7.6	7567	63.1
SS00003976	4,200	1200	3.50	35800	2274	1.8	29557	21.1
SS00004027	20370	4000	5.09	35755	9696	2.1	25210	41.8
SS00000519	7,440	240	31.00	16340	1031	7.2	7217	126.4
SS00000435	3,600	100	36.00	13195	460	7.8	5475	141.0
SS00003693	60	30	2.00	12587	15	4.1	9889	27.3

SS00002464	328	40	8.20	10197	72	4.6	8660	17.7
SS00002590	280	12	23.33	13668	47	6.0	6547	108.8
SS00003274	6	4	1.50	16610	2	2.8	13889	19.6
SS00000437	117	12	9.72	23024	43	2.7	11859	94.2
SS00002663	75	12	6.25	30525	41	1.8	16432	85.8
SS00003356	2,490	1200	2.08	19350	1612	1.5	18537	4.4
SS00001267	580	10	58.00	17646	84	6.9	4138	326.5
SS00000432	398	80	4.98	17668	187	2.1	12764	38.4
SS00000407	4	1	4.00	12050	2	2.4	10696	12.7
SS00003127	15	12	7.50	25340	6	2.5	10169	149.2
SS00000546	1,230	600	2.05	31925	1210	1.0	25412	25.6
SS00002938	21	12	10.50	28371	8	2.5	10159	179.3
SS00000370	11	4	2.75	14298	6	1.9	13413	6.6
SS00002466	120	12	10.00	8749	29	4.1	6122	42.9
SS00003716	1,695	800	2.12	6972	358	4.7	5203	34.0
SS00003244	20	4	5.00	12421	8	2.5	9842	26.2
				695337			492958	41.1

In the above Table III shows the benefit of the proposed policy with company policy, one can see the significant amount of saving in average 41.10%. The largest saving (326.5%), (179.3%), (149.2%), (141.0%), and (126.4%) of the items (SS00001267), (SS00002938), (SS00003127), (SS00000435) and (SS00000519). It is found that one item (SS00003695 have zero effect.

Table IV. Annual Total Cost the Company policy and proposed Policy and % savings category B

Item Code	Purchased Qty per year (D)	Existing Policy Order Quantity per order X	No of order D/X	Annual total cost without purchasing cost =(X/2)*H + (D/X)*S	Economic Order Quantity Q*	No of order of EOQ D/Q*	Annual total cost without purchasing cost =(Q*/2)*H + (D/Q*)*S	Percentage saving (ECP-EOQ)/EOQ*100
SS00002617	3	1	3	4746	2	2	4062.0	16.8
SS00003182	530	100	5	3814	224	2	2839.3	34.3
SS00002245	16	8	2	8054	16	1	6506.6	23.8
SS00003471	16	4	4	5620	10	2	3967.9	41.6
SS00003692	2	2	1	5259	2	1	5105.9	3.0
SS00003575	5	1	5	10650	4	1	5099.0	108.9
SS00004015	5	1	5	10650	4	1	5099.0	108.9
SS00004016	5	1	5	10650	4	1	5099.0	108.9
SS00003583	30	10	3	13075	33	1	7183.3	82.0
SS00003219	23	8	3	7733	19	1	5442.8	42.1
SS00000926	400	100	4	5600	245	2	3919.2	42.9
SS00000731	88	12	7	4100	35	3	2519.9	62.7
SS00003216	88	30	3	5475	61	1	4350.0	25.9
SS00000745	341	30	11	5959	137	2	2494.5	138.9
SS00003153	7	1	7	8844	4	2	3863.7	128.9
SS00000973	424	50	8	4599	172	2	2468.2	86.3
SS00000732	96	10	10	5117	39	2	2467.8	107.4
SS00000102	2	12	1	20000	2	1	4899.0	308.2
SS00003509	4	2	2	3100	2	2	3098.4	0.1
SS00003745	2	2	1	6000	2	1	6000.0	0.0
SS00003299	326	50	7	8291	207	2	3791.2	118.7
SS00003246	20	5	4	16749	23	1	6921.6	142.0
SS00001479	19	5	4	6483	13	1	4224.9	53.4

SS00000796	171	40	4	4116	89	2	3085.2	33.4
SS00002463	50	16	3	5632	36	1	4208.1	33.8
SS00000898	105	120	5	11244	75	1	4205.4	167.4
SS00003662	43	43	1	5903	44	1	5901.7	0.0
SS00003353	30	10	3	4567	19	2	3731.0	22.4
SS00003579	321	321	1	6889	378	1	6798.8	1.3
SS00001564	2,400	300	8	11561	1672	1	4020.1	187.6
				230477			133373.4	72.8

In the above Table IV shows the benefit of the proposed policy with company policy of Category B, we can see the significant amount of saving in average 72.8%. The largest saving (308.2%), (187.6%), (167.4%), (138.90%), and (142.0%) of the items (SS00000102), (SS00001564), (SS00000898), (SS00000745) and (SS00003246). It is found that three store and spare items (SS00003662), (SS00003745) and (SS00003509) have zero effect.
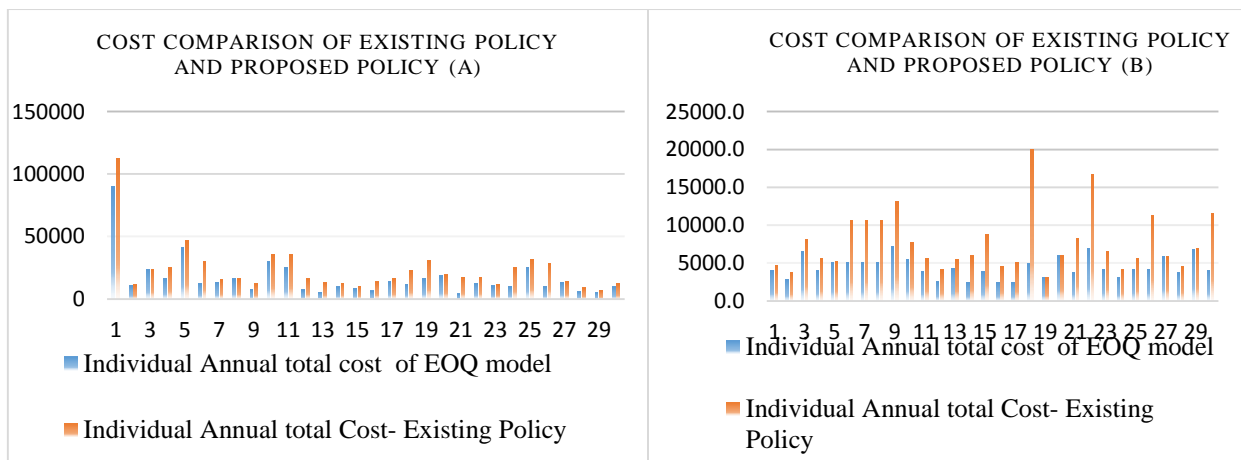
Fig. 4. Item wise cost comparison of the Existing policy and EOQ of Category A and B

A. Safety stock, service level Cost and ROP considering 95% service level

Safety stock also known as buffer stock is calculated, considering the variance in lead time, A 95% service level means the stock out risk is 5%, and has a z-score $Z_{95} = 1.645$

Table V. Safety Stock, ROP and T inventory Cost Considering 95% service level category A

Item Code	Economic Order Quantity Q*	Standard deviation of lead time in month =σLT 15% LT	Service factor Z at 95% service level	Safety Stock SS=Z*σLT* D avg concerning only lead time	ROP including safety level =TL*r +SS	Total inventory cost per year including safety stock and 95% service level = (D/Q*)*S+(Q*/2 +SS) H
SS00002543	2394	1.24	1.64	1276	1953	138359
SS00000496	21	0.18	1.64	9	14	15535
SS00003695	1	0.53	1.64	0	0	32308
SS00000322	1858	0.27	1.64	384	587	19899
SS00002748	1987	1.24	1.64	341	522	48358
SS00000495	92	0.18	1.64	12	18	13872
SS00000036	1344	0.13	1.64	126	193	14651
SS00000959	231	0.44	1.64	51	78	19521
SS00000734	175	0.18	1.64	32	49	8960
SS00003976	2274	0.93	1.64	508	777	36158

Item Code						
SS00004027	9696	0.93	1.64	2360	3611	31346
SS00000519	1031	0.18	1.64	179	274	8469
SS00000435	460	0.09	1.64	45	69	6012
SS00003693	15	0.53	1.64	4	7	12845
SS00002464	72	0.27	1.64	12	18	10074
SS00002590	47	0.18	1.64	7	10	7469
SS00003274	2	1.33	1.64	0	1	16221
SS00000437	43	0.18	1.64	2	3	12448
SS00002663	41	0.27	1.64	5	7	18289
SS00003356	1612	0.93	1.64	316	484	22172
SS00001267	84	0.13	1.64	10	15	4635
SS00000432	187	0.44	1.64	24	37	14405
SS00000407	2	0.18	1.64	0	0	11010
SS00003127	6	0.27	1.64	0	1	10794
SS00000546	1210	1.24	1.64	110	169	27726
SS00002938	8	0.27	1.64	1	1	11094
SS00000370	6	0.53	1.64	1	2	15785
SS00002466	29	0.27	1.64	5	8	7194
SS00003716	358	0.53	1.64	123	188	6987
SS00003244	8	1.99	1.64	1	1	10500
Total inventory Cost of SS with Service Level 95%						613094

Table VI. Safety Stock, ROP and Total inventory Cost Considering 95% service level category B

Item Code	Economic Order Quantity Q*	Standard deviation of lead time in month =σLT 15% LT	Service factor	Safety Stock SS = Z*σLT*D avg concerning only lead time	ROP including safety level =TL*r +SS	Total inventory cost per year including safety stock and 95% service level = (D/Q*)*S+(Q*/2 +SS)H
SS00002617	2	0.66	1.64	0	1	4478
SS00003182	224	0.18	1.64	13	92	2998
SS00002245	16	0.22	1.64	0	2	6607
1SS00003471	10	0.66	1.64	1	11	4563
SS00003692	2	0.22	1.64	0	0	5303
SS00003575	4	0.93	1.64	1	5	5924
SS00004015	4	0.93	1.64	0	3	5594
SS00004016	4	0.93	1.64	0	3	5594
SS00003583	33	0.93	1.64	4	28	8002
SS00003219	19	0.18	1.64	0	1	5497
SS00000926	245	0.18	1.64	10	71	4074
SS00000731	35	0.18	1.64	2	17	2684
SS00003216	61	0.53	1.64	10	73	5059
SS00000745	137	0.13	1.64	7	49	2616
SS00003153	4	0.27	1.64	0	1	3960
SS00000973	172	0.18	1.64	8	61	2587
SS00000732	39	0.27	1.64	4	26	2696
SS00000102	2	0.27	1.64	0	0	5008
SS00003509	2	0.53	1.64	0	1	3316
SS00003745	2	0.27	1.64	0	0	6109

SS00003299	207	0.22	1.64	10	73	3972
SS00003246	23	1.99	1.64	3	20	7736
SS00001479	13	0.27	1.64	0	3	4339
SS00000796	89	0.18	1.64	1	11	3136
SS00002463	36	0.27	1.64	2	11	4392
SS00000898	75	0.18	1.64	2	18	4341
SS00003662	44	0.18	1.64	1	8	6042
SS00003353	19	0.13	1.64	0	3	3805
SS00003579	378	0.93	1.64	41	300	7532
SS00001564	1672	0.18	1.64	51	374	4142
Total inventory Cost of SS with Service Level 95%						142105

B. Effect of service level vs inventory cost.

Service level is the expected probability of not hitting a stock-out during the next replenishment cycle. We are checking different service level and its effect on inventory cost

Table VII. Show the inventory cost at different service level of category A and B items

Service Level	Service factors Z	Total inv. Cost of A items		Service Level	Service factors Z	Total inv. Cost of B items
50%	0	492958		50%	0	133373
60%	0.25	511271		60%	0.25	137104
70%	0.52	531050		70%	0.52	136142
75%	0.67	542038		75%	0.67	134941
80%	0.84	554491		80%	0.84	137846
85%	1.04	569142		85%	1.04	138910
90%	1.28	586723		90%	1.28	140188
95%	1.64	613094		95%	1.64	142105
98%	2.05	643128		98%	2.05	144288
99%	2.33	663639		99%	2.33	145778
99.50%	2.99	711987		99.50%	2.99	149292
99.99%	3.72	765462		99.99%	3.72	153179
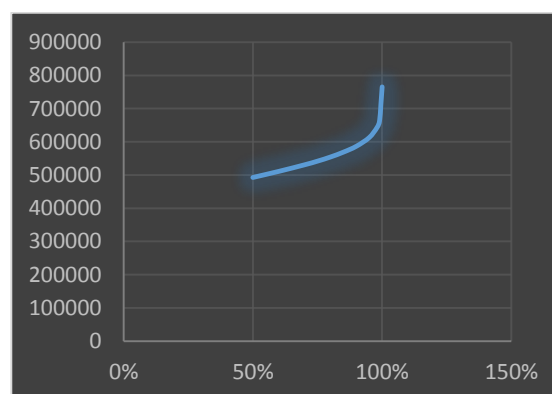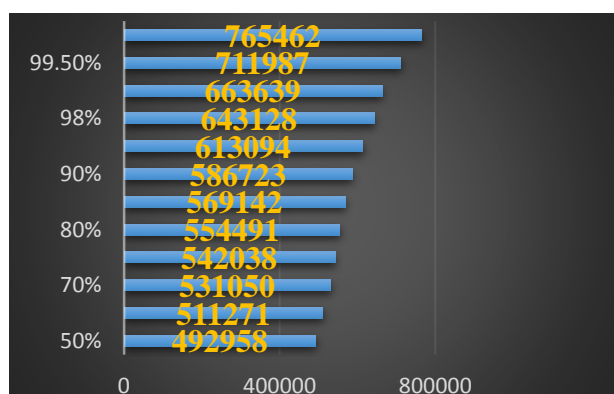
Fig. 5. Service Level relationship with T.C of inventory Category A
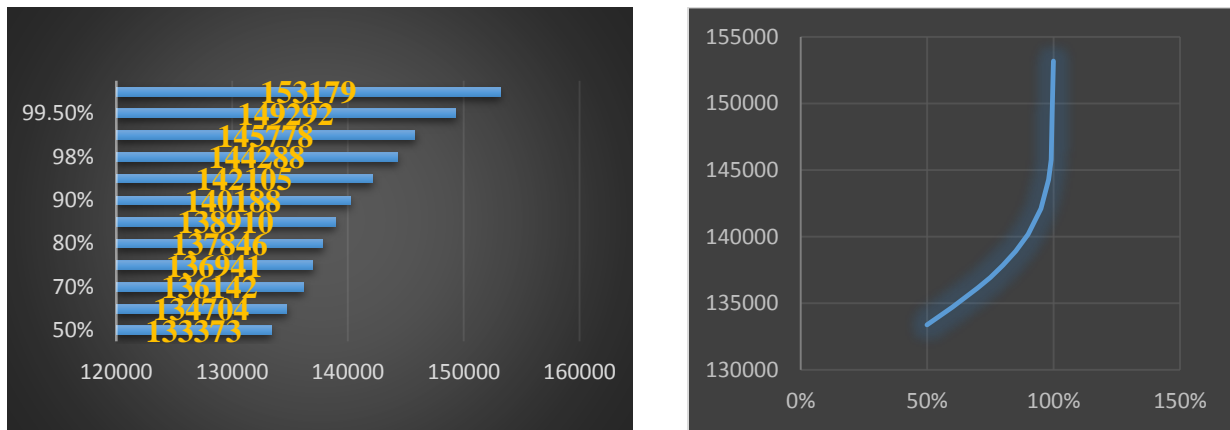
Fig. 6. Service Level relationship with T.C of inventory Category B

In the above tables and Fig. show that if we start from 50% service level and going up-to 95% service level, a very little increase occur in the cost for both category A and B items. If we wish to go from 95% up-to 100% service level then very straight curve bend towards the cost showing that very high jump in the cost in movement of five digits beyond 95% service level.

C. Effect of Service level on Cost on both Category A and B

Table VIII. Show the effect of Service level on Cost of both Category A and B items.

Service Level	Total inv. Cost of A items	Total inv. Cost of B items
50%	492958	133373
60%	511271	137104
70%	531050	136142
75%	542038	134941
80%	554491	137846
85%	569142	138910
90%	586723	140188
95%	613094	142105
98%	643128	144288
99%	663639	145778
99.50%	711987	149292
99.99%	765462	153179
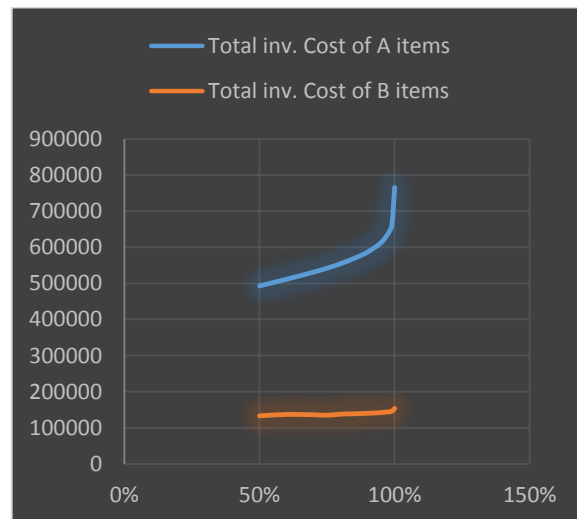
Fig. 7. Effect of Service level on Cost of both Category A and B items.

D. Comparisons of Existing Company Policy, Economic Order Quantity Policy and EOQ with 95% service level Costs

In this section we will generate a summary of Company Existing policy, proposed policy and proposed policy with 95% Service level and then we plot it on grape for more explanation and quick understanding.

Table IX. Comparing existing policy vs proposed policy of category A

Category A	Company Existing policy	Proposed policy	Proposed Policy with 95% service level
SS00002543	112620	90240	138359
SS00000496	11478	10872	15535
SS00003695	23602	23602	32308
SS00000322	24990	16491	19899
SS00002748	46631	41273	48358
SS00000495	29776	12328	13872
SS00000036	15240	13397	14651
SS00000959	16170	16002	19521
SS00000734	12338	7567	8960
SS00003976	35800	29557	36158
SS00004027	35755	25210	31346
SS00000519	16340	7217	8469
SS00000435	13195	5475	6012
SS00003693	12587	9889	12845
SS00002464	10197	8660	10074
SS00002590	13668	6547	7469
SS00003274	16610	13889	16221
SS00000437	23024	11859	12448
SS00002663	30525	16432	18289
SS00003356	19350	18537	22172
SS00001267	17646	4138	4635
SS00000432	17668	12764	14405
SS00000407	12050	10696	11010
SS00003127	25340	10169	10794
SS00000546	31925	25412	27726
SS00002938	28371	10159	11094
SS00000370	14298	13413	15785
SS00002466	8749	6122	7194
SS00003716	6972	5203	6987
SS00003244	12421	9842	10500
Total Cost (T.C) Rs	**695337**	**492958**	**613094**

Table X. Comparing Existing policy vs proposed policy of category B

Category B	Company Existing policy	Proposed policy	Proposed Policy with 95% service level
SS00002617	4746	4062.0	4478
SS00003182	3814	2839.3	2998
SS00002245	8054	6506.6	6607
SS00003471	5620	3967.9	4563
SS00003692	5259	5105.9	5303
SS00003575	10650	5099.0	5924
SS00004015	10650	5099.0	5594
SS00004016	10650	5099.0	5594
SS00003583	13075	7183.3	8002
SS00003219	7733	5442.8	5497
SS00000926	5600	3919.2	4074
SS00000731	4100	2519.9	2684
SS00003216	5475	4350.0	5059
SS00000745	5959	2494.5	2616
SS00003153	8844	3863.7	3960
SS00000973	4599	2468.2	2587
SS00000732	5117	2467.8	2696
SS00000102	20000	4899.0	5008
SS00003509	3100	3098.4	3316
SS00003745	6000	6000.0	6109
SS00003299	8291	3791.2	3972
SS00003246	16749	6921.6	7736
SS00001479	6483	4224.9	4339
SS00000796	4116	3085.2	3136
SS00002463	5632	4208.1	4392
SS00000898	11244	4205.4	4341
SS00003662	5903	5901.7	6042
SS00003353	4567	3731.0	3805
SS00003579	6889	6798.8	7532
SS00001564	11561	4020.1	4142
Total Cost (T.C) Rs	**230477**	**133373**	**142105**

Fig. 8. Company policy, proposed policy and proposed with 95% Safety Stock policy (A)

Fig. 9. Company policy, proposed policy and proposed with 95% Safety Stock policy (B)

IV. CONCLUSION

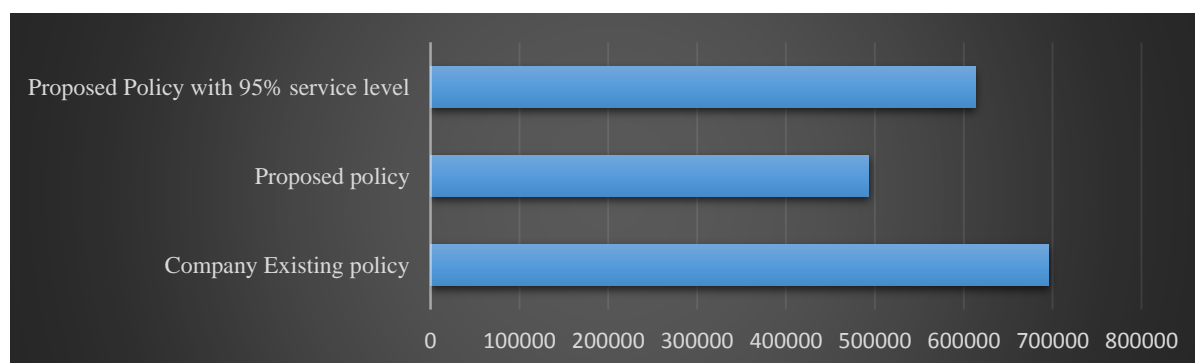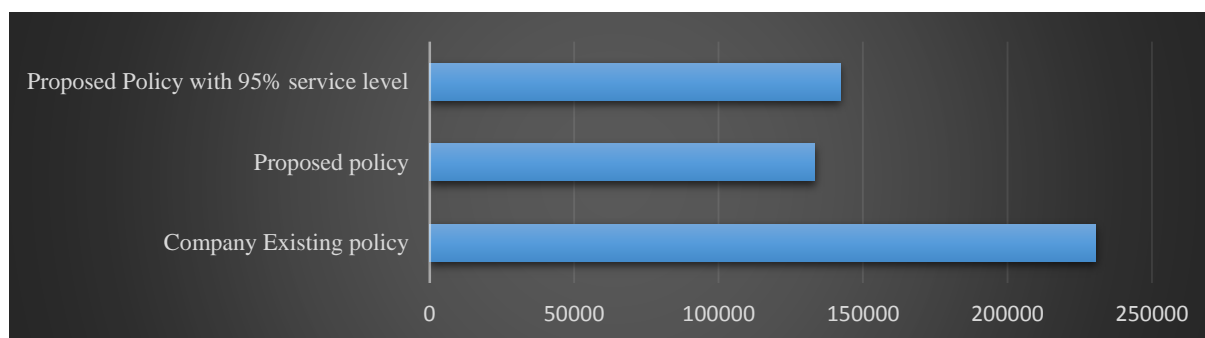In this paper real inventory problem has discussed of the steel mill. We have continued our study by selecting 30 of category A and 30 of category B items for detail analysis. The proposed policy EOQ model gives 41% saving of 30 category A and 73% saving of 30 category B items.

Then inducted the safety stock to the proposed policy by considering 95% service level. From moving the company policy to the proposed policy, considering 95% service level gives 13.41% saving of 30 category A items and gives 62.18% saving of 30 category B items. Also properly defined the reorder point for each items by considering the safety stock and lead time.

Further study can be done by integrating the inventory policy with the major breakdown maintenance activity of the industry. Previously, most of the maintenance model discuss only maintenance activity and neglecting its relationship with Spare parts inventory. Integrating both policy in one model produce some significant insight.

V. REFERENCES

[1]. ASTM, S. (2009). Standard specification for deformed and plain carbon-steel bars for concrete reinforcement. *ASTM A615/A615M-09b.*

[2]. American Society for Testing and Materials. (2015). Standard Specification for Deformed and Plain Low-alloy Steel Bars for Concrete Reinforcement. ASTM International.

[3]. Viswanathan, R. „A Breakthrough in Inventory of Spare Parts‟, The Management Accountant, June 1973, p.396.

[4]. Joseph G.Monks, „Operations Management Theory and Practice‟, McGraw Hill Company, Newyork, p.325.

[5]. Gopalakrishnan, P. Sundaresan, M. „Materials Management – An Integrated Approach‟, Prentice - Hall of India Private Limited, New Delhi, 1999, p.199.

[6]. Accountant Research and Terminology Bulletin, Published by American Institute of Certified Published Accountants, Newyork, 1961, p.28.

[7]. Viyyanna Rao, K. and Prasad, G. „Inventory Management in Andhra Pradesh Public Sector Undertakings‟ Lok udyog, August 1981, p.34.

[8]. Aisyati, A., Jauhari, W. A., & Rosyidi, C. N. (2013). Determination inventory level for aircraft spare parts using continuous review model. *International Journal of Business Research and Management (IJBRM)*, *4*(1), 1-12.

[9]. Smidt-Destombes, K.S., Van Der Heijden, M.C. and Van Harten, "A. Joint optimisation ofmspare part inventory, maintenance frequency and repair capacity for k-out of N system",*International Journal of Production Economics*, Vol. 118, pp. 260-268.2009.

[10]. Croston, J. D. (1972). Forecasting and stock control for intermittent demands. *Journal of the Operational Research Society*, *23*(3), 289-303.

[11]. Syntetos, A. A., & Boylan, J. E. (2005). The accuracy of intermittent demand estimates. *International Journal of forecasting*, *21*(2), 303-314.

[12]. Syntetos, A. A., & Boylan, J. E. (2006). On the stock control performance of intermittent demand estimators. *International Journal of Production Economics*, *103*(1), 36-47.

[13]. Mehdizadeh, M. (2019). Integrating ABC analysis and rough set theory to control the inventories of distributor in the supply chain of auto spare parts. *Computers & Industrial Engineering*.

[14]. Chu, C. W., Liang, G. S., & Liao, C. T. (2008). Controlling inventory by combining ABC analysis and fuzzy classification. *Computers & Industrial Engineering*, *55*(4), 841-851.

[15]. Teunter, R., & Sani, B. (2009). Calculating order-up-to levels for products with intermittent demand. *International Journal of Production Economics*, *118*(1), 82-86.

[16]. Porras, E., & Dekker, R. (2008). An inventory control system for spare parts at a refinery: An empirical comparison of different re-order point methods. *European Journal of Operational Research*, *184*(1), 101-132.

[17]. van Jaarsveld, W., Dollevoet, T., & Dekker, R. (2015). Improving spare parts inventory control at a repair shop. *Omega*, *57*, 217-229.

[18]. de Smidt-Destombes, K. S., van der Heijden, M. C., & van Harten, A. (2009). Joint optimisation of spare part inventory, maintenance frequency and repair capacity for k-out-of-N systems. *International Journal of Production Economics*, *118*(1), 260-268.

[19]. Kilpi, J., Töyli, J., & Vepsäläinen, A. (2009). Cooperative strategies for the availability service of repairable aircraft components. *International Journal of Production Economics*, *117*(2), 360-

[20]. Wong, H., Van Oudheusden, D., & Cattrysse, D. (2007). Cost allocation in spare parts inventory pooling. *Transportation Research Part E: Logistics and Transportation Review*, *43*(4), 370-386.

[21]. Aisyati, A., Jauhari, W. A., & Rosyidi, C. N. (2014). Periodic Review Model for Determining Inventory Policy for Aircraft Consumable Spare Parts. *International Journal of Business Research & Management (IJBRM)*, *5*(3), 2014

[22]. Do Rego, J. R., & de Mesquita, M. A. (2011). Spare parts inventory control: a literature review. *Produção*, *21*(4), 645-655.

[23]. Sani, B. (1995). *Periodic inventory control systems and demand forecasting methods for low demand items* (Doctoral dissertation, University of Lancaster)

[24]. Sani, B., & Kingsman, B. G. (1997). Selecting the best periodic inventory control and demand forecasting methods for low demand items. *Journal of the Operational Research Society*, *48*(7),

[25]. Syntetos, A. A., Babai, M. Z., Dallery, Y., & Teunter, R. (2009). Periodic control of intermittent demand items: theory and empirical analysis. *Journal of the Operational Research Society*, *60*(5),

[26]. Ramaekers, K., & Janssens, G. (2014). Optimal policies for demand forecasting and inventory management of goods with intermittent demand.

[27]. Abbasi, M. (2011). 10 Storage, Warehousing, and Inventory Management. *Logistics Operations and Management: Concepts and Models*, 181.

Performance comparison of Shell and General Electric gasifiers for low quality Pakistani coal

Muhammad Adnan [A*], Muhammad Zaman [A], Atta Ullah [A], Afşin Güngör [B,C]

[A] *Department of Chemical Engineering, Pakistan Institute of Engineering and Applied Sciences (PIEAS), Islamabad, Pakistan*
[B] *Department of Mechanical Engineering, Faculty of Engineering, Akdeniz University, Antalya, Turkey*
[C] *Bucak Technology Faculty, Burdur Mehmet Akif Ersoy University, Bucak-Burdur, Turkey*

Abstract— **Huge emissions of greenhouse gases such as carbon dioxide are of major concern during power generation from coal. Global warming is the main harmful effect of these emission products and it becomes necessary to mitigate the effect of emissions to the environment. Gasification is a way to convert low-value feedstock (coal, biomass and oil waste) into synthetic gas (syngas). Integrated gasification combined cycle (IGCC) power system has been recognized as a rare existing opportunity to utilize low quality fuels with reduced emissions and co-production of power, fuels and chemicals. The conversion of coal into syngas is a process of interest in Pakistan where the huge reserves of low quality coal are present, and at the same time harmful effects of environmental pollution are being faced. Gasifier selection plays a key role in mitigating the air pollution and improving the overall efficiency of the IGCC co-generation systems. In this work, the gasification process has been simulated using coal-entrained flow gasifiers under thermochemical equilibrium with the Gibbs free energy approach. Two typical technologies used in entrained flow gasifiers such as coal dry and coal slurry are simulated using Shell and General Electric (formerly Texaco) gasifiers, respectively in Aspen Plus®. The emphasis is put on performance evaluation of both gasifiers using same low quality Pakistani coal. Models used for the performance evaluation of gasification process on local coals have been validated by same quality coals provided in NETL reports. Thus, the proposed models can be considered as a reliable and useful tool to study and optimize the gasification process for indigenous coals. Sensitivity analysis for 12 % drying level in dry feed gasifier has been performed to study the effect oxygen to coal ratio on output composition of syngas. Effects of temperature of gasifier and oxygen to coal ratio on the cold gas efficiency are also studied in both type of gasifiers using sensitivity analysis. Oxygen consumption rate in both type of gasifiers for low quality coal has also been investigated for the desired syngas composition and operating temperature. In the end the effect of solid concentration in slurry on the output composition of the syngas has been investigated for slurry feed system. Composition of syngas plays a vital role in the co-generation scenario, so this research could provide a guideline for making a decision in the optimal scenario of the IGCC co-generation system.**

Keywords— **Co-generation, General Electric gasifier, IGCC, Low quality coal, Shell gasifier.**
*Corresponding author (chemadnan72@yahoo.com)

I. INTRODUCTION

The rapid industrial growth, increase in population and urbanization coupled with improved living standards has led to an ever-increasing world energy demand, especially electric power. Cheap and clean energy demand have been apriority in modern world. Fossil fuels are still exploited by most of the energy sectors for power production. Coal has emerged as a cheap source of electricity generation. The major electricity generation of developing countries (e.g., Pakistan) depends upon oil, coal and natural gas. Coal contributes around 41 % in the total electricity production of the world [1]. It has been proved that coal has the maximum potential for the production of electricity in future [2]. However, huge emissions of greenhouse gases from coal combustion, such as carbon dioxide are of major concern. Presence of sulfur in the coal also makes the emission control more challenging. Use of low quality coals like lignite containing high sulfur contents becomes even more challenging for power generation. Huge reserves of low quality coal because of their low cost can provide a sustainable solution for power generation if their environmental impacts can be mitigated. According to some estimates, more than about 50% of global coal reserves are of low rank, i.e. sub-bituminous and lignite [3]. In Pakistan, the largest reserve of 175 billion tonnes of lignite coal, is located in the Thar Desert of Sindh. In addition to this, there are other

lignite coal reserves in Lakhra, Sonda, Indus East coalfields in Sindh [4].

Therefore, it is very important to consider power generation technologies which help mitigate the effect of emissions to the environment. IGCC power generation system is a rare existing technology which offers efficient power generation due to possibility of co-firing (i.e., coal with biomass), co-production (electricity, methane, ammonia, etc.) and ease of carbon capture.

Gasification is a vital part and plays a key role in an IGCC power plant [5], [6]. Gasification is a way to convert low-value feedstock (coal, biomass and oil waste) into electricity, steam and hydrogen. Coal and biomass are utilized in the gasification unit for the production of syngas in an efficient way. Selection of proper gasification technology is crucial for optimizing the operation of a future generation IGCC plant, especially with varying coal quality.

Gasification process is significantly affected by the quality of coal. The high heating value (HHV) of the coal has direct impact on the performance of the gasifier [7]. Similarly, the performance of the gasifier and coal dryer is influenced by the moisture content of the coal [8], [9]. Composition and amount of syngas produced from a gasifier and steam requirement for coal drying also depend on the coal type, hence, overall performance of the IGCC plant in term of efficiency improvement and environmental regulations is also influenced by coal quality. Thus, considering the above issues, the comparison study for the utilization of various types of coal in gasification is imperative to analyze the relative performance of different coals with respect to existing gasification technologies.

Thus, to explore a realistic future generation IGCC plant for Pakistani coal, the effects of the coal quality on the gasification process must be investigated. Several previous studies [10], [11], [12], [13] in context to Pakistan have reported on IGCC plants using different low quality coals without any reference to performance of different gasifiers. Most recently [14] considered simulation of dry and slurry gasification using computational fluid dynamic (CFD) technique with special emphasis on reaction taking place in both processes employing a two-dimensional computational fluid dynamic (CFD) model of downdraft gasifier.

In this study, benchmark models of dry feed and slurry feed gasification has been developed in Aspen Plus® and results are in close agreement with reported data [15], [7]. After verification of the models, sensitivity analyses to check the feasibility of indigenous Pakistani coals of diverse qualities have been performed. Analysis for the composition of syngas against temperature of the gasifier for both dry and slurry feed gasification has been performed. Composition of syngas for varied Oxygen/Fuel (O/F) ratio has been investigated for all three coals using dry feed and slurry feed gasification. In the end, cold gas efficiency of gasifier for both dry feed and slurry feed systems has been investigated against varied O/F ratio.

II. METHODOLOGY

This section covers the brief description of entrained flow gasifiers (dry and slurry feed technologies) in general and assumptions considered in this study for both type of processes. Characteristics of Pakistani coals considered in this study and their significance has also been included. In the end of this section, simulation model development and its verification with literature has been presented.

A. Process description

1) Dry feed technology using Shell gasifier
The Shell gasifier typically operates at around 45 bar, with a temperature range of 1400-1600 °C, well above the ash melting point [15]. These gasifiers show high cold gas efficiencies compared to (single stage) slurry-fed entrained flow gasifiers (e.g., General Electric gasifier), as in dry-fed system no water required to be evaporated leading to additional energy consumption [16]. Coal is pulverized and dried to specific moisture level (12% residual moisture in this study) prior to gasification. The dry, pulverized coal is subsequently pressurized using a lock-hopper system to pneumatically feed to the gasifier in dense phase mode using pure nitrogen as a conveying gas. Oxygen to fuel ratio is low for hard coal gasification, but when gasifying lignite, oxygen to fuel ratio is high and steam supply with oxygen is not required [7]. The raw syngas leaving the gasifier is first rapidly cooled to around 900 °C. Further details on Shell gasifier regarding syngas

quenching can be found in [7]. In this work only gasification process has been considered for both dry feed and slurry feed systems, and composition of hot syngas will be analyzed by performing sensitivity analysis of various parameters for Pakistani coals. Vattenfall Buggenum IGCC plant in the Netherlands used Shell gasifier technology [7].

The relatively high gasification temperatures have been assumed to minimize the kinetic barriers to ensure the gasifier gaseous products approach to the equilibrium [17], [18]. In this way the gasification process can be described by means of a thermodynamic model [19]. In this work, an overall equilibrium approach is employed while neglecting the hydrodynamic complexity of the gasifier. Char is supposed to be 100% graphite (conventional substance available in Aspen Plus® database). The ash content turned into slag. The gasifier reactors are simulated as RGibbs adiabatic reactors. In addition, assumptions related to operation of the shell gasifier are listed below.

- Particle size distribution (PSD) before gasifier is maintained at 80 % coal under 100 micrometer
- Nitrogen rich gas has been used as a drying agent at 232 ºC
- Up to 12 % moisture level has been achieved for all type of coals before gasifier
- For comparison purpose the temperature of dried coal is maintained at 71 ºC (160 ºF)
- Nitrogen used for pneumatic flow is 0.125 lb/lb of dried coal [15]
- Oxygen requirement for gasification in base case is 0.6856 lb/lb of dried coal (O_2 purity 95 %) [15]
- Pressure of the gasifier has been maintained at 42.49 bar (615 psia)
- Temperature of the gasifier is fixed at 1371 ºC (2500 ºF) for base case
- Carbon conversion in gasifier is assumed at 99.3 % [15]

Drying of the moistened coal is performed in Rstoic reactor of the Aspen Plus®, where moisture level of dry coal up to 12% and conversion for moisture removal has been adjusted. Flash2 block of Aspen Plus®, has been employed to remove gases along with released moisture and dried coal is fed to the gasifier.. In gasification section, pyrolysis to decompose coal into its constituents like C, H_2O, N_2, H_2, Cl_2 and Ash etc. has been performed in Ryield block. Gasification reactions of the decomposed constituents have been modeled in RGibbs block in the presence of oxygen to produce syngas.

2)Slurry feed technology using GE gasifier

Similar to the Shell gasifier, the GE gasifier uses pulverized coal; however, pulverized coal is mixed with water to produce a slurry feed. The typical range of solid concentration in slurry varies from 35 to 70 wt% depending on the type and quality of the coal [20], [21], [22]. In case of the slurry type of gasifiers, a slurry pump is utilized to feed the slurry into the gasifier. Higher operating pressure up to 70 bar is possible in this type of gasifier.

Oxygen to fuel ratio in this case is relatively high, caused by the fact that some CO and H_2 burning is required to vaporize the water present in slurry. As can be confirmed from the results, the syngas produced by GE gasifier shows relatively high contents of combustion products (i.e. CO_2 and H_2O). The limited lifetime of the refractory in this technology causes low availability. Further details on this technology and its downstream components can be found from somewhere else [7].

The Tampa Electric Polk IGCC power station in the USA uses GE gasifier [7]. Similar to shell gasifier, the high temperature assumption for the gasification minimizes the kinetic barriers and therefore the gaseous products leave from the gasifiers approach to the equilibrium. In this way the gasification process can be considered a thermodynamic model [19]. Similar to shell gasifier, in GE gasifier, an overall equilibrium approach is employed while neglecting the hydrodynamic complexity of the gasifier. Assumptions specific to operation of the GE gasifier in slurry feed system for base case development have been listed below.

- PSD before gasifier is maintained at 80 % coal under 100 micrometer
- Coal concentration in slurry is 45 %
- Coal conversion in decomposer is fixed at 95 %
- Oxygen rate in gasifier is 0.721 lb/lb of coal (as-received) with O_2 purity of 95 % [7]
- Pressure of the gasifier has been maintained at 60 bar
- Temperature of the gasifier is fixed at 1450 ºC
- Carbon conversion in gasifier is assumed at 99 % [7] in base case

Simulation of a slurry based coal gasification has been implemented in Aspen Plus® software package. Coal sizing and screening in the form of slurry; and gasification of coal slurry sections have been considered

during model development in slurry based gasification. Slurry of coal and water is prepared during size reduction of the coal in coal preparation section. Water composition in slurry is adjusted to 55% and left is coal. Slurry leaving from the sizing section enters in Rstoic block where non-conventional PSD sub stream of coal changes to only non-conventional sub stream. In gasification section coal water slurry comes in contact with almost 95% pure oxygen. As discussed in dry coal gasification section before gasification of solid fuels like coal and biomass, solid fuel is required to decompose into its constituents. In case of slurry based gasification, decomposition of coal is performed in Rstoic block instead of Ryield block and products of decomposition have been specified in reaction along with conversion of the coal. All other steps in slurry based gasification are same as in dry coal gasification.

B. Selection of coal:

Three Pakistani coals have been selected which cover qualities of major existing Pakistani coals. HHV of as-received and dry basis coals have been calculated using Dulong equation (1) [23]. Accuracy of Dulong equation was verified first by calculating HHV of (North Dakota Beulah-Zap Lignite) reported in NETL 2011 [15] for both as-received and dry basis. The selected coals of Pakistani origin involve moisture contents 35% to 50.24% and ash contents 3.13% to 14% on as-received basis coal. Since, it is a proven reality now, that coal quality impacts performance of gasification process and resultantly overall performance of the IGCC power plant [7], [24]. Selection of diverse range of low quality coal will help find feasibility of indigenous coal for power generation through gasification technology. Considered coal samples of Thar origin for gasification have been presented in**Error! Reference source not found.**, comprising proximate and ultimate analysis of coal along with HHV both on as-received and dry basis. Size of the coal to be fed to entrained flow gasifier should be under 100 micrometer, hence in this work up to 80 % of the mass of the coal considered for gasification is under 100 micrometer and for Shell gasifier inherent moisture of the coal is reduced to 12 % by weight, in line with NETL report [15].

$$HHV\left(\frac{kJ}{kg}\right) = 337C + 1419(H - 0.125O) + 93S + 23N \tag{19}$$

Where, C, H, O, S and N are percent components of ultimate analysis both for as-received or dry basis HHV calculations.

Table XV: PROPERTIES OF VARIOUS CLASSES OF THAR COAL

Coal identity	Thar lignite A [25]		Thar lignite B [26]		Thar lignite C [26]	
Analysis type	as-received	dry basis	as-received	dry basis	as-received	dry basis
Proximate analysis (wt %)						
Moisture	35.00	0	44.92	0	50.24	0
Fixed carbon	20.00	30.769	21.14	38.381	19.64	39.469
Volatile matter	31.00	47.692	29.58	53.704	26.99	54.240
Ash	14.00	21.538	4.36	7.916	3.13	6.290
Ultimate analysis (wt %)						
Carbon	36.39	55.984	37.96	68.918	34.65	69.634
Hydrogen	4.21	6.477	2.85	5.174	2.76	5.546
Nitrogen	0.64	0.984	0.46	0.835	0.34	0.683
Sulphur	2.00	3.077	0.31	0.563	0.40	0.803
Oxygen	7.76	11.938	9.14	16.594	8.48	17.042
Ash	14.00	21.538	4.36	7.916	3.13	6.290
HHV (kJ/kg)	17061.71[a]	26248.72[a]	15254.87[a]	27695.84[a]	14134.37[a]	28405.03[a]
[a] Calculated by Dulong formula [23]						

C. Model development and verification

For each entrained-flow gasifier i.e. Shell and GE, a generic thermodynamic Aspen Plus® model has been developed. Compared to individual verification cases, such generic thermodynamic models are valid in the range of slightly altered boundary condition. As the operating experience of both gasifiers is present, hence developed thermodynamic models can provide a simple and robust tool to match the performance of the gasifiers. Verification data was found from literature for both the shell gasifier [15] and GE gasifier [7]. Simulation of coal based gasification using recent version of Aspen Plus® (V.11) both for slurry feed and dry feed technologies have been performed in this work. A model is developed and tested by comparing the results predicted by this model with the results of NETL report [15] for shell gasifier and with the results of [7] for GE gasifier, so that accuracy of the developed model can be confirmed, and the developed model can be used for performing further analysis.

During model development a sequential modular approach was used in Aspen Plus® to simulate different stages of the gasification process. In this model, coal sizing and gasification have been simulated using different hierarchy blocks. Peng-Robinson property method was used as a global method and for sizing section SOLID property method has been used. Experimental data of the coal used during simulation of the gasification process in Aspen Plus® has been taken from literature. The following analyses are important to be used in Aspen Plus® simulation.

- Proximate analysis of coal
- Ultimate analysis of coal
- Sulfur analysis
- General analysis
  a) Heat of combustion of fuel
  b) Density of fuel (coal)
- Particle size distribution (PSD) analysis of coal

In simulation, COAL and COALASH are considered nonconventional solid components. The properties calculated for nonconventional components are enthalpy and density. The enthalpy model for COAL, and COALASH is HCOALGEN and for the density model for all components is DCOALIGT in Aspen Plus®.

Flow sheet was developed for both cases i.e., dry feed technology using shell gasifier and slurry feed technology using GE gasifier in Aspen Plus®. Simulations were run for both flow sheets considering various sensitivity analyses. ASU is not included in simulation, 95 % pure oxygen has been considered as an oxidizing agent in gasification process [15]. Locally available Thar coal is considered for predicting feasibility of indigenous resources using the tested model.

The oxygen-to-coal (mass flow rate) ratio and temperature of the gasification are two important parameters in practicing coal gasification. Cold gas efficiency (CGE) and syngas composition at the outlet of the gasifier are two vital indices used for evaluating the performance of gasification. CGE % (2) or the energy efficiency of the gasification process is the ratio between the energy contained by syngas leaving from the gasifier and the coal energy in the stream feeding into the process. Since the main combustible components of the syngas are CO, H_2, CH_4, H_2S and even tar compounds, a high cold gas efficiency does not necessarily imply a high gas quality [27].

$$CGE(\%) = \left(\frac{m_{sg} \times HHV_{sg}}{m_{coal} \times HHV_{coal}} \right) \times 100 \qquad (20)$$

Where, m_{sg} is the mass flow of syngas leaving from the gasifier; m_{coal} is the mass flow of coal fed to the gasifier; HHV_{coal} is the higher heating value of coal as-received basis that is including ash and moisture contents; HHV_{sg} is the higher heating value of the syngas stream leaving the gasifier (wet basis), (3).

$$HHV_{sg} = \sum_{i=1}^{k} X_i \times HHV_i \qquad (21)$$

Where, X_i is the mass fraction of the syngas components (wet basis); HHV_i values of syngas components taken from [28]. The energy parameters, such as HHV_{sg} and CGE, were directly estimated within the Aspen

Plus® model by means of Fortran statements in calculator blocks. The Oxygen/Coal as-received (a.r) was also estimated using Fortran statement during sensitivity analysis.

III. RESULTS AND DISCUSSION

Three different coals of Pakistani origin, comprised of high ash and average moisture (i.e., Thar Lignite A [25]), medium ash and high moisture (i.e., Thar Lignite B [26]), and low as with very high moisture (i.e., Thar Lignite C [26]) are considered in this work to analyze the feasibility of these coals for gasification. The properties of the coal, such as proximate, elemental, and calorific values, are summarized in Table *XV*. Two commercial technologies, dry feed (using Shell gasifier) and slurry feed (using GE gasifier) being used for power generation in the world for gasification of the fuels are considered in this work. Temperature of the gasifier, flow rate of oxygen, extent of drying and solid concentration in slurry impacts the performance of the gasification process. Composition of syngas produced is majorly influenced by these parameters. Moisture contents and ash contents of the feed also affect the output composition of the syngas. In this section various analyses performed are to evaluate the status of the Pakistani lignite coal for gasification feasibility. Comparison of syngas composition at the outlet of the gasifier simulated in this work and reported in DOE reports [15] for shell gasifier has been presented in **Fig. 9a**. Results of syngas composition from both works are in close agreement, hence the developed model can be used for performing further analysis by using operating conditions used by most of the Shell gasifiers for dry feed technology and GE gasifier for slurry feed technology. Slurry feed gasification model has been compared with [7] and presented in **Fig. 9b**. The results from the slurry feed model are also in close agreement with literature.

A. Performance analysis of dry feed gasifier (Shell):

The profiles of the temperatures at the exit of the gasifier from the gasification of the three coals and the cold gas efficiency (CGE) of the gasifier at various Oxygen/ Coal as-received (O/Coal a.r) ratios for dry feed gasification are presented in **Fig. 10**. Compositional analysis of syngas at varied O/Coal (a.r) ratios for all three selected coals of Pakistani origin, is presented in

Fig. 11 and **Fig. 12**. The moisture level in all three coal types under consideration is reduced to 12 %, assumed from the literature [15]. CGE is higher at lower temperatures, as the methane yield is high in the region of carbon presence and decreases abruptly in the carbon-free area reflecting the gasification temperature. Due to kinetic restrictions it is not possible to achieve these high values of CGE in practice [27]. Combustible components of the syngas which exists at high temperature like CO and H_2 are considered on wet basis for CGE evaluation. As the CH_4 has not been considered in CGE evaluation, the trends for CGE at lower O/Coal ratios are at lowest side and peaks of CGE graphs in **Fig. 10b** indicate high temperature in the gasifier and negligible production of CH_4 and H_2S. Hence, at higher temperature in shell gasifier, the CGE of the gasification process is true representation of main components of syngas, like CO and H_2. The HHV of syngas components have been taken from [28] and HHV of coal (a.r) has been calculated from Dulong formula [23].

1) Effect of oxygen to coal ratio on the outlet temperature of the syngas

The outlet temperatures rise of the syngas with increasing O/Coal ratios is observed, regardless of which quality coal has been used as shown in **Fig. 10a**. This arises from the fact that the exothermic oxidation reactions are intensified as the O/Coal ratio increases. It is noted that after 0.43 O/Coal ratio a sharp rise in temperature indicates production of more exothermic compounds like CO_2 and H_2O. Temperature profiles for dry feed gasification presented in **Fig. 10a**, also confirms that for considered low quality Pakistani coals the optimum gasification temperature exist between O/Coal ratio of 0.40 to 0.43. It is also observed from the temperature profiles that temperature rise of Thar Lignite C (TL-C) at higher O/Coal is more, as compared to the other coals, the reason is more fixed carbon present in TL-C at dry basis and more chances of exothermic CO_2 production.
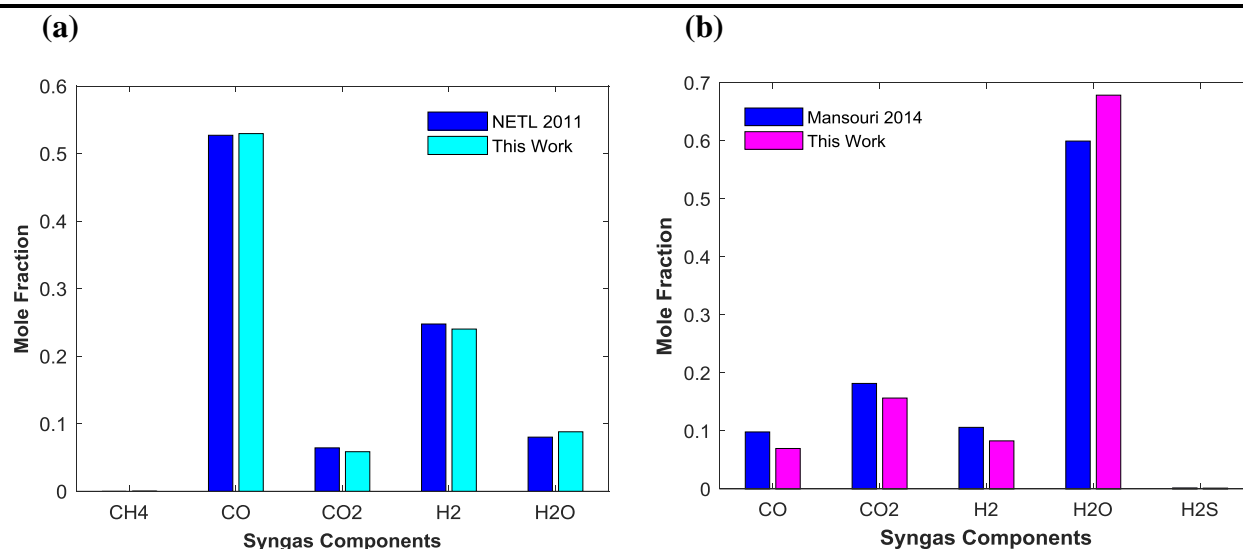
(a) **(b)**

Fig. 9. Comparison of syngas composition from this work, with NETL 2011 report [15] using (a) dry feed technology and, with [7] using (b) slurry feed technology.
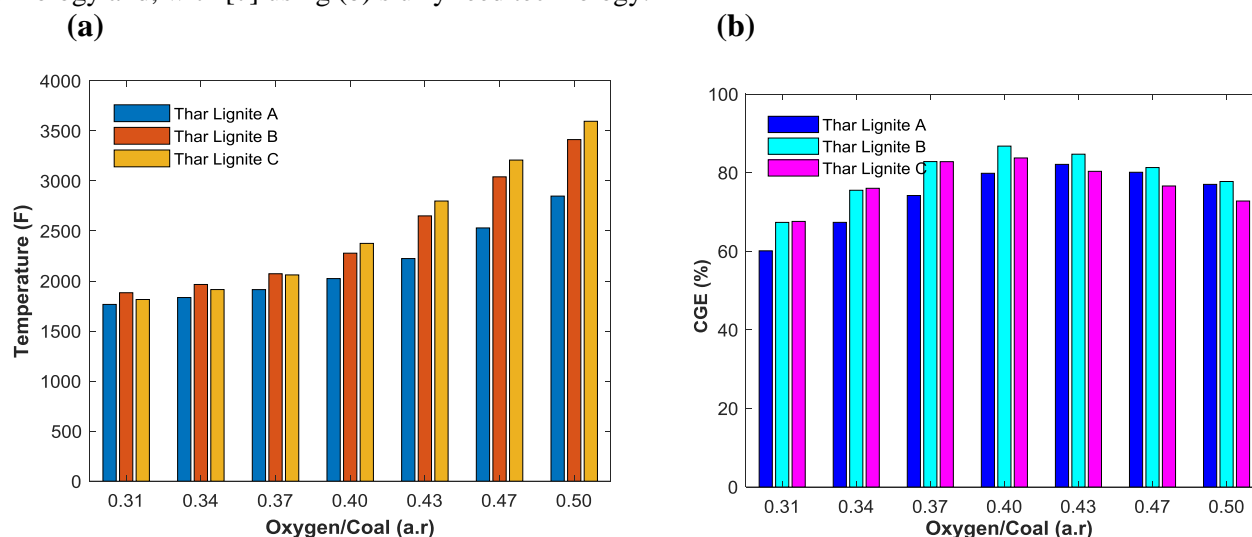
(a) **(b)**

Fig. 10. Profiles for the shell gasifier, (a) Temperature (b) CGE, at the exit of the shell gasifier for various Oxygen/Coal (a.r) ratios.

2)Effect of oxygen to coal ratio on the CGE of the gasification process

The CGE of the dry feed gasifier has been presented in **Fig. 10b** at various O/Coal ratios. In case of dry feed system at low temperature, huge amounts of CH_4 are formed which causes an increase in CGE of the process, but in reality CGE near 90 % is not possible [27]. To see the actual CGE of the process CH_4 formation at early stage of gasification is not considered in CGE calculation that is why the small values of CGE are observed at lower values of the O/Coal ratios. CGE based on HHV of syngas and coal for all three coals is calculated in Aspen Plus using calculator block. As shown in **Fig. 10b**, the CGE for Thar Lignite B (TL-B) and TL-C at O/Coal ratio of 0.40 is maximum with values 86.78 % and 83.76, respectively. Temperature of the gasifier for these CGE was 2277 °F and 2376 °F, respectively. After this point, the temperature rise is observed in gasification process and downward fall of syngas components results in lower CGE at higher O/Coal ratios. When temperature of the gasifier reaches near 2500 °F, the further decrease in CGE for all type of coals is noted, which gives a prediction for actual gasification process using entrained flow gasifier in which high temperature and high carbon conversion is assumed. Carbon contents of Thar Lignite A (TL-A) on dry basis are low as compared to TL-B and TL-C, so exothermic compounds start forming at O/Coal ratio of 0.43 instead of 0.40. It has also been noted from the temperature and CGE profiles for varied O/Coal ratio that TL-B and TL-C are close in carbon contents, hence shown almost same performance. Furthermore as observed at 0.43 O/Coal ratio where all possible reactions take place and represent true dry feed gasification, there is not huge difference in CGE of different quality coals, hence it is proved that in case of

dry feed gasification using shell gasifier the performance of the gasifier is not vulnerable to the quality of the coal.

3)Effect of oxygen to coal ratio on the outlet composition of the syngas

Fig. 11a,
Fig. 11b and **Fig. 12a** present the syngas composition at various O/Coal ratios for coal TL-A, TL-B and TL-C, respectively. **Fig. 12b** expressed the composition of syngas at already confirmed optimal O/Coal ratios of 0.43 for coal TL-A and 0.40 for TL-B and TL-C. In case of TL-A as represented in
Fig. 11a, at lower temperatures and at lower O/Coal ratios, CH_4 formation is high. Similarly, CO_2 and H_2O formation show a rise after a specific O/Coal ratio when combustion reactions instead of gasification reactions commence. At the early stage of the gasification process when O/Coal ratio is not high, formation of CO and H_2 by the reduction reaction takes place. The trends in all type of coals are almost same with varied amounts of the syngas components. For TL-A in
Fig. 11a, the amount of CO produced is less in comparison to other two coals, the reason behind is the less amount of carbon contents in TL-A on dry basis as compared to other coals. Similarly, H_2 mole rate is more in coal TL-A because of more hydrogen existed in that coal on dry basis. It is also observed from
Fig. 11b and **Fig. 12a**, that coal TL-B and TL-C show almost same behavior during gasification. It is obvious because of same characteristics of these two coals after drying up to 12 % moisture contents, as seen fromTable XV. Syngas composition for all three coals after gasification in dry feed gasifier presented in
Fig. 11a,
Fig. 11b and **Fig. 12a** at varied O/Coal ratios provide a foundation for decision making for the selection of different operation parameters for the desired composition of the syngas for downstream co-generation.
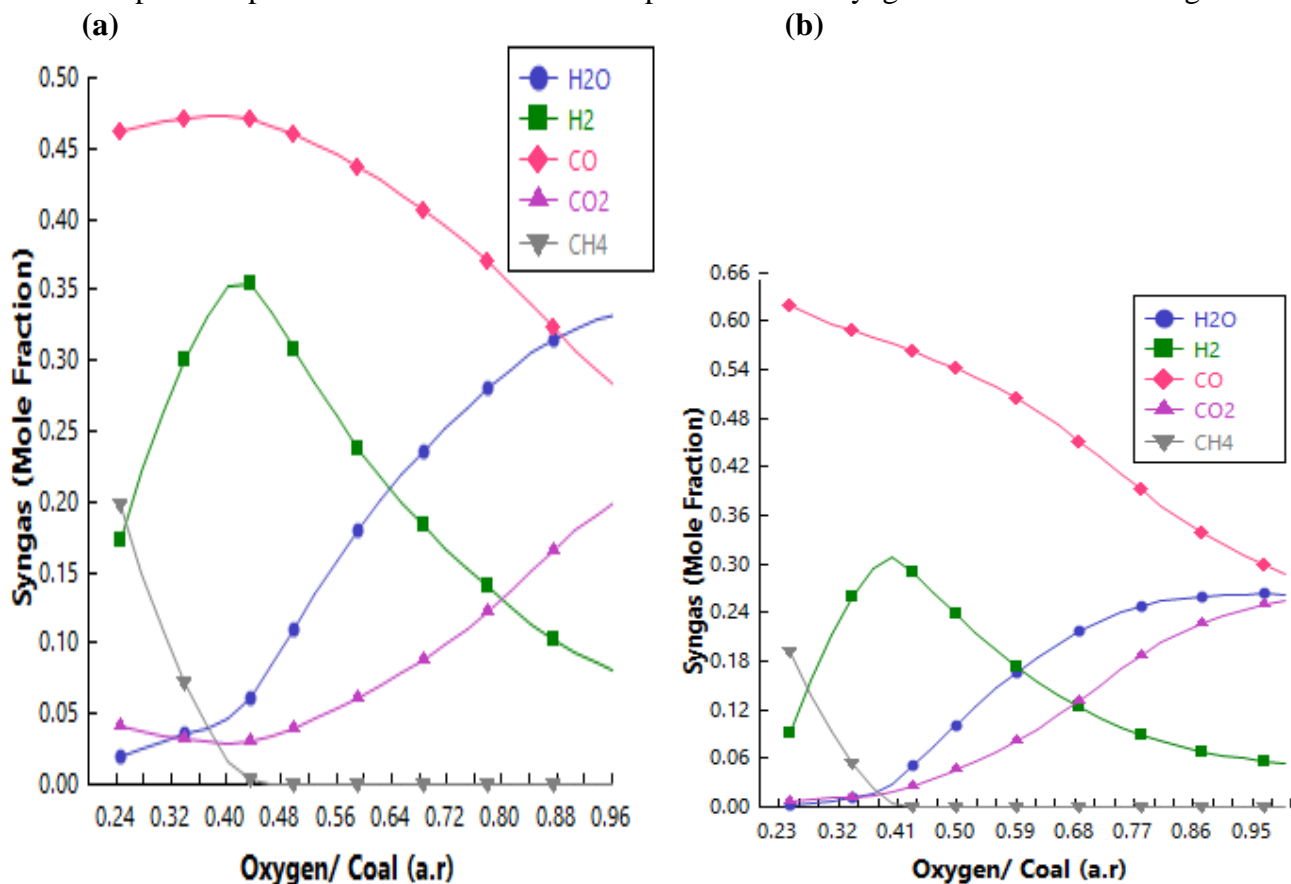

Fig. 11. Syngas composition in dry feed system for varied O/Coal ratio for coal (a) TL-A and (b) TL-B.
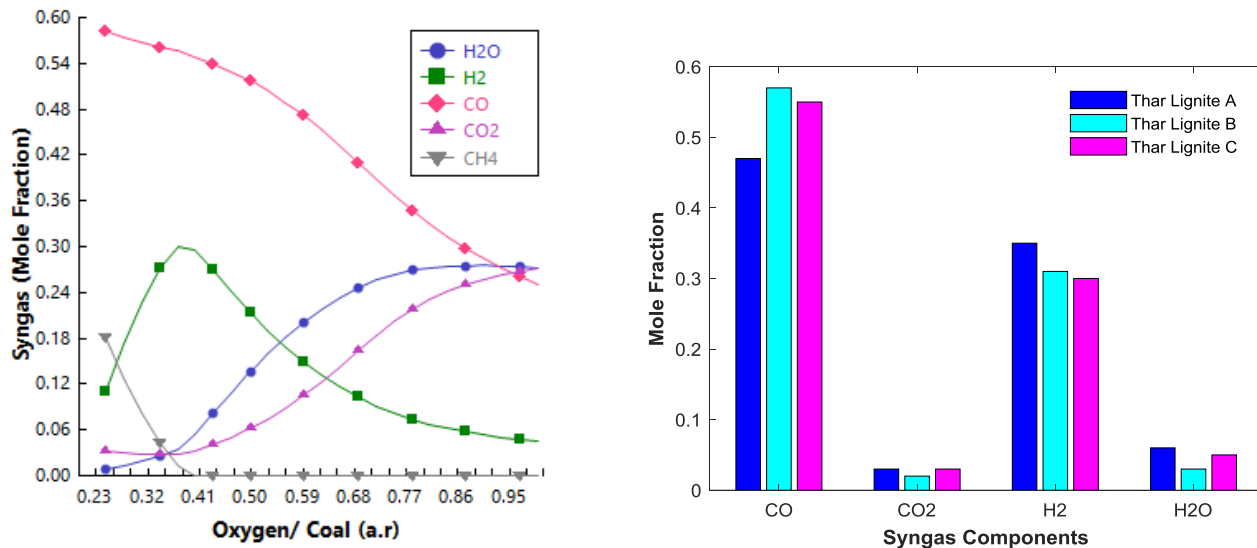
Fig. 12. (a) Syngas composition for varied O/Coal ratio for TL-C coal and (b) Syngas composition at optimal O/Coal ratios.

B. Performance analysis of the slurry feed gasifier

The profiles of the temperatures at the exit of the gasifier from the gasification of the three coals and the cold gas efficiency (CGE) of the gasifier at various (O/Coal) ratios for slurry feed gasification are presented in **Fig. 13**. Compositional analysis of syngas from slurry feed gasifier at varied O/Coal ratios for all three selected coals of Pakistani origin, has been presented in **Fig. 14** and **Fig. 15a**. The solid concentration in these cases explained in the coming sections has been fixed at 45%, taken from literature [7] for low quality coals.

1)Effect of oxygen to coal ratio on the outlet temperature of syngas and CGE of the gasifier

The outlet temperatures rise of the syngas with increasing O/Coal ratios is observed (as shown in Fig. 13a), regardless of which quality coal has been used same as in dry feed system. This arises from the same reason as in dry gasification, that the exothermic oxidation reactions are intensified as the O/Coal ratio increases. It is noted that in case of TL-A, temperature rise at the early stage of the gasification when O/Coal ratio is low is because of low moisture contents of that coal. After 0.7 O/Coal ratio a sharp rise in temperature indicates production of more exothermic compounds, like CO_2 and H_2O. Temperature profiles for slurry feed gasification presented in Fig. 13a, and CGE profiles against O/Coal ratio presented in Fig. 13b, also confirm that for considered low quality Pakistani coals the gasification temperature where higher values of CGE are achieved is in the range of 1500-1600 ^{o}F. Low temperature up to this extent is not suitable for entrained flow gasifiers like GE and Shell where reaction kinetics barriers are assumed to be removed at high temperatures to achieve equilibrium conditions [27]. Temperatures near 2500 ^{o}F can be achieved by employing more O/Coal ratio, as can be seen in Fig. 13a, in which more than 0.91 O/Coal ratio is required to reach temperature near 2500 ^{o}F. Huge amount of oxygen required for gasification of Pakistani coals by employing slurry feed technologies. Huge oxygen consumption causes cost increase of the power plant and result in decreased overall efficiency of the system.

The CGE of the slurry feed gasifier has been presented in Fig. 13b at various O/Coal ratios. CGE based on HHV of syngas and coal for all three coals has been calculated in Aspen Plus using calculator block. As shown in Fig. 13b near 2500 °F temperature as a requirement of the entrained flow gasifiers. The CGE for TL-A is 29 %, for TL-B is 25 % and for TL-C is almost 15 % at O/Coal ratio of 0.91. At 0.91 O/Coal ratio, there is huge difference in CGE of different quality coals, hence it is proved that in case of slurry feed gasification using GE gasifier the performance of the gasifier is vulnerable to the quality of the coal. Very small values of CGE for low quality coals also suggest that slurry feed gasification is not suitable for very low quality coals.

2)Effect of O/Coal ratio on the outlet composition of the syngas
Fig. 14a, **Fig. 14b** and **Fig. 15a** represent the variation in composition of the syngas at various O/Coal ratios for coal TL-A, TL-B and TL-C, respectively. Fig. 15b expressed the composition of syngas at already found point of O/Coal ratio of 0.91 for all type of coals. In case of TL-A as represented in Fig. 14a CO_2 and H_2O formation show a rise after a specific O/Coal ratio (0.91) when combustion reaction instead of gasification reaction commence. At the early stage of the gasification process when O/Coal ratio is not high, formation of CO and H_2 by the reduction reaction takes place. The trends in all type of coals are same with varied amounts of the syngas components. For TL-A in **Fig. 14a**, the amount of CO and H_2 produced is more in comparison to other two coals, the reason behind is the less amount of moisture contents in TL-A on as-received basis as compared to other coals, resultantly temperature suitable for the gasification reaches soon and more CO and H_2 exist at that temperature. Syngas composition for all three coals after gasification in slurry feed gasifier presented in **Fig. 14a**, **Fig. 14b** and **Fig. 15a** at varied O/Coal ratios show almost same behavior but varied composition based on their moisture contents. If slurry feed technology has to be used for power generation these graphs for low quality coals provide a foundation for the decision making for the selection of the process and hint different operation parameters for the desired composition of the syngas for downstream co-generation.

(a) **(b)**
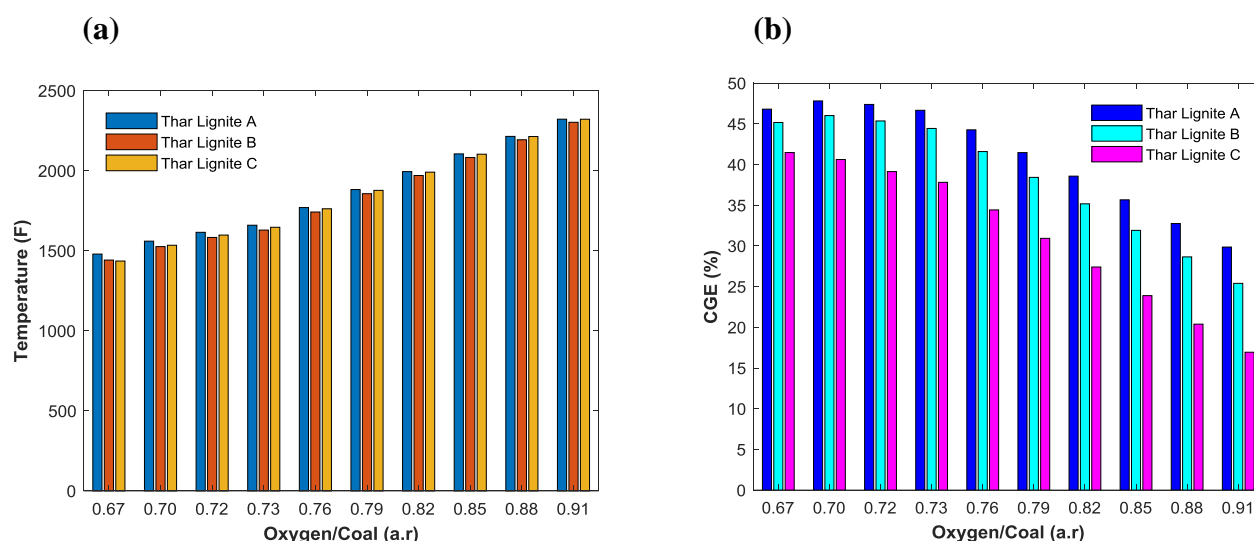
Fig. 13. Profiles for the GE gasifier, (a) Temperature (b) CGE, at the exit of the GE gasifier for various Oxygen/Coal (a.r) ratios.
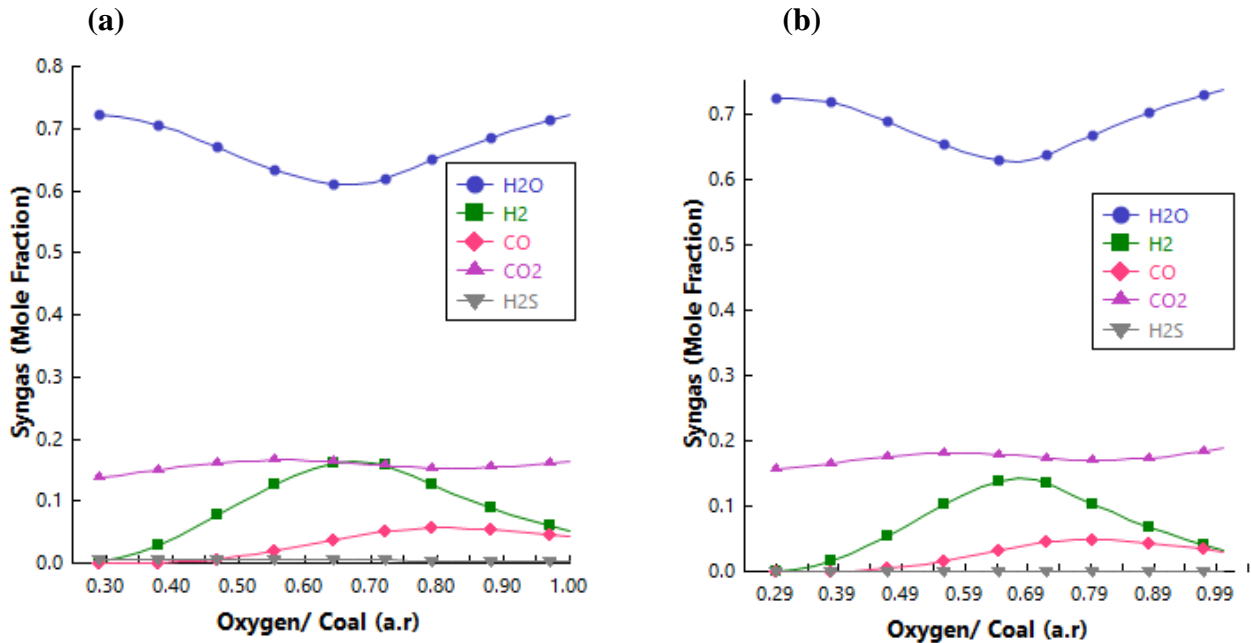
Fig. 14. Syngas composition in slurry feed system for varied O/Coal ratio for coal (a) TL-A and (b) TL-B.
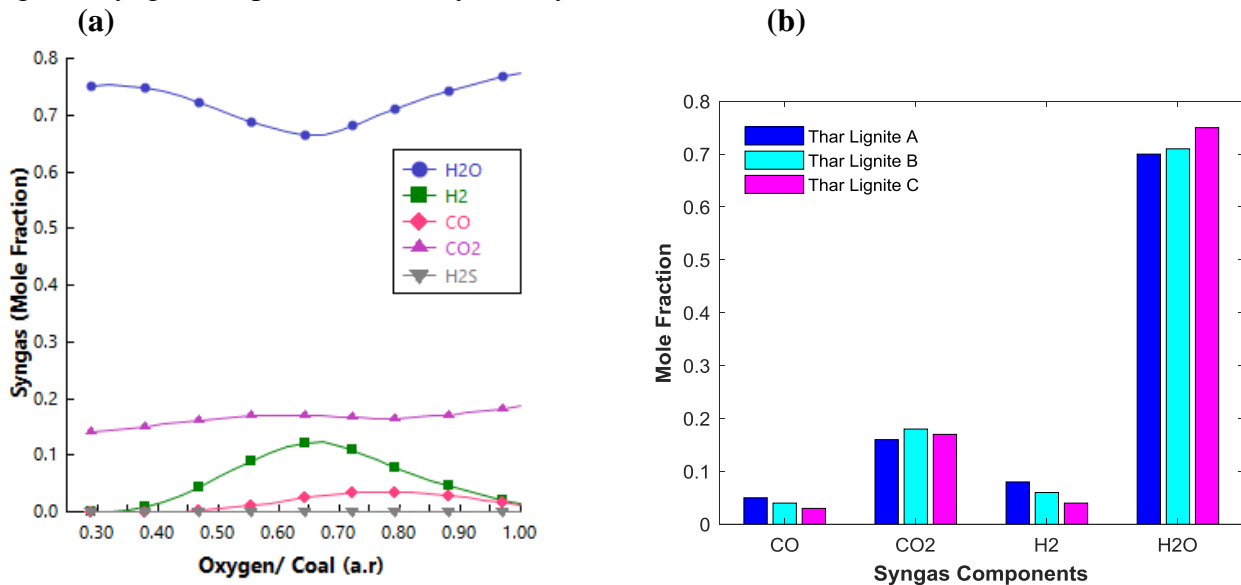
Fig. 15. (a) Syngas composition at varied O/Coal ratio for TL-C coal, (b) Syngas composition at O/Coal ratio of 0.91 for TL-A, TL-B and TL-C.

3)Effect of solid concentration in slurry on the composition of the syngas and CGE of the gasifier

Fuel contents in slurry play an important role on the performance of the gasifier and even overall performance of the IGCC system. **Fig. 16** presents a comparison for two different concentrations of fuel contents in the slurry. **Fig. 16a** with 50% solid contents in slurry shows increased CO, CO_2 and H_2 composition in outlet syngas. Water coming out from the syngas in case of 50% solid contents is less in comparison to 40% concentration as seen in Fig. 16b, but CO, CO_2 and H_2 contents in case of 40% solid contents are less in comparison to 50% concentration. This comparison based on the different concentrations of the fuel in slurry provides a guideline for decision making to adjust the desired concentration of solid

content as per requirements downstream of the process. Similarly, **Fig. 17a** presents a comparison for different solid concentrations of TL-A coal in slurry and it is very obvious from the results that as solid concentration decreases in slurry, amount of CO and H_2 decreases in syngas and resultantly CGE of the gasifier decreases. As the assumed outlet temperature of the syngas is same i.e. 2300 ºF for all solid concentrations, the amount of CO_2 in syngas is almost same. As the amount of water increases in slurry more oxygen is required to vaporize the water and to reach the desired gasification temperature, hence O/Coal ratio increases. The O/Coal ratio for 35%, 45% and 55% solid concentration is 1.145, 0.907 and 0.757, respectively.

(a)   **(b)**
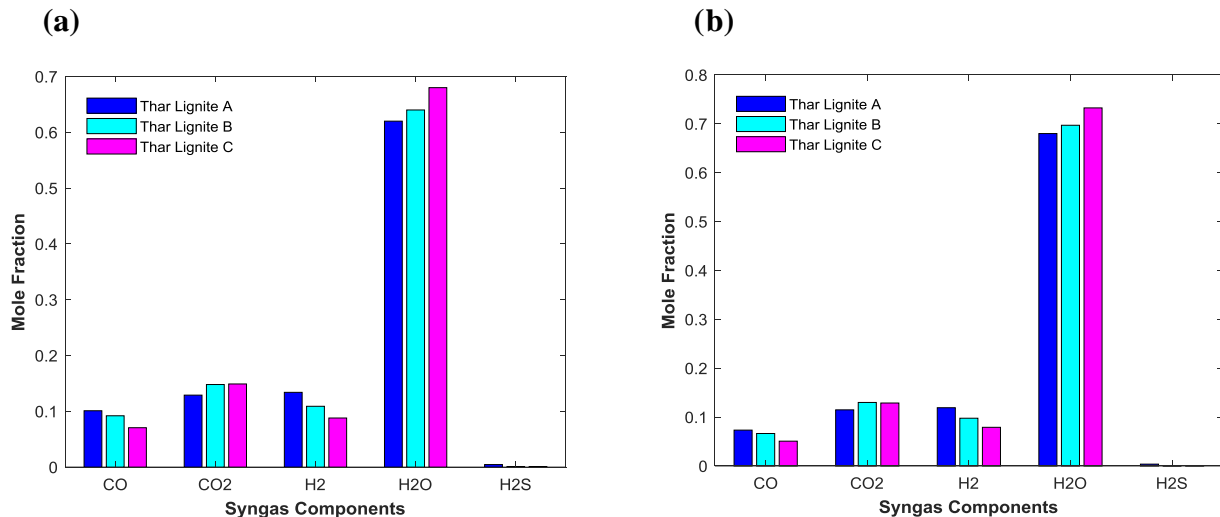
Fig. 16. Syngas composition from gasifier at same input parameters for (a) 50% and (b) 40% solid concentration in slurry.
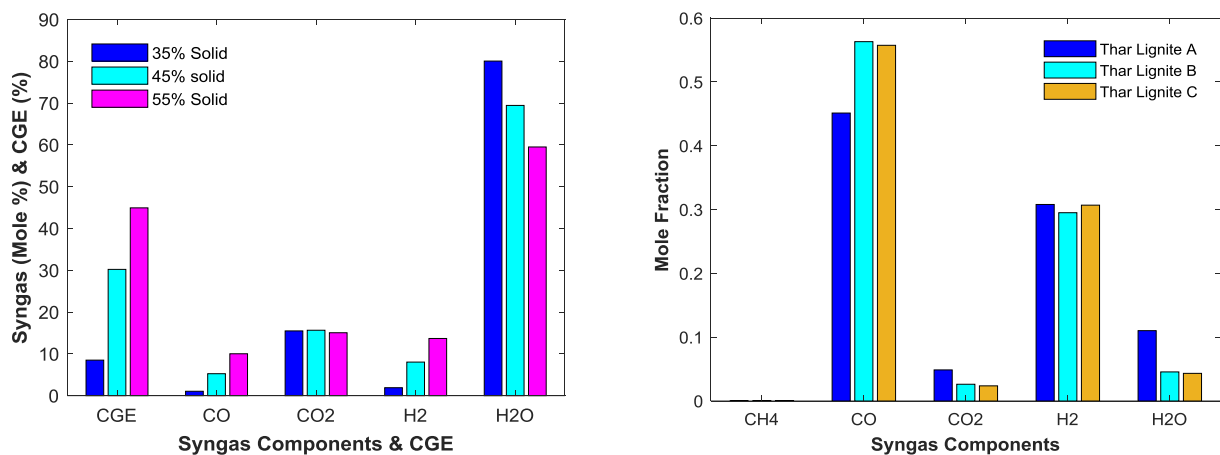
Fig. 17. (a) Syngas composition and CGE comparison for the same coal (TL-A) at same temperature and pressure but different solid concentration in slurry, (b) Mole composition of syngas from different quality coal at 0.6856 oxygen/ dried coal (up to 12%) using Shell gasifier.

For comparison purpose, syngas composition from the Shell gasifier at same oxygen to dried coal ratio of 0.6856 is presented in **Fig. 17b**. It is clear from the results, dry feed gasifier produces more CO and H_2 as compared to slurry feed gasifier.

IV. CONCLUSION

Critical analysis of two commercial gasification technologies using indigenous resources of coal in gasification provide a foundation in decision making for the utilization of these coals. In this study, coal with average, low and very low quality were used with moisture content 35%, 44.92% and 50.24%, respectively, which represent major portion of the existing coal resources in Thar, Pakistan. Based upon the results obtained from the thermodynamics models of gasification process performed using dry feed

technology (using Shell gasifier) and slurry feed technology (using GE gasifier) following conclusions have been drawn.

1) In case of dry feed technology, at 2500 °F temperature and 615 Psia pressure, the CGE for TL-A is 80.40% at 0.46 O/Coal ratio, for TL-B is 85.88% at 0.42 O/Coal ratio and for TL-C is 82.86% at 0.41 O/Coal ratio. From these values it is clear that, as all coals were dried up to 12% moisture content before gasification process, the performance of the dry feed gasifier depends upon the quality of the coal with respect to ash content and carbon content.

2) From above values of O/Coal ratios for different quality coals also confirm that low quality coals require more oxygen to reach desired performance in comparison to high quality coals.

Even huge difference in coal quality of the three considered coals, there is merely a minor difference in the performance of the gasifier with respect to the CGE of the gasifier, proves that dry feed gasification technology is less vulnerable to the quality of the coal.

3) In case of slurry feed gasification technology, near 2500 °F temperature, the CGE for TL-A is 29 %, for TL-B 25 % and for TL-C is almost 15 % at O/Coal ratio of 0.91. The above values of O/Coal ratio to reach up to 2500 °F gasification temperature show that huge amount of oxygen is required to initiate entrained flow gasification reactions as compared to dry feed system. Furthermore, huge difference in CGE for different quality coals proves that in case of slurry feed gasification using GE gasifier the performance of the gasifier is vulnerable to the quality of the coal. Very small values of CGE for low quality coals also suggest that slurry feed gasification is not suitable for low quality coals.

4) When dry feed gasification is compared with slurry feed gasification on same quality coals of Pakistani origin, it has been noted that dry feed gasifier (Shell) shows appropriate performance, and suitable for power generation.

V. REFERENCES

[1] "Market Series Report: Coal 2017 in Analysis and Forecasts to 2022," France, 2017.

[2] "International Energy Outlook 2019," Paris, 2019.

[3] "BP Statistical Review of World Energy. British Petroleum Company," 2012. [Online]. Available: https://scholar.google.com/scholar?hl=en&as_sdt=0%2C5&q=BP+Statistical+Review+of+World+Energy.+British+Petr oleum+company+2012&btnG=. [Accessed: 21-Nov-2020].

[4] "Pakistan's Power Generation Potential," 2008.

[5] Y. Yun, Y. Yoo, and S. Chung, "Selection of IGCC candidate coals by pilot-scale gasifier operation," *Fuel Process. Technol.*, vol. 88, no. 2, pp. 107–116, 2007.

[6] L. M. Abadie and J. M. Chamorro, "The Economics of Gasification: A Market-Based Approach," *Energies*, vol. 2, pp. 662–694, 2009.

[7] M. Mansouri Majoumerd, H. Raas, S. De, and M. Assadi, "Estimation of performance variation of future generation IGCC with coal quality and gasification process - Simulation results of EU H2-IGCC project," *Appl. Energy*, vol. 113, pp. 452–462, 2014.

[8] Y. Ju, H. H. Lee, M. Oh, and C. H. Lee, "Performance Analysis on an Entrained-Flow Gasifier by Coal Moisture," *Chem. Eng. Technol.*, vol. 40, no. 12, pp. 2257–2265, Dec. 2017.

[9] M. Karthikeyan, W. Zhonghua, and A. S. Mujumdar, "Drying Technology Low-Rank Coal Drying Technologies-Current Status and New Developments Low-Rank Coal Drying Technologies-Current Status and New Developments," *Taylor Fr.*, vol. 27, no. 3, pp. 403–415, 2009.

[10] O. Nooruddin, "Simulation and optimization of IGCC technique for power generation and hydrogen production by using lignite Thar coal and cotton stalk," Faculty of Technology, LAPPEENRANTA UNIVERSITY OF TECHNOLOGY, 2011.

[11] K. Younas, K. Hayat, and M. Asif, "Thermodynamic evaluation of IGCC (integrated gasification combine cycle) power plant using thar coal," *Proc. 2015 12th Int. Bhurban Conf. Appl. Sci. Technol. IBCAST 2015*, pp. 419–427, 2015.

[12] K. Younas and M. Asif, "Process simulation and thermodynamic evaluation of integrated gasification combine cycle power plant using low-grade coal," *Int. J. Renew. Energy Technol.*, vol. 7, no. 1, p. 83, 2016.

[13] S. A. Rajper, I. N. Unar, A. Channa, and Z. A. Bhatti, "Investigation of Performance for Entrained Flow Gasifier Through Simulations," *Mehran Univ. Res. J. Eng. Technol.*, vol. 39, no. 1, pp. 97–110, 2020.

[14]   I. N. Unar *et al.*, "Impacts of slurry and dry forms of low-rank coal (lignite) on quality of syngas produced," *Clean Technol. Environ. Policy*, vol. 22, no. 3, pp. 613–625, 2020.

[15]   J. Black, "Cost and Performance Baseline for Fossil Energy Plants Volume 3 Executive Summary : Low Rank Coal and Natural Gas to Electricity," USA, 2011.

[16]   "The Shell coal gasification process for sustainable utilisation of coal," *Shell Global Solutions*, 2006. .

[17]   Z. Yuehong, W. Hao, and X. Zhihong, "Conceptual design and simulation study of a co-gasification technology," *Energy Convers. Manag.*, vol. 47, no. 11–12, pp. 1416–1428, 2006.

[18]   S. - M Chern, L. T. Fan, and W. P. Walawender, "Analytical calculation of equilibrium gas composition in a C-H-O-inert system," *AIChE J.*, vol. 35, no. 4, pp. 673–675, 1989.

[19]   K. G. Mansaray, A. M. Al-Taweel, A. E. Ghaly, and F. Hamdullahpur, "Mathematical Modeling of a Fluidized Bed Rice Husk Gasifier: Part I-Model Development," *Energy Sources*, vol. 22, no. 1, pp. 83–98, 2000.

[20]   C. Chen and E. Rubin, "CO2 control technology effects on IGCC plant performance and cost," *Energy Policy*, vol. 37, no. 3, pp. 915–924, 2009.

[21]   O. Maurstad, H. Herzog, O. Bolland, and J. Beér, "Impact of coal quality and gasifier technology on IGCC performance," in *Proceedings of 8th International Conference on Greenhouse Gas Control Technologies*, 2006.

[22]   S. W and L. J, "Texaco gasifier IGCC base cases," *DOE/NETL*, 2000.

[23]   M. Sawalem, I. Badi, and S. Aljamel, "Ijesrt International Journal of Engineering Sciences & Research Technology Evaluation of Solid Wastes for Utilisation in Biogas Plant in Libya-a Case Study," *Int. J. Eng. Sci. Res. Technol.*, vol. 4, no. 11, pp. 577–583, 2015.

[24]   H. T. Oh, W. S. Lee, Y. Ju, and C. H. Lee, "Performance evaluation and carbon assessment of IGCC power plant with coal quality," *Energy*, vol. 188, p. 116063, 2019.

[25]   S. S. Daood, M. T. Javed, A. H. Rizvi, and W. Nimmo, "Combustion of Pakistani lignite (Thar Coal) in a pilot-scale pulverized fuel down-fired combustion test facility," *Energy and Fuels*, vol. 28, no. 2, pp. 1541–1547, 2014.

[26]   R. Haider, M. A. Ghauri, E. J. Jones, and J. R. Sanfilipo, "Methane generation potential of Thar lignite samples," *Fuel Process. Technol.*, vol. 126, pp. 309–314, 2014.

[27]   M. Gräbner and B. Meyer, "Performance and exergy analysis of the current developments in coal gasification technology," *Fuel*, vol. 116, pp. 910–920, 2014.

[28]   R. Barrera, C. Salazar, and J. F. Pérez, "Thermochemical equilibrium model of synthetic natural gas production from coal gasification using Aspen Plus," *Int. J. Chem. Eng.*, vol. 2014, 2014.

THERMAL ENERGY EFFICIENCY ASSESSMENT OF SMALL AND MEDIUM INDUSTRIES: A CASE STUDY

Kashif Ismail[A], Khurshid Ahmad[B] and Muhammad Hassan[C]

A, B, C USPCASE-University of Engineering and Technology Peshawar

Abstract—**worldwide attention to the reduction of carbon foot prints and energy efficiency (EE) has inspired researchers to design energy efficient thermal processes and systems. Heat energy recovery is one among the most important measures that can help in acquiring both. However, the small and medium industries, which are in significant numbers in Pakistan, are rarely being studied for energy efficiency improvements. In this study, the thermal process of a medium density fiber (MDF) manufacturing industry was studied. Processes like steam generation and consumption, fuel contents, air preheating and thermal power generation were modeled and simulated. It is found that the air preheating option (APH) increased the generated steam capacity from 24.6 to 37.2 $tons/hr$ and reduced flue gas temperature at stack from 400°C to 100°C. It was also found that the fouling resists the exchange of heat at the interfaces significantly, thus not only reducing the steam generation but also increases the stack temperature. Moreover, the combined heat and power model also showed an opportunity for energy efficiency improvement.**
Keywords— **Air Pre Heating, Energy Efficiency, Power Generation, Waste Heat Recovery**

I. INTRODUCTION

In the modern world a country's progress is measured by diversity and sustainability of energy resources along with their efficient and environment friendly utilization. The viability of energy source is measured in terms of efficiency and sustainability. Inefficient practices cause a rise in demand as well as the price of energy. To cope up with inefficient utilization of energy and increased carbon emissions, Energy Management is considered a viable tool and a matter of keen global interest [1]. Owing to the increasing rate of industrialization and multifold increment in population in recent years, the energy demand has been increasing very rapidly. Studies suggest that the energy demand increased by 2.3% in 2018; the highest rise in demand since 2010. Industrialized nation like US, China and India accounted for 70% of the total worldwide energy demand growth. With an alarming population growth rate of about 3%, the increase in Pakistan's energy demand is distressful [2]. Energy management provides us with standards, tools, techniques and procedures which pave the way to what is called Energy Efficiency. Organizations are reported to have saved up to 20% of the energy cost by implying various energy management programs with nominal investment [3]. The inefficient usage of energy comes with a cost in all the Small and medium enterprises. The energy cost is reflected in the increased price of the product and the services Researches suggest that 10 to 40% possible energy savings can be achieved within the available technology in the manufacturing industries by implementing various energy and resources management strategies [4].

Flue gases have enormous amount of heat energy which often leaves the system with unutilized heat energy. In all the process of fuel-fired furnaces, exhaust losses are unavoidable. Fuel Air mixture is burned to produce thermal energy which is utilized up to maximum possible level in the heating devices and its load. The utilized gases then lost via stack to give a space to the fresh charge of combustible gases.

The Exergy puts a limit, means they can't liberate further energy to the load when the furnace and load achieve the same temperature as the combustion products. They have to be rejected as waste heat losses. The greater the exhaust gases temperature, the lower the efficiency. The temperature of the stack gases defines energy efficiency [5].

In order to bring improvement in the energy efficiency waste heat recovery has been proved as an attractive, less costly and an emission free technology for the industrial sectors. Several industries have installed/adopted several waste heat recovery technologies and have upgraded or improved their energy consumption.WHR is an emission free substitute instead of purchasing costly fuels or power generation [6].

II. METHODOLOGY

The methodology for research work has been divided in different phases.

i.   Phase 1
- The first step in phase 1 is familiarization about the plant activities for identification of the main energy consuming units; in process heat industry as in our case (MDF) the steam generation and its consumption at various stages of the process is crucial.
- The next step in the phase 1 is the selection of a simulation tool; **EBSILON®Professional** that has been used for simulation purpose in our research work. EBSILON®Professional is a simulation software used for plant designing, planning and optimization [7].
- The last step in phase 1 is primary data collection from the plant for simulation purposes

ii. Phase 2
- Analysis and simulation of energy consumption of existing plant data.
- Development & Identification of Energy Conservation opportunities

iii. Phase 3 of the methodology includes selection and recommendation of the proposed and promising ideas.

III. RESULTS AND DISCUSSION

Model 01: the plant input data is shown below in the table I

TABLE I: Existing plant data

Fuel type	$tons/day$	NCV(kj/kg)
COAL	50	24080
DUST	20	9048.3
BARK	24	9048.3
CHIPS	40	19340

For this data the existing plant is currently producing a steam of 18 $tons/hr$ with a hot flue gases temperature of 900°C while thermal oil temperature is 280 °C.

We have modeled our plant in EBSILON®Professional for the same data and after simulation we have obtained the following results as shown in the below Fig. 1.
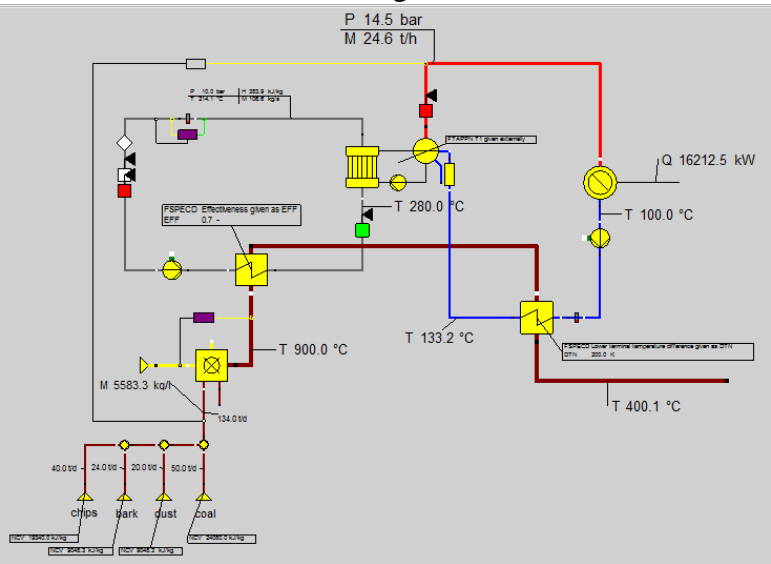
Fig. 1. Model 01.

At final stage the various properties of hot flue gases are shown in the following Fig. 2.
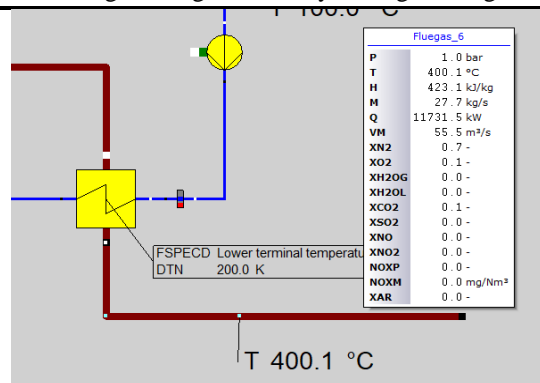
Fig. 2. Flue gases properties at stack of Model 01.

So we have an ample potential to utilize this waste heat for some useful purposes.

Model 02 With APH option: We have modeled our plant with air pre heating option by utilizing the waste heat which is shown below in the Fig. 3.
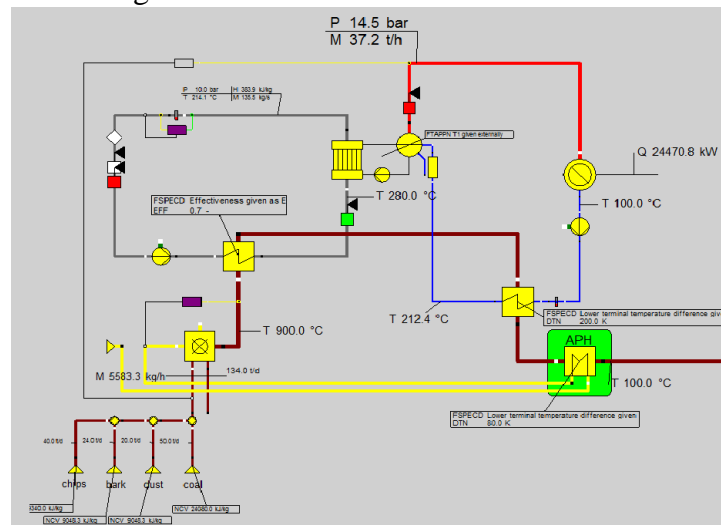
Fig. 3. Model 02 with air pre heating option.

We have noticed that in our first model the flue gases at stack are at 400°C and 1bar so we have utilized that waste heat for air pre heating purposes. Visible changes occurred in our plant model as shown in the Fig. 3 above. The hot flue gases temperature changes after installing APH reduces from 400°C to 100°C; ultimately the waste heat has been recovered and utilized for APH purposes.

APH effects on Steam

The generated steam capacity has been increased from 24.6 to 37.2 $tons/hr$; consequently the heat consuming capacity has also been increased to 24470.8 KW which was 16212.5 KW in our first model.

TABLE II: Comparison between inlet air with and without APH

Parameter	Inlet air to CC without APH	Inlet air to CC with APH
Pressure (bar)	1	1
Temperature (°C)	20	235.12
Enthalpy (kj/kg)	20.10	238.59
Energy flow (KW)	529.22	8149.37
Exergy (kj/kg)	-0.310	65.53
Mass flow (kg/s)	26.32	34.15

Model 03 EBSILON® model with APH and as well as Power Generation option. We have utilized the waste heat in this model for the two purposes which are as followings

1. Air Pre Heating option   2. Power Generation option

So, primarily we have two circuits; one is working for industrial process while at the same time the other

circuit is generating power which can be utilized for industry use.
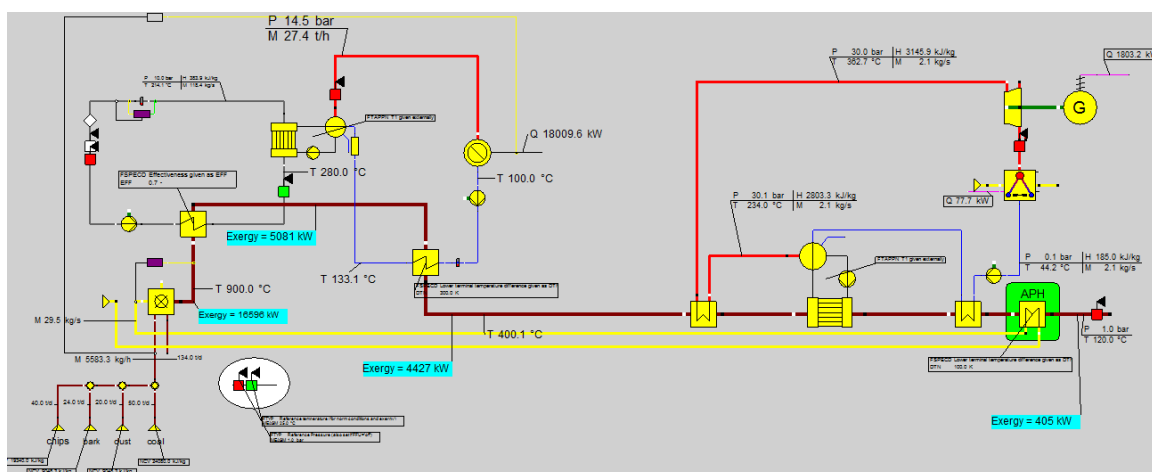
Fig. 4. Model 02 with air pre heating option and power generation option.

Effect on Steam: The generated steam capacity has been increased from 24.6 to 27.4 $tons/hr$; consequently, the heat consuming capacity has also been increased to 18009.6KW which was 16212.5KW in our first model.

Power generation option: With the flue gas properties of 400 °C and mass flow of 27.2 kg/s approximately 1.8 MW of electric power (gross) can be achieved; if an air cooled condenser is used approximately 77 KW of power is needed for that.

Fouling factor plays an important role in heat exchangers, with the addition of fouling factor (i-e 0.8 in our case) the value cross at each component shows significant changes, some of the changes are shown in the TABLE IV *below*.

TABLE IV: Role of fouling factor

Parameter	Design case with no fouling	Design case with fouling factor of 0.8
Generated Power (KW)	1803.2	1778.2
Generated steam (kg/s)	27.4	27.1
Exergy (KW)	17860	17639
Heat flow @stack (KW)	3806.09	4068.60
Stack temperature (°C)	120	129.80

IV. CONCLUSION

In this research work, simulation-based assessments are conducted in order to evaluate the energy efficiency resources or conservation measures in a small & medium enterprise. The plant for the input fuels at current level has been simulated and it is found that for the same data our simulated model has generated 24.6 $tons/hr$ steam as compared to 18 $tons/hr$ in the actual plant. While, the hot flue gases at stack are at 400°C and at 1bar pressure. So, there is an ample potential to utilize this waste heat for some useful purposes like for Air preheating and as well as for power generation purposes.

In the second type, we have developed a simulated model in EBSILON® Professional with air pre heating option utilizing the waste heat. The hot flue gas temperature after installing APH reduces from 400°C to 100°C. The generated steam capacity has been increased from 24.6 to 37.2 $tons/hr$; consequently the heat consuming capacity has also been increased to 24470.8KW which is 16212.5KW in our first model. The air temperature at the inlet of combustion chamber has been changed from 20°C to 235.12°C.

In our third type, i-e model with APH and power generation purposes the flue gas temperature at stack has been reduced to 120°C from 400°C, The generated steam capacity has been increased from 24.6 to 27.4 $tons/hr$; consequently, the heat consuming capacity has also been increased to 18009.6KW which is 16212.5KW in model 01, With the flue gas properties of 400 °C and 27.2 kg/s, approximately 1.8 MW of electric power (gross) has been generated.

Fouling factor plays an important role in heat exchangers. The generated power has been reduced from 1803.2KW to 1778.2KW; the flue gas temperature at stack has been increased from 120°C to 129.8°C, while the energy flow at stack has also been increased to 4068.60KW from 3806.09KW.

Thus, a model with both the APH and Power generation option is the most promising option because using the waste heat for power generation, resulting in independency on power-producing agencies, lower product prices, and an environment-friendly industrial process.

Acknowledgment

References

[1]   I. Dincer, "Environmental Issues: I-Energy Utilization," *Energy Sources*, vol. 23, no. 1, pp. 69–81, Jan. 2001, doi: 10.1080/00908310151092191.

[2]   D. F. Birol, "Energy Efficiency 2019," p. 110, 2019.

[3]   R. Saidur, "A review on electrical motors energy use and energy savings," *Renew. Sustain. Energy Rev.*, vol. 14, no. 3, pp. 877–898, Apr. 2010, doi: 10.1016/j.rser.2009.10.018.

[4]   S. Thiede, G. Posselt, and C. Herrmann, "SME appropriate concept for continuously improving the energy and resource efficiency in manufacturing companies," *CIRP J. Manuf. Sci. Technol.*, vol. 6, no. 3, pp. 204–211, Jan. 2013, doi: 10.1016/j.cirpj.2013.02.006.

[5]   J. I. Chowdhury, Y. Hu, I. Haltas, N. Balta-Ozkan, G. Jr. Matthew, and L. Varga, "Reducing industrial energy demand in the UK: A review of energy efficiency technologies and energy saving potential in selected sectors," *Renew. Sustain. Energy Rev.*, vol. 94, pp. 1153–1178, Oct. 2018, doi: 10.1016/j.rser.2018.06.040.

[6]   "Waste Heat Recovery: Technology and Opportunities in U.S. Industry," p. 112.

Comparative Study of conventional and microwave assisted pyrolysis of corncob

M.Y. Gul , M.Mustafa , and M.Habib

University of Engineering And Technology Peshawar

*Abstract-***Renewable sources of energy are the need of the day in the current energy crises situation. To combat energy crises, energy from the biomass feedstock could be the possible remedy. Lignocellulose biomass feedstock due to its abundance and carbon neutral nature could be utilized for the production of renewable biofuels. Pyrolysis for such utilization is an efficient method for producing liquid biofuels from waste biomass feedstock. A comparative study of conventional and microwave assisted pyrolysis for biofuel formation from corncob is done in the current study. In this study some of the factors like bio oil yield and process variables in the conventional and Microwave assisted pyrolysis were studied. Comparing the two processes, keeping same process variables, a maximum bio oil yield of 6.5% and 9.6% is obtained in the conventional and Microwave assisted pyrolysis respectively. Microwave assisted pyrolysis is proving to be an energetically as well as economically feasible process.**

Keywords **— Bio oil, Feedstock, pyrolysis.**

I. INTRODUCTION

Renewable energy has attracted increasing interest because of the concerns about the high demand on fossil fuels and the global climate change. One of the renewable energy sources is biomass. Biomass represents an abundant carbon-neutral resource for the production of bioenergy and biomaterials, and its enhanced use would address several societal issues [1]. Bioenergy and biofuels derived from biomass feedstocks exhibit lower life-cycle greenhouse- gas emissions than fossil fuels and with little or no competition with food production. The satisfactory feedstocks include agricultural residues, sustainably harvested wood, and municipal and industrial wastes [2]. Bioenergy industry will grow in the next few decades to address societal demands to reduce net carbon emissions, and it will require major changes in supply chain infrastructure [3]. Lignocellulosic biomass, a major biomass. resource, has been recognized as a potentially sustainable feedstock for the production of biofuels and other biomaterials [4]. However, because of the nature of biomass recalcitrance which means the complex structural and chemical mechanisms of plant biomass for resisting assault on its structural sugars from the microbial and animal kingdoms, it would be difficult to convert lignocellulosic biomass by biological processes and the cost could be high [4]. In this case, thermochemical processes could be a better choice to convert lignocellulosic feedstocks more quickly with lesser cost. Thermochemical conversion processes include combustion, gasification, liquefaction, and pyrolysis [5,6]. Combustion is the burning of biomass in air to convert the chemical energy stored in biomass into heat, mechanical power, or electricity [6]. Gasification is the conversion of biomass to a fuel gas by heating in a medium such as air, oxygen, or steam [7]. Liquefaction is generally carried out at relatively low temperatures to produce liquid products [8]. Pyrolysis is a thermal decomposition process occurring in the absence of oxygen, and it is always also the first step to produce primary products in combustion and gasification processes where it is followed by total or partial oxidation of the intermediate products [9]. The products of biomass pyrolysis include solid (char), liquid (bio-oil), and gaseous fuel [10]. The yields of the three-phase products would vary with changing operational parameters. Lower process temperature and longer vapor residence time favor the production of char, higher processing temperature and longer vapor residence time increase the biomass conversion to gas, and moderate temperature and shorter vapor residence time are optimum for liquids production [9]. Pyrolysis consists of a complicated set of reactions involving the formation of radicals [11]. Most of the research on pyrolysis processes has been conducted by using conventional heating sources such as electric and gas heater [12]. However, biomass pyrolysis heated

by microwave irradiation could be a more promising technique because of a number of advantages over conventional pyrolysis.

1.1. Microwave heating mechanism

2.1. Microwaves: In the electromagnetic spectrum, microwaves lie between infrared and radio frequencies. The wavelengths of microwaves are between 1 mm and 1 m with corresponding frequencies between 300 GHz and 300 MHz, respectively [13e15]. The two most commonly used microwave frequencies are 915 MHz and 2.45 GHz [14]. Microwave energy is derived from electrical energy with a conversion efficiency of approximately 85% for 915 MHz and 50% for 2.45 GHz [13]. Most of the domestic microwave ovens use the frequency of 2.45 GHz. Compared with 2.45 GHz, the use of 915 MHz can provide substantially larger penetration depth which is an important parameter in the design of microwave cavity size, process scale up, and investigation of microwave absorption capacity of materials [16].

1.2. Microwave heating

Microwaves cause molecular motion by migration of ionic species or rotation of dipolar species or both [13] to generate heat because of the friction among molecules. Materials that can absorb microwaves are called absorbers or dielectrics, so microwave heating is also referred to as dielectric heating [15]. The extent of microwave heating a material can be determined by a term called loss tangent which is the ratio of dielectric loss factor to dielectric constant of the material [13]. In general, materials can be divided into three types according to their loss tangents: high (> 0.5), medium (0.1-0.5), and low (< 0.1) microwave absorbing materials [16]. The loss tangents of carbon materials such as charcoal, carbon black, and activated carbon, ranging from 0.1 to 0.8, are either comparable to or higher than the loss tangent of distilled water (0.118 at 2.45 GHz and 298 K), so carbon materials are good microwave absorbers that show high capacity to absorb and convert microwave energy into heat [12,17]. Materials can be classified into three categories according to their interactions with microwaves: conductors, insulators, and absorbers. Microwaves are reflected from the surface and thus do not heat metals, which generally have

high conductivity and are classified as conductors [13]. Materials (e.g., glass and ceramics) transparent to microwaves are classified as insulators. Microwave heating offers a number of advantages over conventional heating such as: (1) non-contact heating; (2) energy transfer rather than heat transfer; (3) higher heating rate; (4) material selective heating; (5) volumetric heating; (6) quick startup and stopping; (7) heating from interior of the material body; (8) higher level of safety and automation [13]. Microwave energy is efficient in the selective heating of materials as no energy is wasted in the bulk heating of feedstocks, which is a clear advantage over conventional methods (bulk heating in furnaces) [15]. Therefore, microwave heating has been widely used in various scientific researches and industrial applications, such as food processing, sterilization and pasteurization, different drying processes, rubber vulcanization, and polymerization or curing of resins and polymers [17]. An important characteristic of microwave heating is the phenomenon of hot spot formation, which arises from the inhomogeneity of microwave field (the formation of standing waves) or dielectric property within a feedstock (a blend or a mixture) so that a local temperature inside the feedstock is much higher than the temperature measured in the bulk [15,16]. Hot spots would have significant influence on the yield and characteristics of microwave processing products. To control or utilize the hot spot phenomenon, cavity design is an important factor [15]. The effects of hot spots can be reduced by several techniques, such as increasing the size of the cavity, operating at a higher frequency, equipping a turntable, installing a mode stirrer, and hybrid heating that combines microwave heating with conventional heat transfer through radiation, convection, or conduction [14].

1.3. Microwave pyrolysis

Lignocellulosic biomass, such as crops, wood, agricultural and forestry residues, is mainly composed of cellulose, hemicellulose, and lignin. In general, the cellulose, hemicellulose, and lignin contents of plant biomass are approximately 35-50, 25-30, and 15-30 wt%, respectively [1].

2. METHODOLOGY

2.1 Microwave assisted Pyrolysis:

Figure.1 shows the experimental setup used in the pyrolysis of corn cob wastes. . Particle size range was between 0.425mm< dp < 0.600 mm. Pyrolysis was carried out in a microwave cavity oven (Panasonic model). The heating area of the oven is 46.1 cm × 28.9 cm × 37.7 cm and has a maximum output power of 800 W. In a typical experiment, 100 g dried biomass was added to a two-neck round bottom quartz flask which was placed inside the microwave cavity. The atmosphere was purged for 10 min to create oxygen free environment. Appropriate holes were made in the oven such that the flask can be connected for nitrogen supply and condenser set-up. Water was used as the coolant in the condensers. Since microwave heating assists in fast pyrolysis, a sufficient time of 10 min was kept for all biomass to achieve complete pyrolysis. Due to rapid microwave heating, continuous monitoring of temperature was not possible; however the observed temperature at the end of the pyrolysis reaction was in the range of 400–500 °C. At the end of experiments, the liquid products (bio-oil) remained in the round bottomed flask. All the bio-oil were collected in a single tight sealed Teflon coated container, and analyzed further. The obtained solid bio char in the quartz flask was allowed to cool and then weighed. The non-condensable gases were left into the atmosphere.
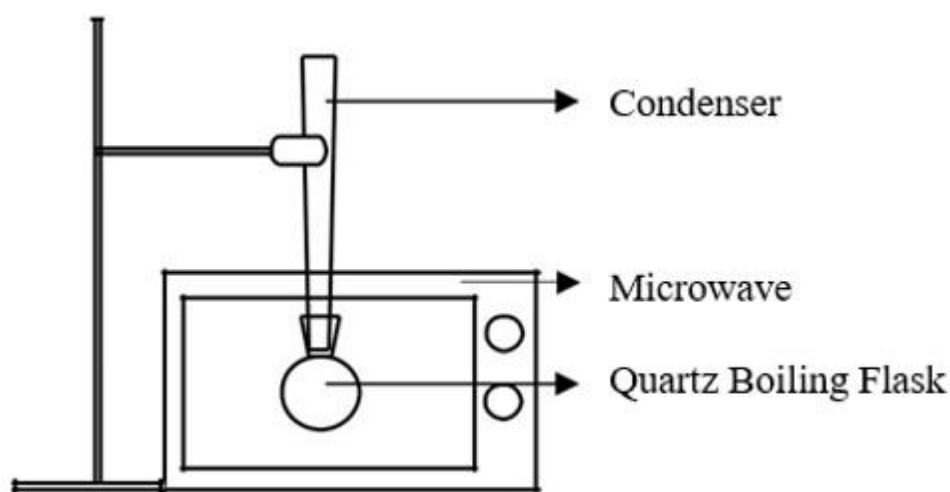
Figure.1 Experimental setup for microwave pyrolysis experiment

2.2 Conventional Pyrolysis:

The Microwave assisted pyrolysis was compared to the conventional pyrolysis of corncob, a work of demiral at al[18]. operated on a very similar features and conditions in which they used 100g of biomass samples in a fixed-bed reactor with a length of 104 mm and an internal diameter of 70mm equipped with a sweep gas (nitrogen) connection. The 600W furnace with an inner volume large enough to contain the whole reactor was employed for heating. The thermocouple was connected to a proportional controlling unit which was capable of maintaining the oven temperature installed into a control panel.

3. RESULTS AND DISCUSSION:

Product Yield

When the reaction temperature was only 180-200°C, bio oil yield was 5% in microwave assisted pyrolysis. However, at the reaction temperature of 480 °C (optimum temperature) liquid yields was approximately 9.6 wt.%, respectively. At a temperature of 600°C, the liquid yield was 6.5%. Therefore, liquid yield substantially decreased with increasing reaction temperature. This may imply that, when product vapors are released by the devolatilization of biomass pyrolysis, more hydrocarbons in the vapors can be converted into permanent gases at higher reaction temperature.

In the conventional pyrolysis, upon heating at 500°C(optimum temperature) a maximum yield obtained was 6.5%

4. CONCLUSION

In this study, a renewable source, corncob, was taken as the biomass sample for the pyrolysis experiments performed in a modified microwave oven under different conditions to investigate the effects of these experiental changes on product yields. Also the results were compared at very similar conditions with the conventional pyrolysis. The results from the present study suggested that the corn cob can be utilized as an energy-rich potential renewable feed stock to produce higher amount of bio-oil hence, the corn cob based bio oil can be used as a suitable feed stock for further upgrading it in to fuel oil via catalytic hydro processing. Finally, it was concluded that the microwave assisted fast pyrolysis is an emerging technology to produce good quality bio-oil.

5. REFERENCES

[1] Ragauskas AJ, Williams CK, Davison BH, Britovsek G, Cairney J, Eckert CA, et al. The path forward for biofuels and biomaterials. Science 2006;311:484-9.

[2] Tilman D, Socolow R, Foley JA, Hill J, Larson E, Lynd L, et al. Beneficial biofuelsethe food, energy, and environment trilemma. Science 2009;325:270-1.

[3] Richard TL. Challenges in scaling up biofuels infrastructure. Science 2010;329: 793-6.

[4] Himmel ME, Ding SY, Johnson DK, Adney WS, Nimlos MR, Brady JW, et al. Biomass recalcitrance: engineering plants and enzymes for biofuels production. Science 2007;315:804-7.

[5] Bridgwater AV, Peacocke GVC. Fast pyrolysis processes for biomass. Renew Sust Energ Rev 2000;4:1-73.

[6] McKendry P. Energy production from biomass (part 2): conversion technologies. Bioresour Technol 2002;83:47-54.

[7] McKendry P. Energy production from biomass (part 3): gasification technologies. Bioresour Technol 2002;83:55-63.

[8] Peterson AA, Vogel F, Lachance RP, Froling M, Antal Jr MJ, Tester JW. Thermochemical biofuel production in hydrothermal media: a review of sub- and supercritical water technologies. Energy Environ Sci 2008;1:32-65.

[9] Bridgwater AV. Biomass fast pyrolysis. Therm Sci 2004;8:21-49.

[10] Demirbas A, Arin G. An overview of biomass pyrolysis. Energy Sources 2002;24:471-82.

[11] Yaman S. Pyrolysis of biomass to produce fuels and chemical feedstocks. Energy Conv Manag 2004;45:651-71.

[12] Lam SS, Chase HA. A review on waste to energy processes using microwave pyrolysis. Energies 2012;5:4209e32.

[13] Haque KE. Microwave energy for mineral treatment processes e a brief review. Int J Min Process 1999;57:1-24.

[14] Thostenson ET, Chou TW. Microwave processing: fundamentals and applications. Compos Pt A-Appl Sci Manuf 1999;30:1055-71.

[15] Jones DA, Lelyveld TP, Mavrofidis SD, Kingman SW, Miles NJ. Microwave heating applications in environmental engineering e a review. Resour Conserv Recycl 2002;34:75-90.

[16] Yin C. Microwave-assisted pyrolysis of biomass for liquid biofuels production. Bioresour Technol 2012;120:273-84.

[17] Menendez JA, Arenillas A, Fidalgo B, Fernandez Y, Zubizarreta L, Calvo EG, et al. Microwave heating processes involving carbon materials. Fuel Process Technol 2010;91:1-8.

[18] Ilknur D, Alper E, Sevgi S, , enso Z et al. Bio-oil production from pyrolysis of corncob (Zea mays L.) science 2012 43-49

Energy Efficiency Resource Assessment for Marble Industry of Peshawar City

Zaeem Ahmed [A], Prof. Dr. M. A. Irfan [B],

[A]*USPCASE UET Peshawar* [B]*UET Peshawar*

Abstract— **Pakistan is a developing country. To meet its energy needs one way is to install new powerplants, the other way is to slow down the growing demand of energy without effecting the economic growth through energy efficiency. Internationally energy efficiency is considered as a resource. Three sample marble industries were studied and checked for inefficient practices. A list of Energy Conservation Measures was provided through energy audits of the industries. The ECMs were checked for their technical and economic feasibility. A potential energy efficiency intervention program was obtained after the economic and technical feasibility study of the ECMs.**
From the energy efficiency program potential, a resource of approximately 5 Million kWh saving per year for Peshawar marble industrial sector was identified through the intervention of energy efficiency program. A total savings of 81.6 Million PKR/year from the marble industry can be achieved for ten years by one-time initial investment of 572.7 Million PKR. The payback of the investment will be 7 years.

Keywords— **Energy Conservation Measures, Energy Efficiency, Energy Savings, Resource.**

I. INTRODUCTION

The most effective way to address energy crises and global climate change issue is to improve energy efficiency. Energy efficiency is basically doing more with less. With the advancements in science and technology the efficiency of equipment's and machines are improving day by day. For example, a 12-watt LED can give you the same number of lumens that a 100-Watt incandescent bulb emits. By switching towards more efficient technology and improving the current technology's efficiency a huge amount of power can be saved from the industrial sector of Pakistan, whose result would reflect in the form of lower energy demand. Energy efficiency is itself a resource. And a large potential for energy savings through energy efficiency is present in Pakistan.

A large portion of energy is consumed by the industrial sector in Pakistan, about 37.46% of the total energy produced is consumed by this sector. Second largest energy consuming sector is transport. While the domestic sector consumes 21.20% of the total energy [1].

A detailed study of Pakistan energy supply and demand side was taken in 2012-13, All the inputs and outputs on supply and demand side were measured in MTOE. The study revealed that if the losses are included at consumer level, the loss of energy that Pakistan is suffering in its power transmission and consumption are about 82% due to inefficiencies. The biggest losses incur on consumer side about (29.24 MTOE), losses in power generation and transmission account for 15.06 MTOE, the losses in transmission and distribution of natural gas 3.79 MTOE, and electricity transmission and distribution losses 1.69 MTOE [2].

It means that for every one unit of energy used we are wasting 4.5 units of energy, which is a huge loss. If we concentrate on minimizing the inefficiencies in the major consuming sectors, we would be able to control and minimize our future projected demands of energy.

II. METHODOLOGY

The methods employed for this study are presented in the steps below:

1. Identification of the Significant Energy Users (SEU's)
2. Detailed Energy Audit of Ashrae level I and level II
3. Evaluation of the costs and benefits of energy efficiency measures
4. Assessing the key barriers and constraints to implementation
5. Design of a practical energy efficiency intervention program
6. Quantifying the energy resource from program potential

III. RESULTS AND DISCUSSION

The saving potential in terms of PKR for the different ECMs is listed below in the table.

TABLE I: Savings potential from the ECMs in Rupees.

S.No.	Details	Imran Marble	Iqra Marble	Karkon Marble	Average Saving potential
1	Savings from Power factor correction (PKR/yr)	28,848	35,328	0	21,392
2	Savings from premium efficient motors (PKR/yr)	162,282	233,892	250,873	215,682
3	Saving from shifting peak to off peak (PKR/yr)	18,781	29,570	20,859	23,070
Total Average savings					**260,144 PKR/yr**

The saving potential of the premium efficient motors in kWh is listed below in the Table:

TABLE II: Saving potential from premium efficiency motors.

Details	Imran Marble	Iqra Marble	Karkon Marble	Average
Savings in kWh/month	1,013	1,460	1,566	1,346 kWh/month
Savings in kWh/year	12,156	17,520	18,792	16,156 kWh/year
Savings in PKR/year	162,282	233,892	250,873	215,682 PKR/year

* Unit cost @13.35 PKR/kWh

The program potential which consists of three Energy Conservation Measures for the marble industrial sector is used to identify the potential of energy savings from the sector. The results of energy efficiency resource assessment of the marble industrial sector of Peshawar are presented in the figures below.
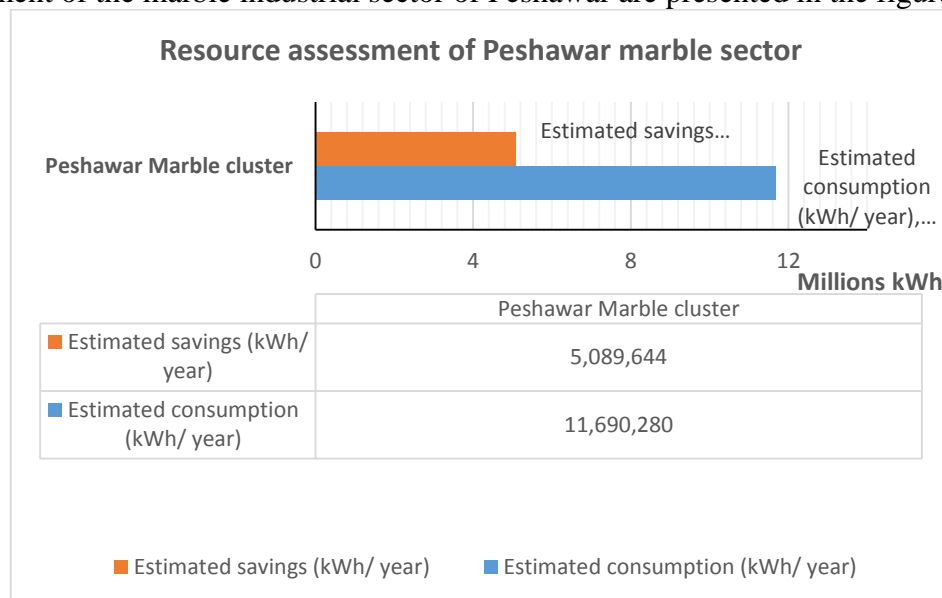
Fig. 1: Energy efficiency resource assessment of Peshawar marble sector.

The estimated units of energy consumed by the whole marble sector of Peshawar is estimated to be 11.69 Million kWh, out of which 5.1 Million kWh of electricity can be saved from this sector by the implementation energy efficiency intervention program.

The estimated savings in Rupees from the individual ECM of the energy efficiency intervention program and the cost of energy consumption by the sector on annual basis are presented in the Figure below:

Fig. 2: Savings comparison of different ECMs and estimated energy consumption.
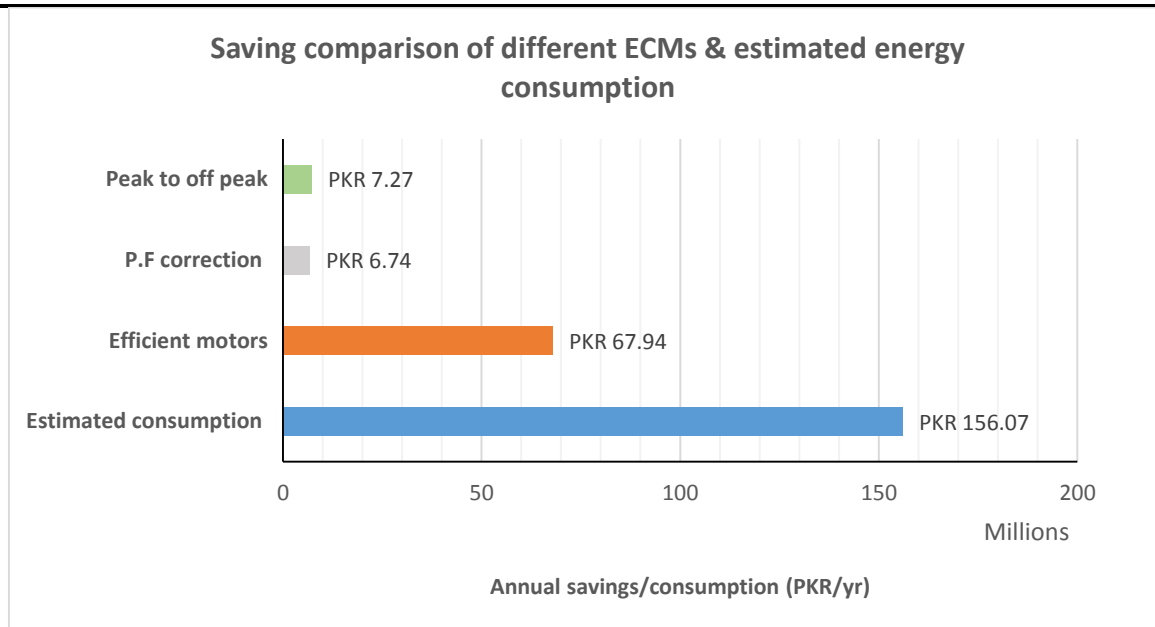
An estimated total of 156.07 Million PKR/ year is spent by the marble sector of Peshawar in paying the electricity bills. A saving of 67.94 Million PKR/ year can be achieved by replacement of less efficient motors with highly efficient ones. A saving of 6.74 Million PKR/ year can be achieved by improving the power factor. Shifting the working hours from peak to off peak can also save 7.27 Million PKR/ year for the marble sector. While the estimated total investment in the highly efficient motors account for 567 Million PKR and an estimated initial investment of 5.2 Million PKR is required for the power factor correction.

A total savings of 81.9 Million PKR/year from the marble industry can be achieved for ten years by one-time initial investment of 572.7 Million PKR. The payback of the investment will be 7 years.

IV. CONCLUSION

The energy efficiency intervention program consists of three Energy Conservation Measures.
1. Power factor correction
2. Highly efficient motors
3. Shifting from peak to off peak hours.

Saving of 6.7 Million PKR/year can be achieved for up to ten years by the marble industrial sector of Peshawar by just correcting the power factor of their facility. The Investment for the power factor correction is estimated to be 5.25 Million PKR. The Payback of this ECM will be 0.8 years.

Savings of 67 Million PKR/year can be achieved for a period of ten years by the marble industrial sector of Peshawar by replacing the low efficiency motors with highly efficient premium class motors. The investment for the highly efficient motors is estimated to be 567.3 Million PKR. The investment would pay back in 8.5 years.

Savings of 7.2 Million PKR can be achieved by the marble industrial sector of Peshawar just by shifting its working hours from peak to off peak. This ECM will not cost any penny to the industry.

As a result of energy efficiency resource assessment of marble sector of Peshawar city an estimated saving potential of 5.1 Million kWh/year of electricity was identified. The proper implementation of the Energy efficiency intervention program could result in savings of 81.94 Million PKR/year, for a period of ten years, with one-time initial investment of 572.7 Million PKR. The investment will pay back in 7 years.

Due to large payback period of the highly efficient motors, the owners of marble industry prefer to purchase motors from second hand market, which costs them less. But due to the use of inefficient motors a huge amount of energy is wasted, which if saved can prove to be a good resource on the energy supply side.

ACKNOWLEDGMENT

V. REFERENCES

[1] Division), M.o.E.P., Energy Year Book. Hydrocarbon Development Institute of Pakistan, 2018.

[2] Farid, N.R. Pakistan energy flow diagram. 2013; Available from: http://www.energyefficiencydatabase.com/energy-flow-diagram.php.

Technical Session 5-B (Google meet/Zoom) **Energy Conservation**	
Session Chair: **Engr. Hafiz Zeeshan Ahmad** Session Co-Chair: **Dr. Muazzam Paracha**	
M. Ihsanullah *(USPCAS-E UET Peshawar)*	Thermal analysis of refused derived fuel for waste to energy conversion
Mohammad Shoaib Fazal *(USPCAS-E UET Peshawar)*	Composition, energy and environmental analysis of the local coal of KP province.
M. Junaid *(USPCAS-E UET Peshawar)*	Hybrid Energy System For Small industries and Large Residential Centers in Peshawar City.
Arsalan Ali *(USPCAS-E UET Peshawar)*	Energy Efficiency Improvements for Power Generation Sector of Pakistan

Thermal analysis of refused derived fuel for waste to energy conversion

Muhammad Ihsanullah[A], Khurshid Ahmad[A], Mohammad Shoaib Fazal[A].

[A]US-Pakistan Center for Advanced Studies in Energy (USPCAS-E), University of Engineering and Technology Peshawar, Pakistan

engrmihsan@gmail.com, khurshid@uetpeshawar.edu.pk,

Abstract-Disposal of municipal solid waste is one of the challenging issues in Pakistan. Such wastes produce leachate and harmful gases which damage our environment. Converting municipal solid waste to refused derived fuel is an exciting technique for producing energy from wastes. In this research, household waste from selected houses in Peshawar Pakistan was quantified and characterized. It was found that the waste consists of 61% food waste, 10% plastic, 12%paper & cardboard, and 3% textile, 14% other non-combustible waste. The analysis showed that per capita waste generation ranges from 0.5 to 0.7 kg. The solid combustible wastes except of food were converted to refused derived fuel (RDF) pellets. The RDF pellets were further characterized using a thermal gravimetric analyzer and calorimetry. The net calorific value of the RDF turned out to be 13 MJ/kg. The backward analysis of energy utilization revealed that food production and cooking accounts for 10.8 MJ per kg of energy which includes energy consumed for transportation, labor, seeds, fertilizers, and cooking. Thus, reducing food waste is of equal importance.

Keywords— Calorific value, characterization, municipal solid waste, refused derived fuel, TGA Analysis

I. INTRODUCTION

The municipal solid waste (MSW) is generated from household, commercial, and institutional activities. MSW consists of food, plastic, clothing, glass metals, wood, tree trimming waste, etc. [1]. It does not include hazardous, industrial, and construction wastes [2]. According to research about 1.3 billion tons of solid waste was generated worldwide in 2012, and it is expected to double in 2025. MSW required more budgets in cities of the developing world. And poor management of MSW in a city badly affects the environment, health, and economy of cities[3].

There are many ways and means, technologies to convert MSW to energy and end-use application[4]. (WTE) technologies include pyrolysis, incineration, anaerobic digestion (AD), and refuse-derived fuel (RDF) pellets[5]. Internationally waste to energy conversion turns out to be only 13% of the total waste produced while 53 % of the waste is managed through landfilling.

Currently, incineration, composting, and recycling are making headway for waste management, and landfilling is no longer the first preference. Initially, the world used the incineration process to reduce the mass of solid waste but these days it is used for energy recovery. Landfills produce biogas which is used as a source of thermal energy and electrical power production. Composting of organic waste is the best choice when mass is taken into account during material recycling [6]. Advanced techniques can solve the problem arising from solid waste. The available waste to energy (WTE) techniques can be very useful for efficient energy recovery. This technique includes fluidized bed combustion, anaerobic digestion, pyrolysis, thermal conversion, plasma technology combustion, gasification, and landfill gas utilization. Specific amounts and compositions of solid waste are addressed by each of the techniques [7].

This research work deals with waste to energy conversion of Peshawar, Pakistan. As refused derived fuel pellets is an option for waste to energy conversion. This paper is about all details and prerequisites about refused derived fuel.

II.   Materials & methods

For this research work, the following methodology was adopted.

    a.   Data collection for waste characterization

    b.   waste characterization of MSW of Peshawar

    c.   Sampling for refused derived fuel pellets

    d.   Refused derived fuel pellets preparation

    e.   Testing of refused derived fuel pellets

A.   Data collection

Data for waste characterization was collected from different areas of Peshawar. For data collection, different areas of Peshawar were selected. For this purpose digital scales were distributed to volunteers. Volunteers collected data separately from all fractions of solid waste.

B.   Waste characterization of MSW

After data collection of the waste, the average of data was taken and by that way, waste characterization was found out.

C.   Refused derived fuel pellets sampling &preparation

Refused derived fuel pellets were prepared from combustible solid waste. For RDF pellets preparation, fractions of MSW was dried and weighted according to the percentage get in waste characterization. After that fractions of solid waste were shredded into powder particles with help of a shredder, after that mixed with calcium hydroxide and then pressed according to the standard size of RDF, and then put to sunlight for drying. Three types of RDF samples were prepared. Details of RDF samples are given below in table No.1.

Table 1: RDF Pellets composition by mass

S.No	Component name	Mass percentage		
01		RDF#01	RDF#02	RDF#03
02	Paper and cardboard	42.43%	Nil	29.5%
03	Plastic	31%	Nil	14%
04	Textile	11.22%	Nil	11%
05	Wood	Nil	56%	25.5%
06	Binder	8%	4%	9.5%
07	Moisture	7.8%	4.5%	10.5%
08	Binder	$Ca(OH)_2$	$Ca(OH)_2$	$Ca(OH)_2$
09	Coal	Nil	35.5%	Nil

Fig. 1:Refused derived fuel pellets

D. Testing of refused derived fuel

Different testing of refused derived fuel pellets was done by different equipment such as proximate analysis was done by Thermo Grivemetric Analyzer, ultimate analysis by X-ray Fluorescence Spectrometer (EDX) of model EDX 7000, calorific values by bomb calorimeter.

III. RESULTS AND DISCUSSION

A. Characterization of municipal solid waste

As for characterization, different houses from different areas of Peshawar were selected, and after that data was collected for 30 days. As municipal solid waste consists of different fractions such as paper, plastic, textile, food waste, etc. the data of these items collected separately and after taking an average of the data are shown in table 2. The term others represent the values of non-combustible.

Table 2: characterization of MSW of three houses

Items	House#01	House#02	House#03	Average
Food waste	64.7%	58.4%	55.9%	69.6(±2.5.)%
plastic waste	8.3%	11.7%	10.7%	10.2 (±0.5)%
Paper and card board	10%		16.3%	12.53(±0.6)%
Textile	5.2%	3.4%	3.6%	4.06(±0.2)%
Others	11.8%	16.7%	14.1%	14.1(±0.6)%

B. Proximate analysis of refuse-derived fuels pellets

Proximate analysis of RDF was carried out for refused derived fuel. The results were obtained from Thermo Grivemetric Analyzer TGA. This analysis was carried out in an Argon atmosphere with a 10-degree per minutes rise in temperature. The results are given below in table No.2.

Table 2: Proximate analysis of refused derived fuel

Name	RDF 1	RDF 2	RDF 03
Moisture content	16.5%	14%	12%
Volatile matter	11.5%	23%	18%
Fixed carbon	35%	33%	37%
Ash content	37%	30%	37%

C. Elemental analysis RDF pellets

We conduct elemental analysis through Energy Dispersive X-ray Fluorescence Spectrometer (EDX) of model EDX 7000. The result of the EDX is given below. For the RDF 01 sample. This graph shows the elements contained in the sample and their percentage. This graph show percentage of aluminum. As usually
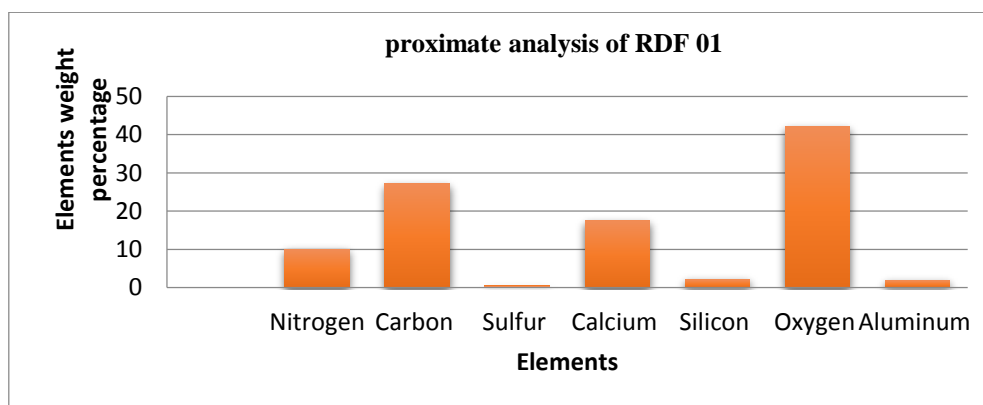
Fig. 2: Elemental analysis graph of Refused derived fuel pellets with the composition of paper, plastic, textile
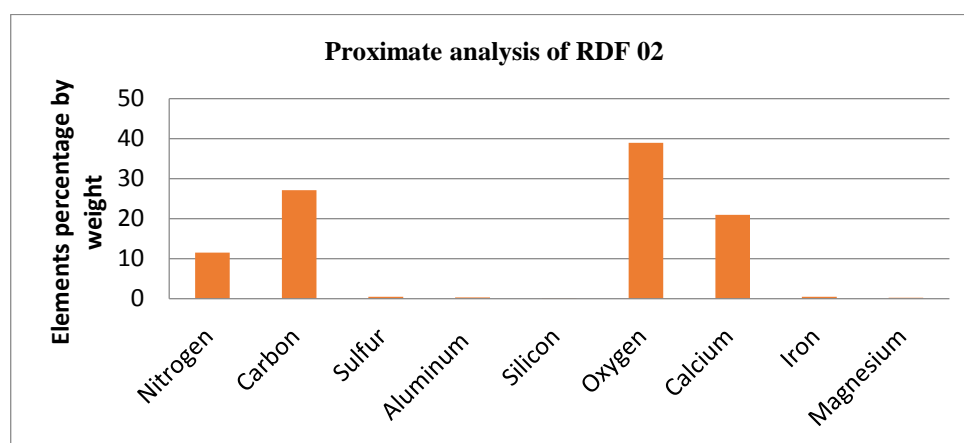

Fig. 3: Elemental analysis TGA graph of Refused derived fuel pellets with the composition of paper, plastic, textile, wood, and coal
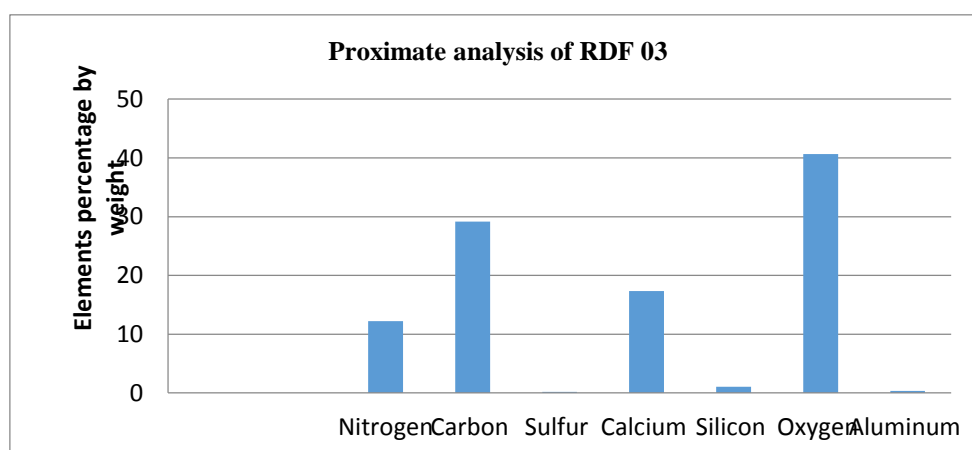

Fig. 4: Elemental analysis of Refused derived fuel pellets with the composition of coal.

E. Calorific value of refused derived fuel pellets

Calorific value is determined by bomb calorimeter. we found the calorific value of RDF pellets 01,02 and 03 12900 kJ/kg,12950 kJ/kg and13065 kJ/kg respectively. The average value of all these RDF is about 13MJ.

F. Energy loss in houses in term of food waste

As municipal solid waste is consists of about 60 percent of food waste. So we calculated the food waste in terms of energy lost. As 1-kilogram food consumes 11 MJ energy from sowing to cooking [8]. As we have already calculated the per capita waste generation for the houses so on that basis we calculated the energy lost in terms of food waste for every house. and found that 27.81MJ energy is wasting on an average basis per house.

IV.   CONCLUSION

Municipal solid waste is collective trash collected from houses, commercial markets, and organizations. It consists of food waste, paper waste, plastic waste, and textile waste, etc. Its waste composition changes considerably from place to place. Waste to energy is an attractive option ecologically and economically which is rapidly increasing associated with energy demand. Waste to energy technologies is thermal conversion such as pyrolysis, incineration, and gasification. From data collection, it was found that MSW consists of about 61% food waste, 10% plastic waste, 12% paper /cardboard, 3% textile waste, and 14% other waste. After the ultimate analysis, it is investigated that sulfur content is varying from 0.2% to 0.4 % which is very less than that of lignite coal. So it is more environment friendly. It was concluded that the calorific value of Refused Derived Fuel (RDF) pellets comprising combustible solid waste is 13MJ.

V.   REFERENCES

[1]Azimi Jibril, J. D. (2012). 3R s critical success factor in solid waste management system for higher educational institutions. *Procedia-Social and Behavioral Sciences,*, 626-631.

[2]Batool, S. A. (2009). The impact of municipal solid waste treatment methods on greenhouse gas emissions in Lahore. *Pakistan. Waste management*, 63-69.

[3]Baum, B. &. (1974). Solid waste disposal. Volume 1. Incineration and landfill.

[4]Bjeldanes, M. N. (1996). Resource recovery In Power Plant Engineering.chen, c. i. (2010). Spatial inequlity in municipal solid waste disposal... *international journel of environmental scinces and technology*, 447?-456.

[5]Clark, M. L. (2102). Land change for all municipalities in Latin America and the Caribbean assessed from 250-m MODIS imagery. *Remote Sensing of Environment, , 126,*, 84-103.

[6]Dowie, W. A. (1998). A case study of an institutional solid waste environmental management system. *Journal of Environmental Management*, 137-146.

[7]Dris, Z. O. (2004). Microstructural effects on the flow law of power-law fluids through fibrous media. *Modelling and Simulation in Materials Science and Engineering*, 995.

[8]Olawolea. (2014). Cooking with Minimum Energy and Protection of Environments and Health.

Composition, energy and environmental analysis of the local coal of KP province

Mohammad Shoaib Fazal [A], Muhammad Hassan [B], Khurshid Ahmad[C], Fahad Ullah Zafar[D] , Muhammad Ihsanullah[E]

U.S.-Pakistan Center for Advanced Studies in Energy, UET Peshawar, Pakistan
Corresponding author email: shoaibfazal146@gmail.com

Abstract—**Fossil fuel such as coal is used as an ultimate source of energy in the world. 186.28 billion tons of coal is estimated in Pakistan, in which approximately 123 million tons are present in KP province, but very little is known about the composition and energy content of this local coal. This research is about the analysis of local coal found in Dara Adam Khel area of KP. Total of 7 samples of coal are analyzed, in which 4 samples are Dara Adam Khel coal, 1 sample is Afghanistan coal and 2 are Quetta coal. The main analysis is proximate, ultimate, energy analysis and also the environmental hazards from local coal. Proximate analysis of four samples of local coal gives Moisture 5.94 to 8.74 percent, Volatile Matter 14.42 to 23.30 percent, Ash content 16.35 to 45.19 percent and Fixed Carbon from 22.77 to 55.49 percent. Elemental analysis gives Carbon content from 60.29 to 74.685 weight percent, Oxygen is 13.9435 to 24.425 weight percent, and Sulfur is 1.1725 to 3.4875 weight percent. The caloric values are from 10,883.4 to 25,757.077 kJ/kg. Main environmental hazards causes by local coal mines are the dust, diseases like influenza, subsidence, production of methane gas, production of carbon monoxide gas, water pollution, vibration due to blasting, noise, erosion and difficulties in labor work.**

Keywords—**Proximate analysis, Ultimate Analysis, Calorific value, Environmental Hazards, KhyberPakhtonhwa, Kilojoules per Kilograms.**

I. INTRODUCTION

Fossil fuel such as coal, is formed from plants and vegetables as a result of high pressures and temperatures which takes millions and billions years. Coal demand is increasing day by day due to energy crises and natural abundance worldwide [1]. Pakistan is one of the coal-rich countries in the world because of its large reservoirs and mines. Pakistan is the sixth coal-rich country in the world [2]. The total estimated coal being formed in Pakistan is 186.28241 billion tons, of which 122.99 million tons is formed in KP province, but very little is known the composition and energy analysis of this local coal. Dara Adam Khel coal has not yet been analyzed [3]. The study is about the analysis of local Dara Adam Khel coal and compared this local coal with coal from Quetta and Afghanistan, which is also analyzed in our study. The Dara Adam Khel coal mines are located in the local mountains of DaraAdamKhel, which is in the Kohat-Peshawar road, close to the north of the Kohat tunnel and south of Peshawar. The main analysis of coal includes proximate analysis, elemental analysis, energy (calorific values) analysis and environmental hazards.

Proximate analysis is the determination of the distribution of products when samples are heated under specific conditions. It involves the determination of moisture content, volatiles, ash and solid carbon using a muffle furnace. The sample is taken about 1 gram. The moisture content is determined under 105°C-110°C for one hour, the weight loss is calculated as the moisture content of coal. Volatile matter is determined by dry bases as the moisture is removed from about 1g of sample and then it is kept at 950°C for seven minutes, the sample weight loss shows us the volatile matter of coal. Ash is determined on dry bases, the sample is stored in the oven at room temperature and gradually increases the temperature to 450-500°C for the first hour, then from 500°C to 700-750°C for the next second hour and then Kept at 750°C for two hours, the residue left at the end is the ash content of coal [4].

Ultimate analysis is also known as elemental analysis of coal. The main elements of carbon, nitrogen, sulfur, oxygen and others are determined in elemental analysis of coal. There are many methods by which to determine elemental analysis, but the method available in KP is SEM EDX. SEM is a scanning electron microscope with which EDX is attached. EDX is electron-dispersive X-ray spectroscopy in which the

sample is bombarded by a high beam. These rays eject electron from the shell of the element, as a result a hole is created that is filled by the outermost electron of the element. In the process of jumping electrons from one shell to another, energy is emitted by the element. Several energy peaks are emitted and printed to give us the elemental analysis of coal [5].

Analysis of the available energy of coal means determining the calorific values (CV), such as the gross calorific value(GCV). Calorific value is the indication of the heat content of coal. The best method for determining the calorific value is the bomb calorimeter. Bomb calorimeter is used to determine the gross calorific value of coal. About 1 gram of sample is burned in high pressure oxygen under certain conditions. The heating value shows the heating value of coal along with the moisture content of the water [4].

Environmental hazards from coal include environmental and health problems caused by local mines. To assess environmental hazards, I visited the local coal mines and researched the working conditions of coal mines, met local people, engineers, technical personnel, manger and workers who worked there. I have collected data on environmental and health issues.

II. METHODOLOGY

Coal methodology consists of several analyses. These analyses tell us about the ranking of coal and the intrinsic properties of the coal. The main analysis of coal consists of proximal analysis, element analysis, energy analysis and environmental analysis.

A. Proximate analysis

Proximate analysis is used to determine moisture, volatiles, ash and fixed carbon in the coal. Proximate analysis of coal followed standard methods which are ASTM and ISO. Equipment used for proximate analysis is muffle furnace.

1) Moisture content

For moisture content, first weigh seven empty silica crucibles and note that, this is the weight of the empty crucible and then take about 1 gram of coal in the silica crucible, this is the initial weight of the coal sample and crucible for moisture content and set the furnace at 105°C when the temperature rises to 105-110°C, keep these samples in the muffle furnace and set the time to one hour. After one hour crucibles removed from the furnace and placed in a desiccator to cool to room temperature. After some time when the temperature drops to room temperature, then weigh the sample with a crucible and record the weight, this is the final weight of the coal after heating. The difference between the initial and final weight divided by the sample weight and multiplied by 100, this gives us a percentage of coal moisture.

$$\%Moisture = \frac{Initial\ Weight - Final\ Weight}{Weight\ of\ Sample} \times 100 \qquad (1)$$

2) Volatile matter

Volatile matter is carried out by means of a moisture-free method, that is, when moisture is removed from the coal sample and then kept below 950°C. The final weight obtained in the moisture content is the initial weight in volatile matter because moisture is removed from the coal and the analysis is performed in the anhydrous state of coal. Record the final weight of the moisture content, that is, the initial weight of volatiles. Gradually increase the temperature of the muffle furnace by 50°C to 950°C, when the temperature rises to 950°C, keep the seven samples of the crucibles in the oven for seven minutes. After seven minutes, remove the crucible from the furnace and place them in the desiccator to cool the temperature of the crucibles to room temperature. Wait sometime, after some time when the temperature has cooled down. Weigh the crucibles; this is the final weight of the coals. % Volatile matter is calculated by the difference between the initial and final weight divided by the weight of the sample multiplied by 100.

$$\%Volatile\ Matter = \frac{Initial\ Weight - Final\ Weight}{Weight\ of\ Sample} \times 100 \qquad (2)$$

3) Ash content

Ash is the residue left over from coal combustion. It is also done on a moisture-free basis to determine the ash content. About 1 gram of coal is placed in the crucible, and then the moisture is removed from the

samples at 105°C for one hour and cooled in a desiccator. Then keep the crucible in the muffle furnace, and gradually increase the temperature of the furnace from room temperature to 450-500°C in the first hour and then gradually increase the temperature of the oven to 700-750°C in the next second hour and keep it temperature over 750 ° C for two hours. This is a total of four hours heating process. After heating for four hours, samples were removed from the oven and stored in the desiccator to cool to room temperature and then weighed and recorded. The weight of the residue divided by the weight of the sample gives the % ash content.

$$\%Ash = \frac{Weight\ of\ Residue\ remaining}{Weight\ of\ Sample} \times 100 \tag{3}$$

4) Fixed carbon

Fixed carbon is the carbon that remains in the sample after volatile matter has evolved from the samples. FC is calculated by the following formula.

$$\%Fixed\ Carbon = 100 - (\%Moisture + \%Volatile\ Matter + \%Ash\ Content) \tag{4}$$

B. Elemental analysis

Elemental analysis is performed by many methods. The chemical method used for elemental analysis of coal is CHNS. But that method is so expensive, time-consuming and not feasible in our province. The method used in this study is X-ray spectroscopy. The equipment used is SEM EDX. SEM is the scanning of electron microscopes. EDX, EDS or EDXS is electron dispersive X-ray spectroscopy. This is a kind of spectroscopy where an X-ray beam is used to pass through samples and then it has detected by a detector used in this method of SEM EDX.

In SEM EDX sample of powder form is used. Sample is attached with the carbon tape and remains in the SEM. Seven samples can be determined at a time. An incident electron beam passes through these samples, electron beam ejects electron from the K shell, and produces a hole.

This hole created by the ejection of the K shell electron due to an incident electron beam is filled by the outer shell electron which is filled by L, M, N etc. When the K shell hole is filled by the outer shell electron, an unnecessary energy is emitted in the form of X-ray energy.

Excess X-ray energy then goes to EDX. EDX system consists of several parts: X-ray detector, pulse processor and multi-channel analyzers. X-ray radiation is detected by a detector. Detector consists of several components. X-ray beam incident on the detector which forms a photoelectron, and produces an electron pair as a result, which produces charge that is pre-amplified and produces Kev which is then much more amplified in the pulse processor. Pulse processor converts charge to voltage which is then displayed in the MCA. Multiple Channel Analyzer shows us different energies of different atoms in the form of Kev (5).
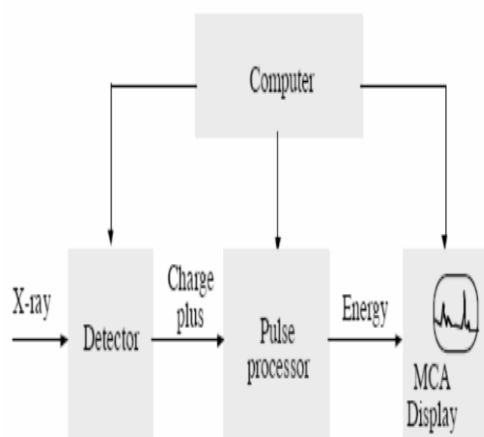
Fig 1 "(a)" EDX system, "(b)" Scanning Electron Microscope

C. Energy analysis

Energy analysis of coal is find out by the determination of calorific values of coal. Calorific value (CV) is the heating value of the coal. Coal Calorific Value is determined by using bomb calorimeter. Bomb calorimeter is the best method to find out Calorific Value in coal.

Bomb calorimeter gives the heating value of coal. About 1 gram of sample is taken into the crucible and

noted, which is placed in a bomb with a lid on. It consists of wire that is the ignition source for the combustion of coal. Wire is attached with electrolyte, which is attached with thermocouple that burns the wire. The wire is also attached with sample, causing combustion of sample. The bomb is tightly covered with a lid and heavy metal, so that constant pressure is exerted on the bomb. Bomb consists of water that is continuously stirred. The temperature is measured by a temperature measuring device. Oxygen is supplied to the bomb using a valve with a pressure of 30 bars. Water is continuously agitated when combustion started and the sample gives all of its heating to the water. The temperature of the water rises for some time until a constant temperature is reached. The mass of water is known, the heating value is determined.
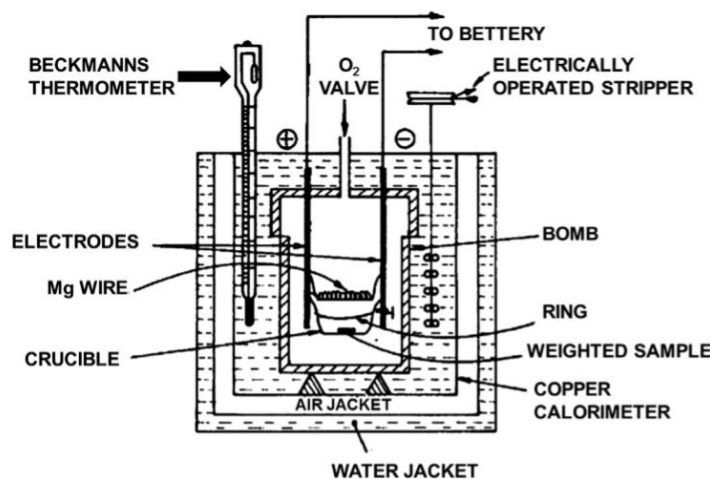

Fig 2 Bomb Calorimeter

D. Environmental hazards

Environmental hazards are the health and environmental problems caused by coal mines in the local mining area. For this purpose I visited the DaraAdamKhel and asked questions about the problems they face regarding their health, difficulties and environment of local people, engineers, workers, miners and administrations working in coal mines. Also investigated the local mines and found the shortcomings in the working conditions of local coal mines.

Fig 3 "(a)" A labor in coal mine, "(b)" Dust from coal mines

III. RESULTS AND DISCUSSION

A. Proximate Analysis

After doing experimental work on the four samples of Dara adam khel coal, one sample of Afghanistan and two samples of Quetta, following the above methodology and doing calculations from formulas and equation, the final results of proximate analysis such as Moisture, volatile matter, ash and fixed carbon contents are as
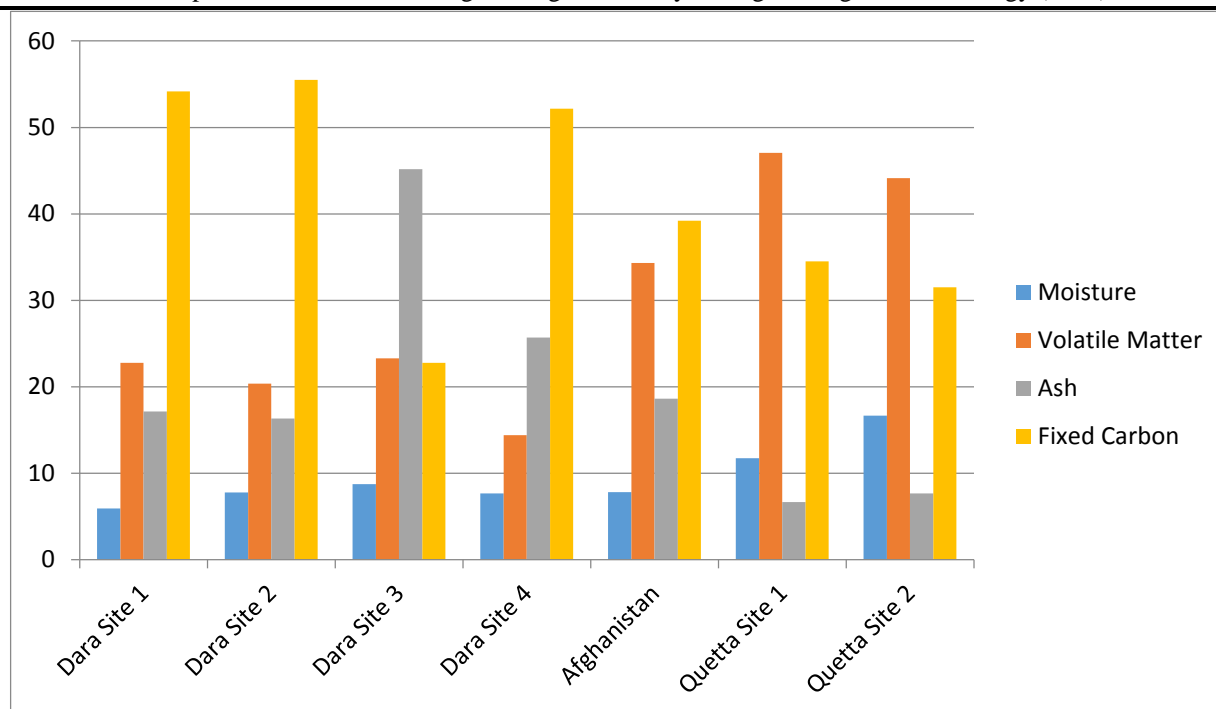
Fig 4 Overall Proximate analysis of seven samples

B. Elemental Analysis

Final results of elemental analysis such as carbon, oxygen, sulfur and other contents of seven samples obtained from SEM EDX are
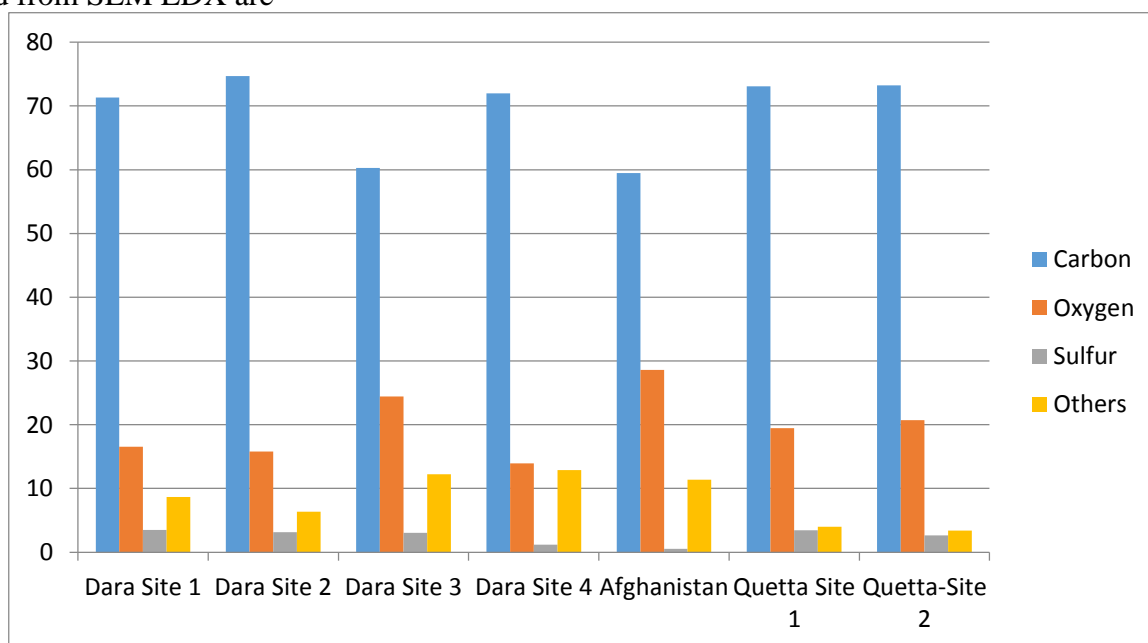

Fig 5 Elemental analysis of seven samples of coal

C.Energy Analysis

After experimental work through bomb calorimeter, the final results of calorific values of seven samples of coal are

Table 16 Calorific values of seven samples of coal

S.NO	Sample	Calorific Value(kJ/kg)
1	Dara Site 1	25,757.08
2	Dara Site 2	23,539.58
3	Dara Site 3	10,883.4
4	Dara Site 4	23,258.42
5	Afghanistan	23,657.77
6	Quetta Site 1	23,357.34
7	Quetta Site 2	23,100.9

D. Environmental hazards

After researching the coal mines and inquiring from local people, engineers, workers, miners and authorities, the following are environmental dangers in Dara Adam Khel coal mines.

• Dust problems in coal mines.

• Caused many illnesses such as chest conditions, influenza caused by dust in the mines.

• Land subsidence.

• Methane gas production..

• Dust and methane cause major damage.

• Carbon monoxide gas production causes a lack of oxygen gas.

• Water pollution.

• Vibrations occur due to explosion when creating new coal mines.

• Noise pollution.

• Erosion of machines, equipment and other useful items.

• The method used in mine creation and exploration is not a standard and expensive method, but it is being worked on, therefore there is risk of accidents, injuries and also deaths.

• Labor uses shovels, etc. To dig and explore coal, so there is a potential for accidents such as rocks and mines falling over their heads and bodies that could cause serious injury.

IV. CONCLUSION

Pakistan is a rich coal country and KP's local coal is also present in very large quantities. In this study, I collected the samples from the local area of Dara Adam Khel and did the analysis and compared this local coal with the Afghanistan and Quetta coal analysis. From proximate analysis, the moisture content of 4 samples of Dara Adam Khel coal from 5.94% to 8.74% and fixed carbon from 22.77 to 55.49%. Elemental analysis of 4 samples of coal, such that carbon content from 60.29 wt% to 74.685 wt% and sulfur from 1.1 wt% to 3.4875 wt%. Energy analysis gives us the result of Dara Adam Khel coal from 10,883.4 to 25,757.077 kJ / kg. The analysis shows that coal of Dara Adam Khel sites 1, 2 and 4 is slightly better than coal from Afghanistan and Quetta and also falls in the good rank of coal which is anthracite and bituminous. While site 3 alone is not better than Afghanistan and Quetta coal and falls in the lagnite coal range.

ACKNOWLEDGMENT

REFERENCES

[1] S. S. P.S., Fuels and Combustion CHAPTER – 4 FUELS AND COMBUSTION 4.1 Introduction 4.2 Requirements of a Good Fuel, October 2010.

[2] P. P. a. I. Board, Pakistan Coal Power Generation Potential, June 2004.

[3] M. S. Malkani, "Coal and petroleum resources of Khyber Pakhtunkhwa and FATA (Pakistan)- An overview," February 2013.

[4] Q. Zhu, Coal sampling and analysis standards, April 2014.

[5] B. Hafner, "Energy Dispersive Spectroscopy on the SEM: A Primer".

Hybrid Energy System for Small industries and Large Residential Centers in Peshawar City

Muhammad Junaid[1], Muhammad Raheel Khan[2]

[1,2.]US Pakistan Center For Advanced Studies in Energy, University of Engineering and Technology, Peshawar, Pakistan

Email : ee.junaid@gmail.com

Abstract— **Energy requirement has increased as result of modernization in style of living. People today relay on energy to personnel gadgets, provide for themselves a conformable environment and expedite their work using technology. Moreover, industrial sector also want energy to power the machinery used to increase their production. It is definite that energy is required, now the question is that what type of energy is required. The answer to this question is that energy is required that is cheap, reliable, and environmentally friendly. At this moment, these three qualities are not available in both renewable as well non- renewable sources of energy. The solution to this problem is that we adopt hybrid energy system that is combination of different sources with advantages more than disadvantages. This hybrid system can reduce cost of electricity provide reliability and do negligible harm to the environment. In this research, four sources of energy are used such as solar, wind, gas generators and sanctioned load from WAPDA. From the analysis we concluded that cost of energy is reduced that is 0.082$/kWh and the second is that reliability of the system is enhanced due to use reliable sources such as Gas generators and WAPDA**.

Keywords— Solar PV, Gas Generator, Hybrid Power System, HOMER, Net Present Cost.

I.   INTRODUCTION

Dependency of our country on fossil fuels for energy is evident from the generation data that is(65%) from crude oil, (33%) from natural gas, (7%) from nuclear plants and remaining from renewable energy sources [1].This data make it evident that large chunk of energy is our country is generated from fossil fuels. It will result in the depletion of natural resources as well as affect the environment. It is the need of the hour that renewable energy resources are utilized, and the share of renewable energy resources is increased in the overall energy matrix. This will not only provide cheap energy to the domestic and industrial users but also reduce the environmental effects of energy generation. [2].Pakistan is blessed with natural resources , clearness index and solar hours are among the longest for solar energy, coastal belt of around twelve hundred kilometers for wind energy, trillions of tons of coal for energy from coal and many rivers with ideal location for hydro energy. Biomass energy is available in rural, which can utilize for generation of thousands of megawatts.

Pakistan is facing a shortfall in meeting the energy requirement of the country. The shortfall is around five to six megawatts. Both residential and industrial users are affected by it, especially in summers.[3].

Peshawar is badly affected by load shedding. Load shedding in summers is from eight to fifteen hours in different parts of the city. Industrial sector is badly affected due to reliance on expansive and reliable energy from public sector energy institutions [4]. Peshawar city is having total load of around 70MW. This load is divided into up to 50 MW residential load and 20 MW industrial load. For this load, the city is dependent on public sector entities for expansive energy.

Residential and industrial sector in Peshawar city is totally dependent on public energy development institutions for energy requirements. Current Cost of electricity /kWh is 0.113$. Through this research work cost of energy will be reduced from 0.113 $/kWh to 0.0824$/kWh. Secondly, carbon emissions will be minimized by use of renewable energy resources and natural Gas as a source of generation. The carbon emissions will be reduced from 7,866,633kg/yr to 4,495,824kg/yr. The proposed system is also shown in the figure 1. Share of renewable resources to fulfill energy requirement is at negligibly low level. Expansive energy from fossils fuels results in expansive electricity for domestic and industrial consumers. Energy crisis has also resulted in load shedding to the residential and indusrial consumers. Industry is being shifted to other countries, which is resulting in unemployment and poverty.

The proposed hybrid energy system that that is intended to provide a cheap and reliable energy to both residential and industrial sector in Peshawar city.

One drawback of renewable energy is its reliability. To reduce the effects of reliability the renewable energy

system can be merged with conventional energy system in a hybrid system to increase the reliability of the system
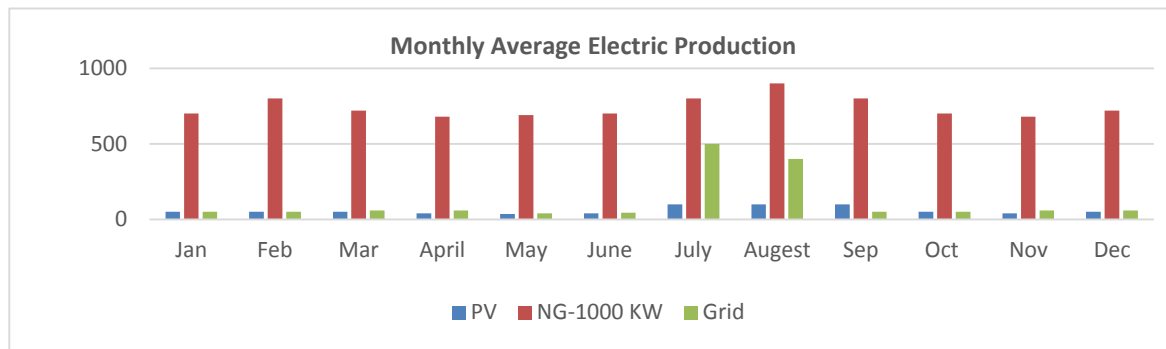

Figure 1.   Monthly Electric production of the system

In this research work hybrid energy system is recommended that is a combination of renewable and nonrenewable energy resources. The energy sources used in the hybrid system are national Grid, Generation from natural gas, solar and wind energy. The system is design to cater the load of 1.5 MW. The system is designed to facilitate small industrial sector and large residential in the Peshawar city. All the analysis is done through HOMER software. The best system was chosen after comparison of simulation results of four hybrid systems that will give cheap, reliable, and environmentally friendly solution to the industry and residential user.

II.   LOCATION DETAIL

The project is designed for the city of Peshawar, capital of province kyber Pakhtunkhwa. Peshawar city is a valley surrounded by hills of Khyber, Mohmand, and semi tribal areas of formally FATA region. Total population of Peshawar is around 5 million by census 2017 [12]. Although district Peshawar is having different resources of energy such as solar, hydro and wind resources due to its adjacent hilly areas. Similarly, adjustment district of Kohat and karak is having a lot of natural resources of natural gas and oil. District karak is having production of natural gas around 80 million cubic feet and oil is 7000 barrels.

III.   METHODOLOGY

The hybrid energy system is modeled by using HOMER software. In this system four sources of energy with the following specification are used.

-National Grid 1800 KVA Sanctioned load

-1500KVA Natural gas operated generator

> Model G3512E TA
> Rated power 1200KW/1500KVA
> Continuous power
> 1500 rpm/ 50Hz.Fuel: Natural gas

-400KW Solar PV system

> Flat plate PV
> Brand SMA
> Rated capacity 400KW
> Each panel: 260 W
> Total 1540 panels

100KVA wind system

> Horizontal axis type
> Rotor dia: 21m

1. Load calculation

Different types of loads were taken in the load calculations, these were equipment's inductive loads, lighting loads and supporting equipment loads such as fans, water supply system, firefighting equipment loads etc.Electrical load was low during the winter season. Load increased as summer season was approaching closer. Maximum load was noted in the month of August. Electrical loads in the peak hours were also considered. The peak load calculated was 1.5 MW maximum in the summer's month of August. All the energy resources were allocated based on this peak load.

2. Calculation of resources   required.

Both renewable as well as non –renewable resources of energy were considered for the hybrid system. Advantages of both resources are tried to be utilized as efficiently as possible and disadvantages were minimized as much as possible. The following resources were used, Solar PV, Wind, Generation from gas through Gas generators and sanctioned load from grid. The resources used are considered based on the weather conditions and geographical location. The problems in the current electricity supply system are considered and addressed in the hybrid system designed. Specially, the issue of reliability andcost are considered as the main target of the hybrid system. To achieve the two targets both renewable and non-renewable resources are used in appropriate portions.

Solar data is required to be accumulated when a hybrid system comprise of solar PV. Solar data is dependent on two factors, solar radiation in the area and cleanness index of the area.

The clearness index is defined as the ratio of the solar radiation that strikes the surface of earth to the solar radiation that strikes the top of the atmosphere. It defines how clear the atmosphere and this constant number are ranging between 0 and 1. Solar data for the city of Peshawar is obtained from NASA database as shown in the below table 1.

Table 1: Average Solar Radiation and Clearness Index of Study Area

Months	Jan	Feb	Mar	Apr	May	Jun	Jul	Aug	Sep	Oct	Nov	Dec
Solar radiation (kWh/m2/day	3	3.77	4.7	6.1	7.31	7.8	6.9	6.21	5.8	5.0	3.7	286

3.   Natural gas requirement and availability

District Peshawar also the provincial capital does not have any explored reserved of natural gas but the adjoining district of Karak and Kohat are blessed with large reserves of natural gas. This natural can be used for generation of cheap electricity for domestic and industrial users.

3) Main components used in the system

Solar Flat PV system composed of Flat PV solar panels polycrystalline are used in the system, total capacity of each panel is 260 Watt and total of 1400 panels are installed with total capacity of 400KW.The connection of the system is a series – parallel combination and sinked with the grid.

The second component of the system is the natural gas generators having capacity of 500KVA each and total capacity of 1500KVA for three generators. The fuel used is natural gas and the generators are prime time generators with long hours of operation. The generators were set for synchronous to serve the major chunk of load. Almost 78% of the load is served by the natural gas generators.

The third source of electricity is the sanctioned load of 1800KW from natural grid. Sanctioned load is obtained from natural grid at a cost of 18.5 Rupees/Unit. The connection will be done from the grid through three wire overhead system and connection at the utility will be done through a three-core cable system.

The fourth component of the system is DC to AC convertor with the capacity of 400KW. This converter is used to convert the DC energy generated by the solar system to AC energy before sinking it with the AC energy from   Grid and Natural gas generators. All the details of the four components are mentioned in the below schematic figure 2.
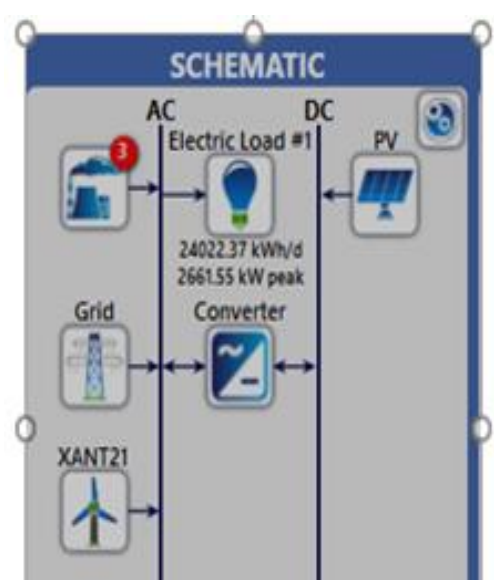
Figure 2.   Schematic Diagram of Hybrid System

IV. SIMULATIONS AND RESULTS

The simulation results obtained from HOMER software are discussed and the best hybrid system is advised on the base of these results. Results are shown in table 2.

Table 2: Detail description of system No. 1

Parameters	Grid-connected multisource generation			
	System #1	System #2	System #3	System #4
COE($/kWh)	0.0824	0.0867	0.0915	0.0938
NPC ($)	9,341,771	9,832,688	10,374,2450	10,635,450
O&M Cost ($)	683,745	748,998.3	745,054	795,350
Gas Generators%	78	86.6	75	0
PV (%)	9.83	0	9.83	9.83
Wind (%)	0	0	3.63	0.00
Grid Purchase (%)	12	13.4	11.6	90.2

In the above four systems, system no 1 is recommended for small industries and residential centers in Peshawar. This system not only adds 9.83% of renewable energy in the systems but also provides the lowest COE, NPC and MC as compared to the other three systems scenarios. Details of the most suitable system is shown in the table 3.

Table 3: cost comparison of the hybrid systems

Component	Capital ($)	Replacement ($)	O&M ($)	Fuel ($)	Salvage ($)	Total ($)
CAT-NG-1500KVA	$150,000.00	$122,507.02	$528,153.69	$ 6,835,504.9	$26,241.57	$7,609,924.08
PV	$325,000.00	$0.00	$129.28	$0.00	$0.00	$325,129.28
Grid	$0.00	$0.00	$1,369,554.94	$0.00	$0.00	$1,369,554.94
System convertor	$27,642.51	$11,727.99	$0.00	$0.00	$2,207.33	$37,163.18
System	$502,642.51	$134,235.01	$1,897,837.91	$6,835,504.94	$28,448.89	$9,341,771.48

Total cost of the system is USD 9,341,771.4. USD 7,609,924.08 is incurred on 1500KVA Gas Generators. USD 325,129.2 is incurred on Flat PV system of 400KW. Purchase cost on Grid is USD1,369,554.9 and total cost on system converter cost is USD 37,163.18.Details of the renewable penetration are shown in the table 4.

Table 4: Renewable penetration

Quantity	KWh/Yr	Units
Renewable	9.4	%
Max Renewable Penetration	108	%

Electric Load production of the system

Production from different sources used in the system is mentioned in the below graph. Gas generating plant is contributing the major chunk of energy that is 78.1 %. Grid is contributing 12% and solar flat PV is adding 9.83%.Electric load production is shown by the table 5 and figure 4 below.

Table 5: Electric load production of the system.

Quantity	kWh/yr	%
Excess Electricity	971	0.0110
Unmet Electric Load	0	0
Capacity shortage	0	0

Production	kWh/yr	%
Generic flat PV	866,380	9.83
CAT -NG-1500kVA	6,886,630	78.1
Grid Purchases	1,059,426	12.0
Total	8,812,436	100

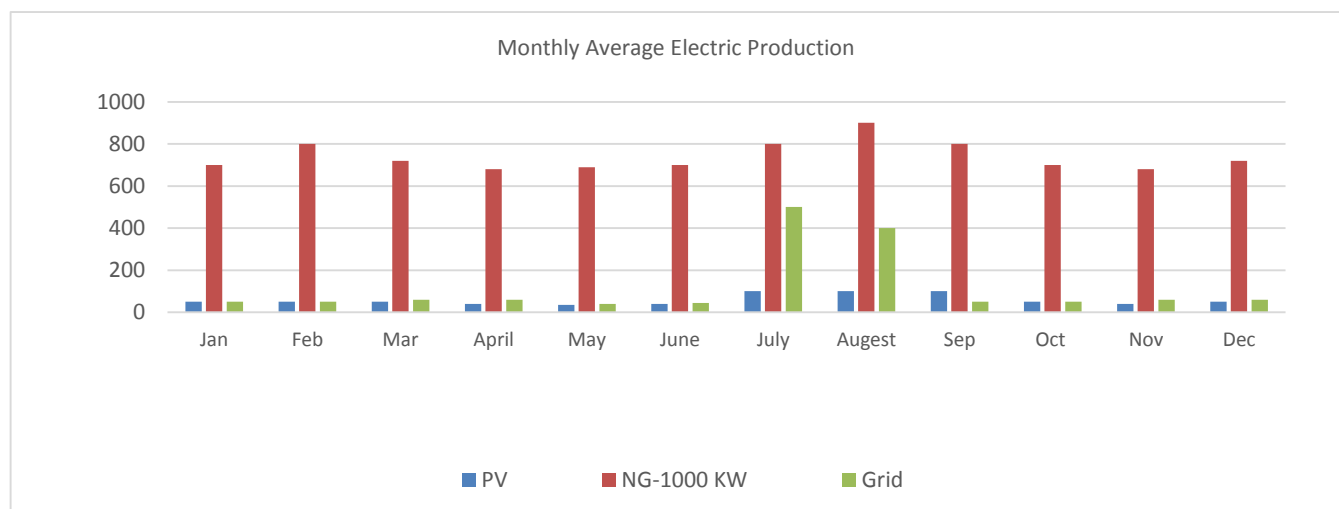| Consumption	kWh/yr	%
AC Primary load	8,768,164	100
DC Primary load	0	0
Deferrable Load	0	0
Grid Sales	31.0	0.000354
Total	8,768,164	100

Figure 4: Electrical load contribution from different sources

Fuel consumption Detail

As natural gas is the only fuel used in the system for Generation of energy, so cost calculations will be done for three 500KVA gas generators. 1762521 cubic meter is the total gas consumed per year for three 500KVA generators. The consumptions per hour and per day are also mentioned in the below table 6 and figure 5.

Table 6: Fuel consumption

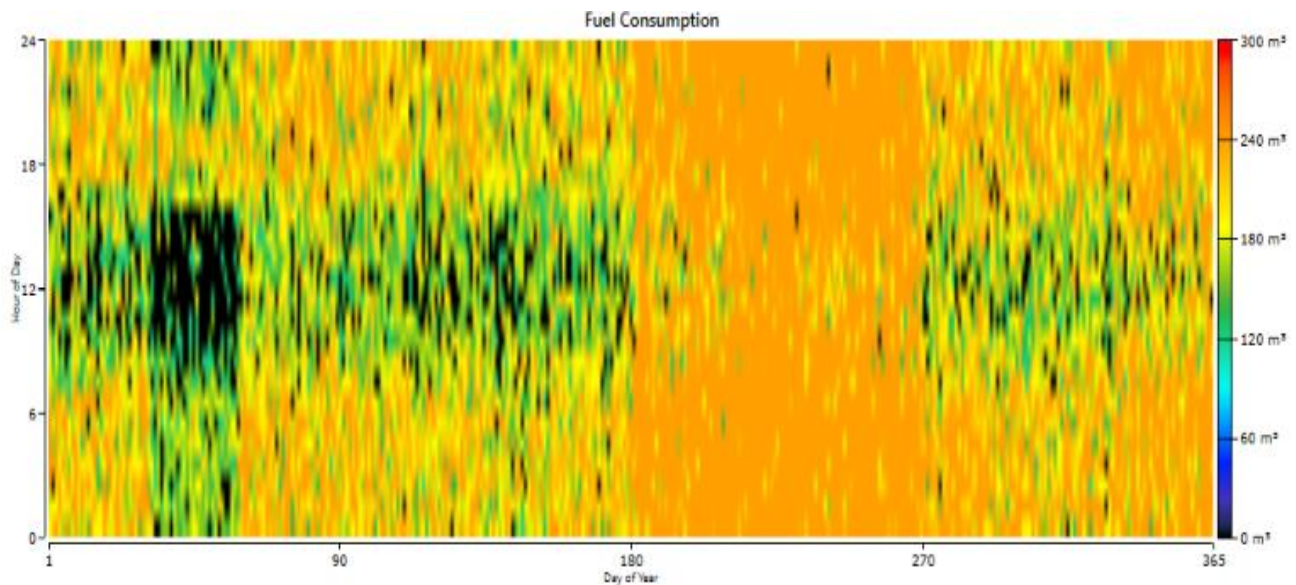| Quantity	Value	Units
Total fuel consumed	1,762,521	m3
Avg fuel per day	4,829	m3 /day
Avg fuel per hour	201	m3 /hour

Figure 5: Natural gas consumption

Electrical specification of three 500KVA Generators:

The parameters of three 500KVA generators are discussed, such as hours of operation, number of starts, operational life and generation cost/ unit is mentioned in the below table 6 and figure 6.

Table 6: Generators output detail

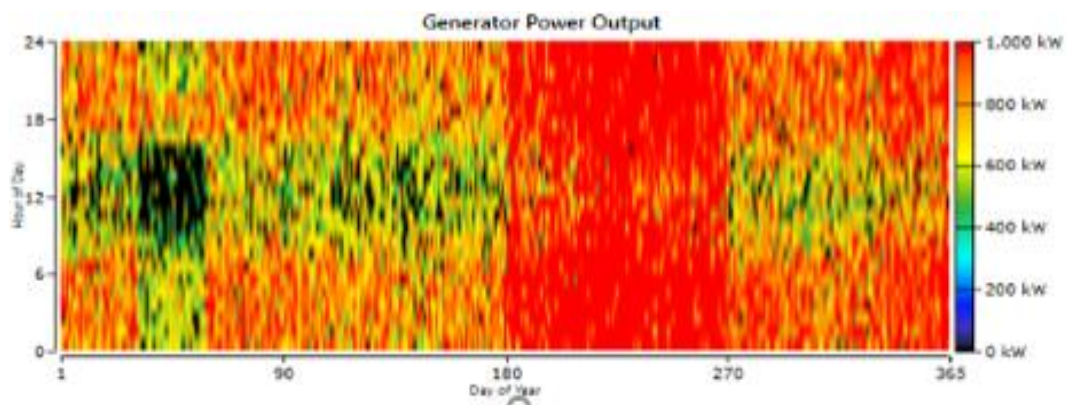| Quantity	Value	Units
Electric Production	6,886,630	kWh/yr
Mean Electrical output	843	kW
Minimum Electrical output	440	kW
Maximum Electrical output	1,000	kW

Figure 6: Specification of 500KVA generator

Parameters of Grid Purchase/Sale

Purchase from Grid and sale of energy to grid is mentioned in the bellow table. The net purchased energy and peak demand are the below table 7 and figure 7.

Table 7: Grid purchase/sale parameters

| Month	Energy Purchased (kWh)	Energy Sold (kWh)	Net Energy Purchased (kWh)	Peak Demand (kW)	$	$
January	36,300	16	36,284	489	$3,629.22	$0
February	61,764	15	61,749	440	$6,175.65	$0
March	30,616	0	30,616	632	$3,061.58	$0
April	30,244	0	30,244	450	$3,024.41	$0
May	33,346	0	33,346	439	$3,334.57	$0
June	25,016	0	25,016	438	$2,501.57	$0
July	136,043	0	136,043	965	$13,604.31	$0
August	335,844	0	335,844	1,465	$33,584.39	$0
September	223,302	0	223,302	1,065	$22,330.23	$0
October	36,674	0	36,674	459	$3,667.44	$0
November	34,708	0	34,708	590	$3,470.80	$0
December	75,569	0	75,569	753	$7,556.89	$0
Total	1,059,426	31	1,059,395	1,465	$105,941.0	$0
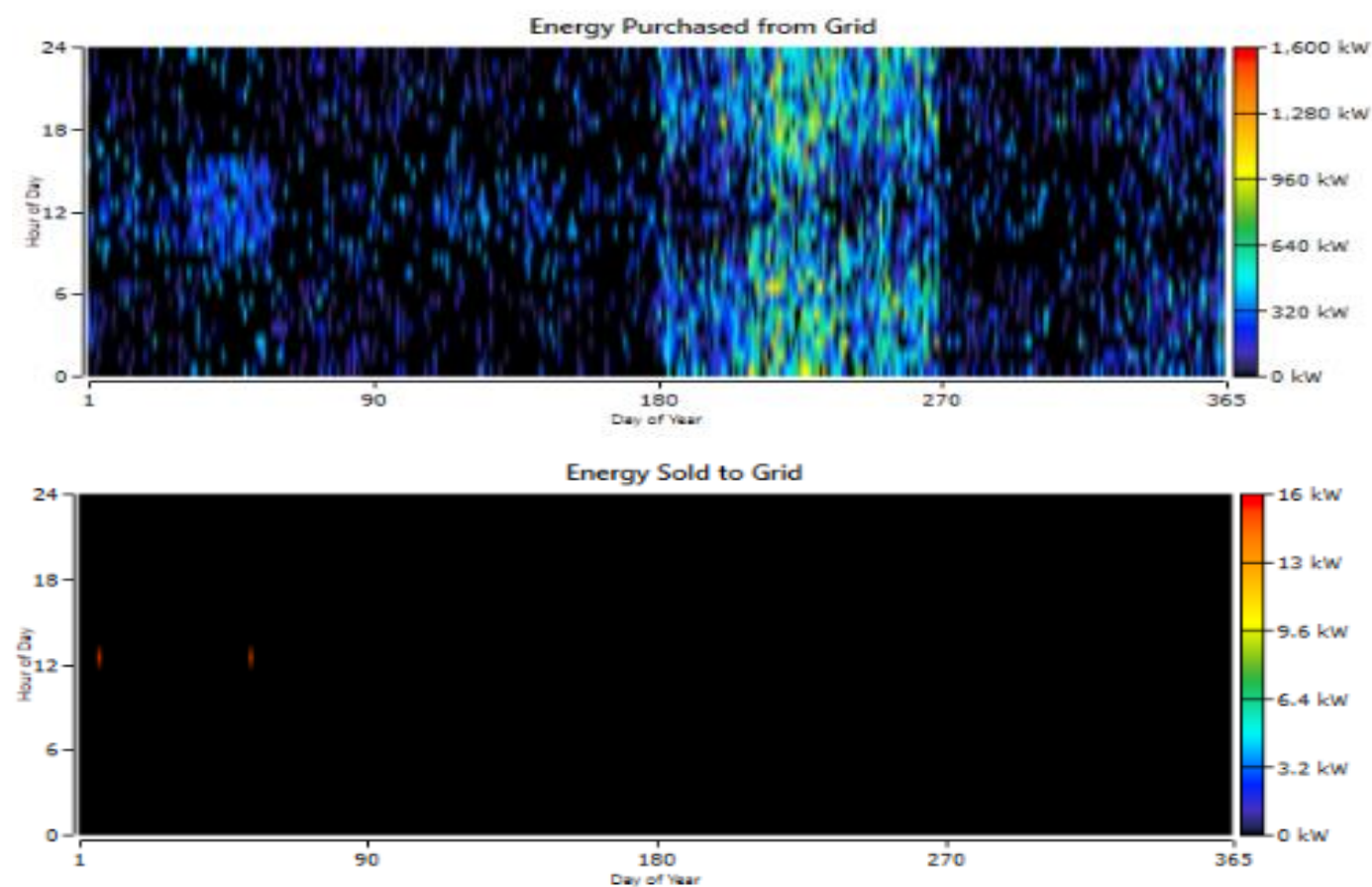
Figure 7: Specification of Grid

Details of system convertor:

System convertor has a capacity of conversion 302KW. The hours of operations will be 4385Hr/Yr.It will produce output of 822,139KWH/Yr. Inverter specification are shown in the table 8 and figure 8.

Table 8: Inverter specification

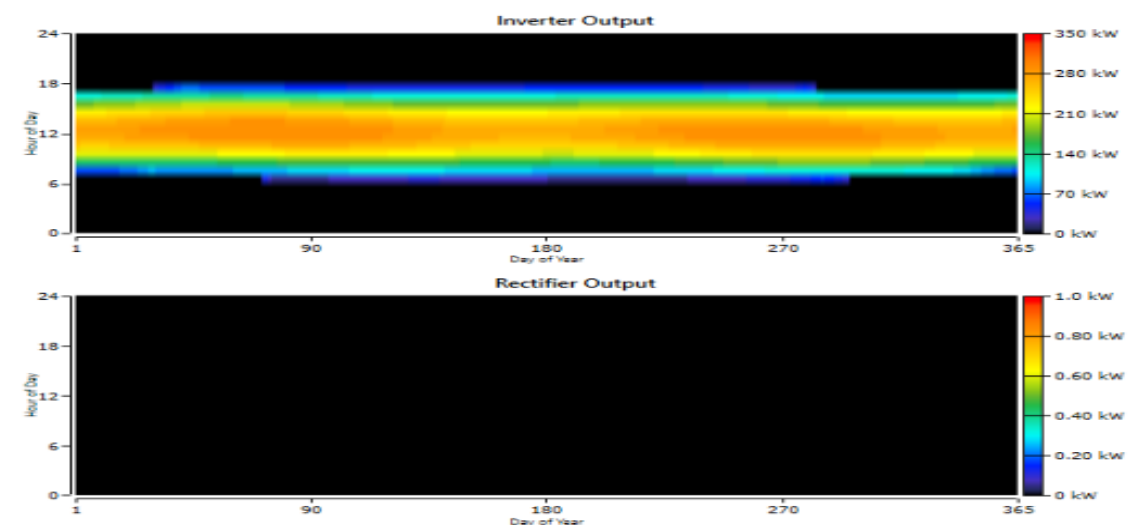| Quantity	Inverter	Rectifier	Units
Hours of operation	4,385	0	hrs./yr.
Energy out	822,139	0	kWh/yr.
Energy In	865,410	0	kWh. /yr.
Losses	43,270	0	kWh. /yr.

Figure :8 System convertor

VI.   Conclusions

This research paper is intended to provide the most economical and reliable solution to energy requirements of small industry and large residential in Peshawar with load requirement of 1.5 MW. This system can be adopted for any other region depending on the conditions with modifications. The best system was selected after detail comparison of four hybrid systems in HOMER software. The proposed system is based on contribution from Grid, Solar and gas generators. The adoption of the system will reduce the cost by $0.1555/kWh to $0.08241/kWh. Grid will only be used for 12% load. Such type of systems adopted by private sector can help reduce the energy crisis in the country and help reduce the import bill spent on crude oil.

VII.   Recommendations

The recommended system can be adopted for an any area with modification as required. It must be noted that space availability must be insured as renewable sources like solar plant will require space of installation. In coastal and hilly areas where wind speed is high, generation from wind can play a major part in fulfilling the load and must be adopted. Collection of data should be made as accurate as possible to

REFERENCES

[1] AL-Kababjie, M.F., &W.H. Hamden. 2013. Performance Evaluation study of Hybrid Generation System

[2] Alam, K. 2015. SBP cuts discount rate to 8%. The Express Tribune. Retrieved from http://tribune.com.pk/story/856894/sbp-cuts-discount-rate-to-8/

[3] Alternative Energy Development Board. 2015. Retrievedfromhttp://www.aedb.org/index.php/ae-technologies/wind-power/wind-re

[4] "Anwari, M., M.I. M. Rashid. I. Hui, T. W. Yee, &C. K. Wee. 2011 Photovoltaic power system simulation for small industry area. In Electrical, Control and Computer Engineering (INECCE), 2011 International Conference on (pp. 263-268). IEEE.

[5] Aziz, M.F., &N. Abdulaziz. 2010. Prospects and challenges of renewable energy in Pakistan. In Energy Conference and Exhibition (Energy Con), 2010 IEEE International (pp. 161-165). IEEE.

[6] Doppio, R. 2008. Geothermal power plants: principles, applications, case studies and environmental impact. Oxford: Butter work-Heinemann.

[7] Elliott, D. 2011. Wind resource assessment and mapping for Afghanistan and Pakistan. National Renewable Energy Laboratory. Golden, Color, USA.

[8] Energy, H.O.M.E.R. 2011. Getting Started Guide for HOMER Legacy (Version 2.68).

[9] Yang HX, Zhou E, Lu, L, Fang ZH. Optimal sizing for standalone hybrid solar-wind system with LPS technology by using

Energy Efficiency Improvements for Power Generation Sector of Pakistan

Prof. Dr. M.A. Irfan [A], Engr. Arslan Ali [B]

[A] =Department of Mechanical Engineering, University of Engineering and Technology Peshawar

[B] = Thermal System Engineering Department, USPCAS-E University of Engineering and Technology, Peshawar

Abstract— This study presents energy efficiency improvement technologies in power generation sector of Pakistan after identifying losses in power sector. Saving potentials also have been estimated after implementing these improvements as a solution. The methodology employed to conduct this study was first to find plant load factor (PLF), plant capacity factor (CF), efficiency, upfront tariff/power generation cost, indigenous fuel option for specific power sector then select the appropriate energy efficiency improvement technology like ultra-supercritical (USC), coal beneficiation (CB), combine heat & power (CHP) etc for that sector from international energy efficiency standards & benchmark studies. The salient results from this research are saving potentials of 2,242.92 GWh annually from renewable power sector including pumped storage hydropower (PSH) potential, 6,769.76 Million PKR savings from CB of indigenous coal, 2,357 Million PKR from USC technology by up gradation of coal fired power plants, 4.48 MMTOE saving from CHP in gas sector and almost 7% capacity factor improvement in nuclear sector by good outage management. Total energy units will increase from 131,275 GWh to 188,527.25 GWh with 43.61% increment and total average power units will increase from 14,985.73 MW to 21,521.37 MW with 43.61% increment. It is recommended to consider these energy efficiency improvement technologies and promote indigenous resources like hydro, Thar coal and Renewable for curtailment of 17.75 Billion USD fuel import bills.

Keywords— Pakistan, Energy Efficiency, Power Sector, Saving Potentials, Solutions.

I. INTRODUCTION

During 2017-18, Primary energy was increased from 80.584 Million tonnes of oil equivalent (MMTOE) to 86.301 MMTOE (6 MMTOE annual increase for FY2017-18) with transformation losses of 27.202 MMTOE. Only 59.099 MMTOE including electricity of 10.957 MMTOE primary energy was converted to useful secondary energy with 53.98% losses. Oil import bill was 9.1 Million USD in 2016-17 which was raised to 11.9 Million USD in 2017-18. More 19.3% Crude oil was imported by refineries as compare to last year. High speed diesel (HSD) consumption was 8.48 million tonnes of oil equivalent (MTOE) in 2017 and was 9.04 MTOE in 2018 with 6.5% increase from last year. RLNG import was 186,672,977 MMBtu in 2017 and 313,902,345 MMBtu in 2018 with 68.2% annual increase (1).

This study is comprised of three major sections. The first section presents the current situation of Pakistan power sector. The second section discusses the inefficiencies in power sector and third section presents is the solutions with energy saving potentials of Pakistan power sector. Current situation of power generation sector of Pakistan describes the installed capacity of power plants, energy potential, current energy efficiency technologies in Pakistan power sector and power development status. Source wise conversion from primary energy to secondary energy in power sector is also mentioned. It gives the idea that how much a primary source like coal, RLNG, gas, Oil, nuclear, hydro is more efficient utilized to produce electricity.

Two kinds of power generation losses are technical and non-technical losses or inefficiencies in power sector of Pakistan. Technical Losses in power sector of Pakistan are lower PLF, huge combustion losses, lower capacity factor, forced outages, etc. Non-technical issues of power generation sector of Pakistan are lack of technical skills, lack of leadership skills, no decision power, management incompetency and irresponsible behavior. Some common technologies like combine heat & power (CHP) in gas-fired power plants as mentioned in Fig. 1., coal beneficiation (CB) in coal, pumped storage hydropower (PSH) in

hydro power, ultra-supercritical (USC) technology in coal, renewable repowering, reduction in refueling outage (RFO) length of nuclear power plant are considered for identify the energy saving potentials from Pakistan power generation sector. It is necessary to analyze the cost as simple payback period of any investment in any energy efficiency improvement opportunity. Simple payback period (SPP) is considered for any investment that shows feasibility of project. More than 10 years of simple payback period is not reasonable but an average 3-5 years is very economical.
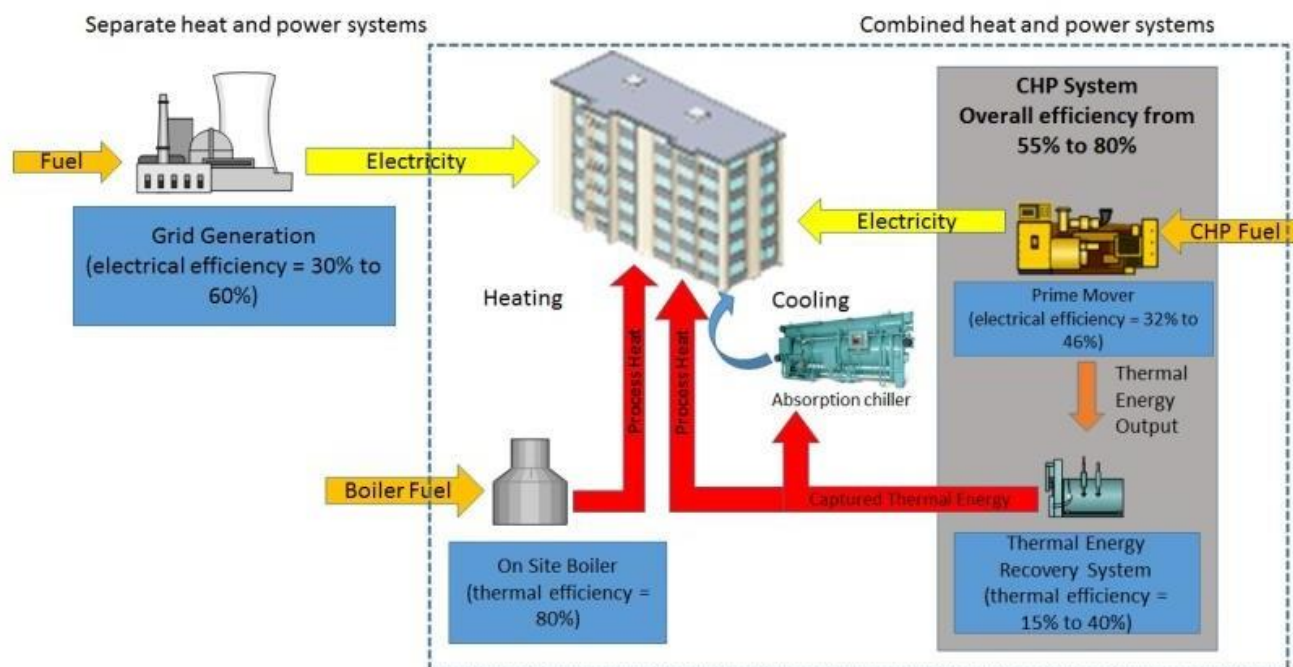

Fig. 1. Separate Heat and Power as compare to CHP (Source: NREL)

II. LITERATURE REVIEW

World's primary energy intensity was 5.1 MJ/USD in 2017 as compare to 5.9 MJ/USD in 2010 that means world is adopting energy efficiency techniques. Contribution of energy intensity reduction of end use electricity is more in the production sector. Many countries like USA, China, India, Germany etc., haves adopted energy efficiency techniques for building, transport, residential and industrial sector but have given less attention towards power generation sector. Main reason for less attention is that power generation system is more complex and difficult to understand the whole process of electricity production (2).

Nowadays average Electricity generation from fossil fuel power plant is 40% efficient (2). China and India are the top two countries constructing more efficient coal fired generation and gas fired generation. They have improved efficiency up to 45% for gas fired generation. These countries are improving 0.7% efficiency annually for coal fire generation from 2010 to 2016 (2). Major economies (Australia, Brazil, Canada, EU, China, India, Indonesia, Japan, Korea, Mexico, Russia, South Africa and United States) have potential of $2.177*10^{10}$ GJ (520 MTOE) saving annual fossil fuel in 2020 (3). In Japan, combine cycle power plants haves been installed with gross thermal efficiency (maximum design value) up to 60%. For more improvements in efficiency in generation system, integrated coal gasification combine cycle (IGCC) power plant is under construction in world other than this Japan has constructed world's most efficient power plant Chubu electric power Co.'s Nishi-Nagoya Thermal Power Plant Unit No. 7-1 with 63.08% efficiency (LHV) (4).

In Japan, thermal power generation capacity was 1, 74,390 MW in 2017 including coal fired power plant of 45,910 MW capacity. By improvements like Ultra Super Critical (USC) pressure boiler, & variable pressure operation equipment, Japan has enhanced efficiencies and load capabilities of their power plants. Kawasaki Thermal Power Station (TEPCO Fuel & Power, Inc.) Unit 2 and 3 entered for operation in January and June 2016 respectively with 61% efficiency. These plants were running at 1600°C of gas turbine inlet temperature (5).
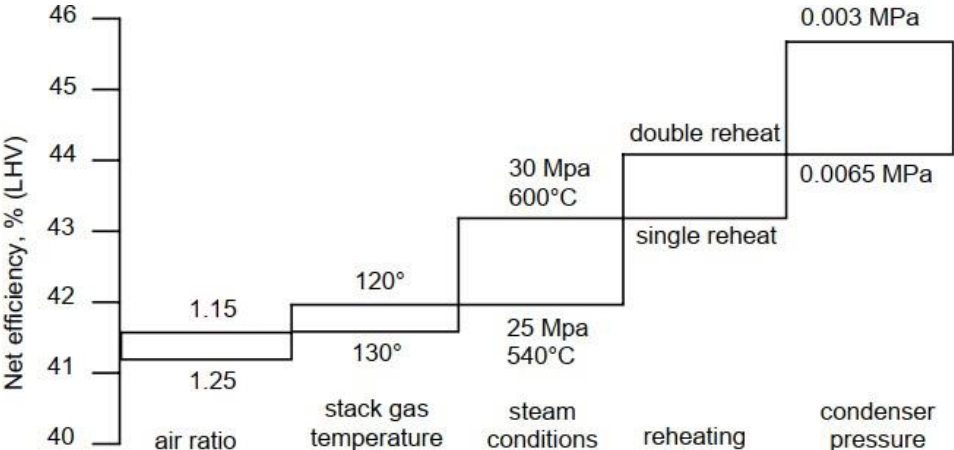
Fig. 2. Effects of various measures for efficiency (LHV) improvements of pulverized coal fired power plants (6)

For Trenton Channel Power plant (USA) the main steam conditions was changed from 2.89 MPa/657.6 K (420 psi/724 °F) to 8.96 MPa/783.15 K (1300 psi/950°F) after expansion built in 1949. And after in 1967 steam conditions was also changed by single reheat unit to 16.547 MPa/810.928 K (2400 psi/1000 °F). By change the steam condition efficiency can be increased as in Figure 2. This energy improvement increased in efficiency from 18.5% in 1924 to 33% in 1967 (7).

III. METHODOLOGY

There are three major sections of methodology that can be seen in Fig. 3. First section is related to current energy review and classification of power sector of Pakistan. Second section is to analyze inherent inefficiencies in power generation sector of Pakistan. Final section is to propose the solution of reducing losses or inefficiencies. It also includes quantify saving potential of primary energy on the basis of those energy efficiency improvement technologies with cost analysis.
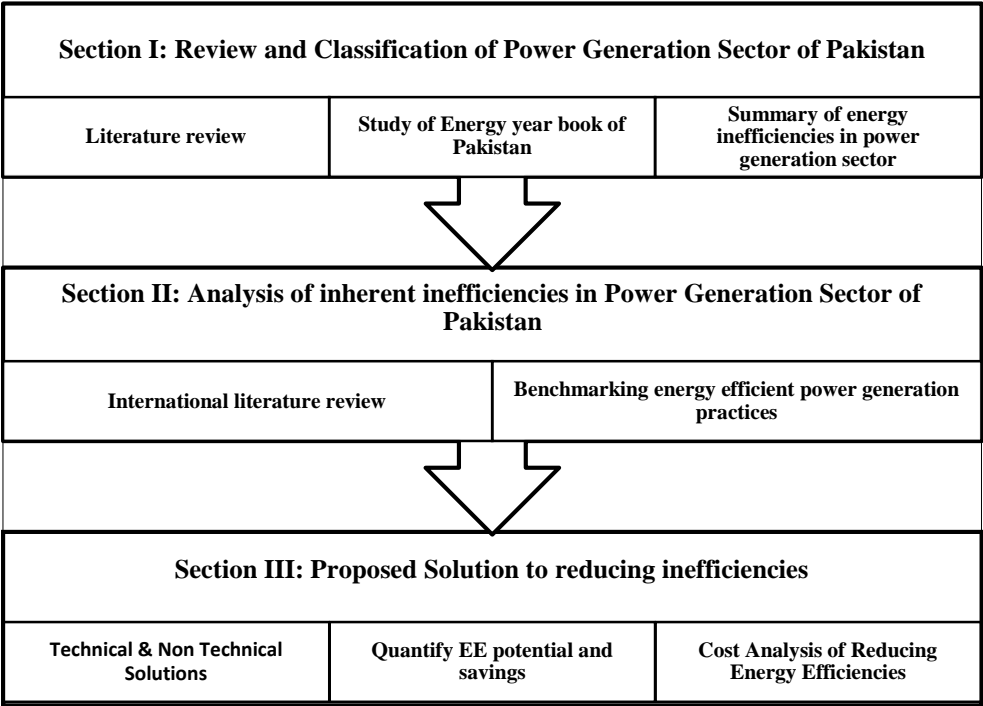

Fig. 3. Three sections of research methodology

First section includes current energy scenario of power generation sector of Pakistan, current power sector development status, current energy efficiency improvements in Pakistan and summary of energy inefficiencies in power generation sector of Pakistan.

Second section of methodology as illustrated in Fig. 3 above is an analysis of inherent inefficiencies of power generation sector of Pakistan. It includes inefficiencies/losses in each system, LCOE/ Upfront tariff comparison of different countries, plant load factor (PLF) & generation cost comparison of Pakistan energy sector and RFO length comparison in Pakistan with USA for nuclear power generation sector.

Third section as in Fig. 3 is a proposed solution to improve the efficiency of power generation sector of Pakistan and quantify saving potential by implementing these energy efficiency technologies. It includes addressing technical inefficiencies, addressing non-technical inefficiencies, challenges in power generation sector of some countries with financials, social & environmental benefits, recommended energy efficiency improvements and cost analysis of energy efficiency retrofits analysis in some countries.

IV. REVIEW AND CLASSIFICATION OF POWER GENERATION SECTOR OF PAKISTAN

Pakistan is generating electricity to fulfill energy demand of country from thermal, nuclear and renewable (including Hydro) power plants. According to Central Power Purchasing Agency Annual Report 2019, Total installed capacity of country is 42,004.3 MW with 61.38% major contribution of thermal power (8). According to USAID report 2007, Pakistan has 122.6 GW annually of wind energy potential. Most prominent location for wind power generation is Gharo-Keti Bandar wind corridor of 60 kmx170 km land area and potential map of wind energy in Pakistan. It was developed by Pakistan metrological department (PMD) with collaboration of AEDB at 100 m height from ground level. Wind speed varies from 5 m/s to 12 m/s at different locations of Pakistan (9) (10).

Pakistan has potential of producing more than 100,000 MW electricity from solar radiations in solar energy potential map of Pakistan. According to Alternative Energy Development Board (AEDB), Pakistan has target to increase of 5% by 2030 of renewable energy which is almost 9700 MW. Southern Punjab, Sindh and Baluchistan has solar energy potential of 2 MWh/m^2 solar radiation per year. Annual average solar radiation in Pakistan is 5.5 KWh/m^2 per day which is more than the value of 4.5 KWh/m^2 solar radiation measured in Naha Okinawa, Japan (11) (12). Pakistan has planned to develop 25,000 MW more power by 2025 for its power sector under the private power infrastructure board (PPIB). For this purpose, letter of intent (LOI) has issued to 37 IPPs construct thermal power projects of 15,469 MW capacity under China Pakistan economic corridor (CPEC) with 36 billion USD investment. (13)

According to hydro planning organization (HPO), Pakistan has 60,159 MW hydro power potential mostly located in KPK, AJ&K, Gilgit Baltistan and only 12% of this potential has been exploited so far. According to vision 2025, Pakistan has planned to achieve 40,000 MW target of hydro energy by 2025. For this purpose WAPDA has considered 72 sites for hydro projects. WAPDA will develop these sites in three phasesAccording to National Action Plan Energy Report 2019, Primary energy intensity of Pakistan has been decreasing continuously by 1.7% annually since 2000. Implementations of energy efficiency technologies/programs like rehabilitation of main plant and conversion to combine cycle, optimum use of additional water head and good outage management in power generation sector have sizeable contribution to lower this primary energy intensity.

V. ANALYSIS OF INHERENT INEFFICIENCIES OF POWER GENERATION SECTOR OF PAKISTAN

In 2009, India was 15% and Philippine was 25% more energy efficient than Pakistan. In Pakistan, obsolete technology and poor infrastructures are causes for energy losses or inefficiencies in power generation systems. In a technical report published with the collaboration of Ministry of Planning Commission & Reforms it was estimated that 2,121 thousand TOE or 93,763 TJ energy saving potential in power generation sector is available. It can be achieved with the investment of $3.3 billion (14) & (15). But Pakistan has less paid very attention on energy efficiency techniques as comparison of energy efficiency of pakistna with different countires can be seen in Fig. 4.

According to Pakistan energy yearbook 2018, Primary energy of 29.747 MTOE was converted to 10.376 MTOE electricity. Due to huge power generation sector losses only 34.88% of primary energy was

converted into electricity with conversion losses of 65.12% (19.372 MTOE). Whereas the overall world has power generation losses of 54.88% in 2012, UK has 56.28% in 2014 and USA has 61.29% in 2018. Such losses are not tenable for a growing economy like Pakistan. It is imperative for Pakistan to identify and mitigate power generation losses. (16), (17) & (14).
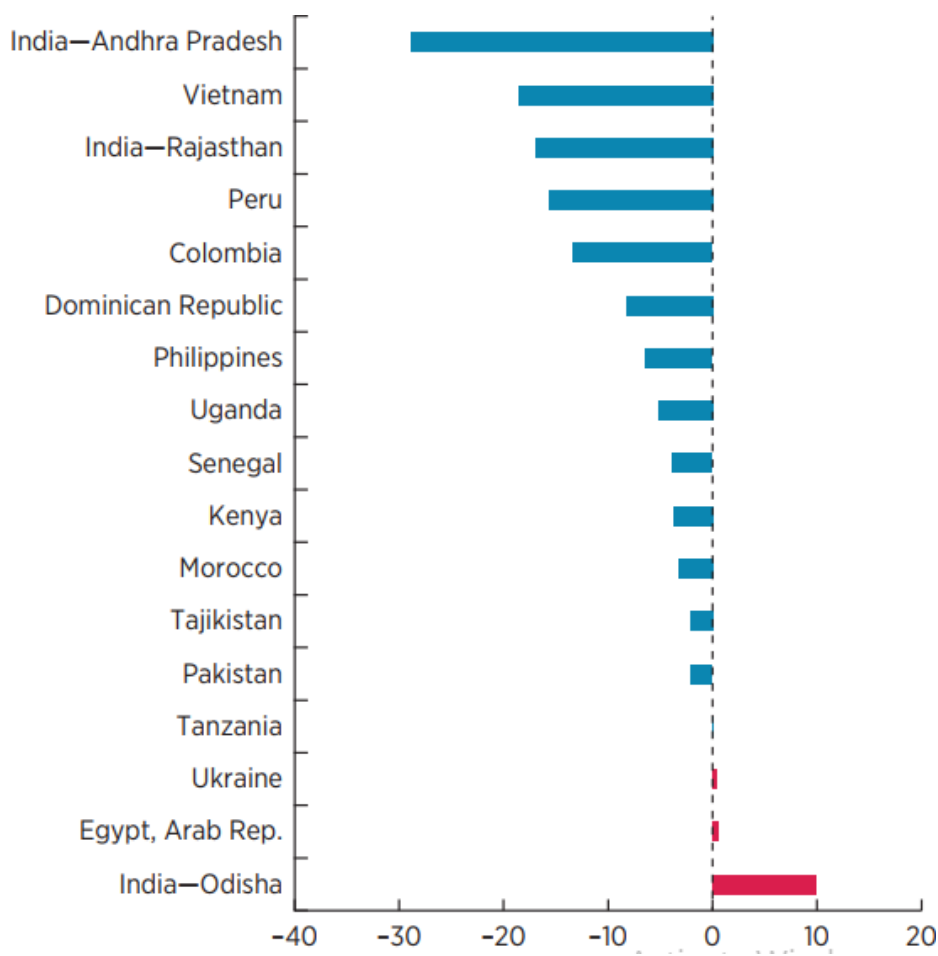

Fig. 4. Progress of Energy Efficiency of Pakistan with other countries 1990-2015
(Source: World Bank Elaboration Based on Rethinking Power Sector Reform Utility Database 2015)

According to Wood Mackenzie report 2019, levelized cost of electricity LCOE (Upfront tariff/ Cost of power generation) on fossil fuel based power generation is 44.5 USD/MWh in India and 48.5 USD/MWh in China (18). Where as in Pakistan average thermal power generation cost was 65.2 USD/MWh in 2018 so saving potential is available in power generation sector of Pakistan including renewable energy sector due huge losses/inefficiencies in power systems (16).

Average PLF is not more than 60% which is less than other many developing countries. Pakistan has potential to increase in PLF that would decrease in overall cost of power generation. Overall PLF in Pakistan power sector is below than acceptable limits especially for public sector utilities.

In India, NTPC Ltd's Talcher thermal power station has achieved more than 90% PLF. China has PLF for its utilities varies from 70% to 90% at different regions and this is also an acceptable limit for PLT (19) (20). Some of energy efficiencies have mentioned in Table I.

TABLE I: INEFFICIENCIES/LOSSES IN EACH SYSTEM (21) & (22)

Category	Inefficiency 01	Inefficiency 02	Inefficiency 03	Inefficiency 04
Thermal power generation	Lower Plant Factors	Poor Steam Conditions	Combustions Losses	High Stack Temperature
Renewables power generation	Lower Capacity Factors	Environmental effects	Insulation Losses in Solar PVs	High Temperature in Solar PVs
Nuclear Power Generation	More Refueling Outage (RFO) Length	Cooling/Coolant System Leakages	Down Time Variations	Over Heating in Core of Reactors and Meltdown Risk
Hydel Power Generation	Lower Capacity Factor	Head Losses	Forced Outages due to Corrosions and Fatigues	Lower Peaking Capabilities

VI. PROPOSED SOLUTIONS TO REDUCE INEFFICIENCIES

Many countries are improving their power generation sector by implementing many energy efficiency technologies some of these have mentioned in Table II, but few of them like pumped hydro in hydro power sector, cogeneration/CHP, SC/USC technologies in thermal power sector, RE repowering, improving RFO length in nuclear power plants, and coal beneficiation in coal fired power plant are more important. In this report only these six energy efficiency technologies will be considered for quantify energy saving potential in power generation sector of Pakistan.

TABLE II: ADDRESSING TECHNICAL INEFFICIENCIES (23), (24) & (25)

Category	Solution 01	Solution 02	Solution 03	Solution 04
Thermal power generation	Plant Up Gradation with CHP	Optimum Combustion Process	Efficient Burner Design	Improve Fuel Capacity
Nuclear power generation	Good Outage Management	Online Inspection of Cooling/ Coolant System	Improve Stabilization & Synchronization with Startup	Optimize Core Mapping
Renewables power generation	Battery Storage	Enhanced Thermal Effects (Solar PV)	Solar Tracking System (Solar PV)	Lower Shading Effects (Wind & Solar)
Hydro power Generation	Pumped Storage	Optimize Penstock Design	Reduce Seepage and Sedimentation	Corrosion and Fatigue Assessments

Pakistan is also have many of non-technical inefficiencies as in Table III. But in this study only technical will be discussed.

TABLE III: ADDRESSING NON-TECHNICAL INEFFICIENCIES (26), (27), (28), (29) & (30)

Category	Solution 01	Solution 02	Solution 03	Solution 04
Policy Issues	Evidence-Based Execution of Energy Efficiency Projects with Planning	Addressing the Problems of Past Energy Efficiency Policies/Programs	Reduce Fuel Imports (Coal Imports for Sahiwal and Port Qasim Power Plant)	Reduce Energy Production Cost (More Energy Production Cost per KWh than buying from IPPs)
Governance Issues	Decision Making Power	Decentralization of Authority	Clear the Role and Functions for all Institutions	Design Incentive Mechanism for Saving Power Generation
Financial Issues	Commercialize Approved Academia Research	Pilot Scale Project after repeated research with Positive Results	Cost Analysis Comparison with World's Best Energy Projects	Micro Financing the EE Retrofits in Power Generation Sector of Pakistan
Political Issues	Five Years Energy Plan Follow up	Fair Merit and Transparent Criteria for Public Investments	Prefer Public Issue and Safety (Environmental Pollution, Land Acquisition, etc)	Endeavor For the well-being of Pakistan
Behavior Issues	Adopting New Technologies	Realize Self - Responsibility of Energy Saving contribution	Energy Saving trainings at each & every level	EE Techniques should be Easy to Adopt
Technical Issues	Improve Labour Skills	Technical Capacity Enhancement	Codes and Standards	Digitalization and Software Based Controls

Hourly load curve Fig. 5 of peak demand of day during 2016-17 which is considered for identify the potential of pumped storage hydropower (PSH). During 2016-17 National Transmission & Dispatch (NTDC) system has peak capacity of 22,600 MW. Pumped hydro potential against this peak capacity is 8,299.2 MWh. This power storage will be considered during off peak demand of country from 11:30 PM to 7:30 AM. Peak demand from 12 PM to 9:30 PM above 24,000 MW is 7,479 MWh against pumped storage hydropower potential of 8299.2 MWh. This report will not cover implementation cost of these potential. It is just highlighting the available saving potential of renewable energy storage. If 22,000 MW is considered as base load then 4,699.2 MWh per day potential is available and for annual saving potential it will be 1,715.208 GWh or 1,396,832.06 TOE annually. (31)
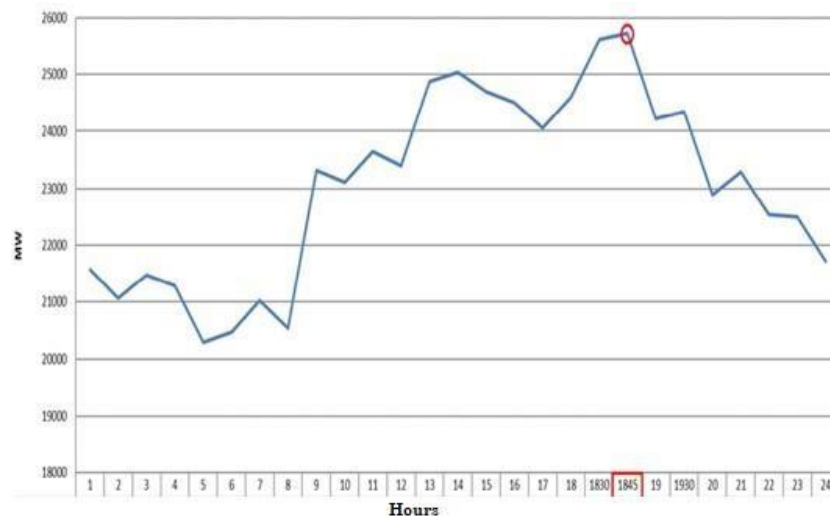
Fig. 5: Load Curve of Peak Demand of Day 2016-2017 (June 3, 2017) (Source: NTDC)

According to Pakistan energy yearbook 2018, Primary energy supply as gas fuel was 10,831,662 TOE (544,654MMCft) and gas-fired plants were generated 39,435 GWh (3,211,586.4 TOE) as final energy as electricity. There was 30% contribution of total electricity from gas-fired power plants. Only 29.64% of primary energy was converted to useful energy as electricity that's why combine heat & power (CHP) energy saving opportunity has been considered for gas fired power plants. Overall efficiency of power station will increase to range of 66-71% after upgrading a gas power plant to CHP. For minimum efficiency limit of 66%, gas-fired power plant has 3,937,310.52 TOE saving potential and for maximum efficiency of 71% power stations has 4,478,899.62 saving potential (32).

Overall Effeciency

$$= \frac{Net\ Electricity\ Generation + useful\ Heat\ Recovered * \frac{1\ KWh}{3.412\ MBtu}}{Fuel\ Input * \frac{1KWh}{3.412MBtu}} \quad (1)$$

Higher heating value (HHV) of coal can improve to 20.24 MBtu/Tonne when 20% reduction in ash is considered by the process of coal beneficiation. It can improve 10% utilization factor, 10-15 % plant load factor and 8-10% increase in HHV of coal. Average higher hating value of Pakistan indigenous coal is 18.74 MBtu/Tonne Indigenous Coal and imported coal is 27.56 MBtu/Tonne. Higher heating value of coal can be found based on proximate analysis. Eq. 3 is used to find coal consumption (Kg/KWh) based on HHV of coal. If indigenous coal will use other than imported coal after washing it can save 6,769.76 million PKR (33), (16).

$$HHV(MJ/Kg) = 0.353FC + 0.1559VM - 0.0078ASH \quad (2)$$

 Where
  FC = % Fixed Carbon in Coal
  VM = % Volatile Matter in Coal
  ASH = % Ash in Coal

$$Coal\ Consumption\ (Kg/KWh) = \left(\frac{3600KJ/KWh}{Plant\ Overall\ Effciency * HHV\ (KJ/Kg)} \right) \quad (3)$$

 Where
  HHV = Higher Heating Value (KJ/Kg)

During 2017-18, only three units (Port Qasim, Sahiwal with design efficiency of 39%, and Lakhra power plants with 35% based on LHV) were generating electricity based on coal fuel. These coal-fired power plants have supercritical technology. Up gradation from supercritical technology (571°/25.5 MPa) to ultra-supercritical technology (600 °C/30 MPa) can improve 1.5-2% efficiency of power station (34). Average 1.5% increase in power plant efficiency can save coal consumption of 0.0187 Kg/KWh according to equation 6.4 and 2,357 Million PKR can be saved from import bills of coal (21).

$$Coal\,Saving\,(Kg/KWh) = (\frac{1}{\eta_{Previous}} - \frac{1}{\eta_{Improved}}) * (\frac{3600 KJ/KWh}{HHV\,(KJ/Kg)}) \quad (4)$$

Where

$\eta_{Previous}$ = Efficiency before retrofit
$\eta_{Improved}$ = Efficiency after retrofit
HHV = Higher Heating Value (KJ/Kg)

During 2017-18, Pakistan has generated 9,880 GWh from 1430 MW installed capacity of nuclear power plants. Operating hours was 6,909.09 hours and average RFO length was 77.12 days. Two important processes start-up & synchronization and core design optimization of refueling outage require proper monitoring and outage management. These processes optimization along with up gradation (15% CF increment) of nuclear power sector can reduced average 20- 25 days of RFO length (16). Capacity factor will increase from 78.81% to 85.72% of nuclear power plants by reducing RFO length from 77.12 days to 56 days (24).

$$Capacity\,Factor = \frac{Total\,Generation\,(MWh)}{Plant\,Capacity\,(MW) * Total\,Time\,(Hours)} \quad (5)$$

According to energy year book 2018, Pakistan has 430 MW installed capacity of solar power plant and average capacity factor was 20%. During 2017-18, solar PV plants has generated 786 GWh. Solar tracking system is one option as solar energy repowering to improve the output yield of solar PVs. Solar tracking system increase output energy by 13-15% increase in global horizontal irradiance (GHI) 13-15% (35) (36).

$$Performance\,Ratio\,(PR) = 100 * (\frac{E_{AC}}{E_{Irradiation} * A_{Array} * \eta_{STC}}) \quad (6)$$

Where

E_{AC} = Energy measure coming from inverter in KWh
$E_{Irradiance}$ = Unshaded irradiance at Module Level in KWh
A_{Array} = Total Surface Area of module in m²,
η_{STC} = Efficiency Standard Test Condition of PV Module

Equation 6 will use to find value of performance ratio. It represents operation quality of PV module system. Performance ratio from Eq. 6 will put in Eq. 7 to find the specific power of PV module in KWh/KWₚ.

$$E = A * \eta * H * PR \quad (7)$$

Where

E = Specific Power (KWh/KWₚ)
A = Area of PV Module (m²)
η = Operational Efficiency of PV Module
PR = Performance Ratio
H = Annual Average Solar Radiation on Tilted Panel (KWh/m²)

Equation 6.8 represents another alternate method to estimate specific power of PV module because above equation 6.6 and 6.7 require operational values of PV system.

$$Specific\ Power\ (KWh/KWp)$$
$$= GHI\ (Global\ Horizontal\ Irradiance) * Area\ of\ PV\ Modules$$
$$- 16.42\%\ other\ system\ Losses\ (8)$$

Where

Average Global Horizontal Irradiance (GHI) for Pakistan = 2,071 KWh/KW$_p$

Eq. 8 gives the value of specific power 1,919.97 KWh/KW$_P$ after 15% increase global horizontal irradiance (GHI) due to solar tracking system. This retrofit will yield 83,895.931 MWh more electricity and utilization factor will improve from 20% to 22.68%.

During 2017-18, Pakistan has generated 2101 GWh from 1,006 MW wind power plant capacity. Average capacity of Wind Turbine Generator was 1.74 MW and total 568.63 number of WTG were installed. 10% increase in rotor diameter as design improvement can be increase from 1.74 to 2.11 MW per WTG find by Eq. 9 due to increase in turbine efficiency and wind power availability. Energy output from 568.63 WTG will increase from 2,101 GWh to 2,544.841 GWh and capacity factor will be improved from 23.85 % to 28.87%.

$$P_{Wind\ Power} = \frac{1}{2}\rho AV^3C_p \quad (9)$$

P $_{Wind\ Power}$ = Wind Power Available (MW)

ρ = Air Density =1.24 Kg/m^3 A = Swept Area (m^2) = πr^2
V = Average Velocity (m/s) = 6-8 m/s C$_P$ = Power Coefficient = 0.4

Capital cost can be considered for cost analysis in upgrading USC technology of coal fired power plants. For example, Sahiwal coal fired power plant of 1320 MW capacity has capital cost of 1535.736 Million USD. This capital cost for super critical technology but for ultra-supercritical technology, more 57.12 Million USD will be required as capital cost. Savings potential from this up gradation with 70% utilization factor will be 12.234 Million USD from imported coal with only 4.66 years simple payback period (37). In 2008, China has upgraded its almost 100 power stations with SC/USC technologies and has saved utilization of 27 million metric ton of standard coal annually. Coal utilization has reduced from 380 gce/KWh in 2003 to 350 gce/KWh in 2008 with avoided 55 million metric CO2 annually. Table 6.7 shows that SC/USC retrofits in China has average 5.34 years of simple payback period. Another case of coal beneficiation has been mentioned in Table 6.7 that in India ash contents was reduced from 40% to 30% and 26.73 Million USD was saved for 500 MW capacity coal-fired power plant (38) & (39).

VII. RESULTS AND DISCUSSIONS

The salient results from this research are saving potentials of 2,242.94 GWh annually from renewable power sector including PSH (Pumped Storage Hydropower), 6,769.76 Million PKR savings from CB (Coal Beneficiation), 2,357 Million PKR from USC (Ultra Supercritical), 4.48 MMTOE from CHP (Combine Heat & Power) and almost 7% CF improvement by RFO (Refueling Outage) reduction. Total energy units will increase from 131,275 GWh to 188,527.25 GWh with 43.61% increment and total average power units will increase from 14,985.73 MW to 21,521.37 MW with 43.61% increment. It is recommended to consider these energy efficiency improvement technologies and promote indigenous resources like hydro, Thar coal and Renewable for curtailment of 17.75 Billion USD fuel import bills.

TABLE IV: RESULTS OF SAVING POTENTIALS FROM ENERGY EFFICIENCY IMPROVEMENTS

Power Generation Sector	Technical Improvements	Saving Potential	Capacity Factor Enhancement
Gas-Fired Power Sector	Combine Heat and Power (CHP)	3.93 MMTOE to 4.48 MMTOE	-
Coal-Fired Power Sector	Coal Beneficiation and Ultra- Supercritical (USC) Technology	6,769.76 million PKR from Coal Beneficiation 2,357 Million PKR from Up-grading to USC	-
Nuclear Power Sector	Optimize start-up & synchronization with core design optimization	Reducing RFO length from 77.12 days to 56 days	Current Value: 78.81% Improved Value: 85.72%
Hydro Power Sector	Pumped Storage Hydropower (PSH)	1,715.208 GWh or 1,396,832.06 TOE Annually	-
Solar Power	Solar Tracking System	83895.931 MWh or 68324.84 TOE	Current Value: 20% to Improved Value: 22.68%
Wind Power	Design Improvement for Enhanced Wind Energy Availability	443,841.05 MWh	Current Value: 23.85% to Improved Value: 28.87%

VIII. CONCLUSION

Gas-fired thermal power plants converted only 29.65% useful energy into electricity with 70.35% power generation system losses. Overall efficiency of power station can be increased to 66-71% after upgrading a gas power plant to CHP and it has 3.93 MMTOE to 4.48 MMTOE energy saving potential. Pakistan renewable power sector can save energy of 2,242.94 GWh annually from including 1,715.208 GWh from pumped storage hydropower (PSH). Proper monitoring and good outage management in nuclear power sector of Pakistan has potential to increase in capacity factor from 78.81% to 85.72%. It means 30.2 GWh more generation annually by reducing 20- 25 days from average nuclear refueling outage (RFO) length During 2017-18, Pakistan has generated electricity by utilizing almost 4,433,081 Tonnes of imported coal. Pakistan has huge coal reserves of 361,512 Million Tonnes but indigenous coal has been not considered for power generation application due to high ash contents with other contamination. Process of coal beneficiation can be reduced 10-15% ash content and it will save 6,769.76 million PKR from import bill. Up gradation from supercritical technology (571°/25.5 MPa) to ultra-supercritical technology (600 °C/30 MPa) can improve 1.5-2% efficiency of power station. That is another techniques to save average 18.7 g/KWh coal from coal-fired power plants and save 2,357 Million PKR from import bill of 17 Billion USD for Primary energy fuels.

REFERENCES

1. Minisrty of Energy (Petroluem Division) . *Pakistan Energy Book 2017-18.* Islamabad : Hydrocarbon Institute of Pakistan, 2018.
2. IEA, IRENA, UNSD, WB, WHO. *Tracking SDG 7: Energy Progress Report* . Washigton DC 20433 : s.n., 2019.
3. IEA/OECD. *Opportunities to Transform The Electricty Sector in Major Economies* . Paris : IEA Publishers, 2010.
4. The Fedration of Electric Power Companies of Japan. *Electricity Review Japan* . Tokyo : s.n., 2018.
5. JEPIC . *Electric Power Industry in Japan* . Tokyo : s.n., 2019.
6. *High Efficiency Electric Power Generation: The Environmental Role.* Beer, Janos. 2009, pp. 3-5.
7. Tillman, David A. *Coal Fired Electricity and Emission Control: Efficiency and Effectiveness* . Cambrige, USA : Joe Hayton, 2018.
8. *Central Power Purchasing Agency Annual Report.* Islamabad : Central Power Purchasing Agency, 2019.
9. Energypedia. energypedia. *Pakistan Energy Situation.* [Online] November 27, 2019. https://energypedia.info/wiki/Pakistan_Energy_Situation.
10. AEDB. AEDB. *Wind Resource Potential.* [Online] 2020. http://www.aedb.org/ae-technologies/wind-power/wind-re.
11. —. AEDB. *Current Status of Solar PV Power Plants.* [Online] 2020. http://www.aedb.org/ae-technologies/solar-power/solar-current-status.
12. JICA & AEDB. *Data Collection Survey on Renewable Energy Development in Pakistan* . Islamabad : s.n., 2013.
13. Ministry of Planning, Development & Reform, Government of Pakistan and UNDP Pakistan. *Suatainable Energy For All: National Action Plan.* Islamabad : Ministry of Planning, Development & Reform, Government of Pakistan, 2019.
14. Haigler Bailly Pakistan & Econoler International . *ADB Technical Assistance Consultant's Final Report.* Islamabad : s.n., 2009.
15. IEA Energy Efficiency. *Authoritative Trackers of Global Efficiency Trends* . Paris : s.n., 2019.
16. Ministry of Energy (Petroleum Division). *Pakistan Energy Yearbook* . Islamabad : Hydrocarbon Development Institute of Pakistan , 2018.
17. Bates, Emma. Energy, Climate Change and Brexit: Avoiding a Future Energy Crisis. *ggs Experts In Countinuous Monitoring* . [Online] November 27, 2018. https://www.ggs-uk.com/energy-climate-brexit/.
18. Wood Mackenzie. India Leads with Lowest Renewable Cost in Asia Pacific. *Wood Mackenzie.* [Online] July 29, 2019. https://www.woodmac.com/press-releases/india-leads-with-lowest-renewable-cost-in-asia-pacific/.
19. Jiang Lin, Xu Liu & Fredrich Kahrl. *Excess Capacity in China 's Power System: A Regional Analysis* . California : s.n., 2016.
20. NTPC . *43RD Annual Report* . New Dehli : s.n., 2018-19.
21. General Electric . GE/Power & RE. *General Electric.* [Online] April 2020. https://www.ge.com/power, https://www.ge.com/renewableenergy.
22. USDOE. USDOE EERE. *EERE.* [Online] April 2020. https://www.energy.gov/eere/office-energy-efficiency-renewable-energy.
23. WAPDA. *WAPDA ANNUAL REPORT* . Lahore : SMS Consultants, 2017-2018.
24. *Key Issues for the Control of Refuelling Outage Duration and Cost in PWR NPP.* XA0055990, 1997.
25. Bryden, K.W. Ragland & K. M. *Combution Engineering* . Boca Raton : CRC Press, 2011.
26. Ministry of Planning, Development and Reform, Govt. of Pakistan. *Sustainable Energy For All; National Action Plan* . Islamabad : s.n., 2019.
27. R. Becque, E. Mackres, J. Layke, N. Aden, S. Liu, K. Managan, C. Nelser, S. M-Stommen, K. Petrichenko, and P. Graham. *Accelerating Building Efficiency: Eight Actions for Urban Leaders.* Washington D.C. : s.n., 2016.
28. Ministry of Water & Power, Govt. of Pakistan . *National Power Policy.* Islamabad : s.n., 2013.
29. Ministry of Energy (Petroluem Division). *Pakistan Energy Year Book.* Islamabad : Hydrocarbon Development Institute of Pakistan, 2018.
30. CPEC Authority. CPEC (China Pakistan Economic Corridor). [Online] October 2017. http://cpec.gov.pk.

31. Planning Power NTDC . *Power Data Referennce Book 2011-2017* . Islamabad : s.n., 2017.

32. NREL. *Chapter 23: Combined Heat and Power Evaluation Protocol.* California : s.n., 2017.

33. Sharpe, Craige D. Zamuda & Mark A. *A Case for Enhanced Use of Clean Coal in India: An Essential Step Towards Energy Security and Environment Protections* . Ranchi : s.n., 2007.

34. NEPRA. Tariff Generation Upfront. *NEPRA* . [Online] May 2020. https://nepra.org.pk/tariff/Generation%20Upfront.php.

35. —. NEPRA. *NEPRA.* [Online] 2020. https://www.nepra.org.pk/#.

36. The World Bank. *Solar Resource Mapping in Pakistan: Solar Modelling Report.* Washington DC : The World Bank, 2015.

37. Reddy, P.Jayarama. *Clean Coal Technologies for Power Generation.* 2013.

38. Tan, Xiaomei. Business and Public Administration Studies. *Super Critical and Ultra Super Critical Coal-Fired Power Generation.* [Online] 2012. https://www.bpastudies.org/bpastudies/article/view/170/318.

39. Craig D. Zamuda, and Mark A. Sharpe. *A Case for Enhaced Use of Clean Coal In India: An Essential Step towards Energy Security and Environmental Protection* . Ranchi, India : s.n., 2007.

Tea Bag Model Using Fe-Coated Chitosan as an Adsorbent for the Dearsenification of Water

Saddam Hussain Dal[A], Khadija Qureshi[B], Muhammad Shuaib Shaikh[C] and Zulfiqar Ali Solangi

[A, B, C]=*Department of Chemical Engineering Department, Mehran University of Engineering and Technology, Jamshoro, Pakistan.*

Abstract— **Arsenic contamination in water is a major problem around the word. It is well known that the ingestion of groundwater polluted with arsenic results in chronic health effects. World Health Organization (WHO) provisional guideline value for arsenic in drinking water is 10 μg/l. There are various treatment techniques for removal of arsenic from water, such as adsorption, filtration, ion exchange and membrane process, reverse osmosis, phytoremediation, chemical precipitation, electrokinetic methods, and electrocoagulation. Among these, because of the low cost, performance, and simplicity, adsorption is an efficient and versatile process. Chitosan is a cationic polysaccharide with an exceptional potential for arsenic adsorption. In this study ferric coated chitosan was synthesized and used as an adsorbent in tea bags for the batch study. The adsorbent was characterized by SEM and FTIR to see the surface texture and functional groups besides this different parameters were studied to investigate the effect of the arsenic removal percentage such as pH(2,4,7,9), contact time(15,30,60,120) in minutes, initial arsenic concentration (50,100,150,200) in ppb, and adsorbent dose(0.25,0.5,0.75,1.0) in grams. The optimized parameters at which maximum arsenic was removed (98%) from water at contact time 60 minutes, adsorbent dose 0.25 g, initial arsenic concentration 50ppb and pH 7.**

Keywords—**Adsorption, Arsenic removal, Batch study, Characterization, Fe-Coated Chitosan, Tea Bag.**

V. INTRODUCTION

Freshwater percentage on the earth surface is limited to 2.5% out of which only 1% is used. Including this, one of the highly important water resources are lakes which are mostly a supply of water consumption for human beings and it is only 0.3% of total surface water body sources. As such, the conditions of lakes are in constant deterioration due to increased anthropogenic activities surrounding them [1]. Arsenic is hazardous in nature. The sources through which human are being exposed are atmospheric air, groundwater as well as food sources too. Arsenic contaminants in water are due to major sources which includes either by geological or by anthropogenic activities [2]. Due to arsenic contaminants it causes many complications in body organs such as, respiratory, nervous, integumentary, hematopoietic, endocrine, cardiovascular, immune, renal, hepatic, reproductive system, and development. Arsenic contaminants if available can be a cause of cancer in the body. Presence of several arsenic caused health effects involving emerging areas such as epigenetics and cancer [2]. In spring water, arsenic contaminants are increasing day by day because of which there are many ill-effects on health totally throughout the world. On the other hand, studies show that, arsenic contaminants effects health of children too i.e. skin lesions, overall health effects and changes within the complete blood count in children exposed to arsenic through beverage in West Bengal, India. This report shows that in one of the most populated country India, children were having genetic damages due to arsenic contaminants [3]. It has been found that there is a big threaten to health i.e. result in bladder cancer. Breast cancer and laryngeal cancer are two diabetes as it has been shown in new data. As a youth, its symptoms include kidney damage, carotid intima-media thickness, and different pulmonary thicknesses in infants. On the other hand, effects in childhood were also witnessing which includes low birth weight, low fetal age, anemia, enhanced apoptosis, and reduced cognitive functions. Along with this Arsenic also damaged DNA and modification of gene and protein expression have also been found [4]. On the planet, Arsenic is one of the lethal elements, putting citizenry in peril by affecting the drinkable water. Twenty-four districts of Sindh, Pakistan were analyzed. From the results, it was found that Sakrand, Shaheed Benazirabad region, Halla, Matairi, Tando Muhammad Khan (TMK), and Nasarpur region have the highest arsenic concentration that was 200 ppb. It is above the limits which are set by the World Health Organization

(WHO) [5]. This analysis highlights, for the main time, the magnitude and severity of As-induced issues supported by related published papers in Pakistan; examines possible sources of As-contamination of aquifers and estimates of As-induced potential health threats in the country on global data [6]. Contaminants of Arsenic if available in ground water will be a major issue which will give rise to many dangerous health issues as already explained. It includes effect on physical body (internal and external cancers) [7]. According to research we can get rid of this fully or we can immobilize arsenic, which includes natural process, sand filtration etc. These methods have advantages as well as disadvantages too. From above methods, two methods have shown good results in removing arsenic contaminants includes in-situ subsurface arsenic immobilization by aeration and the removal of arsenic from aqueous phase [7]. These methods can remove both arsenic contaminants as well as these will affect their chemical treatment and membrane process too. If ions like phosphate, silicate, nitrate, chloride, carbonate, and sulfate are present in them it will help a lot in removing arsenic contaminants [8]. Electrocoagulation (EC) is taken into account as an advantageous process for the removal of As due to simplicity, high removal efficiency, cost-effectiveness, lower chemical requirement, and the feasibility of small-scale operations as compared with other treatment processes [9]. On wastewaters many water purification processes are applied which includes electrolytic chemical treatment, adsorption, biological treatment, and membrane separation. It was observed from the above techniques that advantages on adsorption were following three; its cost was low, it was effectiveness and it was simple [10]. In batch tests, magnetic nanoparticles impregnated with chitosan beads (MICB) synthesized using the chitosan template were investigated for the absorption ability of arsenic. Magnetic nanoparticles impregnated chitosan beads (MICB) synthesized by using the chitosan template was investigated for uptake capacity of arsenic in batch studies. the consequences of varied factors like adsorbent dose, power of hydrogen, time of contact, concentration of arsenic, and co-existing anions in detail were studied systematically on removal of arsenic [11]. A new sorbent of Fe-Mn binary oxide impregnated chitosan bead (FMCB) was manufactured by impregnating Fe-Mn binary oxide into the chitosan matrix. Into chitosan matrix by using a novel sorbent of Fe–Mn binary oxide impregnated chitosan bead (FMCB) was fabricated through impregnating Fe–Mn binary oxide. As a result of which showed that the presence of the FMCB helps in removing arsenic (V) and arsenic (III), which indicates that it is very helpful in removing the arsenic from the real beverage [12]. By using iron-chitosan composites on real-world groundwater to remove arsenic is studied and presented. Under two conditions i.e. equilibrium and dynamic through adsorption at pH 7.0 was studied to see the effect on removing arsenic (III) and arsenic(V). By fitting the equilibrium data to Langmuir adsorption models, evaluation was done on various parameters. For removing total inorganic arsenic right down less than to 10μg/l from real-life arsenic-contaminated ground water samples, adsorbent was also successfully applied [13]. Various technologies for the removal of arsenic from contaminated water supplies have been developed, which includes following four, precipitation, membrane processes, ion exchange and adsorption. A number of adsorbents are used to remove this dangerous arsenic and many other contaminated metals. In this research fe-coated chitosan is synthesized to increase its removal efficiency of arsenic and used in tea bags to study the adsorption of arsenic and batch study were carried out.

VI. MATERIALS AND METHODOLOGY

A. Preparation of Fe-Coated Chitosan Tea Bag Model

1) Materials
For developing the fe-coated chitosan tea bag model, following types of materials were used, that includes the chitosan, tea bags and ferric chloride hexahydrate. Ferric chloride hexahydrate was arranged from the water quality lab Chemical Engineering Department MUET. Whereas the chitosan and Tea bags were purchased commercially from market of standard grade.

2) Preparation of ferric solution
Ferric solution was prepared by taking 0.5406 g of ferric chloride hexahydrate in ethanol and distilled water in the ratio of 1:1 respectively and stirred well.

3) Coating of ferric to chitosan material

Fe-coated chitosan was prepared by initially pouring 10 g of chitosan in 100 ml of ferric solution. The solution was mixed at magnetic stirrer 300 rpm for 2 h. Adsorbent was filtered and dried in muffle furnace at 90°C for 3 h. Fe-coated chitosan was ready.

4) Tea bag model containing fe-coated chitosan

Different grams of adsorbent in tea bags were added. The Tea bags model containing fe-coated chitosan are dipped in arsenic contaminated water, and shaked well are shown in below figure.

Fig.1: Tea bags, Samples, Shaking of samples

B. Batch studies of Tea bag model contained adsorbent

Tea bag model containing fe-coated chitosan has been developed and used to remove the arsenic contaminants from water. Batch study was carried out to investigate the effect of contact time, adsorbent dose, arsenic initial concentration, and pH.

C. Arsenic Removal %age

Formula through which we can find the arsenic removal percentage or percentage filtration is given by:

$$\% \, Removal = \frac{Ci - Cf}{Cf} \times 100 \quad (1)$$

Where Ci stands for water containing arsenic contaminated water and Cf stands for water containing arsenic contaminated water after treatment,

VII. RESULTS AND DISCUSSIONS

A. Characterization of fe-coated chitosan

1) SEM Characterization

Fe-coated chitosan adsorbents surface morphology was performed by scanning the electron microscopy to see the surface behavior of the fe-coated chitosan adsorbent with an accelerated voltage 15kV, and magnification 50 and having diameter i.e. pore equals to 500μm. So now if we want to compare the surface features of fe-coated chitosan which clearly shows the clear surface and on the other hand media pores are smooth before adsorption test. After the adsorption test that surface shows that arsenic adsorption took place at the surface of the media, apparently including within surface region of the pores in the particles of fe-coated chitosan.
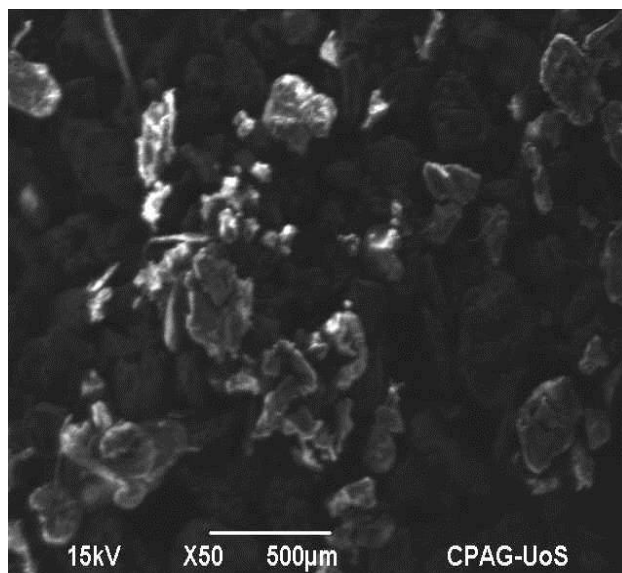
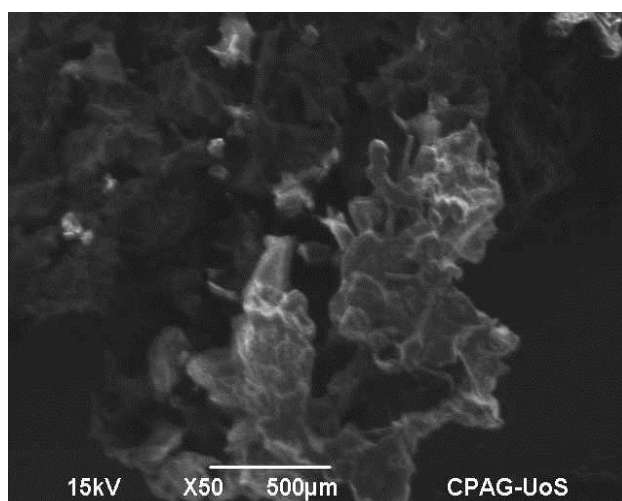Fig. 2: SEM results before adsorption test

Fig. 3: SEM results after adsorption test

2) FTIR characterization

The purpose of FTIR is to know the functional groups and structure of the fe-coated chitosan. Following figures i.e. 3.3, 3.4 and 3.5 shows FITR results of fe-coated chitosan before and after adsorption of arsenic, respectively. These figure shows the behavior of attachment functional groups before and after arsenic removal.
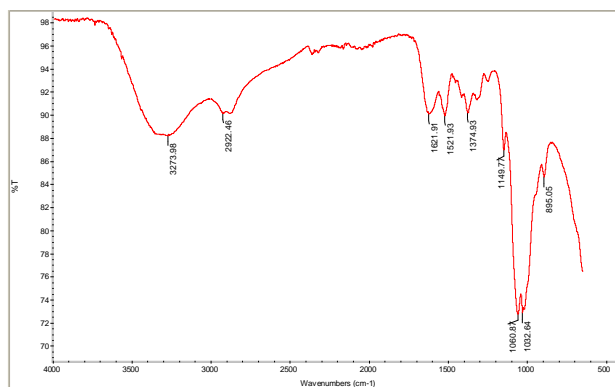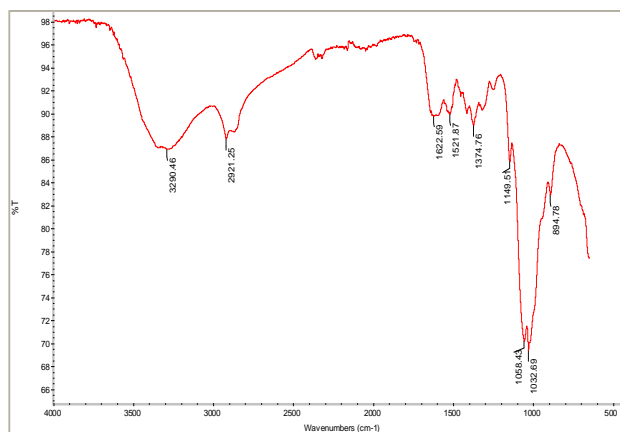

Fig. 4: Before adsorption test
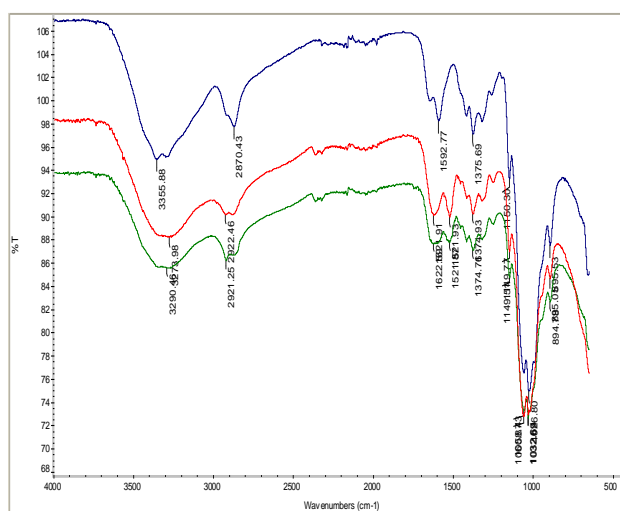
Fig. 5: After adsorption test

Fig. 6: Combined Chitosan & Fe-coated chitosan before & after Adsorption

B. Batch study of tea bag model containing adsorbent

   1) Effect of contact time

Effect of contact time shown in figure 3.6, the adsorption rate of arsenic was observed & to find the optimum time. Other paraments were kept constant such as adsorbent dose 0.25 grams, pH 7, Initial Concentration of arsenic 50 ppb & shaking speed 150 rpm. It was observed that at 60 minutes contact time maximum arsenic was removed which was 98% with an increased in contact time the adsorption rate was reduced.
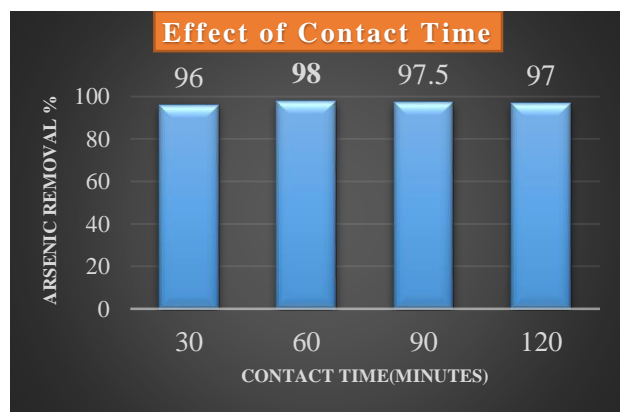

Fig. 7: Effect of contact time

2) Effect of pH

Power of Hydrogen's effect on arsenic adsorption is shown in the figure 3.7, pH was varied between 1 and 9. Other parameters were kept constant such as contact time 60 minutes, Arsenic concentration 50ppb, Adsorbent dose 0.25 grams, and shaking speed 150rpm. It was observed that adsorption of arsenic is highly dependent on pH. The maximum adsorption was 98% at pH 7. With increased in pH 7 to 9 and decreased from pH 7 to 4 adsorption of arsenic was also decreased.

3) Effect of adsorbent dose

To see adsorbent dose effect on removing of arsenic is shown in figure 3.7. The Adsorbent dosage were varied from 0.25 to 1.0 grams. Other parameters were kept constant such as arsenic initial concentration 50ppb, contact 60 minutes, pH 7, and shaking speed 150rpm.The optimized adsorbent dose was 0.25grams at which maximum (98%) arsenic was removed. By increasing the adsorbent dose arsenic removal % was decreased.
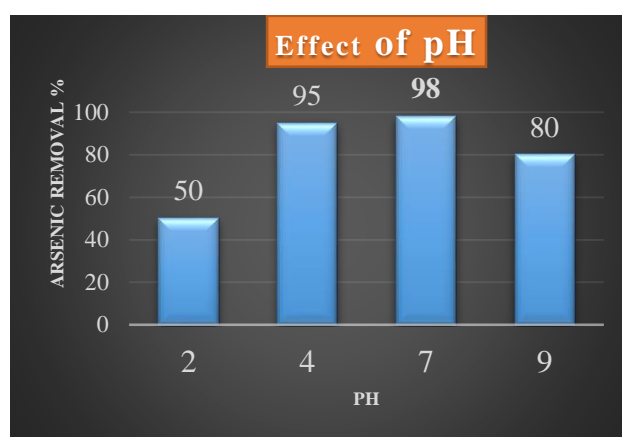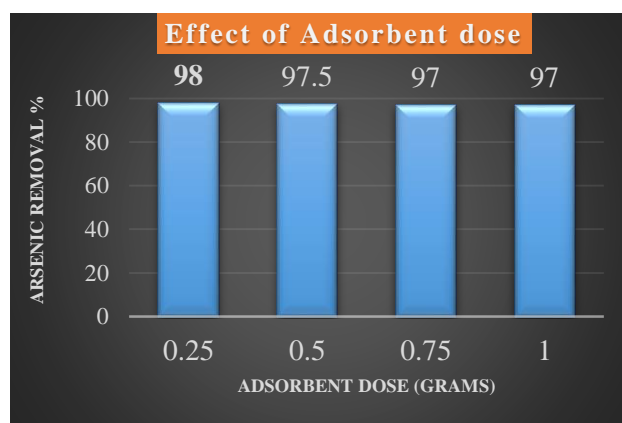

Fig. 8: Effect of pH

Fig. 9: Adsorbent dose effect

4) Effect of arsenic concentration

The arsenic concentration ranged from 50ppb to 200ppb to observe the effect of arsenic. Other parameters were kept constant such as adsorbent dose 0.25grams, time of contact 60 minutes, pH 7, and shaking speed 150rpm. It was observed that maximum arsenic was removed 98% at initial arsenic concertation 50ppb.By increasing the arsenic concentration adsorption of arsenic was decreased.
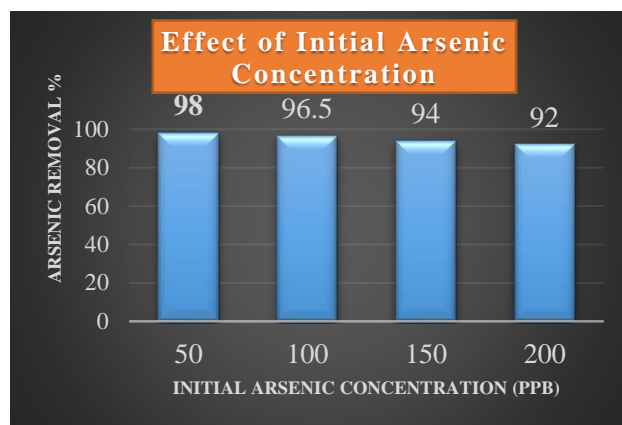
Fig. 10: Effect of initial arsenic concentration

VIII. CONCLUSION

Adsorption of arsenic was investigated by using fe-coated chitosan Tea bag model. The batch study of the adsorbent was carried out for finding the effectiveness of the adsorbent.

Following parameters were optimized in this research, time of contact, adsorbent dose, initial arsenic concentration, and pH.

- In the batch study by fixing the other optimized parameters constant and varying the contact time. From this research it can be concluded that at 60 minutes, maximum percentage i.e. 98% of arsenic contaminants was removed. With an increase in contact time, the removal efficiency of adsorbent was reduced. So, the optimized contact time was 60 minutes.
- In the batch study by fixing the other optimized parameters constant and varying the pH. It can be summarized from the results that 98% of arsenic was removed at pH 7. With an increase and decrease in pH, the removal efficiency of adsorbent was decreased. So, the optimized pH value was at pH 7.
- In the batch study by fixing the other optimized parameters constant and varying the adsorbent dose. After performing tests, it is concluded that the maximum percentage of arsenic (98%) was removed at 0.25 grams. It was also noticed that by increasing the adsorbent dose, the removal efficiency of adsorbent was decreased. So, the optimized adsorbent dose value was at 0.25 g.
- In the batch study by fixing the other optimized parameters constant and varying the initial arsenic concentration. It was seen that 98% of arsenic removal was at 50 ppb. With an increase in initial arsenic concentration, the removal efficiency of adsorbent was decreased. So, the optimized initial arsenic concentration value was at 50 ppb.

IX. REFERENCES

[1]   P. Vasistha and R. Ganguly, "Water quality assessment of natural lakes and its importance: An overview", *Materials Today: Proceedings*, vol. 32, pp. 544-552, 2020.
[2]   K. Mohammed Abdul, S. Jayasinghe, E. Chandana, C. Jayasumana and P. De Silva, "Arsenic and human health effects: A review", *Environmental Toxicology and Pharmacology*, vol. 40, no. 3, pp. 828-846, 2015.
[3]   J. Baig et al., "Evaluation of arsenic and other physico-chemical parameters of surface and ground water of Jamshoro, Pakistan", *Journal of Hazardous Materials*, vol. 166, no. 2-3, pp. 662-669, 2009.
[4]   K. Khan, R. Chakraborty, J. Bundschuh, P. Bhattacharya and F. Parvez, "Health effects of arsenic exposure in Latin America: An overview of the past eight years of research", *Science of The Total Environment*, vol. 710, p. 136071, 2020.
[5]   Z. Bhatti, K. Qureshi, I. Bhatti, I. Unar and M. Khuhawar, "Determination of Arsenic and Health Risk Assessment in the Ground Water of Sindh, Pakistan", *Mehran University Research Journal of Engineering and Technology*, vol. 36, no. 4, pp. 1037-1048, 2017.
[6]   M. Shahid et al., "A meta-analysis of the distribution, sources and health risks of arsenic-contaminated groundwater in Pakistan", *Environmental Pollution*, vol. 242, pp. 307-319, 2018.
[7]   V. Luong, E. Cañas Kurz, U. Hellriegel, T. Luu, J. Hoinkis and J. Bundschuh, "Iron-based subsurface arsenic removal technologies by aeration: A review of the current state and future prospects", *Water Research*, vol. 133, pp. 110-122, 2018.

[8]   S. Jadhav, E. Bringas, G. Yadav, V. Rathod, I. Ortiz and K. Marathe, "Arsenic and fluoride contaminated groundwaters: A review of current technologies for contaminants removal", *Journal of Environmental Management*, vol. 162, pp. 306-325, 2015.

[9]   M. Kobya, R. Soltani, P. Omwene and A. Khataee, "A review on decontamination of arsenic-contained water by electrocoagulation: Reactor configurations and operating cost along with removal mechanisms", *Environmental Technology & Innovation*, vol. 17, p. 100519, 2020.

[10]   F. Bertoni, J. González, S. García, L. Sala and S. Bellú, "Application of chitosan in removal of molybdate ions from contaminated water and groundwater", *Carbohydrate Polymers*, vol. 180, pp. 55-62, 2018.

[11]   J. Wang, W. Xu, L. Chen, X. Huang and J. Liu, "Preparation and evaluation of magnetic nanoparticles impregnated chitosan beads for arsenic removal from water", *Chemical Engineering Journal*, vol. 251, pp. 25-34, 2014.

[12]   J. Qi, G. Zhang and H. Li, "Efficient removal of arsenic from water using a granular adsorbent: Fe–Mn binary oxide impregnated chitosan bead", *Bioresource Technology*, vol. 193, pp. 243-249, 2015.

[13]   A. Gupta, V. Chauhan and N. Sankararamakrishnan, "Preparation and evaluation of iron–chitosan composites for removal of As(III) and As(V) from arsenic contaminated real life groundwater", *Water Research*, vol. 43, no. 15, pp. 3862-3870, 2009.

Process Optimization for Synthesis of Ni-based Energetic Materials

Shafi Ullah Khan[1], Muhammad Imran Ahmad[1,*]

[1]Department of Chemical Engineering, University of Engineering and Technology, Peshawar

Author email: shafi9193@gmail.com

Abstract

This paper presents synthesis of Nickel based energetic materials as a suitable replacement for lead based compounds in terms of safety in handling and processing. Typical mixtures of lead azide, and lead styphnate are toxic, and very sensitive to friction, impact and heat. Nickel hydrazine nitrate (NHN) has been utilized for developing energetic materials due to its low mechanical sensitivity, good stability, and insensitivity towards light. NHN was synthesized in a batch process using hydrazine (80%) and nickel nitrate in the presence of Ethanol (80-90%). Comparison with lead azide and lead styphnate mixtures indicate that NHN is more powerful.

Keywords: Energetic materials; lead azide; lead styphnate.

Introduction

In the past, mercury fulminate (MF) was used in detonators as primary explosives. But later on, a mixture of lead azide (LA) and lead styphnate (LS) with small quantity of Al powder known as ASA are used in detonators to replace Mercury Fulminate because of its ultra-sensitive to friction and impact and also its decomposition with passage of time [1]. Lead Azide has considerable advantage in terms of detonation potential. But it is very highly sensitive due to typical structural features. Lead azide on hydrolysis forms hydrozic acid which is very hazardous. Lead azide reacts with metals like copper to form highly sensitive azides leading to serious accidents on handling [2]. The ASA,though safer than mercury fulminate, is quite sensitive to friction, impact, static electricity etc. In the whole detonator production process, most of the unpleasant incidents had been occurring during handling and drying of lead azide, lead styphnate or ASA and such other manufacturing stages [3]. Lead itself increases toxicity and contamination with sever type of its sensitivity during handling and storage [4]. A primary explosive need to be sensitive enough to initiate a detonator but at the same time it should also be safe enough for manufacturing, drying and handling [5].

After these issues, researchers from ordinance community started thinking about the development of a safer energetic and lead free molecule. Studies have been going on silver azide for specific Initiators. But it is more sensitive to friction stimuli than even lead azide [6]. Many researchers in the field considered a compound of Nickel nitrate with Hydrazine Hydrate as one of

the alternatives. Space and defence industry, with a view to thwart the risks and damages of ASA to their end product, adopted going on Silver azide for specific NHN. Some of the properties of NHN are much better than that of lead azide. Its low mechanical sensitivity, good stability and no effect to light makes it a preferred candidate to replace lead azide and lead styphnate in commercial detonators [7].

1. EXPERIMENTAL PROCEDURE

2.1 Materials

Materials such as nickel nitrate, hydrazine hydrate, ethanol and distil water were used of analytical reagent (AR) grade. RDX prepared locally was used in detonators as high explosive.

2.2 Synthesis of NHN

Nickel hydrazine nitrate (NHN) was prepared on lab scale in a set up already available for LA and LS with some amendments. Before starting preparation of NHN, first of all two solutions were prepared. Nickel nitrate (bright green salt) dissolved with saturate hot water, then add the later solution with 1:1 (Volume ratio) with ethanol (80-99%). After mixing it has a green ethanol solution of $Ni(NO_3)_2$. With the same procedure Hydrazine with 80% mix with ethanol. Hydrazine solution was taken and add drop wise under stirring conditions of the green alcoholic $Ni(NO_3)_2$ solution. Temperature of the reaction would be 50°C and this was achieved indirectly by the cycling of steam with specific flow rate. A deep blue precipitate appears which upon agitation turns purple colour.

The complex salt filtrate is insoluble in ethanol/water which helps fast and smooth precipitation and yield is close to 100%. Vacuum drier is used for drying with max 60°C and for 3-4 hrs.

2.3 Analysis

Experiments have been carried out and achieved the product of NHN more safely and easily than LS and LA. NHN after preparation, vacuum dried and then sample is selected for analysis. Three random samples have been selected from different batches and then the general and structure characteristics of NHN are summed up in the **Table 1**.

Table 1: General Characteristics of Nickel hydrazine Nitrate (Values in brackets are taken from literature).

Molecular formula	Ni H12 N8 O
Molecular weight	278.69
Colour	Purple violet
Crystal density (g/cm^3)	2.1
Average particle size (μm)	12
Nickel content (%)	21.12 (21.06)[a]
Hydrazine content (%)	34.47 (34.45)[a]
Nitrate content (%)	44.48 (44.49)[z]
Moisture content (at 333 K for 10 min) (%)	0.34

Average M.wt of combustion products	27.35
Percent condensable Ni (l)	18
Oxygen-fuel ratio	0.8571

1)

2.3.1 Performance Evaluation

Performance of the produced NHN was checked and examined after passing through some basic tests required for detonators and primers.

2.3.1.1 Flash Sensitivity of NHN

NHN (350mg) was filled and pressed in detonatorat2MPa with dwell time of 2-3 s after 20 mg of RDX with same pressing load. Gun powder of Grade-20placed above the pressed NHN loosely and crimped gently. Relative humidity (45 <R_H< 65%) of process room was ensured throughout the preparation and filling operation. For evaluation the NHN filled detonator was vertically held on 4 mm lead plate and the loose Gun powder was initiated by hot electric wire. Dent to the lead plate was measured in terms of the size of the hole equal to the diameter of the detonator.

2.3.1.2 Friction Sensitivity

Detonators filled with NHN (350mg) and RDX were passed through drop test to check friction sensitivity. A steel ball weight of 110 gram was dropped from a height of 6cm on a detonator fix in a drop test fixture and 100% ignition was observed. While from 4cm, 50% ignition was observed. It indicates that NHN is insensitive to mechanical shock up to 10N.

2.3.1.3 Performance Evaluation

Comparative fire/detonation of lead based detonators/primers used in artillery ammunitions and NHN filled dots under the same conditions as already applied for the later one. Detonator LH3 having dimensions (cap case dia 3.5mm and length is 6.5mm while det case 3.6mm dia and 7mm length) were used for this comparison. Lead based detonators were filled according and then NHN has been used where LS & LA was used. Det cap was firstly pressed with 2MPa (250lbs/cm^2) RDX quantity 20 mg at bottom and then 260 mg of NHN pressed at 2MPa (250 lbs/cm^2) over the pressed RDX. After this, det case was filled/pressed RDX 40mg at 2MPa and then loose 60mg of RDX put on the pressed one so that easy for catching flash from det cap.

This type of filling for both lead based and NHN was carried out initially for 50 nos. Of detonators and passed through static tests like jolting, soaking for 4 hrs, drop test to check sensitivity of the det and then detonation where 4mm lead disc was used to check the hole size created after the detonation. Result observed was satisfactory but during filling, low in gauge was observed which is against the filling procedures.

 But it was observed during filling that due to comparatively less density of NHN, 1.5times more use of NHN than lead based. Now there were two options to control the quantity and gauge issues, one is to study about the pressing load and lessen the load to desire value to control the quantity and the second option is to used little more NHN to overcome the gauge issue with same pressing load.

But it was decided after thorough study that quantity factor will be considered instead of pressing load to achieve better result for artillery projectiles. After this observation, 50 nos. of dets were prepared where 360mg of NHN were used and passed through the above mentioned tests and the results were more satisfactory than the previous one.

After the second procedure, another 100nos. of det were filled and 50nos. passing from same basic tests and the remaining were used in artillery fuses and check the behaviour, especially in detonation of fuse where result was satisfactory.

During processing of detonators, the humidity of the operation shop will be in between 45 to 65 %.

Another 250nos. of the dets were prepared with later procedures and this time all tests were carried out thoroughly and 100nos. were used in static tests and processing/performance/handling/storage were satisfactory and even the workers were feel easy during handling/processing. Some dets were used in fuses and send these fuses with gun firing to check the behaviour in ballistics as well and the results were satisfactory. NHN filled Detonators were then placed in open environment where no humidity and temperature control to check their storage behaviour for one month but there is no difference in their behaviours observed. But the storage should be proper like humidity will be $45 < R_H > 65$. NHN used then in other detonators to check the performance and the result is quite suitable.

2. RESULTS AND DISCUSSIONS

After friction sensitivity test it was concluded that alone NHN filled primers were not suitable for percussion and stab action primers but physically it was tested and check the behaviour of the NHN in percussion and stab action type primers. The results were unsatisfactory and 85% duds were observed.

Density of the NHN was calculated and found 2.1 g/cm^3 which is less than LA/LS. It is found in literature that at 2.1 g/cm^3 the detonation of NHN is 6700 m/s while LA has 3400 m/s. In high explosives, RDX has maximum VOD which is approx. 8300 m/sec. For explosive train/chain, it is necessary that each component in the chain will perform correctly otherwise partial detonation of the artillery ammo will observed.

Different types of primers and detonators used in artillery ammos were filled with NHN instead LA/LS at specific conditions which is recommended for the latter composition and tests have been conducted in house. NHN filled detonators responded to initiation by flash and hot wire stimuli. While in percussion and stab action primers, their behaviours were quite unsatisfactory and it shows that NHN is friction insensitivity.

3. CONCLUSIONS

Nickel hydrazine nitrate is an energetic material usually used as initiators, which can prepare easily compare to LA/LS in required quantity and in high yields with no time with economically available raw materials. Because of its low sensitivity to mechanical shock, the processing, handling and storage of NHN detonators is relatively safe. The size and performance of the NHN detonators are matching with the presently used lead based detonator. From the firing data, it is cleared that NHN can be used in place of LA/LS, without compromising on performance.

It is also observed during trial that it is more power full than LS/LA filled detonators and satisfactory results were observed. There is issue with LS/LA filled Detonators that partial detonation may observed sometimes with High Explosives, but this was not observed with NHN because NHN is 3 times powerful than the latter one according to Literature. And this was physically observed during firing of approx. 1000Nos. Detonators.

Lead based composition is hazardous to health and there is a serious issue with contact of lead and this is minimized up to some extent to use lead free energetic compositions for initiators.

4. ACKNOWLEDGEMENTS

5. REFERENCES

[1] M. B. Talawar, A. P. Agrawal, J. S. Chhabra, C. K. Ghatak, S. N. Asthana, and K. U. B. Rao, "Studies on nickel hydrazinium nitrate (NHN) and bis-(5-nitro-2H tetrazolato-N2)tetraamino cobalt(III) perchlorate (BNCP): Potential lead-free advanced primary explosives," *J. Sci. Ind. Res. (India).*, vol. 63, no. 8, pp. 677–681, 2004.

[2] AN Gupta & N V Srinivasa Rao, "A Safer and Green Detonator with NHN Substituting ASA."

[3] P. P. Spear, Robert J and Elischer, "Studies of stab initiation. Sensitization of lead azide by energetic sensitizers," *Aust. J. Chem.*, vol. 35, pp. 1--13, 1982.

[4] 1 and Jawed Ahmad Usmani2 Ab Latif Wani, corresponding author1 Anjum Ara, "Lead toxicity: a review," vol. 8(2), pp. 55–64.

[5] Z. Shunguan, W. Youchen, Z. Wenyi, and M. Jingyan, "Evaluation of a New Primary Explosive: Nickel Hydrazine Nitrate (NHN) complex," *Propellants, Explos. Pyrotech.*, 1997.

[6] B. Hariharanath, K. S. Chandrabhanu, A. G. Rajendran, M. Ravindran, and C. B. Kartha, "Detonator using nickel hydrazine nitrate as primary explosive," *Def. Sci. J.*, vol. 56, no. 3, pp. 383–389, 2006.

[7] B. Nair, UR and Asthana, SN and Rao, A Subhananda and Gandhe, "Advances in high energy materials," *Def. Sci. J.*, vol. 60, pp. 137--151, 2010.